

Graduate Schools Yearbook **2012**



Editors:

Kim Dam-Johansen

Sindhu Vudayagiri

Krist V. Gernaey

DTU Chemical Engineering

Department of Chemical and Biochemical Engineering

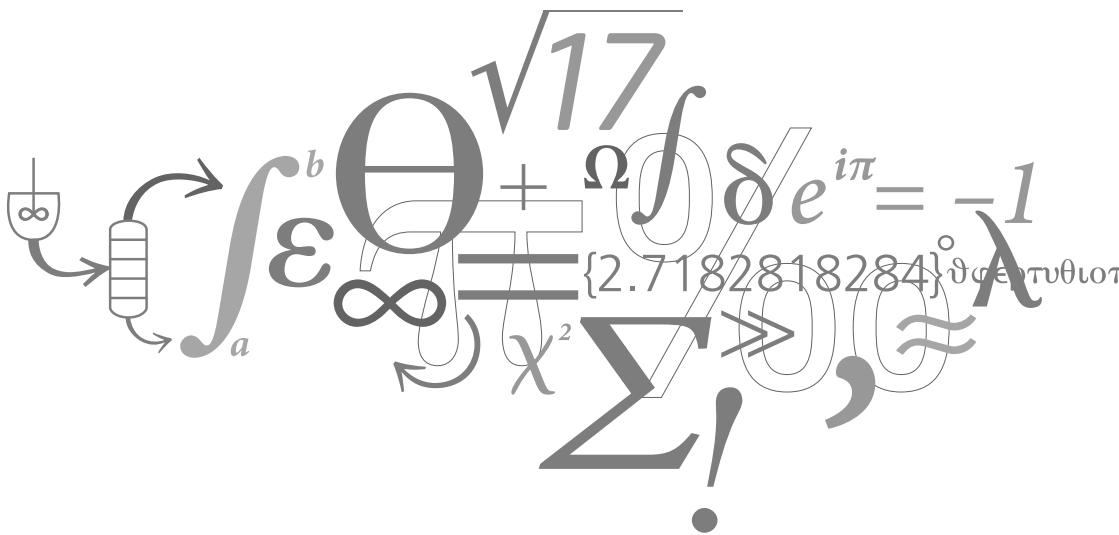
Graduate Schools Yearbook **2012**

Editors:

Kim Dam-Johansen

Sindhu Vudayagiri

Krist V. Gernaey



Address: Department of Chemical and Biochemical Engineering
Søltofts Plads, Building 229
Technical University of Denmark
DK-2800 Kgs. Lyngby
Denmark

Telephone: +45 4525 2800

Fax: +45 4588 2258

E-mail: kt@kt.dtu.dk

Internet: www.kt.dtu.dk

Print: J&R Frydenberg A/S
København
March 2013

Cover: Suzanne Fog

Cover photo: Klaus Holsting

ISBN-13: 978-87-92481-91-7

Preface

In this Graduate Schools Yearbook 2012 the PhD students of the Department of Chemical and Biochemical Engineering present their research projects. Some of the students have just initiated their research and therefore provide a short description of their research project in the Yearbook, whereas others are close to concluding their work and present the most significant project results. We hope that the readers will find the Yearbook interesting and we invite you to contact us in case you would like to receive additional details.

The PhD projects cover all areas of the Department, both at Campus Lyngby and Campus Risø. The total number of PhD students at the Department is now significantly higher than 100. For the years to come, we foresee a consolidation of this level of activity at the Department. One focus area for the forthcoming years will be the initiation of an increased number of industrial PhD projects, since such projects often give unique opportunities to perform experiments on large scale systems, and to start collaboration with new industrial partners.

We wish you a pleasant reading.

Yours Sincerely

Kim Dam-Johansen
Professor, Head of Department

Krist V. Gernaey
Professor, Editor

Contents

Combined Silage Pretreatment and Enzymatic Hydrolysis of Energy Grasses for 2G Bioethanol Production <i>Morten Ambye-Jensen</i>	1
Bioprocess Engineering for the Applications of P450s <i>Marie Andersson</i>	3
Thermodynamic Modeling for CO ₂ Capture Systems <i>Muhammad Waseem Arshad</i>	5
Process Intensification: A Phenomena-based Approach <i>Deenesh K. Babi</i>	7
A Study of Microalgal Symbiotic Communities with the Aim to Increase Biomass and Biodiesel Production <i>Claus Baggesen</i>	11
Temporal Evolution Profiling for enzyme activity determination <i>Andreas Baum</i>	13
Operation and Design of Diabatic Distillation Processes <i>Thomas Bisgaard</i>	17
CO ₂ -Hydrates - Challenges and Possibilities <i>Martin Gamél Bjørner</i>	19
Integrated Microfactories for Enzyme production <i>Vijaya Krishna Bodla</i>	21
Physiological responses of plants and ecosystems to climate change <i>Kristine Stove Boesgaard</i>	23
Monitoring Continuous Fermentation Processes in Microbioreactor Systems <i>Andrijana Bolić</i>	25
Design of Future Municipal Wastewater Treatment Plants: A Mathematical Programming Approach to Manage Complexity and Identify Optimal Solutions <i>Hande Bozkurt</i>	27
Effects of Alternative Fuel Combustion on the Cement Clinker Quality <i>David Bøgh</i>	29
Novel Reactor Design for Organic-Chemical Crystallization of Active Pharmaceutical Ingredients <i>Joussef H. Chaaban</i>	31
Similarity and differences in the Low salinity modeling for carbonate and sandstone reservoir <i>Krishna Hara Chakravarty</i>	33
Synthesis and design of integrated-intensified chemical/biochemical processes <i>Peam Cheali</i>	37
Symbiotic Growth Depressions in Bioenergy and Forage Crops <i>Signe Sandbech Clausen</i>	39
Modelling of phase equilibria and related properties of mixtures involving lipids <i>Larissa Peixoto Cunico</i>	41

Enzymatic Production of Prebiotic Polysaccharides using a bacterial family 11 RGI lyase expressed in <i>Pichia pastoris</i> <i>Inês Rodrigues da Silva</i>	43
Interactions between solid fuels and raw materials in cement rotary kilns <i>Maria del Mar Cortada Mut</i>	45
Line-by-line Modeling of Gas Spectra <i>Vadim Evseev</i>	49
Microalgae with increased synthesis or diminished breakdown of TAG for efficient biodiesel production <i>Camilla Favrholt</i>	53
Systematic Methods and Tools for Computer Aided Modeling <i>Marina Fedorova</i>	57
Cinnamic Acid Derivatized Poly(Ethylene Glycol) as a Stimuli-Adaptable Polymer Material <i>Sarah Maria Grundahl Franke</i>	59
Measurements and modelling of phase equilibrium of oil-water-polar chemicals <i>Michael Frost</i>	63
Enhanced enzymatic cellulose degradation by cellobiohydrolases via product removal <i>Hassan Ahmadi Gavlighi</i>	67
Poly (propylene oxide): A novel silicone-resembling elastomer for dielectric electroactive polymer (DEAP) actuator application <i>Kaustav Goswami</i>	69
On-line Trace Gas Measurement Technique for Biomass Gasification <i>Helge Grosch</i>	73
Enzymatic Production of Human Milk Oligosaccharides <i>Yao Guo</i>	75
Novel Clay/Nanocellulose Biocomposite Films and Coatings in the Context of New Packaging Materials <i>Jon Trifol Guzmán</i>	77
Microbial Enhanced Oil Recovery for North Sea Oil Reservoir <i>Amalia Halim</i>	79
Deposition Build-Up in Grate and Suspension Boilers Firing Biomass <i>Stine Broholm Hansen</i>	81
Integrating resins in enzymatic processes <i>Naweed Al-Haque</i>	85
Combustion Characterization of Bio-derived Fuels and Additives <i>Hamid Hashemi</i>	89
Monolithic Structures and their Influence on Electromechanical Breakdown Phenomena <i>Suzan Hassouneh</i>	91
Mastering Process Intensification across Scales for ω -Transaminase Processes <i>Søren Heintz</i>	93
Thermodynamic and Process Modelling of Gas Hydrate Systems in CO ₂ Capture Processes <i>Peter Jørgensen Herslund</i>	95

Mathematical modeling of vegetable oil crystallization <i>Jeppe Lindegaard Hjorth</i>	99
Are Entangled Polymer Melts Different from Solutions: Role of Entanglement Molecular Weight <i>Qian Huang</i>	103
Property Modeling and Uncertainty Analysis for Reliable Process Design and Sustainability Analysis <i>Amol Shivajirao Hukkerikar</i>	107
Nanoparticle Design using Flame Spray Pyrolysis for Catalysis <i>Martin Høj</i>	111
Climate Change Effects to Plant Ecosystems <i>Cathrine Heinz Ingvorsen</i>	113
A Methodology for Selection of Cascades for Co-product Removal in an ω -transaminase System <i>Krešimir Janež</i>	115
Biomass Burners for Biodust Combustion <i>Joakim M. Johansen</i>	119
Sustainability Assessment of 2nd Generation Bioenergy Production in Ghana <i>Andreas Kamp</i>	121
China's waste crisis and thermal conversion of Chinese waste streams <i>Kasper Bislev Kallestrup</i>	123
Wettability Improvement with Enzymes: Application to Enhanced Oil Recovery under Conditions of the North Sea Reservoirs <i>Alsu Khusainova</i>	125
Nitrogen Cycle Assessments and Greenhouse Gas Emissions in Low-Input Legume Management Systems <i>Petra Lachouani</i>	129
Population Balance Models and Computational Fluid Dynamics: an Integrated Model Framework to Describe Heterogeneity in Fermentors <i>Rita Lencastre Fernandes</i>	131
Speed of sound from Perturbed-Chain Statistical Associating Fluid Theory Equation of State <i>Xiaodong Liang</i>	135
A Development Methodology for Biocatalytic Processes <i>Joana Lima-Ramos</i>	139
Fuel Efficiency and Fouling Control Coatings in Maritime Transport <i>Asger Lindholdt</i>	143
Development of novel cross-linkers for PDMS networks for controlled and well distributed grafting of functionalities by click chemistry <i>Frederikke Bahrt Madsen</i>	145
Inhibition of Gas Hydrate Formation by Antifreeze Proteins <i>Christine Malmos</i>	147
Development of an Electrolyte CPA Equation of State for Applications in the Petroleum and Chemical Industries <i>Bjørn Maribo-Mogensen</i>	151

PDMS microsphere synthesis and theoretical explanation <i>Baoguang Ma</i>	155
Systemic Approach to Sustainability Assessment of Food and Bioenergy Production in a Societal Context <i>Mads Ville Markussen</i>	157
A Systematic Methodology for Design of Emulsion-Based Chemical Products <i>Michele Mattei</i>	159
Multi-Dimensional Population Balance Models of Crystallization Processes <i>Kresten Troelstrup Meisler</i>	163
Operational Aspects of Continuous Pharmaceutical Production <i>Aleksandar Mitic</i>	165
The SolventPro – Computer-Aided Solvent Selection and Design Framework <i>Igor Mitrofanov</i>	167
Optimizing control of the integrated urban wastewater system <i>Ane Loft Mollerup</i>	171
Mechanistic Insight in Hydrodeoxygenation on Nickel Based Catalysts <i>Peter Mølgaard Mortensen</i>	173
Process strategies for implementing (S)- ω -transaminase catalyzed reactions <i>Watson Neto</i>	175
Synthesis and development of novel coating components for exterior wood applications based on sustainable resources <i>Hiep Dinh Nguyen</i>	179
Phytate and Phytase Enzyme Kinetics <i>Anne Veller Friis Nielsen</i>	181
Hydrocarbon Architectures for Fuel Cell Membranes <i>Mads Møller Nielsen</i>	183
Design and Testing of Robust and Efficient Intumescent Coatings <i>Kristian Petersen Nørgaard</i>	187
Deactivation of Selective Catalytic Reduction Catalysts in Biomass Fired Power Plants <i>Brian Kjærgaard Olsen</i>	189
CO ₂ Capture from Cement Production by Carbonate Looping <i>Sharat Kumar Pathi</i>	191
Design of Continuous Reactor Systems for API Production <i>Michael Jønych Pedersen</i>	195
Model of Stickiness in Spray Drying <i>Thomas Petersen</i>	197
Sensitivity Analysis Applied to Kinetics of Enzymatic Biodiesel Production <i>Jason Price</i>	199
Characterization of Residual Particulates from Biomass Entrained Flow Gasification <i>Ke Qin</i>	203

Analysis and quantification of foaming phenomena in wet FGD plants <i>Siqiang Qin</i>	207
Incremental Refinement of Process Design <i>Alberto Quaglia</i>	209
Design and use of scale-down reactors for assessing operational stability of Oxidases <i>Hemalata Ramesh</i>	213
Preheater Design for High Energy Efficiency and Low Emissions <i>Claus Maarup Rasmussen</i>	215
Selective and Efficient Synthesis of Ethanol from Dimethyl Ether and Syngas <i>Dominik Bjørn Rasmussen</i>	219
Large Scale Enzymatic Extraction of Pectic Dietary Fibers <i>Helle Christine Ravn</i>	221
μ -Tools for Development of ω -Transaminase Processes <i>Rolf H. Ringborg</i>	223
Topology optimization in biocatalytic reactions using miniaturized reactors <i>Inês Pereira Rosinha</i>	225
Influence of biomass chemical properties on torrefaction process <i>Suriyati Saleh</i>	227
Upgrading Fuel Properties of Biomass Fuel and Waste by Torrefaction <i>Lei Shang</i>	231
Practical Application of Models in the Urban Water System: Simulation Based Scenario Analysis <i>Laura Snip</i>	235
Climate Change Mitigation by Transport of CO ₂ to Aquifers beneath Croplands <i>Eike Marie Thaysen</i>	237
Catalytic Steam Reforming of Bio-Oil to Hydrogen Rich Gas <i>Rasmus Trane</i>	241
Fast Pyrolysis of Lignin <i>Trung Ngoc Trinh</i>	245
Single Biomass Particle Combustion and Fuel Characterization <i>Anna Trubetskaya</i>	249
Framework for Construction of Multi-scale Models for Biological Wastewater Treatment Processes - Autotrophic Nitrogen Conversion <i>Anna Katrine Vangsgaard</i>	251
Factors affecting surface and release properties of thin PDMS films <i>Sindhu Vudayagiri</i>	255
CO hydrogenation over Cu-Ni catalysts <i>Qiong Xiao Wu</i>	257
Reactor and Process Design for Multi-enzymatic Synthesis <i>Rui Xue</i>	261

An Integrated Methodology for Design of Tailor-Made Blended Products: Lubricant Base Oil <i>Nor Alafiza Yunus</i>	263
Wind Turbine Blade Coatings with Anti-Erosion Properties <i>Shizhong Zhang</i>	267



Morten Ambye-Jensen

Phone: +45 2132 8032
E-mail: morj@kt.dtu.dk

Supervisors: Anne Meyer
Katja Salomon Johansen, Novozymes A/S
Thomas Didion, DLF TRIFOLIUM A/S

PhD Study
Started: November 2010
To be completed: November 2013

Combined Silage Pretreatment and Enzymatic Hydrolysis of Energy Grasses for 2G Bioethanol Production

Abstract

Pretreatment and enzymatic hydrolysis for conversion of lignocellulosic biomass to fermentable sugars is often the most expensive steps in 2nd generation bioethanol production. The aim of this project is to develop a pretreatment method using ensiling combined with enzymatic hydrolysis. Ensiling of biomass has a great potential as storage method for bioenergy feedstock. At the same time the silage process might function as a simple pretreatment method given its moist acidic conditions, and hereby facilitate better enzymatic hydrolysis of the lignocellulosic structure.

Introduction

Ensiling is an anaerobic biological process that conserves biomass. This method of moist forage preservation is widely used for fodder preservation all over the world. The aim of producing silage is to preserve the crop with minimum loss of nutrients and carbohydrates. In a successful silage process, lactic acid bacteria dominate the fermentation process; fermenting free sugars into lactic acid and acetic acid causing the pH to drop which inhibits microbes that decompose polysaccharides, in that way effectively minimizing the degradation of sugars and polycarbohydrates in a crop [1]. The main products from the anaerobic metabolism by lactic acid bacteria can be seen in Figure 1.

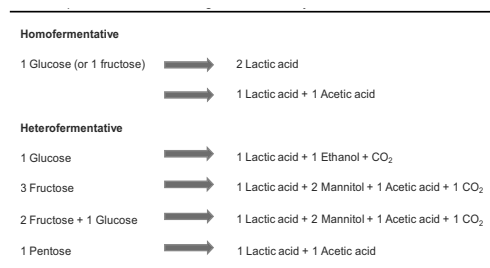


Figure 1: Main products of anaerobic metabolism by lactic acid bacteria

A study by Oleskowicz-Popiel *et al.* [2] at DTU Risø has shown that silage treatment of maize whole crop as well as clover grass is a promising pretreatment method for 2G bioethanol production. The results indicate that

ensiling may serve as sufficient pretreatment for 2G bioethanol production. For example the conversion of cellulose to glucose in maize silage (whole crop) was more than 77%. The ethanol yield after 120 hours was nearby 90% when inoculated with yeast. The results also indicate that further studies on optimization of this method will help to improve the process efficiency. Thus achieved yields are comparable to yields achieved after pretreatment methods using high temperature, high pressure and/or chemicals.

Based on those initial results, it can be concluded that this innovative method has a great potential to be applied in full scale bioethanol production. However, the influence of silage treatment of energy grasses and better understanding of silage process for bioethanol process is necessary to optimize the process, reduce cost and make it industrially.

Hypothesis

A low cost low energy process by means of ensiling and enzymatic hydrolysis can be developed for combined pretreatment and storage in the production of 2G bioethanol from energy grasses:

- The ensiling process can open the lignocellulosic biomass structure and facilitate a <90% conversion of the cellulosic polymers to monomeric sugars in a following enzymatic hydrolysis.
- Efficiency of silage treatment depends on dry matter (DM) at ensiling and use of inoculums, and optimal condition concerning these factors can be identified.

- Efficiency of enzymatic hydrolysis of silage treated energy grass depends on duration, load and enzyme mixture, and optimal conditions concerning these factors can be identified.

The biomass to be used in the project is high yielding forage grass, developed and produced by DLF TRIFOLIUM A/S. This grass, *Festulolium* Hykor, is a hybrid cross between the species *Festuca* and *Lolium*. It grows well in northern temperate regions due to high resistance against cold conditions and yields around 15-17 ton DM/hectare. A characterisation of a first cut harvest of *Festulolium* Hykor can be seen in Table 1.

Table 1: Composition of *Festulolium* Hykor

Biomass component	g/g DM
Free sugars	14.8
Cellulose	29.5
Hemicellulose	20.1
Klason lignin	11.8
Ash	7.7

Several biomasses could be considered. Compared to the use of traditional high yielding annual crops like maize with a high energy content, more diversified perennial pastures like e.g. mix of clover and ryegrass (*Lolium perenne* L.) require fewer inputs (fertilizer, energy for soil treatment), produce more biomass and larger amount of bioenergy/hectare, reduce greenhouse gas emissions more than annual cropping systems, and have the ability to grow on marginal land [3]. Silage of whole crops and pastures is a traditional practice originally developed to “fuel the animal power” on the farm. Increasingly, farmers must consider managing for multifunctionality and include effects on environmental quality in their management decision-making. Thus, investigating ensiling as pretreatment and combined storage method include in principle considerations about managing for emerging ecosystem services such as enhancement of carbon (C) sequestration, mitigation of GHG emissions, and to capitalise on new opportunities, such as bioenergy production, to diversify the traditional cropping systems to achieve these outcomes for the future.

The Silage treatment is carried out using vacuum packaging according to the method of H.E. Johnson *et al.* [4], performed on a Variovac EK10, see Picture 1. Freshly harvested *Festulolium* Hykor is chopped into 2-5 cm pieces and packed in plastic bags, see Picture 2.



Picture 1: Vacuum packaging machine, Variovac EK10

Picture 2: Grass silage bag

Current work

Optimization of the silage treatment. A large factorial design experiment is carried out testing different ensiling conditions of dry matter concentrations and silage inoculants (commercial lactic acid bacteria cocktails) and correlates them to changes in chemical composition and enzymatic cellulose convertibility of the silaged biomass. This test is performed on four cuts over the season to determine seasonal changes and compare these to the effect of dry matter and inoculation.

Acknowledgements

The project is financially supported by The Danish Energy Agency under the programme of EUDP (Energiteknologisk Udviklings- og Demonstrationsprogram)

References

1. D.N. Thompson, J.M. Barnes, T.P. Houghton: *Appl Biochem and Biotech* (2005) 121-124.
2. P Oleskowicz-Popiel, A.B. Thomsen, J.E. Schmidt, *Biomass Bioenergy* (2011)
3. B.S. Dien, H.J.G. Jung, K.P. Vogel, M.D. Casler, J.F.S. Lamb, L Iten, R.B. Mitchell, G Sarath. *Biomass & Bioenergy* (2006) 30(10):880-91
4. H.E. Johnson, R.J. Merry, D.R. Davies, D.B. Kell, M.K. Theodorou, G.W. Griffith, *J Appl Microbiol* (2005) 98(1):106-13.



Marie Andersson

Phone: +45 4525 2958
E-mail: mande@kt.dtu.dk

Supervisors: John M. Woodley
Ulrika Törnvall
Pär Tufvesson

PhD Study

Started: February 2012
To be completed: January 2015

Bioprocess Engineering for the Applications of P450s

Abstract

P450 monooxygenases hydroxylate unactivated hydrocarbons stereo- and regiospecifically, reactions hard to perform via chemical routes. Whole cells is a suitable biocatalyst form due to enzyme restrictions but the whole cell reactions involving P450s still face several challenges, shown to be related to the host cell and the specific reaction performed, e.g. solubility issues, mass transfer limitation and oxygen supply. Strategies proposed to overcome these issues are optimization of the mode of operation, to use a 2-phase system and to design a suitable oxygen supply system.

Introduction

Cytochrome P450 monooxygenases (P450 or CYP) comprise a group of heme-containing enzymes hydroxylating non-activated hydrocarbons in a stereospecific manner, something that is hard to achieve via classical chemistry. The importance of these reactions can be stressed by the hydroxylation of steroids, but hydroxylation of e.g. alkanes, alcohols and fatty acids is also highly interesting in e.g. the polymer industry if the processes can be designed with high yield and productivity. The main biological challenges for these enzymes are the requirement for cofactor, corresponding electron transfer proteins, limited stability and low activity. P450s are mainly dependent on NAD(P)H but NADH is also used by some classes. The use of a host cells cofactor regeneration system provides a major economic advantage as it circumvents the need for stoichiometric amounts of cofactor to be supplied to the reaction. The electron transport from the cofactor to the heme active site has been shown to be another limitation to the system and possible redox partners for heterologously expressed systems are hard to anticipate and needs to be determined experimentally. As in many biocatalytic reactions the stability of the catalyst is also a challenge to P450 processes. Not only has the stability of the monooxygenase but also the redox partner, cofactor and host to be considered. For eukaryotic membrane bound P450s this is a particular challenge. A whole cell system provides a cofactor regeneration system, possibility of coexpression of redox partners and a protected environment to enhance the stability of the catalyst and furthermore it reduces

the cost added to the process by a purified or immobilized enzyme.

Specific objectives

The objectives of the project are to:

- define the requirements and bottlenecks for an industrial relevant process involving P450 monooxygenase
- evaluate mode of operation (growing or resting cells)
- evaluate 2-phase system involving water immiscible organic solvents
- explore oxygen supply strategies
- perform environmental and economic evaluation of a selected process

Results and Discussion

Published whole cell P450 processes above 1L have been summarized in Fig 1. Only one process reaches the biocatalytic productivity target of 10 g product per g cell dry weight and a product concentration of 50 g/L defined to be the requirements for production of pharmaceuticals [1]. This process consists of a *Candida tropicalis* mutant with the native P450 from the host for the hydroxylation of alkanes [2] and is superior compared to the alternative processes.

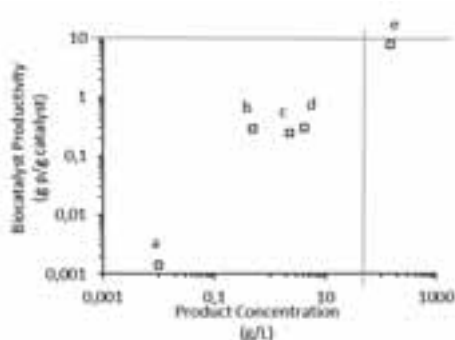


Figure 1: Biocatalyst productivity vs product concentration as reported in literature for whole cell P450 processes above 1L scale.

The mode of operation is one of the first things that can influence the reaction and different options are illustrated in Fig 2. Growing cells are known to be more resistant to solvents but do not allow the fermentation and transformation process to be optimized separately. However, growing cells require more oxygen both for the cell metabolism and a stoichiometric amount to the reaction performed, as illustrated in Fig. 3. Based on reached expression and activity in literature [3], industrial fermenters would only be able to supply 5g cdw/L with the required oxygen demand. However, this would not be enough to reach the economical requirements specified above and cell recycle would be required which would put extra pressure on the stability of the host cell and enzyme itself.

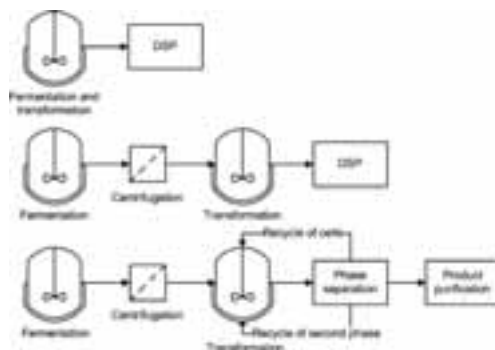


Figure 2: Possible mode of operation of the process. Top; growing cells where fermentation and transformation are performed simultaneously. Middle; resting cells, which enables the fermentation and transformation to be optimized separately. Bottom; suggestion for a process where a second phase is introduced in the transformation step and both solvent and cells are being recycled.

Most substrates for P450 catalyzed reactions are not water miscible and in many cases toxic to the cells and inhibitory to the enzyme. Substrate feeding and 2-phase

systems are suitable solutions to these limitations. However, the requirement of oxygen restricts the solvent selection to non-volatile solvents to avoid an explosive atmosphere. Application of a second phase can also introduce transport limitations of the substrate between the phases. The transport of the substrate and product across the cell membrane can also limit the reaction and this can be avoided either by host cell engineering or chemical disruption of the cell membrane.

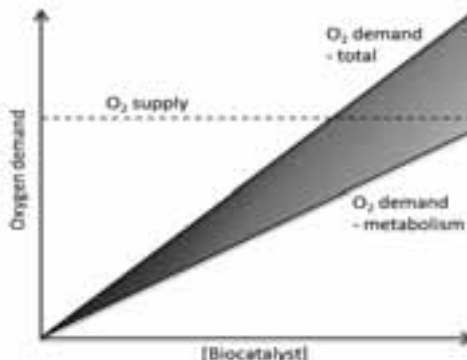


Figure 3: Oxygen requirement for metabolism of growing cells and total requirement for transformation and growing cells limited by the possible supply in a traditional fermenter. Modified from [4].

Conclusions

The activity and stability reached by single component P450s [3] are sufficient for industrial implementation provided that this activity can be maintained for 24h. Based on the required cell density for an economical pharmaceutical process (13 g cdw/L) without cell recycle, this leads to bottlenecks related to the reaction and host cell, such as solubility issues and mass transfer limitations of both substrate and oxygen. Solutions to these limitations can be addressed by introduction of a second phase and increased oxygen supply by e.g. a bubble column.

Acknowledgements

The author would like to acknowledge P4FIFTY financed by the People Programme (Marie Curie Actions) of the European Union's Seventh Framework Programme FP7 under grant agreement no. 289217

References

1. P. Tufvesson, J. Lima-Ramos, M. Nordblad, J.M. Woodley, *Org. Process Res. Dev* (15) (2011) 266-274
2. S. Liu, C. Li, X. Fang, Z. Cao, *Enzym Microb Tech* (34) (2004) 73-77
3. S. Pflug, S.M. Richter, V.B Urlacher, *J. Biotechnol.* (129) (2007) 481-488
4. C.V.F. Baldwin, J.M. Woodley, *Biotechnol. Bioeng.* (95)(2006) 362-369



Muhammad Waseem Arshad

Phone: +45 4525 2866
E-mail: mwa@kt.dtu.dk

Supervisors: Kaj Thomsen
Nicolas von Solms

PhD Study

Started: September 2010
To be completed: September 2013

Thermodynamic Modeling for CO₂ Capture Systems

Abstract

Process simulation of carbon capture processes require the availability of thermodynamic models for CO₂ capture systems which requires accurate experimental data. The solvent systems used for CO₂ capture are usually aqueous solutions of amines, alkanolamines or their blends, ammonia, amino acids and carbonates. These are electrolyte systems so the thermodynamic modeling of these systems can only be done with electrolyte models like Extended UNIQUAC model. In this project, we are investigating an amine based solvent system with two different amines 2-(Diethylamino)ethanol (DEEA) and 3-(Methylamino)propylamine (MAPA). Their mixture at a certain composition splits into two liquid phases on CO₂ absorption with an upper phase lean in CO₂ and a lower phase rich in CO₂. If only the CO₂ rich phase is regenerated, the energy requirements for solvent regeneration can be reduced due to low liquid circulation rate in the stripper. Since, these phase change solvent systems are relatively new and there is a complete lack of experimental data in the open literature, different types of experimental measurements like freezing point depression, vapour liquid equilibrium, heat of absorption etc. are planned together with the thermodynamic modeling of these CO₂ capture systems using the Extended UNIQUAC model.

Introduction

Amine scrubbing has been considered the most feasible route to post-combustion CO₂ capture from power plant flue gases due to its use in many industrial applications e.g. acid gas removal from natural gas, CO₂ removal from reformer gases. However, it is well known that these processes are relatively energy intensive. There is a need to develop solvent systems with improved energy efficiency while retaining the favorable properties of high CO₂ loading capacity, fast reaction rate, low solvent degradation and being environmental friendly.

Specific Objectives

The main objectives of this work are as follows:

1. Experimental measurements of freezing point depression (FPD), vapour liquid equilibrium (VLE) and heat of absorption of CO₂ in aqueous binary and ternary solutions of DEEA and MAPA. The selected mixture composition gives liquid-liquid split on CO₂ absorption.
2. Thermodynamic modeling of above systems using extended UNIQUAC thermodynamic model.

Experimental Work

Heat of reaction is an important parameter for designing unit operations for acid gas removal. In the current

work, enthalpy of absorption of CO₂ in aqueous single amines (DEEA and MAPA) and amine mixtures (DEEA-MAPA) were measured as a function of CO₂ loading, temperature and amine composition. A reaction calorimeter model CPA 112 (ChemiSens AB, Sweden) was used for the measurements. A schematic diagram of the experimental setup is given in Figure 1 [1].

Before starting the experiment, the reactor was evacuated in order to ensure the complete removal of any inert gas present in the reactor. After evacuation about 1200-1500 cm³ of amine solution was fed into the reactor from an amine solution feed bottle and heated to a set temperature. The system was then allowed to reach equilibrium by ensuring when no change in reactor temperature (within $\pm 0.01^\circ\text{C}$) or pressure (within ± 0.01 bar) was observed. When the system attained equilibrium, monitored by the pressure difference in the CO₂ storage cylinders, ~ 0.1 - 0.3 mol of CO₂ was fed into the reactor through the mass flow controller. The system was then allowed to reach a new equilibrium before the next CO₂ feeding sequence could take place. The feeding process was continued until no more CO₂ could enter the reactor at set pressure (the absorption rate equals zero). The pressure and temperature in the reactor and CO₂ storage cylinders were recorded before and after each feeding. The amount of heat added or

removed from the system by the thermostat medium used to keep the system at constant temperature was also recorded. The measurements were taken isothermally at temperatures, 40 and 120°C. The Peng-Robinson equation of state was used to calculate the amount of CO₂ added to the reactor from the pressure difference in the CO₂ storage cylinders before and after each CO₂ feeding. The heat released in each interval was determined by integration of the heat flux curve. The molar heats of absorption were then calculated from the ratio of heat released in a feeding interval to the amount of CO₂ absorbed [2].

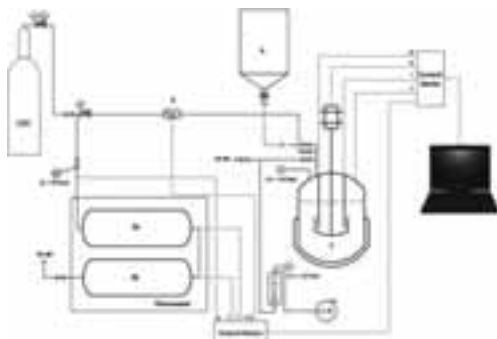


Figure 1: Experimental setup for measuring heat of absorption: 1 - reaction calorimeter; 2a, 2b - CO₂ storage cylinders; 3 - CO₂ mass flow controller; 4 - amine solution feed bottle; 5 - vacuum pump [1].

Results and Discussion

The differential enthalpies of absorption of CO₂ in all the systems studied in this work are presented in Figure 2 for absorption conditions (40°C) and Figure 3 for desorption conditions (120°C). All the measured data were compared with 30 mass% MEA as base case. It can be seen that the heat of absorption is a function of temperature i.e. increases with temperature. For amine mixtures, heat of absorption is also a function of amine composition in the mixture and CO₂ loading.

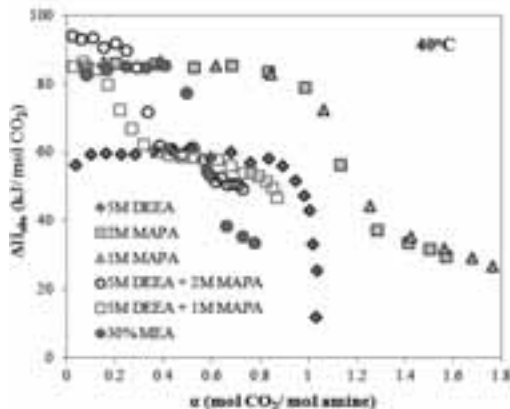


Figure 2: Differential enthalpy of absorption of CO₂ for all the studied systems and 30 mass% MEA at 40°C.

DEEA has shown the lowest heat of absorption among all the studied systems and MAPA has values close to that of 30 mass% MEA at absorption and desorption conditions. Both amine mixtures have shown relatively less heat of absorption compare to 30 mass% MEA. The amine mixtures have also shown low absorption capacity at 120°C.

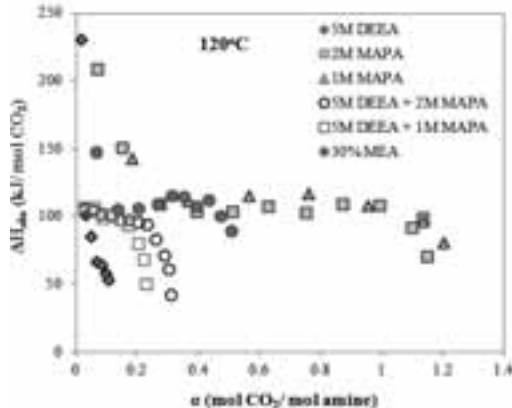


Figure 3: Differential enthalpy of absorption of CO₂ for all the studied systems and 30 mass% MEA at 120°C.

Conclusions

A commercially available reaction calorimeter CPA 112 (ChemiSens AB, Sweden) was used to measure the differential heats of absorption of CO₂ in phase change solvents as a function of temperature, CO₂ loading and solvent composition. The tested systems were 5M DEEA, 2M MAPA, 1M MAPA, 5M DEEA + 2M MAPA and 5M DEEA + 1M MAPA. The measurements were carried out at absorption (40°C) and desorption (120°C) conditions.

Acknowledgements

This Ph.D. is a part of iCap project and financially supported by the European Commission under the 7th Framework Program (Contract No. 241393).

References

1. I. Kim, H.F. Svendsen. *Int. J. of Greenhouse Gas Control* 5 (2011) 390-395.
2. I. Kim, H.F. Svendsen. *Ind. Eng. Chem. Res.* 46 (2007) 5803-5809.

List of Publications

1. M.W. Arshad, N. von Solms, H.F. Svendsen, K. Thomsen. Heat of Absorption of CO₂ in Aqueous Solutions of DEEA, MAPA and their Mixture. GHGT-11, Kyoto, Japan, 2012.
2. M.W. Arshad, K. Thomsen. Freezing Point Depression of Aqueous Solutions of DEEA, MAPA and DEEA-MAPA with and without CO₂ Loading. 2nd ICEPE, Frankfurt am Main, Germany, 2011.
3. P.L. Fosbøl, R. Neerup, M.W. Arshad, Z. Teclé, K. Thomsen. *J. Chem. Eng. Data* 56 (2011) 5088-5093.



Deenesh K. Babi

Phone: +45 4525 2959
E-mail: dkbabi@kt.dtu.dk

Supervisors: Rafiqul Gani
John M. Woodley

PhD Study
Started: September 2011
To be completed: August 2014

Process Intensification: A Phenomena-based Approach

Abstract

Process Intensification (PI) is a means by which the overall improvement of a process can be sustainably achieved through the improvement of key elements within the process, for example energy efficiency and waste reduction. Primarily, PI exists at the unit operations (Unit-Ops) level and two examples of wisely used PI equipment that has been implemented in industry are reactive distillation and dividing wall columns. PI is generally considered during plant retrofit. But the following question should be considered, why consider PI during plant retrofit and not during process synthesis and design? If PI is considered like this then simultaneous synthesis, design and intensification can all be considered during process sthesis. But this is not enough, in order to go beyond existing Unit-Ops and therefore be predictive; one has to operate at a lower level of aggregation. Previously different PI methodologies operated at the Unit-Ops [1,2] and task levels [3] and it was shown how PI can be achieved, but these methods were only able to find solutions based on existing Unit-Ops. Therefore to go beyond the existing Unit-Op solutions one has to operate at the phenomena level which uses key knowledge obtained from the previous developed methodologies. The objective of this work is the development of a systematic methodology which integrates process synthesis and PI.

Introduction

Process Intensification (PI) can be defined as the improvement of a process at the operational, functional and/or phenomena levels that is: (a) Operational- the integration of unit operations for example reaction and separation, (b) Functional (task)- the enhancement of functions for example the finding of a new solvent for an extractive distillation process and (c) Phenomena- the integration or targeted enhancement of phenomena which has an overall impact on the functional and operation levels. PI aims to improve processes without sacrificing product quality, by increasing efficiency, reducing energy consumption, costs, volume and waste as well as the overall improvement of plant safety. The main objectives of process synthesis are as follows: (a) The systematic generation of a process flowsheet to fulfill a particular goal [3], (b) Process analysis/evaluation and (c) The selection of the best flowsheet to achieve a desired goal based on the previous step. In industry, process improvements are primarily done through an evolutionary optimization approach; however with the inclusion of PI into process synthesis, one can further evaluate a process for the inclusion of intensified equipment which can be novel or mature. Currently process synthesis is performed and

then during, for example, plant retrofit, PI is considered. Therefore the objective of this work is the development of a systematic methodology which integrates process synthesis and intensification. This integrated approach has the following benefits: (a) Simultaneous investigation whether the process from process synthesis can be intensified, (b) Investigations are performed at different levels: unit operations→tasks →phenomena and (c) The ability to be innovative and hence propose new designs for intensified equipment.

Discipline

The research conducted in this field is primarily within the field of process systems engineering (PSE).

Methodology

The synthesis, design and intensification methodology is shown in *Figure 1*. The methodology is explained as follows: Step1-6 consists of the problem and objective function definition, the investigation whether a base-case design exist/does not exist, in which case flowsheet alternatives are generated and screened. If a base-case design exists, as is the case for retrofit, then this design is considered as a reference for further improvement. Step 7-8 consists of performing a sustainability analysis

using data obtained from rigorous simulation, which helps in the identification of process bottlenecks. Having this information the phenomena based (PBS) intensification sub-method is entered.

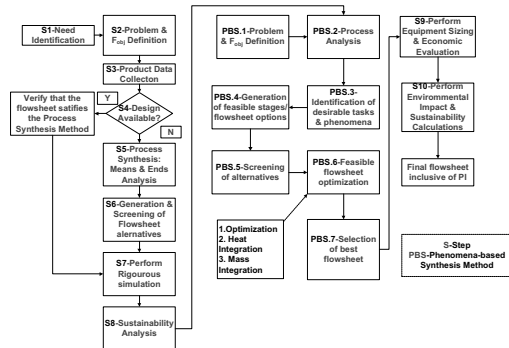


Figure 1 Synthesis, Design and Intensification Methodology

Step 9-10 consist of equipment sizing and economic evaluation followed by a further environmental and sustainability analysis. The PBS sub-method consists of a process analysis for identification of further bottlenecks using a knowledge-based search, the representation of the flowsheet in terms of unit operations, tasks and phenomena, and the identification of phenomena needed to improve the process. The next steps consist of the connection and analysis of the phenomena obtained from the previous step to form a series of building blocks for the generation of unit operations then flowsheet alternatives. These alternatives are then screened using logical, structural and operational constraints and the feasible flowsheets are optimized in order to find the best flowsheet alternative. In this way the final flowsheet is simultaneously synthesised, designed and intensified.

Concepts

In order to move from the flowsheet to the phenomena level one moves down the hierarchy as follows: Flowsheet→Unit-Ops→Tasks→Phenomena. At the phenomena level when further process bottlenecks are identified, then appropriate tasks via the knowledge-base are found in order to overcome these bottlenecks. When these tasks are identified, these are then translated to the phenomena level. Finally a set of individual phenomena building blocks (PB) are obtained, which can then be connected using connectivity rules to form different structures, ultimately forming different intensified flowsheet options. This concept is shown in *Figure 2*. An example of the phenomena mentioned here is as follows: a distillation column non-separative section consists of the following phenomena occurring simultaneously (referred to as a simultaneous phenomena building block): Mixing=2Phase mixing (V-L)=Phase contact=Phase transition (V-L)=Phase separation (V-L) and the 'smiles' representation: $M=2phM=PC(V-L)=PT(V-L)=PS(V-L)$.

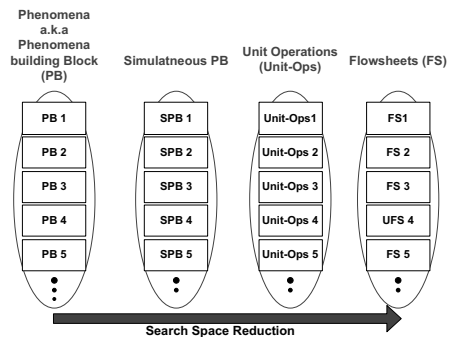


Figure 2 Concept: Connection of phenomena building blocks to form flowsheets

Tools

In applying this methodology different tools are used and are classified as follows:

- Property prediction: ProPred
- Modelling-MoT
- Economic Evaluation: ECON
- Sustainability Analysis: LCA/SustainPRO
- Rigorous simulation: PROII/ASPEN
- Knowledge-base

The first 4 tools are part of a developed integrated computer-aided software (ICAS) developed by CAPEC. The knowledge-base consists of information such as follows: (a) Intensified Unit-Ops and the process bottlenecks that they have been used to overcome and (b) The translation of phenomena into Unit-Ops. If after checking the knowledge-base for a given Unit-Op based on a set of connected phenomena which fulfill process requirements, none is found, then a novel solution is obtained.

Methodologies

This methodology uses information gained from two other process synthesis methodologies which operate at the Unit-Ops and tasks levels in order to perform an accurate process analysis based on thermodynamic insights and to find the means by which tasks and phenomena can be integrated in order to generate intensified flowsheets. These methodologies are process synthesis based on thermodynamic insights [2] and the means-ends analysis [3]. The overall integration is shown in *Figure 3*.

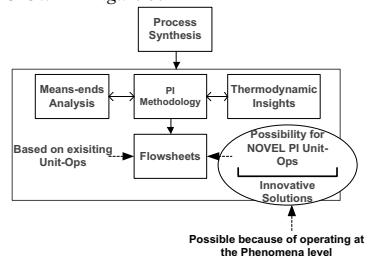


Figure 3 Integration of the methodologies from [2] & [3]

Case study Application

Two case studies are currently being applied to the methodology, the production of methyl-acetate (MeOAc) and the production of di-methyl carbonate (DMC). Here the study related to the production of MeOAc will be highlighted.

Step 1-6: Need identification and problem definition: Production of MeOAc for the production of (example) cleaners for ink processes and the identification of an intensified flowsheet for the production of MeOAc having the lowest operational cost per amount of product produced. The raw materials are acetic acid (HOAc) and methanol (MeOH), the reaction type is an esterification reaction and three azeotropes exist in the system. A base-case design was available through a literature survey which was a multi-step process which had consisted of a reactor, extractor, decanter, several normal and azeotropic distillation columns, and two mass separation agents. Step 7-8: The base design was verified through rigorous simulation and from the application of the sustainability analysis process bottlenecks that were identified were as follows: high energy and solvent usage for separations.

PBS 1-2: The problem definition has already been defined in S1. From a further process analysis and use of the knowledge-base, another bottleneck was identified that is limiting equilibrium reaction. The flowsheet is then decomposed into its constituent Unit-Ops and then represented in terms of a task-based flowsheet. Having the task-based flowsheet and knowing what Unit-Ops exist in the flowsheet, it can then be represented in terms of a phenomena-based flowsheet because the phenomenon present within each Unit-Op has been previously identified. PBS 3: Having all the process bottlenecks (from Step 8 and PBS 2), using the knowledge-base, tasks can be identified in order to overcome these bottlenecks for example because the reaction is equilibrium governed simultaneous removal of a product will shift the equilibrium. After these tasks have been identified, they can then be translated into phenomena via information from the thermodynamic insights [2]. From PBS 3 all the individual phenomena building blocks are obtained, in total 13, which have overcome the identified process bottlenecks. These can now be connected to form simultaneous phenomena building blocks (SPB's) and the total possible options are statistically calculated as follows, where $n_{p,tot}$ is the total number of individual phenomena building blocks (13) and $n_{p,max}$ is the maximum phenomena within an SPB:

$$n_{p,tot} = 13$$

$$n_{p,max} = 9$$

$$NSPB_{max} = \left[\sum_{k=1}^{n=n_{p,max}} \frac{(n_{p,tot} - 1)!}{(n_{p,tot} - k - 1)!k!} \right] + 1 = 4017$$

Using connectivity rules for example heating and cooling cannot exist within a SPB because this is not energy efficient that is $M=H=C=...$, the SBP's are screened and reduced to 58. An excerpt is shown in Table 1.

Table 1 Example of feasible SPB's

SPB	Interconnection Phenomena	In	Out
SPB.1	M	1..n(L)	1(L)
SPB2	M=R	1..n(L)	1(L)
SPB.7	M=R=2phM=PC=PT(VL)	1..n(L,VL)	1(V/L)
SPB.8	M=R=2phM=PC=PT(VL)=PS(VL)	1..n(L,VL)	2(V;L)
SPB.9	M=R=2phM=PC=PT(PVL)=PS(VL)	1..n(L,VL)	2(V;L)
SPB.58	D	1(L;VL,V)	1..n(L;V; VL)

PBS 4-5: These SPB's can then be further to form operations which are then translated into Unit-Ops which form flowsheets, see Figure 2. Each operation must be checked for feasibility to ensure that process requirements are fulfilled, in this case for the production of MeOAc. An example of a process operation not fulfilling process requirements is shown in Table 2.

Table 2 Process operation not fulfilling process requirements

Process Operation	SPB
1	M=C=2phM=PC=PT(VL)
2	M=R=2phM=PC=PT(VL)=PS(VL)
3	M=H=2phM=PC=PT(VL)

The process operation in Table 2 can be translated into a Unit-Op consisting of a condenser (1), reactive section (2) and reboiler (3). However this can fulfill process requirements because within such a Unit-Op non-reactive separation sections are needed where the product is obtained. One of the feasible Unit-Ops obtained from a knowledge-base search, which fulfills process requirements is a reactive distillation column, shown in Table 3, which has a similar configuration to that presented in Table 2 but also includes the non-reactive separations (2 and 4).

Table 3 Process operation fulfilling process requirements

Process Operation	SPB
1	M=C=2phM=PC=PT(VL)
2	M=2phM=PC=PT(VL)
3	M=R=2phM=PC=PT(VL)=PS(VL)
4	M=2phM=PC=PT(VL)
5	M=H=2phM=PC=PT(VL)

Having this structure one can then generate even further alternatives for example, replace one or both of the on-reaction separation sections with a membrane separation. This can be a new alternative because it still fulfill process requirements.

Future Work

The future work related to this thesis is as follows:

- The completion of the remaining steps of the methodology when applied to the case studies
- Further application of the methodology to other case studies.
- The continuous development of the methodology
- Ultimately the development of a computer-aided tool for the automation for applying some of the steps in the methodology

Current Conclusions

The current conclusions of this thesis are as follows:

- A systematic methodology inclusive of process synthesis and intensification (integrated approach) has been developed and presented
- The integrated approach operates at four levels: flowsheet, unit-operations, tasks and phenomena
- The concept of phenomena based PI is promising because it is believed that all intensified flowsheet options can be generated if one operates at this level of aggregation
- The integrated approach has been applied to the production of MeOAc and it can be shown that besides the generation of reactive distillation other option(s) can be generated

References

- [1] P. Lutze, R. Gani, J.M. Woodley, A systematic synthesis and design methodology to achieve process intensification in (bio) chemical processes, *Comp. & Chem. Eng.* 36 (1) (2012), 189-207
- [2] C. Jaksland, R. Gani, K. M. Lien. Separation process design and synthesis based on thermodynamic insights. *Chem Eng Sci*, 1995 (50) 511-530
- [3] J.J. Siirola, Industrial Applications of Chemical Process Synthesis, *Advan. in Chem. Eng.*, 23 (1) (1996), 1-62



Claus Baggesen
Phone: +45 4677 4298
E-mail: cbag@kt.dtu.dk

Supervisors: Claes Gjermansen
Anders Brandt
John Woodley
Krist V. Gernaey

PhD Study
Started: Nov 2010
To be completed: Dec 2013

A Study of Microalgal Symbiotic Communities with the Aim to Increase Biomass and Biodiesel Production

Abstract

Microalgae show great promise as feedstock for production of biodiesel. Many species exhibit fast growth rates reach high cell densities and contain large amounts of lipid. This study investigates the role symbiotic bacteria in microalgal cultures as these can enhance the growth of the microalgae. Results show that growth of the microalgae *Dunaliella salina* greatly benefit from the presence of several species of bacteria.

Introduction

As the price for fossil fuels rise so does the worldwide need for energy as well as the need for energy security. In order to respond to these challenges, research to develop new sources of alternative fuels is growing. Microalgae represent a solution for biomass-derived energy which does not compete with food production and fresh water resources. The fast growth rates as well as high lipid content of some microalgal species make them a promising feedstock for biodiesel production. Furthermore, they grow and thrive in a wide range of habitats, from fresh to hyper-saline waters all over the globe. This makes it possible to find species or strains with optimized growth at almost every location, thus eliminating the need for artificial light, heat etc [1]. Key factors in making microalgal biodiesel a viable product are understanding how and when the microalgae produce lipids as well as understanding what make the microalgae grow fast and develop dense populations, i.e. biomass. Some studies have shown close relation between microalgal growth and the presence of bacteria [2,3][2,3]. It has been shown that bacteria provide vitamin B₁₂ for some algae which cannot synthesize this cofactor [4]. The importance of this relationship has however been disputed[5]. Other studies have shown that microalgal cultures benefit from the presence of bacteria under iron deficient conditions [2], and it has been shown that some bacteria produce siderophores, iron chelators, which can

facilitate iron uptake in microalgae [6]. Most likely interactions other than those which are already known occur between microalgae and bacteria.

It is possible to grow most microalgae under axenic, i.e. pure, conditions, but growing microalgal biomass for biodiesel production will, however, most likely be done in open ponds. Under such conditions it will be of value to understand the interactions between microalgae and microorganisms in the community that will be established.

Specific objectives

The aim of this study is to assess the importance of the symbiosis between microalgae and bacteria in order to increase both growth rate and biomass production as these factors are important if microalgal derived biodiesel shall become viable. This will be done by investigating the effect of bacterial strains on the growth and biomass accumulation in microalgal species which show promise for production of biodiesel. Investigations also cover identification of compounds, produced by the bacteria, which promote microalgal growth as investigations of potential physical contact between microalgae and bacteria.

Experimental procedure

Bacteria which are naturally occurring in most microalgal cultures were isolated from a strain of *Dunaliella salina* (Dunal) Teodoresco and repeatedly restreaked on solid

media to obtain pure strains. To obtain axenic *D. salina* cultures the microalgae were grown in media containing different antibiotics. The bacteria have been identified by means of PCR and gene sequencing. To test the effect of these bacteria on microalgal growth they have been inoculated into axenic cultures of *D. salina*. Growth rates and cell densities were then measured by flow cytometry and compared with those of the corresponding axenic culture as well as the original *D. salina* culture containing a variety of bacterial species.

Results

In order to verify that the presence of bacteria has a beneficial effect on *Dunaliella salina* the growth of axenic cultures was compared with that of the original culture containing both microalgae and bacteria. This series of experiments convincingly showed that the original culture could sustain growth for a longer period (Fig. 1).

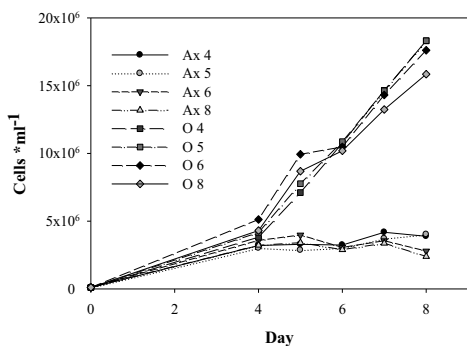


Figure 1: The growth of axenic (Ax) cultures of *Dunaliella salina* compared to the growth of the original culture (O) at different iron concentrations.

Three species of bacteria were isolated and identified from the original culture: *Halomonas* sp., *Marinobacter* sp. and *Pelagibaca* sp. Both M and H are known from other microalgal symbiosis studies [2,6]. The effect of the bacteria, when inoculated into axenic cultures of *D. salina* are substantial (Fig. 2). The inocula of both *Marinobacter* sp. and *Pelagibaca* sp. need to be quite large in order to detect a positive effect on the growth of the microalgal culture. With *Halomonas* sp., however, only a small inoculum is needed.

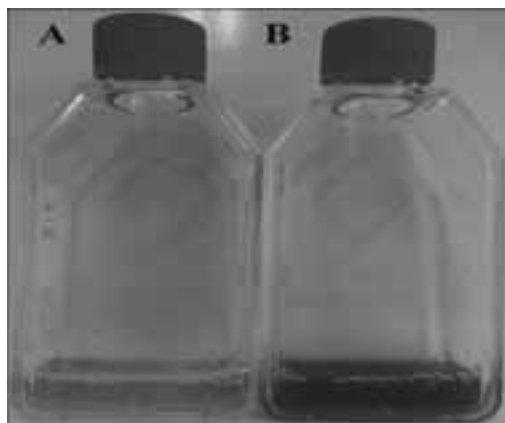


Figure 2: After two weeks of growth, the axenic culture of *Dunaliella salina* (A) has much less color, i.e. less cells, compared to that of an axenic culture with an inoculum of *Halomonas* sp. (B).

Discussion

The results show that the microalgal cultures in the presence of these bacteria reach much higher densities. This may become important in case these microalgae are to be grown as feedstock for biodiesel production. With further research, we believe that it will be possible to determine which bacteria need to be present within the microalgal culture to obtain to maximum densities. Knowledge of the right composition of the community of microalgae and bacteria will be important when growing microalgae in larger scale. Outdoor ponds will probably be the only economically sound strategy for production of microalgal biomass for biodiesel. Such cultures will be susceptible to microbial contamination, but if the composition of the starter culture is balanced deleterious effects of a contamination can probably be countered.

References

1. M. Daroch, S. Geng, G. Wang. Appl Energy (2012).
2. E. Keshtacher-Liebson, Y. Hadar, Y. Chen. Appl Environ Microbiol 61 (6) (1995) 2439-41.
3. Y. Park, K. Je, K. Lee, S. Jung, T. Choi. Hydrobiologia 598 (1) (2008) 219-28.
4. M.T. Croft, A.D. Lawrence, E. Raux-Deery, M.J. Warren, A.G. Smith. Nature 438 (7064) (2005) 90-3.
5. M.R. Droop. J Plankton Res 29 (2) (2007) 107-13.
6. S.A. Amin, D.H. Green, M.C. Hart, F.C. Küpper, W.G. Sunda, C.J. Carrano. Proc Natl Acad Sci U S A 106 (40) (2009) 17071-6.



Andreas Baum

Phone: +45 4525 2943

E-mail: ABA@kt.dtu.dk

Supervisors: Jørn D. Mikkelsen
Per Waaben Hansen, FOSS Analytical

Industrial PhD Study

Started: June 2010

To be completed: May 2013

Temporal Evolution Profiling for enzyme activity determination

Abstract

Replacing cumbersome univariate enzyme activity assays with universal and direct spectroscopic assays promise a better and direct observation of the big picture regarding ongoing enzymatic reactions. The recent advances in multivariate analysis allow substantial alternatives to question the reasonability of traditional enzyme activity assessment. The presented study enables possibilities to monitor various enzymatic reactions continuously by taking all substrate(s) and product(s) into account. By observing temporal spectral evolution the method inaugurates possibilities to also characterize multi component enzymatic systems as complex cellulose blends.

Introduction

Current assay methods for biomass and polysaccharide degrading enzymes are particularly cumbersome mainly due to the complexity of the substrates, and rely on the use of artificial substrates, crude measurements such as reducing end analyses, laborious photometric techniques, which may only measure the reaction indirectly, or employ advanced chromatography-based analyses [1-3]. A main disadvantage of all existing enzyme assays is that they rely on measurement of either the product formation or the substrate consumption, not both at the same time.

The presented study demonstrates a new approach to monitor enzymatic reactions continuously by taking all substrate(s) and product(s) into account. By observing temporal spectral evolution using FTIR the method inaugurates possibilities to also characterize multi component enzymatic systems. The approach does not require any chemical standards or biomarkers, but instead utilizes multivariate analysis to continuously monitor the enzymatic reaction in real time. Thus the method is directly applicable to a wide range of enzymes, even considering complex sample matrices, and may furthermore be highly suitable for automation implying intelligent instrumentation.

At last, the recent advances in multivariate analysis allow substantial alternatives to question the reasonability of traditional enzyme activity assessment.

Method

Fourier Transform Infrared spectroscopy (FTIR) [4] was employed for time-resolved spectra acquisition

(temporal evolution profiles) and chemometric multi way models derived from parallel factor analysis (PARAFAC) [5, 6] were utilized for enzyme activity determination. The multi-linear data structure which is necessary for multi way modeling was constructed as described in Figure 1.

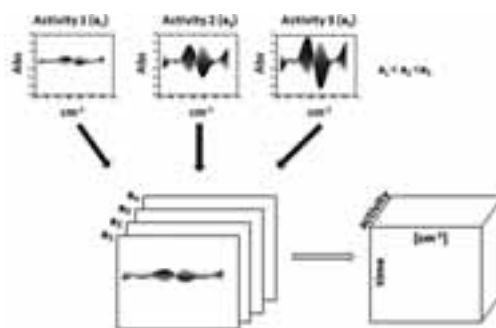


Figure 1: Conversion from two-way to a three-way data structure. All data matrices containing time-resolved spectra for a certain enzyme activity are stacked behind each other to form a tensor. The cubic data structure fulfills trilinearity since all Evolution Profiles are recorded in the same time-scheme.

Parallel Factor Analysis is a numerical decomposition method of multilinear datasets into its Loadings derived from the used measurement dimensions [5].

It can be mathematically described as

$$x_{i,j,k} = \sum_{f=1}^F a_{if} b_{jf} c_{kf} + e_{i,j,k}$$

where a , b and c are elements of matrices A, B and C as they are explained in Figure 2.

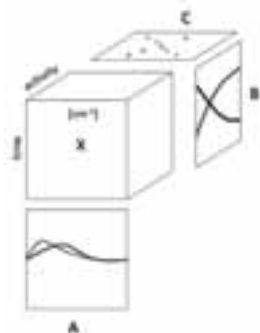


Figure 2. Schematic illustration of a PARAFAC decomposition of time-resolved enzymatic FTIR data. The matrices contain the following information:

A – This matrix contains the true spectra (fingerprints) of the enzymatic system. Here spectral fingerprints representing both the substrate and the product and are illustrated by green and blue color.

B – This matrix contains the kinetic (i.e. time resolved) behavior of substrate(s) and product(s)

C – This matrix contains the information about how abundant the change in spectra in B is considering the pure spectra from A. Those values of that matrix therefore correlate with the used enzyme activity (having opposite slopes for substrate(s) and product(s) if non-negativity constraints are applied to the analysis)

Results

Assuring that substrate(s) and product(s) have distinguishable spectral fingerprints the time-resolved FTIR spectra change simultaneously with the development of the product molecules and thus shape a “landscape” in relation to enzyme activity (Figure 3). Those spectral landscapes each identifying the full enzyme catalyzed reaction accomplished at one particular enzyme level, i.e. one particular enzyme activity, are referred to as temporal *Evolution Profiles* and are illustrated for three different enzyme catalyzed reactions with glucose oxidase (EC 1.1.3.4), pectin lyase (EC 4.2.2.1), and a mixed cellulase preparation, respectively.

The *Evolution Profiles*, each measuring a certain enzyme activity, have been visualized using difference spectra, implying that the first spectrum, and therefore all constant background signals including the water signals, were subtracted from the spectra series. The absorbance of certain bands decreased over time due to

substrate consumption whereas other bands grew over time due to product formation (Figure 3).

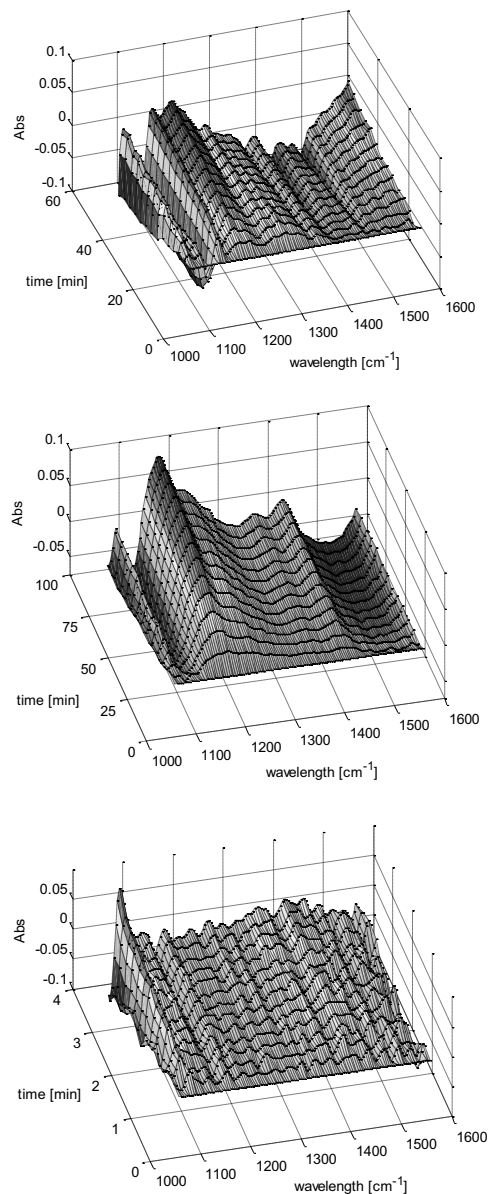


Figure 3. Temporal Evolution Profiles for the enzymatic reactions of pectin lyase (top), glucose oxidase (middle) and a cellulase enzyme blend (bottom). Spectra are displayed as difference spectra, meaning that the background has been subtracted from each series (first spectrum is a vector of zeros).

Except for glucose oxidase, the products being formed cannot be explicitly identified as a single product, but

rather a distribution of products. Nonetheless the various products lead to a combined fingerprint which was measurable by FTIR.

This spectral evolution profiling in real time, combined with chemometric multi-way methodology, i.e. Parallel Factor Analysis (PARAFAC), allows for the detection of spectral changes of both the substrate and the product during the enzyme catalyzed reaction, secondly, PARAFAC can examine the enzyme dosage dependent differences in the Evolution Profiles (e.g. the differences in pectin lyase Evolution Profiles as in Figure 5).

For each enzyme calibration several spectral *Evolution Profiles* were acquired using three replicate measurements. The total amounts of *Evolution Profiles* used for the calibrations of glucose oxidase, pectin lyase and Celluclast 1.5L were 29, 32 and 33, respectively. The calibration for pectin lyase can be seen in Figure 4, while the calibration parameters for the other two enzymatic systems are given in table 1.

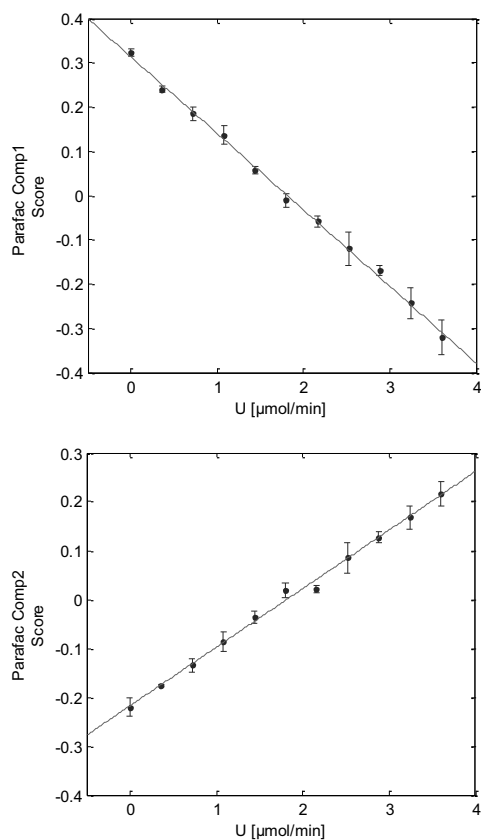


Figure 4: Substrate (top) and product calibration (bottom) for pectin lyase derived from PARAFAC

The multi way scores (Figure 2, Matrix C) were obtained by applying PARAFAC to the tensors of each

of the three enzymatic systems and the known enzyme activities were determined by classical colorimetric and photometric assays.

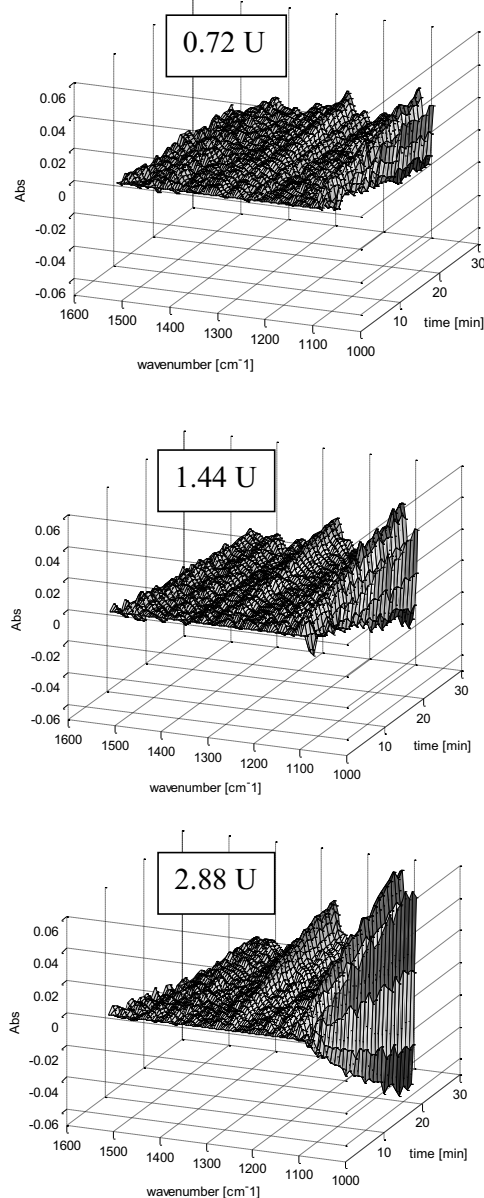


Figure 5: Temporal Evolution Profiles for pectin lyase reaction using different activities. Spectral evolution clearly depends on added enzyme amount (activity).

The unique solution derived from PARAFAC highly correlated with the enzyme activity in each

Table 1: Calibration parameters for the three modeled enzymatic systems

	pectin lyase	glucose oxidase	Celluclast1.5L
Observation time	4.2 min	20.7 min	4.2 min
Number of spectra in each Evolution Profile	15	40	15
Calibration range (per ml Substrate)	0-200 mU/ml	0-6 U/ml	0-80 mU/ml
LOD*	9 mU/ml	277 mU/ml	3.79 mU/ml
R ² substrate calibration	0.998	0.97	0.99
R ² product calibration	0.995	< 0.60	0.98

* LOD only valid for used time of spectral evolution. LOD decreased for extended observation time.

case (table 1). Since the PARAFAC scores were retrieved to encompass one score result for the spectral evolution of the substrate(s) and another one for the product(s), per definition two calibrations should result from the PARAFAC analysis for each enzyme (Figure 4). Overlap of strong fingerprint abundances from the PARAFAC derived solution with substrate depletion bands e.g. gave evidence to identify this PARAFAC Component as a substrate depletion calibration and vice versa. Hence, for pectin lyase and Celluclast 1.5L a set of two calibrations, one for the substrate consumption and one for the product formation could be established, respectively (Figure 4). However, glucose oxidase showed poorer performance than the other enzyme reactions due to lower signal/noise ratio and resulted in only one calibration (substrate calibration). This was due to low amounts of solubilized oxygen (the second substrate) measured at 42 °C even though oxygen supply was kept constant throughout the reaction.

- [4] F.A. Iñón, S. Garrigues, M. de la Guardia, *Analytica Chimica Acta*, 513 (2004) 401.
- [5] R. Bro, *Chemometrics and intelligent laboratory systems*, 38 (1997) 149.
- [6] R. Bro, *Critical reviews in analytical chemistry*, 36 (2006) 279.

Conclusion

A straight forward and universal method to determine enzyme activity has been developed using temporal evolution profiling and spectral fingerprinting. It is applicable to a wide range of enzymes without the need of any external standards as biomarkers, antibodies, Carbohydrate Binding Modules (CBMs) or chemicals, but instead utilizes the multivariate advantage to observe the overall (spectrophotometric) picture of an ongoing enzymatic reaction. The method employs chemometric multi-way methods as PARAFAC and is highly suitable for automation and further intelligent instrumentation.

Using the described approach it was possible to assess the activity of three different enzymatic systems, namely Pectin Lyase, Glucose Oxidase and the multi-component enzymatic preparation Celluclast 1.5L. Concluding, it has high potential to displace traditional assays, such as the very cumbersome colorimetric reducing sugar assays.

References

- [1] A. Hennig, H. Bakirci, W.M. Nau, *Nature methods*, 4 (2007) 629.
- [2] R.K. Bera, A. Anoop, C.R. Raj, *Chemical Communications*, 47 (2011) 11498.
- [3] J.L. Reymond, *Food Technology and Biotechnology*, 42 (2004) 265.



Thomas Bisgaard

Phone: +45 4525 2811
E-mail: thbis@kt.dtu.dk

Supervisors: Jens Abildskov
Jakob Kjøbsted Huusom
Nicolas von Solms
Kim Pilegaard

PhD Study
Started: September 2012
To be completed: August 2015

Operation and Design of Diabatic Distillation Processes

Abstract

Diabatic operation of distillation columns can lead to significant reductions in energy and operation cost compared to conventional (adiabatic) distillation columns, at an expense of an increased complexity of design and operation. The earliest diabatic distillation configuration dates back to the late 70's, and various different configurations have appeared since. However, as it is today, no full-scale diabatic distillation columns are currently operating in the industry. The aim of this project is to shed light on the potential benefits of diabatic operation for given feed mixtures, and to solve some of the barriers for industrial application/acceptance of diabatic distillation columns.

Introduction

Multi-stage distillation is the most widely used industrial technique for continuously separating liquid mixtures. At the same time, conventional distillation columns (CDiC) are energy intensive and operate at Second-Law efficiencies as low as 5-20% [1]. This is because heat is added at the highest temperature (high grade energy) and heat is removed at the lowest temperature (low grade energy), thereby preventing integration of e.g. utility streams. Exergy (available energy) is thus said to be degraded throughout the distillation column.

Despite the fact that distillation is considered a mature technology, alternative configurations are under consideration, primarily due to increased attention paid to environmental issues and resource management. Some examples of demonstrated, alternative distillation configurations are heat-pump assisted distillation columns, reactive distillation columns, and dividing wall columns.

Diabatic distillation columns represent another class of alternatives, in which the heat required to perform the separation is added and/or removed throughout the column, has been proposed as a means to increase the Second-Law efficiency and hence the reversibility of the process. An example is the heat-integrated distillation column (HIDiC) which is illustrated in Fig. 1 with a CDiC. Internal heat transfer in the HIDiC is realized by operating the rectifying section at higher pressure than the stripping section, using vapor recompression. This heat transfer facilitates gradual boil-up throughout the stripper and

condensation throughout the rectifier leading to an improved Second-Law efficiency [2].

The HIDiC uses significantly less utility in form of steam and cooling water compared to the CDiC. Instead, electrical energy needs to be supplied to the compressor. Even though electricity is several times more expensive than supplying energy through steam, this operation can significantly reduce the operation cost of the separation [3].

As a result of the promising features of the HIDiC, extensive efforts have been made to develop this technology during the past 15 years, both theoretically and experimentally [4-6].

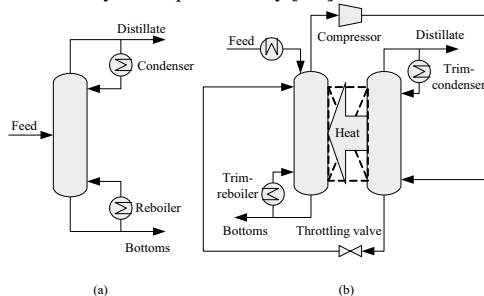


Fig. 1. Schematic representation of (a) Conventional Distillation Column (CDiC) and (b) Heat-Integrated Distillation Column (HIDiC)

However, despite demonstrations of large energy savings of the HIDiC compared to the CDiC and

manageable operability, it has not yet been accepted by industry. This could be due to lack of mature methods for designing these more complex configurations.

Specific Objectives

The objective of this project is to identify the potential benefits of diabatic operation in distillation columns and to clarify the impact on operation and design of diabatization. This includes a clarification of the relation between the type of feed mixture and the feasibility of diabatic operation. Following aspects will also be covered:

- Thermodynamics: It is of interest to gain knowledge about the feasibility of a diabatic distillation column based on a thermodynamic description of the feed mixture components. Considerations on applying rigorous thermodynamic models will also be given.
- Unit Operation Design: How to design the column such a desired separation is obtained.
- Operation and control: Investigate abnormal operation conditions (e.g. steady-state multiplicity) and to synthesize stabilizing control structure(s).
- Sustainability: Compare diabatic and adiabatic operation from an energy account point of view.

The first step in the fulfilling of the objectives is to be able to obtain a detailed, dynamic model of the distillation column configurations of interest. As a result, the first phase of the project consists of modeling and implementation in MATLAB®.

Current Results and Discussion

A simple dynamic model have been developed [7], including following assumptions: (1) Lewis/Randall ideal, binary mixture, (2) tray column, (3) ideal mixing and equilibrium on each tray, (4) negligible changes in sensible heat, (5) equal sized rectifying and stripping sections, (6) negligible pressure dynamics, and (7) linearized liquid flow dynamics.

To illustrate the influence of diabatization on the stationary behavior of distillation columns, Fig. 2 provides an example of the internal flows of a HIDiC and a CDiC.

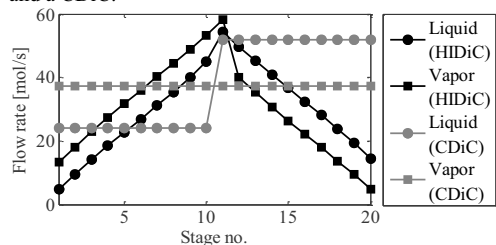


Fig. 2. Example of internal flows of a HIDiC and a CDiC with 20 stages with number 11 being the feed stage. Stages are counted from top to bottom. In the HIDiC, stage 1 and 11, 2 and 12 (so on) exchange heat.

As a result of variations of flows throughout the column sections in a HIDiC, the HIDiC is typically suggested to be designed with variable column section diameters. Dynamic analyses, including considerations on Bristol's Relative Gain Array and Singular Value Analysis, have been carried out on a case-study of a CDiC and a HIDiC. Studies have shown that a higher degree of interaction occur in diabatic operation which e.g. influences the control performance.

Conclusions and Future Work

Diabatic distillation offers promising features in terms of energy usage and operation costs. It is thus an attractive technology from economical and an environmental point of view. The main barriers for industrial implementation, identified in this study, are the design and the operation aspects.

Currently work is conducted on establishing a model database which enables detailed dynamic modeling of various adiabatic and diabatic distillation column configurations. The modeling comprises of extending the previous developed, simple model by increasing the level of detail. The model to be developed will serve as a basis for future work related to this PhD project and hopefully beyond.

Acknowledgement

The author would like to thank the Technical University of Denmark for financing of the study.

References

- [1] G.M. de Koeijer, S. Kjelstrup, *Int. J. Applied Thermodynamics* 3 (3) (2000) 105-110
- [2] M. Nakaiwa, K. Huang, M. Owa, T. Akiya, T. Nakane, M. Sato, T. Takamatsu, H. Yoshitome, *Appl. Therm. Eng.* 18 (11) (1998) 1077-1087
- [3] Z. Olujić, F. Fakhri, A. de Rijcke, J. de Graauw, P.J. Jansens, *J. Chem. Technol. Biotechnol.* 78 (2-3) (2003) 241-248
- [4] M. Nakaiwa, K. Huang, T. Endo, T. Ohmori, T. Akiya, T. Takamatsu, *Chem. Eng. Res. Des.* 81 (1) (2003) 162-177
- [5] M. Gadalla, L. Jiménez, Z. Olujić, P.J. Jansens, *Comput. Chem. Eng.* 31 (10) (2007) 1346-1354
- [6] A.K. Jana, *Appl. Energy* 87 (5) (2010) 1477-1494

List of Publications

- [7] T. Bisgaard, J.K. Huusom and J. Abildskov, *Dynamic Effects of Diabatization in Distillation Columns*, Proceedings of ACD2012, 2012.



Martin Gamél Bjørner

Phone: +45 4525 52886

E-mail: mgabj@kt.dtu.dk

Supervisors: Georgios M. Kontogeorgis
Amir Mohammadi

PhD Study

Started: June 2012

To be completed: June 2015

CO₂-Hydrates - Challenges and Possibilities

Abstract

Despite its importance, accurate modeling for CO₂ and mixtures of CO₂ are still challenging. Traditional approaches model CO₂ either as an inert or as a solvating molecule. Rigorously, however, CO₂ is a quadrupolar molecule and should preferably be modeled as such. A literature survey has been performed over models containing an explicit quadrupolar term, and it has been found that several promising theories have been developed. All models, however, suffer from fundamental problems, moreover it is almost impossible to compare the current models 'as is'.

Introduction

Carbon dioxide, as a solvent or refrigerant, is considered an environmentally harmless chemical. Nevertheless, in recent years carbon dioxide (CO₂) has received a significant amount of negative attention due to its contribution to the global warming and the fact that the amount of CO₂ in the atmosphere continues to rise. This is believed to be largely due to the high amounts of CO₂ emitted to the atmosphere as a result of e.g. electricity production from fossil fuels. Alone in Denmark about 50 million tons of CO₂ is emitted each year. The reduction of the CO₂ emission is considered a high priority.

To understand the problems caused by CO₂, high quality experimental data and accurate models, valid over a wide range of conditions and chemicals, are necessary. For example a novel technique for CO₂ capture using gas hydrates has recently been patented [1]. The operative pressure of the technique, however, is currently too high to be economically profitable. It is believed this pressure could be reduced by specific additives. Such a screening process, however, is expensive and time consuming, and accurate models for CO₂ in mixtures would greatly facilitate this process.

Mixtures of CO₂ and gas hydrates are also a nuisance in the petroleum industry, where the phase equilibrium of mixtures of CO₂ in hydrocarbons, water and glycols are of particular importance [2].

Specific Objectives

This work is part of a project funded by FTP (Danish Technical Research Council). The purpose of the overall FTP project is to acquire a solid experimental and

theoretical basis for understanding and addressing the problems of CO₂ and CO₂ hydrates, for the possible utilization of hydrate formation as a CO₂ capture technology.

More specifically a molecular thermodynamic model for CO₂ will be developed, based on the Cubic Plus Association (CPA) Equation of State (EoS). The model is expected to include a specific quadrupole term and possibly other polar and/or induction terms. These terms should originate from statistical thermodynamic considerations.

It is expected that the applicability of several different terms, related to varying theoretical approaches such as those of Karakatsani et al. [3] and Gross [4], will be evaluated in terms of (at least) the Helmholtz energy.

The proposed model will be first tested for regular mixtures containing CO₂ and alkanes, water and/or glycols and later incorporated in an improved van der Waals-Platteeuw theory for describing CO₂ hydrates.

Complex mixtures containing CO₂ hydrates and inhibitors will be studied both experimentally and using the new model.

Results and Discussion

Despite the importance of CO₂ containing mixtures, accurate predictive modeling of such mixtures still poses a challenge [2]. A reason for this may be that traditional approaches such as the Soave-Redlich-Kwong (SRK) [5] or Peng-Robinson (PR) [6] EoS treat CO₂ as an inert compound. Even in modern equations of state such as the Statistical Association Fluid Theory (SAFT) only dispersive forces are usually considered.

The continued use of such procedures may be attributed to the fact that the behavior often works well when correlating with a (large) interaction parameter (k_{ij}), some predictive character is lost in this way, however, and it is uncertain how well such procedures work when extended to ternary or higher systems.

Other more pragmatic approaches tend to treat CO₂ as a self-associating (hydrogen bonding) or solvating molecule. Such procedures often work very well; resulting in better correlations with smaller interaction parameters for mixtures of CO₂ with water and other polar compounds, and slightly improved correlations for CO₂-hydrocarbon mixtures [2]. Unfortunately these improvements are obtained at the cost of additional pure component parameters and, in some cases, an extra parameter for the binary mixtures.

Rigorously, however, CO₂ has a large quadrupole moment. While quadrupolar forces are very short ranged forces, relative to regular van der Waals forces, they may become important for molecules with a significant quadrupole such as CO₂. The effect of a quadrupole (or a dipole) is that certain molecular conformations are favored more than others. That is, the quadrupole moment causes some local structuring in the fluid. This is believed to be the reason for the unusual phase behavior of mixtures containing CO₂.

For these reasons several quadrupolar terms have been suggested, mainly based on the statistical mechanical theories for polar and quadrupolar fluids developed by Stell et al. [7] and Rushbrook et al. [8] (the so-called u-expansion). Gubbins and Twu presented the first equation applicable for calculation of the phase equilibrium of real mixtures [9].

In recent years several research groups have exploited, the fact that the Helmholtz energy contributions are (assumed to be) independent of each other, that is:

$$A^{\text{res}} = A^{\text{disp}} + A^{\text{assoc}} + A^{\text{chain}} + A^{\text{polar}} + A^{\text{quad}} \dots \quad (1)$$

Eq. 1 is used to combine the quadrupolar terms with the SAFT framework. This approach has been utilized with varying degrees of success. To the best of the author's knowledge the first attempt was made by Walsh et al [10] for a general multipole. Gross [4] used an energetic term very similar to that used by Gubbins and Twu, without adding any extra pure component parameters. Improvements are observed for mixtures of CO₂-hydrocarbons, however, model performance seem to deteriorate for mixtures where cross-interactions are of importance. Two quadrupolar (and polar) terms (a "full" expression and a truncated version) were utilized by Karakatsani et al. based on the theory of Stell et al. [7]. The truncated version, which seems to be the most used, is more computationally efficient at the cost of an additional pure compound parameter. Both models yield comparable results. The model has mainly been investigated for complex mixtures of cross interacting systems. While demonstrating the strength of the approach, this unfortunately makes it quite difficult to assess the model performance for specific system classes. Other authors have contributed with similar

terms, mostly taking their basis in the model of Gubbins and Twu rather than the original papers by Stell et al.

While the different models all struggle with their own problems, there are some more fundamental issues, which are not well understood. For instance, there seem to be no consensus about how cross interactions should be accounted for in the models, and classical mixing rules do not seem to be fully satisfactory. A related problem is how induction effects should be taken into account. Some authors use an effective (adjustable) quadrupolar moment others a separate induction term.

Unfortunately it is difficult to compare the different models directly, since the various authors tend to test their own theory on different systems, thus making a comparison difficult. Moreover, the results are often not even compared to those of the unmodified SAFT version, which is crucial in order to properly evaluate the possible improvements from the theory. By far the most important problem is that very few literature studies have considered multicomponent systems (and multiphase equilibria) which should be considered one of the most challenging targets for al thermodynamic models.

Conclusions

It can be concluded that while several promising models for the quadrupolar moment have been presented in the literature, it is difficult to assess which models perform best, both overall and for specific mixtures. At the same time we can conclude that all models seem to suffer from several fundamental problems, which should be addressed. Future work will consist of a comparative evaluation of the different model terms.

Acknowledgements

The author is grateful to the Danish Research Council for Technology and Production Science (FTP) for funding this project.

References

1. D.F. Spencer, Methods of selectively separating CO₂ from a multicomponent gaseous stream, US Patent 5700311 (1997) and 6106595 (2000).
2. I. Tsivintzelis, G.M. Kontogeorgis, M.L. Michelsen, E.H. Stenby, Fluid Phase Equilibria 306 (1) (2011) 38-56.
3. E.K. Karakatsani, T. Spyriouni, I.G. Economou, AIChE Journal 51 (8) (2005) 2328-2342.
4. J. Gross, AIChE Journal 51 (9) (2005) 2556-2568.
5. G. Soave, Chem. Eng. Sci. (27) (1972) 1197-1203.
6. D.Y. Peng, D.B. Robinson, Ind. Eng. Chem. Fundamen. 15 (1) (1976) 59-64.
7. G. Stell, J.C. Rasaiah, H. Narang, Mol. Phys. 27 (5) (1974) 1393-1414
8. G.S. Rushbrooke, G. Stell, J.S. Høye, Mol. Phys. 26 (5) (1973) 1199-1215
9. K.E. Gubbins, C.H. Twu, Chem. Eng. Sci. (33) (1978) 863-878
10. J.M. Walsh, H.J.R. Guedes, K.E. Gubbins, J. Phys. Chem. 96 (26) (1992)



Vijaya Krishna Bodla

Phone: +45 4525 2967
E-mail: vikb@win.dtu.dk

Supervisors: Krist V. Gernaey
Ulrich Krühne
John M. Woodley

PhD Study

Started: March 2011
To be completed: May 2014

Integrated Microfactories for Enzyme production

Abstract

This project aims to demonstrate for the first time that fermentation and biocatalysis can be integrated. The hypothesis is to construct and operate integrated microscale reactors – so-called microfactories – using a transaminase model system (adapted to the specific microorganism and the biocatalytic reaction) in an intensified process. The integrated microfactory can be used to quickly and effectively screen different process conditions. The first part of this study is to evaluate the effect of miniaturization on biocatalytic reactions and to design and construct a miniaturized reactor, comparing its performance to lab scale reactor.

Introduction

Biocatalysis is becoming increasingly attractive for the production of pharmaceutical intermediates and other products. However, significant efforts are needed to develop processes and biocatalysts to achieve the economic feasibilities and to increase the biocatalyst productivity¹. Miniaturization can help in gaining more process understanding and thus significantly enhance the productivity of some processes¹. The potential for high throughput experimentation for rapid screening of biocatalysts, substrates, reaction conditions, kinetics, reactor and process design is of particular interest. An integrated microfactory has a number of features that are advantageous for rapid screening with respect to improved economy of the proposed process and process development: (1) the method for preparing the catalyst is considerably cheaper as no intermediary purification steps are needed; (2) the system process intensity is inherently enhanced through the continuous operation; (3) large hydrophobic substrates would be easily accessible since the cell membranes are to be lysed. The aim of this study is to design a microfluidic system, for rapid screening, that can mimic or improve the performance of the reaction at larger scale using biocatalytic transamination as a model reaction.

Transaminases (TAMs) (also known as aminotransferases) catalyze the transfer of an amino group from an amine donor, usually an amino acid or a simple amine such as isopropylamine, to an acceptor molecule yielding a chiral amine as well as a co-product ketone (or alpha-keto acid) and require the cofactor

pyridoxal phosphate (PLP) to act as a shuttle to transfer the amine group.



The main challenges are: (1) an unfavourable thermodynamic equilibrium position, requiring processes to shift the equilibrium; (2) substrate and product inhibition; (3) low substrate solubility, giving low volumetric productivities; (4) high biocatalyst cost². The performance is evaluated by varying the operation conditions, i.e. parallel flow, segmented flow, multi-phase system for controlled supply of substrate, varying flow rate, residence time, enzyme concentration etc, which influences the performance of the reaction, and to study the reaction rate and mass transfer rate limitations.

Material selection and Design formats

Poly(methyl methacrylate) (PMMA) is widely used and considered a biologically compatible material also for medical applications, and is therefore used for our application. Reactor configurations that are fabricated and tested are shown in Fig 1.

Computational Fluid dynamics (CFD) simulations

CFD is used to predict the flow behaviour inside the micro-channels and is further also applied to improve our understanding of the diffusional properties of the substrate and product.

Reactor configurations

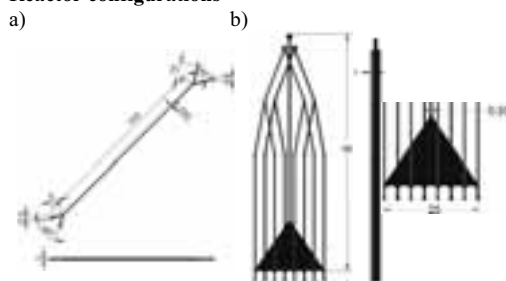


Figure 1: Reactor configurations: a) YY channel reactor, volume 50 μL and b) 8 stream reactor (8S), volume 245.5 μL . The dimensions of the reactors are mentioned along with the front and side views. The bottom part of the 8S reactor is also shown in an exploded view

Residence time distribution (RTD) – YY channel

The CFD model of the reactor configuration was built, simulated and analyzed using the software Ansys Fluent 12.1. Transient CFD simulations were performed by testing 2 different diffusion coefficients of a diffusing species in water. A surface monitor was set to calculate the vertex average mass fractions at the outlet at the specified time intervals. They are presented as a function of time in order to obtain the RTD profiles (Fig 2). Comparing the experimental data from transient experiments to the RTD curves from simulations can give an insight into the diffusional properties of the compounds. The simulation of MBA (Fig 2) corresponds well to the data indicating that the diffusion coefficient of MBA is in the order of 10^{-9} m^2/s . From the simulation for APH (Fig 2), it can be concluded that the simulation doesn't fit with the data at the beginning. The simulation corresponds well with the data at the end where the normalized concentration was closer to 1. Based on understanding that this lag is caused by a slow diffusing species it can be anticipated that the diffusion coefficient of APH is in the order of 10^{-12} m^2/s . Thus it can be concluded that the substrate is diffusing considerably slower than the product.

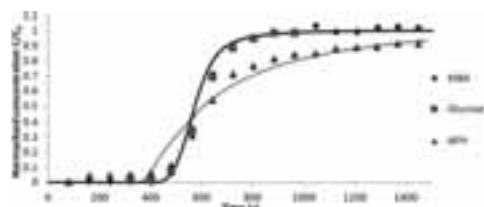


Figure 2: CFD simulations with tested diffusion coefficients of $0.67 \cdot 10^{-9}$ and $0.67 \cdot 10^{-12}$ plotted as continuous lines; Experimental results plotted as dots

An 8 stream reactor configuration was built, as shown in Fig 1, where the 2 inlet streams are subdivided into 8 substreams and combined to form an interdigitated flow (Fig 3). Thus, the 8 stream reactor has 6 more contact surface areas for diffusion compared to the YY channel.

This enables a much faster mixing of streams by diffusion due to reduced diffusion length. The interface where the substrate and enzyme concentrations are non-zero also grows wider along the length compared to the YY-channel. A reasonable expectation is that the product formation should increase with a factor 6 as there are 6 more contact surfaces for diffusion if the species transport was the bottleneck rather than the reaction kinetics. These studies also help in understanding the interaction between the species transport and the kinetic limitations. Experimental results show an increased production compared to the YY-channel reactor and the batch reactor (Fig 4). However the yield was not 6 times higher as expected before. This indicates the shifting of the bottleneck from the species transport limitation to kinetic limitation.

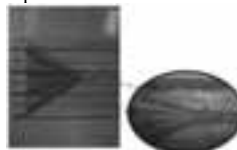


Figure 3: Interdigitated flow of the 8 stream reactor represented by two colored dyes

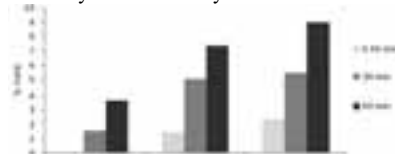


Figure 4: Comparison of experimental results for batch, YY-channel and 8Stream reactor for different residence times

Conclusions and Future Work

Microreactors can prove to be an effective tool as they can be easily fabricated and tested. It has been demonstrated here that combining microreactor technology and computational fluid dynamics (CFD) can be used for rapidly acquiring process data. Reactor configurations built from this knowledge are shown to perform better than the traditional well mixed batch reactor. Experiments at microscale thus will also reduce the process development times for scale-up.

Future work is focussed on obtaining a reactor design that can be used as an effective screening tool. It is intended to build a membrane microreactor with integrated packed bed resins and optimize the performance of the module. This reactor is expected to yield more product because of reduced inhibitions from substrate and product with limited substrate supply and complete product extraction.

References

1. Pollard DJ, Woodley JM, Trends Biotechnol, (2007) 25(2), 66-73
2. Matosevic S., Szita N., Baganz F., J Chem Tech and Biotechnol., (2011) 86, 325–471



Kristine Stove Boesgaard

Phone: +45 5180 1559
E-mail: kboe@kt.dtu.dk

Supervisors: Teis Nørgaard Mikkelsen
Andreas Ibrom
Helge Ro-Poulsen, UC

PhD Study
Started: June 2010
To be completed: May 2013

Physiological responses of plants and ecosystems to climate change

Abstract

Response studies in terrestrial ecosystem physiology have so far focused on average climatic changes. However both observations and model projections indicate that climatic variability will be enhanced in the future, which most likely would lead to more serve responses in the ecosystem. In the natural-ecosystem field facility of CLIMAITE the plant physiological responses of 6 years of climate manipulation of CO₂ enrichment, temperature increase and periodical drought are investigated. Not everything are possible to investigate under field conditions why some plant ecophysiological responses to different climate change scenarios will be based on both field- and laboratory-work. A study in one of the often used ecophysiological approached as lead to the development of a new theory and a way to improve the method.

Introduction

Changes in CO₂ concentration and temperature are expected to have dramatically impact on the precipitation patterns. Higher frequency of extreme event such as summer droughts and heavy precipitation event are pronounced [1].

Photosynthetic uptake of CO₂ is known to be directly influenced by the pronounced increase in atmospheric CO₂ concentration, higher temperature or altered water availability [2]. All physiological responses of elevated CO₂ on plants and ecosystem can divided as a result of increased photosynthesis (A) and decreased stomatal conductance (g_s) [3]. Plants grown in elevated CO₂ have a significantly higher light saturated photosynthesis (A_{sat}) [4]. However, the maximum carboxylation rate (V_{cmax}) and maximum rate of electron transport (J_{max}) in Photosystem II is known to be significantly down-regulated to elevated CO₂ [4].

An increased temperature (by only few degrees) is known to have a positive enzymatically effect on the photosynthesis. However, an increased temperature indirectly leads to an increased transpiration and evaporation from the total ecosystem, resulting in lower water availability for the plants. Water limitation decreases the rate of photosynthesis decreasing the stomatal conductance in the attempt to maintain water in the plant [5].

Combination of higher temperature and increased CO₂ might not cause an effect on the photosynthetic CO₂ assimilation, while the stomatal conductance can

be successfully reduced as a result of the higher availability of CO₂. This combination is hypnotized to be an additive effect.

Water availability is essentially for all plants and drought periods are known to have a negative impact on the photosynthesis. With increased temperature a higher evapotranspiration of the ecosystem occurs, leading to lower soil moisture in short-term. In longer term continuous lower soil moisture can lead to change soil structure and from that changed the field capacity of the soil. A physiological response to higher soil water might be the same as for increased temperature, while low soil moisture also leads to stomatal closure. In combination with CO₂ an additive effect is expected while the closed stomatal but the higher substrate (CO₂) supply for the photosynthesis will equalize the assimilation rate. However it is also possible that the increased CO₂ will be the main driver resulting in a still higher CO₂ assimilation.

Response studies in terrestrial ecosystem physiology have so far focused on average climatic changes. However both observations and model projections indicate that climatic variability will be enhanced in the future, which most likely would lead to more serve responses in the ecosystem.

Specific objective

Two major objectives are addressed to the PhD project; assessing the development of ecophysiological key parameters in the two species after ecosystem

stabilization, do to 6 years of climatic manipulation, and assessing the estimation of important parameters for dynamic ecosystem models for simulation of carbon, water and nitrogen fluxes. Combining the multifactorial CLIMAITE field experiment with controlled environmental laboratory mesocosm experiments, it will be possible to investigate parameters which are complicated (if not impossible) to investigate in the field.

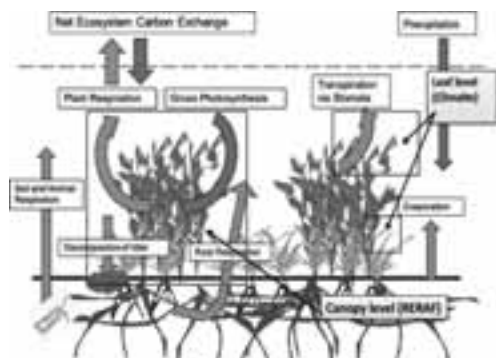


Figure 1: Schematic overview of the responses this project seeks to investigate according to long-term climate manipulations.

Methodology

The field facility of CLIMAITE is a multi-factorial experiment trying to simulate the climate in 2075. The setup includes treatments of un-treated control, elevated CO₂, passive nighttime heating, periodic summer drought and all combination replicated in six blocks in a split-plot design [6] (www.climaite.dk).

The experimental area of CLIMAITE is dominated by two species, heather (*Calluna vulgaris*) and wary-hairgrass (*Deschampsia flexuosa*). Starting in these two species the overall carbon and water-balance of the ecosystem are evaluated. The ecosystem is examined at two levels. In the field leaf level response is examined and in the control growth facility RERAF, at Risø DTU, whole ecosystem responses are investigated.

To investigate and describe the physiological response of the climate changing over time, gas-exchange CO₂ and H₂O method are used. Concentration on leaf level gas-exchange of CO₂ and H₂O can describe a lot of photosynthetic processes and parameters. During the growing season 2011, data have been collected in the field.

Methodological improvements and theory

An often used technique in the monitoring of ecophysiological response is the leaf gas-exchange. The technique is based on the CO₂ and H₂O gas exchange that is exchange through the leaf surface during photosynthesis and respiration processes. One used technique is portable infrared gas analyzers system that allows detection of the leaf gas-exchange on small and single leaves and using well established models [7]

different plant physiological parameters can be estimated. However these systems are not perfect and have their limitations. A major concern using the leaf gas-exchange technique is that there can occur leakages sealing the leaf inside the chamber were the gas-exchange are measured, this can lead to over or underestimations of the physiological parameters – and worse wrong conclusions.

In this PhD project we have developed a leaf adaptor frames (LAF) that can improve the accuracy of the measurement and in the development and investigation of the LAF's a new theory has been developed (manuscript submitted to *Plant, Cell and Environment*, September 2012).

LAF have successfully been used in the field-based work 2010-2012 and data are now being processed and statically analysis has been started aiming a number of publications.



Figure 2: Leaf adaptor frame with attached leaves for *Deschampsia flexuosa*.

Acknowledgment

The work was carried out within the CLIMAITE project, financially supported by the Villum Kann Rasmussen Foundation. Support has also been received from Air Liquid and DONG energy.

References

1. IPCC: The Physical Science Basis. Intergovernmental Panel on Climate Change, Geneva, 2007.
2. H. Lambers, F. Stuart Chapin, T.L. Pons, Plant physiological ecology, Springer, New York, USA, 1998.
3. S.P. Long, E.A. Ainsworth, A. Rogers, D.R. Ort, Ann. Rev. of Plant Bio. 55: (2004) 591-628
4. E.A. Ainsworth, A. Rogers. Plant, Cell and Env., 30: (2007) 258-270
5. B.E. Medlyn, E. Creyer, D. Ellsworth *et al.* Plant, Cell and Env. 25: (2002) 1167-1179
6. T.N. Mikkelsen, C. Beier, S. Jonasson *et al.*, Func Eco, 22 (2008): 185-195
7. G.D. Farquhar, S. von Caemmerer, J.A. Berry, Planta, 149 (1980):178-190



Andrijana Bolić

Phone: +45 4525 2958

E-mail: anb@kt.dtu.dk

Supervisors: Krist V. Gernaey
Anna Eliasson Lantz
Karsten Rottwitt
Nicolas Szita, UCL

PhD Study

Started: March 2010

To be completed: February 2013

Monitoring Continuous Fermentation Processes in Microbioreactor Systems

Abstract

At present, research in bioprocess science and engineering requires fast and accurate analytical data (rapid testing) that can be used for investigation of the interaction between bioprocess operation conditions and the performance of the bioprocess. Miniaturization could provide an attractive tool necessary for obtaining a vast amount of experimental data in a short time. The main objective of this project is to develop a microbioreactor platform for continuous cultivations of *Saccharomyces cerevisiae*, where NIR spectroscopy could be further implemented for rapid on-line measurement of process variables like substrate and biomass.

Introduction

Conventional microbial cell cultivation techniques are no longer sufficient considering the fast development of tools for genetic manipulation of biological systems resulting in a large numbers of strains and conditions that need to be screened. There is a tremendous driving force and interest for development of new techniques, which could provide both high quality data and also a high quantity of experimental data. In recent years, microbioreactors have been researched intensely due to their clear advantages like small volume, little or no need for cleaning, high throughput, high information content and control capabilities [1].

Even though microbioreactors have many advantages, it is important to bear in mind that they also have issues related to their size and handling. Evaporation, proper and reliable stirring, interconnections between micro-scale features and the 'macro world' are just some of the burning problems that need to be solved. In addition, measurements of several process variables in microbioreactors are not straightforward to implement. They rely on analytical methods, which are not sufficiently developed for such a small scale at this point. If the measurements are possible, they are not cheap either.

Another important issue that needs to be addressed is determining the optimal microbioreactor volume while keeping in mind the final objective – application. Does one need a sample or not? Does one talk about cells in suspension or adhered on a substrate? The final microbioreactor design should thus strongly depend on the goal of a specific microbioreactor application.

Microbioreactor Design

To address some of the previously mentioned questions, we are currently developing a microbioreactor platform with 1-2 ml working volume. Considerable effort is placed in developing a system that could provide reproducibility and easy handling at a reasonable cost.

Platform

The microbioreactor surrounding is equally important as the microbioreactor itself. Keeping this in mind, a platform with gas connections, optical fibers for sensing, a specially designed heater and standard temperature sensor was designed and fabricated. It can be seen in Figure 1.



Figure 1: Microbioreactor together with platform

The microbioreactor can be placed on a platform using a 'Lego' approach, which ensures reproducibility in sensing and connections. Furthermore, this configuration lowers the cost per microbioreactor, considering that expensive parts of the system are reusable and placed in the platform, while the

microbioreactor is mostly made from cheap PMMA and has one magnetic ring and two sensor spots.

Microbioreactor and stirrer design

The microbioreactor, made in PMMA, consists of a bottom and top part as shown in Figure 2. The bottom part is made as a negative to the platform and has a thin optically transparent layer to make sure that measurements based on optical properties are possible (pH, DO, OD).



Figure 2: Microbioreactor design

The top part is a cylinder with a shaft in the middle on which a magnetic stirrer is mounted. The microbioreactor also has two tubes for optional aeration. Beside air sparging, there is also the possibility for exploiting surface aeration in which case aeration tubes are removed and connectors are made on the top of the microbioreactor.

The stirrer has two pairs of impeller blades placed at two levels, which can be seen in Figure 3. Each blade can be removed in order to create a different mixing behavior. A permanent magnetic ring, which is magnetized across its diameter, is placed inside the stirrer and is driven by a rotating magnetic field.

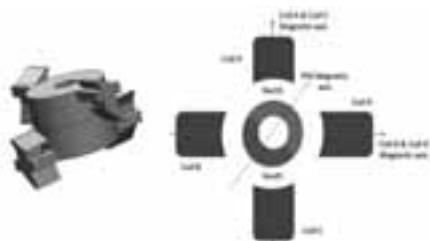


Figure 3: Stirrer design

Electromagnets were incorporated in the mixing device, in order to obtain control over the mixing by changing the speed and direction of the stirrer rotation. In this way, it is possible to prevent formation of a vortex without usage of baffles. The mixing device consists of a base fabricated by micromilling in PMMA (non-magnetic material and part of the platform), illustrated in Figure 1, on which 4 coils (electromagnets) are mounted. The coils are connected to a switch mode power supply, which is controlled by a PC running LabView software. The basic principle of the mixing control is presented in Figure 4.



Figure 4: Mixing control

Results

The mixing capability of the microbioreactor was quantified by experiments where mixing time and volumetric mass transfer coefficient ($k_L a$) were evaluated against different stirrer rotational speeds. The mixing time in a 1 ml microbioreactor was 2 s for a rotational speed of 200 rpm and 0.4 s for 1000 rpm.

The correlation between volumetric mass transfer coefficient and rotational speed during surface aeration in a 1 ml microbioreactor is presented in Figure 5. In another case, where air sparging was applied, the maximum $k_L a$ value obtained was 450 h⁻¹. Furthermore, when mixing was applied with change of direction every 0.2 s at 1000 rpm, the $k_L a$ value was 900 h⁻¹.

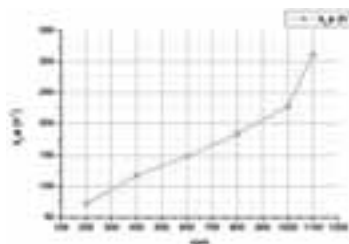


Figure 5: $k_L a$ versus rpm

Conclusion

A flexible and cheap microbioreactor with supporting platform was developed. The device can be operated with surface aeration or gas sparging. It shows flexibility in mixing by changing rpm and direction of rotation. Mixing can be considered almost instantaneous. The volumetric mass transfer coefficient obtained by surface aeration is sufficient for a standard fermentation.

Acknowledgements

This project is supported by the Danish Council for Strategic Research in the frame of the project "Towards robust fermentation processes by targeting population heterogeneity at microscale" (project number 09-065160).

References

1. D. Schäpper, M.N.H.Z. Alam, N. Szita, A.E. Lantz, K.V. Gernaey, Anal. Bioanal. Chem. 395 (2009) 679–695



Hande Bozkurt

Phone: +45 4525 5510
E-mail: hboz@kt.dtu.dk

Supervisors: Gürkan Sin
Krist V. Gernaey

PhD Study

Started: December 2011
To be completed: December 2014

Design of Future Municipal Wastewater Treatment Plants: A Mathematical Programming Approach to Manage Complexity and Identify Optimal Solutions

Abstract

The increasing number of alternative wastewater treatment technologies and stricter effluent limit values imposed by regulations make the early stage decision making for wastewater treatment plant (WWTP) layout design, which is currently based on expert decisions and previous experiences, harder. This study therefore proposes a new approach based on mathematical programming to manage the complexity of the problem and generate/identify novel and optimal WWTP layouts for municipal/domestic wastewater. The decision support tool, that is being developed, will enable the users to select the optimum technology network in early stage decision making by screening among the large number of alternative treatment technologies represented in a superstructure.

Introduction

Since the beginning of the 20th century, development of wastewater treatment technologies has become an important field of engineering activity. In the early stages, wastewater was treated in order to provide sanitation; in the second stage of development, however, WWTPs were focused mainly on removing the major pollutants such as carbon and nitrogen.

The third and current phase of development in municipal wastewater treatment technologies was initiated with the stricter effluent limit values imposed by both emission and immission based regulations. In EU, while The Water Framework Directive (Directive 2000/60/EC) regulates the ecosystems by setting quality objectives, the effluent urban wastewater quality is controlled by the Urban Wastewater Treatment Directive (91/271/EEC). A wide range of parameters were included in the regulations, i.e. organics, nutrients, pathogens, heavy metals, emerging contaminants etc. This resulted in development of new technologies as well as the introduction of new configurations of already existing technologies in the WWTP network. The number of available alternative technologies using physical, chemical and biological means of treatment has increased considerably in order to satisfy the high removal efficiencies required by the regulations. Several configurations of different biological processes exist (Bardenpho, MUCT, A2O, etc. with more than 10

configurations most commonly used in Europe [1]) and other processes like UASB, Anammox, various MBR-based treatment technologies etc. have become available as well.

The fact that the number of alternative wastewater treatment technologies is growing steadily increases the importance of early-stage decision making in WWTP design and retrofitting problems, especially in project development studies, i.e. which WWTP technologies to select for a particular case/project? How to verify the rationale and engineering optimality of the decision? Often – if not always – such decisions are multi-objective and multi-criteria based considering economics, environmental, legal and social constraints. This automatically leads to the following important question: how does a decision maker or an engineer take strategic decisions on which wastewater treatment technologies to use for a particular project and can verify the optimality of such a decision? With increased complexity of the technologies and stricter limit values for effluents, making the most feasible decision became harder.

Objective

This study therefore proposes an approach based on mathematical programming to manage the complexity of the problem and generate/identify novel and optimal WWTP layouts for municipal/domestic wastewater.

Methodology

Currently, the early stage decision making for WWTP design is mainly based on expert decisions and previous experiences. This approach takes values like environmental issues, water reuse, by-product recovery (if possible) and public impacts into account and identifies the alternatives based on experience, similar solutions and brainstorming to come up with the most viable WWTP network [2]. In our new approach based on mathematical programming, which is presented in six steps in Figure 1, a superstructure is built consisting of primary, secondary and tertiary wastewater treatment technologies together with sludge treatment alternatives.

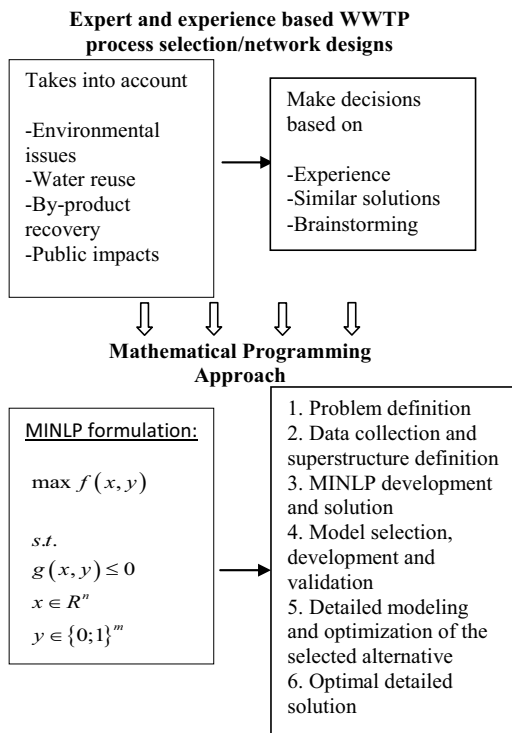


Figure 1: Shift from current approach to mathematical programming approach.

While the primary treatment part is composed of different alternatives of separation units, this structure enables the identification and selection of the optimum technology for the specified conditions among a variety of biological treatment technologies in the secondary treatment section. This part not only covers the activated sludge based configurations of anaerobic, anoxic and aerobic units with several recycle options but also other technologies like SBR, MBR, trickling filters, RBC etc. Tertiary treatment on the other hand, was built mostly by inserting more advanced treatment units such as membrane filtration processes, adsorption, Anammox and Sharon into the superstructure. The units and processes are defined with fixed

conversion/removal rates of the key pollutants (C, N and P) while the sludge production is based on the yield concept.

The tool is developed to formulate the design problem as an MINLP [3], and by using the database of wastewater treatment technologies it generates many alternatives and evaluates their optimality. The methodology is based on the optimization of a superstructure representing different alternatives for primary, secondary and tertiary wastewater treatment units of physical, chemical and biological technologies, as well as for sludge treatment units. Since the tool covers both environmental and sustainability metrics it is a powerful decision making agent for WWTP network design. The objective function covers both capital and operation cost, which includes investment cost components as well as prices for wastewater effluents, utilities, wastes and sludge production.

Conclusion

The design problem will be solved to obtain the optimal wastewater treatment network and the optimal wastewater and sludge flow through the network. This tool enables the optimization of the defined superstructure by the use of a systematic methodology resulting in the design of new WWTPs as well as retrofit of existing plants. Moreover, a generic and functional model for the WWT units and processes has been defined which can be considered as a novel outcome.

Current Status and Future Work

Currently, the superstructure for the domestic/municipal wastewater treatment technology has been developed and the corresponding database for data and models to describe process performance and utility costs is under development. Once the database development is completed, it will be tested as a decision support tool for helping with engineering work including design/retrofitting case studies. Afterwards, the decision support tool will be expanded with the kinetics based wastewater treatment process models- thereby replacing the conversion data with stoichiometry and reaction rates.

References

1. L. Benedetti. Probabilistic design and upgrade of wastewater treatment plants in the EU Water Framework Directive context. PhD thesis, Ghent University, Belgium, (2006) pp. 304.
2. G.T. Daigger. Wastewater Treatment Plant of the Future – Decision Analysis Approach for Increased Sustainability. Presented at the Water Security: Policies & Investments Water Week 2005 Making Decisions on Water Quality. Washington, DC.
3. A. Quaglia, B. Sarup, G. Sin, R. Gani. Integrated business and engineering framework for synthesis and design of enterprise-wide processing networks. *Computers & Chemical Engineering* (38) (2012) 213-223.



David Bøgh

Phone: +45 3618 2893
E-mail: davb@kt.dtu.dk

Supervisors: Kim Dam-Johansen
Flemming Jappe Frandsen
Klaus Hjuler (FLSmidth)
Morten Boberg Larsen (FLSmidth)

Industrial PhD
Started: February 2012
To be completed: January 2015

Effects of Alternative Fuel Combustion on the Cement Clinker Quality

Abstract

Cement production is a highly energy consuming industry. Thus, in order to reduce direct fuel cost and CO₂ emissions, cement producers demand technologies enabling them to substitute fossil fuels with alternative fuels, such as sewage sludge or tires. Substitution of fossil fuels with alternative fuels is not unproblematic, since alternative fuels typically have a higher ash and moisture content than fossil fuels, which may affect clinker formation and quality. This PhD project will improve the understanding of how alternative fuels affect the clinker quality, by a combination of experimental work and modeling.

Introduction

Ordinary Portland cement (OPC) consists mainly of Portland cement clinker (clinker), app. 5% gypsum and up to 5 % other constituents, such as fly-ash, limestone etc. The hydraulic ability of cement originates from clinker, which harden by addition of water.

Clinker consists mainly of alite (3CaO·SiO₂), belite (2CaO·SiO₂), aluminate (3CaO·Al₂O₃) and ferrite (4CaO·Al₂O₃·Fe₂O₃). Alite is the main strength-giving component in cement, dominating both early and late strength development [1]. Strength describes the ability of the cement material to support a certain load, and it is therefore one of the most important parameters to evaluate clinker quality. Belite contributes mainly to the later stages of the cement strength development. Aluminate dominates setting time which is the time from the initial mixing of water and cement until hardening of the material. Ferrite has only minor influence on both the setting time and the strength, but it provides the cement with a greyish or black colour, which is characteristic for OPC [2].

Clinker is produced by burning a mixture of ground limestone, clay, sand and iron ore in a rotary kiln, where the temperature reaches approximately 1500 °C. In order to heat up the materials to the process temperature, fuel is fired in the calciner (60%), and in the kiln main burner (40 %). An outline of the hot part of a cement plant is presented in Figure 1.

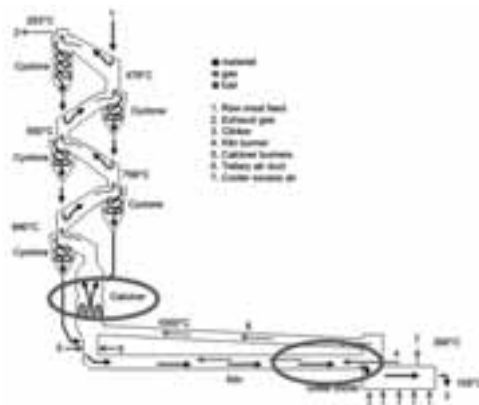


Figure 1: Overview of the pyro part of a cement plant, (calciner, kiln and cooler) where the red circles indicate where fuel is fired.

In total (combining the calciner and main burner), approximately 100 g coal is used per kg cement [3], which corresponds to approximately 350 gram CO₂ per kilo cement. In order to reduce the CO₂ emission and direct fuel cost, cement producers demand technologies which enable them to substitute an increasing amount of fossil fuel with alternative CO₂-neutral fuel.

Combustion of alternative fuels (AF) in the calciner and main burner is not without problems for the product quality, since AF-ash typically contain mineral

components and trace elements in proportions that differ from those being present in the fuel and the raw materials normally used, which may influence clinker quality. Furthermore alternative fuel particles are typically coarser and contain more moisture which affects the temperature profile of the pyro part of the cement plant by decreasing the maximum temperature and increasing the mean temperature which may influence the cement product as well.

Project objectives

The ultimate goal is to develop a method for predicting the effects of alternative fuels combustion, on the resulting clinker quality, in order to avoid a reduced clinker quality when fossil fuel is substituted with alternative fuel by changing the cement plant design or operational parameters.

This is complex, since AF combustion affects the clinker formation and clinker quality in many different ways. The project will focus on the issues regarding combustion of alternative fuel on the clinker quality which is expected to have the most significant effect;

1. Study the effect of a changed temperature profile in the kiln due to AF-combustion in the main burner, and;
2. To study the effect of coarse fuel particles and foreign elements on the clinker quality introduced early and late in the kiln and;
3. To study the effect of changed volatiles circulation (S, Cl and alkali) on the clinker formation and clinker quality.

Experimental Methodology

Tasks 1, 2 and 3 will be addressed by different methodologies. The methodology is established for investigating how ash, added to clinkers already formed, affect the distribution between alite and belite in the product. This investigation simulates combustion of alternative fuels, with high ash content, in the main burner. The procedure is the following:

Industrially produced clinker with a diameter of 1.5-3 cm is used. This specific interval is chosen because 1.5 cm is the minimum size which is possible to cut in half with the available equipment and the diameter of the crucible is 3 cm. The clinker nodules are cut in half for obtaining a flat surface where ash is added. On one of the clinker halves the ash is added while the other clinker half is kept as a reference, as show in **Figure 2**.



Figure 2: Two clinker half. One where ash is added and the other one is kept as a reference.

Both clinker halves are burned at 1500°C in air. After the experiment, the sample is removed from the furnace and cooled in ambient air.

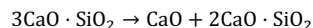


Figure 3: The left side shows a clinker which is embedded vertically in epoxy and the sample is cut along the line. The right side shows a top view of the sample which has been cut in half. This sample is studied by an optical microscope.

The sample is embedded vertically in epoxy, as shown in Figure 3, and it is cut in half in order to obtain a cross section of the clinker, which can be studied in an optical microscope. In order to separate the clinker phases the sample is exposed to hydrogen fluoride (HF) vapor which changes the clinker color.

Future Work

The presented method has been tested for 30 minutes burning time with an ash from sewage sludge. The results show that alite is converted to belite and free lime:



The burning time used for the initial test is much higher than the time ash is in contact with already formed clinker in an industrial plant, therefore the method has to be tested for a shorter burning time (approximate 5 minutes). Furthermore clinker produced by this method has to be compared to industrial produced clinker where ash-rich fuels are fired in the main burner, for evaluating if the method produces clinker which are comparable to industry.

Acknowledgements

This project is an Industrial PhD project performed in corporation between FLSmidth A/S and the CHEC Research Centre with co-funding from The Danish Agency for Science, Technology and Innovation. The project is a part of a research platform on future cement technologies financed by The Danish National Advanced Technology Foundation, DTU and FLSmidth A/S.

References

1. Hewlett, P.C., *Lea's Chemistry of Cement and Concrete*, Elsevier, 1998, p. 243. ISBN: 9780750662567
2. F. W. Locher, Influence of burning conditions on clinker characteristics, *World Cement Technology*, pp. 67–73, 1980
3. <http://wbcsdcement.org/index.php/key-issues/fuels-and-materials/key-performance-indicators>



Joussef H. Chaaban

Phone: +45 4525 2846

E-mail: joc@kt.dtu.dk

Supervisors: Kim Dam-Johansen
Søren Kiil
Tommy Skovby, H. Lundbeck A/S

PhD Study

Started: January 2010

To be completed: January 2013

Novel Reactor Design for Organic-Chemical Crystallization of Active Pharmaceutical Ingredients

Abstract

In the present PhD project a continuous preferential crystallization process for the separation of chiral APIs was developed. Proof-of-Concept experiment using the conglomerate forming amino acid Asparagine monohydrate in water as model system was conducted. The experiment revealed that the enantiomeric composition in the mother liquor during the crystallization process was 50:50 and identical in both crystallizers. Furthermore, crystal growth was observed which shows systematic 3D crystal growth. The yields of solid product obtained were 77% D-AsnH₂O and 58% L-AsnH₂O based on the initial mass of seeds used. The productivities were determined to 1.67×10⁻⁵ g D-AsnH₂O/(g racemate × min) and 1.25×10⁻⁵ g L-AsnH₂O/(g racemate × min).

Introduction

Biological activity and physiological effect of stereoisomers that are non-superimposable mirror-images of each other, i.e. enantiomers, are dependent on the optically active form of such isomers. The majority of active ingredients in the pharmaceutical, biotechnological, agrochemical, food and cosmetic industries are racemic mixtures, i.e. mixture of equal quantity of enantiomers. Only one enantiomer is biologically effective and the other enantiomer can be considered as an impurity comprising 50% of the mixture. Health and environmental side effects are in many cases attributed to the presence of counter-enantiomers. A clear evidence of the consequences of administering racemic drugs is the dramatic incident of the drug thalidomide in the last century¹. During the last decade the commercialization of chiral active ingredients has attracted great attention, which resulted in issuing guidelines for the commercialization of such chiral ingredients by the Food and Drug Administration (FDA), the Japanese authorities and the European Community². Strict regulatory requirements and increasing public demand for the production of chiral active ingredients in optically pure form have sparked the intensive research devoted to the development of reliable and cost-efficient production processes to produce optically pure chiral active ingredients. In this context, two options are available: 1) Enantioselective synthesis (chemical or enzymatic asymmetric synthesis)

or 2) Enantioselective separation of racemic mixtures. The latter option comprises an attractive alternative for the production of optically pure enantiomers⁴. For this purpose there exist alternative technologies which, among others, include Preferential Crystallization³.

Continuous Preferential Crystallization system

The developed coupled continuous preferential crystallization system (CCPC) is illustrated in Figure 1.

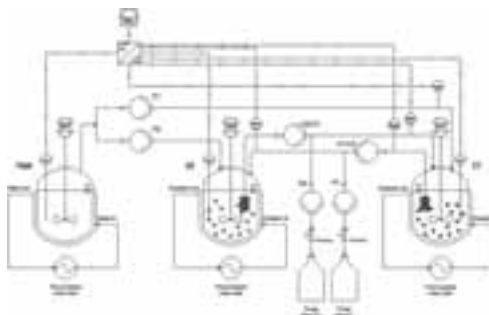


Figure 1: Schematic diagram of the developed coupled CCPC system. Red and blue filled circles indicate growing seed crystals of each enantiomer.

The concept is based on two crystallizers coupled by crystal-free liquid exchange between the crystallizers and feed solution entering the crystallizing solution in

each crystallizer simultaneously. To maintain constant volumes in the crystallizers, withdrawal of mother liquor occurs through purge streams. The purpose of coupling by liquid exchange streams and supplying fresh racemic feed solution is to improve the separation efficiency of the two enantiomers in the overall process. To maintain a constant driving force and thereby a constant overall growth rate throughout the crystallization process, the CCPC system comprises an attractive. It is thus believed that it should provide an improvement of productivity and yield of solid product and maintain a high purity of the solid product. Furthermore, the CCPC system should provide improved control of PSD and polymorphism which in turn eases the downstream processing.

Results and Discussion

To verify the achievement of a steady state in the crystal growth driving force, i.e. supersaturation, and to reveal the applicability of the concept of the CCPC a trial experiment was performed. The model compound used is the conglomerate forming amino acid Asparagine monohydrate (DL-AsnH₂O) in water. Crystal-free liquid solution samples were withdrawn at five minutes intervals after seeding and through the 90 minutes process duration time. The samples were analyzed by polarimetry. The results are shown in Figure 2.

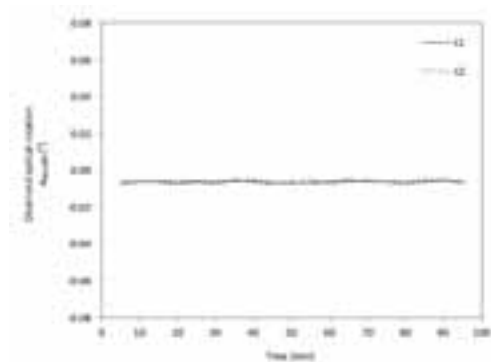


Figure 2: Observed optical rotation signal as function of time for separation of AsnH₂O enantiomers by CCPC.

It is shown that the observed optical rotation is about zero degrees throughout the process. This indicates that the composition of the liquid phase in the crystallizers is indeed racemic as expected. For the process conditions at which the experiment is performed, racemic solid mixture will not occur due to the suppression of the crystallization of the counter-enantiomer.

At the end of the experiment the solid product from each crystallizer was filtered off, washed and dried. To reveal whether crystal growth has occurred or not the solid products were analyzed by SEM and compared to samples of the initial crystals used for seeding.

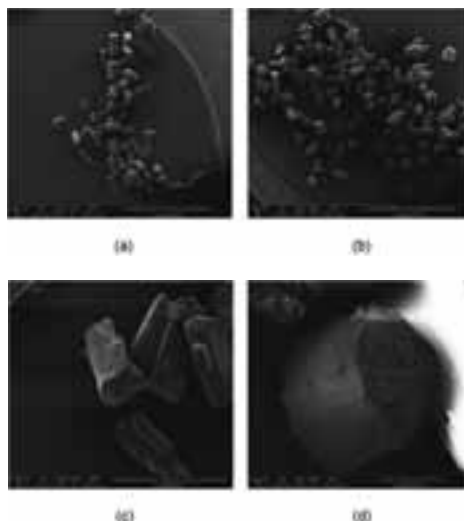


Figure 3: SEM microphotographs of enantiopure seeds and solid product after ended experiment.

Figure 3 (a) and (c) show the seed crystals of D-AsnH₂O before introducing them into the crystallizer. As seen the surface of the crystals is relatively smooth and the crystals are uniform in shape and size. Figure (b) and (d) show the product crystals. It is observed that systematic growth occurs in 3D and the surface of crystals becomes rough facilitating further growth. Furthermore, there are some minor fragments which could indicate adsorption of fragments on crystal surface.

Conclusions

Continuous preferential crystallization enables improved control of the enantiomeric composition in the liquid phase and solid phase growth to ensure separation of enantiopure APIs and their intermediates. It can be concluded that the CCPC system is certainly an attractive alternative for separation of enantiomers from a conglomerate forming system and it also provides several benefits compared to conventional batch crystallization.

Acknowledgments

The author acknowledges the financial and professional support of H. Lundbeck A/S and CHEC Research Center at the Department of Chemical and Biochemical Engineering at DTU.

References

1. G. Blaschke, H.P. Kraft, K. Fickentscher, F. Köhler, *Arzneimittel-forschung* **1979**, 29, (10), 1640-1642.
2. S.C. Stinson, *Chemical and Engineering News* **1995**, 73, (41), 44-74.
3. M.P. Elsner, G. Ziomek, A. Seidel-Morgenstern, *Chemical Engineering Science* **2011**, 66, (6), 1269-1284.



Krishna Hara Chakravarty

Phone: +45 4525 4637
 E-mail: krich@kt.dtu.dk

Supervisors: Kaj Thomsen
 Philip Loldrup Fosbøl

PhD Study:
 Started: September 2012
 To be completed: August 2015

Similarity and differences in the Low salinity modeling for carbonate and sandstone reservoir

Abstract

Carbonate and Sandstone wet ability is dictated by the surface chemistry connected to stability of the water film amid the oil phase and the rock surface. It has been verified, both in the field and laboratory, that seawater is an excellent insertion fluid to improve the oil recovery in many cases. But in some cases particularly it has categorically failed. This work indent to highlight the fundamentals in each and unlist the constraints associated.

Introduction

Water flooding has for a long time been regarded as a secondary oil recovery method. In the recent years, extensive research on crude oil, brine and rock systems has documented that the composition of the injected water can change wetting properties of the reservoir during a water flood in a favorable way to improve oil recovery. But, over the past few years this injection of “smart water” has been consistently raising the same questions¹⁻⁵.

- Are the mechanisms in low salinity water flooding understood?
- Can low salinity water flooding be used in all sandstone fields?
 - If not, when can it be used?
- Will low salinity water flooding improve the oil recovery in all sandstone reservoirs?

Can oil recovery be estimated by existing reservoir simulators?.

Even after significant advancement in number of research projects and publication, why there is no direct answers to these questions?

It is simple because low salinity water flooding cannot be understood by using classic EOR physical fluid flow equations.

- There is no evident miscible process
- Reduction in inter facial tension has not been observed

• Mobility control
$$M = \frac{\lambda_D}{\lambda_d} = \left(\frac{k_{rw}}{\mu_w}\right) \cdot \left(\frac{\mu_b(1)}{k_{ro}}\right)$$

- k_{rw} : Relative permeability at connate water saturation
- k_{ro} : Relative permeability at residual oil saturation
- μ_o : Viscosity of Oil at reservoir conditions
- μ_w : Viscosity of water at reservoir conditions
- M : Mobility ratio

- Favorable mobility control if $M < 1$
 - Reducing k_{rw} or μ_o
 - Increasing k_{ro} or μ_w

- None of these seems to be dominating
- When all other explanations have failed put the blame on chemical mechanism of wetability

Overview

The mechanism behind Low Salinity Effect in carbonate and sandstone reservoirs cannot be explained together as the studies so far has given quiet different results in the two scenarios .Carbonate reservoirs seems to have a more simple mechanism while sandstone reservoirs are likely to have more than one process occurring. For the same it is important to the basic conditions for low salinity effect.

Conditions for low salinity effects

The listed conditions for low salinity effects are mostly related to the systematic experimental work by Tang and Morrow (1999a), but some points has also been taken from the work by researchers at BP (Lager et al., 2007; Lager et al., 2008a).

- Porous medium
 - Sandstones.

Low salinity effects have not been recognized in pure carbonates, but Pu et al. have observed low salinity effects in a sandstone that hold dolomite crystals (Pu et al., 2008).

- Clay must be there
The kind of clay may play a role.
- Oil
 - Ought to contain polar components (i.e. acids and bases)
 - No effect has been observed using refined oil free from polar components.
- Formation brine, FW,
 - Formation water necessarily contain divalent cations, i.e. Ca²⁺, Mg²⁺ (Lager et al., 2008a)
 - Initial FW must be flooded
 - effectiveness is related to initial water saturation,
- Low salinity insertion fluid
 - The salinity is frequently between 1000-2000 ppm, but effects have been observed up to 5000 ppm.
 - Appears to be responsive to ionic composition (Ca²⁺ vs. Na⁺)
- Produced water
 - For a non-buffered scheme, the pH of the effluent water typically increases about 1-3 pH units when injecting the low salinity fluid.
 - It has not been established that raise in pH is needed to observe low salinity effects.
 - In some cases, production of fines have been detected, but low salinity effects have also been reported without visible production of fines (Lager et al., 2008a)
- Permeability decrease
 - Usually a raise in pressure over the core is detected when moving to the low salinity fluid, which may be associated to migration of fines or formation of an oil/water emulsion.
 - There is a lack of experimental evidence to say that observed low salinity effects are accompanied by permeability reduction.
 - Waterflood experiments have been performed without any deviation in end point relative permeability data among high and low salinity water floods, under both secondary and tertiary flood circumstances (Webb et al., 2008).
- Temperature
 - There seems to be no temperature restrictions to where low salinity effects can be observed. The majority of the reported studies have, however, been performed at temperatures below 100 °C.

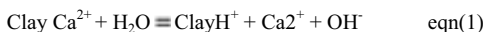
Sandstone Mechanisms:

Laboratory and field tests have shown that enhanced oil recovery can be obtained by performing water flooding at low salinities. The precise method following the amplified oil recovery by low salinity flooding still remains a topic for debate, but various efforts have been

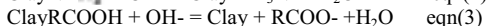
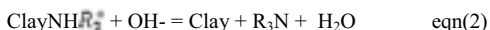
made, and are still being made, to reach a universally accepted understanding. Various mechanisms have been suggested during the last 10 years, and some of them are listed below⁶:

- Migration of fines
- Impact of alkaline flooding
- Multi component ion exchange
- Microscopically diverted flow
- Double-layer expansion

Recently, the desorption of organic material from the clay surface by a local enhance in pH at the clay_water boundary caused by desorption of surface energetic inorganic cations as the low saline fluid invades the porous medium, has been recommended by Austad et al.¹⁰ to play a significant role in the low salinity enhanced oil recovery procedure. Both acidic and basic crude oil components are released from the surface as the pH is increased from 5-6 to about 8-9. In laboratory experiments, the raise in pH is typically established, but due to buffering property in field situations due to presence of CO₂ and/or H₂S, an increased pH is seldom observed. Chemically, the mechanism could be described by the subsequent equations using Ca²⁺ as the active cation:



The local enhance in pH, close to the clay surface, causes reactions between adsorbed basic and acidic material as in an normal acid base proton transfer reaction, as shown by eqs 2 and 3. Both organic acid and base components are partly desorbed from the surface.



The optional chemical mechanism for enhanced oil recovery by low salinity water flooding has been based on three tentative interpretation:

- Clay must be present in the sandstone1
- Polar components (acidic and/or basic material) must be present in the crude oil
- The formation water must contain active ions like Ca²⁺.

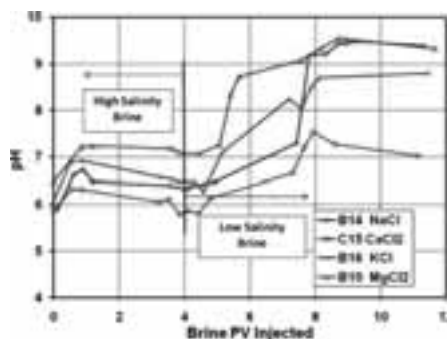


Figure 1. pH change caused by different LS brines⁶

The exclusive chemical property of clay minerals to act as cation swap material is the key feature in the chemical explanation of the recommended low salinity EOR mechanism. The cation swap ability, varies with the kind of clay, and raise in the order kaolinite (3_15 meq/100 g) < illite (10_40 meq/100 g) < montmorillonite (70_120 meq/100 g), for three common clay minerals.⁶

Kaolinite and illite clay minerals are usually found in sandstones, whereas montmorillonite is a frequent mineral in the smectite mineral group and is the major clay mineral in bentonite. Montmorillonite can exist in rather considerable quantities in shale due to volcanic ash deposition. In a mixed-wet sandstone reservoir, polar organic material from the crude oil, has acidic and/or basic functional groups, is adsorbed onto the rock surface, particularly onto the clay minerals.⁶⁻⁹.

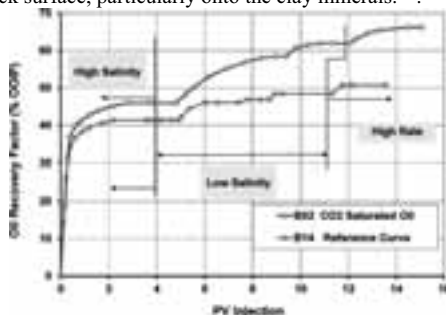


Figure 2. Effect of initial pH on oil recovery by tertiary low salinity flood⁶

Recent laboratory tests have indicated that the wet ability is changed toward a more water-wet condition after flooding with low saline water.^{6,9} Thus, the key objective of the our work is to create experimental chemical evidence for the wettability alteration procedure probably taking place during the low saline water flood. Herein the main insights include:

- The adsorption of the acidic form (pH = 5) is about 4 times greater than the adsorption of the basic form (pH = 8) independent of the salinity.
- The adsorption at pH = 5 decreased steadily as the salinity increased, confirming a competition between the protonated cationic base and cations (especially Ca²⁺) toward the negative sites of the clay.
- The adsorption at pH = 8 decreased as the salinity increased to about 500 ppm, and thereafter, the adsorption has been not affected by the salinity.
- At salinities above 500 ppm, the impact of salinity on the adsorption of quinoline is much less than the effect of pH

Carbonate Reservoir Mechanism :

The model developed according to the work so far comprise the consequence of divalent cations (Mg²⁺ and Ca²⁺) in the presence of SO₄²⁻ on wettability alteration towards extra water-wet situation in chalk and as a

result enhancing oil recovery. From experiments rformed and the following conclusions were drawn⁷:

- It is experimentally verified that Mg²⁺ is also a strong potential formative ion towards chalk surface, which has the possibility to increase the positive charge density of chalk.
- At high temperatures, Mg²⁺ present in seawater can substitute Ca²⁺ from the chalk surface, and the degree of replacement increased as the temperature increased.
- Seawater can recover spontaneous imbibition of water into reasonable water-wet chalk to improve oil recovery from fractured chalk reservoirs. The key parameters in seawater are the potential determining ions: Ca²⁺, Mg²⁺, and SO₄²⁻.
- To advance the oil recovery, sulfate must act together with either Ca²⁺ or Mg²⁺. In both cases, the efficiency increases as the temperature increases.
- A chemical mechanism, which discusses the interplay between the potential determining ions to displace organic carboxylic materials from the chalk surface, is proposed.

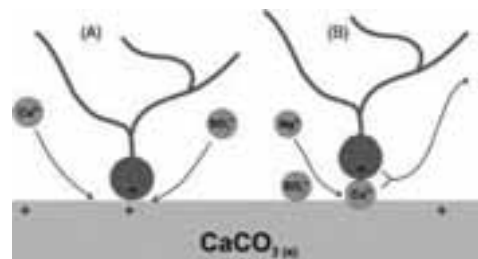


Figure 3: Graphic model of the recommended mechanism for the wettability alteration induced by seawater. (A) Proposed mechanism when Ca²⁺ and SO₄²⁻ are active at lower and high temperature. (B) Proposed mechanism when Mg²⁺ and SO₄²⁻ are active at higher temperatures⁷.

Our View

It is clear from the present research that there is significant complexity and non-linear dynamics in this multi-variable mechanism. We have started our modeling simulation, to understand this issue very fundamentally and very meticulously. Herein we take one hydrocarbon at a time and calculate the all possible reaction and phase transition with each of the ions used in the “smart water” over a varied pressure temperature range. Here in all the relevant thermodynamic parameters are being taken in record to develop a complete database. The same reaction sets are being used through different empirical thermodynamic model SUPCRT92, CHNOSZ etc to ensure the consistency in our result. To ensure that our estimated thermodynamic values are correct we also intend to use DFT-LDA and GGA tools. Through this kind of analysis we can exactly calculate the possible multi ionic exchanges that can actually occur and at what conditions. We also intend to develop a data base for the possible reactions

between the smart water and the different minerals. This will help us quantitatively monitor the possibility of fines formation in any particular given scenario. Once we are done with all these different combinational reaction studies then only we can select out feasible reactions and then try to figure out a more suitable match by modeling more than one mechanism at a time to co-relate with the experimentally observed data using Extended UNIQUAC model⁸.

$$G(T, p) = E^{\text{tot}} + F^{\text{vib}} - TS^{\text{conf}} + pV \quad (2)$$

E^{tot} : Total energy obtained from the electronic structure calculation

F^{vib} : Vibrational energy calculated by the Molecular Dynamics(MD) simulation

T : Temperature

S^{conf} : Configuration Entropy calculated by MD simulation at 0 Kelvin

p : Pressure

V: Volume

G(T,p): Gibbs free energy at a given pressure temperature

This process of detailed calculation is quite likely to take some time but it is very important to continue it in this approach not only from a scientific point of view but also from a commercial point of view as well. In we look in Fig 1 then we clearly observe that in the recent publications directly or indirectly related to Low Salinity Effect (LSE) has been mostly dominated by the use of multiple EOR. So, it clear that majority of the funds are presently being invested to make the optimum use of the different tertiary recovery tools

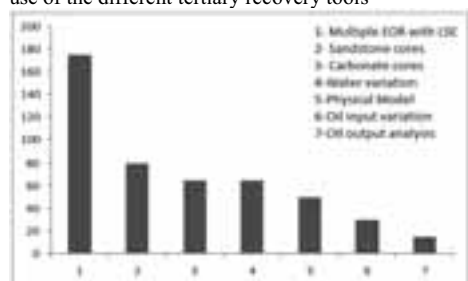


Figure 4: The figure show the number of recent publications and articles in the different sectors of work involving LSE

. Using polymers, CO₂, etc with LSE has been a common practice. Most of the studies are experimental and are not proving any clear trend between the different cores. So, to make an optimum use of the LSE with other tertiary oil recovery, we need to first understanding of this phenomena.

Problems and Challenges:

All most all research articles have tried varying one of the parameters and has observed the output efficiency¹⁻⁶. The cores, ions in water and other physical parameter like pressure temperature has been

consistently varied a lot¹⁻⁵. But, unfortunately barding very few research articles, none have analyzed the difference between in the content of input oil and the oil extracted. The articles which have reported the change on oil concentration has also been not the main issue. So this information is completely unavailable. Moreover the changes in the clay minerals during this has been has also not been studied that well. Moreover there has been very few published research article where an exhaustive simulation has been used. And in these particular articles⁹ (mostly published by Innovation and R&D Center, Shell (China)) use a colossal data base of the core fields and minerals changes during LSE, which are unfortunately made unavailable to the rest.

Conclusion:

We are convinced that a detailed mathematical fundamental analysis is a basic requirement to proceed in this field. Empirical relation and experiments are neither enough to understand this phenomenon nor to use it commercially. The unpredictability gets further increased in experiments on optimized use of multiple EOR. So, a detailed mathematical analysis is a starting requirement. Further implementing the results obtained through this experiment will require geodynamic subsurface model.

References

- (1) Zhang, P. Water-based EOR in Fractured Chalk; Wettability and Chemical Additives; Ph.D. Thesis, University of Stavanger: Norway, 2006; ISBN: 82-7644-293-5.
- (2) Høgenesen, E. J. EOR in Fractured Oil-Wet Chalk; Spontaneous Imbibition of Water by Wettability Alteration; Dr. Ing. Thesis, University of Stavanger: 2005C
- (3) Puntervold, T. Waterflooding of Carbonate Reservoirs; EOR by Wettability Alteration; PhD Thesis, University of Stavanger: Norway, 2008; ISBN 978-82-7644-347-9.
- (4) Standnes, D. C. Enhanced Oil Recovery from Oil-Wet Carbonate Rock by Spontaneous Imbibition of Aqueous Surfactant Solutions; Dr. Ing. Thesis, NTNU: Norway, 2001.
- (5) Strand, S. Wettability Alteration in Chalk - A Study of Surface Chemistry; Dr. Ing. Thesis, University of Stavanger: 2005.
- (6) [x.doi.org/10.1021/ef201435g](https://doi.org/10.1021/ef201435g) | Energy Fuels 2012, 26, 569–575
- (7) Doust Colloids and Surfaces A: Physicochem. Eng. Aspects 301 (2007) 199–208 Colloids and Surfaces A: Physicochem. Eng. Aspects 301 (2007) 199–208
- (8) Thomsen, K. 1997 Aqueous Electrolytes Model Parameters and Process Simulation Type: Ph.d. thesis - Ph.d. thesis
- (9) Wei, L. 2012 Sequential Coupling of Geochemical Reactions With Reservoir Simulations for Waterflood and EOR Studies



Peam Cheali

Phone: +45 4525 2911
E-mail: pche@kt.dtu.dk

Supervisors: Gürkan Sin
Krist V. Gerbaey

PhD Study

Started: May 2012
To be completed: April 2015

Synthesis and design of integrated-intensified chemical/biochemical processes

Abstract

The reduction of fossil fuel feedstock causes a serious challenge on economic growth and environmental sustainability. This motivates the development of renewable technologies to bridge the gap for fuel, chemical and materials production. This project is focusing on the development of methodologies for fast, flexible and future design of integrated-intensified chemical/biochemical processes, with particular focus on a biorefinery case study.

Introduction

Energy supply as well as chemical manufacturing currently depends strongly on the availability of crude oil. Estimations show that the reserves for oil are decreasing rapidly, hence the need for alternative feedstock and processing techniques becomes more urgent. In addition the call for sustainable and environmentally attractive technologies is growing stronger.

A sustainable alternative (Figure 1) is the production of fuels, chemicals and products on the basis of biomass; more specifically lignocellulosic biomass, which is a non-food feedstock and has desirable environmental and price characteristics. Biomass is available in many different forms and there are in principle many processing paths available to produce a plethora of end products resulting in a combinatorial problem.

Moreover, the synthesis and design of intensified chemical and biochemical processing networks is a complex and multidisciplinary problem, which involves many strategic and tactical decisions at business (considering financial criteria, market competition, supply chain network, etc) and engineering levels (considering synthesis, design and optimization of production technology, its feasibility, sustainability, R&D needs, etc), all of which have a deep impact on the profitability of biorefining industries.

Specific Objectives

In this PhD project, an integrated framework for synthesis and design of integrated-intensified chemical

and biochemical processes is presented. The framework is evaluated on biorefinery network design and synthesis. A systematic approach is used to manage the complexity and to solve simultaneously both the business and the engineering dimension of the problem. This allows generation and comparison of a large number of alternatives at their optimal point. The result is the identification of the optimal raw material, multi-product portfolio and process technology selection for a given market scenario, their sustainability metrics and risk of investment under market uncertainties enabling risk-aware decision making.

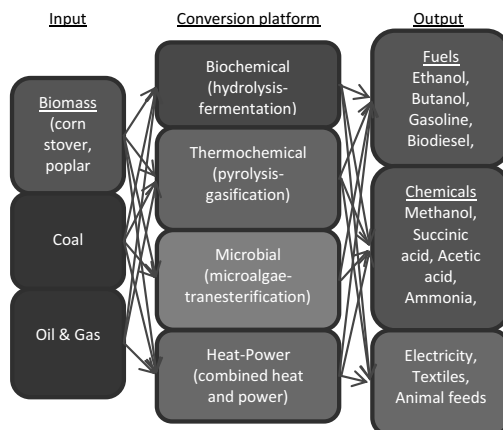


Figure 1: Process network of fuels, chemicals and materials production through different conversion platforms and feedstocks [1]

In particular, the framework will include the following features:

- Development of a library of models and a database for the assessment of performance
- Separation modeling, reactor modelling and kinetics modelling
- Database of processing technology alternatives and intensified processes
- Computer-aided synthesis and design of candidate processing paths in biorefinery networks
- Mixed integer nonlinear programming (MINLP) as well as stochastic programming for selection of optimal biorefinery path

Several case studies of biorefinery networks focusing on production of biochemicals, biofuels (e.g. butanol, ethanol) and an optimal blend of mixtures with fossil fuels will be used to highlight the application of the framework developed above.

Framework

This study follows the integrated business and engineering framework developed earlier (Figure 2, [2]) to find the optimal processing path according to a specific problem definition and specific optimization scenarios.

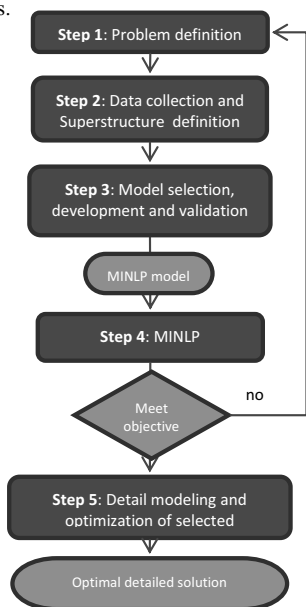


Figure 2: The framework for integrated business and engineering decisions [2]

Step 1, problem definition, aims at defining the problem scope, including selection of objective functions and optimization scenarios with respect to either business strategy, engineering performance or sustainability.

Step 2, data collection and superstructure definition: Collected data on processing technologies are organized in the form of a superstructure, which represents a network of alternative processing technologies.

Step 3, model selection and validation: Selection or formulation of the models relevant to the defined problem and the collected data. All the necessary equations and constraints relevant to each processing technology are formulated in this step.

Step 4, MINLP optimization: The equations, constraints and logical functions defined in the previous step are formulated as an MINLP problem, and are subsequently solved. The objective function has been defined in step 1.

Step 5, detailed modeling and optimization of the selected alternative: Generation of data to validate the result of step 4 on the basis of detailed models and optimization.

Case Studies

Different MINLP optimization scenarios were formulated and solved in GAMS to identify the optimal biorefinery processing route. The objective functions in these scenarios were as follows:

- maximize biorefinery products with or without gasoline blending
- maximize product sales, minimize utility, waste and investment cost with or without gasoline blending

Conclusions

The PhD project is expected to result in the framework implemented as a software platform to serve as enabling technology for facilitating innovation in the biorefinery processing industries. This will contribute to supporting the development of renewable carbon-based technologies and industries.

Acknowledgement

The author kindly expresses his gratitude to the Technical University of Denmark for financial support.

References

1. G. Sin, P. Cheali, K. V. Germaey, R. Gani, 2012, Superstructure based optimization for process synthesis/intensification, OPTICO 1st Technical Meeting, 6.
2. A. Quaglia, B. Sarup, G. Sin and R. Gani, 2012, Integrated Business and Engineering Framework for Synthesis and Design of Enterprise-Wide Processing Networks, Computers and Chemical Engineering, 38, 213-223.



Signe Sandbech Clausen

Phone: +45 4677 4151
E-mail: sicl@kt.dtu.dk

Supervisors: Iver Jakobsen
Mette Grønlund
Ingo Lenk, DLF Trifolium

PhD Study

Started: April 2011
To be completed: March 2014

Symbiotic Growth Depressions in Bioenergy and Forage Crops

Abstract

Phosphorus (P) is an essential nutrient for plant growth. Since P is also one of the least plant-available nutrients in the soil, it is often growth limiting. To solve this problem most plants engage in a symbiotic relationship with arbuscular mycorrhizal (AM) fungi. The symbiosis is usually mutualistic and increases plant uptake of mineral nutrients, especially P, and thereby growth. This is however not always the case as some grasses exhibit symbiotic growth depressions when colonized by certain AM fungi. Currently the P rock reserves used for fertilizer production are depleted in parallel with an increasing demand on global food and bioenergy production. A part of the solution to mitigate the consequences of the phosphate (Pi) resource problem could be to increase the Pi acquisition capacity and efficiency of crop plants. In order to do this a better understanding of the Pi uptake pathways and regulatory mechanisms in crop plants is required. This project aims at characterizing putative direct Pi uptake transporters in the model grass *Brachypodium distachyon* and will test the hypothesis that AM-colonized plants become P limited and hence growth depressed due to impaired function of direct Pi uptake at the root surface.

Introduction

Phosphorus (P) is one of the major macro-nutrients for plant growth and development. Plant roots acquire P from the soil as inorganic phosphate (Pi) which is actively taken up via Pi transporter (PT) proteins. The PTs play a critical role in Pi acquisition from soil solution and Pi translocation within the plant. Even though P may be present in relatively large amount in the soil, it can still be limiting for plant growth. This is mainly because of a very low solubility and mobility in the soil [1]. To overcome this, plants have evolved a range of strategies which increase either Pi uptake capacity or Pi availability in the soil. One strategy is to establish a symbiosis with arbuscular mycorrhizal (AM) fungi. This is an advantage to the plant as the AM fungi offers an alternative and very effective pathway from which P can be acquired from the soil. In arbuscular mycorrhizal (AM) plants two Pi uptake routes are present: the mycorrhizal pathway and the direct root uptake pathway. The symbiotic association occurs in roots of most soil grown plants, and approximately 80% of all terrestrial plants are colonized by AM fungi [2]. AM colonization often leads to dramatically increased plant growth, primarily because the fungal mycelium assists the plant in scavenging P and other nutrients from larger soil volumes than by the root system alone. Nevertheless, there is a considerable functional diversity

in the outcome of the symbiosis, ranging from positive to negative effects [3, 4]. In grasses it has been observed that the colonization in some cases results in growth depression rather than a positive growth response. The observed symbiotic growth depressions were conventionally assigned to carbon drain by the fungi. However, a new hypothesis is that the direct Pi uptake in plants is repressed during AM colonization. This is based on results showing that PT genes in direct pathway are suppressed in AM plants and that some AM non-responsive plants have been shown to have a high mycorrhizal Pi uptake. Therefore the direct uptake is assumed to be down-regulated and this will result in a P limited plant if the AM-mediated Pi uptake cannot fully compensate for the reduced direct Pi uptake.

Since crop plants grown today are supplied with plenty of P fertilizer and have been bred under plenty of nutrient supply they may not be very efficient plants in relation to uptake of P or other nutrients. This provides a global challenge as the mineral phosphate rock (PR) reserves used for fertilizers are non-renewable. Although there is considerable debate about the magnitude of the PR reserves, they must be utilized in a sustainable manner to avoid their depletion on the long term. To maintain optimal crop yields using a reduced amount of P fertilizer, it is necessary to work towards

new crop varieties with superior P utilization capacity. This could potentially be obtained by breeding plants, in which direct and AM mediated Pi uptake become additive rather than alternative. For this reason, an important issue is to clarify how Pi is acquired and how the uptake is regulated in plants.

Plant species

The fully sequenced model grass system *Brachypodium distachyon* (Bd) is used to investigate the activity of the two Pi uptake pathways under different growth conditions using selected AM fungi. *B. distachyon* was first proposed as a model system by Draper et al. in 2001 [5]. Like Arabidopsis, Brachypodium has no agricultural significance, but offers many advantages over current model systems for plant genetic, cellular and molecular biology studies in monocots. Also, the phylogenetic position of Brachypodium makes it a convenient model for functional genomics studies in temperate grasses, cereals, and dedicated biofuel crops. A growing list of genomic resources has been developed and is currently under development (see brachypodium.org).

Method and perspective

A transformation approach is used to manipulate the activity of the Pi transport pathways, firstly by generating over-expression (OE) and knock-down (RNAi) lines of two putative direct phosphate transporters (*BdPT4* and *BdPT8*) along with two control constructs in the model plant. Secondly, the sub-cellular localization will be determined in stable transgenic lines expressing GFP tagged versions of the BdPT4 and BdPT8 proteins. In addition, OE lines of the AM-induced *BdPT7* have been produced. Along with our own transgenic *B. distachyon* lines, two T-DNA tagged mutant lines of *BdPT9* and *BdPT11*, obtained from the WRRRC *Brachypodium distachyon* T-DNA collection will be characterized. All of the transgenic *B. distachyon* lines will be used to investigate the specific roles of the phosphate transporters in Pi uptake. By evaluating the expression of the gene of interest, which should be over- or down regulated as expected in the transgenic lines, specific lines are selected for further analysis. The expression patterns of the transgenic and wild type plants in combination with physiological isotope tracer uptake studies will allow discrimination between Pi uptake via the mycorrhizal and direct pathways. In the selected lines, it will be determined how Pi uptake and/or translocation is affected by the change in expression and the potential for increasing Pi uptake efficiency in plants will be evaluated. Pi uptake efficiency of crops might be improved if a high activity of the direct uptake pathway in mycorrhizal plants is maintained, thereby making the two pathways additive instead of complementary. Finally, the sub-cellular localization of the selected genes will be investigated in transgenic lines, which express the genes fused to GFP. When identified, these lines will be imaged using confocal microscopy for localization. I just returned

from an external PhD stay at Boyce Thompson Institute for Plant Research, Ithaca, NY in Maria Harrison's group where I was trained in confocal microscopy.

All results will be integrated into a model of the proposed regulatory mechanisms and involved genetic components underlying the observed growth depressions in the model grass *B. distachyon*. The experiments will mainly be performed under controlled conditions in climate chambers. The RERAF (Risø Environmental Risk Assessment Facility) phytotron will be used to study the influence of elevated CO₂ and thereby a changed carbon-balance, on the Pi uptake mechanisms.

Results

Thirteen PT genes have been identified in *B. distachyon* and their expression pattern analyzed by qPCR in non-mycorrhizal and mycorrhizal plants grown at different phosphate levels. Based on the expression levels and phylogenetic relationship to other known phosphate transporters, two putative direct transporter genes (*BdPT4* and *BdPT8*) found to be down-regulated at high phosphate levels and in mycorrhizal plants have been selected for further analysis. During the last year two transformation rounds have been performed by *Agrobacterium tumefaciens*-mediated transformation of embryogenic *B. distachyon* callus. T₁ seeds have already been collected from a range of transgenic plant lines which are ready for molecular and physiological studies. At present, more than a hundred transgenic T₀ plants of different lines are growing in the growth chambers to produce transgenic T₁ seeds.

Acknowledgements

The PhD project is part of the Research Project *Can we prevent symbiotic repression of crop performance?* Funded by The Danish Council of Independent Research | Technology and Production Sciences. It involves close collaboration with plant breeders at DLF TRIFOLIUM A/S and plant scientists at Boyce Thompson Institute for Plant Research, Ithaca NY and The University of Adelaide.

References

1. D.P. Schachtman, R.J. Reid, S.M. Ayling, Plant Physiol (116) (1998) 447-453
2. S.E Smith, D.J. Read, Mycorrhizal Symbiosis. Ed 3. Academic Press-Elsevier, 2008
3. S. Ravnskov, I. Jakobsen, New Phytologist 129 (1995) 611-618
4. S.E Smith, F.A. Smith, I. Jakobsen, New Phytol., 162 (2004) 511-524
5. J. Draper, L.A. Mur, G. Jenkins, G.C. Ghosh-Biswas, P. Bablak, R. Hasterok, & A.P. Routledge, Plant Physiol. 127 (2001) 1539-1555

**Larissa Peixoto Cunico**

Phone: +45 4525 5510
E-mail: lacu@kt.dtu.dk

Supervisors: Rafiqul Gani
Roberta Ceriani, UNICAMP
Bent Sarup, Alfa Laval Copenhagen A/S

PhD Study

Started: February 2012
To be completed: January 2015

Modelling of phase equilibria and related properties of mixtures involving lipids

Abstract

Equilibria between vapour, liquid and/or solid phases, component properties and also the mixture-phase properties are necessary for synthesis, design and analysis of different unit operations found in the production of edible oils, fats and biodiesel. A systematic numerical analysis to identify the needs of phase equilibria and related properties in process design and analysis for the production of edible oils and related products has been done and from this analysis the requirements of a database with respect to model development has been established. The consistency of the available VLE data has been checked with six tests while tests for LLE-data and SLE-data are discussed. Phase equilibria calculations based on the molecular models (UNIQUAC, UNIFAC, and NRTL) as well as GC+ approach based UNIFAC-CI method are discussed and compared. The available data in the literature and the well-known property models are adopted and further extended with group-contribution combined with atom connectivity based models. Some of these models are UNIFAC-CI, PC-SAFT and NRTL-SAC. The performance of these predictive models and the sensitivity of design variables developed are analyzed with respect to the uncertainties in the predicted properties. The application of the developed property models are illustrated through case studies involving different lipid compounds and their processing steps. The obtained results are implemented in process simulation software and applied to study industrial problems, for example, from Alfa Laval Copenhagen A/S and to validate the models.

Introduction

Lipids have an important role in plastics, insecticides, herbicides, cosmetics, drugs and food industry. The world's production of oils and fats has grown from 79.2 million tons in 1990 to nearly 176 million tons in the year 2011 [1]. With an increasing trend in the production rates of edible oils, fats and other lipids, correct prediction of the necessary properties (pure component and mixture) has become a major concern and issue. These mixtures handled consist of large complex chemicals such as fatty esters, acids alcohols, glycerides, sterols, etc., with or without the presence of water. While use of experimentally measured property values is highly desirable, laboratory measurements may be time consuming, expensive, and sometimes it may not even be feasible to perform experiments to obtain the necessary data. Therefore, it is more practical and convenient to employ property prediction methods to obtain the needed property information, which can be used in the early stages of process and/or product design. Hence, given the importance of molecular structure, the role of database, property models, and

analysis of property models in terms of accuracy, reliability, predictive power, and thermodynamic consistency is discussed.

Database

For the purpose of modeling of mixture properties, a database CAPEC_Lipids_Mixture_Database containing measured data of mixture properties has been developed. Currently, there are 333 different phase equilibrium systems (which include 92 VLE, 91 LLE, and 70 SLE), and 80 solid solubility systems. The total number of data-points of properties related to phase equilibria is 4500. A detailed description of database is given in Table 1. The data for some acylglycerols is not available in the database, which is mainly due to the fact that it is not possible to experimentally measure properties of these acylglycerols. The activity coefficient values predicted using different well-known GE models (UNIFAC, UNIQUAC, NRTL) for different lipid systems is also stored in the database for their use in phase equilibria calculations.

Table 1: Database (CAPEC_Lipids_Mixture_Database)

PE	Binary	Mult.	Isobaric	Isotherm.	PTX	PTXY
VLE	83	9	68	16	48	42
LLE	9	82	89	2	22	69
SLE	60	10				
Solubility	75	5				

Model Performance Statistics and Analysis of Property Models

The measured phase equilibrium data has been analyzed using the thermodynamic consistency tests together with the performance of well-known thermodynamic models (UNIFAC, UNIQUAC, NRTL) models. In Figures 01 and 02, the results of the model analysis are given for 2 lipid systems. Big deviations were observed for the UNIFAC model based temperature calculation compared to the other models (NRTL and UNIQUAC), as also reported by Coelho et al. [2]. Revisions of UNIFAC parameters have been done many times in the past but still there are missing entries in the UNIFAC parameter table because of the lack of measured data. To overcome this limitation, a method based on GC+ approach (UNIFAC-CI method) is developed to generate the missing UNIFAC group-interaction parameters without the need for new measured data and using only the structural information of the groups.

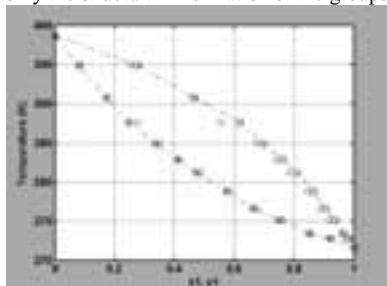


Figure 1: Vapor liquid equilibrium for hexanoic acid(1) + octanoic acid(2) for 1.3KPa. Experimental work [3] (○); NRTL model (□); UNIQUAC model (◇); UNIFAC model(△).

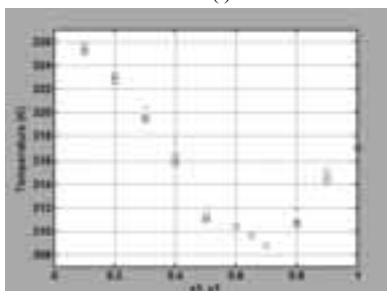


Figure 2: Solid liquid equilibrium for lauric acid(1) + myristic acid(2) for 1.3KPa. Experimental work [4] (○); NRTL model (□); UNIFAC model(△).

Thermodynamic Consistency Test

For vapor-liquid equilibrium data, many consistency tests have been proposed; most of them derived from the Gibbs-Duhem equation. This work considers the most used ones that are also considered by Kang et al. [5]. The program TDE developed at NIST by Frenkel et al. [6] does not reject any VLE data set found to be inconsistent. Rather, it assigns a lower weight (quality factor). If a test fails, the corresponding qualitative test assigns a value for its quality factor ranging from 0.1 to 1.

For Solid-Liquid Equilibrium (SLE) data, our search did not give any established method to check for its consistency. In this work we propose a new test method for thermodynamic consistency tests of SLE data. This test is similar to one of the tests for the VLE data but now including the uncertainty of the pure compound data (the melting point of the compound). Also, considering the same idea proposed in the Van Ness Test[7], where the thermodynamic consistency analysis is made based in how the mathematical activity coefficient model can reproduce the experimental data accurately, a new test method were developed to analyze the intermediate points in SLE. Preliminary test results are given in Table 2[8].

Table 2: Thermodynamic Consistency Test

Compounds	Quality Factor	
	VLE	SLE
Fatty acids	0.004 - 0.680	0.005 - 0.995
Methyl Esters	0.027 - 0.500	0.019 - 0.796
Ethyl Esters	0.024 - 0.500	0.017 - 0.500
Glycerol	0.005 - 0.500	

References

- World production of oils and fats, Available from: <http://www.rea.co.uk/rea/en/markets/oilsandfats/worldproduction> [Accessed 25th August 2012].
- R. Coelho; P. G. Santos; M. R. Mafra; L. Cardozo-Filho; M. L. Corazza, J. Chem. Thermodynamics 43 (2011) 1870–1876.
- E. Müller, H. Stage, Experimentelle Vermessungen von Dampf- Flüssigkeits Phasengleichgewichten, Springer Verlag, Berlin, 1961.
- M.C. Costa; L.A.D. Boros; J.A.P. Coutinho; M.A. Krähenbühl; A.J.A. Meirelles, Energy and Fuels 25 (2011) 3244–3250.
- J.W. Kang; V. Diky; R.D. Chirico; J. W. Magee; C. D. Muzny; I. Abdulagatov; A.F. Kazakov; M. Frenkel, J. Chem. Eng. Data 55 (2010) 3631–3640.
- V. Diky, R. D. Chirico; C. D. Muzny; A. F. Kazakov; K. Kroenlein; J. W. Magee; I. Abdulagatov; J.W. Kang; M. Frenkel, J. Chem. Inf. Model 52 (2011) 260-276.
- H.C. Van Ness; S. M. Byer; R. E. Gibbs, AIChE J. 19 (1973) 238-244.
- L.P. Cunico, A. S. Hukkerikar, R. Ceriani, R. Gani, Submitted to Fluid Phase Equilibria, 2012.



Inês Rodrigues da Silva

Phone: +45 4525 2610

E-mail: ins@kt.dtu.dk

Supervisors: Jørn Dalgaard Mikkelsen
Anne S. Meyer

PhD Study
Started: February 2009
To be completed: February 2013

Enzymatic Production of Prebiotic Polysaccharides using a bacterial family 11 RGI lyase expressed in *Pichia pastoris*

Abstract

Prebiotics are non-digestible carbohydrates that beneficially affect the host by selectively stimulating the growth of a limited number of bacteria in the colon. The waste streams from agricultural industry are a large source of oligosaccharides with potential prebiotic effects. These streams comprise barley bran, sugar beet pulp and potato pulp from the brewing, sugar and starch industries. Modification of oligomers to achieve the desired prebiotic effect requires a number of specific enzymes which can be acquired by cloning and expression in the yeast *Pichia pastoris*.

Aiming for an enzyme able to degrade pectinaceous biomass at elevated temperature we selected a gene encoding a putative rhamnogalacturonan I (RGI) Lyase (EC 4.2.2.-) from *Bacillus licheniformis*. The designed gene was transformed into *Pichia pastoris* and the enzyme was produced in the eukaryotic host with a high titer in a bioreactor. The RGI Lyase was purified by Cu²⁺ affinity chromatography. By use of a statistical design approach, with potato rhamnogalacturonan as the substrate, the optimal reaction conditions for the RGI Lyase were established to be: 61°C, pH 8.1, and 2mM of both Ca²⁺ and Mn²⁺ (specific activity 18.4 U/mg). The addition of both Ca²⁺ and Mn²⁺ was essential for enzyme activity.

Introduction

Functional food ingredients possessing potential health benefits have recently attracted strong attention. Some of the functional food ingredients are prebiotic oligosaccharides. Dietary fibers and prebiotics are non-digestible carbohydrates that beneficially affect the host by selectively stimulating the growth and/or activity of one or a limited number of bacteria in the colon. Oligosaccharides could be obtained as products of hydrolysis of plant derived polysaccharides, or directly from plant cell walls. Rational enzyme catalysed reactions are going to be developed to modify heterogeneous samples of substrates to create 'designed' oligosaccharides with defined structures and high prebiotic potential.

Discipline

The area of research is Enzyme technology.

Specific objectives

To use selective enzyme catalysts to convert polysaccharides into oligomers. Only few commercial enzymes are available for this task. Most of the commercial enzymes in addition contain other enzyme activities which degrade the desired oligosaccharides. Mono-component enzymes can, however, be produced by cloning and expression of suitable enzymes in the

yeast, *P. pastoris*. This process can be performed in the laboratory at our department. Furthermore, the optimal conditions of enzymatically catalyzed reactions have to be worked out as well. This includes up-scaling of the enzymatic reaction in order to deliver sufficient amount of oligosaccharides with potential prebiotic activity.

Results

A gene encoding a putative rhamnogalacturonan I (RGI) Lyase (EC 4.2.2.-) from *Bacillus licheniformis* was the enzyme selected. The designed gene was transformed into *Pichia pastoris* and the enzyme was produced in the eukaryotic host with a high titer in a bioreactor [1]. We have expressed the enzyme of interests with a MW of 68 kDa. The recombinant proteins we want to produce are isolated by diversity screening or identified in genomic databases. The genes are inserted into *P. pastoris* under the control of the AOX1 (Alcohol Oxidase 1) promoter, in order to induce the gene of interest in the presence of methanol [2, 3].

During the fermentation (95 h) the *P. pastoris* growth was monitored by measuring the OD600, which increased from 1.2 to 620. The OD600 increased slowly from 1.2 to 13 during the glycerol phase (21 h). The glycerol fed-batch phase (5 h) was characterized by a strong biomass growth where the OD600 values increased from 13 to 74. In the last phase (69 h), the

methanol fedbatch phase, the OD600 increased to 620, and the RGI Lyase activity increased almost linearly from 0 to 125 U/ml. The overall activity of the fermentation process (4 l working volume after sterile filtration) was 493 kU. At the Cu^{2+} affinity chromatography step the RGI Lyase was successfully attached by the His6-tag and was selectively eluted by the imidazole gradient (at 500mM). The total yield of pure recombinant RGI Lyase was 4.29 g protein. The recovery of pure protein in the Cu^{2+} affinity purification process was 81%, with a total activity of RGI Lyase of 79 kU.

The characterization of RGI Lyase was carried out to evaluate the effect of temperature, pH and ions such as Mn^{2+} and Ca^{2+} . The observed activities varied between 0 and 18 U/mg using potato rhamnogalacturonan as the substrate. The response-surface showed the effect of temperature and pH on the activity of RGI Lyase at high concentrations of Ca^{2+} and Mn^{2+} (2 mM). The set of experiments gave rise to a surface with a bell shaped structure that allowed the determination of optimum pH and temperature of the reaction (Fig. 1).

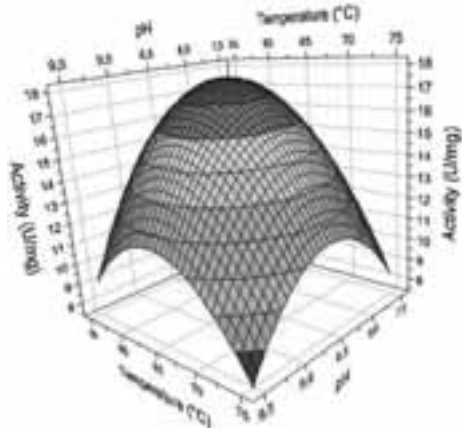


Figure 1: 1st Surface response as a function of Temperature and pH on the RGI Lyase activity. The incubation mixture contained 2mM Ca^{2+} and Mn^{2+} . RGI Lyase activity was measured at pH 8.1 and at a temperature of 61°C. The colours vary from blue (low RGI Lyase activity) to red (high RGI Lyase activity).

Mn^{2+} strongly increased the enzyme activity: from 11 to 18 U/mg, when Mn^{2+} was increased from 0 to 2 mM. Multivariate regression analysis showed that the reaction temperature, Mn^{2+} concentration, and pH significantly influenced the RGI Lyase activity with a statistical significance of $p < 0.001$. The data modeling allowed a definition of the optimum reaction temperature and pH for the enzymatic reaction and also exhibited the positive influence of Ca^{2+} and Mn^{2+} on the RGI Lyase activity. Based on the model, the best factor combination was: temperature 61 °C, pH 8.1 and 2 mM concentration of both Ca^{2+} and Mn^{2+} with a RGI Lyase activity of 17.8 U/mg.

In order to assess the thermal stability of the enzyme, enzyme activity assays were performed at the optimum conditions established above, using 2.5, 5, 15 and 30 min of reaction time, at different temperatures (20, 40, 61, 65, 75 and 80 °C). When plotting Ln (activity) vs. incubation time a linear relationship was observed showing that the thermal inactivation of RGI Lyase followed first order reaction kinetics (Fig. 2). At 55 °C the RGI Lyase had a half life of 25 min and at 61 °C of 15 min. With temperatures higher than 61 °C the RGI Lyase activity decreased significantly with incubation time. The enzyme completely lost catalytic activity after half an hour at 80 °C.

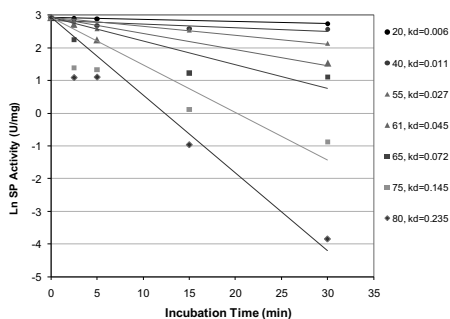


Figure 2: The temperature stability of RGI Lyase was evaluated using temperatures of 20, 40, 55, 61, 65, 75, 80°C and incubation times for 2.5, 5, 15 and 30 minutes. A semilogarithmic linear plot was obtained for time vs. the Ln of the Activity.

Conclusions

This is the first production of a prokaryotic thermostable RGI Lyase in the eukaryotic host *P. pastoris*. The RGI Lyase was active at relatively high temperature (61 °C) and high pH (8.1) and showed dependency of manganese. The enzyme is a good target for genetic engineering modifications to increase temperature optimum and thermal stability, and thus serve the need for improved processes to produce healthy prebiotic oligosaccharides from industrial side-streams.

References

1. Cereghino, J. L. and Cregg, J. M. (2000). "Heterologous protein expression in the methylotrophic yeast *Pichia pastoris*." *FEMS Microbiology Reviews* **24**(1): 45-66.
2. Cereghino, G. P. L.; Cereghino, J. L.; Ilgen, C. and Cregg, J. M. (2002). "Production of recombinant proteins in fermenter cultures of the yeast *Pichia pastoris*." *Current Opinion in Biotechnology* **13**(4): 329-332.
3. Stratton, J.; Chiruvolu, V. and Meagher, M. (1998). *High Cell Density Fermentation*. *Pichia Protocols*. D. Higgins and J. Cregg. New Jersey, Humana Press. **103**: 107-120.



Maria del Mar Cortada Mut

Phone: +45 4525 52920
E-mail: mmarc@kt.dtu.dk

Supervisors: Kim Dam-Johansen
Peter Glarborg
Kim Hougaard Pedersen, FLSmidth

PhD study
Started: September 2011
To be completed: August 2014

Interactions between solid fuels and raw materials in cement rotary kilns

Abstract

The cement industry has an interest in replacing fossil fuels with alternative fuels due to economical considerations and environmental concerns. The combustion of alternative fuels may increase the internal circulation of sulphur and may cause blockages and corrosion. The effect of different degree of volatiles of pine wood on the sulphur release from raw materials and carbon conversion at high temperature in the rotary drum is investigated. Three different sizes of wood cylinders were used and were pre-treated at 300, 500, 700 and 900 °C. It has been found that the sulphur release from the raw meal primarily takes place during devolatilization. Sulphur release was only observed for the virgin wood and wood char made at 300 and 500°C. However when char was combusted under the bed material in a low O₂ environment, small amounts of sulphur was detected but further investigations on this topic needs to be done.

Introduction

The cement industry is an energy intensive industry and the energy costs account for 30-40 % of the total costs of the cement production [1]. In the past decades, the cement industry has had a great interest in replacing fossil fuels with alternative fuels (waste from other industries), partly minimize production cost due to the increase of the fuel prices and partly to minimize the environmental impact.

Alternative fuels cover a large range of fuels, such as industrial and municipal waste, tire derived fuels, plastic and wood waste. The fuels have typically relatively large particles, with different chemical and physical properties. The common characteristics are that they are cheap, CO₂-neutral, and available in large quantities. The most important fuel characteristics to consider when selecting alternative fuels are the heating value, the ash and the moisture content.

The process flow sheet of a modern cement kiln system is illustrated in Figure 1. The traditional firing points in a cement plant are the calciner and the kiln burner. Additional combustion equipments for combustion of coarse alternative fuels have been developed, such as the HOTDISC [2]. However, several cement plants are firing the alternative fuels directly into the material inlet end of the rotary kiln or in the calciner (the large particles may fall into the kiln inlet), because it requires

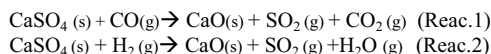
a minimum of investments. Therefore, the combustion of alternative fuels in these conditions has some consequences, which are:

- Direct physical contact between the fuels and the cement raw materials.
- Local reducing conditions in the material inlet end of the rotary kilns.
- Potential of increase internal circulation of sulphur, chlorine and alkali metal species.



Figure 1: Scheme of a modern In-Line Calciner (ILC) cement kiln system [2].

The modification of process conditions due to the combustion of alternative fuels may affect the clinker quality and the process operation. As a consequence of the reducing conditions and high temperature, the sulfates in the raw meal decompose to release SO₂, which will potentially circulate in the kiln system. For instance, the CaSO₄ can be reductively decomposed by CO and H₂ according to reaction 1 and 2 under specific conditions.



High levels of sulphur enhance deposit build-ups and corrosion in a long term. These deposits accumulate typically in the material inlet end of the rotary kiln, or in the riser duct between the calciner and rotary kiln, where they cause blockages. The plant must sometimes be temporarily shut-down in order to remove the deposits [2].

Specific Objectives

The objective of this project is to improve the understanding of the behavior of alternative fuels in the material inlet of the rotary kiln and predict the sulphur release from raw materials due to the direct combustion of alternative fuels or partially combusted in the kiln material inlet.

Experimental

To simulate the process conditions in the material inlet end of an industrial rotary kiln a rotary drum was constructed, a schematic 3D view is shown in Figure 2 [3]. The combustion behaviour and the effect of different volatiles of the fuel on the sulphur release from raw materials at high temperature in the rotary drum have been investigated. The rotary drum is electrically heated by a furnace and the gas is introduced to the furnace through a hole in the roof in order to have a controlled atmosphere and the exhaust gas is cooled and analyzed. The exit concentrations of SO₂, CO, CO₂ and O₂ in the gas are measured and logged during the periods of devolatilization and char combustion. The furnace is equipped with a window for visual inspection, and a sample container allows introduction of solid fuels into the hot rotary drum.

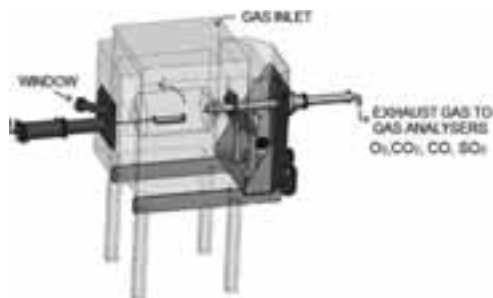


Figure 2: Schematic 3D view of the high temperature rotary drum.

The experiments were performed in an oxygen concentration of 10 vol. % in N₂ with a constant flow of 100 NL/min and at 900 °C. The used cement raw materials were based on a synthetic mixture of coarse quartz sand with a particle size ranging from 0.5 to 0.71 mm and 2 wt. % calcium sulphate, and the mixture was placed in the rotary drum in the desired volumetric filling degree of 5 %.

Pine wood cylinders were used as fuel. The fuel analyses and the lower heating value are shown in Table 1. The initial dimensions of the wood cylinders are: 19, 13 and 8 mm of diameter and 25 mm length.

Table 1: Fuel analyses and lower heating values (LHV) for solid fuels used in the experiments. Notes: VM: Volatile matter, FC: fixed carbon.

	Proximate analysis [wt.%]			Ultimate Analysis [wt.%]			LHV [MJ/kg]
	VM	FC	Ash	C	H	N	
Pine Wood	76.8	22.7	0.5	44.7	5.54	0.04	15.97

The pine wood cylinders were pyrolysed in a horizontal tube reactor under a nitrogen atmosphere for 20 minutes at different temperatures (300, 500, 700 and 900 °C) in order to obtain wood char with different degree of volatiles.

The total release of sulphur and the carbon conversion are calculated for each experiment. The sulphur release during the experiments is quantified by integration of the gas concentration of SO₂ in the gas over the relevant time interval (Equation 1).

$$n_{\text{Sulphur release}} = \int_0^t y_{\text{SO}_2} dt \cdot 10^{-6} \cdot \frac{PV}{RT} \quad (1)$$

where y_{SO_2} is in ppmV, R the gas ideal constant (8.314 J/mol K), P the atmospheric pressure in Pa, T the temperature in K, and V the gas flow in m³/s. The number of moles of SO₂ is subsequently converted to mg. The degree of fuel conversion can be calculated by integration of the concentrations profiles of CO₂ and CO, as shown in Equation 2 by assuming that the fuel conversion is proportional to the carbon conversion.

$$X(t) = \frac{\int_0^t (y_{\text{CO}_2} + y_{\text{CO}}) dt}{\int_0^\infty (y_{\text{CO}_2} + y_{\text{CO}}) dt} \quad (2)$$

Results and discussion

The experiments for the different cylinders and pre-treated fuels were performed using an energy input of 55 KJ. An example of the carbon conversion for the different particle sizes can be seen in Figure 3 for the virgin wood (wood without pre-treatment) and the start and end of the combustion periods is also illustrated.

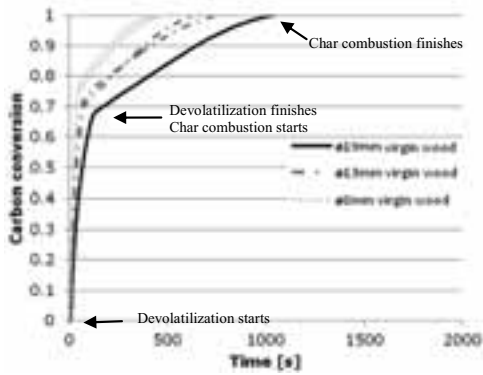


Figure 3: Carbon conversion for different virgin wood particles.

A general trend observed for the different particles with the same pre-treatment is that for the same initial energy input, the total conversion time is shorter for the small particles than for the bigger particles. The time required for the complete combustion is decreasing in the sequence of one cylinder of 19 mm diameter > 2 cylinders of 13 mm diameter > 5 cylinders of 8 mm diameter.

In the case of the cylinders of 13 mm diameter, the carbon conversions for the different pre-treatment temperatures are compared in Figure 4 and Figure 5.

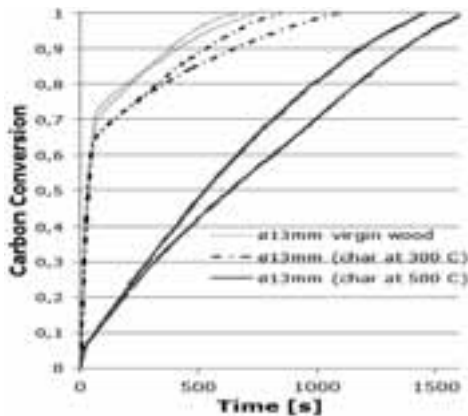


Figure 4: Carbon conversions of the cylinder of ø13 mm for the virgin state, char made at 300 and 500°C.

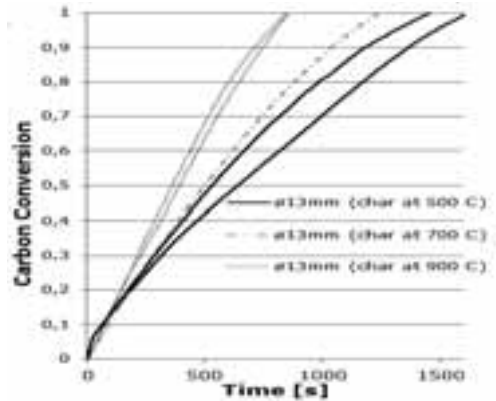


Figure 5: Carbon conversions of the cylinder of ø13 mm for the char made at 500, 700 and 900°C.

It can be seen that the total conversion time is shorter for the virgin wood than for wood char made at 300 °C, and for wood char made at 300°C than at 500°C. Thus, it seems that devolatilization promotes faster char combustion. However, the total conversion time is shorter for wood char made at 700 °C than 500 °C. The reason for this is that most of the wood decomposition takes place at temperatures lower than 500 °C, and no more significant decomposition is produced above 750°C. Increasing the pyrolysis temperature above 500°C increases the yield of gaseous products and decreases residue char production. This effect was also noticed by the weight of the fuel particle after pyrolysis. For example, a cylinder of 13 mm of diameter with an approx. initial weight of 3.6 g, whereas it after pyrolysis at 300, 500, 700 and 900 °C had a weight of 3.09 g, 0.83 g, 0.6 g, and 0.55 g, respectively. Figure 6 summarizes the average time to complete devolatilization for the different pre-treated wood (virgin wood, wood char made at 300 and 500 °C) for the different particle sizes.

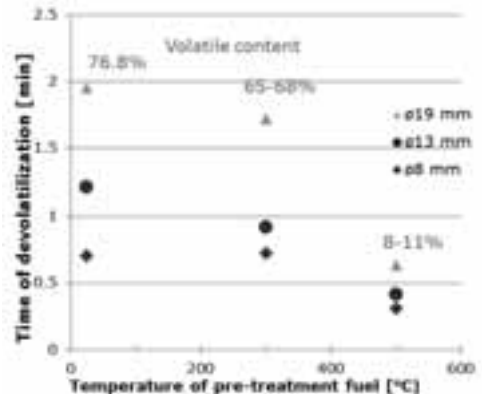


Figure 6: Time of devolatilization vs. the temperature of pre-treatment for the different wood particle sizes.

It can be seen that the devolatilization period is shorted when the temperature of pre-treatment is increased due to the reduced content of volatiles. The total amount of volatiles in the wood chars can be estimated by the mass loss during the treatment.

Figure 7 summarizes the average time to complete the char oxidation for the different pre-treated wood for the different particle sizes.

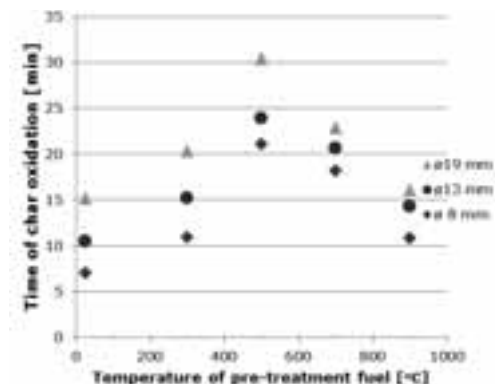


Figure 7: Time of char oxidation vs. the temperature of pre-treatment for the different wood particle sizes.

It can be noticed that the required time to complete char oxidation increases with increasing temperature of the pre-treatment until 500 °C and decreases from 500 to 900 °C. This is because the most of the wood decomposition takes place at temperatures lower than 500 °C. Furthermore, increasing the pyrolysis temperature decreases the production of residue char. The time necessary to complete char oxidation is doubled for the wood char made at 500 °C compared to the virgin fuel.

Figure 8 shows the total sulphur release in form of SO₂ for the different particles sizes for virgin wood and wood char mad at 300 and 500 °C.

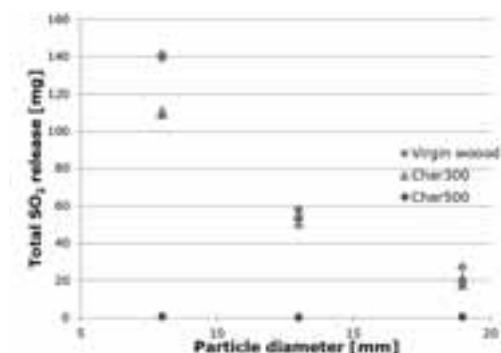


Figure 8: Total sulphur release from the raw materials due to combustion of pine wood cylinders and wood char cylinders of different sizes.

Sulphur release was only observed for the char made at 300 and 500 °C. For the virgin wood and wood char made at 300 °C, smaller particles give a higher sulphur release than larger particles, because their fast devolatilization causes stronger local reducing conditions. There is a significant difference between the volatile content in char made at 300 and 500 °C, which is reflected in sulphur release.

Furthermore, additional experiments were performed to study the sulphur release from wood char in extreme conditions (covered by raw material and in a low oxygen atmosphere). The SO₂ release was detected but in very low concentrations, where the gas analyzer has high uncertainty. Therefore, the results can only be used qualitatively.

Conclusions and Future work

The experimental work shows that the sulphur release from the raw materials primarily takes place during devolatilization. Sulphur release was only observed for the virgin wood, wood char made 300 and 500 °C. A significant difference between the volatile content in wood char made at 300 and 500 °C was detected. This was also reflected in the sulphur release.

However, when char is combusted underneath the bed material in a low O₂ environment, small amounts of sulphur is released. More investigations on the sulphur release by wood char need to be conducted.

Further investigations will consist of characterization and quantification of release of volatiles for different fuels. The effect of different concentrations of pyrolysed gases on sulphur release will also be studied. A model for predicting sulphur release from cement raw materials will also be developed.

Acknowledgements

This project is part of a research platform on future cement technology financed by The Danish National Advanced Technology Foundation, DTU and FLSmidth A/S.

References

1. Cembureau, Activity Report 2008, <http://www.cembureau.be/>. (Accessed on 2/12/2011)
2. FLSmidth HOTDISC™ combustion device. <http://www.flsmidth.com> (Accessed on 2/12/2011)
3. Nielsen, A.R.; Combustion of large solid fuels in cement rotary kilns, DTU, Lyngby, Denmark, 2011. ISBN: 978-87-92481-66-5
4. Koufopoulos, C. A., Maschio, G. and Lucchesi, A.; 1989. Canadian Journal of Chem. Eng. 6 (1989) 75-84.



Vadim Evseev
Phone: +45 5261 6134
E-mail: vaev@kt.dtu.dk

Supervisors: Sønnik Clausen
Alexander Fateev

PhD Study
Started: April 2009
Completed: October 2012

Line-by-line Modeling of Gas Spectra

Abstract

The title of the PhD project is “Optical Tomography in Combustion” and it is developed in three directions: 1) the development of tomographic algorithms for 2D gas temperature profile reconstruction; 2) the development of the multichannel IR spectrometer system for simultaneous spectral measurements at several line-of-sights (described in the Yearbook 2011); 3) the investigation of spectral properties of major combustion species such as CO₂ and CO in the IR spectral range at high temperatures to provide the theoretical background for the development of the optical tomography methods. The work on the latter direction is presented here and published in Ref [5].

Introduction

The title of the PhD project is “Optical Tomography in Combustion” and it is developed in three directions: 1) the development of tomographic algorithms for 2D gas temperature profile reconstruction; 2) the development of the multichannel infrared (IR) spectrometer system for simultaneous spectral measurements at several line-of-sights with a view to application for tomographic measurements on full-scale industrial combustion systems and the application of the developed system for simultaneous exhaust gas temperature measurements at the three optical ports of the cylinder exhaust duct of a large Diesel engine (this part is presented in the Yearbook 2011); 3) the investigation of spectral properties of major combustion species such as carbon dioxide (CO₂) and carbon monoxide (CO) in the IR range at high temperatures to provide the theoretical background for the development of the IR optical tomography methods of combustion diagnostics developed within the first direction of the PhD project.

Within the latter direction in the development of the PhD project the new software was developed for the line-by-line calculations of the transmission spectra of a CO₂/CO mixture. The developed software follows the calculation procedure presented here in “Theory and Methods” and is able to use within reasonable time the most recent but huge CDS-4000 database [1] containing updated high-temperature spectroscopic line-by-line data. The software was used for the line-by-line calculations of the transmission spectra of the CO₂/CO mixture at high temperatures and the results were compared to the measurements in the high-temperature

flow gas cell [2, 3, 4, 5] which were carried out before the PhD project. The results and discussion are presented in journal article [5].

Specific Objectives

The specific objective of this part of the PhD project was the line-by-line modeling of the transmission spectra of CO₂ in the 2.7, 4.3 and 15 μm regions and of CO in the 4.7 μm region at temperatures up to 1773 K (1500 °C), the volume fractions of CO₂ in the range 1-100% and at atmospheric pressure based on the HITEMP [6, 7] and CDS [8, 9, 1] spectroscopic databases.

A detailed description of the line-by-line modeling procedure presented here in “Theory and Methods” was implemented in the new software developed in the PhD project using the C++ Programming Language (Microsoft Visual Studio 2008) which was used for the line-by-line modeling of the transmission spectra of a CO₂/CO mixture with the results and discussion presented in Ref. [5]. It should be noted that this detailed description presented here in “Theory and Methods” is not given in Ref. [5] but it is given in the PhD student’s PhD thesis (Ref. [10]).

Theory and Methods

The effective, or measured, transmittance $\tau(v_0, T_g)$ at any observed wave number v_0 [cm⁻¹] of the slab of a gas mixture at temperature T_g [K] can be calculated as

$$\tau(v_0, T_g) = \int_{v_1=0}^{v_2=\infty} ILS(v-v_0) e^{-\sigma_{true}(v, T_g) n L} dv, \quad (1)$$

(a combination of Eqs. (2) and (3) from Ref. [5]) where $ILS(v-v_0)$ is the instrument line shape function [$1/\text{cm}^{-1}$]; for an FTIR spectrometer used in the measurements in work [5], the ILS was given by

$$ILS(v-v_0) = \frac{1}{R_{spec}} \frac{\sin(\pi(v-v_0)/R_{spec})}{\pi(v-v_0)/R_{spec}} \quad (2)$$

with $R_{spec} = 0.0625 \text{ cm}^{-1}$ [5] (R_{spec} is the half of the nominal resolution of the spectrometer which was 0.125 cm^{-1} [5]), the actual values of integration limits v_1 and v_2 used in (1) should make $ILS(v_1-v_0)$ and $ILS(v_2-v_0)$ sufficiently close to zero and the integral

$$\int_{v_1}^{v_2} ILS(v-v_0) dv$$

sufficiently close to unity at a given value of v_0 (a more detailed discussion on this issue can be found below);

$$[M] = \frac{c_V p}{k_B T_g} \quad (3)$$

is the total concentration [$\text{molecule}/\text{cm}^3$] [11, eq. (2)] of a molecular species under consideration (e.g. CO_2) in the slab of a gas mixture at temperature T_g [K] having length L [cm] (which is supposed to be sufficiently small, actually dL), c_V is the volume part (volume ratio, or mole fraction) [fractions of 1] of the species under consideration, p is the total pressure in the slab of the gas mixture [atm], k_B is the Boltzmann constant;

$$\sigma_{true}(v, T_g) = \sum_{i=1}^{N_T} k_i(v, T_g) \quad (4)$$

is the true absorption cross-section (Sec 3.1 in [5]; cf. eq. (4) in [11]), where v is any wave number [cm^{-1}],

$$k_i(v, T_g) = S_{T_g, i} g(v-v_i^*, T_g) \quad (5)$$

is the *monochromatic* absorption coefficient (Appendix A in [12]),

$$S_{T_g, i} = S_i \frac{Q(T_{ref}) \exp(-c_2 E_i / T_g)}{Q(T_g) \exp(-c_2 E_i / T_{ref})} \times \frac{[1 - \exp(-c_2 v_i / T_g)]}{[1 - \exp(-c_2 v_i / T_{ref})]} \quad (6)$$

is the temperature corrected line intensity [$\text{cm}^{-1}/(\text{molecule cm}^{-2})$] of the i -th transition ($i = 1, 2, \dots, N_T$ is the sequence number of a current transition (or spectral *line*) under consideration and N_T is the total number of transitions under consideration, see also a more detailed discussion on the number of transition under consideration below), S_i is the line intensity [$\text{cm}^{-1}/(\text{molecule cm}^{-2})$] of the i -th transition at a reference temperature $T_{ref} = 296 \text{ K}$ (S_i is taken from the database, see also Fig. 1), $Q(T)$ is the total internal partition sum at temperature T , the values of this function for the four most abundant isotopes of CO_2 and for the other molecular species on the HITRAN/HITEMP databases can be calculated using the Fortran programs for Partition Sums [13], c_2 is the

second radiation constant $= hc/k = 1.4388 \text{ cm K}$ (Appendix A in [12]), E_i is the lower state energy of the i -th transition [cm^{-1}] (taken from the database, see also Fig. 1), v_i is the frequency of the i -th transition (also taken from the database) (not to be confused with v_0 , v_1 and v_2 mentioned above which are NOT v_i at $i = 0, 1, 2$ respectively);

$g(v-v_i^*, T_g)$ is the line shape function caused by Doppler broadening (Gaussian profile), pressure broadening (Lorentzian profile), or a combination of the two (Voigt profile) [14]. The choice of the line profile depends on gas temperature and pressure. A detailed discussion on this issue can be found in [14]. However, a Voigt profile is the most general form of a line shape function as it combines both Gaussian and Lorentzian line shapes. The Voigt profile cannot be evaluated in closed analytical form and a large number of numerical algorithms have been developed in the past [15]. One can use an algorithm presented in e.g. [16]. In this work, an empirical approximation to the Voigt profile as given by (Eqs. (6) and (7) in [14]) was used:

$$\frac{g_V(v-v_i^*, \gamma_{p,i}, \gamma_{V,i})}{g_{V, \max}} = \left(1 - \frac{\gamma_{p,i}}{\gamma_{V,i}}\right) \times \exp\left(-2.772 \left(\frac{v-v_i^*}{2\gamma_{V,i}}\right)^2\right) + \left(\frac{\gamma_{p,i}}{\gamma_{V,i}}\right) \frac{1}{1 + 4 \left(\frac{v-v_i^*}{2\gamma_{V,i}}\right)^2} + 0.016 \left(1 - \frac{\gamma_{p,i}}{\gamma_{V,i}}\right) \left(\frac{\gamma_{p,i}}{\gamma_{V,i}}\right) \quad (7)$$

$$\times \left(\exp\left(-0.4 \left(\frac{|v-v_i^*|}{2\gamma_{V,i}}\right)^{2.25}\right) - \frac{10}{10 + \left(\frac{|v-v_i^*|}{2\gamma_{V,i}}\right)^{2.25}} \right) \frac{1}{2\gamma_{V,i} \left(1.065 + 0.447 \left(\frac{\gamma_{p,i}}{\gamma_{V,i}}\right) + 0.058 \left(\frac{\gamma_{p,i}}{\gamma_{V,i}}\right)^2\right)} \quad (8)$$

where

$$\gamma_{p,i} = \gamma_{air,i} \left(\frac{T_{ref}}{T_g}\right)^{n_{air,i}} (p - p_s) + \gamma_{self,i} \left(\frac{T_{ref}}{T_g}\right)^{n_{self,i}} p_s \quad (9)$$

is the temperature and pressure corrected line half-width at half-maximum (HWHM) [cm^{-1}] of the i -th transition, $\gamma_{air,i}$ is the air-broadened HWHM [$\text{cm}^{-1}/\text{atm}$] at $T_{ref} = 296 \text{ K}$ and a reference pressure 1 atm ($\gamma_{air,i}$ is also taken from the database), $n_{air,i}$ is the coefficient of temperature dependence of $\gamma_{air,i}$ (also taken from the database), $\gamma_{self,i}$ is the self-broadened HWHM [$\text{cm}^{-1}/\text{atm}$] at $T_{ref} = 296 \text{ K}$ and pressure 1 atm (also taken from the database), $n_{self,i}$ is the coefficient of temperature dependence of $\gamma_{self,i}$ (available in the CDSD-4000 [1] and CDSD-HITEMP [8] databases, for the other databases $n_{self,i}$ is assumed to be equal to $n_{air,i}$), p is the

total pressure in the slab of the gas mixture [atm], $p_s = c_V p$ is the partial pressure [atm] of the molecular species under consideration (e.g. CO₂) in the slab of the gas mixture, c_V is the volume part (volume ratio, or mole fraction) [fractions of 1] of the species under consideration;

$$\gamma_{V,i} \approx 0.5 \left(1.0692 \gamma_{p,i} + \sqrt{0.86639 \gamma_{p,i}^2 + 4 \gamma_{D,i}^2} \right) \quad (10)$$

is the HWHM of the Voigt line shape (eq. (14) in [15]) for the i -th transition,

$$\gamma_{D,i} = v_i^* \sqrt{\frac{2 \ln 2 R_{\text{gas}} T_g}{M_w c^2}} \quad (11)$$

is the HWHM of the Doppler feature [cm⁻¹] (eq. (3) in [14]) for the i -th transition, R_{gas} is the ideal gas constant, M_w is the molecular weight [kg/mol] of the isotope of the molecular species under consideration (e.g. M_w of ¹²C¹⁶O₂ is 0.04398982923912 kg/mol), c is the speed of light in vacuum,

$$v_i^* = v_i + \delta_{\text{air},i} p \quad (12)$$

is the pressure-shift corrected frequency of the i -th transition [cm⁻¹], $\delta_{\text{air},i}$ is the air-broadened pressure shift [cm⁻¹/atm] of the transition frequency at $T_{\text{ref}} = 296$ K and a reference pressure 1 atm ($\delta_{\text{air},i}$ is taken from the database, see also Fig. 1).

The format of the databases, such as HITEMP-2010 [7], CDSD-1000 [9], is shown in Fig. 1. The meaning of the notation can be found in the preceding text except Mol_i which is the molecular species identification number ($Mol_i = 2$ for CO₂) and Iso_i which is the isotope identification number (see Appendix A in [12] or table 6 in [17] for details). The spectroscopic data in the databases is a text list sorted with increasing transition frequency ν_i . Databases, such as HITEMP-2010, CDSD-1000, consist of many text files.

The calculation of $\tau(\nu_0, T_g)$ according to the above given procedure is a suggestion of a possible approach to the line-by-line modeling (cf. Sec 2.1 in [4]). The name *line-by-line* is given because the spectroscopic parameters for every transition (or spectral *line*) are used in the calculations. These spectroscopic parameters are given in the databases as shown in Fig. 1. In the procedure described above, only 7 parameters are in use (or 8 parameters if the CDSD-4000 database [1] is used, see above) and they are highlighted each with a certain color in the figure. Databases contain also other spectroscopic parameters which are used in the other models. This issue is out of the scope of this work.

The calculation of $\tau(\nu_0, T_g)$ at a certain ν_0 requires to determine the finite limits ν_1 and ν_2 of the integration in (1). They are determined based on the condition that $ILS(\nu_1 - \nu_0)$ and $ILS(\nu_2 - \nu_0)$ should be sufficiently close to zero and

$$\int_{\nu_1}^{\nu_2} ILS(\nu - \nu_0) d\nu$$

should be sufficiently close to unity at a given value of ν_0 .

Figure 1: Format of the spectroscopic databases, e.g., HITEMP-2010 [7], CDSD-1000 [9]. The meaning of the notation can be found in the text. The CDSD-4000 [1] and CDSD-HITEMP [8] databases include one more parameter, $n_{\text{self},i}$, which is not shown in the figure.

Once ν_1 and ν_2 are determined, it is necessary to determine the range of values for the transition frequency ν_i (ν_i should not be confused with ν_0 , ν_1 and ν_2 mentioned above which are NOT ν_i at $i = 0, 1, 2$ respectively) or, in other words, to choose the transitions for the line-by-line calculations from the database files. That will also give N_T which is the total number of chosen transitions. The range for ν_i is chosen based on the values of ν_1 and ν_2 and the wing cut-off of the line profile as discussed in the following.

A line profile $g(\nu - \nu_i^*, T_g)$, e.g. such as given by Eqs. (7, 8), determines the contribution of i -th transition having frequency ν_i (or pressure-shift corrected frequency ν_i^*) to $\sigma_{\text{true}}(\nu, T_g)$ at a current value of ν ($\nu_1 \leq \nu \leq \nu_2$) that is used in the integration in (1). But this contribution never reaches zero even at $\nu_i^* \gg \nu$ and $\nu_i^* \ll \nu$. It is reasonable to assume that at values of ν_i^* sufficiently different from ν , or such that $|\nu - \nu_i^*| > \Delta \nu_{\text{wing cutoff}}$, a line shape function turns to zero. In this work, $\Delta \nu_{\text{wing cutoff}}$ was determined from the following condition

$$g_V(\Delta \nu_{\text{wing cutoff}}, \max_i \gamma_{p,i}, \max_i \gamma_{V,i}) = C_{\text{wing cutoff}} g_V(0, \max_i \gamma_{p,i}, \max_i \gamma_{V,i}) \quad (13)$$

where a constant $C_{\text{wing cutoff}}$ was taken as, e.g., $C_{\text{wing cutoff}} = 10^{-3}$ or other value. In such a way

$$g_V(\nu - \nu_i^*, \gamma_{p,i}, \gamma_{V,i}) = 0 \quad \text{for} \quad |\nu - \nu_i^*| > \Delta \nu_{\text{wing cutoff}} \quad (14)$$

that is also to be accounted for in addition to Eqs. (7, 8). The range of values for the transition frequency ν_i can now be determined from the condition

$$\nu_1 - \Delta \nu_{\text{wing cutoff}} \leq \nu_i^* = \nu_i + \delta_{\text{air},i} p \leq \nu_2 + \Delta \nu_{\text{wing cutoff}} \quad (15)$$

where Eq. (12) is taken into account.

Results and Discussion

The described above line-by-line procedure for the calculation of the effective transmittance spectrum $\tau(\nu_0, T_g)$ of the mixture of CO₂ and CO using the line-by-line parameters from the HITEMP-1995 [6], HITEMP-2010 [7], CDSD-HITEMP [8] and CDSD-4000 [1] databases is implemented in the software developed in this PhD project using the C++ Programming Language (Microsoft Visual Studio 2008) as a primary tool and MATLAB as an auxiliary tool. The software was used for the line-by-line modeling of

the transmission spectra of the CO₂/CO mixture with the results and discussion presented in Ref. [5].

Conclusions

The title of the PhD project is “Optical Tomography in Combustion” and it is developed in three directions: 1) the development of tomographic algorithms for 2D gas temperature profile reconstruction; 2) the development of the multichannel IR spectrometer system for simultaneous spectral measurements at several line-of-sights (described in the Yearbook 2011); 3) the investigation of spectral properties of major combustion species such as CO₂ and CO in the IR range at high temperatures to provide the theoretical background for the development of the optical tomography methods.

Within the latter direction in the development of the PhD project the new software was developed for the line-by-line calculations of the transmission spectra of a CO₂/CO mixture. The developed software follows the calculation procedure presented here in “Theory and Methods” and is able to use within reasonable time the most recent but huge CDS-4000 database [1] containing updated high-temperature spectroscopic line-by-line data. The software was used for the line-by-line calculations of the transmission spectra of the CO₂/CO mixture at high temperatures and the results were compared to the measurements in the high-temperature flow gas cell [2, 3, 4, 5] carried out before the PhD project. The results and discussion are presented in journal article [5]. The acknowledgements are also mentioned in that article.

References

1. S.A. Tashkun, V.I. Perevalov, *J Quant Spectrosc Radiat Transf* 112 (2011) 1403-1410.
2. A. Fateev, S. Clausen, *Int J Thermophys* 30 (2009) 265-275.
3. A. Fateev, S. Clausen, On-line non-contact gas analysis, Report No. Risø-R-1636(EN), Contract No. Energinet.dk nr. 2006 1 6382, Risø DTU, 2008.
4. V. Becher, S. Clausen, A. Fateev, H. Spliethoff, *Int J Greenhouse Gas Control* 5S (2011) S76-S99.
5. V. Evseev, A. Fateev, S. Clausen, *J Quant Spectrosc Radiat Transfer* 113 (17) (2012) 2222-2233.
6. L.S. Rothman, R.B. Watson, R.R. Gamache, J. Schroeder, A. McCann, *Proc SPIE* (2471) (1995) 105-111.
7. L.S. Rothman, I.E. Gordon, R.J. Barber, H. Dothe, R.R. Gamache, A. Goldman, V.I. Perevalov, S.A. Tashkun, J. Tennyson, *J Quant Spectrosc Radiat Transfer* 111 (15) (2010) 2139-2150.
8. S.A. Tashkun, V.I. Perevalov, Readme for CDS-4000-HITEMP, Laboratory of Theoretical Spectroscopy, V.E. Zuev Institute of Atmospheric Optics, Tomsk. Internet, cited 2012 Nov 23, available from: <ftp://ftp.iao.ru/pub/CDS-4000-HITEMP/Readme%20for%20cdsd-hitemp.pdf>.
9. S.A. Tashkun, V.I. Perevalov, J.L. Teffo, A.D. Bykov, N.N. Lavrentieva, *J Quant Spectrosc Radiat Transf* 82 (2003) 165-196.
10. V. Evseev, *Optical Tomography in Combustion*, PhD Thesis, DTU Chemical Engineering, 2012.
11. T. Fleckl, H. Jäger, I. Obernberger, *J Phys D: Appl Phys* 35 (2002) 3138-3144.
12. L.S. Rothman, et al, *J Quant Spectrosc Radiat Transfer* 60 (5) (1998) 665-710.
13. J. Fischer, R.R. Gamache, A. Goldman, L.S. Rothman, A. Perrin, *J Quant Spectrosc Radiat Transfer* 82 (2003) 401-412.
14. P.W. Morrison Jr., O. Taweechokesupin, *J Electrochem Soc* 145 (1998) 3212-3219.
15. F. Schreier, *J Quant Spectrosc Radiat Transfer* 112 (2011) 1010-1025.
16. S.M. Abrarov, B.M. Quine, *Appl Math Comput* 218 (2011) 1894-1902.
17. L.S. Rothman, et al, *J Quant Spectrosc Radiat Transfer* 96 (2005) 139-204.

List of Publications

1. V. Evseev, A. Fateev, S. Clausen, *J Quant Spectrosc Radiat Transfer* 113 (17) (2012) 2222-2233.
2. M.V. Rimskikh, V.O. Evseev, V.S. Sizikov, *J Opt Technol* 74 (11) (2007) 764-768.
3. S. Clausen, A. Fateev, S. L. Hvid, J. Beutler, V. Evseev, Combustion zone investigation in fuel flexible suspension fired boilers, Experimental, Report No. Risø-R-1751(EN), Risø DTU, 2011.
4. S. Clausen, A. Fateev, K. L. Nielsen, V. Evseev, Fast optical measurements and imaging of flow mixing, Report No. ForskEL 2008-1-0079, DTU Chemical Engineering, 2012.
5. V. Evseev, A. Fateev, V. Sizikov, S. Clausen, IR Tomography in Hot Gas Flows, Report No. ForskEL 2009-1-10246, DTU Chemical Engineering, 2012.



Camilla Favrholdt
Phone: +45 40492708
E-mail: cfav@kt.dtu.dk

Supervisors: Anders Brandt
Claes Gjermansen
John M Woodley
Krist Gernaey

Ph.D. Study
Started: December 2011
To be completed: November 2014

Microalgae with increased synthesis or diminished breakdown of TAG for efficient biodiesel production

Abstract

Triacylglycerol, an energy storage compound in plants and microalgae, is a preferred substrate for the chemical conversion of plant-derived and microalgae-derived oil to biodiesel. Upon nitrogen starvation, microalgae cells accumulate triacylglycerols. Microalgae have emerged as important phototrophic microorganisms for the future biodiesel production due to their rapid growth and high oil content. The objective of this project is to further increase the amount of triacylglycerol produced per cell, to make microalgae biodiesel production economically attractive.

Introduction

The potential use of algae in biofuels applications is receiving significant attention due to limiting fossil fuels. Microalgae are photosynthetic microorganisms that convert solar energy, water and carbon dioxide to algal biomass. Lipids are essential to growth and many microalgae are extremely rich in oil. Polar lipids (primarily phospholipids) are integral part of all cellular membranes, while storage lipids are present in the form of triacylglycerol (TAG). TAG consist of a glycerol backbone esterified with three fatty acids (FAs) and is stored in lipid bodies in the cytosol of cells. A TAG core surrounded by a thinner layer of esterified sterols and an outer shell of hydrophobic short length proteins forms the lipid body.

TAG synthesis enables the microalgal cell to store energy in the form of FAs as well as functioning as a sink to remove excess free FAs. In plants, the *de novo* FA biosynthesis occurs in the plastid and the implicated enzymes are dissociable soluble components (Ohlrogge and Browse 1995).

FAs are synthesized from acetate via a repeated cycle of reactions involving cycles of condensation, reduction and dehydration of carbon-carbon bonds. The acetyl-CoA (ACCase) converts the acetyl-CoA input to malonyl-CoA which then gets transferred to acyl carrier protein (ACP) (figure 1).

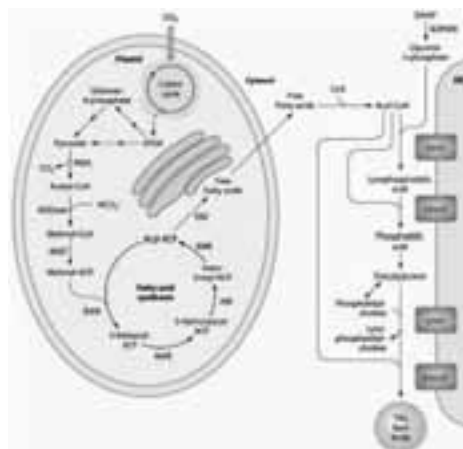


Figure 1. Simplified overview of pathways in microalgal lipid biosynthesis. Metabolites are shown in black and enzymes shown in red (Radakowitz et al. 2010).

or acetyl-CoA with malonyl-ACP to extend the acyl chain with to carbons. First, KASIII catalyzes

condensation from C2 to C4 (Jaworski et al. 1989), and KASI and KASII catalyze carbon-carbon bond formation from C4 to C18. KASI prefers substrates from C4 to C16 and KASII uses C16 substrates to generate C18. After condensation, the 3-keto group is reduced, the acyl chain gets dehydrated and subsequently the double bond is reduced (Ohlrogge and Browse 1995). When produced, the saturated fatty acyl-CoA is exported to endoplasmatic reticulum where TAG synthesis occurs. Higher amounts of FA leads to their incorporation in TAGs and thus deposited in the lipid bodies. Mutant cells with an increased synthesis of FAs may accumulate more TAG due to a higher rate of TAG assembly. In microalgae, cytosolic lipid bodies are built up when growth ceases due to nutritional limitations and cells will then enter stationary phase (Miller et al. 2010). Under nutrient replenished conditions TAGs are rapidly degraded by lipases and the cells use the formed diacylglycerols and FAs as precursors for synthesis of cellular membranes (Kurat et al. 2006). TAG breakdown is initiated by TAG lipases associated with the lipid body membrane (Athenstaedt and Daum 2005). Putatively, lipase mutants defective in TAG breakdown also accumulate additional amounts of TAGs.

Objective

This study aims to increase the synthesis and reduce the breakdown of TAG in *Nannochloropsis oceanica* using a common approach. This involves forward genetic engineering techniques.

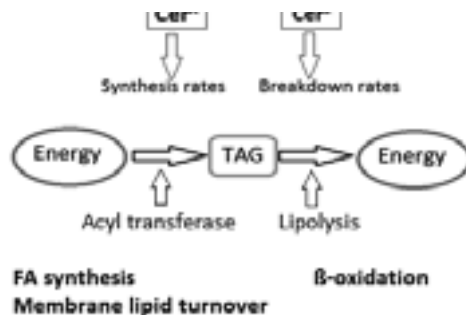
The fatty acid composition of the neutral and polar lipid fraction of the mutants is to be quantified as lipid-derived fatty acid methyl esters (FAME). In order to identify genes that are either up or down-regulated as a consequence of the induced mutations gene expression analyses by cDNA high throughput sequencing is to be carried out.

Project

To select mutants harboring a KAS enzyme with changed activity, preferably a more efficient KAS, I induce DNA mutations by UV radiation and screen for specific mutant phenotypes of microalgae cells that display a higher tolerance to the antibiotic cerulenin, i.e. cerulenin resistant (cer^R) cells (figure 2). Cerulenin is a 12-carbon unit component that inhibits fatty acid synthesis by forming a covalent linkage to a cysteine residue within the active site of KAS. Furthermore, to select mutants with a diminished breakdown of TAG, I screen for cells that are cerulenin sensitive (cer^S phenotype) (figure 2), as FAs derived either from *de novo* synthesis or from

TAG breakdown are essential to promote cell proliferation.

Figure 2. Schematic illustration of biological processes stimulating TAG synthesis or breakdown, and mutant cell phenotypes that may represent changes in reaction rates.



Results and procedures

To study the lipid metabolism in marine microalgae, *N. oceanica* has been chosen as the model microalgae for genetic engineering. *N. oceanica* is one of six species in the *Nannochloropsis* genus (Jinkerson et al. 2012) and these microalgae exhibit high phototrophic biomass and lipid productivities. Furthermore it has a small genome and is genetic transformable. *Nannochloropsis* species is already in use at commercial scale for production of nutraceuticals, especially eicosapentanoic acid (omega-3 FA, EPA) as well as feed for rotifers. Over a period of 7 days in a 2L 'large scale' growth experiment of *N. oceanica* we achieved a biomass production with 0.8 doublings d^{-1} starting at a cell density of 3.8×10^6 cells ml^{-1} and ending with a final concentration of 178×10^6 cells ml^{-1} (day 7) in $\frac{1}{2}$ SWES + B_{12} CO_2 enriched at $22^\circ C$ 18h/8h light/dark cycles and $130 \mu mole m^{-2} sec^{-1}$. Lipid production in these conditions reached $0.12 \mu g/10^6$ cells or 35 % of the algal biomass. Based on Nile red staining (figure 3) we estimate that 70% of the culture makes apolar lipid.

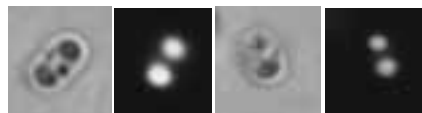


Figure 3. Light microscopy and fluorescence microscopy of Nile red stained wild type *N. oceanica* single cells.

Table 1. FAME analysis of *N. oceanica*, lipid composition, %

C14:0	C16:0	C16:1	C18:0	C18:1	C18:2	C18:3	C20:3	C20:4	C20:5
5.2	39.0	28.3	1.6	14.1	0.9	0.1	0.2	1.7	8.9

The primary storage lipid in *Nannochloropsis* is TAG. The FA composition of *N. oceanica* is shown in table 1. The most abundant chain lengths are C16:0, C16:1 (n-7), and C20:5 (n-3) (EPA), with C16:0 being the highly favorable in biofuel applications.

Generally, microalgae produce little TAG during logarithmic growth and require nutrient deficiency to accumulate significant storage lipid. In contrast, experiments show that the majority of lipid metabolic pathway genes are not significantly upregulated in *Nannochloropsis gaditana* under nitrogen deprivation (Radakovits et al. 2012) This algae has a significant expanded number of genes involved in both fatty acid synthesis and TAG assembly and lipid production may already be abundant within the cell, and existing levels can manage increased metabolic flux. This may explain why *Nannochloropsis* sp constitutively produces TAG even during logarithmic growth (Radakovits et al. 2012).

Selection and screen strategies for cerulenin resistance and sensitivity are established and mutants are now in production. To generate mutants, DNA mutations are induced in cells by irradiate a logarithmic growing *N. oceanica* liquid culture (1×10^5 cells ml^{-1}) with $5000 \mu\text{J cm}^{-2}$ UV light and incubate in dark for 24 hr to avoid photorepair of DNA damage.

After photorepair protection cerulenin resistant mutants are preselected by adding cerulenin to the radiated liquid culture and incubate for a specific number of days, preferably 5-7 days, to facilitate growth of cer^R cells and inhibit other cells (figure 4). Aliquots of the culture are plated on solid medium to obtain cer^R colonies. These colonies will be collected and subjected to growth assay in microtiter plates to verify the cer^R phenotype. After release of selection pressure, cells material from single colonies that continuously display growth in presence of cerulenin will be collected. These cells will be subjected to lipid analysis to distinguish lipid metabolism mutants from cerulenin uptake mutants.

To obtain cerulenin sensitive cells, a liquid culture also subjected to $5000 \mu\text{J cm}^{-2}$ UV radiation will be incubated with a specific concentration of cerulenin that allows growth of wild type cells. This will inactive sensitive cells and active cells can be killed by doing a high temperature treatment (preselection) (figure 4). Afterwards, aliquots of the liquid culture are plated and incubated to obtain single colonies. I collect these colonies and do I microtiter growth screen for cerulenin sensitivity still using a concentration of cerulenin that allows growth of wild type cells.

All high lipid mutants will be characterized with respect to lipid production. I perform several lipid analyses in order to study the lipid metabolism and to determine changes in lipid amount and FA composition. Hopefully a change in the active site of the KAS enzymes responsible for FA synthesis has been introduced, resulting in changes in FA composition, i.e. the appearance of different chain lengths of FAs in mutants. To detect the neutral lipid formation, cells are stained with Nile red and observed using a fluorescence microscope. In addition, the neutral lipid fraction will be analyzed by thin layer chromatography (TLC). To determine the FA composition of the neutral lipid and polar lipid fractions, these will be quantified as lipid-derived methyl esters (FAMES) using GC-MS.

The second main part of this project is to make gene expression analysis. The high lipid mutants will be characterized by gene expression analyses by cDNA high throughput sequencing in order to identify genes that are either up or down regulated as a consequence of the induced mutations.

Conclusion

Nannochloropsis species are leading phototrophic microorganism for the production of biofuels. However, none of the current algal model species are competitive production strains. Therefore, genetic engineering approaches are necessary to further improve strain productivity to increase both autotrophic biomass accumulation rates as well as lipid content per cell. High lipid mutants, generated by reducing TAG degradation rates and increase TAG synthesis rates in each cell, are to be considered as putative feed stocks for the future biofuel production.

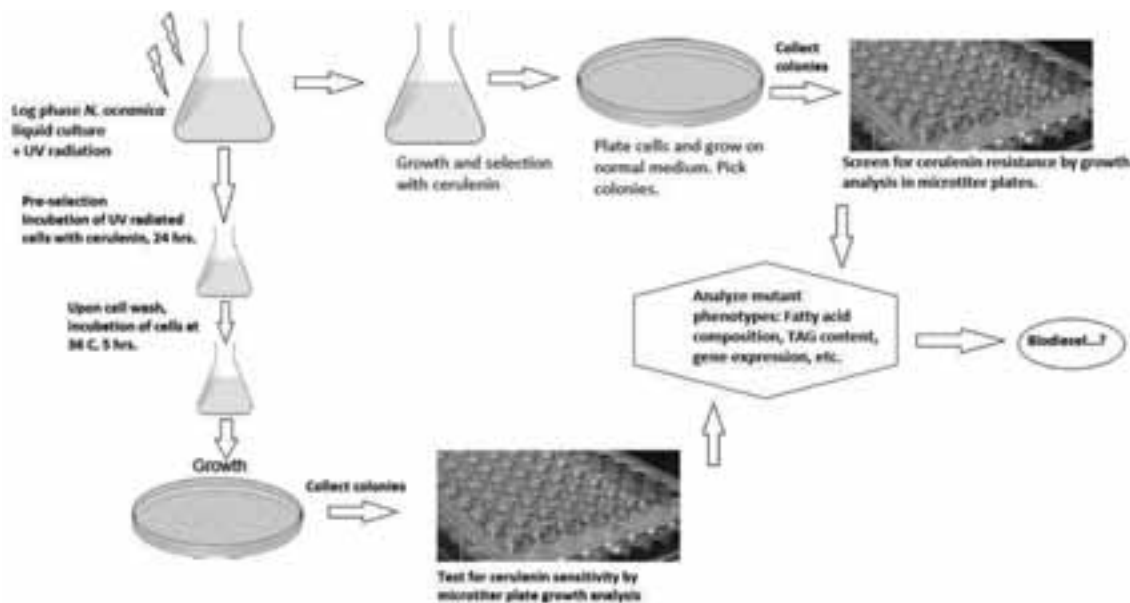


Figure 4. Work flow diagram. See text.

References

Athenstaedt K, Daum G; Tgl4p and Tgl5p, two triacylglycerol lipases of the yeast *Saccharomyces cerevisiae* are localized to lipid particles. *J Biol Chem.* 2005;280(45):37301-9

Jaworski JG, Clough RC, and Barnum SR. A cerulenin insensitive short chain 3-ketoacyl-acyl carrier protein synthase in *Spinacia Oleracea* leaves. *Plant Physiol.* 1989; 90,41-44

Jinkerson RE, Radakovits R, Posewitz MC. Genomic insights from the oleaginous model alga *Nannochloropsis gaditana*. *Bioengineered*, 2012 ; 4:1, 1-7

Kurat CF, Natter K, Petschnigg J, Wolinski H, scheuringer K, Scholz H, Zimmermann R, Leber R, Zechner R, Kohlwein SD; Obese yeast: triglyceride lipolysis is functionally conserved from mammals til yeast. *J Biol Chem.* 2006; 281(1):491-500.

Miller R, Wu G, deshpande RR, Vieler A, Gärtner K, Li X, Moellering ER, Zäuner S, Cornish AJ, Liu B, Bullard B, Sears BB, Kuo MH, Hegg EL, Shachar-Hill Y, Shiu SH, Benning C. Changes in transcript abundance in *Chlamydomonas reinhardtii* following nitrogen deprivation predict diversion of metabolism. *Plant Physiol.* 2010 ;154(4):1737-52.

Ohlrogge J, Browse J. Lipid biosynthesis. *Plant cell*, 1995 7, 957-970

Radakovits R, Jinkerson RE, Fuerstenberg SI, Tae H, Settlage RE, Boore JL, Posewitz MC. Draft genome sequence and genetic transformation of the oleaginous alga *Nannochloropsis gaditana*. *Nat. comm.* 2012 ; 3:686.



Marina Fedorova

Phone: +45 4525 2911
E-mail: mfad@kt.dtu.dk

Supervisors: Rafiqul Gani
Gürkan Sin

PhD Study
Started: April 2012
To be completed: March 2015

Systematic Methods and Tools for Computer Aided Modeling

Abstract

The proposed project will develop methods and tools that will allow systematic development of models and their solution. It will use the modeling framework developed in an earlier project. The framework is a knowledge-based system that is built on a generic modeling language and structured based on workflows for different general modeling tasks. And this framework will be extended in terms of development of new models, re-use of models and development of model-based solution techniques. It will be integrated with the numerical analysis framework for making solution of the wide range of models.

Introduction

Models are playing important roles in design and analysis of chemicals/bio-chemicals based products and the processes that manufacture them. These model-based methods and tools have the potential to decrease the number of experiments, which can be expensive and time consuming, and this is a benefit of working with them.

The idea is in using the modeling systems to either develop new models for final verification by experiments, or evaluate and analyze existing applications to find possibilities for improvements.

The overall objective is to allow the model developer to generate and test models systematically, efficiently and reliably. In this way, development of products and processes can be faster, cheaper and very efficient.

In this work, the generic computer-aided modeling framework is integrated with systematic model derivation framework.

Computer-Aided Modeling Framework

The main objectives of the developed computer-aided modeling framework are to provide structure, guidance and support during model development and application, increase the efficiency of the modeling process, improve the quality and reliability of the models.

This is achieved by structuring the computer-aided modeling framework based on workflows for different general tasks related to model development and application. The modeler is systematically guided through the steps of the different workflows and, at each step, the framework identifies and integrates the

required guidance, tools, database and library connections. The new addition to this framework is the integration of systematic model derivation tools including ModDev and generic template models into the framework as shown in Figure 1.

Proposed modeling framework allows the user to develop new, improve existing, solve and export validated models for third party applications. The framework contains three parts: (i) Model development, (ii) Model identification and validation, (iii) Application using a domain-specific generic template. Depending on the modeling needs and goals, the modeler has a possibility to create a new model in case there is no existing problem-specific model in the library, identify, validate and solve the new model or use existing model from templates library.

The whole structure contains modeling framework, computer-aided tools, methods and libraries including application templates and problem-specific models.

Application and templates library.

This part of the framework describes the using of existing generic modeling templates, which can be chosen from the templates library that includes validated models. Modeler can use the template for his case problem or use the template or its part for extending a model. This is based on idea of model reuse, which emphasizes using a model not only for one specific application but also for future applications involving different needs and levels of details to match different purposes.

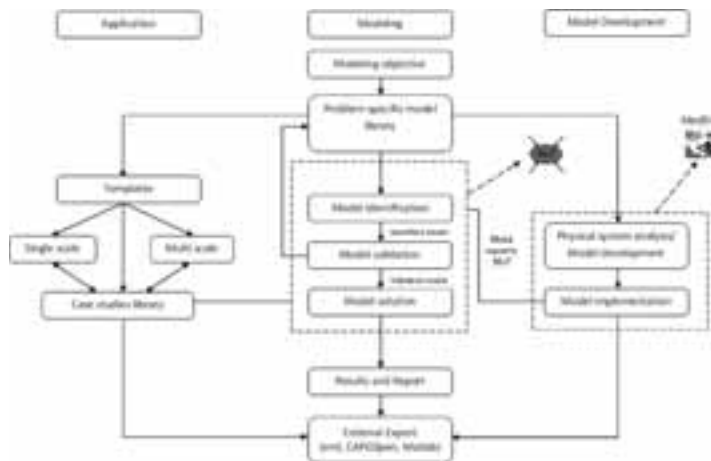


Figure 1: Computer-aided modeling framework with systematic model derivation methodologies.

Modeling template includes model equations, model description, assumptions, solution strategy etc. User will be guided through steps for choosing an appropriate template for his case or will be allowed to change existing template as well.

After a problem specific model equation are formulated following the template of ModDev approach, the model equations are sent to the internal solver of ICAS-MoT [1] for further numerical solution and identification tasks or translated to external computer languages such as Matlab, xml or CAPEOpen in order to be exported for third party application.

Modeling part

This part is based on a generic computer-aided modeling tool named ICAS-MoT [1] developed earlier. It is a computer-aided modeling framework that is structured based on the modeling methodology of in-depth work-flows and data-flows for the different generic modeling tasks required for model development, analyses, identification, discrimination, documentation and application for simulation and optimization.

Following the workflow of this part of the framework user will be able to change existing modeling templates, to pick one of the templates for the case under study, to implement the model that is developed already as well as create a new mathematical model.

Model development

The third part of the modeling framework is using the model development tool – ModDev, which is the part of ICAS.

ModDev is a knowledge-based system that is based on a generic modeling language. It provides a base for manual definition of new variable types and new model blocks as well as a set of fundamental building blocks that assists with knowledge-based information in the creating of new building blocks [2].

Using ModDev modeler is able to describe his case system and the model equations will be obtained by the tool. The resulting mathematical equations can be translated to an appropriate computer language, e.g. mot

file, and sent to internal MoT solver or to be exported to another tool. After creation and validation the model is adding to problem-specific model library. And that will give an opportunity to use this model as a template in other cases.

Conclusions

A computer-aided modeling framework integrating systematic model derivation and development tools has been developed that includes features for model development, model identification and solution, model templates library. Current and future work is looking at increasing the number of problem-specific models in libraries, further development of the computer-aided tools, implementation of two-ways connections among different features of the framework and external export of models in commonly used software languages such as xml, Matlab and CAPEOpen format.

References

- [1] M. Heitzig, Y. Rong, C. Gregson, G. Sin, R. Gani, 2012, Systematic Multi-Scale Model Development strategy for the fragrance spraying process and transport, *Chemical Engineering and Technology*, 35(8), 1381-1391.
- [2] A.K. Jensen, R. Gani, 1999, A Computer Aided Modeling System, *Computers and Chemical Engineering*, 23, 673-678.



Sarah Maria Grundahl Frankær

Phone: +45 4525 56195

E-mail: saf@kt.dtu.dk

Supervisors: Anne Ladegaard Skov
Søren Kiil
Anders Egede Daugaard

PhD Study

Started: May 2009

To be completed: February 2013

Cinnamic Acid Derivatised Poly(Ethylene Glycol) as a Stimuli-Adaptable Polymer Material

Abstract

We created a number of UV-adaptable polymer samples based on cinnamic acid (CA) derivatised poly(ethylene glycol). The samples were irradiated with UV-light and investigated by rheology. We found that dilution of the photo-active CA-group affected the development of the rheological properties. We determined that there is a strong time dependence of the rheological properties and app. 70 hours of irradiation is needed to obtain stable properties.

Introduction

The interest in so-called *smart* materials has been increasing over the last approximately ten years. Several terms are used to cover the area of *smart* materials; stimuli-adaptable, stimuli-responsive, active and designed materials, just to mention a few. [1] A wide variety of materials and stimuli have been published and most well-known is probably shape-memory metal alloys which are in fact temperature responsive metal alloys. Within the field of stimuli-adaptable polymers, materials responsive to temperature changes, electromagnetic radiation, electrical fields, mechanical stimuli, changes in the chemical environment (e.g. pH), electrochemical changes (redox), biological stimuli (eg. enzymes) and changes in the non-covalent interactions have been reported. Many recent reviews thoroughly goes through this growing field.[2,3,4] In general you can distinguish between polymer materials responsive to chemical or physical stimuli of which physical stimuli gives rise to the quickest responses.

The work presented here has focused on making a "physical stimuli"-adaptable material (sensitive to UV) based on the UV-activated cross-linking of cinnamic acid (CA). It is well-known that CA dimerises upon irradiation with UV ($\lambda > 300$ nm) as seen in Figure 1. This reaction has been used by several research groups to make stimuli-adaptable polymers.[5,6,7,8] The CA-group or derivatives thereof (such as cinnamylidene acetic acid) is readily available and relatively low in toxicity and hence very interesting in perspective to bio-applications.

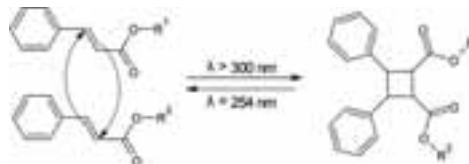


Figure 1: A schematic presentation of the reaction occurring when cinnamic acid (CA) is irradiated with UV-light. When irradiated with λ above 300 nm the double bonds in the CA-groups react to form cyclobutane. Irradiation with $\lambda = 254$ nm cleaves the cyclobutane bonds and returns the material to its original state.[9] (In CA, R^1 is H, but R^1 can also be e.g. polymers).

Specific objective

The specific objective of the presented work was to make a system where the CA-dimerisation was used to make a material which was initially a liquid but cross-link to an elastic material upon irradiation with UV-light. The reversibility of the CA-dimerisation would make it possible to recover the original properties upon irradiation with a shorter wavelength of UV-light.

Firstly it was decided to understand the dimerisation and look into the changes it could induce in a simple polymer system. The information from this study would create the foundation for the development of a more complex interpenetrating network (IPN). An IPN is a combination of two or more polymers which are interlaced at molecular level and which cannot be separated unless chemical bonds are broken.

Table 1: Reaction details and yields from syntheses of cinnamic acid derivatised poly(ethylen glycol) (PEG) polymers.

ID	M _n PEG	PEG	CA	DCC	DMAP	Yield
P4	2000 g/mole (4-armed star)	6.07 g	2.36 g	3.26 g	0.454 g	5.50 g (72%)
P2s	1000 g/mole (linear)	5.00 g	1.93 g	2.72 g	0.373 g	4.18 g (66 %)
P2l	4000 g/mole (linear)	5.00 g	0.483 g	0.689 g	0.0943 g	3.69 g (69%)

Table 2: Composition, irradiation time, intensity of UV-light and distance between sample and UV-light source for samples A, B and C. *t* is the irradiation time, *I* is the intensity of the UV-light ($\lambda=315\text{-}400$ nm) and *d* is the distance from light source to sample.

ID	P4	P2s	P2l	<i>t</i> (h)	<i>I</i> (mW/cm ²)	<i>d</i> (cm)
A	100%	-	-	1	1.98	2.5
B	50%	50%	-	1	1.98	2.5
C	23%	-	77%	1	1.98	2.5

Experimental

General methods. Infrared spectroscopy (IR) was conducted on a Perkin-Elmer Spectrum One model 2000 Fourier transform infrared system with a universal attenuated total reflection sampling accessory on a ZnSe/-diamond composite. The spectra were recorded in the range of 4000-525 cm⁻¹ with 4 cm⁻¹ resolution and 16 scans. UV-spectra were recorded with a BMG Labtech POLARstar Omega micro plate reader in the range from 220 nm to 400 nm. Small amplitude oscillatory shear (SAOS) measurements were made with a TA 2000 Rheometer from TA Instruments set to a controlled strain mode, where the chosen strain value was ensured to be within the linear regime of the materials by means of strain-sweeps. The measurements were done with parallel plate geometry of 10 or 20 mm in the frequency range from 100 Hz to 0.01 Hz at 50°C. The samples were transferred to the rheometer with a pipette as long as they stayed liquid (up to 24 hours of UV-irradiation), after this they were cut in shape and moved with a pair of tweezers. UV-irradiation was carried out with a Sol-Data Ultra Violet Lamp UVA 315-400 nm (mercury vapour lamp) and the intensity of the UV-light was measured with a Sentry® UV-detector (detection range: from 280-400 nm).

Chemicals. 4-armed PEG star (M_n=2000 g/mole) was acquired from Creative PEGWorks and linear PEG (M_n=1000 and 4000 g/mole) was acquired from MERCK-Schuchardt. All other chemicals were acquired from Aldrich.

General procedure for derivatisation of PEG. PEG (4-armed star, 6.07 g, 3.03 mmole, M_n=2000 g/mole) was dried and a solution of CA (2.36 g, 15.9 mmole) and 4-dimethylamidopyridine (0.454 g, 3.64 mmole) in CH₂Cl₂ (3 mL) was added. A solution of N,N'-dicyclohexylcarbodiimide (3.26 g, 15.8 mmole) in CH₂Cl₂ (2 mL) was added dropwise at 0°C. The mixture was left at RT for 15 hours. The product, a white solid, was recovered by precipitation in cold ether (5.50 g,

72% yield), the white solid melted to form a yellow oil at RT. Two linear PEG-polymers were also derivatised with CA and details from the syntheses are summarised in Table 1.

Results and Discussion

Three different CA-derivatised PEG-polymers were prepared by esterification of commercially available PEG-polymers, see Table 1. We prepared a derivatised 4-armed star polymer (P4, M_n=2000 g/mol) and two linear polymers (P2s and P2l, M_n=1000 g/mol and 4000 g/mol, respectively). We mixed the polymers in the ratios mentioned in Table 2 to make the stimuli-responsive materials (**A**, **B** and **C**). In **C** the UV-active groups are diluted compared to **A** and **B** which made it possible to study if the dilution had an effect on UV-activated cross-linking of the CA-groups.

Since we are primarily interested in the cross-linking reaction we ensured that this reaction path was preferred by using a UV-lamp with wavelengths above 315 nm (315-400 nm). The irradiation with UV-light induced detectable macroscopic changes in the samples, as can be seen in Figure 2: Where pictures of the material before and after UV-irradiation are shown. For short irradiation times the samples remain liquids, while for long irradiation times (more than 24 hours) they become solid films. Despite the large change in the macroscopically observed films we were not able to detect the changes with IR-spectroscopy. UV-absorbance spectra of the polymer showed a change upon irradiation with UV-light. This showed that the reaction between the UV-active groups takes place in a sample consisting solely of the UV-active polymer. After irradiation the samples were insoluble and therefore it was not possible to characterize the material with NMR or SEC.

The change in rheological properties (the storage modulus, *G'*, and the loss modulus, *G''*) of the photo-active materials (**A**, **B** and **C**) was investigated using SAOS. The results are shown in Figure 3. All data sets showed terminal relaxation before irradiation with UV-light indicating that the materials are liquids. The terminal relaxation is seen at frequencies (ν) below 50 Hz, where $G' > G''$ and *G'* is proportional to ν and *G''* is proportional to ν^2 . We observe a plateau at low frequencies for *G'* for sample **B** and **C** and ascribed this to the detection limit of the rheometer. After irradiation all data sets showed a plateau at low frequencies. For **A** the observed elastic modulus is low ($G_0 \approx 0.8$ Pa) but the presence of the plateau still clearly shows that a significant change in material properties has taken place. Similarly $G_0 \approx 0.8$ Pa for **B** and $G_0 \approx 0.3$ Pa for **C**. For all samples changes in rheological properties

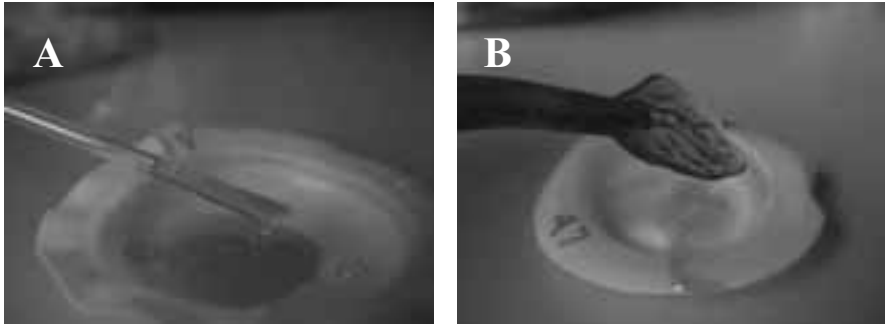


Figure 2: Film formation of P4 after UV-irradiation. A) P4 before UV-irradiation. The material is a liquid. B) P4 after 96 h of UV-irradiation. The material is cross-linked to a film.

were observed after irradiation with UV-light, but the change is most pronounced for **A**. This is most likely closely connected to the concentration of the photo-active CA-group (sample **A** and **B**: 1.59 mole CA/g sample; sample **C**: 0.727 mole CA/g sample) and the structure of the formed network. In **C** the concentration of the photo-active CA-group is reduced to half of what it is in **A** and **B** meaning that the active groups are twice as far from each other. We know that the spatial orientation of the photo-active groups is of great importance and a significant decrease in concentration will therefore reduce the amount of formed dimers. The distance between the cross-linking points is shorter in **A** than in **B** and therefore the network formed with **A** is stronger than **B** and the observed change is bigger.

Based on these results we decided to continue the work with **A**-samples (samples denoted A_T for the time dependence study). In our initial experiments we observed that the development of the mechanical properties of the material was very dependent on the irradiation time. A number of samples (A_T) were made and irradiated with UV-light for up to 120 hours. Rheological data was collected on all the A_T -samples and in Figure 4 a plot of G' and G'' at 0.01, 1 and 10 Hz as a function of the irradiation time (t) is shown. The data shown in Figure 4 shows the structural development of the network which is normally observed during network formation (curing). At low times the curve is steep because the limiting factor here is the collision of the relatively free-moving polymer chains not yet hindered by the network. At longer timescales the curve flattens out because the limiting factor at this point is

the spatial orientation of the active groups. If the active groups are far from each other and the network is reacted to an extent where the flexibility has decreased significantly the likelihood of “left over” active groups to get in close proximity and react is low. The time dependence of the reaction could also be observed simply by looking at the differences between the samples, as mentioned earlier.

The data shows that a plateau is reached with $G' \approx 35000$ Pa and $G'' \approx 10000$ Pa after approx. 70 hours and at larger timescales no profound change is expected. We conducted a control experiment which showed that the four-armed PEG did not cross-link upon UV-irradiation (up to 96 h) at 60°C, and that P4 did not spontaneously cross-link at 60°C (up to 96 h). In other words the UV-active compound is responsible for the observed changes in material properties.

As mentioned before the system presented here is interesting because of its low toxicity and high versatility but also because of its reversibility. We observed that the samples which had been subjected to long UV-exposure times lost their ability to regain their original properties when exposed to UV-light with shorter wavelengths (irradiation with UV-light with $\lambda=254$ nm for up to 96 h). At the same time thorough investigation of UV-spectra of thin films of P4 (treated with UV-light with $\lambda=315-400$ nm for 1 h and then with $\lambda=254$ nm for 1 h) showed reversibility similar to the 40 % reported by Lendlein *et al.*[5], who work with a similar system. This data shows that the long UV-exposure time obstructs the reversibility of the photo-reaction. Optimisation of UV-exposure time and need for reversibility must be made

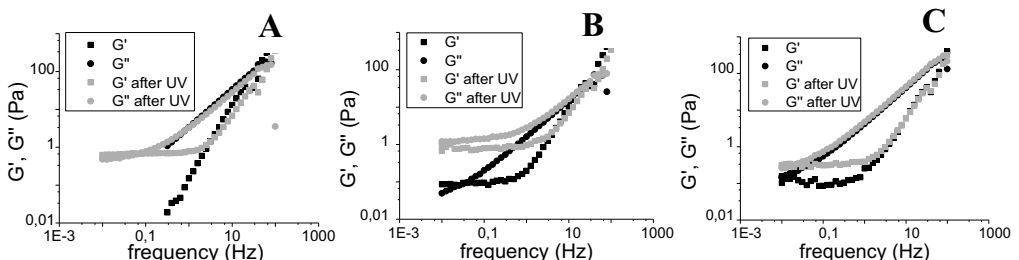


Figure 3: Rheological properties of sample A, B and C before (black symbols) and after (grey symbols) irradiation with UV-light ($\lambda=315-400$ nm) for 1 hour. The measurements were carried out at 50°C with a strain value of 10 %.

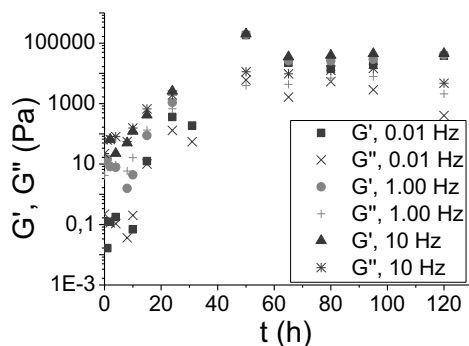


Figure 4: Values for G' and G'' at $\nu=0.01, 1.00$ and 10 Hz for the A_T -samples as a function of the UV-irradiation time (t). After app. 70 hours a plateau is reached at app. 0.01 MPa.

before the material can become useful in applications.

Future work and outlook

The described experiments were carried out a number of times to check reproducibility and we can conclude that the change observed at short timescales proved to be difficult to reproduce. However the long time changes were reproducible. We would like to understand deeper what happens at short timescales and therefore a thorough spectroscopic study has been made. Furthermore we would like to make some proof of concept experiments for the IPN-systems. Our initial experiments show a significant change in material properties upon long irradiation times but we would like to decrease the needed exposure time. There is a need for finding the optimal UV-irradiation time needed for good material properties but at the same time the reversibility of the reaction should not be obstructed and it should be possible to recover the original properties.

Conclusion

A number of mixtures UV-active polymers (P4, P2s and P21) were investigated with rheology before and after irradiation with UV-light. All samples showed a change upon radiation but the change was most profound for sample A. The time dependence of the reaction was studied and we found that an exposure time of app. 70 hours was needed to get stable mechanical properties. After 70 hours a significant increase in G' and G'' was seen. The good control of the reaction rate enables us to follow the network formation closely over time. We observed that the original material properties could not be restored for the samples which had been subjected to long UV-exposure times.

References

1. M.W. Urban. Handbook of stimuli-responsive materials. Wiley Online Library, 2011.
2. JF Liu, MW Urban. Prog. Polym. Sci., 35 (2010) 3–23
3. RJ Wojtecki, MA Meador, SJ Rowan. Nature materials, 10 (2010) 14–27
4. X Yan, F Wang, B Zheng, F Huang. Chemical Society Reviews, 41 (2012) 6042–6065.

5. A Lendlein, H Jiang, O Jünger, R Langer, Nature 434 (7035) (2005) 879–882
6. F. M. Andreopoulos, C. R. Deible, M. T. Stauffer, S. G. Weber, W. R. Wagner, E. J. Beckman, A. J. Russell, J., Am. Chem. Soc., 118 (1996) 6235–6240
7. X. Coqueret, Macromol. Chem. Phys. 200 (1999) 1567–1579
8. K.M. Gattás-Asfura, Weisman; E., F. M. Andreopoulos, M. Micic, B. Muller, S. Sirpal, S. M. Pham, R. M. Leblanc, Biomacromolecules 6 (2005) 1503–1509
9. H Tanaka, K Honda, J. Polym. Sci., Polym. Chem. Ed., 15 (1977) 2985–2689

List of publications

1. SMG Frankær, MK Jensen, AG Bejenariu, AL Skov. Rheol Acta. 51 (2012) 559–567.
2. SMG Frankær, ALH Di Vaia, AE Daugaard, S Kiil, AL Skov. Dansk Kemi. 92 (2011) 24–27.
3. SM Frankær, ALH Di Vaia, AE Daugaard, S Kiil, AL Skov, Nordic Polymer Days, Kungliga Tekniska Högskolan, Stockholm, 2011.
4. SM Frankær, AL Skov, S Kiil. Annual Polymer Day, Technical University of Denmark, 2010.
5. SM Frankær, AL Skov, S Kiil. Dansk Kemingeniør Konference, Technical University of Denmark, 2010.
6. SM Frankær, MK Jensen, AG Bejenariu, AL Skov, O Hassager. Annual Polymer Day, Technical University of Denmark, 2009.
7. SM Frankær, MK Jensen, AG Bejenariu, AL Skov, O Hassager in: Annual Transactions of the Nordic Rheology Society 17 (2009). 18th Nordic Rheology Conference, Reykjavik, Iceland, 2009

**Michael Frost**

Phone: +45 4525 2876
E-mail: mifro@kt.dtu.dk

Supervisors: Georgios M. Kontogeorgis
Nicolas von Solms

PhD Study

Started: June 2011
To be completed: May 2014

Measurements and modelling of phase equilibrium of oil-water-polar chemicals

Abstract

As the exploitable oil resources decrease, more advanced recovery methods are employed in the oil industry. This has led to an increase in used chemicals, in order to ensure a constant and safe production. These chemicals have many applications, and are part of different families like alcohols, glycols, alkanolamines etc.

Due to rising demands from environmental agencies and a wish for a more refined product, it is becoming increasingly important for downstream processing to know/predict the solubility of oil and gas with different complex chemicals. The objective of this project is to further develop the CPA equation of state for use in calculation of solubility between oil and polar chemicals.

Introduction

Chemicals are added in almost all stages of oil and gas production. It is generally accepted that efficient and cost effective oil and gas production is not possible without the use of chemicals. Monoethylene glycol (MEG) and methanol are two of the most widely used production chemicals. They are used as gas hydrate inhibitors to ensure safe production and transportation. The prediction of the distribution of chemicals in oil, water and gas streams is important for the oil industry to ensure reliable production and processing. It is also important information to fulfill the demand from environmental authorities, in order to know the amounts of chemicals and hydrocarbons in a processed water stream for ensuring safety of marine life. Furthermore it is important for efficient design/operation of separation equipment. The partitioning of the chemicals can either be measured experimentally or predicted using a suitable thermodynamic model. The experimental method is expensive and challenging, partly due to the difficulties involved in measurements of such low solubilities. The CPA equation of state proposed by Kontogeorgis et al. [1] has been successfully applied in the past to well defined systems containing associating compounds (such as water, methanol and MEG). It has also, to a first extend, been successfully applied to reservoir fluids in presence of water and polar chemicals, using a characterization method (Pedersen et al. [2]), modified by Yan et al. [3]. In order to understand these complex systems and to further

develop/validate CPA, more experimental data is desirable. This work focuses on producing new experimental data for both well defined multi-component mixtures, as well as for systems containing oil-water-polar chemicals.

Specific Objectives

As basis for the further development of CPA, the aim of this project is threefold:

- Produce experimental data (VLE/LLE/VLLE) for well-defined systems (containing water, hydrocarbons and polar chemicals).
- Further development of equipment for high quality VLE/LLE/VLLE measurements.
- Carry out oil-water-MEG measurements for oil systems not previously studied – emphasis to heavy oils and those with high aromatic/naphthenic content.
- Develop and validate the CPA equation of state based on data generated and relevant literature data.
- It is of special importance to develop an oil characterization method which can be used for a wide range of oils and conditions. This method should account for paraffinic (P), naphthenic (N) and aromatic (A) contents of a reservoir fluid.

Experimental work

Experimental work has been carried out at Statoil research facility in Norway, over the past years. The goal has been to focus on different reservoir fluids from the North Sea, with varying PNA distributions.

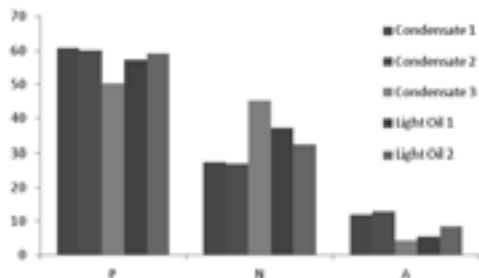


Figure 1: The PNA distribution of 5 reservoir fluids (3 condensates and 2 light oils) from Statoil operated fields in the North Sea.

The properties of the reservoir fluids such as mean molecular weight (MMW), density and C_{10+} fraction is given in Table 1. Mutual solubility data and thermodynamic modeling are presented here only for two of the systems (Condensate 1 and Light oil 1). Example of the composition of a reservoir fluid can be seen in table 2 (Light oil 1).

Table 1: Properties of reservoir fluids

Reservoir fluid	C_{10+} Mass%	MMW g/mol	Density kg/m^3
Condensate 1	40.77	112.7	756.2
Condensate 2	10.47	106.9	738.5
Condensate 3	12.49	97.37	720.5
Light oil 1	91.45	266.0	905.5
Light oil 2	56.97	135.2	778.4

Apparatus and Procedure

The sketch for the experimental setup used in this work is shown in Figure 2.

Mixing and Equilibrium

MEG, condensate and water were mixed at a fixed temperature for 24 hours using a mixing machine in an air heated oven. For binary systems, approximately equal mass of MEG and condensate were added for mixing. The ternary system consists of MEG, condensate and water where the hydrocarbon phase was 50% (mass) and the polar phase was also 50% on mass basis. The polar phase consists of MEG and water where the composition of MEG ranges from 40% to 90% which is of interest to the industrial applications in the North Sea.

Table 2: Composition of a North Sea reservoir fluid (Light oil 1)

Component	Weight %	MW g/mol	Density kg/m^3
Methane	0	16.04	300
Ethane	0.03	30.07	358
Propane	0.13	44.1	508
iso-Butane	0.09	58.12	563
n-Butane	0.22	58.12	585
Neopentane	0	72.15	597
iso-Pentane	0.2	72.15	625
n-Pentane	0.25	72.15	631
C_6 total	0.61	84.9	667.9
n-Hexane	0.57	86.18	662.8
Naphtenes (C_6)	0.04	70.13	750
C_7 total	1.71	92.14	737.1
n-Heptane	0.55	100.2	687.5
Naphtenes (C_7)	1.12	89.16	759.8
Aromatics (C_7)	0.04	78.11	884
C_8 total	2.5	107.14	748.2
n-Octane	1.03	114.23	707.3
Naphtenes (C_8)	1.35	103.79	772.3
Aromatics (C_8)	0.12	92.14	871
C_9 total	2.81	123.24	751.3
n-Nonane	1.82	128.11	721.2
Naphtenes (C_9)	0.67	120.16	787.5
Aromatics (C_9)	0.32	106.17	873
C_{10+}	91.45	317.3	928.3

After mixing the mixture was transferred to two identical glass equilibrium cylinders and was kept for at least 18 hours to attain equilibrium. The equilibrium cylinders contain holes and caps fitted with septa for sampling.

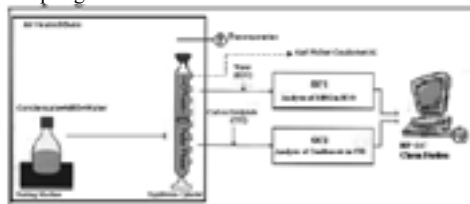


Figure 2: Sketch of experimental setup.

Both mixing and separation were carried out in an air heated oven which was used at the temperature range from 275 K to 326 K in this work. A DOSTMANN P500 thermometer (± 0.1 °C) was used for the temperature measurement.

Sampling and Analysis

At equilibrium, samples from two phases were drawn manually using a preheated syringe and needle. Preheated needle was used to avoid phase separation due to temperature gradient. Two Agilent gas chromatographs (GCs) with different column specifications were used for composition analysis: one for the polar phase (glycol GC) while another for the condensate phase (condensate GC). The gas

chromatographs are connected to a computer which has Chem Station package for data acquisition and quantification.

Polar Phase Analysis

For the polar phase analysis, hydrocarbons were extracted using the solvent extraction method. The solvent used in this work for the extraction of hydrocarbons from the polar phase is carbon disulphide (CS₂) which has negligible solubility in MEG but it is soluble in hydrocarbons. The extract phase is then analyzed on condensate GC using the standard temperature program from ASTM standard D5134-98 with an internal standard 1-heptene diluted in 1-dodecane (C₁₂).

Condensate Phase Analysis

MEG dissolved in condensate was extracted using water and analyzed at glycol GC. The water contents of condensate phase were analyzed using Karl Fisher Coulometer which provides very fast and reliable results, especially for systems with very low solubilities

Thermodynamic Modeling

Thermodynamic modeling is carried out using the CPA equation of state, with the characterization method described by Yan et al. [3]. To be able to use equations of state (EoS) for complex hydrocarbon mixtures, the acentric factor (ω), critical pressure (P_c) and critical temperature (T_c) must be provided for all components in the mixture. Reservoir fluids may contain thousands of different components. Such high numbers are impractical to handle in phase equilibrium calculations. Some components are therefore lumped together and represented as pseudo components. The C_{7+} characterization consists of representing the hydrocarbons with seven or more carbon atoms as a convenient number of pseudo components and finding the corresponding EoS parameters T_c , P_c and ω for each component. Table 3 presents Light oil 1 after characterization.

Both MEG and water have been modeled using four association sites (so-called 4C scheme).

The CPA equation of state uses five pure component parameters, including three for non associating compounds and two for associating compounds. For mixtures containing more than one associating compound, a combining rule is needed for the association parameters. In this work the Elliot Combining Rule (ECR) has been used.

A binary interaction parameter (k_{ij}) is needed for each binary system. For binary interaction parameters between MEG and hydrocarbons, an average value is used. This is done due to lack of relevant experimental data. The binary interaction parameters between water and hydrocarbons are obtained from a generalized expression using a correlation in terms of carbon number as given by the following expression.

$$k_{ij} = -0.026 \cdot N_C + 0.1915$$

Where N_C is carbon number of an alkane. The used binary interaction parameter between MEG and water is -0.115 using ECR.

Table 3: Characterization of light oil¹

Components	Mole %	T_{cm} (K)	P_{cm} (bar)	ω_m
Methane	0.040	190.6	46.0	0.008
Ethane	0.300	305.4	48.8	0.098
Propane	0.810	378.6	47.2	0.105
i-Butane	0.410	415.8	40.1	0.151
n-Butane	1.020	436.3	43.6	0.158
i-Pentane	0.740	460.4	33.8	0.227
n-Pentane	0.900	479.4	38.0	0.217
C ₆	1.920	522.3	34.9	0.244
C ₇	4.920	561.0	36.0	0.229
C ₈	6.210	587.8	33.0	0.269
C ₉	6.090	612.4	29.5	0.317
C ₁₀ -C ₁₁	19.315	675.8	26.4	0.389
C ₁₂ -C ₁₇	14.476	759.9	22.6	0.490
C ₁₈ -C ₂₀	8.423	815.9	20.6	0.556
C ₂₁ -C ₂₄	8.740	861.8	19.0	0.612
C ₂₅ -C ₂₈	7.913	909.7	17.3	0.702
C ₂₉ -C ₃₄	5.518	953.3	15.9	0.775
C ₃₅ -C ₄₁	5.039	1001.1	14.5	0.796
C ₄₂ -C ₅₂	4.203	1056.1	12.8	0.848
C ₅₃₊	3.012	1145.8	9.5	0.912

Results and discussions

In the binary systems only one associating compound (MEG) is present, which means that the only binary interaction parameters needed are those between MEG and each HC fraction. The binary interactions between hydrocarbons are all set to zero.

The mutual solubility of MEG and reservoir fluids using the CPA EoS is shown in table 4. Using a small binary interaction parameter (k_{ij}), between MEG and all hydrocarbons, satisfactory results are obtained for the solubility of hydrocarbons in the polar phase, and for all condensates the solubility of MEG in hydrocarbon phase.

The solubility of MEG in the hydrocarbon phase is highly underestimated for light oils, which might be due to an unexplained increase caused by the lack of information of the C_{10+} fraction (76.64 mole %). The light oils are of naphthenic nature, which might explain the increased solubility of MEG in hydrocarbons, which is not captured by the model.

Table 4: Average deviation from experimental data using the CPA EoS

Reservoir fluid	k_{ij} of MEG-HC	% AAD (HC in MEG)	% AAD (MEG in HC)
Condensate 1	0.02	7	7
Condensate 2	0.00	17	17
Condensate 3	0.04	23	8
Light oil 1	0.02	1	85
Light oil 2	0.02	13	36

In the case of the ternary mixtures of MEG, water and reservoir fluids, the cross association between water and MEG must be taken into account. The Elliott combining rule is used for the MEG/water system, with a $k_{ij} = -0.115$. Binary interaction parameters between water and hydrocarbons used are based on the generalized correlations, where the interaction parameters between all hydrocarbons and MEG have been adopted from the binary system.

CPA EoS can satisfactorily predict the experimental trends and describe the solubilities in both phases with reasonable accuracy. A slight under prediction is observed for the MEG concentration in the hydrocarbon phase, the water solubility in the hydrocarbon phase and hydrocarbon concentration in the polar phase. The under prediction of reservoir fluid solubility in the polar phase and of water solubility in the hydrocarbon phase, can to some degree be explained by solvation, which is not explicitly accounted for in the characterization method.

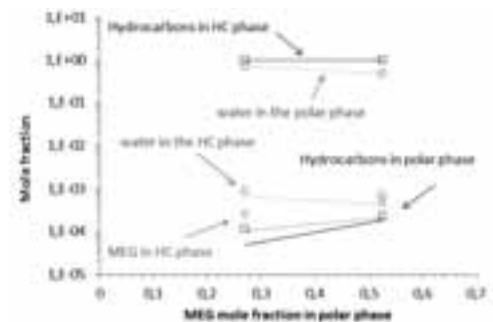


Figure 3: Mutual solubility of MEG - water – reservoir fluid. The points are experimental data and the lines are CPA predictions.

Figure 3 presents experimental data and predictions made with CPA for a mixture of reservoir fluid – water – MEG. This shows that the solubility of condensate and MEG decreases with increasing water content in the polar phase. The modeling results are satisfactory considering that a single and same temperature independent binary interaction parameter is used for all MEG-hydrocarbon pairs.

It is important to mention, that the predictions are as good as for systems of well-defined HC (n-hexane, 2,2,4-trimethylpentane) with MEG and water.

Conclusions

The CPA equation of state has been applied to the systems containing reservoir fluids, MEG and water. The critical properties were calculated using a previously developed characterization method which uses the CPA EoS monomer values.

Using a small binary interaction parameter between all MEG/HC pairs, CPA EoS satisfactorily describes the mutual solubility of the reservoir fluids with MEG. Promising results are obtained with the CPA EoS for both ternary mixtures, with some under predictions of the solubility of MEG and water in the hydrocarbon phase and the solubility of hydrocarbons in the polar phase. The results are in the right order of magnitude, and the predictions are as good as for well-defined hydrocarbons (n-hexane and benzene) with MEG and water. Improved results might be obtained, if binary interaction parameters are used for well-defined HC and MEG, instead of using an average value. Further improvement can be obtained with further investigation of the effect of PNA distribution in the calculations, so that solvation is accounted for explicitly.

Future work

- Development of oil characterization procedure, to account for solvation effects.
- Further experiments with more aromatic/naphthenic oils
- Further experiments of well-defined systems (VLLE/LLE/VLE)
- Construction of new VLLE cell

Acknowledgements

The authors wish to thank the industrial partners in the CHIGP (Chemicals in Gas Processing) consortium for financial support.

References

1. G. M. Kontogeorgis, E. C. Voutsas, I. V. Yakoumis, D. P. Tassios, *Ind. Eng. Chem. Res.* 35 (1996) 4310.
2. K. S. Pedersen, P. Thomassen, A. Fredenslund, *Characterization of gas condensate mixtures, Advances in thermodynamics*, Taylor & Francis, New York, 1989
3. W. Yan, G. M. Kontogeorgis, E. H. Stenby, *Fluid Phase Equilib.*, 276 (2009) 75-85.

List of publications

1. M. Frost, N. von solms, G. M. Kontogeorgis, Poster presentation Presented at ESAT conference, 2012 Postdam
2. M. Frost, G.M. Kontogeorgis, E.H. Stenby, M.A. Yussuf, T. Haugum, K.O. Christensen, E. Solbraa, T.V. Løkken, *Fluid Phase Equilib.* 2012, submitted



Hassan Ahmadi Gavlighi

Phone: +45 4525 2947
E-mail: HAG@kt.dtu.dk
Supervisors: Jørn Dalgaard Mikkelsen
Anne Meyer

PhD Study
Started: June 2009
To be completed: November 2012

Enhanced enzymatic cellulose degradation by cellobiohydrolases via product removal

Abstract

Product inhibition by cellobiose decreases the rate of enzymatic cellulose degradation. The optimal reaction conditions for two *Emmericella (Aspergillus) nidulans*-derived cellobiohydrolases I and II produced in *Pichia pastoris* were identified as CBHI: 52 °C, pH 4.5–6.5, and CBHII: 46 °C, pH 4.8. The optimum in a mixture of the two was 50 °C, pH 4.9. An almost fourfold increase in enzymatic hydrolysis yield was achieved with intermittent product removal of cellobiose with membrane filtration (2 kDa cut-off): The conversion of cotton cellulose after 72 h was ~19 % by weight, whereas the conversion in the parallel batch reaction was only ~5 % by weight. Also, a synergistic effect, achieving ~27 % substrate conversion, was obtained by addition of endo-1,4- β -D-glucanase. The synergistic effect was only obtained with product removal. By using pure, monoactive enzymes, the work illustrates the profound gains achievable by intermittent product removal during cellulose hydrolysis.

Introduction

Cellulose is one of the major building materials in nature and structurally consists of linear macromolecular chains of 1–4-linked β -D-glucopyranose. Cellulose is a major component in plant cell walls, and hence in fibrous plant biomass [1]. Plants of the genus *Gossypium* produce cotton as almost pure cellulose fibers (95 %) to form a protective boll around the plant seeds. From a biotechnological point of view, cellulosic degradation by enzymes is a crucially important process and has a wide range of applications in the food, animal feed, textile, fuel and chemical industries [2].

On the other hand, enzymatic cellulose degradation in nature is slow and moreover requires the action of several different enzymes for complete deconstruction into monosaccharides. In addition to the recently discovered polysaccharide monooxygenase, cellulose-cleaving type of enzymes [3], the important enzymes for hydrolysis of cellulose include exo-1,4- β -D-glucanases or cellobiohydrolases (CBH, EC 3.2.1.91) and endo-1,4- β -D-glucanase activity (EC 3.2.1.4). CBHs catalyze the hydrolysis of the β -1,4 bonds at the ends of the cellulose chains releasing mainly cellobiose: CBHI or Cel7A attacks the reducing ends, whereas CBHII or Cel6A attacks the non-reducing ends of the cellulose polymers, and both enzymes are able to also attack crystalline

cellulose. As the name implies, endo-1,4- β -D-glucanase catalyzes the random cleavage of the internal β -1,4 bonds in the amorphous part of the cellulosic polymers. There are various reasons for the decline in rate during enzymatic hydrolysis of cellulosic material, notably substrate crystallinity, enzyme inactivation (thermal instability), non-productive adsorption of the enzymes to the substrate, and the so-called traffic jam phenomenon by which particularly the action of CBHI molecules has been proposed to be obstructed. Also, product inhibition by cellobiose (and to a lesser degree glucose) is a major reason for the slow reaction rate in cellulosic material degradation [4]. Enhancement of cellulose hydrolysis by product removal using membrane reactors has been reported previously. Various designs involving for example batch reaction with intermittent or continuous product removal in membrane reactors or batch hydrolysis reactors connected to ultrafiltration units containing immobilized β -glucosidase have been systematically evaluated in the past. Based on the available knowledge, membrane reactor technology, which allows the continuous or semi-continuous removal of the cellulose hydrolysis products, seems to be a workable approach for minimizing product inhibition during cellulosic material degradation [5]. However, there is only limited information available about the effect of the technique

of removing the inhibitory cellobiose during cellulose hydrolysis to increase the degradability of cellulose. The objective of this work was to study the increase in cellulose conversion by introducing intermittent removal of cellobiose during extended cellulose hydrolysis (72 h). We used CBHI and CBHII from *Emericella nidulans* (previously known as *Aspergillus nidulans*), cloned in *Pichia pastoris*, and optimized the reaction conditions of the two enzymes to maximize cellulose conversion in the reaction, using cotton cellulose as the model substrate.

Results

The progress curves for enzymatic cellulose hydrolysis of cotton displayed the significant boosting effect of semi-continuous product (cellobiose) removal for CBHI + CBHII catalysis. Hence, after 72 h the conversion of cellulose was approx. 19 % by weight, whereas the parallel reaction run in batch only gave a conversion of approx. 5 % by weight, i.e. approx. a fourfold difference in yields (Fig. 1). As cellobiose diminishes the degradation of cellulosic material by inhibiting enzyme activity, notably cellobiohydrolases [4], our results corroborate that there is significant product inhibition of CBH-catalyzed cellulose degradation in a batch reaction. Since the product inhibition severely decreases the conversion rate of enzyme catalyzed cellulosic reactions the data indicate the potential gains achievable by product removal. In addition, membrane technology allows the removal of product inhibitors while retaining the enzyme in the reactor for reuse. In this case, this “reuse” of the enzyme increased the enzyme productivity (after 72 h) from 0.53 gproduct/genzyme for the batch reaction to 2.37 gproduct/genzyme for the semi-continuous membrane reactor reaction. Likewise, the biocatalytic productivity rate and the bioconversion efficiency increased from 0.0075 to 0.033 gproduct/genzyme h, and from 0.043 to 0.19 gproduct/gsubstrate, respectively, by this approach (calculated for the 72 h reaction). The current set-up did not allow a detailed mechanistic or kinetic examination to firmly establish why the endoglucanase only increased the reaction rate significantly with product removal.

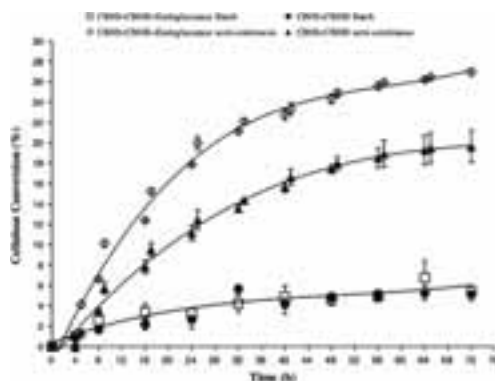


Figure 1. Cellulose conversion (% weight/weight) of cotton during enzymatic treatment for 72 h in different types of membrane reactor mode: Batch and semi-continuous. Data are shown as the mean \pm 1 SD and are derived from two independent repeats

References

1. Zugenmaier P Crystalline cellulose and derivatives: characterization and structures. (2008) Springer, Verlag
2. Bhat MK, Bhat S Cellulose degrading enzymes and their potential industrial applications. *Biotechnol Adv* 15: (1997) 583–620.
3. Quinlan RJ, Sweeney MD, Lo Leggio L, Otten H et al Insights into the oxidative degradation of cellulose by a copper metalloenzyme that exploits biomass components. *Proc Natl Acad Sci USA* 108: (2011) 15079–15084.
4. Andrić P, Meyer AS, Jensen PA, Dam-Johansen K Reactor design for minimizing product inhibition during enzymatic lignocellulose hydrolysis: I. Significance and mechanism of cellobiose and glucose inhibition on cellulolytic enzymes. *Biotechnol Adv* 28: (2010a) 308–324.
5. Andrić P, Meyer AS, Jensen PA, Dam-Johansen K Reactor design for minimizing product inhibition during enzymatic lignocellulose hydrolysis: II. Quantification of inhibition and suitability of membrane reactors. *Biotechnol Adv* 28: (2010b) 407–425.



Kaustav Goswami

Phone: +45 4525 6885
E-mail: kago@kt.dtu.dk

Supervisors: Anne Ladegaard Skov
Ole Hassager

PhD Study
Started: August 2011
To be completed: July 2014

Poly (propylene oxide): A novel silicone-resembling elastomer for dielectric electroactive polymer (DEAP) actuator application

Abstract

A novel very soft but easily handable elastomeric material for EAP purposes was investigated, namely a poly (propylene oxide) PPO network. The elastomer was loaded with fumed silica and commercially available so called core-shell filler consisting of titanium dioxide core and silica shell. The dynamic mechanical behaviour of PPO and composites thereof were examined by shear rheology. Results indicated that incorporation of silica particles improved the stability of the otherwise mechanically poor pure PPO network. Dielectric spectroscopy revealed an increase in the relative permittivity at 10⁴ Hz upon incorporation of fumed silica from 5.4 of pure PPO to 6.2 in the composite, which was about twice that of the commonly used silicone elastomer Elastosil RT625. At low frequencies (10Hz) all composites had relative permittivities on the order of 9-11. Compared to silicone, PPO composites had favorable properties especially in low-frequency applications where very high dielectric permittivities were measured. The incorporation of the core-shell particles was shown not to be favorable for this particular polymer-particle system.

Introduction

Mechanical actuators such as screw jacks, ball screws and roller screws are widely used in converting electrical energy into motion due to their simple design and reliability. However, because of the presence of moving parts grinding against each other they are prone to wear and tear. Dielectric electro active polymers (DEAPs) have emerged as new candidates for actuators due to their light weight, low cost of production, low energy consumption and low heat generation. Moreover, DEAP actuators have no moving parts which drastically reduce wear and thus maintenance becomes easy. They are also commonly nick named artificial muscles as they have similar mechanical properties to human muscle and being the most effective actuators capable of mimicking human muscular tissue functions [1].

In the construction of DEAP actuators a thin film of dielectric elastomer is sandwiched between very thin layers of compliant electrodes which are connected to the power supply for actuation.

The governing equation for actuation of a DEAP actuator is given as [2]

$$p = \epsilon_0 \epsilon_r E^2 \quad (1)$$

where p is the effective pressure acting on the dielectric elastomer due to an applied electric field E , while ϵ_0 and ϵ_r are the permittivity of free space and relative permittivity of the elastomer, respectively. Due to the elastic response of the material, when both electrodes on the opposite surfaces of the elastomer film are connected to an external power source the relation between the strain (S) produced on the elastomer and the applied voltage (V) can be quantified by using the following equation:

$$S = \frac{\epsilon_0 \epsilon_r}{Y} \left(\frac{V}{d} \right)^2 \quad (2)$$

where Y is the elastic modulus of the elastomer and d is its thickness. The main disadvantage of DEAP actuators is the operating voltage which is of the order of kV. From equation 2, it is seen that to lower the required voltage for a particular strain of DEAP, we can decrease either the elastic modulus or the film thickness or alternatively increase the relative permittivity of the elastomer. The influence of elastomer film thickness, elastic modulus and relative permittivity on the electromechanical properties for commercially available

poly (dimethyl siloxane) (PDMS) has already been discussed by Skov et.al [3]. For large scale processing it seems that currently thickness of 40 μ m is the threshold value for thin film actuator prepared from commercially available silicone [4]. PDMS is widely applied as base material for DEAP actuators [2,5–10] due to both its softness, stretchability and excellent actuation response time but the low relative permittivity has a significant negative effect on the operating voltage of the actuator. Therefore the main challenge for development of new systems lies on the fact that the material preferably should have PDMS resembling response time with a high dielectric permittivity [11].

This work is focused on development of a new type of silicone resembling material, namely poly (propylene oxide) (PPO) and composites thereof with the aim of achieving higher dielectric permittivity and hence improved electro-mechanical properties compared to commercially available PDMS. Rheological and characterizations were performed on both this new material and the composites to evaluate PPO as a new generation of electro active polymers.

Experimental

Vinyl terminated PPO of approximate molecular weight 13,500g/mole (Kaneka Silyl ACS 003) was obtained from Kaneka Corp., Japan. The fillers used were hexamethyldisilazane (HMDS) treated fumed silica (AEROSIL® R812) and hydrophobized fumed silicon-titanium mixed oxide filler with titanium dioxide core and silica shell (AEROXIDE® STX801) (core-shell filler), both procured from Evonik Industries. The reported Brunauer, Emmett and Teller (BET) surface area of AEROSIL® R812 and AEROXIDE® STX 801 was 260 \pm 30 m²/g and 55 \pm 15 m²/g respectively. All the other chemicals used in this work were obtained from Sigma-Aldrich.

Standard procedure for preparation of PPO networks. Pentaerythritol tetrakis (3-mercaptopropionate) (crosslinker, 0.244g, 0.5mmol) and 2, 2-dimethyl-2-phenylacetophenone (photo initiator, 0.128g, 0.5mmol) were dissolved in 20-30wt% of toluene. PPO [10g (0.74mmol of reactive group) Mn= 13,500 g/mole]] was added to the toluene solution and the solution was mixed in a SpeedMixer™ at 3500 rpm for 5minutes. The mixture was poured into an 8 cm \times 10 cm steel mould placed over a glass plate lined with Parafilm® M. This setup was kept in a well-ventilated place for 45-60 minutes and subsequently transferred to the UV chamber (λ = 365nm) and irradiated for 45 minutes.

Standard procedure for filled PPO systems. The system was prepared as above for PPO networks. The filler and additional toluene was added to the toluene solution prior to speed mixing. Otherwise the procedure was unchanged.

Results and Discussions

The rubber matrix was prepared through a novel procedure applying thiol-ene chemistry for crosslinking

an α - ω -allylic poly(propylene oxide) (PPO) with a tetrafunctional thiol (pentaerythritol tetrakis(3-mercaptopropionate)). Thiol-ene chemistry [12] is advocated as a “click” reaction due to the high efficiency of the reaction and the mild reaction conditions. The method has been used for preparation of other types of materials and has been found highly effective [13]. The crosslinking takes place through a radical addition mechanism initiated by UV light as shown in Scheme 1.



Scheme 1: Crosslinking of PPO by UV initiated radical thiol-ene chemistry, where R signifies the network.

Pure and filled PPO networks, with two different types of fillers are prepared as shown in Scheme 1. Particle composites were prepared as the pure PPO network, with addition of the different fillers before mixing and UV crosslinking. The contents of the two fillers in the prepared composites can be seen from Table 1.

Table 1: Compositions prepared and their nomenclatures

Nomenclature	Filler (phr)	
	Fumed silica	core-shell filler
PPO	-	-
PPO_30	30	-
PPO_30_1	30	1
PPO_30_2.5	30	2.5

The non-rubber ingredients (such as filler in this case) are, by accepted convention, expressed by parts per hundred rubber (phr). In this convention the filler amount is taken as the ratio against 100 parts (by weight) of rubber. In all the composites, 10g of PP and 30 phr of fumed silica were kept constant and denoted PPO_30. Core-shell filler (1 and 2.5 phr) was added to PPO_30 for preparing PPO_30_1 and PPO_30_2.5 respectively.

The linear viscoelastic (LVE) properties of pure and composite PPO networks were measured in order to characterize the material response in the low strain (1%) limit. Figure 1 shows the LVE diagrams for the prepared networks.

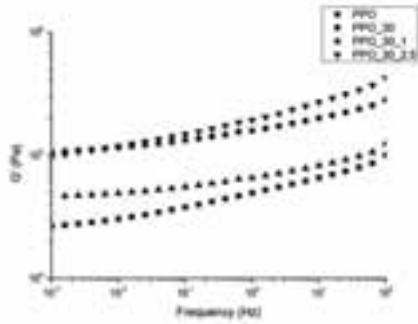


Figure 1: Shear storage modulus versus frequency for pure PPO and filled PPO networks at 23°C

Table 2: LVE data for PPO and filled PPO networks.

Sample Name	Storage modulus (kPa) at 0.001 Hz
PPO	26.5
PPO_30	106.1
PPO_30_1	46.6
PPO_30_2.5	97.4

In table 2 the shear storage moduli values at low frequencies are extracted for comparison. As evident from table 2 the value of the storage modulus (G') at the plateau terminal region (0.001Hz) is approximately 26 kPa for pure PPO which is very low compared to commercially available PDMS elastomers as well as non-filled silicone elastomers[14]. The storage modulus G' for Elastosil RT 625 is reported as 77kPa [3] in very thin films. This clearly indicates that the PPO networks obtained are softer than traditional PDMS. The PPO networks are very sticky but nevertheless their films can be easily handled in a given thickness where a silicone elastomer would be very difficult to handle. On addition of 30 phr fumed silica into the soft PPO network, the storage modulus G' increases to 106kPa due to the hindrance in chain movement imposed by the filler.

From Figure 2(a), a pronounced increase is seen in the dielectric constant of the PPO composites at the low frequencies ($10^1 - 10^2$ Hz) with respect to the pure PPO, which is accompanied by a parallel increase of the dielectric losses (Figure 2b). Such an increase, which shows up as a low frequency dispersion in the dielectric spectra of all the composites, can be ascribed to a Maxwell-Wagner polarization, which is caused by a limited displacement of charges induced by the electric field in correspondence of interfaces between different phases, and which can be indicative of the presence of inter-phases in these systems. Some studies have already revealed that the presence of inter-phases inside a material increases the dielectric permittivity.

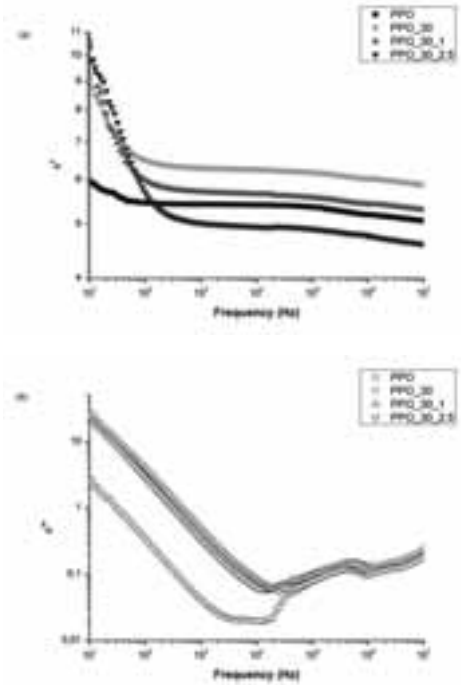


Figure 2: Dielectric spectroscopy plot (a) real part of permittivity versus frequency (b) imaginary part of permittivity versus frequency for PPO and the composites.

For instance, at the interface between matrix and filler in a particulate composite or between two immiscible phases in a polymer blend, there can form intermediate interaction regions provided of their own polarization properties, which can play a major role in determining the final permittivity of the material [15–18]. In our case, such polarization effect is significant due to the presence of interfaces between the PPO matrix and the ceramic fillers. Indeed it is found, as the filler amount is increased, that the interface polarization effect increases due to formation of even higher numbers of interfaces, while no such polarization effect is observed for the pure PPO system. Differently, in the region of the medium-high frequencies ($10^2 - 10^7$ Hz), where the dielectric response mainly depends on the bulk polarization processes [11], the spectra of ϵ' are almost flat for all materials, and we observe only slight variations in the value of the dielectric constant of composites with respect to that of the pure matrix. From Figure 3(a) the relative dielectric constant for pure PPO at 10^4 Hz can be determined to be 5.4, which is about 1.8 times higher than pure or fumed silica reinforced PDMS [3]. Fumed silica is a low dielectric constant material and it is not able to significantly affect the response of the matrix compared to for example lead magnesium niobate-lead titanate [8] or pure titanium

dioxide [7], which instead here is used as SiO₂ encapsulated particles.

Nevertheless, when fumed silica is incorporated into the PPO system, as in PPO_30, the relative permittivity at 10⁴ Hz increases to 6.2. However, on addition of the core-shell filler into the system the relative permittivity drops to 5.6 at 10⁴ Hz for PPO_30_1 and 4.9 for PPO_30_2.5. Concerning the dielectric losses, Figure 2(b) evidences the presence of differences between the pure matrix and its composites only at low frequencies, where the aforementioned interfacial polarization component is active, while at frequencies over 100 kHz all the studied formulations are equally, and slightly, dissipative.

Conclusion

This study reveals the potential of filler reinforced PPO composite as new actuator material. Results from shear rheology show enhancement in the mechanical stability of PPO composites over pure PPO network. Relative permittivity of PPO-fumed silica composite at 10⁴ Hz is observed to be 6.2, which is almost twice as that of commercially available PDMS.

References

- [1] R. Shankar, T. K. Ghosh, R. J. Spontak, *Soft Matter* **2007**, *3*, 1116.
- [2] R. Pelrine, R. Kornbluh, J. Joseph, *Sensors and Actuators A: Physical* **1998**, *64*, 77–85.
- [3] A. L. Skov, A. Bejenariu, J. Bøgelund, M. Benslimane, A. D. Egede, in *Proc. SPIE* (Eds.: A. Lakhtakia, Y. Bar-Cohen, H.A. Sodano, N.C. Goulbourne, V.K. Varadan, M. Tomizuka, A.L. Gyekenyesi, T. Kundu, K. Farinholt, T.E. Matikas, S.F. Griffin, C.-B. Yun, Z. Ounaies, J.P. Lynch), **2012**, p. 83400M–83400M–10.
- [4] S. Vudayagiri, M. D. Junker, A. L. Skov, *Accepted in Polymer Journal* **2012**, *Manuscript*.
- [5] R. Pelrine, R. Kornbluh, J. Joseph, R. Heydt, Q. Pei, S. Chiba, *Materials Science and Engineering: C* **2000**, *11*, 89–100.
- [6] J. D. W. Madden, N. A. Vandesteeg, P. A. Anquetil, P. G. A. Madden, A. Takshi, R. Z. Pytel, S. R. Lafontaine, P. A. Wieringa, I. W. Hunter, *IEEE Journal of Oceanic Engineering* **2004**, *29*, 706–728.
- [7] F. Carpi, D. De Rossi, *IEEE Transactions on Dielectrics and Electrical Insulation* **2005**, *12*, 835–843.
- [8] G. Gallone, F. Carpi, D. De Rossi, G. Levita, A. Marchetti, *Materials Science and Engineering: C* **2007**, *27*, 110–116.
- [9] M. Benslimane, H.-E. Kiil, M. J. Tryson, in *Proc. SPIE* (Eds.: Y. Bar-Cohen, M.N. Ghasemi-Nejhad, Z. Ounaies, V.K. Varadan, M. Tomizuka, K.J. Peters, P.J. Shull, M.B. McMickell, T. Kundu, K.M. Farinholt, A.A. Diaz, W. Ecke, J. Li, H.F. Wu, T.E. Matikas), **2010**, pp. 764231–764231–11.
- [10] M. Y. Benslimane, H.-E. Kiil, M. J. Tryson, *Polymer International* **2010**, *59*, 415–421.
- [11] F. Carpi, G. Gallone, F. Galantini, D. De Rossi, in *Dielectric Elastomers as Electromechanical Transducers* (Eds.: F. Carpi, D. De Rossi, R. Kornbluh, R. Pelrine, P. Sommer-Larsen), Elsevier, Amsterdam, **2008**, pp. 51–68.
- [12] C. E. Hoyle, C. N. Bowman, *Angewandte Chemie (International ed. in English)* **2010**, *49*, 1540–73.
- [13] A. B. Lowe, *Polymer Chemistry* **2010**, *1*, 17.
- [14] A. L. Larsen, K. Hansen, P. Sommer-Larsen, O. Hassager, A. Bach, S. Ndoni, M. Jørgensen, *Macromolecules* **2003**, *36*, 10063–10070.
- [15] M. S. Ozmusul, R. C. Picu, *Polymer Composites* **2002**, *23*, 110–119.
- [16] M. G. Todd, F. G. Shi, *Journal of Applied Physics* **2003**, *94*, 4551.
- [17] M. G. Todd, F. G. Shi, *IEEE Transactions on Dielectrics and Electrical Insulation* **2005**, *12*, 601–611.
- [18] G. Gallone, F. Galantini, F. Carpi, *Polymer International* **2010**, *59*, 400–406.

**Helge Grosch**

Phone: +45 4677 5417
E-mail: hgch@kt.dtu.dk

Supervisors: Alexander Fateev
Sønnik Clausen

PhD Study

Started: December 2011
To be completed: December 2014

On-line Trace Gas Measurement Technique for Biomass Gasification

Abstract

Although concentration of trace gases in the producer gas of biomass gasification is quite low, their on-line analysis plays an important role in process control and optimization. The non-intrusive techniques of FTIR and UV spectrometry are used for this purpose in this project. Spectral absorption databases of the trace gases of interest at different temperatures are built up for both techniques and are used as reference data for trace gas quantification in on-line measurements at different types of gasifiers.

Introduction

Interest in biomass gasification is continuously growing in recent years. In the process of biomass gasification, the raw material is converted into gaseous products including H_2 , CO , CH_4 , CO_2 and others (so-called producer gas). These products can be used for the production of more complex organic chemicals, upgrading to the synthetic gas (primarily CH_4) or as a feeding fuel gas for a range of power plants. This is feasible, since the two-step process (gasification of biomass and combustion of the producer gas) has a higher energy yield than the combustion of the biomass itself [1]. In all applications of the producer gas its quality plays an important role because impurities in the gas may cause several problems like reduced conversion efficiency, pure gas quality and corrosion.

To achieve a high producer gas quality, it is first of all necessary to be able to quantify the gas composition, i.e. concentrations of major and minor gas species. For the gasification process, it is also important to be able to monitor any changes in the producer gas composition in real time, which is why the on-line gas measurements have an important role in process control and optimization. While there are already measurement techniques available to perform on-line gas analysis for the major gas compounds, the focus in this project is laid on the measurement of trace gases components with typical concentrations in the range of few tens of parts per million (ppm).

The scope of the project is, to develop an on-line optical measurement technique for trace gas components important in various gasification processes and prove the technique on gasifiers available at DTU.

In the project, the methods of ultraviolet (UV) and infrared (IR) spectroscopy are used.

Experimental Techniques

Both IR and UV spectroscopy are minimally invasive techniques. Both techniques work according to the principle of gas absorption spectroscopy. This means that each gas component has an individual absorbance structure. The spectral ranges used in this project are 180 nm - 370 nm (UV) and 1400 nm – 10 000 nm (IR).

The challenges of these techniques in this project are: establishing an optical set-up on the gasifier site and the build-up of spectroscopic absorption databases of the important trace gases, which is essential for an accurate analysis of complex experimental data. The databases have to be built up based on measurements with gases of interest on a so-called reference flow gas cell in the laboratory. This set-up of the reference flow gas cell allows the production of various gas mixtures of nitrogen with gases of interest at temperatures up to 525°C. Thus, the reference spectra of the single gases of interest can be measured at different concentrations and temperatures with use of UV and FTIR high-resolution spectrometers. Another challenge in the project is the interference of compounds of large concentrations (e.g. water, CO , tar, particles) with the compounds of interest in the same spectral range. With measurements at high resolution and use of modern data analysis tools, this problem can, in principle, be solved, by identifying single spectral features of the trace gases within of the total spectrum.

Next to the on-line measurements, the already established gas extraction measurements are also

conducted to be able to verify the techniques at the test site.

Results and Discussion

In a first step, the trace gases relevant to gasification process have been identified through literature research and first on-line/gas extraction measurements at the low-temperature circular-fluidized bed (LT-CFB) gasifier.

Important compounds mentioned in the literature are: nitrogen containing (e.g. NH_3 , NO_2 , HCN) [2], sulfur containing (e.g. H_2S , CS_2 and OCS) [3] and aromatic hydrocarbons (e.g. benzene, phenol, naphthalene and higher polyaromatic hydrocarbons) [2]. Other compounds such as Cl-containing (e.g. H_3CCl) are also subject of investigations. These compounds were identified by other (mainly extractive) methods, but their on-line detection is still a challenge. Their appearance in the producer gas depends among others on the process temperature, chemical reactions in the gasifier and the fuel (type of biomass). This means that every type of biomass and gasifier influence the quality of the producer gas and therefore amount of the trace gases.

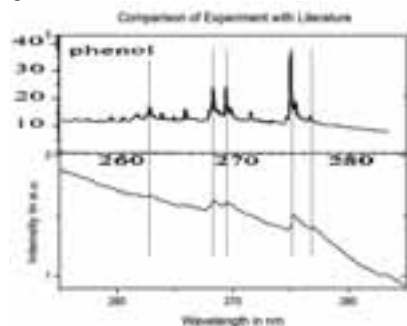


Figure 1: Comparison of the UV absorption cross sections of phenol from Trost et al. [4] (upper graph) and extraction measurements at the LT-CFB (lower graph)

In first experiments at the LT-CFB gasifier the gas extraction measurements showed characteristic fine structures. A comparison between published phenol absorption cross sections from Trost et al. [4] at 20.5°C with the obtained absorption spectra at the LT-CFB gasifier are shown in Fig.1. Since the positions of the major peaks are in agreement, it can be concluded that phenol is present in the producer gas. Nevertheless, the fine structures do not fully agree. The reason for this is that the available data from the literature were obtained at 20.5°C with no interference of other gases and a resolution of 0.11 nm. At measurements at the LT-CFB, the temperature in the gas extraction line was 150°C, the spectral resolution 0.335 nm and other gases were present which gave a slope in the measured absorption spectra. It also needs to be mentioned, that the characteristic structure of phenol absorption only appeared in the gas extraction measurements (which

cooled the gas from approx. 530°C to 150°C) including a dilution with nitrogen. In cross-stack UV absorption measurements no phenol structure has been observed because strong absorption by tar components and temperature.

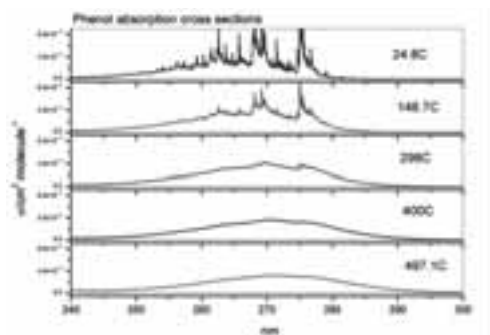


Figure 2: UV phenol absorption cross sections 0,019 nm at various temperatures.

Since the fine structure is changing with the temperature, it is necessary to compare these results with results from the laboratory. Therefore, reference measurements at different temperatures were conducted, see Fig. 2. With these data it is possible to derive the concentration of phenol.

Conclusion and Future Goals

It can be concluded, that the first measurements at the LT-CFB gasifier were successful and a database for the UV spectrometry is built up. In the case of the on-line measurements, first experience and results have been gained. But still many challenges have to be mastered.

In the future, IR spectral database gases of interest will also be created. These databases for IR and UV spectrometry will be used in the experiments with the LT-CFB gasifier as well as a two stage gasifier called VIKING. In the case of the two stage gasifier, different compounds, e.g. naphthalene, are in the focus.

Acknowledgements

Project acknowledgments to Energinet.dk Project Nr. 2011-1-10622.

References

1. P. Basu, Biomass Gasification and Pyrolysis, Academic Press, Burlington USA, p. 22
2. P. Ståhlberg, M. Lappi, E. Kurkela, P. Simell, P. Oesch, M. Nieminen, Sampling of contaminants from product gases of biomass gasifiers, Research Notes 1903, VTT Energy, 1998
3. R. Ma, R. M. Felder, J. K. Ferrell, Ind. & Eng. Chem. Res., 28 (1) (1989) 27-33
4. B. Trost, J. Stutz, U. Platt, Atmo. Environ. 31 (23) (1997) 3999-4008



Yao Guo

Phone: +45 4525 2935
E-mail: yg@kt.dtu.dk

Supervisors: Jørn Dalgaard Mikkelsen
Carsten Jers

PhD Study
Started: August 2010
To be completed: December 2013

Enzymatic Production of Human Milk Oligosaccharides

Abstract

Human milk oligosaccharides (HMOs) are complex glycans that are present at high amounts in breast milk. The structural complexity of HMOs confers unique benefits on human health ^[1], e.g. protection of infants against infections and diarrhea. Only trace amounts of these oligosaccharides are present in bovine milk-based infant formula. In order to produce genuine HMOs, this project explores a sustainable way to develop an enzymatic process capable of converting certain kinds of food materials into the desired products.

Introduction

Human milk is usually the sole nutrition source for the first few months of human life. Not only does it contain the essential nutrients for the infants to grow and thrive, but also it provides health benefits beyond traditional nutrients. These distinctive benefits, e.g. serving as prebiotics to nourish desirable bacteria in the human intestines ^[1], protection of infants against infections and diarrhea ^[2], are attributed to human milk oligosaccharides (HMOs). HMOs are the third largest component in human milk after lactose and lipid. The building blocks of HMOs are D-glucose, D-galactose, N-acetylglucosamine, fucose and sialic acid (Figure 1).

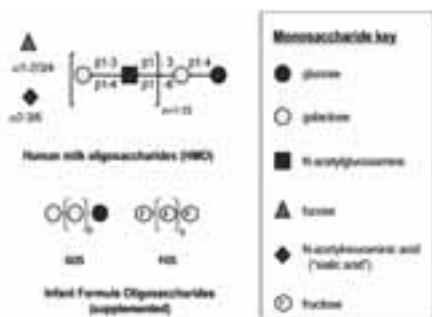
more complex structures of HMOs, lactose is elongated with N-acetylglucosamine repeat units (polyglucosamine). Lactose and polyglucosamine backbone could be further sialylated or fucosylated in varied linkages. Hence, HMOs differ in molecular weight and structure. Approximately 200 distinct oligosaccharides have been identified in human milk ^[3]. The beneficial effects of HMOs depend on specific oligosaccharide structures, which include prebiotic, anti-adhesive, glycome modifying and immunomodulatory effects as well as brain development.

Specific Objective

The beneficial effects of HMOs have led to attempts to mimic these using inexpensive alternatives such as galactooligosaccharides (GOS), fructooligosaccharides (FOS), and inulin. While they possibly have prebiotic effects, the fact that many of the traits of HMOs are structure-specific renders them unlikely to effectively mimic HMOs. In this project we aim to develop an enzymatic process for production of some of the key HMOs for supplementation of infant formula. The specific objective of the present PhD study is to develop novel food grade enzymes capable of generating HMOs from side-streams in the agricultural and food industries.

Figure 1: Structural composition of human milk and infant-formula oligosaccharides

Lactose forms the reducing end of HMOs, in which galactose could be sialylated or fucosylated to form sialyllactose or fucosyllactose, respectively. These trisaccharides constitute the short chain HMOs. To form



The research focuses on identification of enzymes with desired properties by screening of fungal collections (Figure 2) as well as bioinformatics approaches. Identified enzymes will be further optimized via molecular evolution and then investigated for their applicability in biosynthesis of HMOs. By

using several food materials as substrates, desired oligosaccharides will be produced in a reactor.

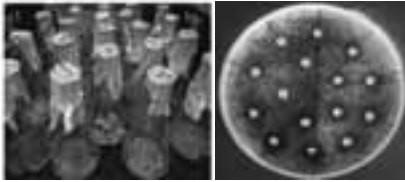


Figure 2: Diversity screening of interesting enzymes from fungal strains

References

1. Gyögy P, Norris RF, Rose CS. Archives of biochemistry and biophysics. 1954, 48: 193–201.
2. Ruiz-Palacios GM, Cervantes LE, Ramos P, et al. Journal of Biological Chemistry. 2003, 278: 14112–14120.
3. Lars Bode. Nutrition Reviews. 2009, 67 (Suppl.2): S183–S191.



Jon Trifol Guzmán

Phone: +45 4525 6196
E-mail: jotg@kt.dtu.dk

Supervisors: Peter Szabo
Ole Hassager
Anders Egede Daugaard

PhD Study

Started: October 2012
To be completed: November 2015

Novel Clay/Nanocellulose Biocomposite Films and Coatings in the Context of New Packaging Materials

Abstract

During recent years several efforts have been made into bio-based and renewable resources. Among all the resources the packaging and more specifically the packaging for food application has started to awake the interest of the scientific community. Now the biopolymers are far away from being useful for this application due to the lack of right technical properties, such as mechanical properties and barrier properties but the addition of novel nanoreinforcements as nanocellulose, cellulose nanofibers or whiskers, organically modified layered silicates or other kind of nanoreinforcements could enhance the properties of the biopolymer enough to have the right technical parameter for this application.

Introduction

The use of petrol-based products for packaging applications represents a serious global environmental problem, not only from the point of view of the raw material but also due to the lack of biodegradability of the most part of the petrol-based products. In recent years novel bio-based materials have been exploited to develop edible and biodegradable materials.

However, the use of edible and biodegradable polymers as PLA has been limited because of problems related to material performance (such as brittleness, poor gas and moisture barrier), processing (such as low heat distortion temperature) and costⁱ but the addition of some nanoreinforcements as nanocelluloseⁱⁱ, nanoclaysⁱⁱⁱ and others^{iv} could enhance enough the biomaterials properties for these applications. Nowadays a big effort is being made into the field of the reinforced composites for food packaging applications^v

During recent years several researches into cellulose nanofibers reinforced polymers has been done^{vi}. There are several publications reporting the influence of the nanocellulose into the mechanical properties of the polymers^{vii},^{viii} but apart from the mechanical properties an improvement on barrier properties has been reported^{ix}. There is not a uniformity of results in cellulose nanofibers based composites since there are several factors which can affect the result of the

composites: a) the aspect ratio and nature of the cellulose nanofiber, b) the compatibility, dispersion and load of the reinforcing agent and c) the nature of the matrix, among others.

The first nanoclay composite was obtained by Toyota in 1993^x but improvement in nanocomposite properties has not been reported until 2002^{xi}. The addition of small amounts of nanoclays in the polymeric matrix has been reported to improve some properties^{xii} as the barrier properties (up to 60%^{xiii}), mechanical properties^{xiv} especially at low clay loading and also gives fire retardant behavior^{xi}. The barrier properties especially for oxygen are key parameters to develop edible films for food packaging applications since the permeability to oxygen is related to the shelf life of the food.

Recently novel nanoclay/nanofibers nanopapers have been developed which are reported to have great mechanical and gas barrier properties^{xv}. This material has been reported to have fire retardant effect^{xvi}.

Specific Objectives

The research will be focused on the development of nanoclay/nanofiber reinforced films for food packaging applications. The cellulose nanofibers could enhance the mechanical properties of the films meanwhile the nanoclays could improve the barrier properties.

Conclusions

Although nowadays the use of biopolymers for food packaging applications has some difficulties for some technical parameters, the addition of nanofillers can enhance the properties of these bio based materials enough to be able to be used in this application.

Acknowledgements

The author wants to thank the Marie Curie Initial Training Network for funding the research. The PhD fellow is very grateful to Professor Iñaki Mondragón Egaña whom dedication to science during his life is an example for everybody.

-
- ⁱ Madhavan Nampoothiri, K., Nair, N. R., & John, R. P. (2010). An overview of the recent developments in polylactide (PLA) research. *Bioresource technology*, 101(22), 8493–501. doi:10.1016/j.biortech.2010.05.092
- ⁱⁱ Eichhorn, S. J., Dufresne, a., Aranguren, M., Marcovich, N. E., Capadona, J. R., Rowan, S. J., Weder, C., et al. (2009). Review: current international research into cellulose nanofibres and nanocomposites. *Journal of Materials Science* (Vol. 45, pp. 1–33). doi:10.1007/s10853-009-3874-0
- ⁱⁱⁱ Sinha Ray, S., & Okamoto, M. (2003). Polymer/layered silicate nanocomposites: a review from preparation to processing. *Progress in Polymer Science*, 28(11), 1539–1641. doi:10.1016/j.progpolymsci.2003.08.002
- ^{iv} Aider, M. (2010). Chitosan application for active bio-based films production and potential in the food industry: Review. *LWT - Food Science and Technology*, 43(6), 837–842. doi:10.1016/j.lwt.2010.01.021
- ^v Azeredo, H. M. C. D. (2009). Nanocomposites for food packaging applications. *Food Research International*, 42(9), 1240–1253. doi:10.1016/j.foodres.2009.03.019
- ^{vi} Abdul Khalil, H. P. S., Bhat, a. H., & Ireana Yusra, a. F. (2012). Green composites from sustainable cellulose nanofibrils: A review. *Carbohydrate Polymers*, 87(2), 963–979. doi:10.1016/j.carbpol.2011.08.078
- ^{vii} Kowalczyk, M., Piorkowska, E., Kulpinski, P., & Pracella, M. (2011). Mechanical and thermal properties of PLA composites with cellulose nanofibers and standard size fibers. *Composites Part A: Applied Science and Manufacturing*, 42(10), 1509–1514. doi:10.1016/j.compositesa.2011.07.003
- ^{viii} Liu, D. Y. (2009). Characterisation of solution cast cellulose nanofibre - reinforced poly(lactic acid). *eXPRESS Polymer Letters*, 4(1), 26–31. doi:10.3144/expresspolymlett.2010.5
- ^{ix} Lavoine, N., Desloges, I., Dufresne, A., & Bras, J. (2012). Microfibrillated cellulose - its barrier properties and applications in cellulosic materials: a review. *Carbohydrate polymers*, 90(2), 735–64. doi:10.1016/j.carbpol.2012.05.026
- ^x Kojima, Y., Usuki, A., Kawasumi, M., Okada, A., Kurauchi, T. and Kamigaito, O. (1993), One-pot synthesis of nylon 6–clay hybrid. *J. Polym. Sci. A Polym. Chem.*, 31: 1755–1758. doi: 10.1002/pola.1993.080310714
- ^{xi} Sinha Ray, S., Maiti, P., Okamoto, M., Yamada, K., & Ueda, K. (2002). New Poly(lactide)/Layered Silicate Nanocomposites. 1. Preparation, Characterization, and Properties. *Macromolecules*, 35(8), 3104–3110. doi:10.1021/ma011613e
- ^{xii} Alexandre, M., & Dubois, P. (2000). Polymer-layered silicate nanocomposites: preparation, properties and uses of a new class of materials, 28(March), 1–63.
- ^{xiii} Svagan, A. J., Åkesson, A., Cárdenas, M., Bulut, S., Knudsen, J. C., Risbo, J., & Plackett, D. (2012). Transparent films based on PLA and montmorillonite with tunable oxygen barrier properties. *Biomacromolecules*, 13(2), 397–405. doi:10.1021/bm201438m
- ^{xiv} Sengupta, R., Chakraborty, S., Bandyopadhyay, S., Dasgupta, S., Mukhopadhyay, R., Auddy, K., & Deuri, A. S. (2007). A Short Review on Rubber / Clay Nanocomposites With Emphasis on Mechanical Properties, 21–25. doi:10.1002/pen
- ^{xv} Wu, C.-N., Saito, T., Fujisawa, S., Fukuzumi, H., & Isogai, A. (2012). Ultrastrong and high gas-barrier nanocellulose/clay-layered composites. *Biomacromolecules*, 13(6), 1927–32. doi:10.1021/bm300465d
- ^{xvi} Liu, A., Walther, A., Ikkala, O., Belova, L., & Berglund, L. a. (2011). Clay nanopaper with tough cellulose nanofiber matrix for fire retardancy and gas barrier functions. *Biomacromolecules*, 12(3), 633–41. doi:10.1021/bm101296z

**Amalia Halim**

Phone: +45 4525 2892
E-mail: amah@kt.dtu.dk

Supervisors: Alexander Shapiro
Anna E. Lantz, DTU Systems Biology
Sidsel M. Nielsen

PhD Study

Started: February 2012
To be completed: January 2015

Microbial Enhanced Oil Recovery for North Sea Oil Reservoir

Abstract

Some microorganisms living in petroleum reservoirs produce substances like gases, surfactants, polymers and/or acids, facilitating enhanced oil recovery (EOR). Therefore, selective stimulation of certain microbial species may be an inexpensive method for additional oil recovery. In addition, microbes can selectively plug reservoir formation, thus divert the flow of the injected water into regions of the reservoir with low permeability-high oil saturations. However, plugging effect by bacteria may also cause reduction in reservoir formation permeability. The first experimental study focused on bacteria penetration in core plug samples to understand how deep bacteria can travel through porous media and the effect of bacterial plugging.

Introduction

It was credited to Beckman in 1926, who found that microorganism could be used to release oil from porous media[1]. Numerous mechanisms have been proposed in the literature through which microorganism can be used for enhanced oil recovery process[1]. However, the mechanism are poorly understood and the effectiveness of each mechanism for different reservoir parameters is also unknown[2, 3]. Recent publications on the bacteria-fluid-porous media interaction classified the mechanisms into two broad categories: 1) alteration of oil/water/rock interfacial properties and/or wettability[2-5], 2) changes in flow behavior due to bioclogging or selective plugging[2-4, 6]. The initial study focused on bacteria penetration as the North Sea chalk reservoir formation has relatively small size of pore throats, which is almost comparable with the bacteria cell size. The plugging effect caused by bacteria is also investigated by monitoring the pressure during bacteria injection.

Specific Objectives

The main goal of the project is to understand the factors that influence the growth, propagation, and movement of bacteria within porous formations; and how this may aid in improving oil production.

The preliminary test focused on core flooding experiment to investigate whether bacteria can pass through the porous media and the mechanism of the bacteria movement within porous media. Two bacteria species, *Bacillus licheniformis* 421 and *Pseudomonas*

putida K12, representing spore forming and non-spore forming bacteria, were used for this purpose.

Experimental Work

Each individual core was then cleaned by flooding with toluene and absolute ethanol to remove any organic material inside the core. After cleaning, the core was dried in the oven at 80°C overnight. The dry weight and wet weight were measured in an analytical balance to calculate core porosity. The dry core was assembled in sterile Hassler core holder. Approximately 7 pore volumes (PV) of 75% ethanol were injected in order to sterilize the core plug. The saturated 75% ethanol core was left overnight inside the core holder. The core was then flooded with sterile 7PV MQ water to displace the 75% ethanol and the effluent was collected every PV to cross check for possible contamination. Injection pressure and pressure difference were monitored throughout this process. The recorded pressure difference during MQ flooding was used to calculate initial permeability using Darcy's Law. The core was injected with bacteria inoculum in synthetic seawater (SS) media. Various bacteria concentrations were tested to see the plugging effect of the bacteria. The effluent was collected every PV for bacteria enumeration. An illustration of core flooding experiment is depicted in figure 1

Inoculum preparation and bacteria enumeration

The bacteria inoculum were grown in the enrichment media for 24 hours then diluted with 0.85% NaCl. The optical density (OD) of the bacteria solution was

adjusted to the desired value at the wave length 600nm using a spectrophotometer. Approximately 10% (v/v) bacteria solution was inoculated into SS media for core flooding experiment. The bacteria and SS media were

homogenized by a vortex for 3 minutes. Bacteria enumeration was conducted by serial dilution plate method using enrichment media.

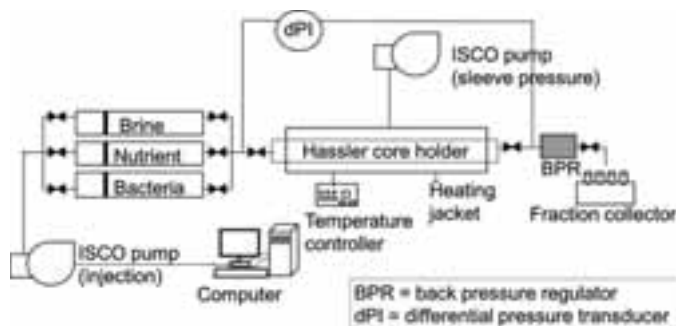


Figure 1. Core flooding experiment

Result and Discussion

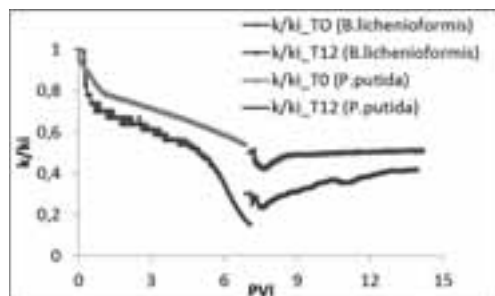


Figure 2. Permeability changes by *B. licheniformis* 421 *B. licheniformis* 421 and *P.putida* during injection and after 12 days of incubation (normalized permeability)

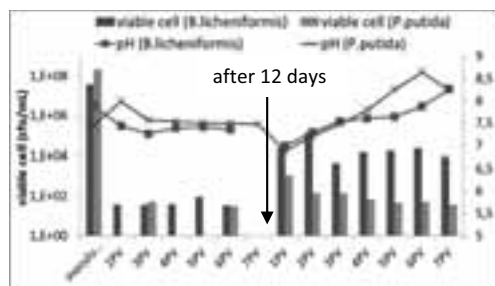


Figure 3. Viable *B. licheniformis* 421 and *P.putida* cells detected on the effluent during injection and after 12 days of incubation

In figure 2, the core permeability is expressed as core permeability at given time during injection (k) divided by initial permeability (k_i). Core permeability is damaged continuously when bacterial population is injected for both spore forming and non-spore forming bacteria. After 12 days of incubation (starvation), permeability does not return to initial condition (k_i),

even after the bacterial population is flushed by approximately 7PV of brine. The permeability is stabilized at a constant level (ca. 0.5 of k_i for spore forming bacteria and ca. 0.6 of k_i for spore forming bacteria). The plate count method (figure 3) revealed that fewer viable cells of the non-spore forming bacteria were detected in the effluent compared to spore forming bacteria, even when the inoculum concentration of the non-spore forming bacteria was higher. This may indicate that survival/motion of bacteria can be mainly due to spores formations.

Conclusion

Bacteria cell and/or other substances (eg: extra polymeric substances/EPS) damaged the porous medium and caused constant reduction of permeability. The spore forming bacteria have a bigger chance for survival compared to non-spore forming bacteria. In addition, a stable colony may have formed during the incubation period. When the core is flushed by injecting brine after the incubation period, the bacteria cells continue to exist (but not grow), thus the permeability did not return to initial condition.

References

- Lazar, I., I.G. Petrisor, and T.F. Yen, Petroleum Science and Technology, 25 (2007) 1353-1366.
- Kowalewski, E., et al., Journal of Petroleum Science and Engineering, 52 (2006) 275-286.
- Armstrong, R.T. and D. Wildenschild, Transport in Porous Media, 92 (3) (2012) 818-835.
- Afrapoli, M.S., et al., Journal of Petroleum Science and Engineering, 69 (2009) 255-260.
- Karimi, M., et al., Colloids and Surfaces B: Biointerfaces, 95 (2012) 129-136.
- Afrapoli, M.S., S. Alipour, and O. Torsaeter, Transport in Porous Media, 90 (2011) 949-964.



Stine Broholm Hansen

Phone: +45 4525 2846

E-mail: sha@kt.dtu.dk

Supervisors: Peter Glarborg
Peter Arendt Jensen,
Flemming Frandsen
Bo Sander, DONG Energy

PhD Study

Started: January 2010

To be completed: August 2014

Deposition Build-Up in Grate and Suspension Boilers Firing Biomass

Abstract

In the short term, the most promising way to reduce the CO₂ emission from heat and power production is to replace fossil fuels with renewable fuels such as biomass and waste. However, compared with fossil fuels, biomass and waste are difficult to handle in terms of pre-treatment, boiler operation, and solid residues. In particular, the content of inorganic species such as S, Cl and K are a concern due to enhanced propensity for deposition and corrosion. The objective of this project is to develop an engineering model that predicts the rate of deposit build-up and shedding during full-scale suspension firing of wood and/or straw. The model will be validated against full-scale experimental data, which have been reviewed as part of the project.

Introduction

To reduce CO₂ emissions and reduce the dependency of fossil resources, the use of biomass for power production is increased in Danish power plants. Utilization of biomass for power production do often increase the rate of formation of ash deposits, which are difficult to remove especially in the boiler chamber and on superheater coil surfaces compared to those formed during coal firing [1]. To support the development of biomass combustion equipment, deposit probe measurements have been performed in the last 20 years on many of the biomass fired power plant boilers in Denmark [2-16].

The objective of this project is to develop an engineering model that predicts the rate of deposit build-up and shedding. The input to the model should be the local flue gas concentration, the flue gas chemistry, the particle size distribution and chemistry of the fly ash particles and local temperatures. The project is limited to deposit build-up and shedding during suspension firing of biodust. The model will be validated against the experimental data from the full-scale probe measurements of deposit build-up biodust suspension firing. These experimental data has as part of the project been reviewed and compared to the data obtained during grate-firing. This was done in order to determine similarities and differences in the deposition behaviors of the two firing technologies and to gain an idea of the influences of fuel type and boiler operation conditions on the deposition and shedding rates and the deposits chemistry.

Discipline

Reaction and Transport Engineering

Experiments Performed In Denmark

The experiments reviewed in this study have been conducted at several Danish CHP plants, both grate [2-8] and suspension fired [9-16]. In the investigated grate fired units, straw is the primary fuel. The straw is fed to the boiler on a grate on which the combustion takes place. Primary combustion air passes through the grate, and the temperature in the fuel-bed on the grate is typically in the range 1000-1200 °C [17]. From the grate, only a small fraction of the ash (typically < 20 wt%) is entrained with the flue gas [18].

In biomass suspension-fired units, both wood and straw pellets have been utilized as fuels. The fuel is milled to obtain small particle sizes (< 2 mm) before entering the furnace together with the preheated primary combustion air. The combustion then takes place in suspension, at temperatures up to 1600 °C [17]. A small fraction of the fuel ash particles may end up in the bottom ash, while most of the fly ash particles will be transported through the furnace with the flue gas [17].

The data set from the full scale measuring campaigns include quantification of the rate of deposit formation, chemical analyses of fuels, ash and deposits [2-16], and in a few cases corrosion studies [3] and shedding observations [6,8,14,16]. A few mature deposits collected on super heater tubes in grate boilers was also studied [4,5].

Both simple probes, as well as more advanced probes have been applied in the conducted experiments. When using the simple probe, the deposits mass is determined by extracting the probe after each experiment and subsequently remove the deposits for weighing and analysis [2,4]. The more advanced probe, used in later studies, provides the possibility of online quantification of mass and heat uptake along with measurement of the flue gas temperature. The deposit formation and shedding can be observed by a video camera [5,6,13,15,16].

Rates of Deposit Build-up

Two definitions of the rate of deposit formation [$\text{g}/\text{m}^2/\text{h}$] have been employed; (i) the Integrated Deposit Formation rate (IDF-rate) and (ii) the Derivative-based Deposit Formation rate (DDF-rate) [13].

The IDF-rate, which is the only measure available from the simple probe, is determined by determining the deposit mass on the probe, at a given time after the probe is introduced to the boiler. The deposit mass is then divided by the probe surface area and the total exposure time, and the rate [$\text{g}/\text{m}^2/\text{h}$] is determined.

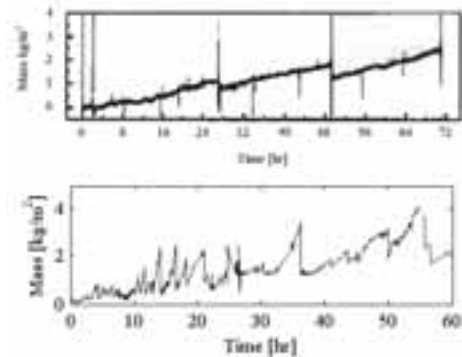


Figure 1: Deposit mass uptake signal from advanced probe in grate firing of straw (upper figure) and suspension firing of straw/wood (lower figure). Flue gas temperature $\approx 800\text{ }^\circ\text{C}$ in both cases [8,13].

In Figure 1, the deposit mass buildup on the advanced probe as function of time is seen for a grate-firing case and a suspension firing case. It is seen that the method of determining the IDF rate can be termed adequate for the grate firing gases, as the rate of deposit buildup seem stable. However, determining an IDF-rate from the probe signals obtained during suspension firing may be a quite difficult task due to fluctuations in the signal. However, within the first hours of the experiments the fluctuations are small and a representative IDF-rate may be estimated. In order to describe the deposit buildup in suspension firing in a more representative manner, the DDF-rate has been introduced by Bashir et al. [13]. The DDF-rate describes the deposit buildup rate between major shedding events and can be obtained by monitoring the mass uptake signal from the advanced probe. The DDF-rate has been

employed in recent studies on suspension firing [13,15,16].

Deposition Rates in Grate and Suspension boilers

The rates of deposit buildup have been compared for the two combustion systems. For comparison sake, the IDF-rates are used for both systems. Thus, for suspension firing, estimated IDF-rates as reported by the authors are employed. It is found that the IDF-rate levels for grate and suspension fired units are comparable, as most IDF-rates are in the range $0\text{-}100\text{ g}/\text{m}^2/\text{h}$ for both technologies. This is not an obvious result since during grate firing only up to 20 wt% ash is entrained while 80-90 wt% of the ash is expected to end up in the fly ash during suspension firing [18].

In order compare the deposit buildup for different fuel and combustion systems an ash propensity has been calculated. The ash propensity is defined as the percentage of total ash flux which deposits on the probe. It is found that for grate fired units up to 6 % of the entrained ash may deposit on the probe, while for suspension fired units only up to 0.6 % is deposited. The difference in the ash propensities of the two combustion systems may be explained by differences in the chemical composition of the fly ashes.

In Figure 2, fuel and fly ash compositions (of the 5 major elements) are compared for each of the two firing technologies, to gain an idea on how the ash transformations occur in or near the combustion zones.

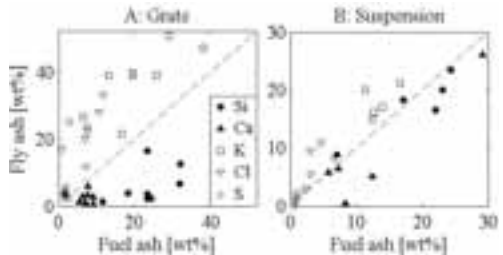


Figure 2: Fly ash composition vs. fuel ash composition. Points on or near the diagonal line indicate that the fuel and fly ash compositions are similar. A: Grate, straw [2,7]. B: Suspension, straw/wood mixtures [9,12,13]

It is seen in Figure 2 that for grate-firing, the fly ash is rich in K, Cl and S and depleted of Si and Ca compared to the fuel ash. This is contrary to suspension-firing, where the fly ash to a large extent resembles the fuel ash, as seen by the distribution of points close to the diagonal line. Only a slight enrichment of K, Cl and S is found in this combustion system. The differences of the chemical composition results in different melting behaviors and thereby stickiness of the fly ash particles as well as of the formed deposits.

The differences in ash deposition propensity may also be caused by the physical form of the fly ashes. In grate fired units, K and Cl dominate the fly ash composition and is expected to appear as KCl vapors or aerosols, which will easily stick to heat transfer surfaces. In suspension fired units K and Si dominates

and are mainly found as solid or possibly molten K-silicates [1].

The influence of flue gas temperature and fuel composition has been examined for both grate and suspension firing. In both systems, it is found that an increased deposition rate can be expected when the flue gas temperature is increased. See Figure 3.

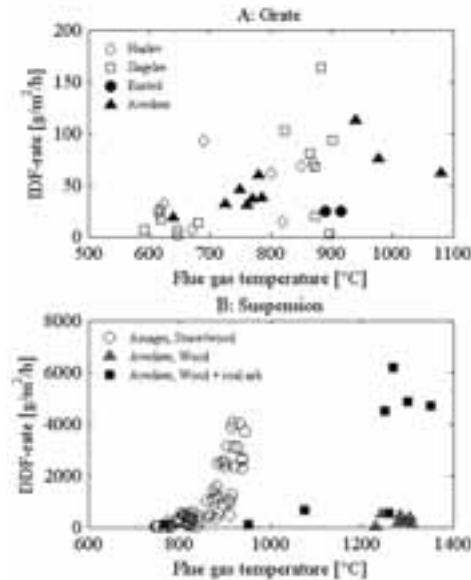


Figure 3: Rates of deposit build-up on probes in A: grate fired boilers (IDF-rates) and B: suspension fired boilers (DDF-rates)

The scattering of the data in Figure 3A for grate fired units is to some extent explained by variations in fuel composition. It is found that increases in the fuel ash K-content also leads to an increased deposition rate.

For suspension fired units, the deposition rate increases with straw share in straw/wood mixtures. Experiments with pure wood or low contents of straw all leads to low DDF-rates.

Modeling Deposit buildup

With respect to the modeling of deposit build-up, several mechanisms contribute to the formation and growth of a deposit layer. These mechanisms are illustrated in Figure 4. These mechanisms have been described and modeled for deposition on a probe in a full scale straw-fired grate boiler [20]. Although differences in combustion conditions and ash properties have been observed between grate and suspension firing of biomass the modeling approach used in ref [20] is expected to be applicable to the conditions in a suspension fired boiler. The different rates of deposition found in suspension firing are expected to be described by the model with adequate description of the input parameters (temperatures and particle sizes, concentrations and chemistry)

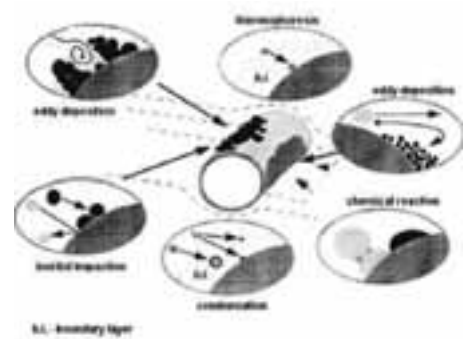


Figure 4: Mechanisms that control deposition and maturation of ash deposits [19].

Deposits Chemistry

In Figure 5, typical examples of the chemical composition of deposits formed on probes near super heater tubes can be seen for three firing cases. Comparing the compositions of deposits formed in straw firing in grate (Figure 5A) and suspension (Figure 5B), it is seen that the fuel compositions of the two straws were similar. The compositions of the deposits formed in the two cases of straw combustion were however different, as the deposits from suspension firing contains more Ca and Si and less K than the deposits from grate firing. This is as could be expected based on the fly ash chemistry examined previously.

Two cases of suspension firing are seen in Figure 5B and Figure 5C; with straw and with wood as fuel, respectively. It is seen that wood contains more Ca and less Si and Cl than straw. These differences are also found in the compositions of the deposits. The deposit

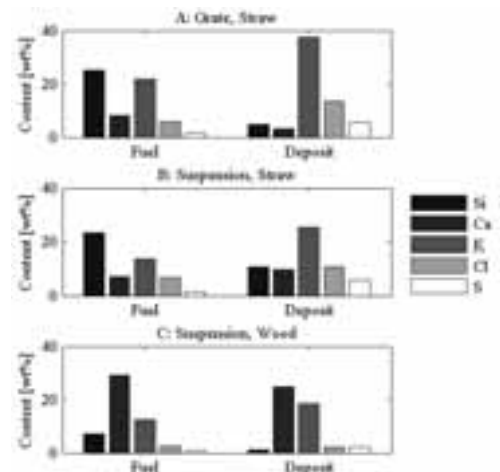


Figure 5: Typical compositions of fuels and deposits collected near superheaters in three firing cases. A: Straw in grate-firing [2]. B: Straw in suspension firing [12]. C: Wood in suspension firing [9]

structure obtained during wood firing may be different from that obtained during straw firing, depending on temperature. For wood-firing in suspension, deposits have been collected at flue gas temperatures 800 and 1300 °C. The deposits obtained at 1300 °C were dominated by Si, Ca and K, while S appears. At 800 °C the deposits were composed of mainly K and Ca, but also Cl and S appears (similar to Figure 5C) [16].

Shedding

Once the deposits are formed on a heat transfer or probe surface physical and chemical transformations may occur within the deposit, depending on temperature, chemistry and structure of the deposit [19]. These internal changes are important for the strength and the melting behavior of the deposit and thereby on the mechanism of deposit removal. The strength of the deposit is to some extent determined by the degree of sintering. Sintering is a solidification process serving to consolidate the individual ash particles [19]. Table 1 summarizes various shedding mechanisms and the types of deposit for which they occur.

Table 1: Occurrence of the deposit removal mechanism depending on the type of deposit. Adapted from [19]

Mechanism	Deposit type			
	Powdery	Lightly Sintered	Heavily sintered	Liquid Slag
Erosion	++	+	-	-
Gravity Shedding	++	+	-	-
Melting	-	-	-	++
Thermal Shock	-	+	++	-
Mechanical shock	++	++	+	-

Shedding behavior has been studied in three cases of biomass combustion; (i) straw fired grate boiler (iii) suspension firing of straw/wood and (iv) suspension firing of wood.

It is observed that in straw fired grate boilers, the flue gas temperature largely determines the type of shedding occurring as shedding by melting is observed at high flue gas temperatures (>1100 °C) [8]. At lower temperatures the removability of the deposits is influenced by the probe surface temperature and the exposure time. Increasing the probe temperature and/or the exposure time will lead to stronger deposits [6].

For suspension fired units firing, shedding by debonding seems to be the primary deposition mechanism at high temperatures, both for straw/wood mixtures (up to 1000°C) [14] and pure wood as fuel (up to 1300°C) [16]. At lower flue gas temperatures around 800°C, two different observations are made. In the case of straw/wood mixtures as fuel, shedding by debonding is observed [14]. When pure wood is fired in a different boiler a steady deposit mass is obtained on the probe. Shedding by debonding does not seem to occur in this case [16]. Whether this difference in shedding behavior at the low temperatures is caused by the chemical differences of the deposits or by operational parameters of the two boilers is unknown at this point. From the

shedding studies, it seems that both fuel composition and operational parameters, especially temperature, are important parameters in the shedding behavior of deposits.

With respect to models of sintering and shedding by de-bonding, only scarce data are available [19] and this will be a major challenge in the project.

Acknowledgement

The PhD study is part of the GREEN research center (Power Generation from Renewable Energy) funded by the Danish Strategic Research Center. The PhD study is co-funded by the MP2T Graduate School and by DONG Energy Power.

References

1. Bryers R.W. Prog. Energy Combust. Sci. 22 (1996) 29-120.
2. Jensen P.A. et al. Energy Fuels 11 (1997) 1048-55.
3. Michelsen H.P. et al. Fuel Proc. Techn. 54 (1998) 95-108.
4. Hansen L.A. et al. Fuel Proc. Techn. 64 (2000) 189-209.
5. Jensen, P.A. et al. Energy Fuels 18 (2004) 378-84.
6. Jensen P.A. et al. Final Report - Ash Deposit Formation and Removal in Biomass-fired Boilers. Fundamental Data Provided with Deposit Probes. Energinet.dk PSO-4106 (CHEC R0603) (2006).
7. Hansen J. et al. Deposit probe measurements in the Avedøre and Ensted straw fired grate boilers. CHEC Report R0705 (PSO 4792) (2007).
8. Zbogor A. et al. Energy Fuels 20 (2006) 512-19
9. Skrifvars B.-J. et al. Fuel 83 (2004) 1371-1379
10. Tobiasen L. et al. Fuel Proc. Techn. 88 (2007) 1108-17.
11. Jensen P.A. et al. Measurements on the 800 MW_{th} Avedøre oil, gas and wood co-fired suspension boiler - Analysis of emission, burnout, deposit and FTIR measurements from April 2005. Energinet.dk PSO 6526 (Appendix E) (2008)
12. Bashir M.S. et al. Fuel Proc. Tech. 97 (2012) 93-106
13. Bashir M.S. et al. Energy Fuels 26 (2012) 2317-30
14. Bashir M.S. et al. Energy Fuels *submitted* (2012)
15. Bashir M.S. Characterization and Quantification of Deposit Build-up and Removal in Straw Suspension-Fired Boilers. PhD Thesis, Technical University of Denmark, 2012.
16. Wu H.; et al. Full-scale deposition measurements at Avedøre Power Plant unit 2 during suspension-firing of wood with and without coal ash addition. CHEC Report, 2012.
17. Van Loo S (ed). The Handbook of Biomass Combustion and Co-firing. Earthscan (2008)
18. Nielsen H.P. Deposition and High-Temperature Corrosion in Biomass-Fired Boilers. Ph.D. Thesis, Technical University of Denmark, 1998
19. Zbogor A et al. Prog Energy Combust. Sci 35 (2009) 31-56
20. Zhou H et al. Fuel 86 (2009) 1519-33



Naweed Al-Haque

Phone: +45 4525 2990

E-mail: nah@kt.dtu.dk

Supervisors: John M. Woodley

Rafiqul Gani

Par Tufvesson

PhD Study

Started: November 2009

To be completed: December 2012

Integrating resins in enzymatic processes

Abstract

Mild operating conditions with high regio and stereo selectivity present biocatalysis as an attractive alternative for integrating it into chemical synthesis. However, in some cases, the activity of the biocatalyst is compromised at industrial relevant substrate and product concentrations. Using porous solid resins as a reservoir for substrate and product is an innovative option for integrating *in-situ* substrate feeding and product removal. A framework is developed in this project for guiding the integration of resin by both mathematical and heuristic approach.

Introduction

For many processes in the chemical and pharmaceutical industries, the easiest means for chemical production by using the conventional chemical synthetic route. However with the development of biocatalysts, greener technologies have become more accessible to industry. Biocatalysis has become increasingly common in all industrial sectors such as chemicals, fuels, food and pharmaceuticals [1]. The obvious advantage of this technology is selectivity which is necessary to obtain a high yield of a specific product. The other advantages of operating in benign operating conditions make it an alternative worth investigating. However in bioprocesses, especially in bioconversions, the substrate and the product may inhibit or damage the biological catalyst or interfere with other components in the reaction medium above a critical concentration [2]. This limitation can be overcome with methods such as slow release of substrates combined with *in-situ* product removal (ISPR) using porous resin [3].

This innovative technology will behave such that the resin will act as a 'reservoir' for the substrate and the product. The substrate via mass transfer will diffuse into the solution. The slow release will maintain the aqueous concentration to be below the inhibition level. The biocatalyst will react with the substrate(s) producing the required product(s). Subsequently the product will be recovered by means of ISPR. At the end of the reaction, the product is eluted to give a high concentration solution [4]. Such an approach will be investigated in this project. This therefore represents an innovative way of process integration.

Figure 1 illustrates the general scheme for this process.

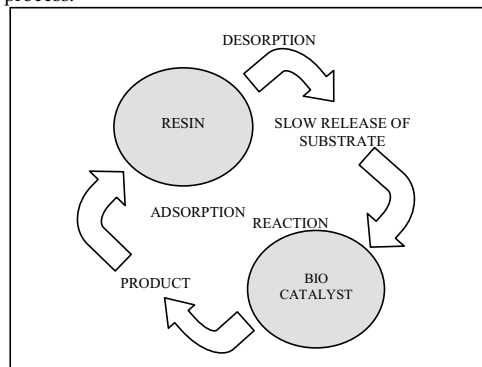


Figure 1 Principle of a resin based ISPR using the slow release mechanism

The objective of this project is to create a framework for a systematic method for guiding the implementation of this technology. The framework will include tools to characterize the reaction, guides for the selection of a suitable resin for a high intensity solid-liquid enzyme catalyzed reaction scheme and finally process evaluation in order to describe the trade-offs of supply and removal as well as resin capacity. The framework will be exemplified with industrially relevant enzymatic reactions, specifically ω -transaminase catalyzed reaction for the syntheses of chiral amines and alcohol dehydrogenase for the syntheses of enantiopure alcohols.

Framework for integrating resins into a bioreactor

When, how and why? The three basic questions that arise when considering implementing any process strategy. Introducing resins is a very interesting option to overcome kinetic limitations, but perhaps it is not applicable in all cases. If a resin is required then how can one choose the resin in a logical way? Some guidelines need to be in place in order to guide the selection procedure. Furthermore the critical question is does integrating resins prove to be beneficial in terms of yield? These three fundamental questions need to be addressed in a systematic way. In order to address these questions a methodological framework has been developed. It is a hierarchical framework where the output of each step becomes the input of the subsequent step. Figure 2 illustrates the workflow of the framework for integrating resins in a bioreactor.

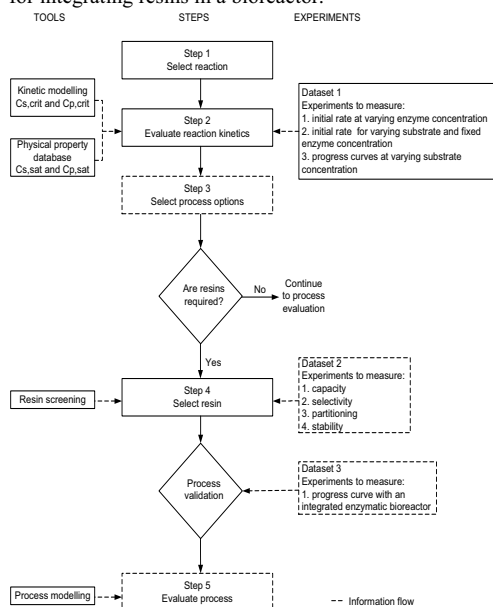


Figure 2 Methodological framework for integrating resins in a bioreactor

Case Study: ω -transamination of acetophenone

To illustrate the methodology, the reaction kinetics of the transamination (TAm) of acetophenone (APH) and co-substrate 2-propylamine (IPA) to produce (S)-1-phenylethyl amine (PEA) and co-product acetone (ACE) is used. Figure 3 below illustrates the reaction scheme.

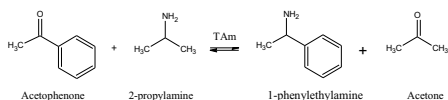


Figure 3 Transamination catalysed by ω -transaminase

Chiral amines are of great importance for the production of chiral drugs. However, the productivity of the catalyst is limited due to substrate and product

inhibition for which special considerations have to be taken into account for scaling up [5]. In view of that, it presents an interesting case study where it would be beneficial to integrate the substrate feeding and product removal using porous resins.

Kinetic modelling for characterizing the reaction

The reaction mechanism follows the ping-pong bi-bi mechanism where there is an exchange of amines. However, in this reaction, both substrate and product inhibit the catalytic activity. The kinetic model with the aid of the King and Altman methodology has been expressed in Equation 1 as follows:

$$\frac{d}{dt}[\text{PEA}] = \frac{[E_t] \cdot K_{cat} / K_{cat} \left([\text{IPA}] \cdot [\text{APH}] - \frac{[\text{ACE}] \cdot [\text{PEA}]}{K_{EQ}} \right)}{K_{cat} \cdot K_{iPH} \cdot [\text{IPA}] \left(1 + \frac{[\text{PEA}]}{K_{SPEA}} \right) + K_{cat} \cdot K_{iPA} \cdot [\text{APH}] \left(1 + \frac{[\text{APH}]}{K_{SAPH}} \right) + K_{cat} \cdot \frac{K_{PEA} \cdot [\text{ACE}]}{K_{EQ}} \left(1 + \frac{[\text{APH}]}{K_{SAPH}} \right) + K_{cat} \cdot \frac{K_{ACE} \cdot [\text{PEA}]}{K_{EQ}} \left(1 + \frac{[\text{PEA}]}{K_{SPEA}} \right) + K_{cat} \cdot [\text{IPA}] \cdot [\text{APH}] + K_{cat} \cdot \frac{K_{PEA} \cdot [\text{IPA}] \cdot [\text{ACE}]}{K_{EQ}} + K_{cat} \cdot \frac{[\text{ACE}] \cdot [\text{PEA}]}{K_{EQ}} + K_{cat} \cdot \frac{K_{iPA} \cdot [\text{APH}] \cdot [\text{PEA}]}{K_{PPEA}}} \quad [1]$$

List of abbreviations

- Kcat: Catalytic turnover [min⁻¹]
- K_{m,i}: Michaelis constants [mM]
- K_{S,i}: Substrate inhibition constant [mM]
- K_{P,i}: Product inhibition constant [mM]
- i : Reactants APH, IPA, PEA and ACE

A robust methodology for estimating kinetic model parameters has been discussed elsewhere [6]. With the aid of the kinetic model, an operability space was possible to be simulated as shown in Figure 4.

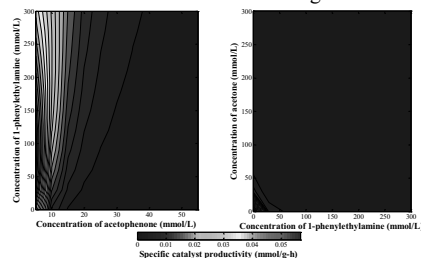


Figure 4 Catalyst activity synthesis of PEA using IPA as amine donor. A) Modeled catalyst activity at different product and substrate concentration. B) Modeled catalyst activity at different product and co-product concentration (APH concentration is kept constant at 5 mM applying a substrate feeding strategy).

From Figure 4, it can be seen that the reaction is heavily inhibited at substrate concentration (APH) above 5 mM and product concentration (PEA) above 30 mM. It also indicates the necessity of the removal of co-product acetone for shifting the reaction in the synthesis direction.

Selection of resin

For the success of this process technology, careful consideration has to be made when screening for a resin.

The resin comprising of porous polymeric matrix differs by diameter of the particle, pore sizes, hydrophobicity, functional groups etc. In this study, the resins have been divided into two groups: (i) neutral resins which work primarily on hydrophobicity, (ii) ion exchange resins which work primarily on charged compound. The screening of the resins is done in a heuristic approach where the appropriate resin is selected based on the fulfillment of certain criterion specific for substrate supply and product removal strategy. The criterions are listed in Table 1.

Table 1 Selection criterion for selecting resin

High capacity for substrate
Low selectivity for non-inhibitory substrate and product to bind with the resin
Moderate partitioning for inhibitory substrate and product
Negligible affinity for enzyme (if soluble)
Reasonable cost
Re-usable

A rational methodology for screening resins based on the criterion mentioned in Table 1 is shown below in Figure 5. The screening is decomposed into three hierarchical steps where the result of each of the step becomes the input for the subsequent step. The experimental data is broken down into 4 sub sets to match the different steps of the screening. Two types of database are used here. The first to provide physical properties of the reactants and the second is a database containing information about commercially available resins.

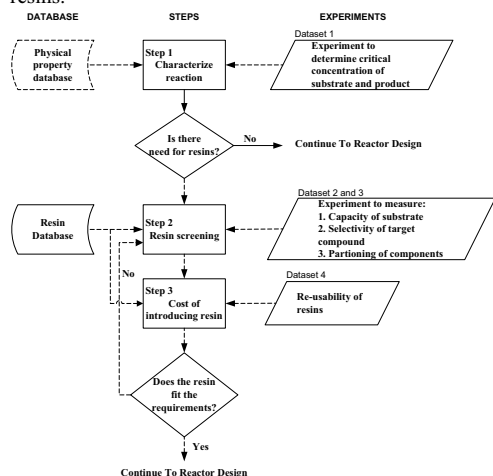


Figure 5 Proposed methodology for selecting resin

With the aid of the proposed methodology, Lewatit AF5 resin was selected for integrating it in the bioreactor.

The resin showed superior quality than the other tested resins. Table 2 displays the results of the screening.

Table 2 Screening of resin

Capacity [mol _{PEA} /kg _{resin}]	Selectivity for PEA		Partitioning coefficient	
	IPA	ACE	APH	PEA
2.3	2.88	1.97	3.45	0.1

For the resin to be cost effective, the resin has to be stable for re-using. Figure 6 illustrates the stability of the resin.

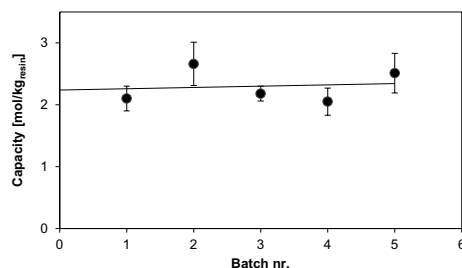


Figure 6 Stability of the resin for re-using

From Figure 6, it can be that the resin was quite durable and resistant to the different solvents and could in principal be used several times.

A resin loading of 40 % (V/V) was selected for testing the process. The resin was packed in an external column and linked to a membrane reactor according to the scheme in Figure 7.

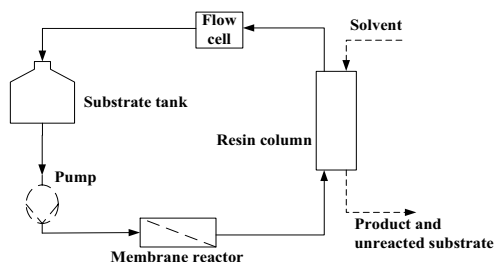


Figure 7 Process flowsheet for the synthesis of chiral amines using an integrated resin bioreactor

Following synthesis, the product was eluted from the resin using acetonitrile. The result of the experimental validation is shown in Figure 8. For comparison an experiment was performed without the resin integrated in the reactor. The integrated resin bioreactor enabled the reaction to reach equilibrium conversion.

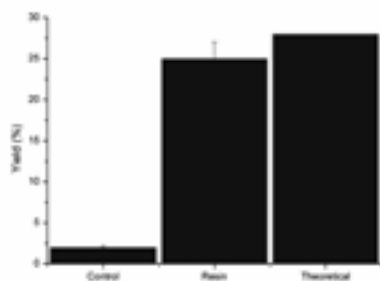


Figure 8 Yield achieved with the integrated resin bioreactor

Process evaluation

From previous chapters it has been assessed that the reaction is limited by substrate and product inhibition and therefore it would be desirable to introduce an integrated approach of substrate feeding and product removal using porous resins as an auxiliary phase in a batch reactor. There are two phenomena that take place in this process. First, the interaction of the different compounds with the enzyme (reaction) and second the interaction of the different compounds with the resin (partitioning) and third the substrate and product flux.

Mass balance in aqueous phase:

$$dC_{APH}/dt = -Q_{SS}/V - r_{PEA} \quad [2]$$

$$dC_{PEA}/dt = -Q_{PR}/V + r_{PEA} \quad [3]$$

Substrate and product flux:

$$Q_{SS} = k_{SS} * A * \text{mass} * (C_{APH, \text{resin}} - P_{APH} C_{APH, \text{aqueous}}) \quad [4]$$

$$Q_{PR} = k_{PR} * A * \text{mass} * (P_{PEA} C_{PEA, \text{aqueous}} - C_{PEA, \text{resin}}) \quad [5]$$

Partitioning model

$$q^* = q_{\max} C_{\text{eq}}^n / (P + C_{\text{eq}}^n) \quad [6]$$

The mass transfer coefficients for substrate supply and product removal were estimated using dynamic experiments as shown in Table 3.

Table 3 Estimated mass transfer coefficients

Parameter	Estimated value (m/min)	R ²
k _{SS}	1.19E-5	0.97
k _{PR}	5.43E-4	0.99

It can be seen that the mass transfer coefficient for substrate supply was smaller than for product removal. This is in agreement with other studies using cyclohexanone as a solvent [6] and moreover the substrate APH is more hydrophobic than PEA and thus is bound firmer to the resin.

With the aid of the process model, it was possible to simulate different scenarios. A critical consideration for using resins is the optimal amount of resins that is required. Figure 9 illustrates the simulation for different volume ratios.

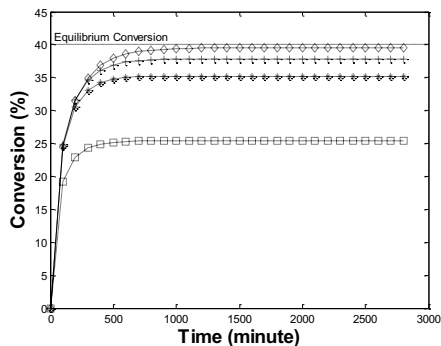


Figure 9 Asymmetric synthesis of 1-phenylethylamine using resin as an auxiliary phase at different volume ratio square symbols (10% V/V), diamond (30% V/V), plus (50% V/V), star (70% V/V)

Based on Figure 9, it can be seen that a volume ratio of around 40% is sufficient to achieve high conversion.

Conclusion

The framework presented here provided guidance from kinetic modeling, selection of resin and process modeling in a systematic manner for integrating resins in enzymatic reactors exemplified with a transaminase catalyzed case study. The integration of resin provided a positive impact in terms of achieving the high conversion. Moreover with the aid of the developed framework, greater insight has been gained about the process and also aided in designing better experiments. The framework can potentially be extended to not only other solid phase geometries but as well to different types of auxiliary phases such as organic solvents.

Acknowledgement

The author kindly acknowledges Technical University of Denmark and the project AMBIOCAS financed through the European Union Seventh Framework Programme (Grant Agreement no. 245144) for the financial support.

References

- Woodley JM. Trends. Biotechnol 26 (6) (2008) 321 – 327.
- Kim P-Y, Pollard DJ, Woodley JM. Biotechnol. Prog 23 (1) (2007) 74 – 82.
- Hilker I, Alphand V, Wohlgemuth R, Furstoss R. Adv. Synth. Catal. 346 (2-3) (2004) 203 – 214.
- Tufvesson P, Lima-Ramos J, Jensen JS, Al-Haque N, Neto W, Woodley JM. Biotech. Bioeng. 108 (7) (2011) 1479 – 1493.
- Al-Haque N, Santacoloma P, Neto W, Tufvesson P, Gani R, Woodley JM. Biotech. Prog. 28 (5) (2012) 1186 – 1196.
- Shin JS, Kim BG. Enzyme Microb. Technol. 25 (3 – 5) (1999) 426 – 432.

**Hamid Hashemi**

Phone: +45 4525 2809

E-mail: hah@kt.dtu.dk

Supervisors: Peter Glarborg
Jakob Munkholt Christensen**PhD Study**

Started: May 2011

To be completed: May 2014

Combustion Characterization of Bio-derived Fuels and Additives

Abstract

Combustion characterization of bio-derived alcohols and mixtures of natural gas with different additives at high pressure and intermediate temperature is the major aim of this project. For this purpose, some experiments on a high pressure laminar flow reactor are done. Furthermore, development of a reaction mechanism to address involved processes is in progress.

Introduction

In recent years, natural gas has attracted interest as an alternative fuel for use in conventional internal combustion engines. Longer ignition times and slower flame speed resulting in unburned hydrocarbons and performance deficiencies are main challenges in the use of this fuel in such engines. To address these problems, it has been suggested to adjust the combustion properties of natural gas via additives for suitable performance in engines. On the other hand, alcohols have potential as high-quality diesel fuels / additives as they appear to reduce soot formation. One probable scenario to have more “green” engines in mid time is to use bio-fuels in combination with natural gas. Knowledge about combustion characteristics of the mentioned fuels and their combination will facilitate chemical modeling of combustion processes involved in internal combustion engines and other heavy duty applications of natural gas.

Few data are available for combustion characteristics of bio-derived alcohols at high pressures. These limitations influence development of appropriate reaction mechanisms for modeling. Furthermore, effects of additives on natural gas combustion at high pressure and intermediate temperature, attractive for ignition in internal combustion engines, are not investigated thoroughly. In the unique high-pressure flow reactor setup at DTU Chemical Engineering, it is possible to investigate combustion of the natural gas with different compositions and also effects of additives on it. It is possible to achieve up to 100 bar pressure in the reactor while isothermal part is been kept at 900 K temperature.

Objectives

Obtaining characteristic data from combustion of bio-derived alcohols, additives, natural gas, and their mixtures at high pressure and intermediate temperature is the major aim of this project. Furthermore, it is desired to modify the current reaction mechanism [1] to address combustion of the mentioned mixtures of fuels. Finally, the implication for use of the selected fuels in diesel engines will be addressed.

Results and Discussion

An experimental and numerical investigation into ethanol oxidation at high pressures and intermediate temperatures has been done. Figures 1 and 2 show results of the experiments in the flow reactor in reducing conditions. Results indicate that major fuel/oxidant consumption starts around 725 K and around 90% of oxygen is consumed at that temperature. At stoichiometric conditions (figures 3 and 4) however the ignition starts at a higher temperature of 750 K, and while all ethanol has been consumed at higher temperatures, almost 30% of oxygen remains untouched. It mainly because of the thermal decomposition of ethanol to other species, while these intermediate species require more time to oxidize which is not provided in the corresponding residence time. According to the results (not shown here), higher temperatures facilitate oxidation of CO to CO₂. Figures 5 and 6 show results at oxidizing conditions. Ethanol consumption started at 725 K and it almost vanishes completely at 750 K. Concentration of O₂ also confirms ignition there.

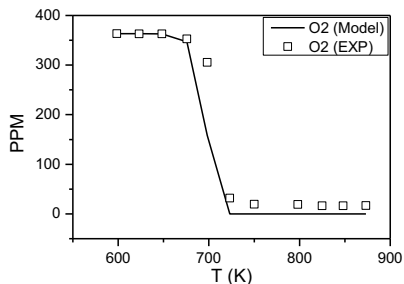


Figure 1: Results of reducing experiments with ethanol/O₂/N₂ (0.525% ethanol and 0.0363% O₂ in N₂) at 50 bar.

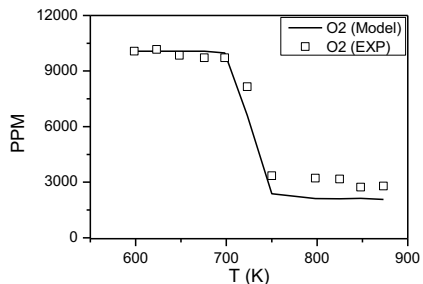


Figure 4: Results of stoichiometric experiments with ethanol/O₂/N₂ (0.347% ethanol and 1.008% O₂ in N₂) at 50 bar.

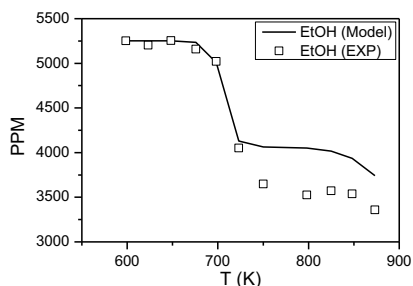


Figure 2: Results of reducing experiments with ethanol/O₂/N₂ (0.525% ethanol and 0.0363% O₂ in N₂) at 50 bar.

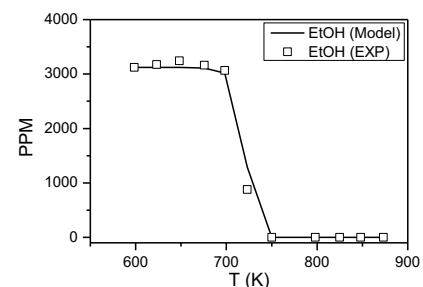


Figure 5: Results of oxidizing experiments with ethanol/O₂/N₂ (0.312% ethanol and 9.830% O₂ in N₂) at 50 bar.

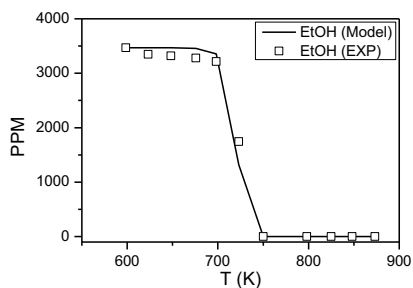


Figure 3: Results of stoichiometric experiments with ethanol/O₂/N₂ (0.347% ethanol and 1.008% O₂ in N₂) at 50 bar.

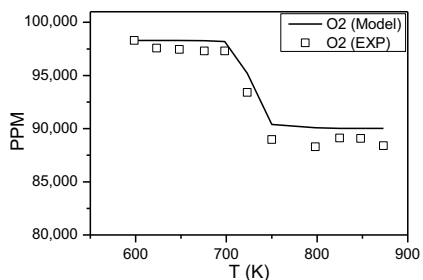


Figure 6: Results of oxidizing experiments with ethanol/O₂/N₂ (0.312% ethanol and 9.830% O₂ in N₂) at 50 bar.

Conclusion

Further work on combustion chemistry of ethanol especially at reducing conditions is suggested. Meanwhile, valuable data would be obtained via ongoing experiments on Natural gas and its interaction with additives such as DME, which are expected to lead to improvement in the current reaction mechanism.

Acknowledgement

Funding from the European Graduate School is gratefully acknowledged.

References

1. V. Aranda, J. Christensen, M. U. Alzueta, A. Jensen, P. Glarborg, S. Gersen, Y. Gao, P. Marshall, To be published, 2012.



Suzan Hassouneh

Phone: +45 4525 6195
E-mail: shas@kt.dtu.dk

Supervisors: Anne Ladegaard Skov
Ole Hassager

PhD Study
Started: August 2012
To be completed: January 2015

Monolithic Structures and their Influence on Electromechanical Breakdown Phenomena

Abstract

Dielectric electro active polymers (DEAP) have gained much ground in many different applications, such as wave energy harvesting, valves and loudspeakers. A lot of research has been focused on the use of polydimethylsiloxane (PDMS) as DEAP materials due to its high dielectric constant and fast response. The aim of this project is to adhere the DEAP films in multiple layers to make the elements more robust, prolong the life time and increase the energy density of the final product.

Introduction

DEAPs can be used as actuator, generators and sensors and consist of thin elastomeric films coated with compliant electrodes connected to a circuit. When applying a voltage the film deforms due to the electrostatic forces between the electrodes, so the film contracts in thickness and expands in area (Figure 1) [1].

Danfoss Polypower A/S (DPP) is one of the only producers of DEAP worldwide, due to the complexity of the processing. DPP uses PDMS as their elastomer and the films are manufactured in a roll-to-roll process, where the elastomeric mixture is coated on a corrugated carrier web. The film cures directly on the carrier web and the corrugations are thereby imparted in the PDMS film [2].

The films are subsequently delaminated from the carrier web and transferred to a liner. The films are coated with a thin layer of metal electrodes on the corrugated surface [2].

Due to the corrugations the film only elongates in one direction when a voltage is applied as shown in figure 1. This is due to the anisotropic stiffness. The corrugated pattern is also strictly required for the electrodes to survive the actuation, since the electrodes are made from metals such as silver. The corrugations make the deformation of the electrodes to become minimal.

Specific objectives

For applications the films are stacked, rolled or folded to increase the energy density, robustness and prolong the lifetime. It is desired to make the multilayers act as a monolithic structure and since the films are corrugated on one side and flat on the other there are three different configurations the films can be laminated as shown in figure 2.

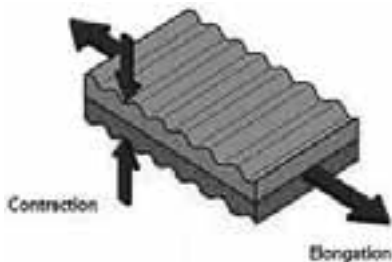


Figure 1: Corrugated DEAP laminate. When a voltage is applied, the film will contract in thickness and elongate in the compliant direction and stiffens along the corrugations.

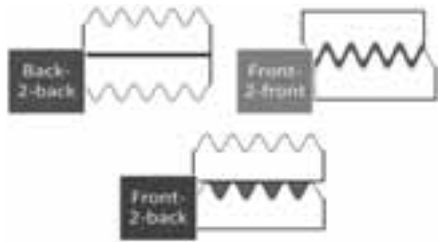


Figure 2: The different configurations for the adhesion of the films. The back-2-back configuration is where the flat sides are adhered together. The corrugated sides are adhered together in the front-2-front configuration and for the front-2-back configuration a corrugated side is adhered with a flat side.

The aim of this study is therefore to investigate methods to adhere the films in the different configurations with a minimal change in the electromechanical properties. Therefore the electromechanical properties of the monolithic structures are investigated and compared to single films.

Results and discussion

The adhesion of the films in the different configurations differs, since the surfaces differ. For the back-2-back configuration different methods were investigated. The first method is by air plasma treatment of the surface, which will make the surface hydrophilic. The methyl groups in the PDMS are exchanged with silanol groups (-OH) when the films are exposed to the air plasma [3]. After the plasma treatment the films are placed on top of each other and a condensation reaction occurs and the films are adhered covalently together.

The equipment was homemade setup, consisting of a vacuum chamber, a power source and a water cooling system. The samples were plasma treated for 1 minute at 50 W and 0.5 mbar pressure.

The second approach is to use an amino silane as glue after the plasma treatment. Bis(3-(trimethoxysilyl)propyl)amine is the amino silane used and after the plasma treatment two drops are placed on the film and another film is placed on top of it, as depicted in figure 3.

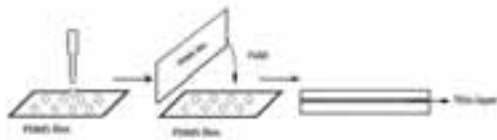


Figure 3: Adding the amino silane in a thin layer as glue between the PDMS films.

It was possible to adhere the PDMS films together with both approaches. A frequency sweep is performed for a single film, an air-plasma treated laminate and an amino

silane adhered laminate, to compare the mechanical properties of the different approaches to a single film.

Figure 4 illustrates that the storage modulus is larger for the amino silane adhered laminate (filled triangles) compared to the single film (filled squares) and the air-plasma treated laminate (filled circles).

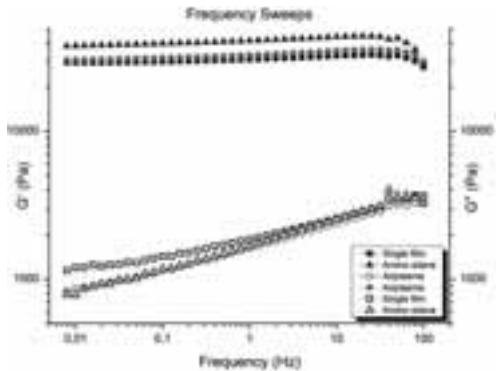


Figure 4: Frequency sweeps of a single film, and air-plasma treated laminate and amino silane adhered laminate.

This indicates that the amino silane adhered laminate is stiffer and that the adhesion is stronger. This change in stiffness is not desired, since it will influence the performance of the final product.

Conclusions

The adhesion of DEAP films in a monolithic structure will enhance the overall performance of the final product. Two methods were investigated for the back-2-back configuration, which showed that the laminate is stiffer when an amino silane is used as glue, which is unfavorable for DEAPs.

The future work will be to investigate the electrical properties of the laminates, compare the results and determine the best adhesion method. Furthermore, adhesion methods for the other configurations will be investigated.

Acknowledgement

The author would like to thank the Danish National Advanced Technology Foundation for the financial support.

References

1. X. Zhang, C. Löwe, M. Wissler, B. Jähne, G. Kovacs, *Advanced Engineering Materials* 7 (5) (2005) 361-367
2. H.-E. Kiil, M. Benslimane, *Proceeding SPIE*, vol 7287, (2009)
3. M. A. Eddings, M. A. Johnson, B. K. Gale, J. *Micromec.Microeng* 18 (2008) 067001

**Søren Heintz**

Phone: +45 4525 2949
E-mail: shein@kt.dtu.dk
Supervisors: Krist V. Germaey
John M. Woodley
Ulrich Krühne
Pär Tufvesson

PhD Study

Started: September 2012
To be completed: August 2015

Mastering Process Intensification across Scales for ω -Transaminase Processes

Abstract

The scope of this project is the development of miniaturized platforms to provide novel tools to accelerate the development phase of bio catalytic processes. It is expected that the platforms will serve multiple purposes in the process development phase, for example fast and easy optimization of process conditions or rapid feasibility screening of new and modified biocatalysts. The chosen reaction system for the platform development is specifically based on ω -transaminase. This specific biocatalyst is of interest due to the complexity of the reaction, which involves two substrates and two products as well as several enzymes, and generally highly unfavorable reaction equilibrium.

Introduction

Enantiomerically pure compounds of chiral amines are important intermediates in pharmaceutical and agricultural applications [1]. Because of their role in those applications they have to be produced in a safe manner and follow regulatory restrictions defined by, e.g. FDA and EMA.

Production of chiral amines with high enantiomeric excess (*ee*) is quite challenging, especially with conventional methods of chemical synthesis. In most cases it is only desired to produce one of the enantiomers of the chiral compounds, the active ingredient. The other enantiomer is considered an impurity and can potentially be harmful.

Biocatalysis provides an alternative to conventional chemical catalysis methods. Biocatalysts have the advantage of high selectivity (enable high *ee* values), and can potentially use a wide array of substrates while forming relatively few by-products [2].

Some limitations in the application of biocatalysts have to be overcome, before such a biocatalytic process option is to be extended to more general application in large scale processes [2]. The main challenges are related to (1) identify methodologies or processes to reduce the effect of biocatalyst inhibition by substrates and products at high concentrations; (2) moving the thermodynamically unfavorable equilibrium toward the products; (3) lack of sufficient thermo stability; (4) the cost of the biocatalyst and – closely linked with it – reuse of the catalyst [3].

This project has its focus on the development of miniaturized platforms and toolboxes, which provide novel methods means to achieve fast screening of new processes, thereby resulting in a reduction of the process development time. A main driving force for developing the miniaturized platforms is the reduced quantity of expensive and/or scarce resources needed for evaluation of potentially promising process candidates at micro-scale. In addition, miniaturized reactors allows real time monitoring and better control, as well as improved safety of the process [4][5][6].

The general principle of the development of biocatalyst based processes is illustrated in the development cycle in figure 1. The development cycle identifies the major areas of development and the key decisions which have to be taken during the development and optimization phase of a process [2].

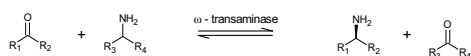
Mainly the definition of general methods and procedures for the process development will be covered in this project, along with a proof of concept.



Figure 1: Development cycle of biocatalyst based processes [2].

This PhD project is performed as part of an EU FP7 project (BIOINTENSE – Mastering bioprocess integration and intensification across scales), the main processes to be studied are ω -transaminase (ω -TA) facilitated processes used for the production of chiral amines.

ω -TAs transfer an amine ($-\text{NH}_2$) group from an amine donor (e.g. an amino acid or simple amines), to a prochiral acceptor ketone – yielding a chiral amine and a co-product ketone or alpha-keto acid [3]. The general principle of an ω -TA facilitated reaction is shown in scheme 1.



Scheme 1: The general principle of the ω -TA facilitated reaction [3].

ω -TA are of interest due to the complexity of the 2 substrates and 2 products. Furthermore, the equilibrium of ω -TA is in many cases located towards the substrate side. ISPR integration is considered as one possibility to move the reaction equilibrium towards the product side. The general strategy is that the developed technology can easily be modified for implementation into other biocatalyst facilitated processes, along with synthesis routes of fine chemicals.

Novel sensor technologies will also have to be implemented into the micro-reactor platforms in order to provide on-line measurement and control of the system, such that the current bottlenecks of analytical methods can be avoided (e.g. time delay on HPLC measurements). The focus will mainly be kept on the implementation of optical sensors, so the impact of the sensors on the process is avoided. Sensors which will be in focus are glucose, pH, temperature and NIR/IR.

The potential for large scale process operation will also be tested and general tools to evaluate whether scale-up or numbering-up is the better choice will be investigated. Such tools should also help give a fast and

reliable indication of the economic feasibility of the process that is under development.

Specific objectives

The main objectives which will be covered in this project are:

- Specification of general protocols for the decision making during process development and optimization with miniaturized platforms.
- Development of the miniaturized platforms and integration of analytical methods and measurements.
- Performance of process evaluation across scales and definition of general scale-up vs. numbering-up decision making procedures.

Conclusion

Currently, development and optimization of industrially relevant biocatalytic processes is quite time consuming, and in some cases the available quantities of substrates and/or catalyst are quite sparse and expensive. The development of miniaturized platforms is therefore important for the rapid design of new processes using minimal quantities of raw materials. New tools for fast optimization with regard to screening of process conditions are therewith provided.

Integration of on-line measurements and control is a parallel important step in view of the practical usefulness of the miniaturized platforms. This is caused by considerable time delays of current standard analytical methods, e.g. HPLC, which makes the process evaluation and/or control difficult.

The developed technology and procedures should be general applicable for biocatalyst based processes even though ω -TA catalyzed reactions are in focus in this project.

Acknowledgements

The PhD project is financially supported by the EU FP7 project BIOINTENSE – Mastering bioprocess Integration and intensification across scales.

References

1. S. Panke, M. Held, M. Wubbolts, Current Opinion in Biotechnology 15 (2004) 272-279.
2. A. Schmid, J. S. Dordick, B. Hauer, A. Kiener, M. Wubbolts, B. Witholt, Nature 409 (January 2001) 258-268.
3. P. Tufvesson, J. Lima-Ramos, J. S. Jensen, N. Al-Haque, W. Neto, J. M. Woodley, Biotech. & Bioeng. 108 (7) (2011) 1479-1493.
4. B. O'Sullivan, H. Al-Bahrani, J. Lawrence, M. Campos, A. Cázares, F. Bagamz, R. Wohlgenuth, H. C. Hailes, N. Szita, Jour. of Molecular Cat. B: Enzymatic 77 (2012) 1-8.
5. K. Geyer, J. D. C. Codée, P. H. Seeberger, Chem. a European Jour. 12 (2006) 8434-8442.
6. M. Miyazaki, H. Maeda, Trends in Biotech. 24 (2006) 463-470.



Peter Jørgensen Herslund

Phone: +45 4525 2863
E-mail: pjhe@kt.dtu.dk

Supervisors: Nicolas von Solms
Kaj Thomsen
Jens Abildskov

PhD Study
Started: February 2010
To be completed: June 2013

Thermodynamic and Process Modelling of Gas Hydrate Systems in CO₂ Capture Processes

Abstract

The fluid phase behaviour, of the binary system comprised of water and tetrahydrofuran (THF) is modeled by use of the Cubic-Plus-Association (CPA) equation of state. It is found that only by allowing cross-association between water and THF, may the full qualitative behaviour of the fluid phase equilibria in this system be described by CPA. Based on the results presented in this work, it is suggested to model this binary system considering THF as cross-associating only, with two association sites. The use of a temperature dependent binary interaction parameter and a correlated binary cross-association volume then allows for both accurate vapour-liquid and liquid-liquid equilibria descriptions over large ranges of temperature and pressure.

Introduction

Tetrahydrofuran (THF) is a cyclic ether compound with the chemical formula $c\text{-(CH}_2\text{)}_4\text{O}$. THF is, among others, used as a precursor in polymer production, a solvent for polymers, e.g. poly vinyl chloride (PVC) and also as a cleaning agent for semi-conductors [1]. However, THF has recently received growing attention due to its ability to form gas clathrate hydrates at moderate conditions of temperature and pressure.

Several publications are available in the literature, presenting THF as a potential thermodynamic promoter in hydrate-based pre- [2-5] or post combustion [2,3,6-9] capture of carbon dioxide (CO₂).

In this work the Cubic-Plus-Association (CPA) equation of state (EoS) is used to model both the vapour-liquid equilibria (VLE) and the liquid-liquid equilibria (LLE) of the binary system.

Modelling results for both VLE and LLE behaviour are presented. This work presents only a condensed part of a thorough investigation, which is currently under preparation for publication.

Model

The CPA equation of state combines the physical term from the cubic Soave-Redlich-Kwong (SRK) EoS with an association term similar to that found in the Statistical Associating Fluid Theory (SAFT) models.

On pressure explicit form, the CPA EoS may be expressed as Eq. 1 [10]:

$$P = \frac{R \cdot T}{V_m - b} - \frac{\alpha(T)}{V_m \cdot (V_m + b)} - \frac{R \cdot T}{2 \cdot V_m} \cdot \left[1 + \frac{1}{V_m} \cdot \frac{\partial \ln g}{\partial (\frac{1}{V_m})} \right] \times \sum_i x_i \sum_A (1 - X_{Ai}) \quad (1)$$

Where R is the universal gas constant and T is temperature. V_m denotes the molar volume, $\alpha(T)$ is the temperature dependent SRK energy parameter and b is the SRK co-volume parameter. g is the hard sphere radial distribution function. A_i denotes association site A on component i . x_i is the mole fraction of component i , X_{Ai} is the fraction of sites, type A on component i , not bonded to other sites.

When extending CPA to binary or multi component mixtures, the classical van der Waals one fluid mixing rules, with "classical" combining rules, are applied for the SRK parameters, $\alpha(T)$ and b , whereas the CR1 combining rules are applied for the two association parameters. Further details of the model and the applied mixing- and combining rules may be found elsewhere in the literature [10].

Association

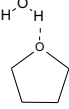
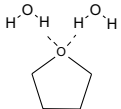
Here, association defines hydrogen bonding occurring between electron donating sites and electron accepting sites on two molecules.

Water is modeled as a self-associating compound using the 4C association scheme as defined by Huang

and Radosz [11]. When using this association scheme, water is assigned two electron donating sites and two electron accepting sites. The five CPA pure component parameters for water are available elsewhere in the literature [10] and these have been adopted in this work.

THF is modeled as a non self-associating compound but is allowed to cross-associate with water via either one or two electron donating sites situated on the oxygen atom. The modelling scenario, where THF is assigned a single association site, is named Model 1. The other scenario, with two association sites on THF, is denoted Model 2. Table 1 illustrates the types of association allowed between water and THF in the two investigated scenarios.

Table 1: Cross-association allowed in the two modelling approaches presented. Model 1 has a single electron donating site on THF, whereas Model 2 has two electron donating sites on THF.

Model	Cross-association
1	
2	

In addition to the cross-association illustrated in Table 1 water molecules are always allowed to self-associate.

Parameter Regression

Three pure component parameters for THF have been regressed as a part of this work. These parameters are obtained by correlating the CPA EoS to pure component vapour pressure- and saturated liquid density data [12]. The reference data have been limited, in terms of reduced temperature, to the interval $0.30 < T/T_c < 0.93$, where T_c equals 540.2 K for THF.

With THF being a non self-associating compound, the two self-association parameters, ϵ^{Aibj} and β^{Aibj} , take values of zero for this compound. When applying the standard CR1 combining rules in order to estimate the binary cross-association parameters with water, $\beta^{Aibj}(cross)$ takes a value of zero, inhibiting all cross-association. In order to solve this, the modification to the CR1 combining rule, presented by Folas et al. [13], is utilized in this work.

The binary parameters that can be correlated thus become the binary interaction parameter, k_{ij} , and the binary cross-association volume, $\beta^{Aibj}(cross)$.

Since the obtained k_{ij} 's turned out to be highly temperature dependant, attempts were made applying a temperature dependency on the correlated k_{ij} 's. By doing this, a total of 3 binary parameters are finally adjusted simultaneously. In the following sections, Model 1 with a constant value for k_{ij} is denoted Model

1A. When a temperature dependent k_{ij} is used, the notation is changed to Model 1B. The same goes for Model 2 that changes notation to 2A and 2B.

A constrained optimisation algorithm has been implemented in order to regress binary parameters in CPA and thereby to correlate the experimental VLE data available in the literature [14-21]. The optimisation algorithm is based on a FORTRAN implementation of the simulated annealing (SA) global optimisation algorithm presented by Goffe et al. [22] (source code available via [23]). The objective function, to which the SA algorithm is applied, is defined by the sum of absolute differences between calculated and experimental boiling point temperatures, or boiling point pressures as well as calculated and experimental vapour phase compositions (if available). As an example, when correlating P_{xy} data, the objective function is defined by Eq. 2.

$$OBJ = \sum_i \left(\left| \frac{P_{calc,i} - P_{exp,i}}{P_{exp,i}} \right| + \left| \frac{y_{calc,i} - y_{exp,i}}{y_{exp,i}} \right| \right) \quad (2)$$

If T_{xy} data are available, the pressures in Eq. 2 are exchanged with temperatures. If only T_x or P_x data are available, the second term in the sum is omitted.

In order to assure complete miscibility in the liquid phase at low pressures, constraints have been applied in the form of stability tests (Gibbs energy minimisation) on the liquid phase in temperature and pressure regions close to the experimental boiling point data. A penalty function has been imposed such that any finding of liquid-liquid phase splits, where the experimental data show a single liquid phase, results in a step increase in the objective function.

Finally the experimental LLE data at approximately 0.5 MPa presented by Riesco and Trusler [24] have been considered. A constraint has been set assuring liquid phase stability at 0.5 MPa up to temperatures of approximately 345 K. This constraint has been implemented in the form of stability tests for multiple compositions at the above conditions of temperature and pressure.

Results and Discussion

The obtained model parameters will be presented elsewhere in the literature in a publication currently under preparation. Here, only a selection of the obtained results is presented in graphical form. Figure 1, Figure 2 and Figure 3 compares the model performances with a selection of the experimental data used in the binary parameter regression.

Figure 1 clearly shows how CPA Model 1A (dashed lines) performs well at the lowest temperature ($T = 298.15$ K) but loses accuracy as the temperature increases. By applying a temperature dependency on the regressed k_{ij} (CPA Model 1B – solid lines), the azeotrope in the experimental data is well described in terms of composition and the boiling point pressure descriptions at the two high-temperature data sets are significantly improved.

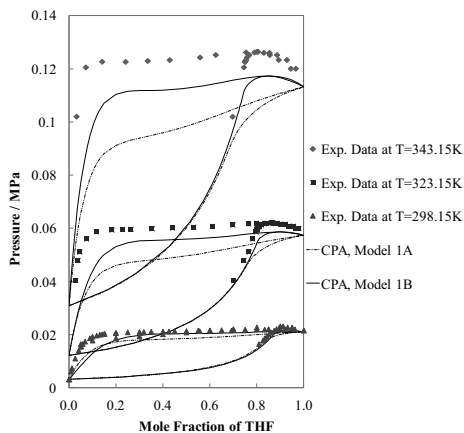


Figure 1: Comparison of Model 1A and 1B with experimental boiling point and dew point pressures as functions of the tetrahydrofuran (THF) mole fraction in the binary system of water and THF. Experimental data from [14,15,17,19].

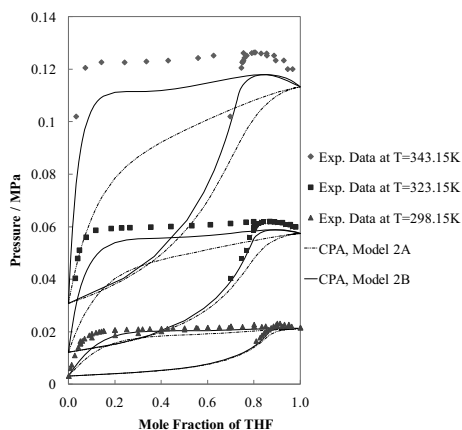


Figure 2: Comparison of Model 2A and 2B with experimental boiling point and dew point pressures as functions of the tetrahydrofuran (THF) mole fraction in the binary system of water and THF. Experimental data from [14,15,17,19].

Similar results are seen in Figure 2 for CPA Model 2A (dashed lines) and 2B (solid lines). Generally, both Model 1B and Model 2B underestimate the boiling point pressures at the two high-temperature data sets. This is a direct cause of the liquid-phase stability criterion set in the parameter regression work. By lowering the temperature in this criterion, the high temperature VLE descriptions may be improved, however the cost will be a liquid-liquid split stretching into the VLE region at $T = 343.15$ K. Hence the above results are the best possible compromise enabling a

description of both VLE and LLE with a single set of parameters.

Figure 3 shows T_{xy} descriptions of the VLE at a pressure of 0.1 MPa. Model 1B and Model 2B are compared in this figure. Despite Model 2B having two sites for cross-association with water, and Model 1B only a single site, the two models perform almost identical. Only in the low THF concentration region, at THF mole fractions below 0.2, does the differences between the two models become visible.

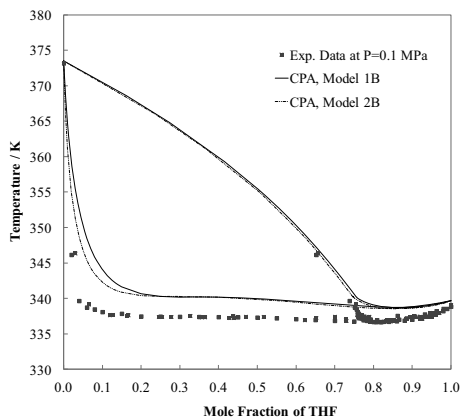


Figure 3: Comparison of Model 1B and 2B with experimental boiling point and dew point temperatures as functions of the tetrahydrofuran (THF) mole fraction in the binary system of water and THF. Experimental data from [14,18,20,21].

It is seen that Model 2B describes the boiling point temperature more accurately than Model 1B in systems with low THF content.

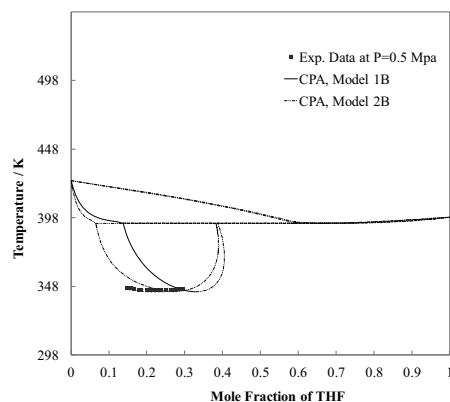


Figure 4: Comparison of Model 1B and 2B with experimental liquid-liquid separation temperatures as functions of the tetrahydrofuran (THF) mole fraction in the binary system of water and THF. Experimental data from [24].

No actual LLE data were included in the binary parameter regression. Hence the LLE descriptions of Model 1B and Model 2B illustrated in Figure 4 and Figure 5 are true predictions made by the CPA EoS. Only when using a temperature dependant k_{ij} does CPA predict LLE with the obtained parameters. Hence Model 1A and 2A predicts no LLE in the illustrated conditions of temperature and pressure.

Figure 4 shows the predicted LLE (and VLE) at $P = 0.5$ MPa. It is seen that both models predict the lower critical solution temperature (LCST) at approximately $T = 345$ K, which was also set as a constraint in the parameter regression. Moreover, Model 2B predicts the phase compositions more accurate than Model 1B.

Figure 5 illustrates the predicted LLE at $P = 6.0$ MPa. Again both models predict the LCST well, however Model 2B is more accurate in terms of phase compositions. Model 1B does however predict the upper critical solution temperature (UCST) more accurate than Model 2B, despite the deviation of approximately 50 K compared to the experimentally determined UCST.

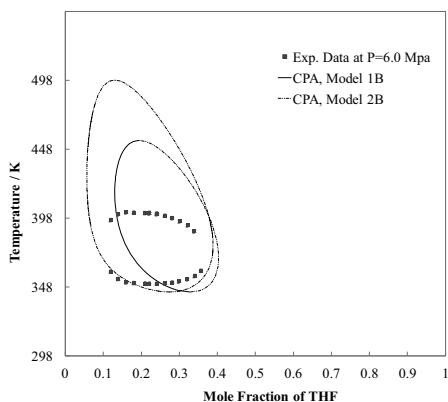


Figure 5: Comparison of Model 1B and 2B with experimental liquid-liquid separation temperatures as functions of the tetrahydrofuran (THF) mole fraction in the binary system of water and THF. Experimental data from [24].

Conclusion

Based on the results of this work, it is suggested to model this binary system considering THF as cross-associating only, with two cross-association sites. The use of a temperature dependent binary interaction parameter, k_{ij} , and a correlated binary cross-association volume, β^{Aij} , then allows for both accurate VLE and LLE descriptions over large ranges of temperature and pressure. A total of three binary parameters were regressed to experimental VLE data.

Acknowledgements

The financial contributions to this work from the iCap project (EU FP7) and the Department of Chemical and Biochemical Engineering (MP₂T) at The Technical University of Denmark, are greatly appreciated.

References

1. H. Matsuda, N. Kamihama, K. Kurihara, K. Tochigi, K. Yokoyama, *Journal of Chemical Engineering of Japan* 41 (3) (2011) 131-139.
2. P. Linga, R. Kumar, P. Englezos, *Chemical Engineering Science* 62 (2007) 4268-4276.
3. P. Linga, R. Kumar, P. Englezos, *J. of Hazardous Materials* 149 (2007) 625-629.
4. J. Zhang, P. Yedlapalli, J. W. Lee, *Chemical Engineering Science* 64 (2009) 4732-4736.
5. H. J. Lee, J. D. Lee, P. Linga, P. Englezos, Y. S. Kim, M. S. Lee, Y. D. Kim, *Energy* 35 (2010) 2729-2733.
6. S.-P. Kang, H. Lee, *Environ. Sci. Technol.* 34 (2000) 4397-4400.
7. S.-P. Kang, H. Lee, C.-S. Lee, W.-M. Sung, *Fluid Phase Equilibria* 185 (2001) 101-109.
8. P. Linga, A. Adeyemo, P. Englezos, *Environ. Sci. Technol.* 42 (2007) 315-320.
9. C. Giavarini, F. Maccioni, M. L. Santarelli, *Fuel* 89 (2010) 623-628.
10. G.M. Kontogeorgis, M.L. Michelsen, G.K. Folas, S. Derawi, N. von Solms, E.H. Stenby, *Ind. Eng. Chem. Res.* 45 (2006) 4855-4868.
11. S. H., Huang, M., Radosz, *Ind. Eng. Chem. Res.* 29 (11) (1990) 2284-2294.
12. Design Institute for Physical Property Data (DIPPR). Diadem Pro.
13. G. K., Folas, G. M., Kontogeorgis, M. L., Michelsen, E. H., Stenby, *Ind. Eng. Chem. Res.* 45 (2006) 1527-1538.
14. V. A., Shnitko, V. B., Kogan, *Journal of Applied Chemistry of the USSR (Zhurnal Prikladnoi Khimii)* 41 (6) (1968) 1235-1242.
15. R., Signer, H., Arm, H., Daeniker, *Helvetica Chimica Acta* 52, 8 (1969) 2347-2351.
16. H. M., Lybarger, H. L., Greene, *Advances in Chemistry Series* 115 (1972) 148-158.
17. J., Matous, J. P., Novak, J., Sobr, J., Pick, *Collection Czechoslov. Chem. Commun.* 37 (1972) 2653-2663.
18. W., Hayduk, H., Laudie, O. H., Smith, *Journal of Chemical and Engineering Data* 18 (4) (1973) 373-376.
19. C., Treiner, *Journal de Chimie Physique* 70 (9) (1973) 1183-1187.
20. E., Sada, T., Morisue, K., Miyahara, *Journal of Chemical and Engineering Data* 20 (3) (1975) 283-287.
21. J., Lampa, J., Matous, J. P., Novak, J., Pick, *Collection Czechoslov. Chem. Commun.* 45 (1980) 1159-1167.
22. W. L., Goffe, G. D., Ferrier, J., Rogers, *Journal of Econometrics* 60 (1/2) (1994) 65-99.
23. SIMANN.F, <http://www.netlib.no/netlib/opt/simann.f> (Acquired July 2012).
24. N., Riesco, J. P. M., Trusler, *Fluid Phase Equilibria* 228-229 (2005) 233-238.



Jeppe Lindegaard Hjorth

Phone: +45 2912 4460
E-mail: jelhj@kt.dtu.dk

Supervisors: Søren Kiil
John Woodley
Rasmus Leth Miller, AAK

Industrial PhD Study – Aarhus Karlshamn
Started: May 2011
To be completed: April 2014

Mathematical modeling of vegetable oil crystallization

Abstract

The present project concerns improved control and prediction of crystal characteristics in vegetable oils and fats used in the food industry, particularly the confectionary area. The project aims to improve the understanding and predictability of crystal characteristics in terms of polymorphism, nucleation and growth kinetics and particle size distribution using a mathematical model. This model will include mass and population balances for each chemical species together with solid-liquid equilibrium models used to determine the crystallization driving force present in the systems. It is to be developed using experience from literature and experimental work as the fundament, and will function as an iterative tool in the sense that it should be used to prove or disprove constructed hypotheses.

Introduction

To date very little research has been done in the field of predicting crystallization behavior of triacylglycerol (TAG) systems, the main component in vegetable oils and fats. Vegetable oils and fats are added to a wide array of foods to obtain the right structure and behavior, this includes chocolate, margarine, ice cream, bread etc. In this project the main focus will be on fats and oils used in the confectionary industry.

Often when mixing specific TAGs in well-defined ratios, interesting and valuable phenomena are observed including eutectic behavior, increased texture and polymorphic stability, or molecular compound formation [1]. Obtaining some degree of predictability of the behavior of such systems could serve as a first approach to develop new products tailored to the public demands for example by replacing trans and saturated fats with healthier alternatives without losing the texture and thermal behavior required in the end product.

Triacylglycerol morphology

As triacylglycerols crystallize, complex solid structures are formed resulting in fats having up to six different polymorphic configurations, as seen in cocoa butter, with distinct physical properties including melting temperature, heat of fusion, solubility, etc [2]. The large number of polymorphs is a consequence of packing patterns of the TAG molecules in the crystalline layers. Three main polymorphs are usually recognized together with a few sub-polymorphs. The main polymorphs are denominated α , β' and β with increasing stability from

left to right. The stability of the polymorphs is often correlated to the miscibility between various TAGs. When mixing TAGs in the α -form, exhibiting loose packing patterns, these are often seen to crystallize together, forming only one solid α -phase. However, as more stable crystals are formed the packing patterns become more specific and different TAGs may be unable to adapt to each other's crystal structures, resulting in more solid phases upon mixing. This is illustrated in Figure 1, showing a binary TAG phase diagram. These considerations greatly complicate solid-liquid equilibrium (SLE) calculation for such systems.

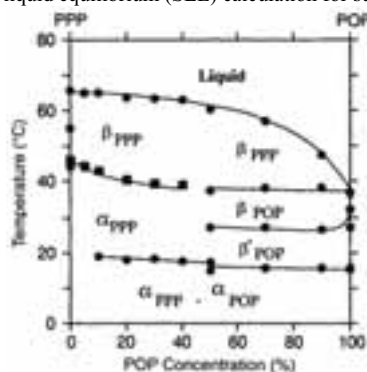


Figure 1: Phase diagram for the binary mixture *sn*-1,3-dipalmitoyl-2-oleoylglycerol (POP) and tripalmitoylglycerol (PPP) [3]

Solid-Liquid Equilibrium

Information about the equilibrium existing between different phases in the system is valuable as it provides a way of quantifying the driving force towards crystallization of the various TAGs and polymorphs. Such SLE calculations are complex due to the various polymorphic states and are further complicated by the nature of the oil systems chosen in the present project. These systems are comprised of an array of TAGs ranging in number from 10 to more than 30 and are thus very different from most model systems used in literature consisting of a limited number of very pure TAGs. Yet, promising results have been published in this field and a similar approach used in present project has allowed for relatively good correlation between experiments and simulations. The SLE model aims to minimize the Gibbs free energy of the system, while assuming non-ideal solid phases and an ideal and completely miscible liquid phase, in accordance with literature[4]. The SLE can be calculated once the activity coefficients of the included TAGs are known. This task is carried out using the Margules 2-suffix model which works well for mixtures with similar chemical composition, molar volume and shape

$$RT \ln \gamma_i = -g^E + \sum_{j=1, j \neq i}^N A_{ij} x_j \quad (1)$$

$$g^E = \sum_{i=1}^N \sum_{j=i+1}^N A_{ij} x_i x_j \quad (2)$$

This activity coefficient model is indeed one of the simplest and more advanced models exist. Yet, due to the sparse amount of data and the appertaining low quality present in literature for TAG systems there is at this point no incentive to incorporate such advanced models [5].

The Margules 2-suffix model requires the interaction coefficients A_{ij} of the involved species. As a first approach these parameters have been estimated using an equation developed in an earlier Ph.D. thesis [5]. This equation predicts the various interaction parameters based solely on the length of the fatty acids comprising the TAGs. This approach obviously is not flawless and some TAG interactions are not predicted very well, e.g. stearic acid and oleic acid both contains 18 carbon atoms and are thus predicted to interact ideally. Yet oleic acid contains a cis-double bond and has a very different spacial structure compared to stearic acid and ideal interactions are unlikely.

Figure 2 depicts the simulated SFC (solid fat content) curve assuming ideal and non-ideal mixing behavior in the solid phase, respectively. A clear shift towards a lower final SFC value is observed for the non-ideal mixing. Nonetheless, the value is still somewhat higher than the experimental equivalent. Allowing for multiple solid phases could very well lower the SFC value further, as eutectic phase behavior lowers the melting point and thus the driving force toward crystallization of a mixture, ultimately resulting in a lower SFC value at a given temperature. This hypothesis has been tested using Michelsen's tangent criterion [6]. This method

evaluates whether the addition of an extra, infinitesimal solid phase, has the possibility to lower the Gibbs free energy of the system, already in equilibrium. If that is the case, another solid phase is added, and the SLE is solved for the new multiphase system.

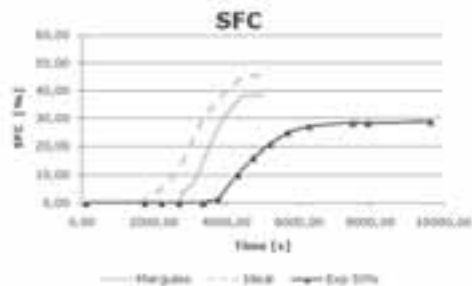


Figure 2: Experimental SFC curve compared to simulated curves for ideal and non-ideal mixing in the solid phase.

At this point the complete SLE model, including the tangent criterion is being tested for a 6 component mixture. For this system the Gibbs free energy is further reduced by addition of another solid phase, giving rise to a 3-phase system. Compared to the equivalent system, restrained to only one solid phase, the SFC value is lowered as expected. The appearance of more than one solid phase could then partly explain why the simulated SFC content is too high, and the tangent criterion will be implemented in the model to accommodate such phase splits.

Together with the improvements described above, it is believed that better estimates of the interaction parameters are needed to arrive at acceptable SLE results. This can be achieved by fitting the SLE model to experimental data. These data should represent the equilibrium conditions in the system and should not be affected by kinetics. For this reason SFC curves are a good choice. Figure 2 shows the SFC curve of an oil system from cooling is started until a final SFC value is reached. The first part of the curve is governed both by kinetics and thermodynamics but the SFC value at the final plateau should be governed only by thermodynamics. Hence this value seems an appropriate mark for the performance of the SLE model and thus the fitted interaction parameters.

Fitting the interaction parameters to experimental data is rather challenging given the number of interaction parameters needed fitting in the oil systems of interest, see Table 1. From the table it is evident that the oil composition can be approximately described by a couple of TAGs (marked in bold). The interaction parameters for these four dominant TAGs will then be fitted first, allowing some deviation from the experimental results, and the minor TAGs will then in turn be added to the model.

Table 1: TAG composition of the investigated oil, S = stearic acid, P = palmitic acid, O = Oleic acid, Li = Linoleic acid

TAG	Amount [%]
SSS	0.3
PPP	2.4
SSO	0.6
PPO	8.3
POP	3.8
SOS	0.4
POS	4.2
PLiP	3.4
POO	11.9
SOO	9.9
OOO	54.8

Finally, the fitted parameters will be validated by mixing various oils, rich in specific TAGs.

Crystallization model

A rather advanced model has been developed. This model is based on mass balances, the described SLE model, assuming complete miscibility in the liquid phase and non-ideal mixing in the solid phase(s), and a population balance, describing the particle size distribution as a function of applied temperature profile and TAG composition. Several mechanisms are included to account for the observed crystallization pathway. These comprise nucleation, growth, aggregation and possibly breakage at a later stage. An array of experiments has been conducted to evaluate these phenomena and determine how they are described most satisfactorily for TAG systems.

According to classical theory, primary nucleation can be described using the following equation

$$\frac{dN_i^j}{dt} = J_{0,i} \exp\left(\frac{-16\pi\sigma_i^j v_{m,i}^j}{3k^3 r^3 (\ln S_i^j)^2}\right) \quad (3)$$

The interesting features of this equation is the dependency of the nucleation rate, $\frac{dN_i^j}{dt}$, on the surface tension, σ_i^j , and the supersaturation, S_i^j . Moreover it has been argued that the induction time, describing the time needed from cooling is initialized to crystals appear, is inversely proportional to the nucleation rate [7]. Thus a straight line should be obtained by plotting the induction time vs. supersaturation. Indeed this technique yields straight lines, but apparently two straight lines with different slopes are appearing instead of just one, see Figure 3. Interestingly, this phenomena has also been observed in literature as the initial nucleation mechanism switches from homogeneous to heterogeneous [7]. As industrial grade oils are usually considered to contain some impurities, homogeneous nucleation is only observed at very high supersaturations (left side of the plot), rendering the presence of impurities unimportant. In this regime the nucleation rate is highly dependent on the

supersaturation and the steep slope is a consequence of large surface tension. On the other hand the heterogeneous regime is much less sensitive to supersaturation as the present impurities accommodate nucleation due to lowered surface tension. To further support these findings, additional impurities were added to the experiments, yielding heterogeneous nucleation, having approximately the same surface tension but a lower induction time, which could be interpreted as a higher nucleation rate (dashed line). Conclusively this indicates that the classical nucleation expression can be used to determine the nucleation onset for TAG mixtures, although secondary nucleation mechanisms are thought to be responsible for nucleation once crystallization has been initialized.

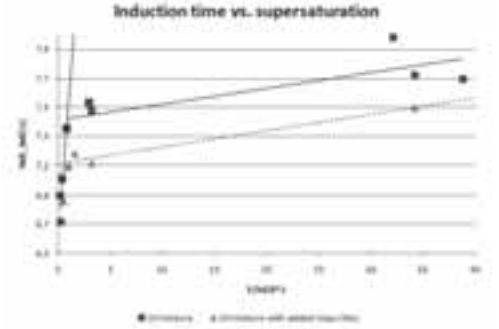


Figure 3: Induction time vs. supersaturation for the same oil mixture with and without additional impurities added.

Much like the nucleation phenomena, growth mechanisms of TAG systems have been investigated. The BCF model, taking both diffusion and integration kinetics into consideration can be expressed as

$$\text{Diffusion: } \frac{dm_c}{dt} = k_d A (C - C_i) \quad (4)$$

$$\text{Integration: } \frac{dm_c}{dt} = k_i A (C_i - C^*)^i \quad (5)$$

Literature suggests that these systems are controlled by kinetics governing integration of molecules into the crystal, once they reach the crystal surface. In that case the interfacial concentration, C_i , equals the bulk concentration, C [8]. Then by plotting the growth rate as a function of supersaturation in the right form it should be possible to determine kinetic order of the integration step, see Figure 4. Again two different regimes seem to be present. At high supersaturation (right part of the plot) a line with a slope very close to 1 emerges, which is consistent with findings in literature. Yet as the supersaturation is lowered (higher crystallization temperature) another dependency is observed. It seems that the diffusion kinetics can no longer be neglected. The observed behavior can be explained by considering the temperature dependence of the kinetic constants. Generally the diffusion constant is seen to be more

temperature dependent than the integration constant, so naturally at some temperature, a mechanistic shift will be observed. Thus, both kinetic constants should be determined and both equations should be included. Furthermore, it seems legit to assume a kinetic integration order of 1.

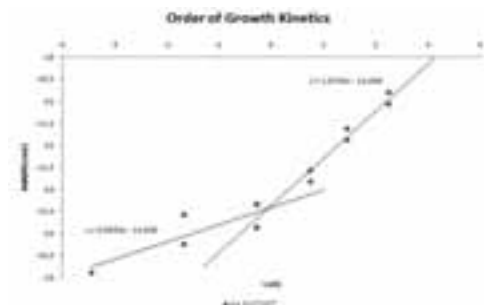


Figure 4: Linear growth rate vs. supersaturation for several temperatures (supersaturations)

The interplay between the various crystallization mechanisms covered so far can be very hard, if not impossible, to predict without model simulations. The implemented population balance beautifully binds the different “building blocks” together and creates a more complete picture and graphic representation of the interactions in the model. Take for example a crystallization event with and without the ability to form aggregates as shown in Figure 5. Both simulations have the same end points but rather different pathways. When aggregation is allowed, the system crystallizes slower as a result of larger crystals having a lower total surface area, which in turn slows down the growth rate.

Conclusion

Although complex vegetable oil systems are investigated in present project, it has been shown that much information can be extracted in terms of thermodynamic and kinetic data. The newly implemented population balance will furthermore serve as a tool to investigate the interplay between thermodynamics and kinetics as the crystal size distribution ties together the different events and provides a more complete picture of the crystallization. Together with the population balance, a robust SLE model able to accommodate non-ideal mixtures and multiphase systems is being implemented and combined with the acquired knowledge regarding nucleation and growth, it seems that a strong, predictive and versatile model foundation is being shaped. The predictive power of the model is of great importance as it is likely to prove a valuable tool when investigating various theories and ultimately as a first approach when designing new vegetable oil products for the industry.

Acknowledgement

The author acknowledges the great financial, professional and collegial support of AarhusKarlshamn

and CHEC Research Center and PROCESS at the Department of Chemical and Biochemical Engineering at DTU.

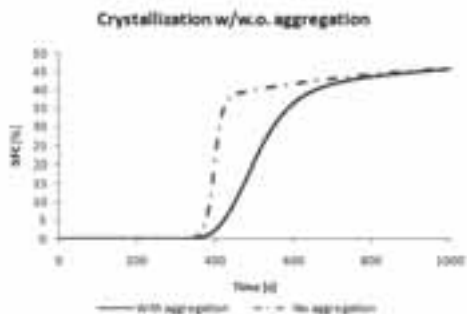


Figure 5: Crystallization of the exact same system with the ability to form aggregates turned on and off, respectively.

References

1. Sato, K., *Crystallization behaviour of fats and lipids -- a review*. Chemical Engineering Science, 2001. **56**(7): p. 2255-2265.
2. Nissim Garti, K.S., *Crystallization and Polymorphism of Fats and Fatty Acids*1988: Marcel Dekker.
3. Minato, A., et al., *Synchrotron radiation X-ray diffraction study on phase behavior of PPP-POP binary mixtures*. Journal of the American Oil Chemists' Society, 1996. **73**(11): p. 1567-1572.
4. dos Santos, M., G. Le Roux, and V. Gerbaud, *Phase Equilibrium and Optimization Tools: Application for Enhanced Structured Lipids for Foods*. Journal of the American Oil Chemists' Society, 2011. **88**(2): p. 223-233.
5. Wesdorp, L.H., *Liquid - Multiple Solid Phase Equilibria in Fats*, in *Ph.D. Thesis* 1990, Delft University of Technology.
6. Santos, M.T.d., et al., *Solid-Liquid Equilibrium Modelling and Stability Tests for Triacylglycerols Mixtures*, in *Computer Aided Chemical Engineering*, C.A.O.d.N. Rita Maria de Brito Alves and B. Evaristo Chalbaud, Editors. 2009, Elsevier. p. 885-890.
7. Hsien-Hsin Tung, E.L.P., Michael Midler, James A. McCauley, *Crystallization of Organic Compounds*. 1st ed 2009: Wiley.
8. Mazzanti, G., A.G. Marangoni, and S.H.J. Idziak, *Modeling of a two-regime crystallization in a multicomponent lipid system under shear flow*. The European Physical Journal E, 2008. **27**(2): p. 135-144.



Qian Huang

Phone: +45 4525 6809

E-mail: qh@kt.dtu.dk

Supervisors: Ole Hassager
Anne L. Skov
Henrik K. Rasmussen,
DTU Mechanical Engineering

PhD Study

Started: February 2010

To be completed: February 2013

Are Entangled Polymer Melts Different from Solutions: Role of Entanglement Molecular Weight

Abstract

In this work we compare the extensional rheology of the entangled linear polystyrene melts with polystyrene solutions to evaluate the influence of entanglement molecular weight. We found that the polystyrene melts and solutions which have the same number of entanglements per chain behave similarly in the oscillatory shear flow, but differently in the extensional flow. The polystyrene solutions are more strain hardening than the melts, especially at lower concentration, which may due to their higher values of entanglement molecular weight. At Weissenberg number bigger than 1, the steady-state viscosity of the solutions shows a plateau region, while the viscosity of the melts still decreases monotonically.

Introduction

The possible existence of a qualitative difference on extensional steady state viscosity between polymer solutions and melts is still an open question. Experiments on entangled polystyrene solutions [1] showed that the extensional steady state viscosity initially decreased with increasing the strain rate; but when the strain rate became higher than the order of inverse Rouse time, it started to increase. In contrast, experiments on entangled polystyrene melts [2] showed that the extensional steady state viscosity decreased monotonically even at the strain rate higher than the inverse Rouse time. Such contradiction also exists in model predictions. The tube model [1] that includes the mechanisms of chain stretch and convective constraint release reasonably described the above behavior of polystyrene solutions. However, it could not capture the monotonic thinning behavior of polystyrene melts. The interchain pressure model [3] captured the monotonic thinning of polystyrene melts. However, it did not specify the difference between melts and solutions.

When an entangled polymer melt is diluted in some solvent, one obvious change is that the number of entanglements per chain decreases and the entanglement molecular weight M_e increases. The purpose of the present work is to directly evaluate the influence of M_e on the rheological behaviors of entangled polymer melts and solutions. We carefully synthesized two nearly monodisperse polystyrenes with molar masses of 285 and 545 kg/mole, respectively. We then prepared three binary blends from either of the two polystyrenes and a

2 kg/mole styrene oligomer. The chains of the oligomer are far below the entanglement molecular weight and therefore the three blends are equivalent to solutions. The two melts and the three solutions have been measured in uniaxial extensional flows using a filament stretching rheometer. We will show the difference between the melts and solutions in nonlinear rheology which is directly related to their different M_e .

Samples Preparation

The two polystyrenes PS-290k and PS-550k have been synthesized by living anionic polymerization at DTU Nanotech with the polydispersity index of 1.09 and 1.12 respectively. The styrene oligomer OS-2k was bought from Sigma-Aldrich. The polydispersity index was 1.08. The polystyrene solutions were made from either PS-290k or PS-550k diluted in OS-2k. The solutions were prepared by dissolving both the polystyrene and the oligomer in tetrahydrofuran (THF) and stirring at room temperature overnight. When the components were well dissolved and mixed, the THF solution was cautiously put into methanol drop by drop and the blends were recovered by precipitation. Finally the blends were dried under vacuum at 50°C for a week. Considering that the methanol may partly dissolve OS-2k during precipitation at room temperature, the concentrations of all the polystyrene solutions were determined by the peak areas of the bimodal curve in size exclusion chromatography (SEC). For each polystyrene solution, two randomly picked parts were checked in SEC in order to make sure the concentration is homogenous.

The entanglement molecular weight M_e of the polystyrene solutions is calculated as [1]

$$(M_e)_{\text{solution}} = (M_e)_{\text{melt}} (c/\rho)^{-1}, \quad (1)$$

where ρ is the density of the polystyrene melt, $c=\rho\phi$ and ϕ is the weight fraction of the polystyrene in the solution. We take $M_e=13.3\text{kg/mol}$ for polystyrene melts as reported by Bach *et al.* [2]. The number of entanglements per chain is calculated as $Z=M/M_e$, where M is the molecular weight of the polystyrene. The properties of the polystyrene melts and solutions are listed in Table 1.

Table 1: The properties of the polystyrene samples

Sample	Compo -nents	ϕ [wt%]	Z	M_e [g/mol]
PS-550k	550k	100%	41.0	13300
PS-290k	290k	100%	21.4	13300
Solution-1	290k+2k	72%(±1%)	15.4	18472
Solution-2	290k+2k	44%(±1%)	9.4	30227
Solution-3	550k+2k	58%(±1%)	23.8	22931

Linear Viscoelastic Properties

The linear viscoelastic (LVE) properties of the polystyrene melts and solutions were obtained from small amplitude oscillatory shear flow measurements. An 8mm plate–plate geometry was used on an ARES–G2 rheometer from TA instruments. The measurements were performed at different temperatures between 110 and 170 °C. For each polystyrene sample the data were shifted to a single master curve at 130°C using the time–temperature superposition procedure. Figure 1 presents the LVE data fitted with the continuous Baumgaertel-Schausberger-Winter (BSW) relaxation spectrum [4] for PS-290k, Solution-1 and Solution-2. Similar data and BSW fittings for PS-550k and Solution-3 are shown in Figure 2. The LVE properties obtained from the BSW spectrum are list in Table 2, where G_0 is the plateau modulus, τ_c is the crossover relaxation time, τ_{\max} is the maximum relaxation time, and η_0 is zero-shear-rate viscosity. The Rouse time τ_R in the table is obtained from the linear theory [5].

Table 2: The LVE properties obtained from the BSW spectrum at 130°C

Sample	G_0 [Pa]	τ_c [s]	τ_{\max} [s]	τ_R [s]	η_0 [Pa. s]
PS-550k	250000	0.4	61540	779	2.8796E9
PS-290k	250000	0.4	6890	216	3.2352E8
Solution-1	129600	0.075	391.4	19	9.5824E6
Solution-2	48400	0.024	22.83	2.4	2.1359E5
Solution-3	84100	0.051	1113	31.2	1.7569E7

Startup and Steady-State Elongational Flow

The extensional stress of the polystyrene samples was measured by a filament stretching rheometer (FSR). Before the elongational measurements, all the polystyrene samples were molded into cylindrical test specimens using a special mould with a fixed radius $R_0=2.7\text{mm}$. The mould was connected to a vacuum pump.

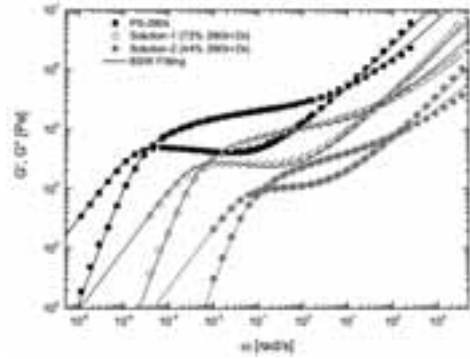


Figure 1: LVE data fitted with the BSW spectrum for PS-290k, Solution-1 and Solution-2 at 130°C.

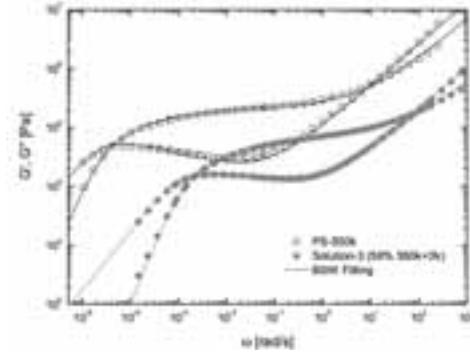


Figure 2: LVE data fitted with the BSW spectrum for PS-550k and Solution-3 at 130°C.

The initial length L_0 of the cylindrical test specimens was controlled by weighing a proper amount of the samples before putting them into the mould. The L_0 of each cylindrical test specimen was varied between 1.3mm and 1.6mm, giving an aspect ratio $A_0=L_0/R_0$ between 0.48 and 0.59. The polystyrene melts were pressed at approximately 150°C and annealed at this temperature for 15min under vacuum to ensure that the polymer chains were completely relaxed. The polystyrene solutions were pressed at approximately 130°C and annealed for 15min under vacuum as well. The samples were checked by SEC again after the extensional stress measurements to ensure that there was no degradation or concentration change.

All the polystyrene samples were pre–stretched to a radius R_p ranged from 3mm to 4mm at either 160°C (for the melts) or 140°C (for the solutions) prior to the elongational experiments. After pre–stretching the temperature was decreased to 130°C for the extensional stress measurements of the melts. As for the solutions the temperature was decreased to either 110°C or 120°C according to their different glass transition temperature T_g . Nitrogen was used in the whole procedure.

During the elongation, the force $F(t)$ is measured by a load cell and the diameter $2R(t)$ at the mid-filament plane is measured by a laser micrometer. At small

deformation in the startup of the elongational flow, part of the stress difference comes from the radial variation due to the shear components in the deformation field. This effect may be compensated by a correction factor as described in Rasmussen *et al.* [6]. The Hencky strain and the mean value of the stress difference over the mid-filament plane are then calculated as

$$\epsilon(t) = -2 \ln(R(t)/R_0), \quad (2)$$

$$\langle \sigma_{zz} - \sigma_{rr} \rangle = \frac{F(t) - m_f g / 2}{\pi R(t)^2} \left(1 + \frac{\exp(-5\epsilon / 3 - \Lambda_0^3)}{3\Lambda_0^2} \right)^{-1}. \quad (3)$$

The strain rate is defined as

$$\dot{\epsilon} = d\epsilon / dt, \quad (4)$$

which is kept as a constant during extension. The extensional stress growth coefficient is defined as

$$\bar{\eta}^+ = \langle \sigma_{zz} - \sigma_{rr} \rangle / \dot{\epsilon}. \quad (5)$$

Figure 3 shows the measured extensional stress growth coefficient as a function of the time at 130°C for PS-290k, Solution-1 and Solution-2. The solid lines in the figure are predictions from the LVE parameters in the BSW spectrum. Similar plots for PS-550k and Solution-3 at 130°C are shown in Figure 4. Solution-1 and Solution-3 were originally measured at 120°C, while Solution-2 was originally measured at 110°C. In Figure 3 and 4 they are shifted to 130°C using the time-temperature superposition. It seems that the strain hardening effect is much more pronounced in the solutions especially at low concentrations compared with the melts. The extensional steady-state viscosity is plotted as a function of the strain rate in Figure 5 for all the polystyrene samples at 130°C. The steady-state viscosity shows a monotonic thinning for the two melts PS-290k and PS-550k, which is in agreement with Bach *et al.* [1]. But the three solutions show obviously different behaviors compared with the melts. The steady-state viscosity of Solution-1 seems to have three regions. It initially decreases with increasing the strain rate in the first region. It then goes to a plateau region while the strain rate keeps increasing. Finally it decreases again with even faster strain rate in the third region. Solution-2 and Solution-3 only have the plateau region which may due to the limited strain rates.

Discussion

When a polystyrene melt is diluted, the entanglement molecular weight increases according to Eq.1. It would be interesting to compare the behaviors of the molecules in shear and extensional flows with different M_e under the same number of entanglements Z . In Figure 6, Solution-3 which has $Z=23.8$ is compared with the melt PS-290k which has $Z=21.4$ in the oscillatory shear flow. Since the glass transition temperatures T_g of the solution and the melt are quite different, they are compared under non-dimensional parameters so that the crossover point at the high frequency part of Solution-3 in Figure 2, and the similar point of PS-290k in Figure 1, are shifted to overlap each other in Figure 6. It can be seen

that with the same value of Z , the G' and G'' data of the melts and solutions can be superimposed with each other. Since Solution-3 has a slightly larger number of entanglements than PS-290k, their G' and G'' curves are not completely overlap in the low frequency part.

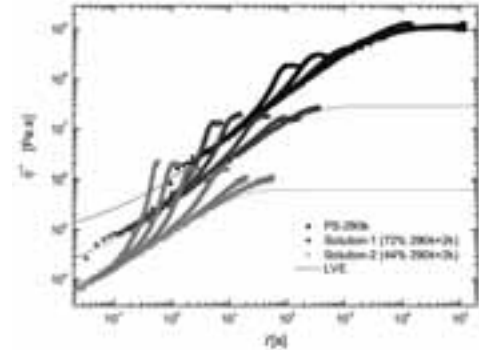


Figure 3: The measured extensional stress growth coefficient as a function of the time for PS-290k, Solution-1 and Solution-2 at 130°C.

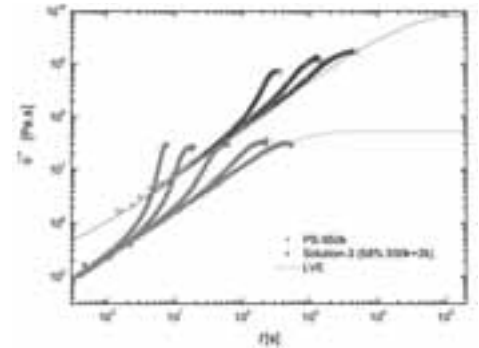


Figure 4: The measured extensional stress growth coefficient as a function of the time for PS-550k and Solution-3 at 130°C.

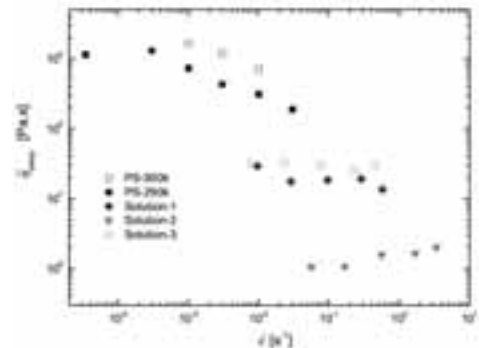


Figure 5: The extensional steady-state viscosity as a function of the strain rate for all the polystyrene samples at 130°C.

The behaviors of Solution-3 and PS-290k in extensional flow are compared in Figure 7, also under non-dimensional parameters which scale the same way as in Figure 6. In Figure 7, the melt and solution have obviously different behaviors in extensional flow, while they behave similarly in shear flow as shown in Figure 6. As already mentioned in Section 3.2, the strain hardening effect is indeed more pronounced in the solutions compared with the melts in Figure 7, where they have almost the same LVE predictions.

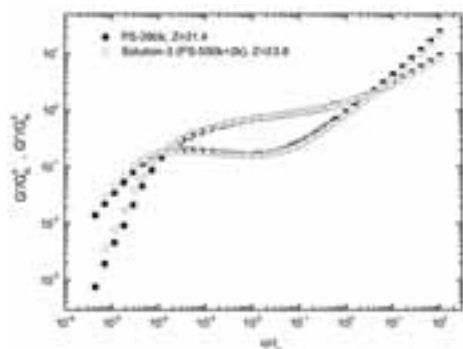


Figure 6: Comparison of Solution-3 and PS-290k in the oscillatory shear flow.

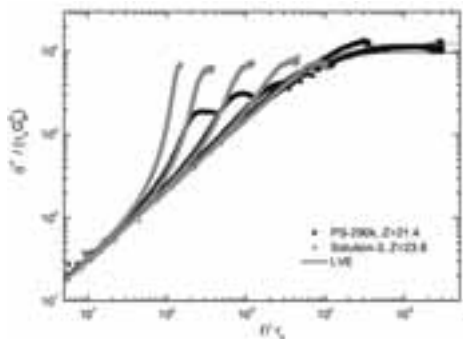


Figure 7: Comparison of Solution-3 and PS-290k in the startup of extensional flow.

Figure 8 compares the non-dimensional steady-state viscosity of the melts and solutions, but normalized by the time scale of τ_R . The Weissenberg number is defined as $Wi_R = \dot{\gamma} \tau_R$. It can be seen that at $Wi_R > 1$, where the polymer chains are stretched, the non-dimensional steady-state viscosity of the solution is higher than the melt. This observation indicates that with the higher values of M_e , the polymer chains in the solution is more flexible and could be stretched further. Moreover, in Figure 7, the non-dimensional stress growth coefficient in the startup of the flow is almost the same for Solution-3 and PS-290k, due to their same Weissenberg number as shown in Figure 8. However, with the lower value of M_e , the extensibility of PS-290k seems rather limited and the flow turns to a steady state much earlier than Solution-3.

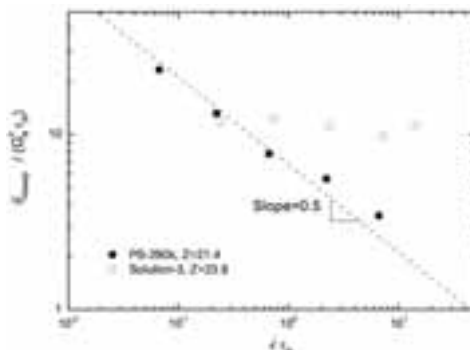


Figure 8: Comparison of Solution-3 and PS-290k in the steady-state extensional flow.

Conclusion

The two nearly monodisperse polystyrene melts PS-290k and PS-550k, and the three polystyrene solutions made from either PS-290k or PS-550k diluted in OS-2k, have been measured in the uniaxial extensional flow using the FSR. The polystyrene melts and solutions which have the same number of entanglements per chain behave similarly in the oscillatory shear flow, but differently in the extensional flow. The polymer chains of the solutions are found to be more strain hardening than the melts, especially at lower concentration, due to their higher values of entanglement molecular weight. At $Wi_R > 1$, the non-dimensional steady-state viscosity of the solutions shows a plateau region, while the viscosity of the melts still decreases monotonically. Further investigation on the influence of the solvents will be required.

References

1. P. K. Bhattacharjee, J. P. Oberhauser, G. H. McKinley, L. G. Leal, T. Sridhar, *Macromolecules* 35(2002) 10131–10148.
2. A. Bach, K. Almdal, H.K. Rasmussen, O. Hassager, *Macromolecules* 36(2003) 5174–5179.
3. M.H. Wagner, S. Kheirandish, O.Hassager, *J. Rheol.* 49(6) (2005) 1317–1327.
4. M. Baumgaertel, A. Schausberger, H. H.Winter, *Rheol. Acta* 29 (1990) 400–408.
5. A.E. Likhtman, T. C. B. McLeish, *Macromolecules* 35 (2002) 6332–6343.

**Amol Shivajirao Hukkerikar**

Phone: +45 4525 2817
E-mail: amh@kt.dtu.dk

Supervisors: Gürkan Sin
Jens Abildskov
Rafiqul Gani
Bent Sarup, Alfa Laval, Denmark

PhD Study: Industrial PhD
Started: July 2010
To be completed: June 2013

Property Modeling and Uncertainty Analysis for Reliable Process Design and Sustainability Analysis

Abstract

The main objective of this project is to develop group-contribution⁺ (GC⁺) approach based property prediction models to provide reliable estimates of pure component properties together with uncertainties of estimated property values needed in the design of chemical processes and sustainability analysis. In total 21 thermo-physical properties and 22 environment-related properties of pure components, which include normal boiling point, critical temperature, normal melting point, LC₅₀, LD₅₀ among others have been modeled and analysed. For parameter estimation and uncertainty analysis, the CAPEC database, the US EPA database, and the USEtox database are used. Important issues related to property modeling such as reliability and thermodynamic consistency of predicted properties, selection of most suitable property model, and effect of quantity of data on parameter estimation have been analysed. To analyse the effects of uncertainties of property estimates on the quality of design and the sustainability analysis of processes, a systematic methodology for performing analysis of sensitivity of process design due to uncertainties of property estimates is developed. This methodology provides: a) list of properties with critical importance on the design; b) acceptable levels of accuracy for different property prediction models; and c) design variables versus properties relationships. The application of this methodology is illustrated through several studies of designs of various unit operations found in chemical processes.

Introduction

Physical and thermodynamic properties of pure components are needed to carry out tasks such as, process design, computer aided molecular/mixture design among others. Environment-related properties, on the other hand, form the basis for performing environmental impact analysis to determine the most sustainable process design alternative. The experimental values of properties of many important pure components have not been measured (due to limitations and constraints such as cost, time, feasibility etc.) and hence they must be estimated. Predictive methods such as GC⁺ method (combined group-contribution (GC) method [1] and atom connectivity index (CI) method [2]) are generally suitable to estimate the needed property values. For assessing the quality and reliability of the chemical product/process design, an engineer needs to know the uncertainties of the estimated property values resulting from the property models. With this information, the engineer can then perform better-informed design calculations by taking into

account these uncertainties. Hence, this work aims to develop GC⁺ based property prediction models to provide reliable estimation of properties together with uncertainties of property estimates so that their effects on the quality of product/process design can be analysed. A systematic methodology for analyzing sensitivities of process design due to uncertainties in property estimates is also developed and its application is highlighted through several case studies.

Property Modeling and Uncertainty Analysis

For property modeling and uncertainty analysis, a systematic methodology is developed and used [3]. The developed methodology includes: (i) a parameter estimation to estimate property model parameters; and (ii) an uncertainty analysis [4] to establish statistical information about the quality of parameter estimation, such as parameter covariance, standard errors, and confidence intervals. For modeling of thermo-physical properties, large data-sets of experimentally measured property values of pure compounds are taken from the

CAPEC database [5]. For modeling of environment-related properties, databases of US EPA [6] and USEtox [7] are used. In this work, Marrero and Gani GC-method [1] based and CI method [2] based property models have been considered. In total 21 thermo-physical properties and 22 environment-related properties have been analyzed. The models for environment-related properties have been developed to assist process synthesis, design, and analysis of sustainable processes.

Results

Model performance statistics: The model performance statistics for selected thermo-physical property models is summarized in Table 1 and it can be seen that most of the data have been fitted to a good accuracy. Table 2 provides model performance statistics for selected environment-related properties.

Table 1. Performance statistics for selected thermo-physical property models [3]

Property	N ^a	R ²	SD ^b	AAE ^c	ARE ^d
T_b K	3510	0.99	7.9	6.17	1.44
T_c K	858	0.99	10.77	7.72	1.23
P_c bar	852	0.96	2.38	1.40	3.90
V_c cc/mol	797	0.99	11.65	7.97	2.05
T_m K	5183	0.94	19.16	15.99	5.07

Table 2. Performance statistics for selected environment-related property models [8]

Property	N ^a	R ²	SD ^b	AAE ^c	ARE ^d
$LC_{50}(FM)$	809	0.78	0.70	0.49	19.29
$LogWs$	4681	0.78	0.99	0.73	--
LD_{50}	5995	0.73	0.43	0.35	16.40
PEL	425	0.74	0.78	0.44	12.61
$ERAc$	470	0.77	0.67	0.51	8.88

T_b = Normal boiling point, T_c = Critical temperature, P_c = Critical pressure, V_c = Critical volume, T_m = Normal melting, $LC_{50}(FM)$ = fathead minnow LC50 (96-hr), $LogWs$ = aqueous solubility, LD_{50} = oral rat LD50, PEL = permissible exposure limit (OSHA-TWA), $ERAc$ = Emission to rural air, ^aN = Data-points, ^bSD = Standard deviation, ^cAAE = Average absolute error, ^dARE = Average relative error.

Figure 1 shows residual distribution plot for T_b (similar plots have been obtained for other analysed properties). It can be observed that residuals follow a normal distribution curve with mean zero suggesting a good fit of the experimental data used in the regression as well as the assumption of normal distribution of random errors is valid behind the followed approach.

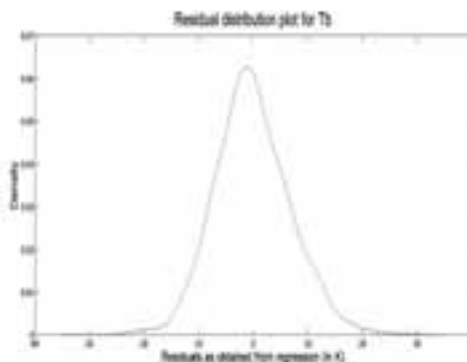


Figure 1. Residual distribution plot

Reliability and thermodynamic consistency of developed models: The reliability of developed property models has been tested by comparing model prediction uncertainties with reported range of experimental measurement uncertainties (see Table 3) for the properties with related available data from DIPPR 801 database.

Table 3. Comparison of average prediction error with average measurement error

Property	Data-points	Average meas. error	Average pred. error
T_b K	1306	6.32	6.17
T_c K	402	7.95	7.72
P_c bar	293	1.20	1.40
V_c cc/mol	234	22.30	7.97
T_m K	1385	5.10	15.99
G_f kJ/mol	258	4.60	5.24
H_f kJ/mol	704	6.31	1.77
H_{fus} kJ/mol	520	0.47	2.79
Flash point K	111	27.96	8.97

G_f = Gibbs free energy, H_f = Enthalpy of formation, H_{fus} = Enthalpy of fusion.

From Table 3, we notice that for most of the properties the prediction error is lower than (or at least comparable to) the average measurement error.

A plot of predicted values of T_b and T_c versus n -alkanes is shown in Figure 2. The experimental data available for T_b and T_c are also shown. In agreement with the basic physical principles, throughout the homologous series, the critical temperature of n -alkanes is always greater than their normal boiling point as the carbon number increases.

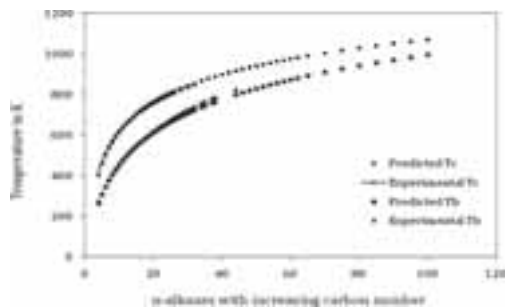


Figure 2. T_b versus T_c for n -alkanes

Selection of the most suitable property model: The selection of most suitable property model for a particular property can be done by studying the behaviour of property of certain class of chemicals with increasing molecular weight. This is illustrated for the case of $LC_{50}(FM)$. Figure 3 shows plots of various molecules types (such as alcohols, amines, multifunctional chemicals etc.) with increasing molecular weight versus their experimental values of $-\text{Log } LC_{50}(FM)$. It can be seen that these plots are linear in nature suggesting that the property $LC_{50}(FM)$ can be modeled using a linear form of the model. Similar analysis have been performed for other environment-related properties with the objective of providing an accurate and reliable property estimation of environment-related properties.

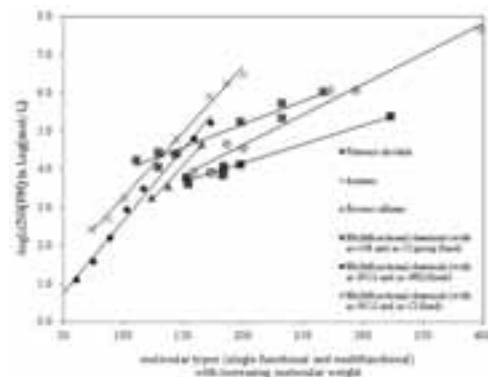


Figure 3. Plot of molecule types versus their $-\text{Log } LC_{50}(FM)$ values

Effect of quantity of data on the prediction performance of property models: The accuracy and reliability of GC-method based property models is largely determined by the quantity and quality of the data used in the parameter estimation. While developing a GC-model, very often, the experimental data-set of property is divided into training and validation sets. In our view, this is a disadvantage since the validation set is to be formed by randomly selecting the experimental data-points making some of the model parameters (that is,

group contributions) unavailable. This affects the application range of the property prediction method due to the lack of necessary experimental data that was made unavailable during the random selection process. Also, when all of the available experimental data-points are used in the parameter estimation step, it results in lower uncertainties of estimated model parameters and hence lower uncertainties of predicted property values [3],[4]. To illustrate this point, we have considered here a cross validation analysis (see Table 4) for property models of LD_{50} and $LC_{50}(FM)$. From Table 4, comparison of the AAE for training sets and test sets show that the predictive capability of the model for LD_{50} is fairly good. This is mainly due to the large amount of available experimental data of LD_{50} used for the training purpose. For $LC_{50}(FM)$, it can be observed that the AAE for test sets calculated using the model parameters as obtained by regression of the whole data-set are much better than those that are calculated using the parameters estimated using the training set. This illustrates that large quantity of the data when used for regressing the parameters of the GC-model, results in better quality of parameter estimation which in turn results in better model performance.

Table 4. Cross-validation analysis results for property models of LD_{50} and $LC_{50}(FM)$

property	Total data-points	AAE of training sets (with 80% of the data-points)	AAE of test sets based on parameters estimated using training sets	AAE of test sets using parameters estimated using whole data-set
LD_{50}	5995	0.3460	0.3811	0.3499
$LC_{50}(FM)$	809	0.4117	0.9169	0.4770

Sensitivities of process design due to uncertainties of property estimates

To evaluate the effects of uncertainties of predicted property values on the process design, a systematic methodology is developed. The methodology provides the following results: a) list of properties with critical importance from process design point of view; b) acceptable levels of accuracy for different thermo-physical property prediction models; and c) design variables versus properties relationships. Figure 4 illustrates the application of this methodology as applied to extractive distillation of acetone+methanol mixture using water as an entrainer. The y-axis shows deviation of design variable from its base case value and x-axis represents errors of predicted property values. It can be seen from Figure 4 that sensitivity of reflux ratio to prediction errors of vapour pressure is significant. If the

deviation in reflux ratio (say 20%) at a particular error (say +0.25%) of vapour pressure of acetone is not acceptable, then user needs to collect a higher accuracy data and use this data in regression to obtain improved model for vapour pressure with desired accuracy level (i.e., error < 0.25%). The sensitivities of process design of several other unit operations have also been analysed and summarized in Table 5.

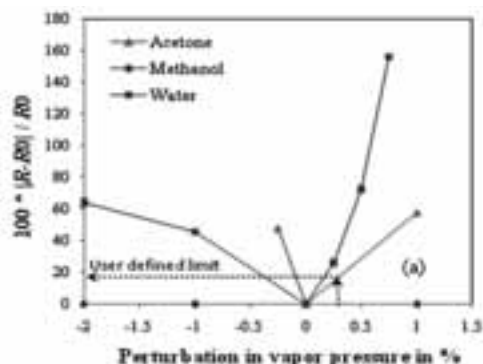


Figure 4. Effect of errors of vap. pressure on reflux ratio

Table 5. Analysis of sensitivities of process design

Unit operation (chemical system involved)	Reference for problem data / required task	Properties involved in the analysis	Variables considered for sensitivity analysis / most important properties (ranked)
Extractive distillation (Acetone +Methanol+ Water)	Gil et al.(2009) / separate acetone from methanol [9]	$P^s, T_c, P_c, H_{vap}, \mu, \text{viscosity, surface tension, density}$	Reflux ratio, number of stges, solvent atage / P^s of acetone and water, H_{vap} of acetone, Density of acetone.
Short-path evaporator (Glycerol + Mono-, Di-, and Tri-glyceride)	Sales-Cruz & Gani (2006) / separate glycerol from the mixture [10]	$P^s, T_c, P_c, H_{vap}, \mu, \text{specific heat } (C_p), \text{acentric factor } (\omega), \text{ and } \gamma$	Distillate (glycerol) flow rate / P^s of glycerol, γ of glycerol, ω of di-glyceride, P_c of di-glyceride C_p of glycerol and di-glyceride, T_c of glycerol, H_{vap} of di-glyceride.
Flash process (methanol and water)	ICAS-MoT® / Separate methanol from the mixture [11]	P^s, T_c (used in the correlation for H_{vap}), and ρ	Product (methanol) flow rate / T_c of methanol, P^s of methanol, ρ of methanol Volume of the flash tank / T_c of methanol, ρ of methanol

Conclusions

A systematic methodology for property modeling and uncertainty analysis is developed and used to develop

GC+ based models for the estimation of various pure component properties. In total, 21 thermo-physical properties and 22 environment-related properties have been analyzed. The developed property models provide reliable and accurate estimation of properties, together with uncertainties of predicted property values. This information allows one to perform better-informed product-process design by taking into account the effects of these uncertainties on the final design. Important issues related to property modeling such as reliability and thermodynamic consistency of the predicted properties have been addressed. The work on the performance improvement of selected important property models by introducing new structural parameters in the property model is underway. For performing analysis of sensitivity of process design due to uncertainties of property estimates, a systematic methodology is developed and applied for the design of several unit operations found in chemical industry. Our current and future work is focused on the development of models for lipid processing technologies for improvement in their design and performance. In this context, process modeling and analysis of deodorization process is taken as a first example.

Acknowledgements

This research work has received funding from the European Union Seventh Framework Programme [FP7-MC-ITN] under grant agreement no. 238013.

References

- [1] J. Marrero, and R. Gani, Fluid Phase Equilibria, (2001), 183-208.
- [2] R. Gani, P. Harper, and M. Hostrup, Ind. and Engg. Chem. Res., (2005), 44, 7262-7269.
- [3] A. Hukkerikar, B. Sarup, A. Ten Kate, J. Abildskov, G. Sin, R. Gani, Fluid Phase Equilib. 321 (2012) 25-43.
- [4] G. Seber, C. Wild, Nonlinear Regression, New York: Wiley, 1989.
- [5] T. Nielsen, J. Abildskov, P. Harper, I. Papaconomou, R. Gani, J. Chem. Eng. Data. 46 (2001) 1041-1044.
- [6] U.S. Environmental Protection Agency. <http://www.epa.gov/nrmrl/std/qsar/qsar.html> (accessed September 12, 2012).
- [7] USEtox™ model. <http://www.usetox.org/> (accessed September 12, 2012).
- [8] A. Hukkerikar, S. Kalakul, B. Sarup, D. M. Young, G. Sin, R. Gani, J. Chem. Inf. Model. 52(11), 2823-2839.
- [9] I.D. Gil, D.C. Botia, P. Ortiz, and O.F. Sanchez, 2009, Industrial Engineering and Chemical Research, 48, 4858-4865.
- [10] M. Sales-Cruz and R. Gani, 2006, Chemical Engineering Research and Design, 84, 583-594.
- [11] Integrated Computer Aided System (ICAS 14.0), CAPEC, DTU, Denmark.



Martin Høj

Phone: +45 4525 2842

E-mail: mh@kt.dtu.dk

Supervisors: Anker Degen Jensen
Jan-Dierk Grunwaldt, Karlsruhe Institute
of Technology

PhD Study

Started: September 2009

To be completed: December 2012

Nanoparticle Design using Flame Spray Pyrolysis for Catalysis

Abstract

Flame spray pyrolysis (FSP) is a novel method for synthesizing metal oxide nanoparticles. Nanoparticulate materials have very high surface area, which is advantageous for heterogeneous catalysis. This work focuses on applying FSP made catalysts in two processes: Hydrotreating of diesel and selective oxidation of propane to propene, two very different areas of heterogeneous catalysis employing sulfide and oxide catalyst, respectively.

Introduction

Liquid fed flame spray pyrolysis (FSP) is a one-step synthesis method for preparation of nanoparticles [1]. Metal compounds are dissolved in an organic solvent and the solution is sprayed as micrometer sized droplets with high velocity oxygen and ignited with a small premixed methane-oxygen flame [2].

The solvent and metal compounds evaporate and combust to form atomically dispersed vapors, which nucleate to form clusters when reaching cooler parts of the flame. The formed clusters grow by surface growth and sintering [3]. This result in non-porous nanoparticles, which form agglomerates and aggregates with high inter particle porosity [1]. The flame process gives high maximum temperature and a short residence time with thermally stable, homogeneous nanoparticles as the product.

Hydrotreating

Hydrotreating is performed at oil refineries in order to remove sulfur and nitrogen from the heterocyclic compounds in which these elements typically occur in crude oil [5]. Industrial hydrotreating catalysts contain Co or Ni promoted MoS₂ as active phase, on an alumina support [5]. The sulfide phase is obtained after sulfiding an oxide precursor, which can be prepared by FSP.

Oxidative dehydrogenation of propane

Demands for short chain olefins like ethylene and propylene are expected to increase in the near future [4]. Current production methods include steam cracking, fluid catalytic cracking and catalytic dehydrogenation.

Oxidative dehydrogenation of propane to propylene is a desirable exothermic process; however, a catalyst with sufficient activity and selectivity for industrial production of propylene by this method has not been discovered yet [4]. The most promising catalyst

candidates are supported vanadium and molybdenum oxide [4], which can be prepared by FSP.

Specific objectives

The objectives of my project are to prepare catalytically active nanomaterials using the FSP method, evaluate the catalytic activity and selectivity and investigate the physical and chemical structure using spectroscopy, X-ray diffraction and electron microscopy.

Results and discussion

Hydrotreating

Seven CoMo/Al₂O₃ samples were synthesized by FSP where all three metallic elements were sprayed in one flame. Different Mo loadings (8 to 32 wt.%) and Co/Mo ratios 1/3, 2/3 and 1/1 were investigated [6].

The catalysts had specific surface areas between 221 and 90 m²/g, decreasing surface area with increasing transition metal loading. This corresponds to average particle sizes of 7 to 13 nm, showing that nanoparticles were the product of the FSP synthesis.

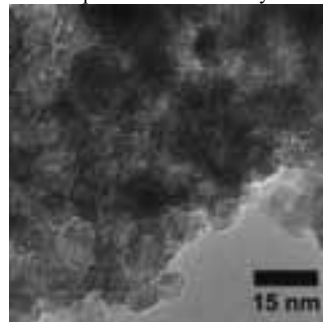


Figure 1: TEM image of 16 wt.% Mo sulfide sample.

The activities of the catalysts for removal of heterocyclic sulfur and nitrogen were measured after sulfidation. The best catalysts contained 16 wt.% Mo with Co/Mo = 1/3, which HDS activity was 75 % of a commercial reference catalyst (see Fig. 2). Increasing the Co content in the FSP material caused a small drop in activity, while increasing or decreasing the Mo content resulted in significantly lower activity.

TEM images of the sulfided catalysts showed a significant increase in MoS₂ particles size with increasing Mo content, explaining the lower activity of high Mo loaded catalysts.

X-ray diffraction (XRD) and UV-vis reflectance spectroscopy showed that the oxide precursor contained γ -Al₂O₃ with some CoAl₂O₄, while MoO₃ was XRD amorphous. The CoAl₂O₄ is unwanted since the Co in this form does not promote the MoS₂ active phase.

Using two-nozzle FSP where Co and Al were sprayed in separate flames resulted in significant reduction of CoAl₂O₄ spinel as determined with UV-vis [7]. Raman spectroscopy identified supported MoO_x species and CoMoO₄ on the oxide catalyst. With two-nozzle FSP the catalytic activity improved from 75 to 91 % of a commercial reference catalyst.

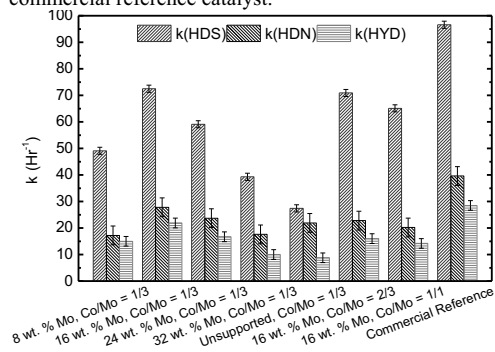


Figure 2: Activity of FSP made CoMo catalysts.

Oxidative dehydrogenation of propane

A new setup with three sequential reactors in series/by-pass configuration has been constructed for evaluating oxidative dehydrogenation catalysts.

Several alumina supported vanadia [8], molybdena and mixed vanadia/molybdena [9] catalysts with varying amounts of transition metal have been synthesized by FSP. The catalysts had surface areas between 140 and 180 m²/g, showing that the products are nanoparticles. The vanadia and molybdena were XRD amorphous while the support was γ -Al₂O₃. UV-vis and Raman spectroscopy identified supported VO_x and MoO_x monomers and oligomers.

The catalysts were highly active for oxidative dehydrogenation. Using low amounts of vanadia propene yields of up to 12 % was achieved at conversion of 33 % at temperatures around 500 °C (see Fig. 3). The conversion and yield could be interpreted in terms of a kinetic model which allowed the determination of the optimum temperature and contact times for high propene yield [10].

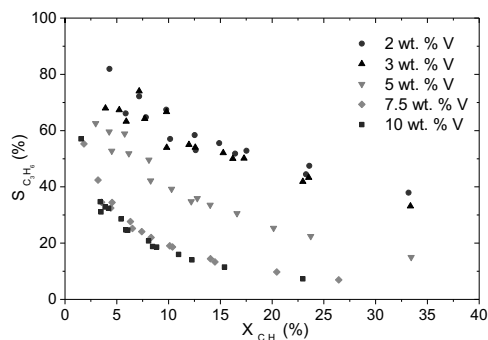


Figure 3: Propene selectivity as function of propane conversion for VO_x/Al₂O₃ catalysts.

Conclusion

FSP is a promising new method for preparation of catalytically active nanoparticles. The prepared hydrotreating catalysts show high activity for initial experiments with a new synthesis method and high propene yields were achieved in oxidative dehydrogenation of propane.

Acknowledgements

DSF grant 2106-08-0039. M. Brorson and P. Beato (Haldor Topsøe A/S) for hydrotreating activity tests and Raman. J. B. Wagner and T. W. Hansen (DTU CEN) for TEM. L. Mädler and D. Pham (University of Bremen) for two-flame FSP. S. Mangold and A. Boubnov (ANKA synchrotron) and DanScatt for XAS.

References

1. R. Strobel, and S.E. Pratsinis, *J. Mater. Chem.* 17 (2007) 4743-4756.
2. L. Mädler, H.K. Kammler, R. Mueller, S.E. Pratsinis, *J. Aerosol Sci.* 33 (2002) 369-389.
3. H.K. Kammler, L. Mädler, S.E. Pratsinis, *Chem. Eng. Technol.* 24 (2001) 583-596.
4. F. Cavani, N. Ballerini, A. Cericola, *Catal. Today* 127 (2007) 113-131.
5. H. Topsøe, B.S. Clausen, F.E. Massoth, in: J.R. Anderson, M. Boudart (Eds.), *Catalysis: Science and Technology*, vol. 11, Springer, Berlin, 1996.
6. M. Høj, K. Linde, T. K. Hansen, M. Brorson, A. D. Jensen, J.-D.Grunwaldt, *Appl. Catal. A* 397 (2011) 201-208.
7. M. Høj, D. K. Pham, M. Brorson, L. Mädler, A. D. Jensen, J.-D.Grunwaldt, *Catal. Lett.* Submitted (2012).
8. M. Høj, A. D. Jensen, J.-D.Grunwaldt, *Appl. Catal. A* In press (DOI: 10.1016/j.apcata.2012.09.037).
9. M. Høj, T. Kessler A. D. Jensen, J.-D.Grunwaldt, In preparation (2012).
10. M. Høj, J.-D.Grunwaldt, A. D. Jensen, *Appl. Catal. A* Submitted (2012).
11. M. Høj, J. M. Christensen, A. D. Jensen, J.-D. Grunwaldt, *Dansk Kemi*, 93:10 (2012) 19-21.



Cathrine Heinz Ingvordsen

Phone: +45 23669751
E-mail: cahi@kt.dtu.dk

Supervisors: Rikke Bagger Jørgensen
Teis Mikkelsen
Michael Lyngkjær, KU-Science
Pirjo Peltonen-Sainio, MTT, Finland

PhD Study

Started: January 2011
To be completed: April 2014

Climate Change Effects to Plant Ecosystems

Abstract

The climate is currently changing with a speed not observed earlier. Climate change affects the world's natural plant ecosystems and consequently the food production systems. Prognoses for Denmark reveal drastic changes with increased temperature and extreme weather events. In this PhD project preliminary results indicate a 28.9 % decrease in spring barley grain yield under expected levels of temperature and CO₂. This drastic decrease is a significant challenge to the agricultural sector that has to feed the increasing world population in a sustainable way.

Introduction

Plant ecosystems consist of plant populations wherein the individual plants are sessile and populations only migrate slowly over time. For this reason plant ecosystems are highly dependent on the surrounding environment, why climate change and biotic stressors as plant pathogens and herbivores strongly affects the agro-ecosystems.

Climate change has, within the last years, lead to decrease agricultural production, and the question is, if food production in the future climate can feed the rapidly growing population of the world [1, 2]. In Denmark the prognoses foresee increase in the summer and winter temperatures together with increased levels of the greenhouse gasses carbon dioxide (CO₂) and ozone (O₃). It is also foreseen that Denmark more frequently will experience extreme weather events such as drought, heat waves and flooding [3]; events that can be devastating for plant ecosystems. The underlying mechanisms of climate change impact on plant ecosystems have been studied only in recent years, where the effects of the changed climate have become measurable. These studies and the ones to come are of great importance to understand and mitigate climate change effects to plant ecosystems.

The PhD project is part of the NordForsk network 'Sustainable primary production in a changing climate' [4] which comprise plant breeders and scientists from Sweden, Finland, Norway and Denmark.

Specific Objectives

This PhD project aims to identify suitable plant genetic resources to mitigate the expected biotic and abiotic

stressors of the future climate. The pace of possible genetic adaptation as a result of the altered environment will moreover be evaluated. Spring barley (*Hordeum vulgare*) and spring oilseed rape (*Brassica napus*) are used as models for crop plants as molecular tools are applicable. The future environmental conditions will be mimicked in the technically advanced phytotron, RERAF (Risø Environmental Risk Assessment Facility) [5].

Results and Discussion

Half way into the project one experiment (1) has been completed and two experiments initiated (2 and 3).

1) To explore the genotypic variance in tolerance to climate change, 140 barley accessions have been screened in RERAF under single and double factor climate scenarios as envisaged by the Intergovernmental Panel on Climate Change (IPCC, scenarios A1FI) [6]. In collaboration with Nordic plant breeding stations of the NordForsk network the 140 accessions have also been tested for field resistance to the fungal diseases net blotch, caused by *Pyrenophora teres*, spot blotch caused by *Bipolaris sorokiniana*, rust caused by *Puccinia hordei* and leaf spot caused by *Ramularia collo-cygni*. Further have 50 oilseed rape accessions been tested for resistance to wilt caused by *Verticillium longisporum* and Phoma caused by *Leptosphaeria maculans*. Results on climate tolerance and fungal resistance are entered into a DNA marker (SNP) association study to link phenotypic traits to DNA markers.

2) In order to analyse the tolerance of barley to extreme climate events, 22 barley accessions from the above 140

barley accessions are studied under the extreme event 'heat wave'. Plants entering the heat wave are grown in single and double factor treatments mimicking the IPCC scenarios [6]. Results on yield and photosynthesis are to enter into the marker association study.

3) To study adaptive genetic changes to fast changes in the climate, amplified fragment length polymorphism analysis has been performed on the first and fifth generation of a unique plant material (four cultivars of oilseed rape and barley) that have been selected over five plant generations in the single and double factor climate scenarios [7]. Identification of outlier loci will reveal genetic markers that have been selected for over generations [8] and indicate the potential for rapid adaptation [9].

Add 1) During cultivation of the barley accessions differences between the climate treatments were noticeable (Fig. 1). As earlier observed a raised $[CO_2]$ level induced increased growth, and elevated temperature caused decreased growth compared to ambient conditions (fig. 1; b, c, d) [10]. The treatment with a combination of elevated $[CO_2]$ and temperature showed plant vigour in between the single factor treatments (fig. 1; a, b, c, d).

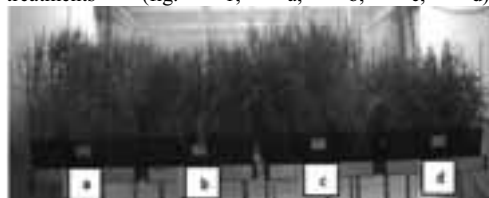


Figure 1: The cultivars Anakin, Columbus and Simba from Sejet Plant breeding Station grown 68 days in different atmospheres. a. 700ppm $[CO_2]$, 24°C, b. 385ppm $[CO_2]$ (control), 19°C c. 700ppm $[CO_2]$, 19°C d. 385ppm $[CO_2]$, 24°C.

The grain yield pooled over all accessions supported the visual observations (fig. 2). All treatments were found significant from the control treatment in regard to grain yield.

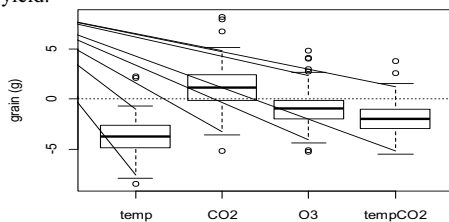


Figure 2: Relative treatment effects for 140 spring barley accessions grown under +5°C above ambient (temp), a $[CO_2]$ of 700 ppm (CO2), a $[O_3]$ of 100-150 ppb (O3) and the combined treatment of +5°C and 700 ppm $[CO_2]$ (tempCO2). The production in the ambient control treatment is the dashed line (0). Ambient conditions were 19°C/12°C (day night), 385 ppm $[CO_2]$ and 0 ppb $[O_3]$.

In grouping of the 140 accessions a stronger response to increased $[CO_2]$ was identified for the group of cultivars (intensively bred) than for the group of landraces (less

bred and with supposedly high genetic diversity). This result suggests the photosynthetic apparatus to have been targeted in the breeding process.

In the association study the traits identified in the screens will be associated with molecular markers. The association to a known DNA sequence allow for fast identification of specific traits in a genetic resource. This genetic resource can then be exploited in the development of cultivars for use in the future environment.

Conclusions

Interesting preliminary results have been produced and more results are underway. The preliminary results add to the general understanding of climate change being a severe threat to the world's food supply. Additionally crop genotypes for the future have been suggested.

Acknowledgements

The author thanks the NordForsk network 'Sustainable primary production in a changing climate' for funding, her supervisors for scientific discussions and repeatedly encouragement. She also thanks everyone at Risø for the positive working environment.

References

1. Tilman D., Cassman K. G., Matson P. A., Naylor R. & Polasky S (2002). *Nature* 418:671-677.
2. Foley J. A., Ramankutty N., Brauman K. A., Cassidy E. S., Gerber J. S., Johnston M., Mueller N. D., O'Connell C., Ray D. K., West P. C., Balzer C., Bennett E. M., Carpenter S. R., Hill J., Monfreda C., Polasky S., Rockström J., Sheehan J., Siebert S., Tilman D. & Zaks D. P. M. (2011). *Nature* 478: 337-342.
3. M. Trnka, J. E. Olesen, K. C. Kersebaum, A. O. Skjelvåg, J. Eitzinger, B. Seguin, P. Peltonen-Sainio, R. Rötter, A. Iglesias, S. Orlandini, M. Dubrovský, P. Hlavinka, J. Balek, H. Eckersten, E. Cloppet, P. Calanca, A. Gobin, V. Vučetić, P. Nejedlik, S. Kumar, B. Lalic, A. Mestre, F. Rossi, J. Kozyra, V. Alexandrov, D. Semerádová & Z. Žalud. *Glob Change Biol* 17 (2011) 2298-2318.
4. <http://www.risoe.dtu.dk/nordforsk.aspx>
5. http://www.risoe.dtu.dk/business_relations/Product_s_Services/Risk_Assessment/BIO_RERAF.aspx
6. IPCC, in: R.K. Pachauri, and A. Reisinger (Eds.) IPCC, Geneva, 2007, Switzerland, p. 104.
7. Frenck, G. Ph.D. Thesis. (2010) Technical University of Denmark and Aarhus University.
8. A. Pérez-Figueroa, M. J. García-Pereira, M. Saura, E. Rolán- Alvarez & A. Caballero, *J Evol. Biol.* 23 (2010) 2267-2276.
9. A. Bonin, P. Taberlet, C. Miaud & F. Pompanon, *Mol Biol. Evol.* 23 (2006) 773-783.
10. E. A. Ainsworth, P. A. Davey, C. J. Bernacchi, O. C. Dermody, E. A. Heaton, D. J. Moore, P. B. Morgan, S. L. Naidu, H. Y. Ra, X. Zhu, P. S. Curtis, and S. P. Long, *Glob Change Biol* 8 (2002) 695-709.



Krešimir Janeš

Phone: +45 4525 2992
E-mail: kreja@kt.dtu.dk

Supervisors: Krist V. Gernaey
John M. Woodley
Pär Tufvesson

PhD Study
Started: December 2010
To be completed: November 2013

A Methodology for Selection of Cascades for Co-product Removal in an ω -transaminase System

Abstract

Production of optically pure chiral amines using transaminases is an attractive alternative to conventional synthetic methods, which yield low enantio-purity and require costly purification processes. Two reaction strategies have been demonstrated: kinetic resolution and asymmetric synthesis. The latter approach has the advantage of a theoretical yield of 100% as compared to 50% for resolution strategies [1]. However, a major challenge for asymmetric synthesis is overcoming the unfavourable thermodynamic equilibrium for many of the most interesting reactions. In order to achieve high enough yields at conditions typical for pharmaceutical processes (>50 g product/L, etc.) the product and/or co-product formed during the reaction must be selectively removed (so called *in-situ* co-product removal (IS(C)PR)). Several different alternative co-product removal strategies have been suggested, all of which have different impacts on the overall process. One strategy is to use a second enzyme reaction to remove the co-product in a so called enzymatic cascade [2]. Many different enzymes and reactions have been suggested for how this can be done but still there are no decision tools available to help select the most appropriate cascade systems.

Introduction

The role of biocatalysis is becoming more and more important in the pharmaceutical industry because it offers an interesting alternative to present synthesis methods. For many biocatalysis processes it is necessary to run the reaction under high substrate concentrations in order to meet high productivity demands and achieve economic feasibility. However, the disadvantage of high substrate and product concentrations is that they can cause process limitations. Some of these limitations are caused by the biocatalyst and its inability to handle high concentrations of product, i.e. toxicity or product inhibition occurs. Protein engineering can be used to overcome these problems [3, 4]. Another process limitation which cannot be addressed by protein engineering is the thermodynamic equilibrium of the reaction. In the case when the substrate side of the reaction is favored, high product concentration will stop the progress of the reaction. Shifting the unfavorable equilibrium definitely has many advantages, especially for the industrially relevant reactions where high yields are expected. One of such examples is investigated ω -transaminase reaction shown in Figure 1.



Figure 1. Simplified general scheme of ω -transaminase reaction and equilibrium shift strategy of co-product removal

Continuous removal of one or more products from the reaction mixture can shift the thermodynamic equilibrium towards product formation [5, 6]. However, not all ISPR technologies can address this problem adequately. Traditional ISPR technologies like extraction, adsorption, evaporation, etc. are lacking sufficient selectivity and ability to decrease product or co-product concentration to low enough levels.

Enzymes as ISPR/IS(C)PR

To illustrate the ISPR for shifting equilibrium, a case study using ω -transaminase in production of chiral amines has been chosen using an LDH/GDH cascade system to shift the equilibrium (Figure 2). This is a system which favors the substrate side of the reaction and K'_{eq} is $4 \cdot 10^{-5}$. It is obvious that there is a strong

need for implementing an equilibrium strategy for this system. To shift the equilibrium, product or co-product has to be removed. Unfavorable thermodynamics demands at least two ISPR/IS(C)PR criteria to be fulfilled: selectivity and ability to remove product or co-product to extremely low concentrations. Selectivity is important to maintain equilibrium shift. Lack of selectivity means possible removal of substrate and shifting the equilibrium back to the substrate side. The second demand of removing product/co-product is extremely important to the shifting of the equilibrium. The amount of product/co-product remaining in the reaction mixture depends on K'_{eq} of the reaction and also on the desired yield (Figure 3). For the ω -transaminase case, a desired yield of 95%, starting substrate concentrations of 500 mM 1-phenylethanone and 1200 mM alanine, and the maximum allowed concentration of residual product or co-product is 1.27 μ M.

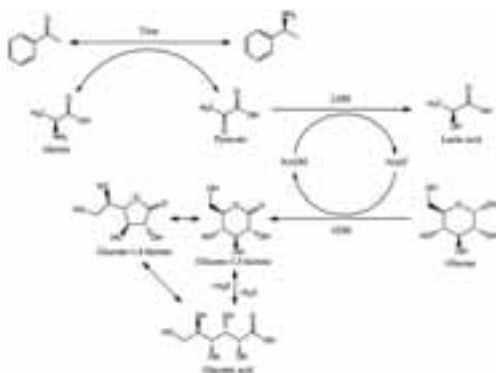


Figure 2. An example of in situ co-product removal in a ω -transaminase reaction by lactate dehydrogenase (LDH) and glucose dehydrogenase (GDH); pyruvate is degraded by an LDH catalyzed reaction and nicotinamide adenine dinucleotide (NADH) is recycled by a sacrificial GDH catalyzed reaction.

Furthermore, another challenge that is required of ISPR/IS(C)PR technology is to remove the product/co-product relatively fast at already quite a low concentration. This means that all technologies, whose driving force is proportional with the concentration of the component to be removed, are inadequate to remove it fast enough. Adsorption, extraction, evaporation and even chemical reaction are techniques whose driving force is proportional to the concentration of the component that needs to be removed and thus cannot be effectively used. Different technologies that utilize other characteristics of the component to be removed like electrodialysis, pervaporation or other membrane technologies lack selectivity in this case. It has also been reported that an electromagnetic field can cause protein unfolding [7] which makes it a poor *in situ* technology. In general, usage of membrane technologies in free enzyme systems is limited to UF membranes,

which are characterized by high fouling and pressure drop. Alternatives are immobilization of enzymes or whole cell processes.

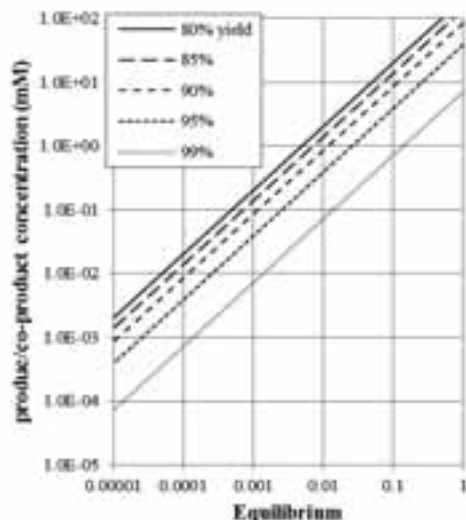


Figure 3. The amount of allowed product or co-product remaining in the reaction mixture as a function of K equilibrium and desired yield

One of the possibilities of shifting equilibrium is ISPR/IS(C)PR by enzymes. There are many examples in the literature where these cascade enzymatic reactions are used in ISPR to shift thermodynamic equilibrium [8, 9, 10, 11]. Enzymatic cascades are the only technology that satisfies previously addressed ISPR/IS(C)PR criteria. They are extremely selective and can reduce the concentration of product/co-product to extremely low values, and furthermore an even lower concentration can be achieved starting already from a low concentration if the K_m value of the enzyme is low enough.

Specific Objectives

In the current work a methodology is developed for choosing a feasible cascade system that will meet process requirements under process relevant conditions. Decisions are based primarily on two parameters: relative stability and specific reaction rate under process relevant conditions. Other parameters such as thermodynamic constraints, kinetics, selectivity, pH change, cascade enzyme compatibility and downstream processing have been considered and are discussed to obtain a holistic overview and understanding of the process. The methodology has been applied to an ω -transaminase system which is thermodynamically challenged ($K'_{eq} = 4 \cdot 10^{-5}$). The enzymes compared for co-product removal are dehydrogenases: lactate dehydrogenase (LDH) (EC 1.1.1.27), alanine dehydrogenase (AlaDH) (EC 1.4.1.1) and as co-factor recycling enzymes: glucose dehydrogenase (GDH)

(EC 1.1.1.47) and formate dehydrogenase (FDH) (EC 1.2.1.2).

The method reviews the potential solutions for transaminase co-product removal and identifies currently best cascade candidates. The methodology identifies current bottlenecks for all investigated cascade systems and provides feedback for future process/enzyme improvement and development.

Results and Discussion

It is very important to evaluate enzymes at concentrations that mimic to some extent current or future industrial process conditions. Working in such conditions and evaluating enzyme stability and activity differs from usual laboratory conditions which are usually milder. For an industrial process to be economically feasible, more than 50 g product/L is needed.

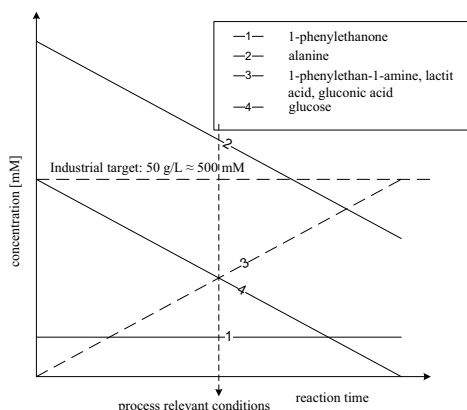


Figure 4. Simplified progress curves of the proposed industrial process of an ω -transaminase reaction using the LDH/GDH cascade system for equilibrium shift and the proposed method of choosing process relevant conditions

An industrial process has been taken into consideration where ω -transaminase is used to produce 1-phenylethylamine, and the LDH/GDH cascade system is used to shift the equilibrium. (Figure 4) The proposed time for this reaction is 24 h under which substrate is converted into 50 g product/L which roughly corresponds to 500 mM. To avoid a two phase system, the concentration of ketone substrate, 1-phenylethanol was kept under maximum miscibility, 30 mM, throughout the whole reaction time (line 1). An excess of amino donor is given (line 2) to push to some extent the thermodynamic equilibrium towards the product side. Reaction products 1-phenylethylamine, lactic acid and gluconic acid are produced in the reaction and their concentration rises to 500 mM (line 3). The starting substrate concentration for sacrificial GDH reaction is 500 mM and is reduced when the reaction takes place (line 4). An approximation of the

reaction (progress) curve to line has been made to simplify the process of choosing process relevant conditions. After approximately 12 hours of reaction time a point was chosen to represent conditions under which cascade enzymes were investigated.

Two important parameters were followed: relative stability and specific reaction rate. Results are shown in figure 5.

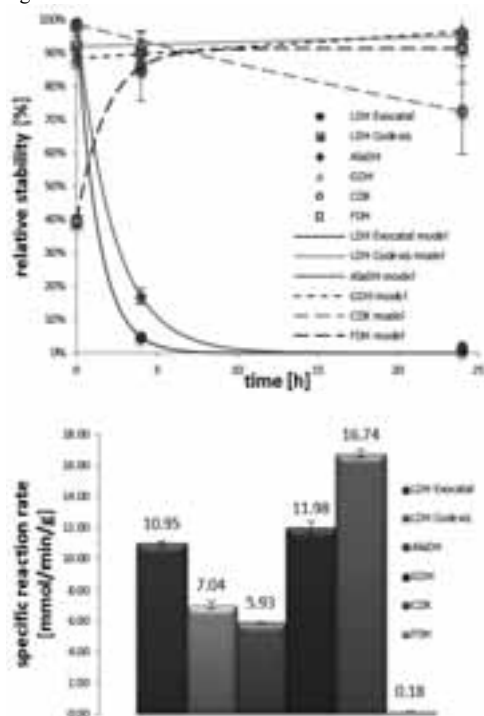


Figure 5. Relative stability and specific reaction rate of the investigated cascade reactions under their respective reaction conditions

Results show increased stability under the respective reaction conditions for all investigated enzymes except LDH from Evocatol and AlaDH. These results should be interpreted together with specific reaction rate results which show how much of the cascade enzyme should be added to the reaction mixture and therefore they determine the cost of cascade enzymes.

From figure 5, it can be concluded that LDH Codexis is the only pyruvate enzyme which shows adequate stability over 24 hours. From co-factor regenerating enzymes GDH, CDX and FDH show satisfactory stability where CDX is engineered GDH.

Theoretical aspects

The current choice of enzymes has many drawbacks. Both enzymes produce salts which remain in the reaction mixture and which need to be removed afterwards. Alternative enzymes can either recycle

pyruvate back to pyruvate (AlaDH) or produce volatile or gaseous products (FDH). GDH has another major disadvantage of producing gluconic acid and therefore changing pH of the reaction mixture. Based on a 50 g product/L calculation, 500 mM of gluconic acid is produced which corresponds to a pH value of 2.08. This significant pH change requires pH control which then involves dilution problems and as a consequence a concentration step is again required. It is therefore the future objective of this methodology to identify possible alternative enzymatic cascades which show promise regarding their robustness, kinetic, thermodynamic, stability requirements, as well as downstream processing, pH change and interference with other reaction mixture components

Conclusions

Methodology has identified the LDH/GDH cascade system (both enzymes from Codexis) currently as the best option for an equilibrium shifting strategy in ω -transaminase catalyzed reactions. This conclusion is based on experimental determination of both specific activity and relative stability. However, this doesn't necessarily mean that this cascade choice is going to be the best option for the future.

Future Work

- Identification of theoretically interesting cascade enzymes for shifting the thermodynamic equilibrium
- Validation of alternative enzymatic cascades based on theoretical aspects: thermodynamics, pH change, downstream processing and identifying overall process bottlenecks
- Application of the method on different systems for shifting thermodynamic equilibrium and validation

Acknowledgments

The support from the AMBIOCAS project financed through the European Union 7th Framework Programme (Grant agreement no.: 245144) is acknowledged.

References

1. Höhne M, Kühl S, Robins K, Bornscheuer U T. (2008). Efficient Asymmetric Synthesis of Chiral Amines by Combining Transaminase and Pyruvate Decarboxylase. *ChemBioChem* 2008, Vol. 9: 363-365
2. Tufvesson P, Lima-Ramos J, Skibsted J J, Al-Haque N, Neto W, Woodley J M. Process considerations for the asymmetric synthesis of chiral amines using transaminases. *Biotech. Bioeng.* (2011) Vol. 108: 1479-1493
3. Lutz S, Beyond directed evolution – semi-rational protein engineering and design. *Curr. Opin. Biotechnol.* (2010) Vol. 21: 734-743
4. Bommarius A S, Blum J K, Abrahamson M J. Status of protein engineering for biocatalysts: how to design an industrially useful biocatalyst. *Curr. Opin. Biotechnol.* (2011) Vol. 15: 194-200
5. Heemrema L, Roelands M, Goetheer E, Verdoes D, Keurentjes J. In-situ product removal from fermentations by membrane extraction: Conceptual process design and economics. *Ind. Eng. Chem. Res.* (2011) Vol. 50: 9197-9208
6. Wang K, Lu Y, Liang W Q, Wang S D, Jiang Y, Huang R, Liu Y H. Enzymatic synthesis of galactooligosaccharides in an organic-aqueous biphasic system by a novel β -galactosidase from a metagenomic library. *J. Agric. Food Chem.* (2012) Vol. 60: 3940-3946
7. Freedman K J, Jürgens M, Prabhu A, Ahn C W, Jemth P, Edel J B, Kim M J. Chemical, thermal and electric field induced unfolding of dingle protein molecules studied using nanopores. *Anal. Chem.* (2011) Vol. 83: 5137-5144
8. Truppo M D, Rozelli J D, Turner N J. Efficient production of enantiomerically pure chiral amines at concentrations of 50 g/L using transaminases. *Org. Process Res. Dev.* (2010). Vol. 14: 234-237
9. Fuchs M, Koszelewski D, Tauber K, Kroutil W, Faber K. Chemoenzymatic total synthesis of (S)-Rivastigmine using ω -transaminase. *Chem. Commun.* (2010) Vol. 46: 5500-5502
10. Cassimjee K E, Branney C, Abedi V, Wells A, Berglund P. Transaminations with isopropyl amine: equilibrium displacement with yeast alcohol dehydrogenase coupled to *in situ* cofactor regeneration. *Chem. Commun.* (2010) Vol. 46: 5569-5571
11. Yun H, Kim B G. Asymmetric synthesis of (S)- α -methylbenzylamine by recombinant *Escherichia coli* co-expressing omega-transaminase and acetolactate synthase. *Biosci. Biotechnol. Biochem.* (2008) Vol. 11: 3030-3033



Joakim M. Johansen

Phone: +45 4525 2830
E-mail: jjoha@kt.dtu.dk

Supervisors: Peter Glarborg
Peter A. Jensen

PhD Study

Started: September 2011
To be completed: August 2014

Biomass Burners for Biodust Combustion

Abstract

In the strive for a CO₂-neutral energy profile the exploitation of biomass in central and decentral heat and power plants has continuously increased in recent decades. This PhD-project aims to establish a scientific basis for the development of a new generation of biodust burners for utility boilers. The project focuses on particle ignition and flame stabilization through parametric studies both in full-scale measurements and from a CFD (Computational Fluid Dynamics) point of view. This article will introduce the reader to the philosophy behind and the methods used to achieve these goals.

Introduction

In recent decades, central power and heat production through thermal conversion of biomass has gained ground concurrently with the political agenda both on a national and an international level. The development of high efficiency biomass plants are required in order to balance the fluctuating power production from wind mills and other alternative energy sources, while still striving towards a CO₂-neutral energy profile. In addition, thermal plants are a necessary need in the provision of district heating.

Development and implementation of high efficiency biomass combustion technology is arguably the best near-term solution to provide stable and CO₂-neutral centralized power and district heating to larger cities and industrial areas.

Biomass differs from conventional solid fossil fuels (traditionally coal) in a number of essential areas including both chemical composition and physical structure and appearance. Thus, direct utilization of existing high efficiency pulverized power or combined heat and power facilities is not an option when considering biodust as an energy source.

The fibrous nature of the biomass complicates particle pretreatment implying larger and oddly shaped fuel particles; changing the aerodynamics and particle size distributions. In addition, the larger fraction of volatile matter changes the conditions at which a stable flame is achieved. A turbulent development of the technology aiming to convert existing high efficiency burner installations has been conducted in Denmark throughout the past couple of decades. However,

technical difficulties lower the efficiency and limit the operation flexibility both with regards to biomass type and quantity.

Objectives

This work aims to establish a scientific basis for the development of a new generation of biomass burners designed to facilitate simultaneous high power efficiency and fuel flexibility combined with good particle burn-out and stable flame capabilities of dedicated biodust fueled plants. The project will link fuel properties to flame properties, considering both fluid dynamic effects due to the differences in particle characters and chemical effects due to changes in the chemical composition and kinetics.

Content

The project will include full scale combustion measurements from relevant plants operated by the industrial partners: Dong Energy Power and Vattenfall. This will include advanced in-situ high speed thermal imaging, optical and extractive probe measurements of the flame, burner area, and fuel conveying system. Close coordination with other work-packages will ensure thorough fuel characterization of a range of different biomass fuels. Flame detection by state of the art diagnostic techniques will be evaluated for optimized operational control.

Fundamental research will be conducted in pilot, bench and/or lab-scale facilities both at DTU Chemical Engineering and during an external stay at Stanford University, Department of Mechanical Engineering.

This will form the basis for modeling work applicable to computational fluid dynamics calculations taking both chemical kinetics and aerodynamic differences between fossil fuels and biodust into account, for the development of novel burner designs.

Swirling Jets

Swirling jets are the main objective of this work. Multiple independent wall mounted burners introduces both fuel and combustion air to the furnace. A fuel-air mixture is introduced to the furnace through a central tube. Secondary and tertiary air is introduced at high velocities (60–80 ms) through annular inlets surrounding the central tube. By angling the secondary air stream relative to the primary jet, introduces a tangential velocity component, stabilizing the flame. As the angular-to-linear-momentum ratio reaches a critical value, described by the non-dimensional swirl number, S , vortex breakdown will occur and a toroidal recirculation will be established in the central region of the jet. Controlling this toroidal recirculation pattern is a key element in the concept of swirling jet combustion of pulverized solid fuels, the effect is illustrated in Figure 2. By introduction of a proper recirculation, intense mixing and combustion may be achieved along with good flame stability. The backward motion ensures a convective heat flux through burning matter from the hot jet back to the nozzle exit at reverse velocities close to the forward motion of the primary jet. This significantly raises the temperature in the near burner field facilitating early ignition and close flame attachment. However, the high degree of mixing in the high temperature zone significantly increases the formation of thermal NO_x .

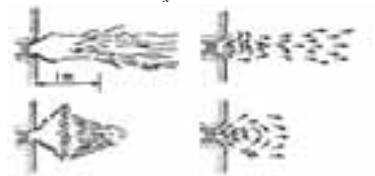


Figure 1: (Top) Low swirl flame, long flame and high degree of main jet penetration. (Bottom) High swirl flame, short flame and large recirculation zone [1].

Full-Scale Campaigns

Full-scale data from pulverized flame burners are scarce in the literature and most present studies have been conducted on either coal or co-fired flames. The need for data obtained from dedicated biodust combustion is important in the development of future designs of high efficient and fuel flexible power plants utilizing sustainable solid fuels, i.e. biomass.

The interpretation of full-scale measurements can be difficult and the exact influence of each parameter almost impossible to assign. The idea behind the upcoming full-scale campaigns is to investigate the influence on biodust ignition and flame stabilization of large variations in central parameters, e.g. fuel load,

particle sizes, swirl, etc. The process parameter influence will be evaluated by in-flame measurements on key values: temperature, velocity fields, imaging techniques in both in the ultra-violet, visible, and infra-red spectra, extractive gas probe and particle sampling, etc.

The experiments are to be carried out in two different full-scale wall fired utility boilers capable of burning 100 % biodust: Amagerværket and Herningværket operated by Vattenfall and Dong Energy Power, respectively. The equipment are of zeroth and first generation biodust burners, i.e. coal burners fueled with biodust and coal burners with physical modification aiming to optimize the process for biodust combustion.

Specialized equipment has been developed for the purpose of requiring flame measurement data from within the flame. Water cooled probes with multiple channels for installation of various measurement equipment have been designed and constructed specifically to this task. Entering the boiler through the burner itself will make it possible to observe changes along the centerline of the flame and thereby provide much wanted flame data for model evaluation.

CFD as an Engineering Modeling Tool

CFD is a widely used method for combustion purposes. As the computational power becomes more readily available the complexity and expectations from the simulation results increases accordingly. As a consequence the models are correspondingly advance and therefore computational demanding. A classical engineering approach to system designs is through parameter studies of simplified models where key parameters are adjusted systematically and with relatively large magnitude for qualitative assessment of the system response – this serves as the primary philosophy for the CFD part of this project.

Numerical modeling tools in the form of CFD simulations will be employed on generic burner geometries for qualitative analysis of a parametric study using the commercial code FLUENT and in cooperation with Clausthal University of Technology. This will provide valuable information on the understanding of the mechanisms taking place when disturbances are introduced to such a system. Correlation to the full-scale results will hopefully open up new ways of utilizing a tool where precision and high degrees of details have conventionally been considered as alpha and omega. This part is in the outlook.

Acknowledgements

This PhD project is part of the GREEN Research Center (Center for Power Generation from Renewable Energy) financed by the Danish Strategic Research Council.

References

- [1] J. M. Beér, J. Chomiak, and L. D. Smoot, *Prog. Energy Combust. Sci.*, 10(2):177-208, 1984

**Andreas Kamp**

Phone: +45 2133 0517
E-mail: ankam@kt.dtu.dk

Supervisors: Hanne Østergård
Simon Bolwig, DTU Management

PhD Study

Started: August 2011
To be completed: November 2014

Sustainability Assessment of 2nd Generation Bioenergy Production in Ghana

Abstract

The PhD project aims to investigate the potential for developing 2nd generation (2G) bioenergy production based on Ghana's hitherto unused agro- and agro-industry-based biomass resources. A multi-disciplinary approach is undertaken to evaluate the environmental consequences for selected case study combinations of biomass production scale, conversion technology and type of biomass co-production. A systems perspective where outputs are considered collectively rather than isolated from co-products is applied. Two publications on systems perspective in bioenergy sustainability assessment methodology have been submitted. Data collection is ongoing.

Introduction

Ghana has a growing economy and energy demand usually increases with economic growth. New bioenergy technologies using hitherto unused biomass from agriculture and agro-industry provides Ghana with the opportunity to meet the growth in energy demand and increase energy security by being less dependent on imports. Basing energy production on biomass resources must however, take into consideration competing uses and availability of the feedstock, the requirement of inputs to biomass production and conversion including their origin, and the substitutability of bio-based energy carriers with fossil-based carriers.

In 'Biofuel production from lignocellulosic materials – 2GBIONRG', a research project funded by DANIDA, systems analysis with a multi-disciplinary approach is undertaken to evaluate the environmental and socio-economic consequences of 2nd generation bioenergy production in Ghana. The project identifies and studies a selection of case systems that are characterised by different combinations of biomass production conditions, utilised feedstock(s) and energy conversion technologies:

1. Municipal waste converted to biogas and/or liquid biofuel
2. Small-scale, staple food residues converted to biogas
3. Large-scale, staple food residues converted to biogas and/or liquid biofuel

4. Agro-industrial residues converted to biogas and/or liquid biofuel
5. Large-scale, energy crop residues converted to biogas and/or liquid biofuel

The cases are assessed in a systems perspective meaning that outputs are considered collectively, e.g. biogas as well as food. This perspective builds on two underlying principles: 1) Residues, when used as a resource, cannot be considered for free in terms of inputs required for their provision (Kamp & Østergård, 2012b) and 2) Optimisation of an integrated system may be hindered by attempting to optimise just a subsystem.

Specific objectives

The PhD project will provide in-depth environmental sustainability assessments for three of the identified systems. In order to provide assessments that are directly applicable for decision-making, the following analyses will be carried out:

- Mapping of Ghana's natural resource flows on a country scale based on the eMergy methodology.
- Mapping of energy supply and demand in the different systems chosen.
- Development of a model for integrated energy and environmental analysis of the selected bioenergy systems and of the country.
- Assessment of a set of indicators for each of the chosen cases based on energy, material and labour flows up- and downstream from the bioenergy

production process, considered in a life-cycle perspective.

Preceding the case study work, the abovementioned systems perspective approach is treated specifically in Kamp & Østergård (2012a,b).

Materials and methods

The analytical framework approach used is SUsustainability Multi-method, Multi-scale Assessment (SUMMA) (Ulgiati et al. 2011). In SUMMA, a portfolio of indicators is calculated based on an inventory of identified inputs and outputs. The indicators/methods will include but are not limited to:

Emergy: An upstream method that assesses the accumulated, direct and indirect exergy use in provision of a product or service, converted to solar equivalent Joules (seJ). It includes work by natural and human systems alike. The transformity indicator (seJ/J) indicates the efficiency of a process in converting (scattered) solar energy to (concentrated) available energy. Inputs are considered as fully or partly renewable according to the fraction of renewable energy sources used in their creation.

Energy Return On (energy) Invested (EROI): An upstream indicator, EROI compares the output of energy to the inputs of commercial energy, often converted to primary (fossil) energy equivalents for quality adjustment. The output:input ratio indicates the efficiency of fossil fuel use in an energy provision process.

Global Warming Potential: GWP Indicates the greenhouse gas (GHG) emission impacts from a system over a given time period (e.g. 100 years), converted to CO₂-equivalents. A downstream indicator.

The inventory for each case system is based on interviews carried out with farmers, industrial managers and other stakeholders in Ghana, on literature study and cooperation with project partners.

Preliminary results and discussion

In Kamp & Østergård (2012b) the algebra of emergy accounting is examined in detail and an addition to existing rules is suggested. The addition concerns how to account for inputs that are outputs of co-production processes and is relevant for other life-cycle assessment methods as well. Such outputs are expected to be used increasingly as inputs in bioenergy production. Typically, the original inputs for these outputs are allocated according to energy content, mass or price. This approach may fail in its choice of allocation basis, e.g. if allocation is based on price, manure is considered value-less when it is in fact a precious carrier of energy and nutrients. We suggest avoiding allocation and instead include upstream co-production processes and their additional outputs in the system boundary when practically possible. As an example, X could represent inputs to pig production, Y additional inputs to biogas

production, A manure, B pig meat and C biogas. (Fig. 1).

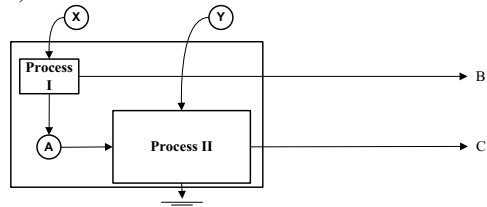


Figure 1: Output C is based partially on a residue A from a co-production Process I. In a systems perspective, inputs to Process I and thereby to the products A and C cannot be separated from inputs to product B.

Recently, interviews among small-scale, traditional farmers was carried out to obtain knowledge of material, energy and labour inputs required for biomass production and to identify the availability of residue types and amounts. More interviews are needed for reasonable representativeness. The preliminary results indicate high dependence on commercial fertiliser, agrochemicals and direct work, and little or no present use of residues of which some are concentrated during harvest operations. Based on the present understanding of the small-scale system, only biogas appears a viable 2nd generation option.

Future work

In 2013 interviews with representatives of the agro-industry-based and the energy crop-based systems will be carried out and further research will be done in the small-scale system. By mid-2013 the assessment model will be established and detailed work on how the different systems can be improved can begin.

Acknowledgements

The work is made possible through the support of 'Biofuel production from lignocellulosic materials' DFC no. 10-018RISØ.

References

1. S. Ulgiati et al. Ecological Modelling 222 (2011) 176-189

List of Publications

2. A. Kamp, H. Østergård in: Brown MT, editor. Emergy Synthesis 7: Proceedings of the 7th Biennial Emergy Research Conference. Gainesville, USA (2012): Center for Environmental Policy, University of Florida; 2012, (2012a) submitted.
3. A. Kamp, H. Østergård, Ecological Modelling, (2012b) accepted.



Kasper Bislev Kallestrup

Phone: +45 4525 2843
E-mail: kbka@kt.dtu.dk

Supervisors: Kim Dam-Johansen
Weigang Lin

PhD Study

Started: December 2011
To be completed: November 2014

China's waste crisis and thermal conversion of Chinese waste streams

Abstract

China currently one possess the capacity to treat less than 80% of their total output of municipal solid waste (MSW). This represents a serious environmental and social risk. In this PhD, the amount and characteristics of China's MSW is investigated and so are the potential solutions to the problem. One potential solution to be investigated is thermal and mechanical homogenization of MSW, followed by cement kiln co-firing.

Introduction

China has experienced a rapid increase in wealth in the last two decades, and this has brought along a rapid increase in solid waste generation. Waste collected and transported has risen from 31.3 ton in 1980 to almost 158 million ton in 2010. In 2010 22% of all MSW generated in China was dumped without any treatment. Of waste actually treated, simple landfilling is still the main disposal route, accounting for 85% of treated volume. This is for China a serious social and environmental problem. Enormous amounts of waste are being stockpiled in locations with no leachate or fume control. Dumpsites are typically places in areas of relative poverty, acting to further increase the social divide between the wealthy and the poor. In this PhD study, the national and provincial accounts on MSW are investigated and so are the possible solutions for closing the capacity gap. Particular attention will be paid to thermal conversion of MSW.

Specific Objectives

The objective of the PhD study is to investigate waste treatment in China and propose technological solutions that apply well to Chinese waste and its unique thermochemical and mechanical properties.

- What is the state of waste management in China?
- What is the macro and chemical composition of Chinese MSW?
- What is thermal conversion behavior of single particles and bulk MSW?
- What place can thermal conversion have in the future of China's MSW management system.

At this point, work has been conducted to answer the first two questions, while the rest have not been considered yet.

Results and Discussion

Waste collected and transported in urban areas has risen from 31.3 million ton in 1980 to almost 158 million ton in 2010 according to the National Bureau of Statistics of China. This is equivalent to collection of 236 kg/capita. Of this collected amount, 22% is not treated. This means that 35 million tons of the waste that enters the official waste handling system in urban China is dumped without treatment. Add to this that fact that a lot of waste is not even collected and it is apparent how far China is from having a functioning waste handling system. Figure 1 show the distribution of the volume of untreated waste in China. It reveals how some of the highly developed provinces like Shandong, Zhejiang, and Jiangsu have able to build treatment facilities at the same rate as their waste production has increased, while others, such as Guangdong, have not. Guangdong dumped 5.4 million ton MSW in 2010.

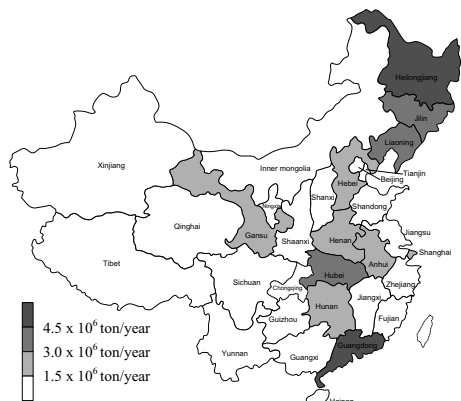


Figure 1: Distribution of untreated MSW among Chinese provinces

Figure 2 shows the composition of MSW as found in 9 recent (2007+) studies from around China. It shows that food waste is the dominant fraction comprising between 51% and 74% of the total. As a consequence, the moisture level of MSW in China is very high, ~50%, and heating values are low, often between 3.9 – 6.5 MJ/kg.

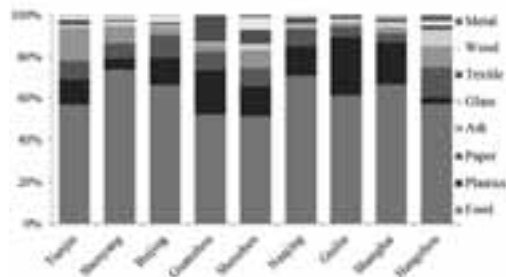


Figure 2: Composition of MSW in various Chinese cities [1, 2].

This makes traditional grate fired incineration difficult without drying, separation, or other pre-treatment process.

Planned work

In this remainder of this PhD study if thermal pre-treatment, utilizing waste heat from cement kilns, could allow for less energy-intensive mechanical homogenization of MSW.

This will be investigated by macro-TGA of thermal conversion dynamics of selected components of MSW subject inert atmosphere and atmospheres with slight oxygen content. Authors often describe MSW's organic part as mix of 5 components; Food waste, Paper, Plastics, Textile fiber, and Wood/timber. These categories may then be "contaminated" with almost every possible inorganic compound.

By comparing results from experiments with single components behavior with that of a "real" MSW mix, we hope to describe and model the correlation between them to a point where estimation of behavior of an arbitrary MSW mix is possible.

Acknowledgements

I wish to thank the Sino-Danish center for Education and Research and Technical University of Denmark for financial support, and the Chinese Academy of Sciences for their hospitality and support.

References

1. J. Tai, W. Zhang, Y. Che, D. Feng, Waste management 31 (8) (2011) 1673-1682.
2. D. Zhang, S. Tan, R. Gersberg, Journal of Environmental Management 91 (8) (2010) 1623-1633.



Alsu Khusainova

Phone: +45 4525 2982
E-mail: sukh@kt.dtu.dk

Supervisors: Alexander A. Shapiro
John M. Woodley

PhD study

Started: December 2011
To be completed: November 2014

Wettability Improvement with Enzymes: Application to Enhanced Oil Recovery under Conditions of the North Sea Reservoirs

Abstract

The main goal of the present work is to establish possible mechanisms in which enzymes may enhance oil recovery. Improvement of the brine wettability of the rock and decrease of oil adhesion to it by addition of an enzyme is one of the possible mechanisms of enzymatic action. This mechanism has been investigated experimentally, by measurements of the contact angles. Different enzyme classes, such as esterases/lipases, carbohydrases, proteases and oxidoreductases, provided by Novozymes, as well as two commercial mixtures have been investigated. Overall, the group of esterases/lipases has demonstrated the best performance in terms of wettability alteration.

Introduction

Enzymes are proteins synthesized by living organisms and catalyzing specific biochemical reactions [1]. They are widely used for different applications, but only recently have been introduced into the field of enhanced oil recovery (EOR). Enzymes are reported to have a potential to increase recovery [2, 3, 4], but the mechanisms by which enzymes enhance extraction of oil from natural rocks are still poorly understood. Lately it was found that certain types of enzymes can alter wettability state of the rock towards more water-wet condition [3, 5], while the water-wet state is believed to be the most favorable for the waterflooding accomplishment and for overall oil recovery.

In case of the petroleum reservoir wettability reflects interaction between oil, brine and rock surface and appears to be a function of the interfacial tensions between oil-brine, oil-rock and brine-rock. Based on this statement, the following hypotheses may be proposed a priori regarding the phenomena leading to wettability alterations of the rock surface after addition of enzymes.

1. Change of oil composition. In the system crude oil–[brine+enzyme]–rock oil can be used as a substrate, and water as a reagent. A specific enzyme may catalyze the reaction of hydrolysis (chemical reaction with water). For example, esterase is a group of enzymes that catalyze cleavage of the ester fragments (which may be present in particular crude oil components) into acid and alcohol during hydrolysis. Consequently, application of the esterase in crude oil–[brine+enzyme]–rock system

may produce additional amount of interfacially active compounds, such as acid and alcohol. Alteration of oil composition will result in change of its properties (e.g. acidity) that will be reflected in change of type of interactions of oil with the rock and of oil with the brine solution.

2. Modification of the rock surface by adsorption of enzymes. Enzymes are of a protein nature and therefore appear to be interfacially active molecules [1]. The adsorption potential of enzymes is explained by the fact that side chains present on their surfaces are physico-chemically very different. They may be hydrophilic or hydrophobic; negatively, positively and neutrally charged. Reservoir rocks are composed of different minerals that also have different surface charges. Hence, enzymes are expected to interact actively with the minerals, for instance, with calcite, which is usually positively charged at $\text{pH} < 9.5$ and negatively at $\text{pH} > 9.5$ [6]. Up to the knowledge of the authors there is no data available on adsorption of enzymes on calcite, since most of the work on enzyme-mineral interactions is focused on negatively charged mica [7, 8], although there was the evidence of protein adsorption on carbonate surface [9].

3. Adsorption of enzymes onto the oil-water interface. Interfacial activity of proteins also results in formation of the adsorbed protein films on oil-water interfaces [10, 11]. Similar to surfactants, enzymes might cause decreasing of the interfacial tension between oil and brine, which will facilitate oil recovery.

Specific Objectives

In the majority of the previous studies commercial mixtures containing components other than enzymes (e.g. surfactants) were applied for investigation of the enzymatic EOR. It is very difficult to ascribe observed positive effects particularly to enzymes. The main goal of this work is to test ability of the different classes of ‘pure’ enzymes to enhance oil extraction from the reservoir rock in the presence of brine. Wettability alteration has been selected as a screening criterion. Among different techniques, determination of the contact angles is the most suitable measure for wettability screening, since it keeps the balance between accuracy, timing and simplicity. Calcite has been used to mimic carbonate rock characteristic of the North Sea petroleum reservoirs. Further discussion will be focused on crude oil -[brine+enzyme]-calcite system.

Results and Discussion

Fifteen enzyme samples belonging to different enzyme classes, such as esterases/lipases, carbohydrases, proteases and oxidoreductases, provided by Novozymes, have been investigated. Two commercial mixtures containing enzymes: Apollo-GreenZyme™ and EOR-ZYMAX™ have also been applied. The North Sea dead oil and the synthetic sea water were used as test fluids. Internal surface of a carbonate rock has been mimicked using calcite crystals.

Two types of outcomes can be obtained from the contact angle experiments. The first is contact angle value and the second is adhesion behavior. Contact angle measurement (Fig. 1) is one of the most common techniques applied for wettability assessment; however, observation of adhesion behavior of fluid–fluid–solid system also provides good qualitative information on wettability. Adhesion test was introduced by Buckley and Morrow [12]. The placed oil drop was allowed to contact with the mineral in the presence of brine for 2 minutes and afterwards the needle still contacting the oil was moved down trying to detach the drop from the mineral. Three ways of behavior for the attached drops were observed (Fig. 2):

1. Adhesion behavior: oil sticks to the surface, the link between the needle and oil breaks and oil drop is left on the surface;

2. Non-adhesion behavior: the oil drop does not attach to the crystal and stays on the needle leaving the clean mineral surface;

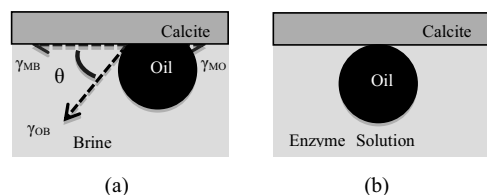


Figure 1: Scheme of the oil drop before (a) and after (b) addition of the enzyme

Note! The contact angle is measured through the densest aqueous phase.

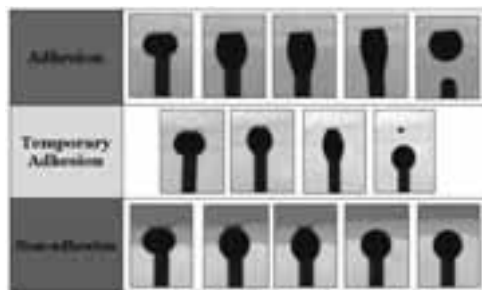


Figure 2: Illustration of types of adhesion behavior

3. Temporary adhesion: oil initially sticks to the calcite surface, but while the needle is moving down, the oil drop detaches from the surface and stays on the needle leaving an oil spot on the mineral.

In order to assess effect of enzymes on wettability state of calcite the oil–brine–calcite system was investigated first. The adhesion behavior of the oil drops was observed. The contact angles varied within $38^{\circ} \pm 7^{\circ}$, which corresponds to the weakly water-wet state according to the classification introduced by Anderson [13]. Consequently, the system has a potential for the wettability improvement. Initial adhesion behavior and contact angle value of 38° will be used as a reference value in the further discussion.

The enzymes are usually distributed as components in the complex mixtures with solvents, stabilizers and surfactants. Direct experimenting with these mixtures may lead to misinterpretations. To avoid this problem, ‘pure’ enzyme samples were used in current study. Such a sample consists of enzyme (2-5%wt), stabilizer (25-30%wt) and water (63-75%wt). It must be highlighted that concentrations discussed below are concentrations of such enzyme products, but not of the pure enzymes. For comparison, separate experiments with purified enzymes, i.e. enzymes with no additives, and stabilizer were conducted to exclude effect of the stabilizer. These experiments confirmed that the enzyme, not the stabilizer, is a working component.

Summarized adhesion map is given in Figure 3. The results revealed that each type of enzymes has a distinct behavior.

Lipases. The most surface-active enzymes belong to the group of lipases/esterases, in accordance to the previous findings [5]. A majority of the lipase samples turned calcite into an absolutely non-adhesive state at the concentration of 1%. Temporary adhesion was mainly observed for the concentration of 0.5%. Few samples could still provide temporary adhesion at 0.1%, while for other enzymes at this concentration calcite adhered oil. Two samples can be highlighted in particular, as they completely prevent adhering of oil to the mineral surface at the concentration of 0.5 %.

The results on adhesion behavior are in a good agreement with the contact angle measurements. The most active enzymes among the lipases at non-adhesion

	1% (wt/wt) of product				0.5% (wt/wt) of product				0.1 % (wt/wt) of product			
	Grey Calcite	Yellow Calcite	White Calcite	Freshly Cleaved Calcite	Grey Calcite	Yellow Calcite	White Calcite	Freshly Cleaved Calcite	Grey Calcite	Yellow Calcite	White Calcite	Freshly Cleaved Calcite
Lipases/Esterases												
NS 44024												
NS 44029												
NS 81249												
NS 44034												
NS 44037												
NS 44044												
NS 44053												
Carbohydrases												
NS 81251												
NS 81252												
Proteases												
NS 81253												
NS 44010												
NS 44055												
NS 44051												
Oxidoreductases												
NS 81234												
NS 44071												
Commercial Products												
NS 44008												
Apollo-GreenZyme												

Figure 3: Summarized adhesion behavior of calcite minerals in the presence of various enzyme products (N/A – information is not available, N/R – not reasonable)

conditions showed 100% reduction of the water contact angle – from 38° to 0° (Fig. 1b), whereas 0° degree implies absolute water-wetness, considered to be ideal case for the oil recovery. The results on the contact angle measurement corresponding to the temporary adhesion behavior at enzyme product concentration of 0.5% can be divided into the two groups. The first group corresponds to absolute decrease of contact angle to 0°, and second corresponds to significant, but not absolute drop of contact angle (approximately 42 % and 79% or 22° and 8°, respectively). Overall, decrease of the enzyme content causes increase in the contact angle values, and ability of the enzymes to change the wetting state of calcite appears to be proportional to the amount of an enzyme in the brine.

In previous studies only lipases were applied as ‘pure’ enzymes [5]. In this work three additional classes of enzymes were investigated in order to attempt broadening the group of potential enzyme candidates for EOR applications.

Carbohydrases. Generally addition of the carbohydrases into the brine solution did not show any effect on adhesion. The only “positive” observation was temporary adhesion state of the grey calcite at 1% for one of the samples. Assessment of the contact angles supported these results: reduction of contact angle in the oil-[brine+carbohydrase]-calcite systems were not larger than 10%, which is comparable to the experimental error.

Proteases. This group of enzymes showed intermediate performance between carbohydrases and lipases. Even though addition of proteases caused some positive changes in the wettability state of calcite, white responses were very non-homogeneous. The only

pattern could be established, that grey and yellow calcite crystals are less “sticky” than the pure calcite with no additives. At the concentration of the protease products of 1% the non-adhesion behavior could be observed for the calcite with additives, while minerals turned only to the temporary adhesion state. The same trend was observed for 0.5%: crystals with additives demonstrated temporary adhesion, while white calcites adhered oil. In cases of non-adhesion and temporary adhesion, the contact angle decreased for about 76%, while no significant reduction of the contact angle was observed in other cases. Overall, proteases have some potential in terms of EOR, however, their selective effect on different minerals makes them less desirable biological agents.

Oxidoreductases. This group of the enzymes has not introduced any wettability alteration.

Commercial mixtures. Two commercial enzyme-based mixtures, Apollo-GreenZyme™ and EOR-ZYMAX™, were included into the enzyme screening list. Based on the adhesion behavior and the contact angle experiments, it may be concluded that EOR-ZYMAX™ does not have any ability to change wettability of the mineral surface. On the contrary, Apollo-GreenZyme™ has demonstrated absolute non-adhesion behavior with decline of the contact angle values by, on average, 60% (approximately 15°) for all the calcite minerals at all the investigated concentrations.

Visual observations during the experiments revealed that mechanisms underlying wettability alteration under the influence of ‘pure’ enzymes and Apollo-GreenZyme™ are different. In order to get some additional ideas on working mechanisms reference

experiments were accomplished by substituting enzymes with protein (BSA) and surfactant (SDS). Performance of the enzyme mixtures provided by Novozymes was analogous to results obtained for oil–[brine+BSA]–calcite system, that implies importance of protein nature of enzymes. The proposed working mechanisms for these enzymes are adsorption of enzymes onto the mineral and/or formation of additional interfacially active oil compounds. Application of Apollo-GreenZyme™ resembled more the oil– [brine + SDS]–calcite system, where working mechanisms are adsorption of surfactant and drastic decrease of IFT between oil and the SDS solution. Thus, for Apollo-GreenZyme™ mixture containing the surfactant, wettability improvement may be both due to enzyme and surfactant that is difficult to distinguish.

Conclusions

1. Enzymes have a potential to EOR due to ability to improve wetting behavior of the mineral surfaces.
2. Lipases changing wettability of calcite from weakly to absolutely water-wet state are the most successful group of enzymes. Particularly, non-specific esterase product turns the mineral surface into non-adhesive state at concentrations of 0.1–0.5% wt.
3. Mechanisms underlying wettability alteration under the influence of esterases/ lipases are adsorption of enzymes onto the mineral and/or formation of additional interfacially active oil compounds.
4. The commercial product Apollo-Greenzyme™ has also demonstrated potential for EOR application, but the results are very mixed. Working mechanisms in this case are different compared to ‘pure’ enzyme products.
5. Crude oil-[brine+lipase]-calcite system behaves similar to crude oil-[brine+protein]-calcite system, while crude oil-[brine+Apollo-Greenzyme™]-calcite system is more similar to crude oil-[brine+surfactant]-calcite system.
6. Influence of the stabilizing part of the enzyme product on improvement of wettability has been excluded and effect of the enzyme has been confirmed.

Acknowledgements

The Danish National Advanced Technology Foundation is kindly acknowledged for support of the project. Novozymes, Mærsk Oil and Gas AS and DONG AS are kindly acknowledged for support of the project and supply of the enzymes, oil and rock samples. Dr. T. Zunic (the Geological Museum University of Copenhagen) is kindly acknowledged for providing the mineral samples and extensive consultancies. Apollo Separation Technologies and VH Biotechnology are acknowledged for supply of the samples of the commercial enzyme mixtures.

References

1. V. Hlady, J. Buijs, H.P. Jennissen, *Methods Enzymol.* 309 (1999) 402–429.
2. Q.X. Feng, X.P. Ma, L.H. Zhou, D.B. Shao, X.L. Wang, B.Y. Qin, *SPE* 107128 (2007).
3. L. He, Z. Zhongnong, *SPE* 114281 (2011).
4. W.K. Ott, T. Nyo, W.N. Aung, A.T. Khaing, *SPE* 114231 (2011).
5. H. Nasiri, K. Spildo, A. Skauge, Conference proceedings, International Symposium of the Society of Core Analysis, Noordwijk, Netherlands, September 27 – 30, 2009.
6. M.M. Thomas, J.A. Clouse, J.M. Longo, *Chem. Geology* 109 (1993) 201–213.
7. S. Demaneche, J.-P. Chapel, L.J. Monrozier, H. Quiquampoix, *Colloids and Surfaces B: Biointerfaces* 70 (2009) 226–231.
8. U.H. Zaidan, M. B.A. Rahman, M. Basri, S.S. Othman, R.N.Z.R.A. Rahman, A.B. Salleh, *Applied Clay Science* 47 (2010) 276–282.
9. N.N. Denisov, L.A. Chtcheglova, S.K. Sekatskii, G. Dietler, *Colloids and Surfaces B: Biointerfaces* 63 (2008) 282–286.
10. S.G. Baldursdottir, M.S. Fullerton, S.H. Nielsen, L. Jorgensen, *Colloids and Surfaces B: Biointerfaces* 79 (2010) 41–46.
11. C.J. Beverung, C.J. Radke, H.W. Blanch, *Biophysical Chemistry* 81 (1999) 59–80.
12. J.S. Buckley, N.R. Morrow, Conference proceedings, SPE/DOE 7th Symposium on Enhanced Oil Recovery, Tulsa, Oklahoma, 1990, 871–877.
13. W.G. Anderson, *Journal of Petroleum Technology* 38 (1986) 1125–1144.



Petra Lachouani

Phone: +45 2133 1955
E-mail: alac@risoe.dtu.dk

Supervisors: Henrik Hauggaard-Nielsen
Per Ambus

PhD Study
Started: September 2010
To be completed: August 2013

Nitrogen Cycle Assessments and Greenhouse Gas Emissions in Low-Input Legume Management Systems

Abstract

Open nitrogen cycles in agriculture have negative effects like nitrate leaching and connected eutrophication of aquatic ecosystems as well as increased nitrous oxide emissions, a greenhouse gas (GHG) 300 times more potent than CO₂. This project seeks to optimize agricultural nitrogen use and close the agricultural nitrogen cycle while maintaining food production and productivity.

Introduction

Nitrogen (N) is the most important plant nutrient for crop productivity in most agroecosystems. Therefore the introduction of Haber-Bosch derived N fertilizers into agriculture resulted in a sharp increase in yield per ha. This development led to undesired side-effects like decreasing soil organic matter content and nitrate leaching with subsequent eutrophication of natural ecosystems, groundwater contamination, and made agriculture widely dependent on fossil fuel reserves.

Legumes obtain N through biological nitrogen fixation (BNF), rather than through fossil energy-derived fertilizer N. However, legumes are not generally considered as climate change mitigation option.

Specific Objectives

Quantifying N₂-fixation in annual and perennial legume cropping systems is the first step to assess the cropping system. Subsequent residue incorporation and release of N through soil microbial decomposition will be studied with focus on soil N dynamics, potential N₂O emissions and optimization of N transfer efficiency to subsequent cereal crops.

Project Outline

For legumes to be effective N suppliers for future cropping systems several points have to be considered:

- High SNF fixation rates [1]
- Microbial decomposition, synchronized N release time and transfer efficiency to subsequent crop
- Potential risks of nitrous oxide (N₂O) emissions after soil incorporation.

The present study focuses on management options:

Intercropping offers the advantage of covering more niches in a field and therefore complements resource use. Intercropping is potentially a management option to tighten the nitrogen cycle, reduce greenhouse gas emissions and mitigate climate change [2].

Brassica species can be intercropped with legumes. The breakdown of Brassica-derived glycosinolates has an influence on the soil microbial biomass and the release of carbon and nutrients from the microbial biomass pool is facilitated (biofumigation) [3]. There are indications that nitrification can be inhibited in the short-term. Biofumigation could be used in nutrient management.

Temporal dynamics after incorporation of residues will be evaluated [4].



Figure 1: Annual intercropping experiment at Risø

Annual Field Experiment

To study the effects of interspecific interactions on N₂-fixation and soil N use an annual intercropping experiment is conducted at Risø DTU. Fig. 1 shows the experiment in which grain legumes (faba bean, pea) and Brassica are intercropped (seeding density: legume 100%, cereal 50%) with oat in a completely randomized plot design with 4 replicates. Atmospheric N₂ fixation is measured at significant growth stages using ¹⁵N natural abundance methodology (EA-IRMS). Common agronomic parameters are monitored as well as soil N in the topsoil (0-10 cm). The experiment is conducted twice in 2011 and 2012 to cover inter-annual variation.

Perennial Field Experiment

The effects of perennial legume-grass mixtures on atmospheric N₂ fixation, short-term use of soil N sources and N₂O emissions are studied in a 2-year field trial at Flakkebjerg, Denmark. A grass-perennial legume (white clover, red clover and alfalfa) mixture gets undersown to spring barley. Atmospheric N₂ fixation is measured at significant growth stages using ¹⁵N natural abundance methodology (EA-IRMS) and N₂O emissions are measured (sampling from field chambers and GC analysis) during campaigns after soil incorporation of the sward. Furthermore soil N is monitored in the topsoil (0-10 cm).

Fig. 2 shows barley yield data from 2010, indicating an increase of the straw yield in case of barley-grass treatments, while undersown legume seems to have no effect on the barley yield. However, we hypothesize that the biomass yield and nitrogen fixation in the subsequent year is positively influenced by legumes.

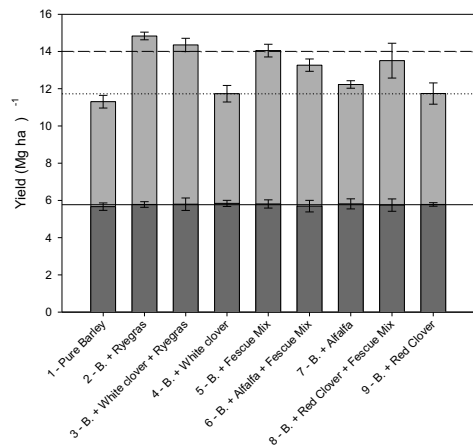


Figure 2: Barley yield 2010 in the perennial field experiment in Flakkebjerg (n=4). Treatments are shown on the x-axis (all treatments contain barley). Dark columns show the grain yield component, while the light columns show the straw yield component. The full line indicates average grain yield, the dotted line

indicates average straw yield and the dashed line indicates average straw yield of grass-grass intercrop.

Greenhouse experiment – Nitrogen fixation

To accurately calculate biological nitrogen fixation in the Annual Field Experiment and the Perennial Field Experiment using the ¹⁵N natural abundance method, reliable reference values of plants grown only supplied with air-nitrogen are needed.

There are indications however [5], that the reference values (b-values) thus obtained bias biological nitrogen fixation calculations potentially due to different microbial strains in the field than in the inoculums in the greenhouse. Furthermore b-values obtained by plants grown in association with single strains seem to differ significantly from plants grown in association with a Rhizobium community. This community situation however reflects more accurately field conditions.

This expected bias is to be quantified by a greenhouse experiment with different plants (faba bean, pea, red clover, white clover, alfalfa and lupine) as well as different single strains and soil community extracts.



Figure 3: Faba bean grown in the greenhouse at Risø, in association with different Rhizobium inoculants.

Acknowledgements

This PhD study is part of the SOLIBAM project (Strategies for Organic and Low-Input Integrated Breeding and Management) which is funded by the European Commission under the SEVENTH FRAMEWORK PROGRAMME with the grant number FP7 KBBE – 245058.

References

1. Peoples MB, Herridge DF, Ladha JK (1995). Plant Soil 174:3-28
2. Hauggaard-Nielsen H, Mundus S, Jensen ES (2009). Nutr Cycling Agroecosyst 84:281-291
3. Gimsing AL, Kirkegaard JA (2009). Phytochem Rev 8:299-310
4. Ambus P, Jensen ES (2001). Commun Soil Sci Plant Anal 32:981-996
5. Carlsson G, Palmborg C, Huss-Danell K (2006). Acta Agr. Scand. 56:31-38

**Rita Lencastre Fernandes**

Phone: +45 4525 2993

E-mail: rlf@kt.dtu.dk

Supervisors: Krist V. Gernaey
Anker D. Jensen
Ingmar Nopens, Ghent University**PhD Study**

Started: November 2009

To be completed: December 2012

Population Balance Models and Computational Fluid Dynamics: an Integrated Model Framework to Describe Heterogeneity in Fermentors

Abstract

Traditionally, cells in a microbial population are considered identical and characterized by averaged properties in studies of fermentation processes. However, research has shown that a typical microbial population in a fermentor is heterogeneous. The aim of this Ph.D. project is to establish a model framework where Population Balance Models (PBM) and Computational Fluid Dynamics (CFD) are integrated in order to describe heterogeneous microbial populations in stirred-tank reactors. This contribution focuses on the proof-of-concept of the integration of a PBM in a CFD model for describing the anaerobic growth of a yeast population in a spatially heterogeneous reactor. The proposed *in silico* tool allows for exploring the complex interplay between flow conditions and the dynamics of a cell population.

Introduction

A heterogeneous microbial population consists of cells in different states, and it implies a heterogeneous distribution of activities (e.g. respiration, product efficiency). Furthermore, cell-to-cell variability implies different responses to extracellular stimuli. This will result in the development of a heterogeneous population with a possibly different structure when the microbial population is subjected to changes in the surrounding environment, relatively to when growing under a constant extracellular environment. In fact, this difference in the population structure may explain the lower productivities and higher viability obtained for cultivations in large-scale reactors where substrate and oxygen gradients are observed, relatively to cultivations in well-mixed bench scale reactors [1].

This PhD project aims at understanding and modeling the development of heterogeneous microbial populations subjected to varying environmental conditions. Given the short time frame of a typical cultivation (i.e. days, weeks), the contribution of genetic drift to the development of heterogeneity within a population was assumed negligible, and the focus of this project is set on understanding and modeling phenotypic heterogeneity.

Specific Objectives

In a first part of this PhD project, a PBM describing the dynamics of cell size and cell cycle position

distributions in response to varying substrate availability was proposed.

The second part of the project focused on integrating the PBM in a CFD model, yielding a model framework that can describe the cell population (in terms of cell size distributions for two cell cycle stages) and the extracellular environment cells experience at different locations in an a spatially heterogeneous reactor. A flexible simulation tool for exploring the interplay between cells and environment should result from the mentioned model integration. In order to avoid the computational burden associated to complex 3D CFD calculations for turbulent flows (such as the ones found in stirred tank reactors), focus was shifted to the microscale.

In order to achieve this goal, the following specific objectives were defined:

- Design a microbioreactor where biomass is accumulated (not washed-out) and substrate gradients are observed.
- Implement the CFD model and solve the flow problem for the designed microbioreactor
- Integrate the PBM describing the cell population, as well as the coupled unstructured model describing the consumption of glucose (substrate) and product (ethanol), into the CFD model.

- Investigate the effect of flow rate on the local cell size distributions and overall reactor performance.

Continuous flow-through microreactor

The microreactor consists of a sequence of spherical chambers connected in the center by a channel (Fig.1). An inlet mass flow rate of 3.6 and 0.36 $\mu\text{l/h}$, containing glucose (20 g/l), was applied. Such flow rates are within the operation range of a commercial microfluidic syringe pump. The ethanol and biomass concentrations at the inlet are 0 g/l.



Figure 1: Schematic representation of the designed microreactor. Due to the existence of two symmetry planes (xz and xy planes), only a quarter of the reactor was simulated and is illustrated.

Model formulation

The anaerobic fermentation of *Saccharomyces cerevisiae* in a continuous microreactor is used as case study. Cell growth and division are tightly coupled, and are modulated according to the substrate availability. The regulation of growth ensures that cells attain a critical size before initiating the division process [2, 3]. In the particular case of *S. cerevisiae*, two critical sizes corresponding to the regulation points START (committing to budding, or budding transition) and division have been identified.

Using cell size as population descriptor allows, thus, for describing the distribution of cellular states. Moreover, a better description of the cellular state is obtained by determining the distribution of cells in cell cycle phases, i.e. by measuring DNA distributions [4]. A PBM based on cell size as model variable, which is applied to different stages (i.e. subpopulations) corresponding to the non-budding and budding (cell cycle) phases, was developed (with a starting point in previous work by Hatzis and Porro [5]) in the first stage of this PhD project and applied for describing a batch cultivation (see *List of Publications*).

Generally, the link to the extracellular environment is accounted for by including substrate dependency in the growth function as well as transition functions (budding and division) for each of the stages. In this case, the critical transition sizes defining the progression from non-budding to budding stage, and cell division, are defined as functions of the local glucose concentration. The unstructured model describes the fermentation of glucose (substrate) to ethanol. The local consumption rate is estimated based on an average yield of biomass on substrate and the concentration of biomass present at

a given location in the microreactor and at a given time point. The rate of formation of ethanol is estimated in a similar fashion. This concentration of biomass is calculated as the zeroth moment of the total cell size distribution. The updated concentrations of glucose and ethanol are used for recalculating the substrate factor which serves to determine the single-cell growth rates, a term in the PBM.

Model implementation

The fixed-pivot technique [6] was used to discretize the PBE, using an evenly distributed grid with 20 pivots. The commercial software by ANSYS® CFX (v. 12.1) was used, and the PBM was implemented using the expression language (CEL). The geometry was defined with ICEM CFD 12.1, and a hexahedral mesh with 32159 elements and 36535 nodes was generated. Diffusion was not considered in the simulations.

Results and Discussion

The glucose concentration profiles for the two simulation cases are presented in Figure 2 a). Glucose is supplied at the inlet of the reactor and is consumed along the reactor as cells use it for growth, resulting in the production of ethanol. Due to the higher residence time for the slowest flow rate (0.36 $\mu\text{l/h}$) simulation, the consumption of glucose is higher in this case and the glucose concentration found in the last spherical compartments (closest to the outlet) is residual. Oppositely, in the case of the higher flow rate, a significant part of the supplied glucose is not consumed, and a high glucose concentration is found at the reactor outlet. In both cases, the glucose concentration at the walls of the spherical compartments is nearly zero, indicating that cells, present in these zones of the reactor, experience glucose depletion.

Due to the lower flow rate, and thus higher residence time, more biomass is observed for this simulation (0.36 $\mu\text{l/h}$) than for the higher flow rate case (3.6 $\mu\text{l/h}$) (Figure 2b). In the latter case, it is clearly visible that biomass does not accumulate evenly on the spherical wall: higher concentrations are found in a wall region closer to the exit of each compartment as illustrated in Figure 2b). This may be explained by the low flow velocities (nearly zero) observed in these zones, preventing cells from being transported to other parts of the reactor. Cell death is not considered in the model. Therefore, most cells will remain in these zones unless an alteration in the flow pattern is imposed and they are transported out of these regions.

Ethanol is formed as glucose is consumed when growth takes place. Not surprisingly, ethanol concentration (Figure 2c)) is highest at the locations where both biomass and glucose are present. When comparing the three profiles in Figure 2, it is possible to observe that generally the highest ethanol concentrations are found in the *interface* between the central stream supplying glucose on the one hand and the biomass accumulated closer to the spherical compartment walls on the other hand.

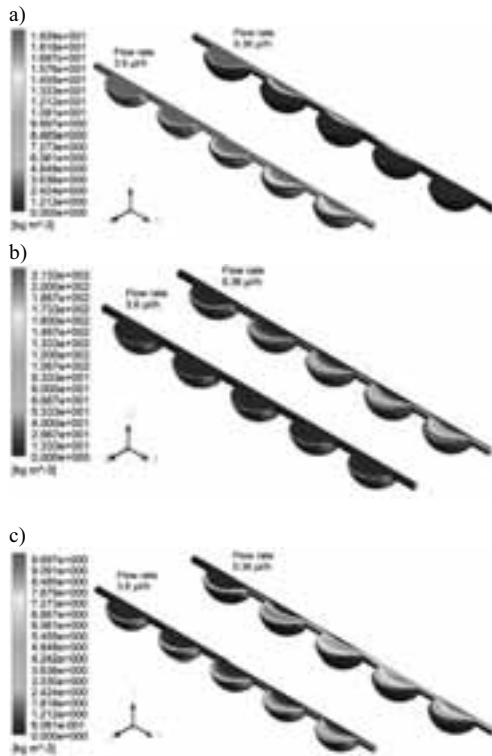


Figure 2: Concentration profiles for a) glucose, b) total biomass, and c) ethanol, for the two feed flow rates.



Figure 3: Illustration of the selected planes and probe locations: a) five yz planes perpendicular to the central channel were defined at the center of the spherical compartments; b) for each plane a point probe (green) was defined at the same location on the given yz plane.

In order to investigate locally the interplay between the flow conditions and population dynamics, five locations in the reactor were selected and the cell size distributions for the non-budding and budding cells predicted for each location were compared. The selected locations correspond to five points probes at the same relative position in each of the five spherical compartments as illustrated by the green pointers in Figure 3. Due to their similar location relatively to the center of the spherical compartments, the flow velocity, at the five probe points, is the same. The average cell

size distributions for the two (cell cycle) subpopulations were, in addition, determined for the reactor outlet plane, and compared to the ones for the probe point locations (Figure 4).

For both simulated flow rates, a greater share of smaller cells is found in the compartment closest to the inlet (point A), where the highest glucose concentration is observed. The smaller non-budding cells forming a peak with a mode around the pivot 6 (see Figure 4 a) and b)), are smaller than the non-budding population given as initial conditions. These cells have most likely resulted from the division of budding cells into non-budding cells with approximately half the size. The bigger cell size peak may correspond to non-budding cells transported from neighboring zones, where, due to lack of glucose, growth is residual and thus cells preserve the characteristics of the initial cell size distribution. The percentage of cells in this larger cell size peak for the non-budding subpopulation increases for the probe locations closer to the outlet (Figure 4 a)), suggesting that a fraction of these non-budding cells in the latter compartments may consist of cells that are transported from previous compartments. In the case of the lower flow rate simulation, the transport contribution to the overall behavior is considerably smaller, and consequently the larger size peak of non-budding cells (Figure 4 b)) is very similar for all locations.

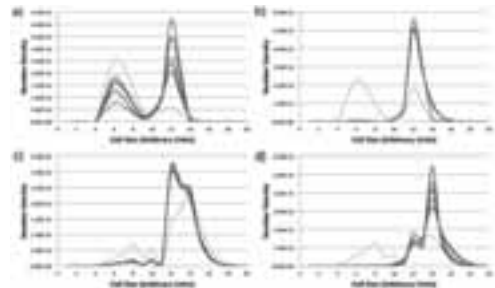


Figure 4: Local distributions predicted for the point probe locations on plane A (orange), plane B (red), plane C (green), plane D (purple), and plane E (blue), as well as average distribution predicted for the reactor outlet plane (grey): a) Non-budding subpopulation for the high flow (3.6 $\mu\text{l/h}$) simulation; b) Non-budding subpopulation for the low flow (0.36 $\mu\text{l/h}$) simulation; c) Budding subpopulation for the high flow (3.6 $\mu\text{l/h}$) simulation; d) Budding subpopulation for the low flow (0.36 $\mu\text{l/h}$) simulation.

Slightly bigger cells are observed for the budding population (Figure 4 c) and d)) in comparison to the non-budding one, as it would be expected based on the model formulation. Similarly to the non-budding cells, two distinct subpopulations (peaks) are also visible for the budding cell population, in both simulation cases, corresponding to a peak with mode around pivot 12, and another peak with mode in pivot 14 (the same mode as the initial distribution of budding cells). In the case of the lower flow rate (0.36 $\mu\text{l/h}$), the fraction of budding

cells with a bigger size seems to vary with the location (Figure 4 d)). As previously mentioned for the non-budding population, these cells are most likely not growing, or growing at a very low rate. A significant decrease in the glucose concentration to near depletion levels is observed, for this lower flow rate, when comparing the first (A) and second (B) compartments. It is, thus, not surprising that the fraction of bigger non-growing budding cells is substantially higher for the second and following compartments.

Summarily, in regions where cell growth takes place (and thus cell cycle transitions occur) relatively high budding indexes are observed and a smaller size subpopulation of non-budding cells is observed. For the lower flow rate, although a significant higher hold-up of biomass within the reactor is achieved. A large fraction of this biomass is not metabolically active (i.e. growing at very low rates, or not growing), due to the existence of spatial glucose gradients. This explains the fact that ethanol concentration at the reactor outlet is in the same order of magnitude for the two flow rate simulations, although the biomass concentration is approximately two orders of magnitude higher for the case of the lower flow rate (0.36 $\mu\text{l/h}$).

Conclusions

In this case study, a PBM describing the distribution of cell size for cell cycle stages, and its dependence on the available substrate concentration, was coupled to a fluid dynamic model that describes the transport of the supplied substrate and the biomass throughout the reactor. The interpretation of the results is challenging as the transport of the cells along the fluid streams has to be considered together with biological phenomena (growth, budding and division) taking place locally. The study contributes to the development of modeling tools for successful prediction of the dynamic behavior of total protein content distributions of a yeast population under non-ideal mixing conditions, as found in large-scale fermentors as well.

Acknowledgements

The Danish Council for Strategic Research is gratefully acknowledged for financial support in the frame of the project "Towards robust fermentation processes by targeting population heterogeneity at microscale" (project number 09-065160).

References

- [1] S.-O. Enfors, M. Jahic, A. Rozkov, B. Xu, M. Hecker, B. Jürgen et al. *J. Biotechnol* 85 (2) (2001) 175-185.
- [2] I. Rupeš. 2002. Checking cell size in yeast. *Trends in Genetics*, 18, 479-485.
- [3] D. Porro, F. Sreenc. 1995. Tracking of individual cell cohorts in asynchronous *saccharomyces cerevisiae* populations. *Biotechnology Progress*, 11, 342-347.
- [4] L. Alberghina, C. Smeraldi, B. M. Ranzi, and D.
- [5] C. Hatzis and D. Porro. *J. Biotechnol* 124 (2) (2006) 420-438.

- [6] S. Kumar and D. Ramkrishna. *Chem Eng Sci* 51 (8) (1996) 1311-1332.

List of Publications

1. D. Schäpper, R.L. Fernandes, A.E. Lantz, F. Okkels, H. Bruus, K.V. Gernaey *Topology Optimized Microbioreactors*, *Biotechnol. Bioeng.* 108 (4) (2011) 786-796
2. R. Lencastre Fernandes, M. Nierychlo, L. Lundin et al. Experimental methods and modeling techniques for description of cell population heterogeneity, *Biotechnol. Adv.* 29 (6) (2011) 575-599
3. M. Carlquist, R. Lencastre Fernandes, S. Helmark, A.L. Heins, K. V. Gernaey, A. Eliasson Lantz *Physiological heterogeneities in microbial populations and implications for physical stress tolerance*. *Microb Cell Fact* (2012) 11:94
4. R. Lencastre Fernandes, U. Krühne, I. Nopens, A.D. Jensen, K.V. Gernaey. Multi-scale modeling for prediction of distributed cellular properties in response to substrate spatial gradients in a continuously run microreactor. *Comp Aid Chem Eng I.A. Karimi and Rajagopalan Srinivasan (Editors), Proceed. 11th Int. Sys PSE.* (2012) 31:545-549
5. R. Lencastre Fernandes, M. Carlquist, L. Lundin, A.L. Heins, A. Dutta, S.J. Sørensen, A.D. Jensen, I. Nopens, A. Eliasson Lantz, K.V. Gernaey. Cell mass and cell cycle dynamics of an asynchronous budding yeast population: experimental observations, flow cytometry data analysis and multi-scale modeling. *Biotechnol Bioeng.* (2012) (doi:10.1002/bit.24749)
6. R. Lencastre Fernandes, V. Bodla, M. Carlquist, A.L. Heins, A. Eliasson Lantz, G. Sin, K.V. Gernaey. Applying mechanistic models in bioprocess development. *Adv Biochem Eng/Biotechnol. State of the Art of M³C.* Ed: C.-F. Mandenius, N. Titchener-Hooker. (2012) (in press)



Xiaodong Liang

Phone: +45 4525 2891
E-mail: xlia@kt.dtu.dk

Supervisors: Georgios Kontogeorgis
Kaj Thomsen
Wei Yan (DTU Chemistry)

PhD Study
Started: August 2011
To be completed: July 2014

Speed of sound from Perturbed-Chain Statistical Associating Fluid Theory Equation of State

Abstract

The advanced equation of state (EoS) models CPA and PC-SAFT were evaluated for their performance on speed of sound in hydrocarbons, alcohols and CO₂. The results reveal that PC-SAFT captures the curvature of speed of sound better than cubic EoS, and has good accuracy for small molecules. However, the accuracy gets worse as the chain gets longer. Two approaches have been proposed to improve PC-SAFT on describing speed of sound: (i) putting speed of sound data into parameter estimation; (ii) putting speed of sound data into both universal constants regression and parameter estimation. The results have shown that the second approach can significantly improve the speed of sound prediction for long chain molecules.

Introduction

The speed of sound can be used to characterize the heterogeneous or homogenous mixtures or to estimate the density of reservoir fluids down hole. Specifically SONAR (Sound Navigation and Ranging) uses sound propagation to navigate, communicate with or detect objects on the surface of the water or in sub-sea regions. It can even provide some measurements of the echo characteristics of the “targets”. It is possible for a thermodynamic model, which can describe the speed of sound for a wide range of mixtures accurately, to be used to analyze these characteristics and then determine what they are. This will be very useful in quick detection of oil and gas leak around sub-sea well and in clear mapping of oil in sea water column during the oil cleanup processing.

Equations

The speed of sound can be calculated from an EoS model as [1]:

$$u = \sqrt{\frac{V^2 C_p \left(\frac{\partial P}{\partial V}\right)_{T,n}}{M_w C_V}} \quad (1)$$

Where V , M_w , C_p , C_V and $(dP/dV)_{T,n}$ are total volume molecular weight, isobaric heat capacity, isochoric heat capacity and the derivative of pressure with respect to total volume respectively. The calculations of C_p and C_V can be done as:

$$C_V = (C_p^{ig} - R) - T \left(\frac{\partial^2 A^r}{\partial T^2} \right)_{V,n} \quad (2)$$

$$C_p = (C_p^{ig} - R) - T \left(\frac{\partial^2 A^r}{\partial T^2} \right)_{V,n} + T \left(\frac{\partial P}{\partial T} \right)_{V,n} \left(\frac{\partial V}{\partial T} \right)_{P,n} \quad (3)$$

The precise description of the first- and second-order derivatives of Helmholtz free energy with respect to temperature and total volume makes it a challenge for any EoS model, as pointed out by Gregorowicz et al. [2]. For instance, most of the classical equations of state (EoS), such as SRK [3] and PR [4], fail in describing speed of sound reliably in wide temperature and pressure range. This may be due to the intrinsic nature of these EoS, usually applied only to phase equilibria calculations, to the sensitivity of the second order derivative properties performed to a given function, or to the physics behind these properties. A way to discern some of these uncertainties could be to use a molecular-based EoS; these equations should ideally not depend on the particular properties under study and should retain the microscopic contributions considered when building the equation.

Advanced EoS models

Classical thermodynamic models used by oil industry are semi-empirical and not suitable for mixtures containing water and other polar chemicals. The Cubic-Plus-Association (CPA) [5] and Statistical Associating

Fluid Theory (SAFT) [6-10] equations of state, contain an association term. These advanced equations of state have been proven to be useful tools for describing complex mixtures, and they have been already used in the petroleum and chemical industries.

The CPA EoS can be expressed for mixtures in terms of pressure P as:

$$P = RT/(V_m - b) - a(T)/[V_m(V_m + b)] - \frac{1}{2} RT/V_m [1 + \rho(\partial \ln g / \partial \rho)] \sum_i x_i \sum_{A_i} (1 - X_{A_i}) \quad (4)$$

The PC-SAFT EoS can be expressed in terms of residual Helmholtz free energy as:

$$\frac{a^r}{RT} = \frac{a^{hc}}{RT} + \frac{a^{disp}}{RT} + \frac{a^{assoc}}{RT} \quad (5)$$

Where subscripts hs , $chain$, $disp$ and $assoc$ denote the contributions from hard-sphere, chain, dispersion and association respectively.

In this work, the simplified PC-SAFT EoS, proposed by von Solms et al. [10] in order to simplify and reduce the computational time is used. From this respect, it is not a new EoS, rather a simplified version in terms of mixing rules of the original PC-SAFT EoS [9], which means that the pure component parameters of the original and simplified PC-SAFT are the same.

$$\begin{aligned} \frac{a^{hc}}{RT} &= \bar{m} \frac{a^{hs}}{RT} - \sum_i x_i (m_i - 1) \ln g_{ii}^{hs}(d_{ii}) \\ &= \bar{m} \frac{4\eta - 3\eta^2}{(1-\eta)^2} - (\bar{m} - 1) \frac{2 - \eta}{2(1-\eta)^3} \end{aligned} \quad (6)$$

$$\frac{a_1^{disp}}{RT} = -2\pi\rho I_1(\eta, \bar{m}) \sum_i \sum_j x_i x_j m_i m_j \left(\frac{\epsilon_{ij}}{kT} \right) \sigma_{ij}^3 \quad (7)$$

$$\begin{aligned} \frac{a_2^{disp}}{RT} &= -\pi\rho\bar{m} \left(1 + Z^{hc} + \rho \frac{\partial Z^{hc}}{\partial \rho} \right)^{-1} I_2(\eta, \bar{m}) \\ &\quad \sum_i \sum_j x_i x_j m_i m_j \left(\frac{\epsilon_{ij}}{kT} \right)^2 \sigma_{ij}^3 \end{aligned} \quad (8)$$

$$\frac{a^{assoc}}{RT} = \sum_i x_i \sum_{A_i} \left(\ln X_{A_i} - \frac{X_{A_i}}{2} + \frac{1}{2} \right) \quad (9)$$

The detailed expressions of these terms can be found in original literature [9-10] or the book of Kontogeorgis and Folas [11].

Average Absolute Deviation (%AAD)

In this work, the percent average absolute deviation of the speed of sound (u) is defined as:

$$\%AAD(u) = \frac{1}{N^{exp}} \sum_{i=1}^{N^{exp}} \left| \frac{u^{calc}}{u^{exp}} - 1 \right| \times 100\% \quad (10)$$

Specific Objectives

The purposes of this work are (i) to validate whether the PC-SAFT model can capture the speed of sound curvature by comparing the results to SRK and CPA;

(ii) to study if it is possible to improve the performance of simplified PC-SAFT [9-10] for speed of sound by putting this data into parameter estimation or by refitting the universal constants, while keeping the same number of the pure component parameters.

Results and Discussion

Model evaluation

We have conducted evaluations of the performances on the speed of sound in normal hydrocarbons, associating and polar compounds using the classical cubic equation of state SRK [3], and the advanced CPA and PC-SAFT models. The results are showed in Figures 1-4 for Methane, n-Hexane, Methanol and CO₂ at one specific temperature respectively.

It can be seen that PC-SAFT [9-10] performs better than other two models in wide temperature and pressure ranges. PC-SAFT can describe the speed of sound with good accuracy for small molecules like Methane, Methanol and CO₂, and it perform also well for long hydrocarbons qualitatively. So PC-SAFT was taken as a start model to develop new approaches to calculate the speed of sound due to its capability of capturing the curvature shown in the Figures 1-4.

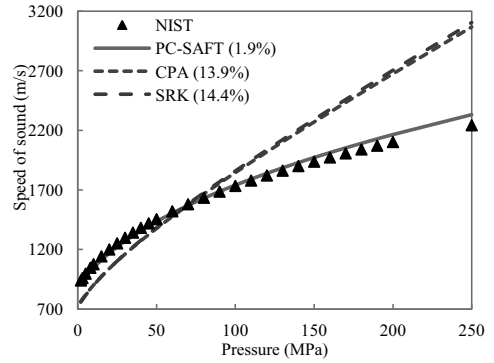


Figure 1: Speed of sound in Methane at 150K

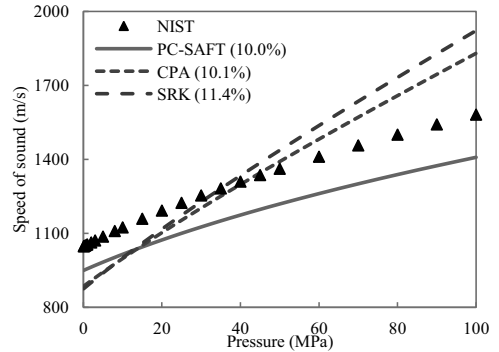


Figure 2: Speed of sound in n-Hexane at 300K

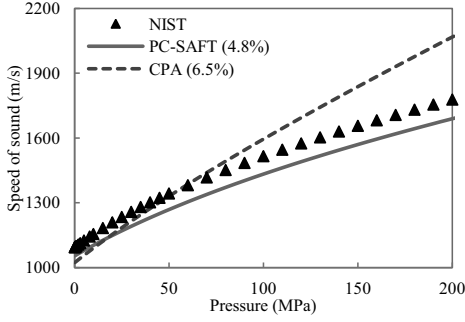


Figure 3: Speed of sound in Methanol at 300K

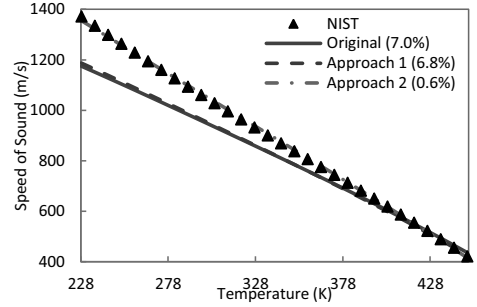


Figure 5: Speed of sound in saturated n-Hexane

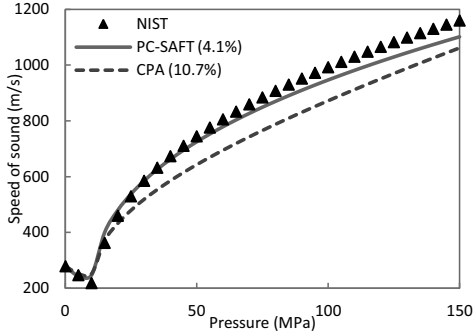


Figure 4: Speed of sound in CO₂ at 323.15K

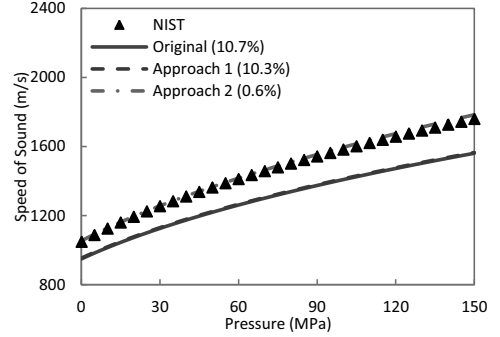


Figure 6: Speed of sound in n-Hexane at 300K

Model improvements

In this work, we have studied two approaches: (i) Putting speed of sound data in the pure component parameters estimation; (ii) Putting speed of sound data into both universal constants regression and pure component parameter estimation. They are denoted as Approach 1 and Approach 2 hereafter in this work. The objective function used in this work is:

$$f_{\min} = w_p \sum_i^{N_p} \left(\frac{P_i^{\text{exp}} - P_i^{\text{calc}}}{P_i^{\text{exp}}} \right)^2 + w_\rho \sum_i^{N_\rho} \left(\frac{\rho_i^{\text{exp}} - \rho_i^{\text{calc}}}{\rho_i^{\text{exp}}} \right)^2 + w_u \sum_i^N \left(\frac{u_i^{\text{exp}} - u_i^{\text{calc}}}{u_i^{\text{exp}}} \right)^2 \quad (11)$$

Where P , ρ and u are vapor pressure, liquid density and speed of sound respectively; N and w with the corresponding subscript are total experimental points and weights of the objective function respectively. Equal weights are used in this study. This objective function is minimized in both approaches by applying a Levenberg-Marquardt algorithm.

The original PC-SAFT, Approach 1 and Approach 2 models are compared in Figures 5-11, from which it can be seen that Approach 2 indeed improves the speed of sound description significantly.

It is shown in Figure 6 that the new approach has good predictive capacity into high pressure ranges, since only the data of saturated liquid is putted into the parameter estimation.

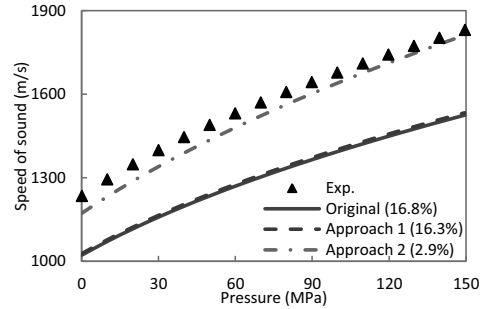


Figure 7: Speed of sound in n-Pentadecane at 323.15K

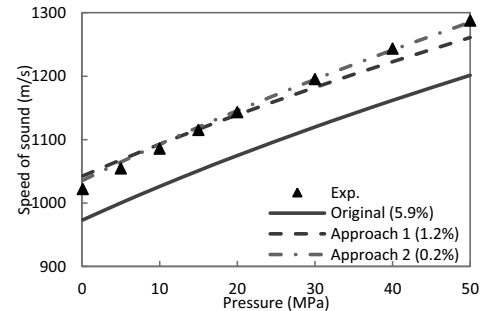


Figure 8: Speed of sound in Methanol at 323.15K

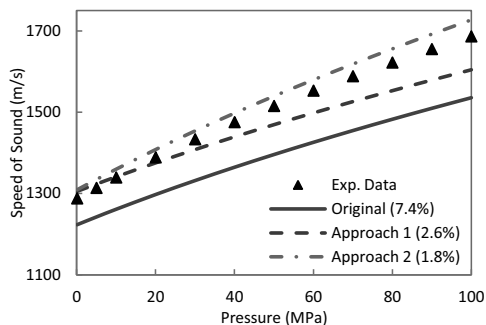


Figure 9: Speed of sound in 1-Hexanol at 303.15K

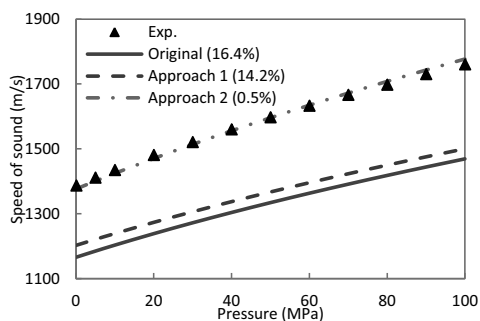


Figure 10: Speed of sound in 1-Dodecanol at 303.15K

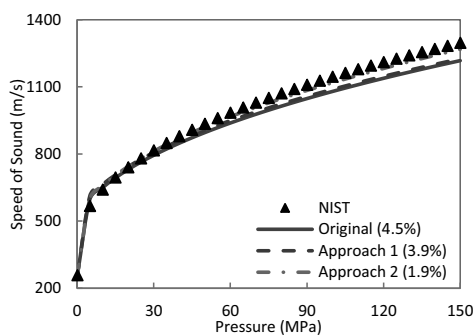


Figure 11: Speed of sound in CO₂ at 273.15K

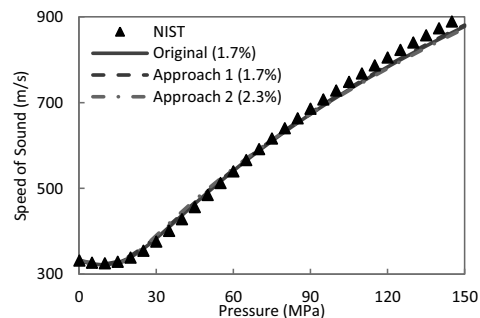


Figure 12: Speed of sound in CO₂ at 473.15K

We can see from Figures 8-9 that the association term plays an important role, since Approach 1 gives very good results compared to non-associating hydrocarbons shown in Figure 6. However, it is shown in Figure 10 that the importance of association term gets smaller when the chain gets longer. Equivalently speaking, the physical term dominates the contribution for long chain molecules.

The original PC-SAFT can describe speed of sound for small molecules, as discussed above, especially at high temperatures, as validated in Figures 11-12 for CO₂, which is treated as a non-associating compound in this work.

Acknowledgements

This PhD project is funded by the Danish National Advanced Technology Foundation (DNATF) and the Department of Chemical and Biochemical Engineering, Technical University of Denmark.

References

1. M.L. Michelsen, J.M. Mollerup, Thermodynamic Models: Fundamentals & Computation Aspects. Tie-Line Publications, Holte, Denmark, 2007, p.63.
2. J. Gregorowicz, J.P. O'Connell, C.J. Peters, Fluid. Phase. Equilibria., 116 (1996) 94-101.
3. G. Soave, Chem. Eng. Sci., 27 (1972) 1197-1203.
4. D.Y. Peng, D.B. Robinson, Ind. Eng. Chem. Fundam. 15 (1976) 59-65.
5. G.M. Kontogeorgis, E.C. Voutsas, I.V. Yakoumis, D.P. Tassios, Ind. Eng. Chem. Res., 35 (1996) 4310-4318.
6. W.G. Chapman, K.E. Gubbins, G.Jackson, M. Radosz, Ind. Eng. Chem. Res., 29 (1990) 1709-1721
7. S.H. Huang, M. Radosz, Ind. Eng. Chem. Res., 29 (1990) 2884-2294
8. S.H. Huang, M. Radosz, Ind. Eng. Chem. Res., 30 (1991) 1994-2005
9. J. Gross, G. Sadowski, Ind. Eng. Chem. Res., 40 (2001) 1244-1260.
10. N. von Solms, M.L. Michelsen, G.M. Kontogeorgis, Ind. Eng. Chem. Res., 42 (2003) 1098-1105.
11. G.M. Kontogeorgis, G.K. Folas, Thermodynamic models for industrial application. John Wiley & Sons Ltd, New York, U.S.A., 2010.
12. NIST Chemistry Webbook, <http://webbook.nist.gov/chemistry>.



Joana Lima-Ramos

Phone: +45 4525 2990

E-mail: jlr@kt.dtu.dk

Supervisors: John M. Woodley
Pär Tufvesson

PhD Study

Started: March 2010

To be completed: March 2013

A Development Methodology for Biocatalytic Processes

Abstract

While biocatalysis is a useful tool to assist with organic synthesis, to date few reports have documented the economics or environmental profile of such processes. As a relatively new technology often biocatalytic processes do not immediately fulfill the required process metrics that are the key for an economically feasible or a greener process at an industrial scale (high concentration, high reaction yield, high space-time-yield, and high biocatalyst yield). However, these process metrics can often be attained by improvements in the reaction chemistry, the biocatalyst, and/or by process engineering. Hence, it is necessary to implement process development in an intelligent way (and not by trial-and error, as is currently done), and the development of a systematic methodology to lead the research focus for each area (chemistry, biology and engineering) from the early stages of process development allowing a better use of resources and to shorten development time.

Introduction

During the last few decades considerable progress has been made in biotechnology research, which is ultimately reflected in the increasing number of bioprocesses that have been implemented at an industrial scale [1]. Among the bioprocesses, around 150 biocatalytic processes (i.e. enzyme and whole-cell biocatalysis) have been applied in the production of different chemicals, mainly optically active intermediates such as fine chemicals and pharmaceutical intermediates. Indeed, using alternative substrates, energy sources and innovative synthetic routes, these processes, have brought many innovations to the chemical, textile, food, health care and pharmaceutical industries [2].

Biocatalytic processes have emerged as an attractive complementary technology to chemical synthesis, due to high selectivity (enantio-, regio-, chemo- and substrate), leading to more efficient processes, the possibility to tailor the biocatalyst properties using molecular biology tools and mild processes conditions (temperature, pH, aqueous reaction media, ...). In the last decade, joint efforts between protein engineers, chemists and more recently process engineers have given rise to new opportunities for biocatalysis (enzymatic chemical synthesis), including opportunities in the bulk chemical and biofuel sectors. However, despite the many potential advantages displayed by biocatalytic processes (such as exquisite selectivity) and

the increasing number of processes running on a commercial scale, this is still a relatively underutilized technology, since many of the biocatalytic processes do not fulfill the required metrics (both economic and environmental profile).

A key reason for this is the complexity of the development process. Interestingly this complexity, which arises from the need for integration of biological and process technologies, is also the source of the greatest opportunities. Indeed protein engineering, amongst other technologies, offers a superb complement to process technology. Potentially this is one of the biggest advantages of biocatalysis when compared with conventional chemical catalysis, where all the reaction bounds are fixed by physical and thermodynamic properties of the reaction compounds. Therefore, the main avenue that still remains to be explored by process engineers is how to promote process development in a smart way rather than on an *ad hoc* basis, as is frequently the case today.

This PhD project aims at developing a systematic methodology, integrating economic and environmental evaluation and applying engineering tools (e.g. kinetic modeling) to define a set of minimum target values for process metrics and assist process development for biocatalytic processes. When applied, this methodology has a decisive role in helping to identify many of the process bottlenecks up-front and in a straightforward

way. This methodology can justify and to guide efforts, research and resources.

Specific objectives

The following specific objectives were defined:

- To develop a systematic methodology for biocatalysis that is able to guide the conceptual process synthesis, and quickly evaluate different process options at early development stage;
- To understand the process and the reaction constraints, identifying the important challenges when developing a new process, such as setting targets and guidelines for the process metrics;
- To identify suitable process techniques (eliminating some less favorable options);
- To access the decision making, regarding process flowsheet (including co-solvent selection, reactor configuration, electron donor/acceptor selection, ISPR and/or ISSS technique selection, among others), biocatalyst formulation (crude extract, purified enzyme or whole-cell and soluble or immobilized), and to guide research during catalyst developing providing guideline for biocatalyst stability and activity at relevant working conditions;
- By accomplishing the previous objectives, this methodology would be able to detect where the research efforts should be focused.

Methodology

The proposed systematic methodology is outlined Figure 1 including inflow information and internal flow and the tools suggested for each step. This methodology is an iterative, since decisions made in an early step are affecting the following steps and therefore a sensitivity analysis (including a what-if analysis) is required in order to avoid process sub-optimization.

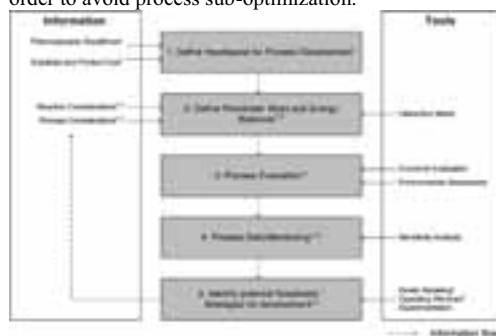


Figure 1: Overview of the proposed methodology for process early stage. Numbers 1,2, 3 refer to case studies of the same number, and are shown in each individual sequence step.

Information

The quality of the design is very much dependent on the quality of the information gathered. For this systematic methodology it is proposed a hierarchical classification of the process and reaction characteristics that influences the process viability.

Reaction considerations: describe the key characteristics to understand the interaction between the substrates, products and other reaction components (e.g. thermodynamic equilibrium, physical properties of the different compounds according with the process units of operation, the state-of-art for the specific activity of the biocatalyst used).

Process considerations: describe the characteristics that can affect the process flowsheet, mass and energy balances. These should be in agreement with the reaction considerations assumed above. Further, the process considerations should be ideally dealt in a hierarchical structure according: operation mode, reactor type, compound characteristics (including concentration of substrates, products and other compounds) and catalyst formulation, if applied process technology options (including capacity and selectivity) and process control.

Tools developed in this project

Operating windows: Operating windows are a tool to quantify and visualize process performance and feasibility. When combined with sensitivity analysis, operating windows can identify the needs for biocatalyst and process development. Furthermore it highlights the process constraint with the greatest impact on process feasibility. This tool allows the engineer to set up the biocatalyst and process requirements, while understanding where the bottlenecks are, channeling the efforts to solve them in a time-saving and strategic away.

Economic Evaluation: To perform an economic evaluation to flowsheets, and with the mass and energy balances already computed, it is necessary to calculate the operation and capital costs (or OpEx and CapEx, respectively) and . The methodology presented by Tufvesson and co-workers was followed [3]. The economic evaluation is performed based on an output of 1 kg of final product (i.e. € per kg of product).

Environmental Assessment: There are several different approaches to quantify the process environmental performance and improvements for chemical production processes. The application of one approach over another it is mostly dependent on the stage of development of the process and on the amount of information available. Green chemistry metrics are mostly preferred when little detail is known, as they are attempts to measure the process chemistry and efficiency in a straight forward and easy to use way. However, these metrics do not distinguish between waste types and emissions generated or resources used upstream or downstream of the evaluated process step. Performing a full LCA during process development might only be possible at a later stage when there are limited possibilities of changing the process design. Nevertheless, the understanding of the contribution each process stage (e.g. catalyst production, raw materials, downstream process) to the environmental performance is essential, and should be regarded with special care.

Description of methodology

1. Define Headspace for Process Development: In the first step, the headroom for downstream process (DSP), biocatalyst activity, and/or other process technologies to enhance the reaction performance is determined. To compute the headspace available it is required to compile the information about the thermodynamic equilibrium constant (K_{eq}), the purchasing substrate(s) cost, and the production cost of the product produced by the competing technology (or if not available the expected selling price of our product of interest).

For an economically feasible process, the product selling cost (C_p in €mol_p^{-1}) has to be higher than purchasing cost of the substrate (C_s in €mol_s^{-1}) used to produce the product P. The amount of substrate required can be translated through the reaction yield (Y in $\text{mol}_p \text{mol}_s^{-1}$). The maximum theoretical reaction yield is determined by the K_{eq} for the given reaction. Therefore, any effort made to shift the thermodynamic equilibrium, in order to obtain a higher reaction yield, must be reflected in increasing the headroom between the substrate purchasing cost and the product production cost in order to, at least, pay off the implementation of this given process technology.

2. Define Flowsheet, Mass and Energy Balances: The information compiled is now put together in a form of flowsheet. Following, mass and energy balances are performed based on the flowsheets generated and addressing the information compiled. Here the amount of the raw materials (reactants, reagents, solvent and catalysts), (co-)products and energy is computed for each identified flowsheet.

3. Process Evaluation: The main goal of this step is to identify the process effectiveness while determining the main process challenges. In this step, the different process options are evaluated in terms of their economic and environmental profile, based on the mass and energy balances computed in previous. Through these evaluation tools, the most unfavorable process options can be eliminated in this step.

4. Process Debottlenecking: The previous steps can already rule-out some of the less attractive process configurations, throughout process evaluation. However, even processes that were not yet discarded, should be submitted to a sensitivity analysis and consequent process re-evaluation to identify the important parameters, that need to be optimized (and/or modified) to attain process success. These parameters are both those considered at the process considerations and the process metrics used to build the mass and energy balances (i.e. reaction yield, concentration, space-time-yield and biocatalyst yield). This step identifies process bottlenecks and important parameters in the flowsheet. Further, research targets for the different process considerations and (to some extent) reaction considerations can be identified.

5. Identify strategies for development: The optimization can be done for a certain process metric (e.g. reaction yield or space-time-yield) when their relationship with the variables assumed in reaction and

process considerations is known. Process optimization can be attained through kinetic modeling, and/or using operating windows. These tools are used for analyzing the process. Modeling and simulation techniques (including operating windows) can be used for exploring alternative routes and hypothetical process modifications.

An iterative methodology is required at this point, to assure that the process implementation is performed at the most optimized conditions. This iterative process, also helps to understand the trade-offs between the variables previously assumed. Hence, the optimized operating space where the process metric can be maximized should be identified in this step. In this way more focused experiments can be performed in order to validate the hypothesis.

Finally, the outcome of the process optimization is condensed to potential process flowsheets identifying the research areas (e.g. reaction design, biocatalyst improvement, solvent selection, ISPR capacity and selectivity, ...) were one should canalize efforts and resources in order to attain an industrially viable and competitive process.

Introduction to case studies

In this thesis three case studies have been selected in order to build, test and verify the methodology developed here. Valuable contributions have been obtained from each case study not only for improved process understanding but also to refine the requirements and outcome of each step of the proposed methodology.

The case studies are:

1. Caprolactam production by multi-enzymatic system in a whole-cell biocatalyst;
2. Chiral amine production using ω -transaminase;
3. Long chain aliphatic alcohol production by a bi-enzymatic system.

For the first case study (see sequence step indicated by the number (1) in Figure 1), the establishment of a feasible flowsheet and mass and energy balances was of great importance, since very little information is known about this process. This case study highlights the importance of structured approach to compile the information required. As an outcome this case study compares different catalyst formulations to be used in a multi-enzymatic system (free-enzyme, whole-cell, immobilized), while setting targets for catalyst stability.

The case study chose was the synthesis of caprolactam. Caprolactam is a monomer of the polymer Nylon-6 (or polycaprolactam) used in several different applications. The conventional chemical synthesis of caprolactam is by Beckmann rearrangement, which entails several disadvantages (such as high toxicity of the raw material and harsh reaction conditions), which can be overcome in a biosynthetic route. The biocatalytic route (Figure 2) is likely to improve the Environmental Health and Safety (EHS) process profile as the process runs at milder conditions.

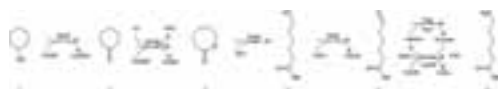


Figure 2: Enzymatic cascade for biosynthesis of caprolactam. 1) cyclohexanol 2) cyclohexanone 3) 6-hexanolactone 4) 6-hydroxy-hexanoic acid 5) 6-oxo-hexanoic acid 6) 6-amino-hexanoic acid or caprolactam. KRed – ketoreductase; BVMO – Baeyer-Villiger monoxygenase; TAm – transaminase; AlaDH – Alanine Dehydrogenase

The second case study had a later starting point (see sequence step indicated by the number (2) in Figure 1), and it intends to explain how to use operating windows as a tool for process development and optimization. This tool was applied to identify suitable process conditions for the assessment of feasible process configurations. The methodology comprises: reaction characterization (such as physicochemical properties, kinetics, and stability); identification of the main variables and analysis of their dependence and boundaries; and sensitivity analysis, comparing operating windows from alternative processes.

This tool was demonstrated for synthesis of optically pure chiral amines using ω -transaminase (Figure 3). The challenges encountered in this process include potentially unfavorable thermodynamic equilibria, low biocatalyst activity and stability, as well as substrate and product inhibition. To overcome these limitations there are several possible process solutions as well as solutions via biocatalyst development and improvement. Potential process solutions include operating at substrate excess (e.g. addition of an excess of amine donor), application of *in-situ* product removal (ISPR) and *in-situ* co-product removal (IScPR). Operating windows identify a potential operating space, defining guidelines for process and biocatalyst development, and assisting in the choice of the most suitable process option.

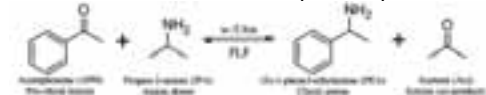


Figure 3: Model transaminase catalyzed reaction

The third case study (see sequence step indicated by the number (3) in Figure 1), aims the development of a second-generation process, strive for reductions in costs and improved environmental profile by attaining higher process efficiency. The proposed methodology was used to identify process bottlenecks in the running processes, aiming savings in the operation costs, and set targets for improvement intending a successfully and economically viable scale-up.

The continuous enantioselective reduction of aliphatic ketones in biphasic systems [4] was chosen as a case study (Figure 3). This system displays several disadvantages, such as: low substrate solubility, high viscosity of the ionic liquid used as solubiliser, low stability of the cofactor used and low enzyme utilization, leading to low concentrations and biocatalyst

yield ($\text{g}_p/\text{g}_{\text{Catalyst}}$) preventing an economic successful scale-up. Hence, a second-generation process was developing aiming the identification of bottlenecks, proposing alternatives to overcome these bottlenecks and applying kinetic modeling to evaluate the feasibility of the proposed solutions.

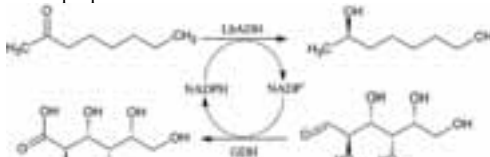


Figure 4: Model transaminase catalyzed reaction

Acknowledgments

This PhD project is founded European Union through the 7th Framework people Programme through the Marie Curie Initial Training Network (ITN) BIOTRAINS (Grant agreement no.: 238531).

References

- [1] B. Hermann, M. Patel, Today's and tomorrow's bio-based bulk chemicals from white biotechnology, *Appl. Biochem. Biotechnol.* 136 (2007) 361-388.
- [2] G. Frazzetto, White biotechnology, *EMBO Rep.* 4 (2003) 835-837.
- [3] P. Tufvesson, J. Lima-Ramos, M. Nordblad, J.M. Woodley, Guidelines and cost analysis for catalyst production in biocatalytic processes, *Org. Process Res. Dev.* 15 (2011) 266-274.
- [4] S. Leuchs, S. Na'amnieh, L. Greiner, Enantioselective reduction of sparingly water-soluble ketones: Continuous process and recycle of the aqueous buffer system, *Green Chem.* (2012).

**Asger Lindholdt**

Phone: +45 4525 2837
E-mail: Asli@kt.dtu.dk

Supervisors: Søren Kiil, DTU
Kim-Dam Johansen
Diego M. Yebra, Hempel A/S
Stefan M. Olsen, Hempel A/S

PhD Study

Started: December 2011
To be completed: December 2014

Fuel Efficiency and Fouling Control Coatings in Maritime Transport

Abstract

The purpose of this project is to investigate the surface friction for marine coatings as the surface friction relates to a vessel's fuel consumption, maneuverability and speed. Experimental designs have been evaluated which has resulted in a design consisting of cylindrical rotor setups placed in the sea and a laboratory cylindrical rotor setup. The design is believed capable of increasing the knowledge in the field of long term drag performance for marine coatings beneficial from both an industrial and academic point of view. The laboratory test setup has been tested and proven capable of measuring significant differences in drag due to increasing surface roughness.

Introduction

The maritime transport sector is responsible for transporting huge amounts of goods all around the world which unfortunately has the negative side effect that vast amount of fuel is being consumed causing harmful emission of e.g. CO₂, NO_x and SO_x particles. Surface friction constitutes a large part of a vessel's total resistance which, however, depends on several factors such as e.g. the condition of the marine coating and the vessel's speed. Marine biological fouling is known to have an undesirable effect regarding increasing vessel drag. Marine coatings are often today being evaluated based on static exposure of coated objects followed by hydrodynamic drag measurements in e.g. a towing tank. As larger vessels is only rarely static (e.g. in ports) a static test is only a mediocre method when evaluating marine coatings. Static exposure followed by hydrodynamic exposure has been applied and is a step closer, as compared to only static exposure, to resembling the conditions a vessel is exposed to during voyage. However, further improvements are desirable in order to evaluate the long term drag performance of marine coatings and also resemble the conditions coatings experience more accurately. The purpose of this project is to expand the boundaries with respect to hydrodynamic drag measurements with focus on long term aging of marine coatings under conditions resembling the ones vessels experience during voyage.

Specific Objectives

The objectives of this project are to develop an experimental method capable of resembling the aging process of marine coatings well. During this aging process it is desired to continuously measure drag and determine the surface friction coefficients for a number of marine coatings and their development over time.

The laboratory cylindrical rotor setup, which is seen in Fig. 1, is currently being finalized. The system consists of a large tank where the rotating cylinder is placed and a static cylinder is placed outside the inner rotating cylinder. The torque sensor is used to measure the torque due to rotation of the system and the surface friction can be determined by measuring the effects due to top and bottom of the cylinder and shaft contribution.

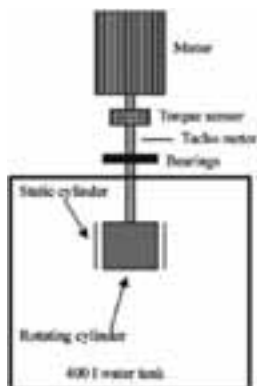


Figure 1: Laboratory cylindrical rotor setup

The seawater setup is seen in Fig. 2 where continuous drag measurements occurs which shall be combined with laboratory drag measurements near the test site.

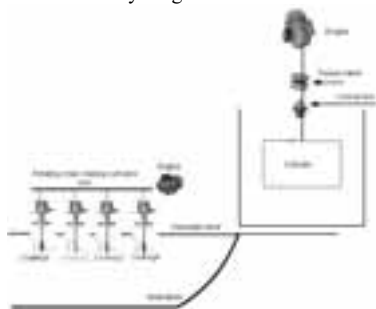


Figure 2: Cylindrical seawater test setup

The advantage of the seawater setup compared to other setups applied in the field of marine coating's drag determination is that the coating's aging process resembles the one a ship experiences due to the hydrodynamic exposure in the sea. Furthermore, the drag measurements are recorded continuously resulting in a large amount of drag measurements over time as opposed to only a limited number of measurements.

Results and Discussion

The cylindrical rotor setup has shown that a difference in surface friction between a smooth surface and a surface roughened with sandpaper P60 can be measured, see Fig. 3.

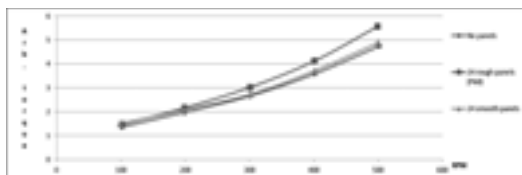


Figure 3: Torque and RPM for no panels, 24 rough panels and 24 smooth panels.

The data which is expected to be obtained will be used to estimate fuel savings for various ship operating profiles based on the choice of marine coatings. Furthermore, drag shall be correlated with biological fouling measurements such as area coverage on coating, thickness and type of biological fouling (e.g. slime, barnacles).

Conclusions

The test setup being developed has proven capable of measuring significant surface friction differences between smooth and mechanically rough surfaces. This indicates that the test setup will be able to measure surface friction development over time for marine coatings being hydrodynamically exposed in the sea.

Acknowledgements

This PhD project is supported both financially and knowledge wise from Hempel A/S which is greatly appreciated.

References

1. M.P. Schultz, G.W. Swain, *Biofouling* 15 (2000) 129-139.
2. G.W. Swain, B. Kovach, A. Touzot, F. Casse, C.J. Kavanagh, *Journal of Ship Production* 23 (3), (2007) 164-170.
3. D.M. Yebra, S. Kiil, K. Dam-Johansen, *Process in Organic Coatings* 50 (2004) 75-104.
4. C.E. Weinell, K.N. Olsen, M.W. Christoffersen, S. Kiil, *Biofouling* 19 (Supplement) (2003) 45-51.

**Frederikke Bahrt Madsen**

Phone: +45 4525 6809
E-mail: frbah@kt.dtu.dk

Supervisors: Anne Ladegaard Skov
Søren Hvilsted
Anders E. Daugaard

PhD Study

Started: August 2011
To be completed: August 2014

Development of novel cross-linkers for PDMS networks for controlled and well distributed grafting of functionalities by click chemistry

Abstract

An azide-containing vinyl cross-linker for silicone networks has been developed. The cross-linker has through Cu(I) catalyzed 1,4-cycloaddition been reacted with six different alkyne-containing chemical groups which each possess a particular functionality. The functional cross-linkers have been utilized to prepare novel polydimethylsiloxane (PDMS) films. TGA showed that a ferrocene functionality increased the thermal degradation temperature of PDMS. It was furthermore shown that the incorporation of only 0.25 wt% of the push-pull dipole, ethynyl-4-nitrobenzene, increased the dielectric permittivity of PDMS by 35 %. The contact angle of PDMS films was increased from 108° to 116° by the introduction of a small poly(pentafluorostyrene) chain.

Introduction

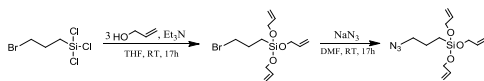
Polydimethylsiloxane (PDMS) is the most widely used siloxane polymer. PDMS elastomers have numerous and widespread applications such as membranes, adhesives, dielectric elastomers and for biomedical applications. PDMS owes its many excellent properties to the presence of methyl groups along the Si-O-Si backbone which gives the polymer high thermal stability, low surface tension, high gas permeability and biological and chemical inertness[1]. Due to the many excellent properties of PDMS it is of great interest to extend the range of applications even further. Modification of PDMS networks by covalent grafting of functionality will change the properties and improve the applicability of PDMS films within many areas.

The cross-linking of PDMS into an elastomer is frequently obtained by hydrosilylation where vinyl groups of one component react with hydrosilane groups of the other component in a platinum catalyzed reaction. In this work, a novel silicone compatible vinyl cross-linker containing an azide functionality is prepared. The vinyl groups allow for cross-linking reactions with hydride-terminated PDMS molecules whereas the azide-group allows for modification of the PDMS network either before or after network cross-linking. The azide-moiety opens up for click reactions, in this case the copper-catalyzed cycloaddition of an azide group and an alkyne (CuAAC) forming a 1,4-disubstituted-1,2,3-triazole [2–5]. The azide group on the cross-linker

therefore enables reactions with various types of alkyne-functional molecules and thereby significantly widens the functionality that can be introduced to PDMS elastomers. Introduction of 4-methylumbelliferone will provide the PDMS network with a fluorescent tag at the cross-linking site that can be used to visualize the distribution of incorporated functionality and create luminescent PDMS films. A push-pull dipole that potentially enhances the dielectric permittivity of the silicone elastomer can be inserted from an ethynyl-4-nitrobenzene and thus improve the dielectric elastomer performance. The incorporation of ferrocene will provide PDMS films with potential applications within the optical, magnetic or electronic field. Different kinds of drugs or therapeutics for biomedical applications will also be possible by the introduction of an estradiol functionality. Recently it has been shown that introduction of trifluoromethyl groups improve the oil and solvent resistance of PDMS films[6]. Therefore bis(trifluoromethyl)phenyl and a short poly(pentafluorostyrene) chain will be inserted in the PDMS network.

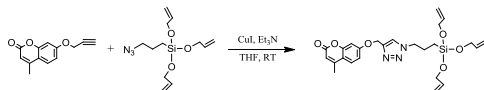
Results and discussion

The azide-functional, silicone compatible vinyl cross-linker was synthesized in two steps via the silyl ether reaction between (3-bromopropyl)trichlorosilane and allyl alcohol and subsequent substitution of bromine with azide as illustrated in Scheme 1.



Scheme 1: Synthesis of the azide-functional vinyl cross-linker.

The alkyne-functional molecules used in the click reactions with the azide cross-linker are shown in Table 1. A general reaction scheme for the click reaction is illustrated in Scheme 2.



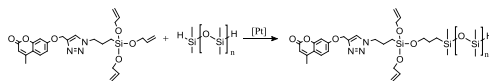
Scheme 2: General reaction scheme for click reaction between the azide cross-linker and alkyne exemplified by 4-methylumbelliferone.

The click reaction was used to prepare a variety of different functional cross-linkers as shown in Table 1.

Table 1: Alkynes and functional cross-linkers from click reactions.

Alkyne	Click-products

The PDMS networks were prepared from the cross-linkers shown in Table 1, hydride terminated PDMS and a platinum catalyst according to Scheme 3.



Scheme 3: Cross-linking reaction between cross-linker and hydride terminated PDMS.

Thermal gravimetric analysis (TGA) was used to investigate the effects of the different functional cross-linkers on the thermal stability of the PDMS films.

The TGA measurements revealed that the PDMS samples have different decomposition temperatures depending on the incorporated functionality with the ferrocene giving the highest initial degradation temperature (540 °C) due to higher thermal stability of ferrocene which increases the degradation temperature of the PDMS film. The dielectric properties were determined by dielectric relaxation spectroscopy (DRS) for the films prepared with the azide-functional and ethynyl-4-nitrobenzene cross-linker. It was found, that the dipolar nature of the nitrobenzene cross-linker, due to the nitro group, increases the dielectric properties of the film from 2.3 for films with no functionality to 3.1 for films with the nitrobenzene functionality which corresponds to an increase of 35 %. This increase is remarkable since the content of this dipolar cross-linker is only around 0.75 wt% corresponding to 0.25 wt% of the pure dipole molecule. Furthermore the contact angle of the PDMS films was shown to be increased from 108° to 116° by the incorporation of a small poly(pentafluorostyrene) chain.

Conclusion

A novel silicone compatible cross-linker that allows for click reactions and thereby grafting of various molecular functionalities onto PDMS networks has been developed. The functionalization of PDMS networks was demonstrated by the successful synthesis of a number of diverse functional cross-linkers that were used to create PDMS films with altered properties.

Acknowledgements

The authors wish to acknowledge the Danish National Advanced Technology Foundation for financial support.

References

1. J. E. Mark, in: J.M. Zeigler, and F.W.G. Fearon (Eds.) *Silicon-Containing Polymers*, American Chemical Society, 1990, p. 47-68.
2. H. C. Kolb, M. G. Finn, K. B. Sharpless, *Angew. Chem. Int. Ed. Engl.* 40 (11) (2001) 2004-2021.
3. P. Wu, A. K. Feldman, A. K. Nugent, C. J. Hawker, A. Scheel, B. Voit, J. Pyun, J. M. J. Fréchet, K. B. Sharpless, V. V. Fokin, *Angew. Chem. Int. Ed. Engl.* 43 (30) (2004) 3928-3932.
4. M. Meldal, *Macromol. Rapid Comm.* 29 (12-13) (2008) 1016-1051.
5. W. H. Binder, R. Sachsenhofer, *Macromol. Rapid Comm.* 29 (12-13) (2008) 952-981.
6. B. Li, S. Chen, J. Zhang, *Pol Chem* 3 (2012) 2366-2376.



Christine Malmos

Phone: +45 4525 2892
E-mail: mmos@kt.dtu.dk

Supervisors: Nicolas von Solms
John M. Woodley

PhD Study
Started: August 2011
To be completed: July 2014

Inhibition of Gas Hydrate Formation by Antifreeze Proteins

Abstract

Antifreeze proteins (AFPs) have shown in the literature to be promising green and environmentally benign inhibitors for gas hydrate formation. Especially insect AFPs express high antifreeze activities which is their ability to prevent ice from freezing. In this study we showed that AFP from the long horn Danish bark beetle, *Ragium mordax*, can perform as an effective kinetic hydrate inhibitor (KHI) on the same level as the commercial synthetic inhibitor polyvinylpyrrolidone (PVP).

Introduction

Gas hydrates are crystalline solid compounds of gas molecules and water which forms at low temperature and high pressure. In the oil and gas industry gas hydrates block flow lines and pipelines in oil and gas production causing huge production losses and safety problems.

Hydrate formation is a stochastic time-dependent process consisting of the steps of nucleation and growth. Several theories and hypothesis are suggested in order to describe the nucleation mechanism of hydrates. One is by Sloan et al. 2007 the 'labile cluster nucleation' hypothesis. A labile cluster is an unstable entity (cavity occupied by a guest molecule) that readily undergoes changes. According to the hypothesis the nucleation of hydrates proceeds in 4 steps which are shown in Figure 1.

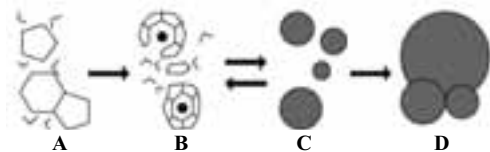


Figure 1: Schematic model of hydrate cluster growth. [1]

First pressure and temperature are at hydrate forming conditions but no gas is dissolved. Then gas dissolve into the water and labile clusters form. These clusters undergo agglomeration and finally hydrate growth begins when the size of clusters reaches a critical value. [2]

Hydrate formation was visually observed and pictures taken during the hydrate formation experiment with natural gas and water corresponding to the steps illustrated in Figure 1 are shown in Figure 2.

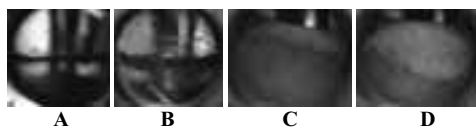


Figure 2: Photographs of hydrate nucleation and growth.

To provide flow assurance the industry use thermodynamic inhibitors as methanol, which are uneconomical and not environmentally friendly as large amounts are needed.

Low dosage hydrate inhibitors are developed as an alternative which can be applied in much lower concentrations. Most of these suffer from low biodegradability which means that they cannot be applied in the North Sea.

Recent studies have shown that antifreeze proteins may hold a promising potential to work as a low-dosage hydrate inhibitors in both natural gas [3-6] and methane gas [7,8] systems while at the same time being environmentally benign. AFPs protect organisms from deep freezing temperatures by preventing ice from growing upon cooling below the melting point. Especially AFPs from insects show considerable higher antifreeze activities than AFPs from other organisms. The long horn Danish bark beetle *Ragium mordax*

(RmAFP) can express antifreeze activity in excess of 8°C which is more than other insect proteins.[9]

Specific Objectives

The objective of this PhD project is to investigate if AFPs can be applied in field conditions to control the formation of gas hydrates i.e. can AFPs substitute conventional types of chemicals like methanol as hydrate inhibitors.

This objective will be achieved by setting up laboratory scale experiments to simulate realistic hydrate formation scenarios using three different experimental apparatus: high pressure micro-Differential Scanning Calorimeter (HP- μ DSC), Rocking Cells, and a pressurized stirred autoclave. Different types of water soluble polymeric commercial low-dosage hydrate inhibitors will be evaluated and the performance will be compared to AFPs. Synergy effects between inhibitors and other production chemicals will be studied and an evaluation of health, safety and environmental matters related to AFPs will be carried out. Finally a feasibility study will be carried out to investigate if AFPs can be implemented in field applications.

In this study methane hydrate inhibition using AFP from *Ragium mordax*, two amino acids: L-threonine and L-valine, Bovine Serum Albumin (BSA) and the synthetic inhibitor PVP (MW 10.000) in the new equipment Rocking Cells were investigated.

The two amino acids and the non- antifreeze protein BSA were used as test controls. In AFP-I (type I AFP that exists in fish) hydroxyl groups of threonine residues have been shown to be essential to make antifreeze protein-ice interaction permanent. Replacement of the threonine hydroxyl-groups with methyl-groups (threonine to valine mutation) indicated that the hydrophobic methyl-group could be involved in water exclusion at the adsorption site of the protein. This means that the hydrophobic methyl-group could be important in the antifreeze inhibition mechanism of ice.[10]

Equipment and method

Measurements of the onset of hydrate nucleation temperatures by constant cooling experiments were studied in Rocking Cells. The aim was to obtain the difference in delay of hydrate nucleation for synthetic and biological KHIs compared to a non inhibitor system in order to investigate how effective AFP is as an inhibitor. The methodology applied is based on the precursor (memory effect) method described by Duchateau et al. [11]. The results obtained are compared to results using fresh solutions. All inhibitors were tested in a concentration of 2770 ppm.

The hydrate nucleation experiments were conducted in a Rocking Cells produced by PSL Systemtechnik (Figure 3). The apparatus consists of 5 test cells placed on a cell drive in the cooling bath. Each cell has a working pressure up to 200 bar. The temperature is

adjusted by the external cooling bath in the range -20°C to +60°C.

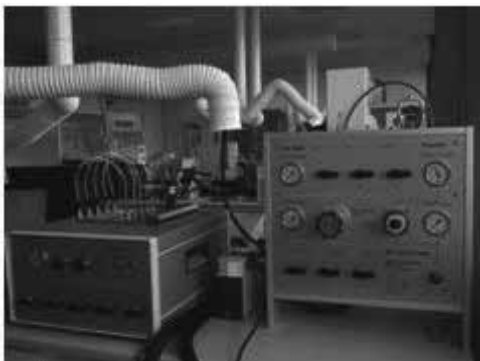


Figure 3: Rocking Cells produced by PSL Systemtechnik. The picture shows the Rocking Cells setup consisting of the cooling bath with 5 test cells and the high pressure panel.

The stainless steel test cells with a volume of 40 ml and have a stainless steel ball that freely rolls over the entire length of the cell when it is rocking. The cells can rock with an angle of -45° to $+45^\circ$. The measuring principle is based on a uniform rocking movement of the test cells. When the cell is rocked the ball inside the cell is rolling along the length of the cell and thereby blends the test mixture. Through movement of the ball shear forces and turbulences are created in the cell. Thereby the conditions in the pipelines can be reproduced.

Each test cell was loaded with 10 ml of test liquid. To eliminate the air in the cells they were evacuated. All the systems were initially pressurized to 95 bar of methane gas. For the non inhibitor systems, the constant cooling/heating cycle was from 20.5°C to 2°C to 20.5°C. For the KHI experiments the 13°C to 2°C to 14°C in order to maintain the stability of the protein while fully melting the hydrates in the cells. The equilibrium temperature for the methane-water system at this pressure was determined using laboratory experiments by standard slow hydrate dissociation [12]. Experiments conducted resulted in an equilibrium temperature of 12.9°C.

The experiments were programmed and temperature and pressure data were logged throughout the experiment. Two cycles were set up for each experiment in order to perform a non precursor and precursor test.

The cells were set to rock and cooling at a constant rate. During cooling down the pressure decreases at a constant rate as the temperature decreases until hydrate nucleation which is observed as a fast pressure drop. The temperature at which hydrate nucleates is called the onset temperature, T_o .

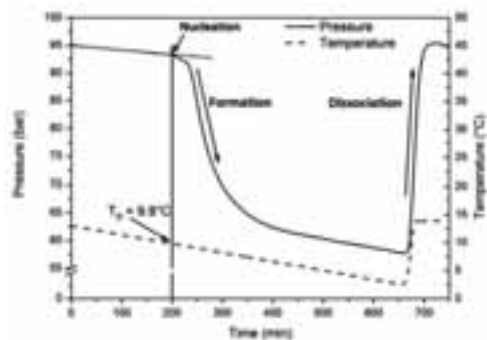


Figure 4: Temperature and pressure recorded during the constant cooling test of PVP10 in 50 mM NaCl-MilliQ. The red line indicates the pressure decrease as the temperature decreases. The measured pressure will deviate from the red line as hydrates nucleate. This is indicated by a black arrow pointing at the onset temperature (T_o).

We maintained the temperature at 2°C for 1h to ensure complete conversion to hydrates. The cells were then heated at a fast rate in order to dissociate the hydrates. The temperature was maintained for 30 min to ensure fully dissociation of the hydrates before repeating the cycle for the precursor test. As the pressure and temperature reach the initial setting and stabilizes all the hydrates are dissociated.

Results and Discussion

Previous studies showed that AFPs do inhibit hydrate nucleation and change the growth profile of hydrates [4,5,7,8]. How effective AFPs delay hydrate nucleation depends on the AFP type and concentration.

In Figure 5 and Figure 6 onset hydrate nucleation temperatures for non-precursor tests and precursor tests are shown.

In both the non-precursor test and precursor test the results show that L-valine and L-threonine do not exhibit any KHI effect in the form of amino acids as they do not delay hydrate nucleation compared to the non-inhibitor system. It should be noted that only one AFP non-precursor test was performed due to limited amount of AFP. Although, AFP shows a very promising result as a KHI compared to PVP.

The ranking of the KHI performance in both the non-precursor and the precursor constant cooling test method, using the onset hydrate temperatures was clearly:

AFP = PVP10 > BSA > L-threonine = L-valine = 50mM NaCl in MilliQ water

As can be seen from Figure 5 and Figure 6 the observed onset hydrate nucleation temperatures are very similar for the non-precursor and precursor test indicating that the memory effect did not affect the nucleation.

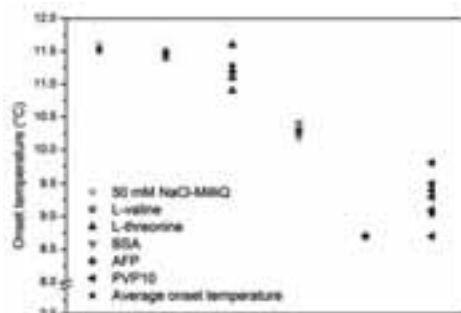


Figure 5: Onset hydrate nucleation temperatures for non-precursor constant cooling tests using KHIs at a concentration of 2770 ppm.

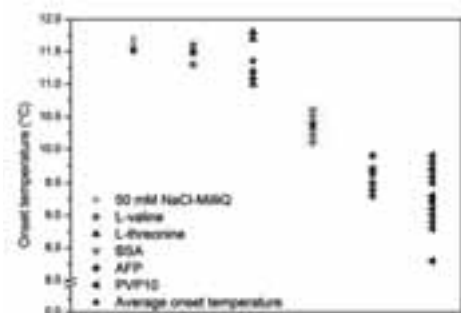


Figure 6: Onset hydrate nucleation temperatures for precursor constant cooling tests using KHIs at a concentration of 2770 ppm.

Daraboina et al. 2011 observed a similar result for PVP and AFP for inhibition of natural gas hydrates. Using an isothermal nucleation procedure to obtain the nucleation time (time delay of hydrate formation) it was shown that PVP and AFP obtained very similar nucleation times using both a stirred tank and the HP μ DSC. [4,5] This indicates that the AFPs are performing similar for both methane systems (SI hydrates) and natural gas systems (SII hydrates).

For antifreeze proteins at equimolar concentrations an increase in size of protein decreases the solubility of the protein in the water phase which will lead to increased antifreeze activity [10]. We speculate that the observed KHI effect of BSA could be due to decreased solubility as the molecular weight of BSA (67 kDa) is significantly higher compared to RmAFP (14 kDa).

In Figure 7 and Figure 8 normalized hydrate growth profiles for the non-precursor tests and the precursor tests are shown.

The controls MilliQ water + NaCl, L-valine and L-threonine show very similar growth profiles in both the non-precursor test and precursor test.

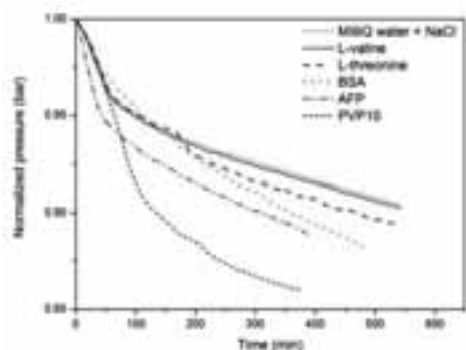


Figure 7: Hydrate growth profiles for non-precursor constant cooling tests using KHIs at a concentration of 2770 ppm.

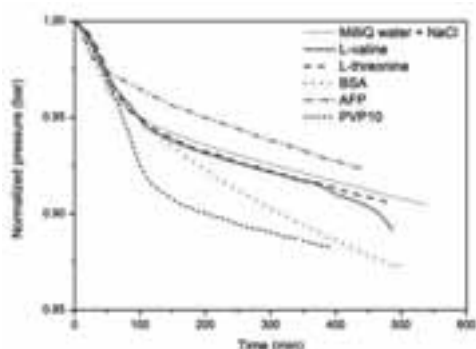


Figure 8: Hydrate growth profiles for precursor constant cooling tests using KHIs at a concentration of 2770 ppm.

In the non-precursor test BSA shows increased growth compared to the controls. AFP shows even more hydrate growth and grows fast initially in contrast to the other KHIs. However, the greatest growth of hydrates is observed when using PVP10 whereas the controls showed the least growth. This indicates that the KHIs promote hydrate growth although they significantly delay hydrate nucleation.

In the precursor test the growth profile of AFP changes significantly by showing the least growth of hydrates which means AFP changes from promoting to inhibiting the hydrate growth. Again, PVP10 shows significant growth but BSA shows even greater growth although at a slower rate. Inhibition of methane hydrate growth was also reported by Jensen et al. 2010 when using similar methodology and the insect AFP, *Tenebrio molitor*. In addition the AFP performed as a more effective inhibitor compared to PVP. However, both KHIs were performing as inhibitors of hydrates growth.[7]

Our study shows that AFP performs as an effective hydrate nucleation inhibitor, while a reference protein (BSA) and amino acids did not show significant inhibition activity.

Conclusions

In both hydrate nucleation tests the AFP from the long horn Danish bark beetle, *Ragium mordax*, (RmAFP) perform as an effective hydrate nucleation inhibitor at the same level as the synthetic inhibitor PVP. All inhibitor systems promoted the hydrate growth except the AFP in the precursor test which showed to inhibit the growth.

By comparing onset nucleation temperatures and growth profiles it is observed that no clear correlation between the effectiveness of KHIs. However, AFP in the precursor test performs as an effective inhibitor in both hydrate nucleation and growth.

Further tests are needed to verify the performance of the AFP. To simulate realistic scenarios moreover, experiments are planned to be carried out in different salinity levels in order to simulate the variations observed in the fields. The biodegradability of AFP compared to synthetic inhibitors will be studied as it is of great importance for selection of future KHIs.

Acknowledgements

The project is a part of the advanced technology project 'Biotechnology in Oil Recovery', funded by the Danish National Advanced Technology Foundation, the Technical University of Denmark, Maersk Oil A/S, Dong Energy A/S, Novozymes A/S, Danish Technological Institute and Roskilde University.

References

1. Jr E.D. Sloan, C. Koh, Clathrate hydrates of natural gases, CRC Press, Boca Raton, USA, 2007, p. 133.
2. R.L. Christiansen, Jr E.D. Sloan, Annals of the New York Academy of Sciences 715 (1994) 283-305.
3. L. Jensen, K. Thomsen, N. von Solms, Energy Fuels 25 (2011) 17-23.
4. N. Daraboina, P. Linga, J. Ripmeester, V.K. Walker, P. Englezos, Energy Fuels 25 (2011) 4384-4391.
5. N. Daraboina, J. Ripmeester, V.K. Walker, P. Englezos, Energy Fuels 25 (2011) 4392-4397.
6. H. Ohno, R. Susilo, R. Gordienko, J. Ripmeester, V.K. Walker, Chem. Eur. J. 16 (2010) 10409-10417.
7. L. Jensen, H. Ramløv, K. Thomsen, N. von Solms, Ind. Eng. Chem. Res. 49 (2010) 1486-1492.
8. S. Al-Adel, J.A.G. Dick, R. El-Ghafari, P. Servio, Fluid Phase Equilib. 267 (2008) 92-98.
9. E. Kristiansen, C. Wilkens, B. Vincents, D. Friis, A.B. Lorentzen, H. Jessen, A. Løbner-Olesen, H. Ramløv, J. Insect Physiol. 58 (2012) 1502-1510.
10. E. Kristiansen, K.E. Zachariassen, Cryobiology 51 (2005) 262-280.
11. C. Duchateau, J.-L. Peytavy, P. Glénat, T.-E. Pou, M. Hidalgo, C. Dicharry, Energy Fuels 23 (2009) 962-966.
12. B. Tohidi, R.W. Burgass, A. Danesh, K.K. Ostergaard, A.C. Todd, Annals of the New York Academy of Sciences 912 (2000) 924-931.



Bjørn Maribo-Mogensen

Phone: +45 4525 2869
E-mail: bmm@kt.dtu.dk

Supervisors: Georgios M. Kontogeorgis
Kaj Thomsen

PhD Study
Started: August 2010
To be completed: March 2014

Development of an Electrolyte CPA Equation of State for Applications in the Petroleum and Chemical Industries

Abstract

Complex mixtures of associating/polar components and electrolytes are often encountered in the oil- and gas and chemical industry. By modeling the phase behavior of these mixtures it is possible to reduce the environmental impact of natural gas processing, to optimize the performance of CO₂ capture and sequestration, and to improve purification of complex chemicals in the pharmaceutical and biochemical industries. This PhD project works on developing a new equation of state for modeling phase behavior of complex mixtures containing electrolytes.

Introduction

Complex mixtures of associating/polar components and electrolytes are often encountered in the oil- and gas and chemical industry. It is well-known in the oil- and gas industry that electrolytes have a substantial effect (typically decreasing) on e.g. solubilities of gases in water-hydrocarbon mixtures (salting-out effect), and furthermore, the presence of electrolytes may enhance the inhibitory effect of methanol and glycol on the formation of gas hydrates in natural gas pipelines, thus allowing for problem-free flow. In the pharmaceutical and biochemical industry, electrolytes, associating and polar compounds are present during downstream processing. Electrolytes are also very important to the energy industry e.g. with regards to wet flue gas desulphurization or CO₂ capture from power plants using aqueous solutions of alkanolamines.

Specific Objectives

A new equation of state for electrolytes in mixed solvents will be developed based on the Cubic Plus Association (CPA) equation of state (EoS). The equation of state must be thermodynamically consistent and predict that ions are present in the liquid phase. We aim to develop a new model for the static permittivity in mixed solvents with salts, and assess the performance and importance of including various models for the electrostatic interactions.

Theoretical Background

The most widely used thermodynamic models are the cubic EoS such as Soave-Redlich- Kwong (SRK), where the liquid-vapor equilibrium is modeled using Eq. (1) [1, p. 42]:

$$P = \frac{RT}{V_m - b} - \frac{a(T)}{V_m(V_m + b)} \quad (1)$$

Where P is the pressure, T is the temperature, V_m is the molar volume, and the parameters a and b are calculated from pure component parameters using e.g. the van der Waals one-fluid mixing rules shown below:

$$a = \sum_i \sum_j x_i x_j [a_i(T) a_j(T)]^{0.5} (1 - k_{ij}) \quad (2)$$

$$b = \sum_i \sum_j x_i x_j \left(\frac{b_i + b_j}{2} \right) \quad (3)$$

While the cubic EoS performs well for predicting vapor-liquid equilibrium at both high and low pressures for simple compounds such as hydrocarbons, it is usually not applicable to mixtures also containing polar or associating compounds, especially for multicomponent mixtures. Despite the shortcomings, cubic EoS are the most widely used models due to e.g. their relatively simple implementation and large parameter databases. Additionally, advanced mixing rules for the equation parameters can yield much better agreement with experimental data.

The cubic EoS gives a macroscopic description of repulsive and attractive intermolecular forces. Through the Helmholtz energy it is possible to extend the EoS to incorporate new terms that describe other intermolecular forces, such as association (hydrogen bonding) and electrostatic interactions as illustrated by Eq. (4):

$$A' = A'_{SRK} + A'_{Association} + A'_{Electrostatic} \quad (4)$$

Other physical properties can be determined from derivatives of the Helmholtz energy – e.g. is it possible

to calculate the pressure using Eq. (5):

$$P = \frac{RT}{V_m} - \left(\frac{\partial A^r}{\partial V} \right)_{T,m} \quad (5)$$

The association term is calculated using a model for the hydrogen bonding. A popular chemical model originates from the perturbation theory of SAFT (Statistical Associating Fluid Theory) where the association energy is expressed as Eq. (6) [1, p. 202]:

$$A^r_{Association} = \sum_i n_i \sum_{A_i}^{Association\ Sites} \left(\ln X_{A_i} - \frac{X_{A_i}}{2} + \frac{1}{2} \right) \quad (6)$$

In which n_i is the amount of molecule i and X_{A_i} is the fraction of the sites A on molecule i not bonded to other molecules, which can be calculated from Eq. (7):

$$X_{A_i} = \left(1 + \frac{1}{V_m} \sum_j x_j \sum_{B_j} X_{B_j} \Delta^{A_i B_j} \right)^{-1} \quad (7)$$

Where $\Delta^{A_i B_j}$ is the association strength between site A on molecule i and site B on molecule j .

Electrostatic Forces

A salt such as NaCl will fully dissociate into its ionic constituents Na^+ and Cl^- when placed in a highly polar solvent such as water. This introduces new intermolecular interactions; namely the energy of charging the ions and the long-range electrostatic forces between the ions using Coulombs law:

$$F(r) = \frac{1}{4\pi} \frac{1}{\epsilon_r \epsilon_0} \frac{q_i q_j}{r^2} \quad (8)$$

Where ϵ_0 is the vacuum permittivity, ϵ_r is the relative static permittivity of the medium, q_i is the elementary charge of molecule i , and r is the separation distance between the two charges.

The electrical potential E of a charged sphere with q_i charge in a medium can be calculated from Eq. (9):

$$E = \frac{1}{4\pi\epsilon_r \epsilon_0} \int_{\sigma_i}^{\infty} \frac{q_i}{r^2} dr = \frac{1}{4\pi\epsilon_r \epsilon_0} \frac{q_i}{\sigma_i} \quad (9)$$

The work of charging the ions gives a contribution to the Helmholtz energy as shown in Eq. (10):

$$A^E = -\frac{N_A}{8\pi\epsilon_r \epsilon_0} \sum_i \frac{n_i q_i^2}{\sigma_i} \quad (10)$$

Once ions are charged, the forces between ions must be accounted for using Eq. (8). There are two widely used models for that account for electrostatic interactions; the Debye-Hückel theory developed by Debye and Hückel in 1923 [2] from linearization of the Poisson equation, and the MSA (Mean Spherical Approximation) derived by Blum in 1975 [3] from statistical mechanics. While literature suggests that the Debye-Hückel theory can only describe electrostatic forces in dilute solutions, we showed that the original Debye-Hückel and the MSA theories actually provide a similar description of the Helmholtz energy of the electrostatic interactions even at high concentrations [4]. Since the Debye-Hückel theory provides an explicit expression for the Helmholtz

energy, the electrolyte CPA equation of state is based on Debye-Hückel shown in Eq. (9) [1, p. 470]:

$$A^r_{DH} = -\frac{1}{4\pi} \frac{k_B T}{N_A} \sum_i n_i q_i^2 \sum_i^N n_i q_i^2 \chi_i \quad (11)$$

Where k_B is the Boltzmann constant, N_A is Avogadro's constant, and χ_i is given by Eq. (12):

$$\chi_i = \frac{1}{d_i^3} \left[\ln(1 + \kappa d_i) - \kappa d_i + \frac{1}{2} (\kappa d_i)^2 \right] \quad (12)$$

Where d_i is the distance of closest approach of molecule i , and the inverse Debye length κ is calculated from Eq. (13):

$$\kappa^2 = \frac{1}{k_B T} \frac{1}{\epsilon_r \epsilon_0} \frac{1}{V} \sum_i^N n_i q_i^2 \quad (13)$$

The process of creating an EoS from models of the various intermolecular forces is illustrated in Figure 1:



Figure 1 The electrolyte CPA EoS consists of contributions from short-range forces (SRK), hydrogen-bonding (Wertheim), Ion charging (Born) and Coulombic interactions (Debye-Hückel).

Results and Discussions

The following sections present the results in various stages of the project until now.

The Importance of the Born Model

Inchekel et al. [5] showed that the Born term serves to balance out the Debye-Hückel term, but at the same time other groups [6,7] have obtained excellent results without including the Born term. The importance of the Born model was assessed by evaluating the contributions to the activity coefficient at infinite dilution and low pressure. The partition coefficients $K_i = y_i/x_i = \phi_i^l/\phi_i^v$ of ions in a vapor phase, a non-polar phase, and a polar phase was investigated by plotting the individual contributions to $\ln \phi_i$ in the different phases as shown in Figure 2:



Figure 2 Contributions to $\ln \phi_i = \left(\frac{\partial}{\partial n_i} \frac{A^r}{RT} \right) - \ln Z$

From the results shown in Figure 2 it can be concluded that the Born model is required to capture a high driving force for the ions towards the polar phase, and is therefore crucial for accurate description of the vapor-liquid-liquid phase equilibrium in the oil-gas-brine system.

Modeling Static Permittivity of Mixed Solvents

The static permittivity has been identified as the most important physical property for calculating the electrostatic interactions [4]. However, the previous work on electrolyte EoS have all used empirical correlations to determine the static permittivity. While the use of correlations may be acceptable for binary water-salt solutions in activity coefficient models, they must be used with care when applied to prediction of solubility in complex mixtures containing water, alcohols and even multiple salts. A new theoretical model has been derived to predict the static permittivity as a function of temperature, pressure, and composition.

Prediction of the Static Permittivity of Hydrogen-Bonding Fluid Mixtures with Salts

The zero-frequency limit of the relative permittivity of a material, also known as the static relative permittivity, or the dielectric constant, is a measure of the ratio of capacitance of a medium relative to the capacitance of vacuum [8]. The static permittivity has been used to correlate solubility and speciation of neutral compounds and pharmaceuticals [9] and to predict the scaling propensity of produced water containing gas hydrate inhibitors [10]. Online measurements of the permittivity are used for non-destructive sensing of moisture content of soils and food [11], and also serves as a valuable resource for assessment of water saturation in geological formations and determination of the hydrocarbon content in the presence of fresh formation water or water with unknown salinity[12].

The theoretical background for predicting the static permittivity of polar compounds from molecular properties relies on the famous papers by Onsager[13] and Kirkwood[14]. Fröhlich[15] introduced the Kirkwood g-factor accounting for the local structure in Onsager's relations and Hasted[11] extended the formulation to mixtures as shown in Eq. (14).

$$\frac{(2\epsilon_r + \epsilon_\infty)(\epsilon_r - \epsilon_\infty)}{\epsilon_r(\epsilon_\infty + 2)^2} = \frac{N_A}{9\epsilon_0 k_B T V} \sum_i n_i g_i \mu_{i,0}^2 \quad (14)$$

The infinite frequency permittivity ϵ_∞ is calculated from the Clausius-Mossotti [8] shown in Eq. (15):

$$\frac{\epsilon_\infty - 1}{\epsilon_\infty + 2} = \frac{1}{3\epsilon_0} \frac{N_A}{V} \sum_i n_i \alpha_{0,i} \quad (15)$$

The molecular polarizability α_0 and the vacuum dipole moments μ_0 may e.g. be obtained from the CRC Handbook of Chemistry and Physics. Based on the probability of association P_{ij} (calculated from the Wertheim association theory), the coordination number of molecule j around central molecule i , we may calculate the the Kirkwood g-factor used in Eq. (14) from the geometrical model shown in Eq. (16):

$$g_i = 1 + \sum_j \frac{z_j P_{ij} \cos \gamma_{ij} \mu_{j,0}}{P_i \cos \theta_{ij} + 1 \mu_{i,0}} \quad (16)$$

The relation between the dipole-dipole angle γ_{ij} , and the bonding angle in the following shell θ_{ij} is defined by simple trigonometric relationships. Using the new

model, we obtain good predictions with the static permittivity of pure compounds over wide temperature and pressure ranges, but the results may be improved by fitting θ_{ij} to ϵ_r at 25°C as shown in Figure 3. The results for binary mixtures of water-methanol and the ternary mixture of water-methanol-ethylene glycol are shown in Figure 4 and Figure 5, respectively.

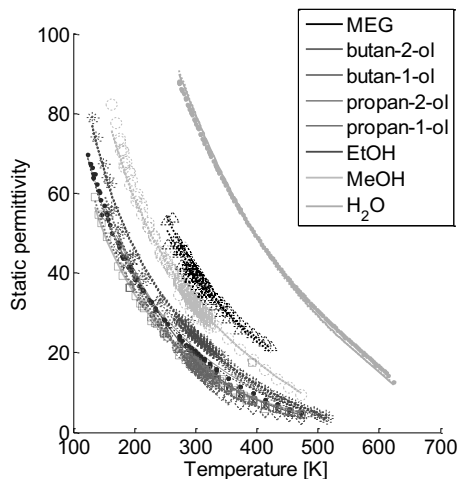


Figure 3 Experimental data for the static permittivity and the predictions from the new model. Data are from the Landolt-Börnstein database [16].

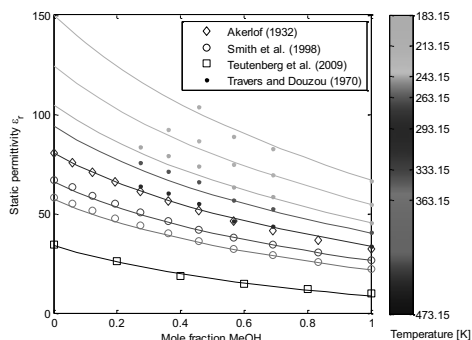


Figure 4 Static permittivity of mixtures containing water and methanol. The results at 473.15K were determined at a pressure of 100 bar. Data from [17-20]

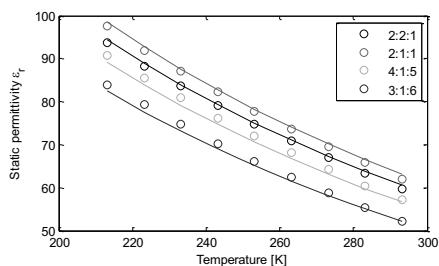


Figure 5 The predicted static permittivity of mixtures of water:ethylene glycol:methanol at different volume fractions measured at 20°C [21].

A modification of Eq. (14) to neglect water in the hydration shells of the ions enables prediction of ϵ_r in mixtures containing salts as shown in Figure 6.

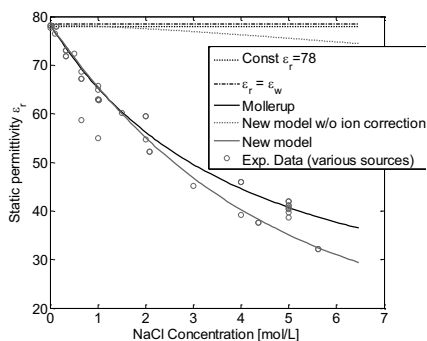


Figure 6 Predicted ϵ_r of water-salt mixtures using empirical models (black lines) and the new model with and without correction for ion hydration (assuming 8 H_2O in the shell of Na^+ and Cl^-). Data from [22]. See [4] and [23] for the empirical correlation by Mollerup.

Conclusions

The thermodynamic framework for an equation of state for electrolytes and associating molecules has been developed. It is based on the Debye-Hückel model and uses the Born model to ensure that ions move towards the polar phase. The key physical property for models of the electrostatic interactions is the static permittivity and a new predictive model has been developed as an alternative to the commonly used empirical correlations. The new model is capable of predicting the static permittivity of mixed solvents with salts over wide temperature and pressure ranges. Work continues in order to perform parameter estimation for a set of fully dissociated salts and apply the equation of state to calculation of salting out of gases and gas hydrate inhibition as a function of salt conc. and temperature.

Acknowledgement

This work is funded by the Department of Chemical and Biochemical Engineering and the CHIGP consortium (DONG Energy, Statoil, GASSCO, BP, Petrobras)

References

- G.M. Kontogeorgis, G.K. Folas, Thermodynamic Models for Industrial Applications-From Classical and Advanced Mixing Rules to Association Theories, Wiley, 2010
- P. Debye and E. Hückel, Physikalische Zeitschrift 24, 1923, 179-207
- L. Blum, Mol. Physics, 30 (5), 1975, 1529-1535
- B. Maribo-Mogensen, G. M. Kontogeorgis, K. Thomsen, Ind. Eng. Chem. Res., 51 (14), 2012, 5353-5363
- R. Inchekel, J.-C. de Hemptinne, W. Fürst, Fluid Phase Equilibria, 271 (1-2), 2008, 19-27
- C. Held, L. F. Cameretti, G. Sadowski, Fluid Phase Equilibria, 270 (1-2), 2008, 87-96
- A. Galindo, A. Gil-Villegas, G. Jackson, A. N. Burgess, J. Phys. Chem. B., 103 (46), 1999, 10272-10281
- B. K. P. Scaife, Principles of Dielectrics, Oxford Press, 1998
- J. V. Walter and J. Schott, Letters to Nature, 332 (14), 1988, 635-638
- E. Djarnali, A. T. Kan, M. B. Tomson, J. Phys. Chem. B, 2012, 116 (30)
- J. B. Hasted, Chapter 5 in Davies, Mansel, 1972, p. 121-162
- B. R. Spies, Surveys in Geophysics, 17 (4), 1996, p. 517-556
- L. Onsager: Electric Moments of Molecules in Liquids, J. Am. Chem. Soc., 1936, 58 (8), 1486-1493
- J. G. Kirkwood: 1939, J. Chem. Phys, 7, 911-920
- H. Fröhlich: 1948, Trans. Faraday Soc., 44, 238-243
- Landolt-Börnstein Database Volume IV/17, IV/6
- G. Akerlof, Journal of the American Chemical Society, 1932, vol. 54, p. 4125-4139
- F. Travers, P. Douzou, J. of Physical Chemistry, 1970, 74, 2243-2244
- R.L. Smith Jr. et al. Fluid Phase Equilibria 144 1998 315-322
- T. Teutenberg, S. Wiese, P. Wagner, J. Gmehling, J. of Chromatography (2009), 1216, 8480-8487
- F. Travers, P. Douzou, T. Pederson, I. C. Gunsalus, Biochemie (1975), 57, p. 43-48
- Y. Y. Akhadov, Dielectric Properties of Binary Solutions: A Data Handbook, Elsevier, 1980
- M. L. Michelsen, J. M. Mollerup, Thermodynamic Models: Fundamentals & Computational Aspects, Tie-Line Publications, Holte (Denmark), 2007

List of Publications

- B. Maribo-Mogensen, G. M. Kontogeorgis, K. Thomsen, Ind. Eng. Chem. Res., 51 (14), 2012, 5353-5363
- V. Darde, B. Maribo-Mogensen, WJM van Well, E. H. Stenby, K. Thomsen, Int. J. Greenhouse Gas Control, 10, 2012, 74-87
- X. Liang, B. Maribo-Mogensen, K. Thomsen, G. M. Kontogeorgis, Ind. Eng. Chem. Res, 51 (45), 2012, 14903-13914



Baoguang Ma

Phone: +45 4525 6809
E-mail: baom@kt.dtu.dk

Supervisors: Anne Ladegaard Skov
Søren Hvilsted

PhD Study

Started: Aug 2011
To be completed: Aug 2014

PDMS microsphere synthesis and theoretical explanation

Abstract

Crosslinked polydimethylsiloxanes (PDMS) are widely applied and studied in many applications due to their low surface energy and hydrophobic surfaces. In this work, crosslinked PDMS microspheres are prepared by mechanical stirring of PDMS elastomer and crosslinking agent in an aqueous surfactant solution and cured at 80°C. The mean diameter of the PDMS microspheres are measured by mastersizer and compared with the Hinze-Kolmogorov theory.

Introduction

Polydimethylsiloxanes (PDMS) have attracted much attention due to the excellent properties, such as water repellency and low surface energy.^{[1][2]} Though PDMS microspheres have been produced by microfluidics with monodisperse sizes^[3], it is not possible to produce PDMS microspheres in a large scale due to the limitation of microfluidic devices. The preparation of PDMS microspheres from emulsion and the resulting size distribution have not been investigated, as well as the theory behind the distribution has not been probed.

Specific Objectives

In this study, for the purpose of producing PDMS microspheres, mechanical stirring of PDMS elastomer and crosslinking agent is carried out to create the emulsions in the aqueous surfactant solution and then cured at high temperature. The mean diameter and size distribution of PDMS microspheres are compared with theoretical values predicted by Hinze-Kolmogorov theory.

Results and Discussion

In order to investigate the PDMS microsphere size distribution by means of diameter and the yield of PDMS microsphere by weight, eight samples are prepared by mixing Sylgard 184 at the ratio of 10:1 (elastomer to curing agent) by varying surfactant concentration. The viscosity of the samples changes significantly with the mixing ratio. Sample ID, surfactant concentration, mean diameter and microsphere yield are listed in Table 1. The Sample ID is related to the surfactant concentration, e.g. S3P1

refers to 3% (wt) sodium dodecyl sulfate (SDS) and 1% (wt) polyvinyl acetate (PVA) are used in the aqueous solution.

The diameter distribution of PDMS microspheres with various surfactant concentrations is illustrated in Figures 1.1 and 1.2. Figure 1.1 shows that the diameter of PDMS microspheres usually falls between 10 μ m and 1000 μ m, while the PDMS microspheres mean diameter is around 100 μ m for all samples. Also, the content of most probable distribution of PDMS microspheres, ranging from 95 μ m to 110 μ m, varies from 6% to 9.5% by using different concentration of surfactant. Moreover, by using PVA as surfactant, PDMS microspheres with more narrow distribution can be produced compared to that without PVA surfactant. However, without the presence of SDS, as listed in Table 1, no PDMS microspheres can be obtained, which indicates that the presence of SDS is the key factor in the technique. In order to investigate the effect of SDS concentration on the yield of PDMS microspheres solutions with 1%, 3% and 5% SDS are prepared. The PDMS microsphere yield percentage is calculated by using eq. (1.9) and the results are listed in Table 1. From Table 1 we can see that the yield of PDMS microspheres is around 70% for the experiments with PVA, while the yield is only around 50% without PVA.

Compared to the systems that use only SDS surfactant in the solution, the PDMS microspheres can be more stable by interacting with PVA due to the strong interaction between PVA and PDMS^[4,5]. Also, the amount of PDMS loss in the synthesis could be reduced, as we will discuss it in the optimization part. On one

hand, PVA can increase the interaction between water and PDMS as an assistant surfactant. Such interaction will increase the stability of PDMS droplets before they PDMS microspheres and producing a higher yield of PDMS microspheres; on the other hand, some may argue that PVA will be crosslinked to the PDMS network, and such crosslinking will increase the PDMS microsphere yield significantly. In fact the PDMS network will not be affected by the presence of PVA, since PVA is not crosslinkable without the presence of particular crosslinking agent, such as glutaraldehyde.^[4]

Table 1: PDMS microspheres mean size and yield from varying surfactant concentrations

Sample ID	PVA (%)	SDS (%)	Mean size (μm)	Microsphere yield (wt%)	Surface tension (mN/m)
S0P0	0	0	/	0	72.9
S1P0	0	1	120	41.6	37.3
S3P0	0	3	104	47.4	32.3
S5P0	0	5	102	54.4	32.0
S0P1	1	0	/	0	52.4
S1P1	1	1	105	25.3	37.9
S3P1	1	3	107	69.4	36.2
S5P1	1	5	89	71.3	36.1

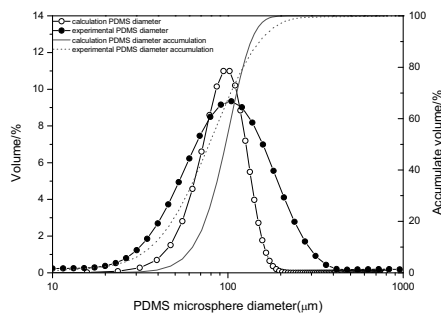


Figure 1: Comparison between simulation and experiment of PDMS microsphere diameter (Sample S3P1). Dots represent the size distribution while lines stand for volume accumulation

From the theoretical distribution of PDMS microspheres in Fig 1[6], we can see that the most probable distribution is around 100μm with a volume fraction of 11% according to Hinze-Kolmogorov theory. Meanwhile, hardly any PDMS microspheres are larger than 200μm or smaller than 30μm, most of the PDMS microspheres fall between 30μm and 200μm. Also, the logarithmic asymmetric theoretical distribution indicates a small possibility of primary particles to form a large

cluster larger than 200μm, but moderate possibility to form a small cluster smaller than 30μm.

For the experimental distribution of PDMS microspheres, it can be observed that the most probable distribution, ranging from 95μm to 110μm, has volume fraction of 9.5%. The diameter of PDMS microspheres falls between 30μm and 200μm, indicating a broad distribution of PDMS microspheres in the experiment. However, the symmetric theoretical distribution indicates that the same possibility of primary particles to form a large cluster or a small cluster.

For the case shown in Fig 1, the theoretical volume fraction is 11% for the most probable distribution, compared to that of experimental value is 9.5%, indicating that the theory fits the experimental data quite well. The deviation in volume fraction is only 13% for the most probable distribution, ranging from 95μm to 110μm. Such deviation reveals that the stability of PDMS mixture has not been considered to the theory.

Conclusions

Compared to other turbulent systems^[6], the agreement between experimental and theoretical value is satisfactory. The deviations of most of physically turbulent systems are around 50%, sometimes larger than 100%. For our system, the deviation is only 13% for the most probable distribution. Only 10% of total volume fraction below 30μm and above 200μm can not be predicted by theory, when theoretical accumulative volume fraction is compared with that of experimental.

Though the effect of chemical reaction has been overwhelmed by mechanical stirring in the turbulent system, it becomes the dominating factor in the 2h curing in an oven of 80°C. Unlike the physical emulsions in the turbulent system, the PDMS microspheres could be filtered and subjected to other application after the curing procedure.

References

1. Turner, J. S. & Cheng, Y.-L. *Macromolecules* 33 (2000) 3714–3718.
2. Lim, K. T. & Webber, S. E. *Macromolecules* 32 (1999) 2811–2815
3. Peng, S. *et al.* Magnetically responsive elastic microspheres. *Applied Physics Letters* 92 (2008) 012108 .
4. Shin, M.-S. *et al.* Swollen behavior of crosslinked network hydrogels based on poly(vinyl alcohol) and polydimethylsiloxane. *Journal of Applied Polymer Science* 85, (2002) 957–964
5. Farid, O. Investigating membrane selectivity based on polymer swelling. (2011) at <<http://etheses.nottingham.ac.uk/1774/>>
6. Hinze, J. Fundamentals of the hydrodynamic mechanism of splitting in dispersion processes. *AICHE Journal* 1 (1955)289–295.



Mads Ville Markussen

Phone: +45 2132 6535
E-mail: mvil@kt.dtu.dk

Supervisors: Hanne Østergård

PhD Study

Started: January 2010
To be completed: February 2013

Systemic Approach to Sustainability Assessment of Food and Bioenergy Production in a Societal Context

Abstract

Modern agricultural systems are highly depending on fossil fuels and other non-renewable resources that are foreseen to come in short supply in the future. The aim of this project is to assess the sustainability of agricultural systems from a systemic perspective and to suggest principles for future development. In four case studies different methodologies are applied to systems of different scales. A main finding of the project is that contemporary sustainability assessment tools are poorly adapted at taking future socio-economic conditions into account.

Introduction

Food is among the most basic needs for any society and having sufficient food is a prerequisite for maintaining social stability. Throughout the 20th century industrialisation of agriculture made it possible to increase food production in roughly the same pace as demand which helped the human population to increase by more than 400% in one century. Key elements of the industrialisation of agriculture were the access to cheap and plentiful oil and synthetic and mineral fertilizers. However, the sources of these resources are limited in stock and their production is expected to go into decline in the near future [1, 2]. It is in this perspective that this project was undertaken.

Specific Objectives

The objective is to develop new perspectives on how to assess the sustainability of food and bioenergy systems. This is obtained by using different sustainability assessment tools on four different food system cases. The specific objectives are:

(1) To assess the Food energy returned on fossil energy invested (Food-EROI) of the Danish food production system considering both agricultural production, transportation of agricultural inputs and outputs and the processing of food. (2) To assess the potentials for average Danish organic dairy farms in becoming self-sufficient with liquid fuels and electricity and supply a surplus of energy to the surrounding economy. (3) To assess and compare resource consumption and environmental impacts of

two English organic vegetable production and supply systems, where one of the systems is a small scale very low input farm with direct marketing of its produce to local consumers, and the other system is a large scale vegetable producer that supplies its produce through the supermarket system. (4) To assess and compare resource consumption and environmental impacts of two low input wheat and bread production systems in France. Objective (3) and (4) are part of the EU FP7 project SOLIBAM.

Results and Discussion

Food energy returned on fossil energy invested (Food-EROI) is suggested as a useful indicator for assessing the dependency of a food system to fossil fuels. Fossil fuel and in particular oil is the most important resource for powering the global industrialised economy, and at the same time their global production are foreseen to go into a terminal decline during the next decades. This indicator is applied to the Danish food production system including production, processing and distribution. The results show that more than 330 PJ of fossil energy is used in the production of approximately 60 PJ of food energy. In other words for each J of fossil fuel used, 0.18 J of food energy is produced, transported and processed. This result underlines the enormous role that fossil fuels plays in producing our food, and consequently that our food production is highly vulnerable to foreseen future constraints on fossil energy supply.

Biofuels are by many thought to be a desirable substitute for fossil fuels. In a theoretical model of energy use, conversion and production the potentials for Danish organic dairy farms to become self-sufficient with energy and supply excess energy to the society is analysed. The results show that based on current production practices approximately 20 % of the cultivated areas should be used to bioenergy crops to achieve farm gate self-sufficiency with liquid fuels and electricity. This raises the concern that biofuels may in fact not be able to supply significant amounts of net-energy to the society taking into account that one fifth of the land is needed just to supply enough energy to power agriculture's own production. This is not taking into account the energy needed to process and distribute the food, which suggest that if significant amount of surplus energy should also be produced to the economy, then even more land should be dedicated to bioenergy crops.

As for the third and fourth specific objective work is still in progress and results has not been finalized. The study combines two approaches to sustainability assessment; Life Cycle Assessment (LCA) and Emergy assessment. The study is based on data collected on two farms in England and two farms in France regarding the growing systems, production practises, resource use and labour use. LCA is a widely used sustainability assessment methodology that is especially adapted to map emission/pollution in a life cycle perspective. Emergy assessment is a donor side perspective that studies systems based on their consumption of resources coming from both human and natural systems and where all inputs are quantified based on the amount solar equivalent joules (seJ) that has ultimately been used to provide the resource [3].

Conclusions

A key finding in this Ph.D. project is that contemporary methods of sustainability assessment, including those applied in the project, are poorly suited at taking future development of socioeconomic conditions into account.

From a complex systems macro perspective a future decline in the use of fossil fuels will necessarily mean large scale adaptations on all levels of society [4], bearing in mind that fossil fuels is the paramount dominating energy source for the global economy. A reduced energy throughput would lead to a contraction of energy consuming activities (i.e. the industrial economy), and fundamentally change socio-economic conditions. The results from the individual studies in this project support this conception: The systems studied in the project would all be fundamentally compromised by constrained access to fossil fuels.

In general the sustainability assessment tools are designed and used to assess the sustainability and resource consumption under current socio-economic conditions and there is an implicit assumption that future conditions will be similar to current conditions or at least develop regularly according to a business as

usual trajectory. This constitutes a paradox since a main goal of sustainability assessments is to identify or suggest systems that are sustainable; i.e. systems that can be sustained under future conditions.

References

- [1] S. Sorrell, J. Speirs, R. Bentley, A. Brandt and R. Miller, (2010). Global oil depletion: A review of the evidence. *Energy Policy*, 38:5290-5295.
- [2] D. Cordell, J. Drangert and S. White, (2009) The story of phosphorus: Global food security and food for thought. *Global Environmental Change*, 19:292-305.
- [3] H.T. Odum, *Environmental accounting - Emergy and environmental decision making*. John Wiley & Sons, Inc, New York, 1996
- [4] H.T. Odum and E.C. Odum (2006). The prosperous way down. *Energy*, 31:21-32.

List of publications

M. Markussen, H. Østergård. Can agriculture again be a net-energy producer?. In: *International Society for Ecological Economics (Eds.), Advancing Sustainability in a Time of Crisis, ISEE CONFERENCE 2010 (2010)*

H. Østergård, M. Markussen. Viability of biofuels as influenced by agricultural production system. In J. Ramos-Martín, M. Giampietro, S. Ulgiati, S. G. F. Bukkens (Eds.), *Can we break the addiction to fossil energy? Proceedings of the 7th Biennial International Workshop Advances in Energy Studies*, Barcelona, Spain, 19.21 October 2010

M. Markussen, H. Østergård. Sustainability assessment of farming in perspective of diminishing global emerge flows – A case study. In: *Center for Environmental Policy Department of Environmental Engineering Sciences University of Florida (Eds.), Seventh BIENNIAL EMERGY EVALUATION and RESEARCH CONFERENCE*. January 12 through January 14, 2012, Gainesville, Florida

M. Markussen, M. Kulak, T. Nemecek, H. Østergård. Assessing sustainability of a low-input single-farm vegetable box-scheme using emergy and LCA methodology. In *SETAC and NOR LCA (Eds.), SETAC*



Michele Mattei

Phone: +45 4525 2959
E-mail: micu@kt.dtu.dk

Supervisors: Rafiqul Gani
Georgios Kontogeorgis

PhD Study
Started: August 2011
To be completed: July 2014

A Systematic Methodology for Design of Emulsion-Based Chemical Products

Abstract

The consumer oriented chemical based products are used every day by millions of people. They are structured products constituted of numerous chemicals, and many of them are emulsions where active ingredients, solvents, surfactants and additives are mixed together to determine the desired target properties. These products are still mainly designed through trial-and-error based experimental techniques, therefore a systematic approach for design of these products can significantly reduce both time and cost connected to the product development by doing only the necessary experiments. The methodology consists of a model-based framework, involving seven hierarchical steps, with associated models, tools, structured databases and algorithms. Two conceptual case-studies have been developed to highlight the application of the methodology.

Introduction

The chemical industry is changing, going beyond commodity chemicals to higher value added products [1]. These structured products are still mainly designed on an experimental base, with a consequent large amount of time and money needed. A systematic methodology for design of these products is then considered a big improvement since the whole design procedure speeds up, saving time and money, and the optimum formulation can be identified, since a broad spectrum of alternatives has been virtually investigated. Such a procedure has been successfully developed recently with regards to liquid formulated products [2]. Many of the consumer oriented products, however, especially household and personal care products, are emulsion and therefore a different methodology is needed for their design. Moreover, data regarding several important both pure component and mixture properties are not available in the open literature and/or appropriate models for their prediction are not readily available. Consequently, dedicated pure component and mixture property models are needed.

Specific Objectives

The objective of this project is to develop a systematic methodology for the design of emulsion-based chemical products, with associated tools, models, structured databases and algorithms, to be afterwards implemented into a computer-aided framework to allow virtual

formulation design and verification of emulsified products. In this way, the design and development of these products can be made less costly and introduced to the market earlier, while using the experimental resources only for verification of the product.

The methodology consists of seven hierarchical steps: starting with the identification of the consumer needs and their translation into appropriate target properties; then building up the formulation by adding, one-by-one, the different classes of chemicals needed for specific functions: from the active ingredients (defined as the ingredients satisfying the main needs of the product), passing through the solvents, the emulsifiers, until the additives; and finally determining the composition of the formulated product, as illustrated in Figure 1.

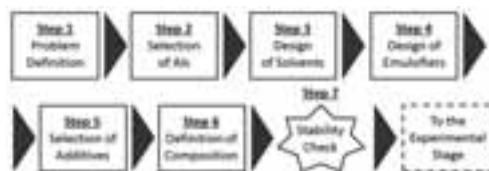


Figure 1: Work-flow of the methodology for design of emulsion-based chemical products.

The selection of the active ingredients and of the additives is done through rule-based selection criteria, centered on structured databases, where the relevant

properties (e.g. safety- or toxicity-related), if not available, are predicted through dedicated pure component property models. The design of the solvents and of the emulsifiers, driven by selection criteria based on the functional properties of the chemical as well as consideration of effectiveness, safety, toxicity and cost, is done through a data-model based computer aided molecular design technique. Once all the most advantageous ingredients have been chosen, the recipe candidates are identified through a knowledge-based mixture design method, where economic considerations are included together with appropriate boundaries related to solubility, stability, toxicity and safety issues. A special database of chemicals, classified according to their function and associated properties has been developed. Also, a model library consisting of pure component and mixture property models have been developed so that the needed functional properties can be reliably predicted when their data cannot be found in the database. Table 1 gives an overview of the models needed for the target properties defined at Step 1 of the methodology in relation to the two case-studies developed so far: a sunscreen lotion [4] and a hand wash [5].

Table 1: Performance criteria considered in this work and translation into target properties and symbols

Performance Criteria	Target Property	Symbol
Cost	Cost	C
Flammability	Open cup flash point	T_f
Foam-ability	Critical micelle concentration, surface tension	CMC, σ
Solubility	Hansen and Hildebrand solubility parameters	$\delta_D, \delta_P, \delta_H, \delta_T$
	Hydrophilic-lipophilic balance (surfactants only)	HLB
Skin care	Hansen and Hildebrand solubility parameters	$\delta_D, \delta_P, \delta_H, \delta_T$
Spray-ability	Density, kinematic viscosity	ρ, ν
Spread-ability	Density, kinematic viscosity	ρ, ν
Stability	Critical micelle conc., cloud point (non-ionic surf.)	CMC, T_C
	Critical micelle conc., Krafft temperature (ionic surf.)	CMC, T_K
	Toxicity	Toxicity parameter

One of the main issues to face when applying this methodology, though, is the availability of the needed properties. Experimental data are often scarce and therefore the development of dedicated models for reliable prediction of pure component and mixture properties is necessary [3]. Table 2 and 3 give a detailed summary of the pure component and mixture property models, respectively, used in this project, where the highlighted rows indicate the newly developed models in this project.

Table 2: Pure component properties considered in this project and models employed for their estimation. Highlighted in grey, the property models developed for this project.

Pure Component Property	Model Used
T_C	M&G GC ⁺ method - This work
C	Correlation
CMC	M&G GC ⁺ method - This work
ρ	Modified Rackett EoS
μ	M&G GC ⁺ method
$\delta_D, \delta_P, \delta_H$	M&G GC ⁺ method
δ_T	M&G GC ⁺ method
HLB	Definition
ν	Definition
T_K	QSPR method
T_f	C&G GC method
σ	M&G GC ⁺ method
LC_{50}	M&G GC ⁺ method

Table 3: Mixture properties considered in this project and models employed for their estimation. Highlighted in grey, the property models developed for this project.

Mixture Property	Model used
C	Linear mixing rule
ρ	Linear mixing rule on the molar volume
μ	GC(UNIFAC)-based method
	Dedicated model (emulsions only)
$\delta_D, \delta_P, \delta_H$	Linear mixing rule
δ_T	Linear mixing rule
T_f	GC(UNIFAC)-based method
σ	GC(UNIFAC)-based method
	GC-based method (emulsions only) - This work
T_f	Linear mixing rule

Results and discussion

One of the main objectives of this project, as already pointed out, concerns the property modeling. As from Table 2 and 3, two pure component properties and one mixture property have been modeled in this work and all the models are group-contribution based methods. In particular, the Marrero&Gani GC⁺ method [6] has been applied. In this method, like other M&G methods, a physio-chemical property is predicted considering that each compound can be described by groups at three levels: first order-groups, second-order groups and third-order groups. The (first) basic level uses contributions of first-order groups that describe a wide variety of organic compounds. The higher (second) level provides additional structural information, not provided by the first-order groups and thus corrects the estimates at the first level. A further correction

(adjustment) to the predictions is provided through the third-level, where the contributions of parts of the structure of complex molecules are calculated.

The M&G estimation model has the form of the following equation:

$$F(\xi) = \sum_i^{NG1} N_i C_i + y \sum_j^{NG2} M_j D_j + h \sum_k^{NG3} O_k E_k$$

Where $F(\xi)$ is a function of the estimated property ξ ; C_i is the contribution of the first-order group of type i ; N_i is the occurrence of the first-order group i ; D_j is the contribution of the second-order group of type j ; M_j is the occurrence of the second-order group j ; E_k is the contribution of the third-order group of type k ; O_k is the occurrence of the third-order group k ; y , h are binary variables, $NG1$, $NG2$ and $NG3$ are the number of first-, second- and third-order groups, respectively.

In the first estimation level, the values of y and h are assigned to zero since, in this level, only first-order groups are involved. In the second level, constants y and h are assigned unity and zero values respectively, because only first- and second-order groups are involved. Finally in the third level, since all groups orders are involved, both constants are equal to one.

The abovementioned approach has been applied for the modeling of three properties: critical micelle concentration and cloud point as pure component properties of surfactants and surface tension of the mixture between water and surfactant. The M&G GC⁺ approach, strictly, is applicable only to pure component properties, but in this particular case, even though all these properties are peculiar of the mixture between water and surfactants, estimating them at constant temperature (and pressure) and since the second component is fixed as water, it is possible to model these properties as pure component properties of the surfactant. In the following Figure 2, 3 and 4 the results of the modeling are shown.

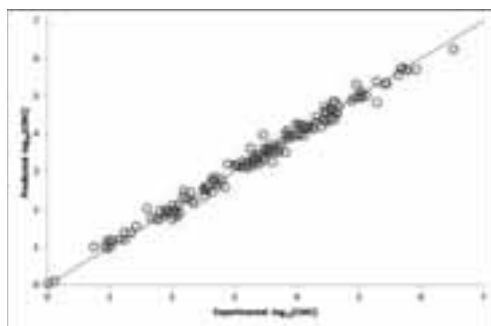


Figure 2: Predicted critical micelle concentration versus experimental data for all components used for the parameter regression, using the GC-based method

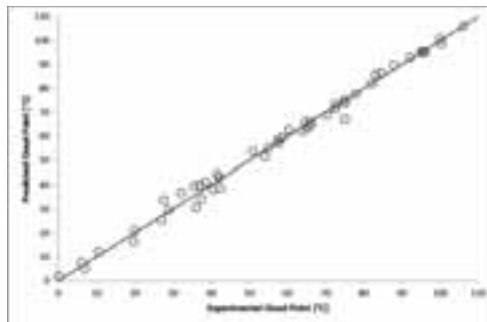


Figure 3: Predicted cloud point versus experimental data for all components used for the parameter regression, using the GC-based method

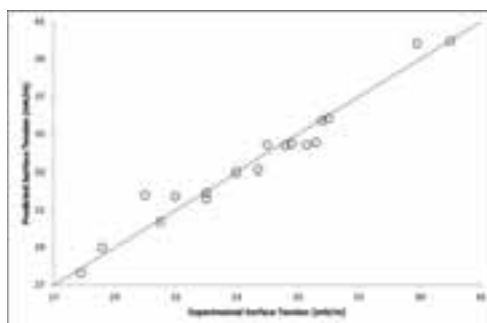


Figure 4: Predicted surface tension versus experimental data for all components used for the parameter regression, using the GC-based method

On the basis of the property models developed in this project and others considered for the different target properties, dedicated structured databases for all the categories of ingredients and appropriate algorithms, it has been possible to test the methodology with two conceptual case-studies dealing with a UV sunscreen and a hand wash. The results are listed in Table 4 and 5.

Table 4: Candidate overall composition for and emulsified UV sunscreen

Category	Ingredient	Weight %
Active Ingredients	Avobenzone	0.99%
	Octyl Salicylate	1.22%
	Zinc Oxide	8.56%
Solvents	Butyl Acetate	32.4%
	Water	54.9%
Emulsifier	Octyl Esaethylene Oxide	0.09%
	α -Tocopherol (antioxidant)	0.34%
Additives	Heptylparaben (preservative)	0.59%
	Leavo-Menthol (aroma)	0.91%

Table 5: Candidate overall composition for an emulsified hand wash

Category	Ingredient	Mole %
Active Ingredients	Sodium Laureth Sulfate	7%
	Octyl Ethaethylene Oxide	7%
Solvents	Jojoba Oil	27%
	Water	49%
Emulsifier	Cocamidopropyl Betaine	3.5%
	Rose Oil (aroma)	2.5%
Additives	CI 17200 (pigment)	1.5%
	Triclosan (anti-microbial agent)	1.5%
	Polyquaternium 7 (softener)	0.5%
	Sodium Benzoate (preservative)	0.5%

Conclusions and Future Work

A model-based framework for emulsion-based chemical product design has been developed and has been applied to two case-studies: the design of an emulsified UV sunscreen and of an emulsified hand wash. The application range of the methodology, however, is broad: once the formulation-structure and the structure-property relationships are available and the consumer assessments are given by the knowledge-base, any emulsion-based product can be designed through it. Uncertainties in the prediction of the composition of the formulated product, however, are likely, and therefore a final stage of verification by experiments is necessary. The work-flow methodology with associated models, tools, structured databases and algorithms have been developed and they are being implemented into a computer-aided framework for emulsion-bases formulation design.

Future work will be the development of new pure component property models, particularly relative to ionic surfactants, as well as of new mixture property models dedicated for emulsions. Moreover, phase diagram of both binary mixture of water and surfactants (to have a better understanding of the geometrical shape of the emulsion, driving several physio-chemical properties of it) and of ternary mixtures of oil, water and surfactants (to have a better understanding of the miscibility gaps and therefore of possible boundaries on the composition) are needed. The description of them through UNIFAC, if possible, or through modern associative equations of state (as PC-SAFT, CPA, *etc.*) is considered a crucial step in the development of a complete methodology for the design of emulsion-based products. More case-studies are planned, some of which including also the second experimental-based stage for verification and/or further refinement. Finally, the

whole methodology will be highlighted as implemented in the software “The Virtual Process-Product Design Laboratory” (Virtual PPD Lab) as a new feature, allowing users to perform virtual formulation design and verification for emulsified products.

References

- [1] E.L. Cussler and G.D. Moggridge, *Chemical Product Design*, Cambridge University Press, 2011
- [2] E. Conte, R. Gani and K.M. Ng, 2011, *AIChE Journal* 57: 2431
- [3] G.M. Kontogeorgis and R. Gani, *Computer Aided Property Estimation for Process and Product Design*, Elsevier, 2004
- [4] M. Mattei, G.M. Kontogeorgis and R.Gani, *Proceedings of the 11th Symposium of Process System Engineering*
- [5] M. Mattei, M.Hill, G.M. Kontogeorgis and R.Gani, *Proceedings of the 2012 AIChE Fall Annual Meeting*
- [6] J. Marrero and R. Gani, 2001, *Fluid Phase Equilibria*, 183-184: 183.

**Kresten Troelstrup Meisler**

Phone: +45 4525 2912
E-mail: kretm@kt.dtu.dk

Supervisors: Rafiqul Gani
Krist V. Gernaey
Nicolas von Solms

PhD Study
Started: March 2011
To be completed: September 2014

Multi-Dimensional Population Balance Models of Crystallization Processes

Abstract

The kinetics in crystallization operations are modeled and used in population balance models. Such models allow obtaining a better insight into the mechanisms of the crystallization and can be useful for process analysis, operational policy design and optimization of crystallization operations. A systematic approach for the use of collected data is suggested in order to analyze the crystallization processes.

Introduction

Crystallization is an efficient separation process for separation of compounds, which are solid in their pure form at the given separation conditions [1]. These operations involve multiple phenomena and understanding of these phenomena and interactions have gained interest as it is recognized that this affects several properties of the final product. The polymorph, the size distribution and derivative properties of these (such as filterability) are strongly influenced or even governed by the kinetics of the chemical system.

Modeling these phenomena and their interaction through a population balance approach could help the understanding and hence the optimization and design of crystallization operations. In order to accommodate the wide range of crystallization systems being in operation, a generic procedure is established for the systematic development of models for use in design, analysis and simulation of crystallization operations.

Specific Objectives

The project aims at developing models for the description of crystallization operations including the necessary phenomena in order to describe a process completely. A multi-dimensional population balance approach is used: The crystals are described with variations in the growth rate for different directions, and by also considering nucleation, breakage and agglomeration the description of the kinetic phenomena is concluded. The kinetics are used for the constitutive equations in the population balance model and, in combination with mass and energy balances, the crystal size distribution from the operation can be calculated.

With this result the simulation and practical operations can be compared and the models and experiments can be evaluated. In case of a mismatch between the experimental result and the model result it is possible to re-evaluate the parameters for the model.

Results and Discussion

A framework has been established for handling multiple crystallization-oriented scenarios [2]. The framework combines the advantages of data-based and model-based analysis in a general approach. The approach is illustrated for a data-based problem in Figure 1. The approach allows multiple crystallization based scenarios to be handled such as parameter estimation and model generation for crystallizers, operational policy analysis and data translation of data types in order to extract information of crystal size distribution.

In order to establish the kinetics of the crystallization operations, kinetic data are necessary. For industrial operations different technologies are used in order to monitor crystallization operations. The use of the data from these sources allows a better understanding of the process; however, these data must be translated in order to give the necessary information. This data-translation can be non-trivial, which for example is the case for the translation of Focused Beam Reflectance Measurements (FBRM) from which a chord length distribution is obtained. This chord length distribution is not directly transferable to a particle size distribution and several challenges have been identified for the translation of data from FBRM measurements. Guidelines for experiments from which the necessary data can be

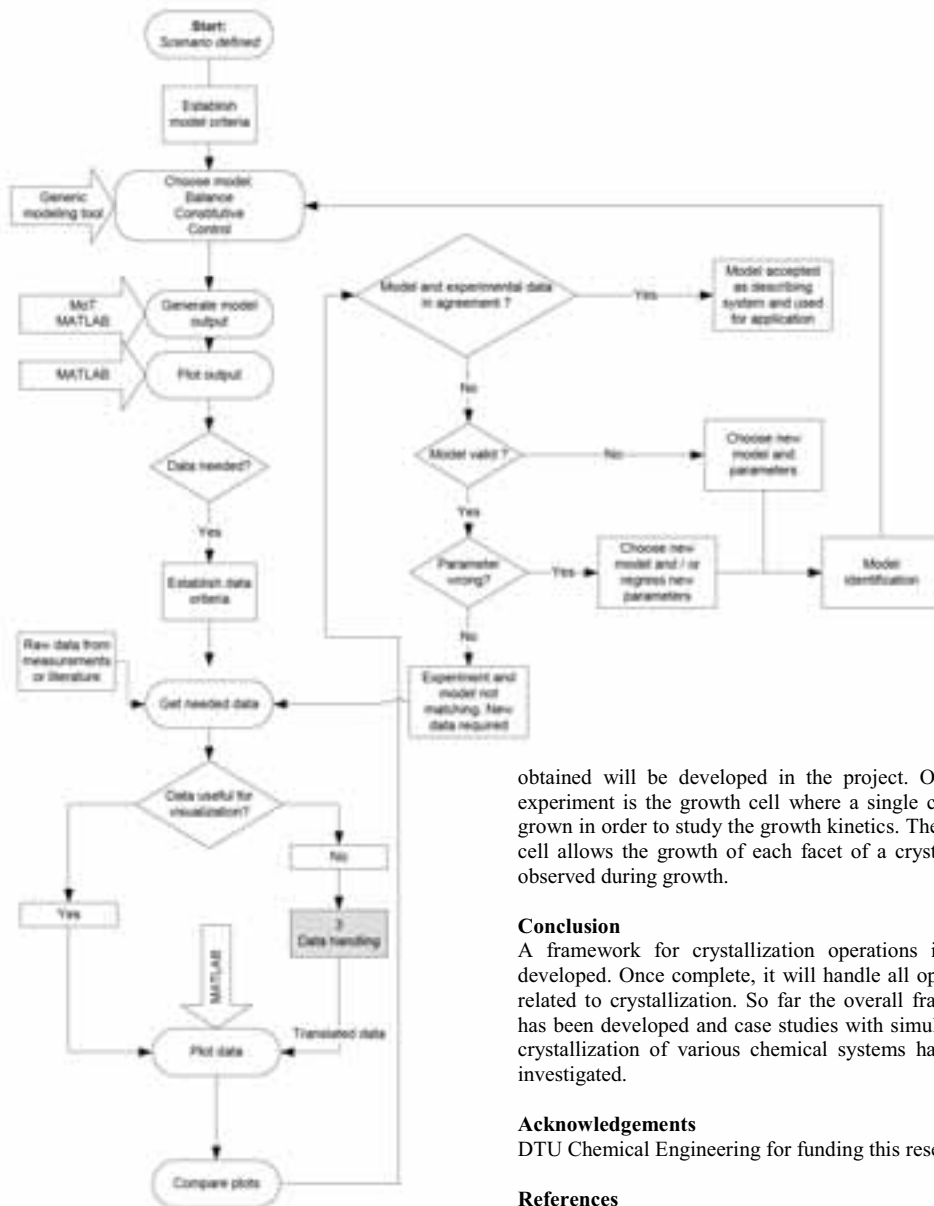


Figure 1: The proposed framework for crystallizer modeling

obtained will be developed in the project. One such experiment is the growth cell where a single crystal is grown in order to study the growth kinetics. The growth cell allows the growth of each facet of a crystal to be observed during growth.

Conclusion

A framework for crystallization operations is being developed. Once complete, it will handle all operations related to crystallization. So far the overall framework has been developed and case studies with simulation of crystallization of various chemical systems have been investigated.

Acknowledgements

DTU Chemical Engineering for funding this research

References

- [1]: Samad, N. A. F. A.; R. Singh; G. Sin; K. V. Gernaey and R. Gani: **A generic multi-dimensional model-based system for batch cooling crystallization processes**, Computers and Chemical Engineering 35, 2011 p. 828-843
- [2]: Meisler, K. T. ; N. A. F. A Samad; K. V. Gernaey; N. von Solms and R. Gani: **Generic Model and Data Based Framework for Analysis and Development of Crystallization Processes**, Conference contribution, AIChE Annual Meeting, 2011



Aleksandar Mitic

Phone: +45 4525 2949
E-mail: asmi@kt.dtu.dk

Supervisors: Krist V. Gernaey
Kim Dam-Johansen

PhD Study
Started: November 2010
To be completed: November 2013

Operational Aspects of Continuous Pharmaceutical Production

Abstract

Establishment of continuous production is a great challenge in modern pharmaceutical industry. Traditional batch and semi-batch processes have plenty of disadvantages which can be avoided by applying eco-friendly and economical continuous manufacturing. Furthermore, process analytical technology (PAT) can reach its full benefits in this type of production system. The main aim of this PhD thesis is to accelerate slow chemical reactions in the production of zuclopenthixol, a product of H. Lundbeck A/S, as well as to complete continuous manufacturing and establish in-line process monitoring and control. Production of zuclopenthixol involves several steps: Grignard alkylation, hydrolysis, liquid-liquid separation, dehydration and hydroamination. Applications of mini- and micro-sized devices, as well as microwave assisted organic synthesis (MAOS) have been tested.

Introduction

Organic synthesis is essential for the production of an important class of pharmaceuticals. Implementation of organic chemistry on an industrial scale is a great challenge. To date, pharmaceutical manufacturing is mainly based on batch and semi-batch processes. However, besides their flexibility and versatility there are many disadvantages compared to continuous production, such as the risk of occurrence of hot-spots, non-ideal mixing, undesirable temperature gradients, difficulties in implementing PAT applications, and so on.

The main aim of this PhD project is to complete continuous manufacturing of zuclopenthixol, with the main focus on acceleration of slow chemical reactions. Figure 1 depicts the current process flow sheet for production of this API.



Figure 1: Zuclopenthixol production flow sheet

Different process solutions are tested with the main focus on micro- and mini-sized devices. For instance, Grignard alkylation is a very fast reaction which occurs

almost in the mixing zone [1]. Application of a mini-sized tubular reactor by forcing laminar flow has proven to be a great choice. This reaction is followed by immediate hydrolysis of the obtained intermediate product. After hydrolysis, water and water soluble by-products should be separated before performing the dehydration reaction. To this purpose, a membrane PTFE micro-separator is used which shows a very high efficiency in practice [2, 3]. Furthermore, N714 Allylcarbinol is dehydrated in N746 Butadiene which is a starting reactant for a very slow hydroamination reaction. The dehydration reaction is carried out in a tubular reactor under increased pressure (5 bars) which allows higher temperature of the reaction media and a higher reaction rate at the same time. The last step of the process, the hydroamination of N746 Butadiene, shows quite a good efficiency under microwave irradiation.

Specific Objectives

In order to complete continuous production of zuclopenthixol, it is necessary to increase the reaction rate of the last hydroamination step. Selectivity of the last step should be improved, as well, because just the cis-isomer is desired.

In general, acceleration of slow reactions in organic synthesis can be performed by applying different methods. Pressure increase has already been demonstrated as a good choice in the dehydration reaction. Sometimes, applications of homogeneous catalysis are defined as good manufacturing practices,

but difficulties in finding suitable purification methods of final products are a major drawback of this approach. Furthermore, combination of heterogeneous catalysis and pressure increase is a good approach for very slow reactions, but possible deactivation of chemical catalysts due to a long-time exposure at very high temperatures actually forms a limitation to this approach.

In the last decade of the 20th century a new approach has been introduced, the so-called microwave assisted organic synthesis (MAOS). This is a modern and a very efficient way for speeding up of slow chemical reactions. The main advantages of this approach are faster heating caused by electromagnetic radiation and the specific temperature profile inside reactors.

Results and Discussions

An increase of the overall yield has its bottleneck in the dehydration step. Applications of hydrochloric acid result in equal amounts of cis- and trans-N746 Butadiene. A more sophisticated approach was established by using thionyl-chloride which has an acidic role, then triethylamine, as a stereo-selective agent, and dichloromethane as the most suitable solvent. A very low temperature (-78°C) is applied. As a result, 70% of the desired cis isomer is obtained.

Furthermore, acceleration of the slow hydroamination reaction might be performed in several ways. The first experimental runs were done in batch mode by using toluene as a solvent. The results showed a very high conversion of N714 Butadiene at 90°C in 24 hours (90%). Further temperature increase caused degradation of the clopenthixol isomers whereas longer reaction times at lower temperatures caused polymerization of N746 Butadiene. Hence, the main idea was to find a sufficiently low reaction time with optimal high reaction temperature.

Small scale trials in microwave ovens have been done. For this purpose a Biotage Initiator was used. All the samples were up to 1 ml and with excess of 1-(2-hydroxyethyl)piperazine (HEP), a compound which shows a good absorption of microwave irradiation. Different temperatures were tested, from 80°C to 250°C, as well as different reaction times: from 20 min to 5 hours. All the experiments were carried out in 2 different solvents, THF and toluene. The main aim of the experimental runs was to find the best conditions for performing the reaction, and thereby just qualitative analyses were done. The obtained results showed almost total conversion of N746 Butadiene at 120°C during 5 hours, as depicted in Figure 2. The API degradation increases rapidly with further temperature increase. More precise analyses will be done in the future.

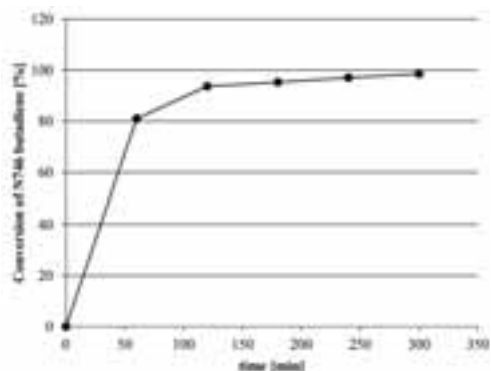


Figure 2: Optimal reaction conditions for N714 Butadiene hydroamination in clopenthixol by using microwave assisted organic synthesis

Conclusions and future work

Applications of micro reactor technology, as well as, microwave assisted organic synthesis, have shown great advantages in the zuclopenthixol production. The Grignard alkylation and the dehydration reaction are carried out in mini-scale tubular reactors with increased yields and lower reaction times. Furthermore, a micro-scale liquid-liquid separator with PTFE membrane showed great results in practice, as well. Microwave assisted organic synthesis (MAOS) and its “stop and flow” continuous regime implied great advantages in the hydroamination reaction. Nevertheless, further investigations should be done.

After establishing completely continuous production of zuclopenthixol, on- and in-line monitoring and control will be applied. For this purpose spectroscopic methods (NIR) and MATLAB[®] Simulink will be used. In addition, further options for process simplification might be tested. Indications that a Wittig reaction could be used in order to avoid the Grignard alkylation, hydrolysis and dehydration [4], sound very promising and experiments for this reaction will be done in the near future as well.

References

1. A. E. Cervera-Padrell, J. P. Nielsen, M. J. Pedersen, K. M. Christensen, A. R. Mortensen, T. Skovby, K. D. Johansen, S. Kiil, K. V. Gernaey, *Org. Process Res. Dev.* 16 (2012) 901-914
2. J. G. Kralj, H. R. Sahoo, K. F. Jensen, *Lab Chip* 7 (2007) 256-263
3. A. E. Cervera-Padrell, S. T. Morthensen, D. J. Lewandowski, T. Skovby, S. Kiil, K. V. Gernaey, *Org. Process Res. Dev.* 16 (2012) 888-900
4. E. Sinkovec, M. Krajnc, *Org. Process Res. Dev.* 15 (2011) 817-823

Acknowledgment

DTU is acknowledged for financial support of the project. H. Lundbeck A/S is acknowledged for financial and technical support of the project.



Igor Mitrofanov

Phone: +45 4525 2817

E-mail: igm@kt.dtu.dk

Supervisors: Prof. Rafiqul Gani, CAPEC
Assoc. Prof. Gürkan Sin, CAPEC
Assoc. Prof. Jens Abildskov, CAPEC

PhD Study

Started: November 2010

To be completed: October 2013

The SolventPro – Computer-Aided Solvent Selection and Design Framework

Abstract

This paper presents a systematic integrated framework for solvent selection and solvent design. The framework is divided into several modules, which can tackle specific problems in various solvent-based applications. In particular, five modules corresponding to the following solvent selection problems are presented: 1) solvent selection and design for organic synthesis, 2) solvent selection and design for separation processes, 3) solvent screening and design of solvent mixtures for pharmaceutical applications, 4) solvents in phase transfer catalysis process and 5) ionic liquids selection and design as solvents. The application of the framework is highlighted successfully through case studies focusing on solvent replacement problem in organic synthesis and solvent mixture design for ibuprofen respectively.

Introduction

Solvents are widely used in a myriad of applications as reaction mediums, reactants or carriers in the chemical industry in general. In the pharmaceutical industry, for instance, it is common to using anti-solvents in crystallization processes to precipitate the active ingredient, while other solvents are still required for the final formulation. In other words, solvents play an important role in both process and product design. Nevertheless, solvent selection and design represent a complex problem, which requires decision making at early stages of the design process to identify the best candidates. Decisions will be taken depending on different multi-objective criteria such as process feasibility and economics. An important aspect is also the environmental impact, a crucial factor in the disposal of huge amounts of industrial solvents, which must match the requirements of the “Green Chemistry Principles” [1].

Currently, solvent selection problems are still solved based on trial-and-error procedures. Such procedures imply getting results that may not be optimal. From a mathematical point of view, the possibilities are in thousands and, by considering solvent mixtures, the combinatorial problem grows even more. A systematic approach is then highly desirable. Although systematic model-based methods have been proposed [2, 3], they need to be extended in terms of modelling and problems they can solve. The solvent selection framework that is presented here is based on the combination of

knowledge from industrial practice, computer-aided tools, and molecular design (CAMD) principles and it is intended for solvent selection and design in product design as well as process design applications.

Framework

The proposed systematic approach is depicted in the framework in fig. 1, where it can be noted that there are 7 modules to cover all possible solvent screening/design problems. In this paper, modules I, II, III, IV and VI are being presented.



Figure 1: Framework for solvent screening and Design.

Software

An important feature to highlight of the SolventPro software is the development of problem specific templates for various solvent related problems such as, solvents for organic synthesis (including complex reaction systems), solvent-based separations

(separations involving vapour-liquid, liquid-liquid and/or solid-liquid equilibrium systems), solvents for phase transfer catalysis (PTC) reactions, solvents for pharmaceutical industry (API solubility), solvents in formulations (as part of cosmetic and other solvent based formulations), and as cleaning agents. The goal of the template is to guide the average user through the essential and desirable steps in solvent selection and design. The expert may also use the general interface and create their own template for the types of solvent related problems they usually solve.

Module I

This module is dedicated to solvent selection and design for organic synthesis. It uses the solvent selection methodology developed by Gani et al. [1, 2] The methodology involves five steps for each reaction:

1. Problem identification: an objective for the given system is chosen by identifying the actual functions of the solvent.
2. Search criteria definition: the solvent functions that satisfy the operational needs of the process are defined in terms of a set of search criteria (R-indices), which, in turn, are defined in terms of physical and chemical properties.
3. Performing the search: the search step consists of the generation and property identification of solvent candidates and the assignment of the RS-indices following the reaction-solvent properties.
4. Score table assignment: the scores are assigned to each solvent based on the calculated values of RS indices that is, giving a weight to each of the calculated RS indices.
5. Matrix of solvents: after the scores table has been generated, a short list of feasible solvents is obtained for each reaction step and presented as a matrix with rows of solvents and columns of reactions. The best solvent should appear in more than one column.

Module II

This module is dedicated to solvent selection for separation processes in the pharmaceutical industry. One of the important tasks is often the identification of a pure solvent or anti-solvent for a specific Active Ingredient (API). Solvents, lipids and other compounds are commonly employed in product formulation as well as in API processing. In addition, it might be needed to design solvent mixtures to improve the solubility performance. This module consists of the following steps:

1. Preliminary solvent screening by CAMD approach: here the design constraints are imposed on important properties, such as, the solubility parameter, melting and boiling temperatures.
2. Secondary screening: this is achieved by ranking the candidates in decreasing order of solvent power, which is calculated through an appropriate model for activity coefficient.

3. Solubility verification: here the solubility of the API is calculated with different rigorous models (UNIFAC, NRTL-SAC, PC-SAFT).

4. Solvent mixture design: this step is needed to improve the solubility performance of the system. Two non-ideal mixing effects can occur, 1) a decrease or 2) an increase of solubility. In both cases a model-based procedure is used to identify the best mixture for the assigned purpose.

5. Final selection/verification: a proper experimental design can be set-up to identify the best from the remaining few candidates.

Module III

Ionic liquids (ILs) are potential solvents for liquid extraction processes. ILs are characterized as designer solvents [3] since it is possible to fine-tune their intrinsic thermo-physical properties by simply replacing the cation and/or the anion for a specific application such as extractive distillation and liquid-liquid extraction. This module includes a database of organic solvents (ca. 1300 compounds) and ionic liquids (ca. 1000 compounds) and a search engine based on chemical properties of the compounds, including their characterization in terms of UNIFAC and other group-contribution method parameters so that solubility and other needed calculations with ICAS can be performed.

Module IV

The fourth module is solvent selection in phase-transfer-catalysis. As pointed out by Piccolo et al (*Modeling and design of reacting systems with phase transfer catalysis, ESCAPE-21, conference proceedings*), a typical biphasic system can be decomposed into four sub-systems: a) water-organic solvent equilibrium, b) inorganic salt (source of reactive anion)-water, c) phase transfer catalyst-organic solvent, d) phase transfer catalyst-water. For each sub-system, data have been collected and representative models to calculate the liquid phase activity coefficients and from it, the solubilities and phase equilibrium, have been developed and tested for the systems of interest. The sub-system models are integrated in a continuous reactor model so that a quick evaluation of the process behaviour at different operational conditions is possible.

This module makes use of a model-based strategy for selection of the best organic solvent in PTC-based reacting systems where the organic solvent plays an important role since solubility of different forms of the PTC in the organic solvents affects ultimately the catalyst partition coefficients. Through this module, it is possible to find opportunities for improving reacting system performance and replacement of solvents.

Module VI

The sixth module is dedicated to solvent selection for separation processes. This module contains set of templates (Table 1) for different solvent-based separation problems (such as extractive distillation,

azeotropic distillation etc.) and is based on the technique called Computer Aided Molecular Design (CAMD), where building blocks for organic chemicals are combined together to form chemically feasible molecules and then evaluated (tested) for their solvent properties.

Table 1: Target properties for different templates

Property	S1 (Solvent)		S2 (Solvent)		S3 (Solvent)		S4 (Solvent)	
	Target	Value	Target	Value	Target	Value	Target	Value
MW	115.17	350.31	473.7	309.36	433.16	698.1	73.06	212.17
Tm [K]	350.31	473.7	309.36	433.16	698.1	73.06	212.17	426.1
Tb [K]	473.7	309.36	433.16	698.1	73.06	212.17	426.1	541.12
Sol.Par [Mpa0.5]	27.72	6.99	15.72	17.53	23.95	10.06	9.88	504.66
HPSP	6.99	15.72	17.53	23.95	10.06	9.88	504.66	521.6
HHSP	15.72	17.53	23.95	10.06	9.88	504.66	521.6	776.62
SP	27.72	6.99	15.72	17.53	23.95	10.06	9.88	84.93
HPSP	6.99	15.72	17.53	23.95	10.06	9.88	504.66	178.1
HHSP	15.72	17.53	23.95	10.06	9.88	504.66	521.6	313.2
SP	27.72	6.99	15.72	17.53	23.95	10.06	9.88	84.93
HPSP	6.99	15.72	17.53	23.95	10.06	9.88	504.66	178.1
HHSP	15.72	17.53	23.95	10.06	9.88	504.66	521.6	313.2
SP	27.72	6.99	15.72	17.53	23.95	10.06	9.88	84.93
HPSP	6.99	15.72	17.53	23.95	10.06	9.88	504.66	178.1
HHSP	15.72	17.53	23.95	10.06	9.88	504.66	521.6	313.2

Case studies

The solvent selection framework and the developed methods/tools have been implemented as software called SSF. It contains the database, property model libraries, links to other tools such as ICAS-ProPred for property prediction, ICAS-ProCAMD for computer aided molecular design, among others. The reported case studies are solved through SolventPro.

Solvent replacement for multistep organic synthesis

The objective of this case study is to find replacement solvents for each reaction step (see figure 2).



Figure 2: Reaction scheme

1. Problem definition. The objective is to find replacement for Dimethylformamide (DMF) and Dichloromethane (DCM) that fulfills the solvent properties but are more benign with respect to environment, health and safety. Reactions are taking place in liquid phase. The reactants are in solid form, addition of solvent will decrease the concentration of the solid reactants in solution thereby increasing reaction rate and yield. The physical properties of the involved compounds are first estimated (using ICAS-ProPred) and reported in Table 1. The names of the compounds are not given for reasons of confidentiality.

Table 2: Physical properties of reactants and products predicted through ICAS-ProPred.

Species	MW	Tm[K]	Tb[K]	Sol.Par [Mpa0.5]
C1	115.17	350.31	473.7	SP: 27.72 HPSP: 6.99 HHSP: 15.72
C2	309.36	433.16	698.1	SP: 17.53
DMF	73.06	212.17	426.1	SP: 23.95 HPSP: 10.06 HHSP: 9.88
C3	541.12	502.99	779.6	
C4	504.66	521.6	776.62	
DCM	84.93	178.1	313.2	SP: 20.37 HPSP: 7.6 HHSP: 4.07

MW – molecular weight, Tm – melting point, Tb – boiling point, SP – Hildebrand solubility parameter, HPSP – Hansen polar solubility parameter, HHSP – Hansen hydrogen bonding solubility parameter

2. Search criteria definition

Stage 1: solvents need to dissolve reactants and products ($17 < SP < 24$); solvents must be liquid within the range 200-380 K ($260 \text{ K} < T_m$ and $T_b > 380 \text{ K}$).

Stage 2: solvents need to dissolve reactants ($17 < SP < 25$) and need not dissolve products; solvents must be liquid within the range 180-260 K ($180 \text{ K} < T_m$ and $T_b > 260 \text{ K}$). In both reaction steps solvents must have better environment health and safety properties.

3. Performing the search, Scoring table assignment and Final matrix of solvents. The solvents satisfying the search criteria are generated using ICAS-ProCAMD and verified through ICAS-ProPred and CAPEC-database. Results are:

Stage 1: 3-pentanone, 2-hexanone, Cyclohexyl acetate, Cyclopentanone, 2-ethyl-1-butanol, Diacetone alcohol, 4-methyl-2-pentanol, 2-ethoxyethanol, 1-heptanol, 2-methoxyethanol, 1-hexanol.

Stage 2: 3-pentanone, Di-n-Propylamine, Methyl ethyl ketone, n-butylamine, 2-Pentanone, Ethyl acetate, Methyl isobutyl ketone, n-pentyl amine, 3, 3-dimethyl-2-butanone, diethylamine, Methyl Isopropyl Ketone, Isopropyl acetate, Pyrrolidine, n-Butylamine, Ethyl Isopropyl Ketone.

Then RS-indices are obtained using a rule-based algorithm and translated into scores according to the scoring algorithm. Eventually the final matrix of solvents is reported in table 3:

Table 3: Solvents matrix. Detailed solution of this problem as well as solutions of multi-step reaction problems can be obtained from the authors

Name	Stage 1	Stage 2	Total score
3-pentanone	1	1	104
Pyrrrolidine	1	0	70
2-methoxyethanol	0	1	70
Cyclopentanone	0	1	62

Solvent mixture design for Ibuprofen

In this case study, a solvent mixture for ibuprofen is designed. The first step is the preliminary screening by Pro-CAMD and the determination of the activity coefficient at infinite dilution of the API, which is needed for solvent power (SP) calculation. Solvent power is calculated with an extended NRTL-SAC model, which requires parameters for the four conceptual segments. Every compound is represented by these parameters and usually experimental data has been recommended [6]. In this paper, however, these parameters are predicted through a GC⁺ model. The combination of the GC⁺

By ordering the solvent candidates in decreasing order of SP, the best candidates are chosen and rigorous solubility calculations are carried out to identify the best solvents needed in dissolution processes for instance and the best anti-solvents needed in crystallization processes for instance. The three best solvents were found to be N, N-dimethylacetamide, trichloroethylene and pyridine, while the three best anti-solvents were dichloromethane, n-octane and methanol. model with the NRTL-SAC constitutes the UNISAC model, which has been implemented in this module to allow model-based solvent mixture design.

The next step consists of fixing one solvent from the best candidates, defining the desired solubility profile for the solvent mixture and performing the mixture design. For crystallization to be carried out, a solvent mixture that causes a solubility decrease is needed. The points on figure 3 represent the desired solubility profile and the curves the fittings resulting from the design procedure. In a similar way solvent mixtures that can enhance solubility can also be found.

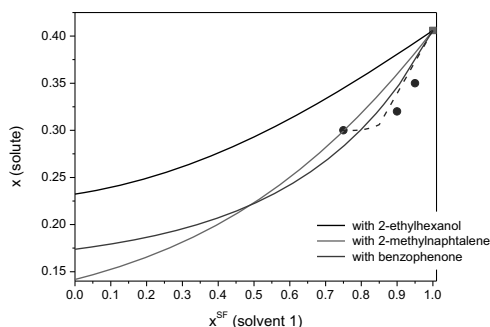


Figure 3: Solvent mixture design graph

Conclusions

An integrated computational tool for solvent selection and design has been developed and showed good performances for different common solvent-based processes. Further features will be added to the tool in order to extend the domain of application.

References

- [1] Anastas, P.T., Warner, J.C., 1998. Green Chemistry: theory and practice, Oxford: Oxford University Press, U.K.
- [2] Gani, R., Jimenez-Gonzalez, C., Constable, D.J.C., 2005. Method for Selection of solvents for promotion of organic reactions. Computers and Chemical Engineering 29, 1661-1676.
- [3] Folic, M., Gani, R., Jiménez-González, C., Constable, D.J.C., 2008. Systematic Selection of Green Solvents for Organic Reaction Systems. Chinese Journal of Chemical Engineering. 16(3), 376-383.
- [4] Gani, R., Nielsen, B., Fredenslund, A., 1991. A group contribution approach to Computer Aided Molecular Design. AIChE J., 37, 1318-1332.
- [6] Chen, C.-C., Song, Y., 2004. Solubility Modelling with a Nonrandom Two-Liquid Segment activity coefficient model. Ind. Eng. Chem. Res. 43, 8354-8362.
- [5] Rodríguez H., Gurau G., Rogers R. D., 2009. Ionic Liquids: Growth of a Field through the Eyes of I & EC Division, Innovations in Industrial and Engineering Chemistry, chapter 11, pp 389-400.

List of publications:

1. **Conference Proceedings:** I. Mitrofanov, S. Sansonetti, J. Abildskov, G. Sin, R. Gani, 2012. The Solvent Selection framework: solvents for organic synthesis, separation processes and ionic-organic synthesis. 22nd European Symposium on Computer Aided Process Engineering. Elsevier Science, 2012. p. 762-766 (Computer Aided Chemical Engineering, Vol. 30)



Ane Loft Mollerup

Phone: +45 4525 2907
 E-mail: molle@kt.dtu.dk

Supervisors: Gürkan Sin
 Peter Steen Mikkelsen, DTU Environment
 Dines Thornberg, Udviklingssamarbejdet
 Niels Bent Johansen, Københavns Energi

Industrial PhD Study

Started: August 2011
 To be completed: August 2014

Optimizing control of the integrated urban wastewater system

Abstract

Design and assessment of control in wastewater systems has to be tackled at all levels, including supervisory and regulatory level. This project aims at developing a methodology for determining the best control structure and technique for an integrated system of both sewer system and wastewater plants, when optimizing towards defined objectives.

To test different control structures and control techniques a simplified model of a case study area in Copenhagen is made, calibrated and validated.

Introduction

This research will use a model-based approach to generate and evaluate control strategies. The existing models of the sewer system that are used by the utilities in their planning are very detailed involving complex phenomena that makes them not suitable for control applications. Therefore a simple model is developed in MATLAB® to be used for testing different control configurations are control techniques. This model is calibrated and validated according to the detailed model, to ensure an equal degree of accuracy with respect to the modelled overflows.

Specific Objectives

At this stage the specific objective is to develop a model that can be used for examining for example the importance of the pairing between measurements and actuators.

The Model

The sewer system is modelled in MATLAB® using the virtual tank approach [1], which is mainly based on mass balances. There are the following elements in the model:

- Virtual tanks
- Real tanks
- Pumping stations
- Interceptor pipes
- Overflow structures, internal and external

A schematic representation of the model is shown in Fig. 1.

A virtual tank is a representation of a subcatchment with its connected surface area and its pipe volume.

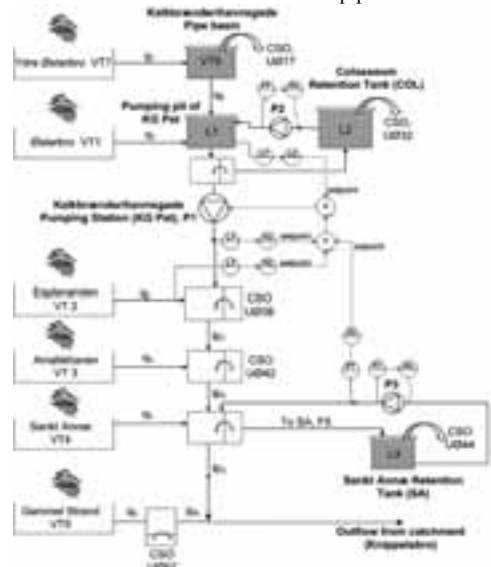


Figure 1: A schematic representation of the model.

The global mass balance for a virtual tank is expressed as:

$$dV_i/dt = q_{in} - q_{out} \quad (1)$$

Where q_{in} is the inflow coming from other tanks, virtual tanks and the dry weather flow (household wastewater) as well as the effective rainfall runoff and q_{out} is the outflow from the virtual tank, empirically modelled as:

$$q_{out} = \beta_i V_i \quad (2)$$

The parameter β_i [s^{-1}] is a volume/flow conversion coefficient. This parameter has no physical meaning and can only be determined from calibration.

Parameter Estimation using Monte Carlo simulations

Initially a maximum likelihood estimation (MLE) method is tried for the parameter estimation. However, due to the very non-linear behaviour of the model, MLE cannot be performed satisfactory without a good initial guess on the parameter values.

Therefore Monte Carlo (MC) simulations are made to try and narrow down the parameter ranges of interest. The number of simulations and hence subsets of parameters to be sampled from the sampling space is chosen to be 5000. The sampling technique used is Latin Hypercube Sampling (LHS). The lower and upper bounds are determined from expert knowledge and can be seen from Table 1.

Table 1: Upper and lower bounds for the parameters to be used in LHS sampling.

	β_1	β_2	β_3	β_4	β_6	β_7
Lower bound	0.001	0.001	0.250	0.100	0.001	0.001
Upper bound	0.500	0.100	0.500	0.200	0.500	0.500

Each of the 5000 sets of parameters are simulated and the costs associated are calculated from:

$$S(y, \theta) = \text{SUM}(((y - \hat{f}(\theta))^2 / \sigma^2)) \quad (3)$$

Where the outputs are the overflows and the filling of the two retention tanks, Colosseum and Sankt Annæ.

Results and Discussion

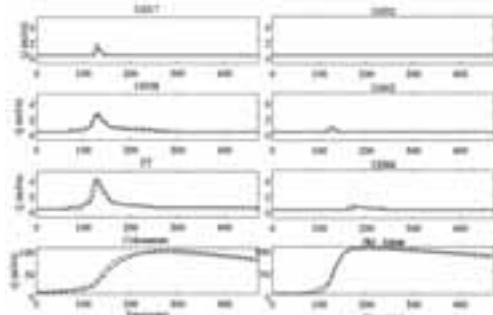


Figure 2: Results from the simulation with parameters found from MC simulations.

From Figure 2 it can be seen that the model captures the right dynamics of the system and therefore the parameters can be assumed to be in the correct range.

Based on this an MLE can be performed and finally a validation is made, which can be seen from Figure 3.

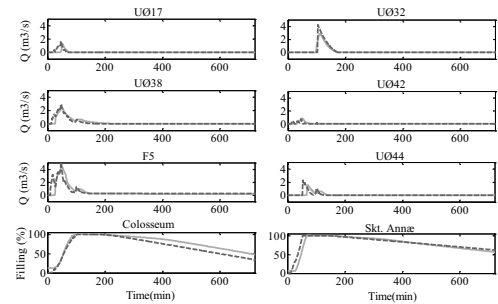


Figure 3: Plot of the validation results

Conclusions

The dynamics that are to be captured with the model are highly non-linear. Therefore it is important to have a good initial estimate of the model parameters when doing the parameter estimation. To get this, a useful method is to apply brute force by making Monte Carlo simulations of subsets of parameters, sampled from within specified boundaries.

The simple model is validated and is shown to perform well with respect to the timing and sizes of the overflows from the system.

Next step is to use the model for analysing the importance of the pairing between measurements and actuators on the performance of the control.

Acknowledgements

This project is initiated and co-financed by Copenhagen Wastewater Innovation.

The research is supported by The Danish Agency for Science, Technology and Innovation under the Industrial PhD programme (Project number 11-109494). The support is gratefully acknowledged.

References

- [1] C. Ocampo-Martinez. Model Predictive Control of Wastewater Systems, Springer-Verlag, London, 2010.

List of Publications

A. Mollerup, M. Iglesias, N.B. Johansen, D. Thornberg, P.S. Mikkelsen and G. Sin, Model-Based Analysis of Control Performance in Sewer Systems, Proceedings of the 17th Nordic process control workshop, Lyngby, DK., 2011, p. 123-127.

A. Mollerup, M. Grum, D. Muschalla, E. van Velzen, P. Vanrolleghem, G. Sin and P.S. Mikkelsen. Integrated Control of the Wastewater System – Potentials and Barriers. Water 21 (submitted) (2012).

**Peter Mølgaard Mortensen**

Phone: +45 4525 2809
E-mail: pmm@kt.dtu.dk

Supervisors: Anker Degn Jensen
Jan-Dierk Grunwaldt
Peter Arendt Jensen

PhD Study

Started: August 2010
To be completed: October 2013

Mechanistic Insight in Hydrodeoxygenation on Nickel Based Catalysts

Abstract

A prospective route for the production of alternative fuels is the conversion of biomass to bio-oil through flash pyrolysis followed by catalytic upgrading through hydrodeoxygenation (HDO). Nickel based catalysts on different supports have been tested in a batch reactor at 275 °C and 100 bar for HDO, using phenol as model compound for bio-oil. Phenol was found to initially be hydrogenated to cyclohexanol and then deoxygenated to cyclohexane. Ni/ZrO₂, Ni/SiO₂, and Ni/Al₂O₃ were found as the best performing deoxygenation catalysts, with ZrO₂ as the overall best performing support for nickel catalysts. On a series of Ni/SiO₂ catalysts, the effect of nickel crystallite size was investigated. Here it was found that the rate of deoxygenation could be linked to the fraction of available low coordinated nickel sites on the catalyst, indicating that these sites are the most active for HDO.

Introduction

Pyrolysis of biomass followed by hydrodeoxygenation (HDO) of the produced bio-oil has been identified as a prospective route to engine fuels. Through pyrolysis practically any source of biomass can be converted into bio-oil [1]. Despite of the higher energy density than the original biomass, bio-oil has a lower heating value compared to crude oil, a low shelf storage time, is viscous and polar, making it unsuitable as an engine fuel. These characteristics are all associated with high contents of water (10-30 wt%) and oxygen containing organic compounds (30-40 wt% oxygen) in the oil [2]. It will be advantageous if bio-oil can be upgraded to a product similar to conventional crude oil through HDO, where hydrogen is used to remove the oxygen functionality in the bio-oil. To accomplish this, a suitable catalyst is required and recent research has indicated that nickel based catalysts could be interesting candidates for this task [3]. We have investigated the mechanistic details of a set of Ni catalysts for HDO of phenol as a model compound of bio-oil.

Specific Objectives

The objectives of the project are to develop catalysts for HDO, which should be evaluated both with respect to activity, stability, and resistance towards impurities in bio-oil. The two later will be tested on a high pressure continuous flow liquid/gas reactor system which has been constructed within the frame of the project.

Experimental

Ni catalysts were all prepared through incipient wetness impregnation on the relevant supports and then calcined at 400 °C. The active carbon was Daihope 009, the SiO₂ was from Saint-Gobain NorPro type SS6*138, the ZrO₂ was from Saint-Gobain NorPro type SZ6*152, the Al₂O₃ was from Sasol type Puralox TH 100/150, the spinel was produced from the Al₂O₃ mixed with MgO, and CeO₂ and CeZrO₄ were from AMR Ltd.

The experiments were performed in a 300 ml batch reactor from Parr, type 4566, constructed of Hastelloy C steel. In an experiment the catalyst was initially loaded in the reactor and hereafter a mixture of phenol in water (as a model system for bio-oil) was added. This was heated to 275 °C in a hydrogen atmosphere, giving a final pressure of 100 bar. The heating rate was in the order of 10-15 °C/min. During the experiments, hydrogen was added continually to maintain the pressure, if needed. To stop the experiment, the reactor was lowered into an ice bath.

Analysis of the product was done with a Shimadzu GCMS/FID-QP2010UltraEi fitted with a Supelco Equity-5 column. Identification was made on the mass spectrometer (MS) and quantification was done on the flame ionization detector (FID).

Results and Discussion

Nickel was tested as catalyst for HDO of phenol on a series of supports in the batch reactor. Generally, it was observed that the reaction proceeds through the reaction

scheme in Figure 1 (solid arrows). However, as the conversion of cyclohexanone into cyclohexanol and cyclohexene into cyclohexane are very fast reactions, the effective reaction scheme could be described as: phenol \rightarrow cyclohexanol \rightarrow cyclohexane. On this basis a kinetic model was developed which described the system on the basis of two parameters: the rate constant of hydrogenation (k_1) and the rate constant of deoxygenation (k_2). These can be correlated to the turn over frequency (TOF) of respectively hydrogenation (TOF_{Hyd}) and deoxygenation (TOF_{Deox}).

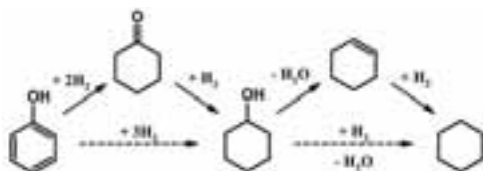


Figure 1: Reaction scheme for phenol HDO.

Figure 2 summarizes the results from HDO of phenol with nickel on different supports. Ni/CeO₂ was found as the best performing hydrogenation catalyst (largest TOF_{Hyd}), but this catalyst was also found practically inactive toward HDO. Ni/ZrO₂, Ni/SiO₂, and Ni/Al₂O₃ were found as the best performing deoxygenation catalysts, decreasing in activity in that order.

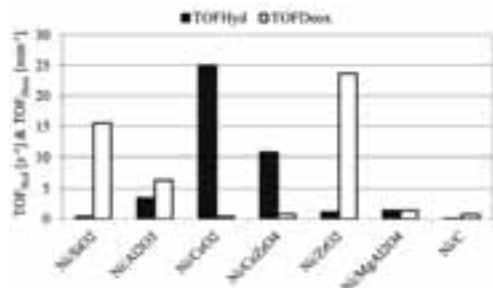


Figure 2: Yield and conversion over nickel based catalysts. The experiments were made with 1 g of catalyst in 50 g phenol. T=275 °C, P=100 bar, reaction time=5 h.

Ni/C was found to be practically inactive. This shows that the nickel catalysts only are active when the nickel is in the vicinity of an oxide support. This indicates that the activation of the oxy-compound takes place on the oxide, probably through heterolytic dissociation. Hydrogen activation on the other hand most likely takes place on nickel crystallites [1,3].

Ni/SiO₂ was investigated with varying nickel dispersion (i.e. Ni crystallite size) as seen in Figure 3. The results show that the TOF_{Hyd} decreased with dispersion, while the TOF_{Deox} increased with dispersion. Figure 3 also shows the relative fractions of different sites on nickel crystals as function of dispersion

developed on the basis of the surface population model by Benfield [4]. Comparing the trend of TOF_{Deox} to the fraction of available low coordinated sites (step & corner) shows that they behave similarly as function of the dispersion. This indicates that the deoxygenation probably preferably takes place on the low coordinated nickel atoms.

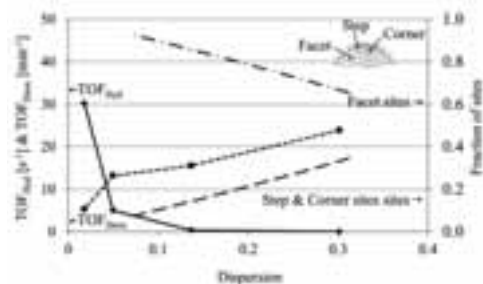


Figure 3: TOF of Ni/SiO₂ catalyst with varying dispersion (determined by TEM) compared to the fraction of step, corner, and facet sites on a crystal. The experiments were made with 1 g of catalyst in 50 g phenol. T=275 °C, P=100 bar, reaction time=5 h.

Conclusions

Among the tested nickel catalysts, Ni/ZrO₂ was found as the best performing HDO catalyst, with balanced rates of hydrogenation and deoxygenation. The presence of an oxide support is of key importance for the catalyst performance, as the oxy-compound activation takes place on this through heterolytic dissociation. Furthermore, the actual deoxygenation site on nickel can possibly be linked to the low coordinated sites (step/corners) on the crystallite. This insight can be used for better design of HDO catalysts.

Acknowledgments

The present work is financed by DTU and The Catalysis for Sustainable Energy initiative (CASE), funded by the Danish Ministry of Science, Technology and Innovation.

References

1. P.M. Mortensen, J.-D. Grunwaldt, P.A. Jensen, A.D. Jensen, *Appl. Catal. A*, 407 (1-2) (2011) 1-19.
2. Q. Zhang, J. Chang, T. Wang, Y. Xu, *Energy Convers. Manage.*, 48 (1)(2007) 87-92.
3. V.A. Yakovlev, S.A. Krhromova, O.V. Sherstyuk, V.O. Dundich, D.Y. Ermakov, V.M. Novopashina, M.Y. Lebedev, O. Bulavchenko, V.N. Parmon, *Catal. Today* 144 (3-4) (2009) 362-366.
4. R. E. Benfield, *J. Chem. Soc. Faraday Trans.* 88 (8) (1992) 1107-1110

List of Publications

1. P.M. Mortensen, J.-D. Grunwaldt, P.A. Jensen, A.D. Jensen, *Appl. Catal. A*, 407 (1-2) (2011) 1-19.

**Watson Neto**

Phone: +45 4525 52958
E-mail: wan@kt.dtu.dk

Supervisors: John M. Woodley
Pär Tufvesson

PhD Study

Started: June 2010
To be completed: May 2013

Process strategies for implementing (*S*)- ω -transaminase catalyzed reactions

Abstract

The implementation of new biocatalytic processes can be a very challenging procedure which might require several stages of characterization and evaluation before implementation. Several process parameters, with different weights on the final economics, need to be considered alongside. Process design and economic evaluation represent a very important part of the early process development stage. However, often the parameters set at these initial stages are purely theoretical. Therefore a lab scale characterization of the different process options and strategies assumed during the design step is important in order to eliminate unfeasible process options and to correct the parameters previously assumed. This work illustrates the lab scale characterization of different process options using as case study the process development for production of chiral amines through enzymatic synthesis with (*S*)- ω -transaminase.

Introduction

Over the past decades, the use of biocatalysis to produce fine chemicals and pharmaceutical intermediates has significantly increased. A major contribution to this trend has been the discovery and isolation of enzymes from a variety of different biological sources. This has broadened the scope of biocatalysis which nowadays allows the regio- and enantio-selective synthesis of many compounds, potentially with green credentials [1-4]. The technology therefore has many potential advantages over classical chemical synthesis to prepare fine chemical and pharmaceutical intermediates.

However, despite the advantages, there are some important challenges associated with this technology. First it is necessary to find a suitable enzyme or group of enzymes that are able to catalyze production of the desired compound. Secondly, often the naturally occurring enzyme does not meet the requirements of the process conditions, where high substrate and product concentrations as well as high selectivity and productivity demands of the catalyst (g product per g biocatalyst), are key to economic feasibility at an industrial/commercial level [5]. Also, it is very common that the wild type enzyme is not stable at operating conditions (temperature, pH, substrate and product concentration). This brings additional challenges for process engineers when designing the process. A way out, is to consider multiple process options including different strategies that can potentially help overcome

these limitations. These strategies can include for instance the use of protein engineering to improve the wild type enzymes (increase activity or stability), the immobilization of catalyst to allow catalyst recycling and facilitate separation, the use of controlled release of substrate (fed-batch or *in-situ* substrate supply – ISSS) to decrease substrate inhibition or the use of *in-situ* product (ISPR) and co-product removal (IScPR) to respectively control product inhibition and shift equilibrium.

The different strategies can be virtually evaluated (having process economics in mind) and a small number of feasible process options are selected. In order to validate the strategies assumed in these process options, the parameters assumed need to be tested and characterized at lab scale.

This work focuses on the case study of (*S*)- ω -transaminase (*S*- ω -TAM) to produce chiral amines which are important building blocks for the chemical and pharmaceutical industries.

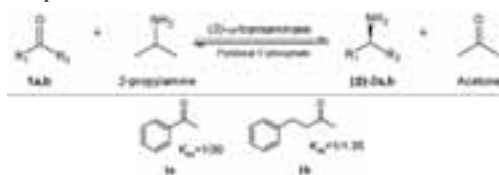


Figure 1: Overview of the biocatalytic transaminase reaction using 2-propylamine as amine donor.

Transaminases are one of the enzymes that have received much attention from industry and academia in the past years. These enzymes are able to transfer amine groups (-NH₂) from an amine donor to an amine acceptor (a pro-chiral ketone), yielding a chiral amine and a co-product ketone (Figure 1). They are known to be dependent on the co-factor pyridoxal-5'-phosphate (PLP) and to be severely inhibited by both the ketone substrate and the chiral product. Also, the unfavorable equilibrium ($K_{eq} \ll 1$) and low water solubility of the substrate and product is often pointed as a major bottleneck [6].

Given these limitations, a feasible process using this biocatalyst needs to take into account different strategies and tools to overcome them. Table 1 summarizes a selected list of potential strategies for successful production of chiral amines using S- ω -TAM. This process option considers the use of protein engineering tools to improve the wild type enzyme towards its selectivity (increase enantiomeric excess) and to alleviate substrate and product inhibition (broaden the operating window). Complementary to this, process engineering tools such as ISSS, ISPR and IScPR can be applied in order to further improve the process.

Table 1: Process strategies for successful production of chiral amines using transaminase.

Limitations	Strategies	Tools
Selectivity (<i>ee</i>)	A+(C,D)	Directed evolution
Product inhibition	A+B	Use auxiliary phase
Substrate inhibition	A+(C,D)	Controlled feeding
Unfavorable Eq.	E	Remove co-product
Low solubility	B,C, D	Use auxiliary phase
Enzyme separation	F	Immobilization onto resins

A: Enzyme development; B: *In-situ* product removal; C: *In-situ* substrate supply; D: Fed-batch; E: Amine donor excess; F: Enzyme immobilization

This mode of operating, combining protein and process engineering tools to improve the process, brings several advantages over the operating mode in which protein engineering alone is used to improve the process (enzyme is designed to fit process requirements). This can result in a biocatalyst which has a reduced range of substrate it can operate with. Also the enormous effort and qualified human resources as well as the time that is required to change numerous amino acids in the protein can be very labor intensive and this is reflected in the process costs [7].

On the other hand, process engineering tools alone cannot deal for instance with a severely inhibited and unspecific enzyme and this motivates a combined approach in which protein and process engineering tools are considered in parallel (Figure 2). This allows decreasing in the number of required rounds for enzyme development which eventually reflects positively in the process costs.

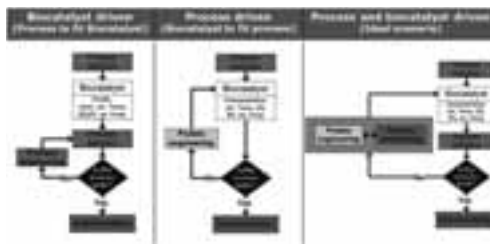


Figure 2: Routes for implementation of a biocatalytic process

Results and Discussion

I. Process definition

During the process design and economical evaluation, the process targets are initially set and the required yield or productivity is defined. In this work we focus on the production of (*S*)-1-phenyl-ethylamine (PEA) from acetophenone (APH) and the production of (*S*)-3-amino-1-phenyl-butane (APB) from benzylacetone (BA) using in both cases 2-propylamine (IPA) as amine donor. The production objective was set to approximately 30 g/L of each product.

II. Biocatalyst screening and characterization

Once defined the process objectives, the next task consists in selecting and characterizing the most suitable mutants inside the enzyme library available. For this purpose, this work has been done in collaboration with c-LEcta GmbH which supplied the first (*S*)- ω -transaminase mutant (ATA 40). This enzyme has been characterized for inhibition profile regarding substrates and product. The result for inhibition profile (Figure 3) shows a very poor performance for concentration of substrate and product higher than 10 mM. Also the selectivity (*ee*) was far from the ideal 100% (data not shown). In order to use this enzyme in the process, it was further developed by c-LEcta GmbH and several new mutants were generated and ATA 47 was selected for further characterization.

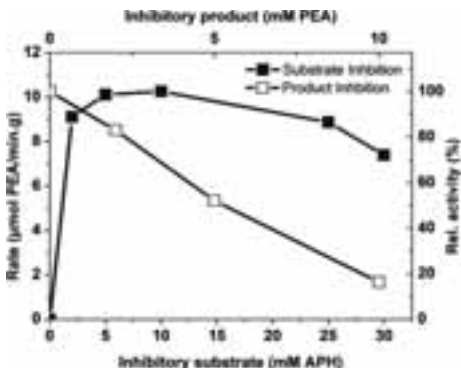


Figure 3: Substrate and Product inhibition for ATA 40 (c-LEcta GmbH)

This new mutant showed better substrate and product tolerance (Figure 4). It showed also improved activity in comparison with ATA 40 and an *e.e.* of approximately 100% (data not shown).

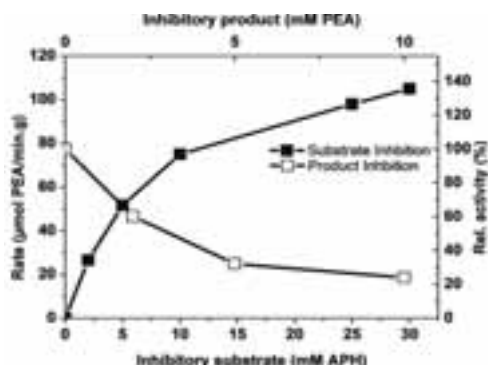


Figure 4: Substrate and Product inhibition for ATA 47 (c-Lecta GmbH)

The production over time for the two mutants showed significant differences between them. The ATA 40 yielded 0.7% of PEA after 30 hours reaction while 16% of yield was achieved for ATA 47 in the same conditions (Figure 5). Although the later showed higher yield, this value was still far away from the equilibrium yield (26%). This can be explained by the strong inhibitory effect caused by the product, which justifies the need for ISPR.

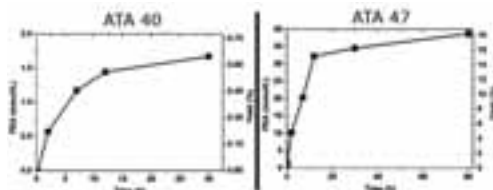


Figure 5: Production of (S)-1-phenyl-ethylamine over time for ATA 40 and 47.

III. The use of process engineering tools (ISSS, ISPR, IScPR and fed-batch)

Using the most suitable mutant (ATA 47), several experiments combining the different strategies were carried out and evaluated based on the final productivity (g product/L).

Several strategies have been previously reported for ISSS and ISPR. The most common consists in using organic solvents or polymeric resins to both supply the inhibitory substrate and deal with its solubility problems (acting as substrate reservoir) and to remove the inhibitory product [8-11]. This work is regarding the use of polymeric resins as auxiliary phase. A potential resin was previously selected from a library (data not shown) where the resin AF 5 from Lewatit was selected due to its relatively higher selectivity for the products over the substrates.

The resin was loaded in the reactor at two different concentrations: 100 g/L and 150 g/L. The lower resin loading allowed 20-25 mM of product and substrates for both reaction systems while 150 g/L of resins reduced the concentrations in aqueous phase to below 10 mM (Figure 6).

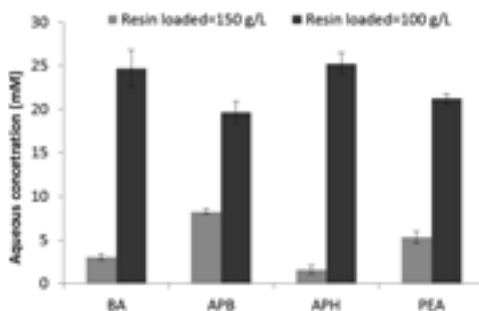


Figure 6: Productivity after 48 h reaction ATA 47 using different process strategies with 150 g/L of resin loading.

A setup of 2 ml (operating volume) reactors where run in parallel, where a control, consisting in 1 M IPA, approximately 300 mM of the substrate ketone, 8 mM of cofactor PLP and 100 mM pH 7 phosphate buffer (run at 30 C with 400 rpm agitation) was compared with:

- ISPR only: where the resin was initially added into a reaction mixture similar to the control.
- ISSS+ISPR: the ketone substrate was previously loaded onto the resin, and the saturated resin was added to reactor (containing all the components except for the ketone substrate).
- ISSS+ISPR+IScPR: similar procedure as in *b* but with nitrogen sweeping in the reactor.
- Fed-batch+ ISPR+IScPR: similar to *c* with exception for the ketone substrate that was fed to the reactor using a syringe pump.

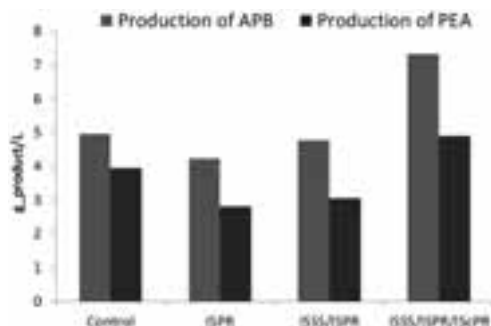


Figure 7: Productivity after 48 h reaction ATA 47 using different process strategies with 100 g/L of resin loading.

The results summarized in Figures 7 and 8 (for 100 and 150 g/L of resin loading, respectively) showed an increasing tendency in productivity for both reaction systems (production of PEA and APB) as the different strategies were combined.

The highest productivity was achieved when fed-batch was combined with ISPR and IScPR (Figure 8) yielding approximately 25 g/L of APB, contrasting with the production of PEA which didn't pass 5 g/L.

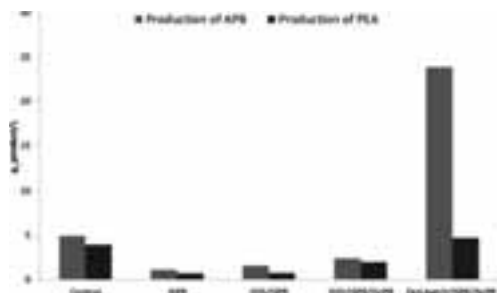


Figure 8: Productivity after 48 h reaction ATA 47 using different process strategies with 150 g/L of resin loading.

It was observed that less than 50% of the produced chiral amines were actually removed by the resin (data not shown). This suggested inefficiency of the resins and need for further characterization or screening for a more selective auxiliary phase.

Conclusions:

The process engineering tools considered as a strategy to improve this process were tested at bench scale and the results evidenced their potential to enhance the biocatalyst performance. The combination of protein and process engineering tools (fed-batch+ISPR+IScPR) allowed the production of 5 fold higher product concentration (25 g/L) than the control using the latest mutant (ATA 47), and approximately 30 fold higher than the control using the initial mutant (ATA 40).

The results also suggested the need for further studies in order to find the most suitable resin loading. It was observed that higher resin loading decreased substrates availability in aqueous phase thus limiting the enzyme activity. On the other hand, lower resin loading resulted in the opposite: very high substrate and product concentration available in aqueous phase, which causes inhibition to the enzyme, also limiting its activity. A compromise need to be found. Ultimately, the enzyme can be further developed to open even more its operating window.

Another alternative which is now being studied is to use ion exchange resin (cation) instead of hydrophobic. This is expected to result in better resin-product affinity. However, in order to be implement this, it is required some changes in the process, such as the use of a different amine donor (to prevent its interaction with the ion exchange resin) and it is also required to use

immobilized enzymes in order to prevent their contact with the resins.

This process option, which is now being characterized and evaluated, will be compared with the one here reported and the most promising strategy will be used to redesign the process and further develop it at higher scale.

References:

1. Woodley, J. M., *Advances in biochemical engineering/biotechnology* 2000, 70, 93-108.
2. Schmid, A.; Hollmann, F.; Park, J. B.; Buhler, B., *Current Opinion in Biotechnology* 2002, 13, (4), 359-366.
3. Rogers, P. L.; Jeon, Y. J.; Svenson, C. J., *Process Safety and Environmental Protection* 2005, 83, (B6), 499-503.
4. Razor, J. P.; Voss, E., *Applied Catalysis a-General* 2001, 221, (1-2), 145-158.
5. Tufvesson, P. r.; Lima-Ramos, J.; Nordblad, M.; Woodley, J. M., *Organic Process Research and Development* 2011, 15, (1), 266-274.
6. Tufvesson, P.; Lima-Ramos, J.; Jensen, J. S.; Al-Haque, N.; Neto, W.; Woodley, J. M., *Biotechnology and Bioengineering* 2011, 108, (7), 1479-1493.
7. Bornscheuer, U. T.; Huisman, G. W.; Kazlauskas, R. J.; Lutz, S.; Moore, J. C.; Robins, K., *Nature* 2012, 485, (7397), 185-194.
8. Schmoelzer, K.; Maedje, K.; Nidetzky, B.; Kratzer, R., *Bioresource Technology* 2012, 108, 216-223.
9. Straathof, A. J. J., *Biotechnology Progress* 2003, 19,(3).
10. Kim, P.-Y.; Pollard, D. J.; Woodley, J. M., *Biotechnology Progress* 2007, 23, (1).
11. Truppo, M. D.; Rozzell, J. D.; Turner, N. J., *Organic Process Research & Development* 2010, 14, (1).



Hiep Dinh Nguyen

Phone: +45 9175 1192
E-mail: hing@kt.dtu.dk

Supervisors: Georgios Kontogeorgis
David Löf, PPG Industries
Anders Egede Daugaard

PhD Study

Started: August 2012
To be completed: July 2015

Synthesis and development of novel coating components for exterior wood applications based on sustainable resources

Abstract

The trend for removing dependence on fossil based resources for industrial products, and development of sustainable, environmentally benign alternatives is increasing. This Ph.D. project is part of a HTF project that aims for preparation of a green biobased wood coating system. The Ph.D. project is focused on synthesis of novel biobased components to replace current petrochemical ingredients in a water based alkyd coating system. Specifically, the project aims to synthesize alkyd resins based on renewable materials and produce alternative solutions to curing and stabilization of the coating system.

Introduction

Wood has been used for many thousands of years in furniture and building construction. Due to its versatility and renewable characteristic, wood can satisfy present and future demands for sustainable construction material. Without protection, wood exposed outdoors suffers from being attacked through many different processes such as UV light, moisture and microorganisms. Coatings have long been used in protecting wood as well as giving it a more appealing appearance. The amount of wood consumed annually over the world is huge, and so is the total market for coating products illustrating the potential of the project.

A coating system consists of the following primary components. The base of the system is the binder. Its role is creating a tough and continuous film adhering strongly to the wood surface that needs to be coated. The second part is the solvent, which acts as an environment for the formulation. The third major component is fillers, such as colored pigments, particles to give reinforcement or particles that reduce the cost of the coating. Last but not least, additives are put into the coating system for other purposes. That could be a biocide to eliminate degradation of the coating system by microorganisms. It could also be a UV stabilizer that protects the lignin in the wood from harmful UV light.

Most coating systems today are fossil based, non sustainable, and contain toxic biocides that are regulated (Biocidal Products Directive, EU directive 98/8/EC). There are only a few non fossil based coating systems, but currently the overall performance of such systems

are not comparable to state of the art fossil based systems. In addition to this, the trend for removing dependence on fossil resources for industrial products, and development of sustainable, environmentally benign alternatives is increasing (e.g. EU White paper, "European Bioeconomy 2030"). Since there are no products on the market now that fulfill present consumer requirements and demands from the future, a new generation of highly durable, state of the art biocide free wood coating systems 100% derived from renewable resources need to be investigated. Such a coating system is the main objective of the HTF project named "Superior BioBased coating System for Exterior Wood Applications". This HTF project combines the efforts of many participants working in different areas required for the development of such a biobased system. The project includes Departments of Biology and Science at Copenhagen University, Dyrup (PPG), Palsgaard, Emmelev, the Danish Technological Institute and Department of Chemical and Biochemical Engineering at DTU. The purpose of this Ph.D. project in relation to the overlying HTF project is synthesis of novel biobased components for the exterior wood paint formulation.

Specific Objectives

One of the main points in this project is synthesis of novel alkyd binders from renewable material. Alkyds are popular in coatings due to the versatility of the method, the ease of use and for economical reasons. It is estimated that around 1 million tons of alkyds are

produced annually [2]. The term alkyd has the origin from the AL of polyhydric alcohols and the CID in polyprotic acids (or polybasic acids, which is modified to KYD) [2]. In fact, alkyds are based on a polyester grafted with fatty acids, which gives a typical structure as illustrated in Figure 1.

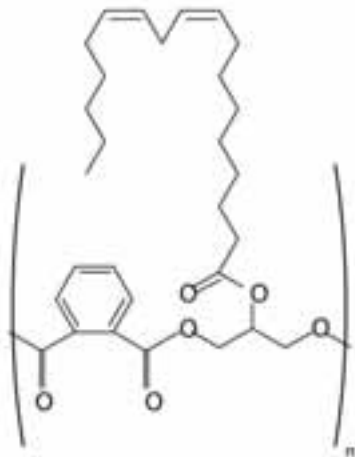


Figure 1: The structure of a typical alkyd produced from phthalic anhydride and glycerol grafted with linoleic acid.

As can be seen from the Figure 1, alkyds are made from three components, polybasic acids, polyols, and fatty acids. Phthalic acid and iso phthalic acid are the two most frequently used polybasic acids, and they are produced from fossil resources. Interestingly, the other parts of the alkyd binder are obtainable from renewable resources. Oils from vegetables and plants have been the sources of fatty acid and polyols, such as linoleic acid and glycerol for alkyd synthesis. Some of the oils frequently used in alkyds are linseed oil, manhaden oil, safflower oil, sunflower oil, dehydrated castor oil, soybean oil, coconut oil and tung oil. These raw materials makes alkyds a good starting point for a biobased coating, since a large amount of the raw materials are available from a biosource or biobased in essence. The challenge of making an alkyd completely biobased thus resides with finding alternatives for the petrochemical part, which account for 50wt% of the alkyd composition [1].

In the early part of this Ph.D. project the focus will be on replacement of the fossil based part of the alkyd binder with biobased alternatives. Initially, a screening of different possible candidates will be conducted to evaluate the possibilities for preparation of binders, the film forming properties of such binders and the quality of the coatings.

The candidates for this early test should be easy to obtain in large quantity and have adequate structures that contribute to the desired mechanical properties of

the synthesized product. In addition to availability, the components should facilitate the preparation of binders of appropriate molecular weight, which plays an important role in the properties of the obtained alkyd. This issue will be addressed through careful synthesis and thorough characterization.

During this early stage of the Ph.D. project also the alkyd synthesis process is considered. Normally, alkyds are synthesized by two kinds of process. The first one is “the fatty acid process” or the “one stage process”, which is a direct polyesterification between polybasic acids, polyols and fatty acids. The second one is called the “monoglyceride process” or the “two stage process”, in which vegetable or plant oils are first converted into monoglycerides by transesterification with polyols. Alcoholysis is then followed by polyesterification with polybasic acids. While the fatty acid process has the advantages of better reproducibility and control of molecular weight of the resins, the monoglyceride process is more economic. However, the two processes are carried out at high temperature and require a lot of energy, and this issue will be taken into consideration.

In addition to preparation of a biobased binder, alternatives for the other petrochemical components in the coating formulation should also be investigated during the project in collaboration with the other participants in the HTF project. From an environmental perspective the alkyd curing poses a problem since cobalt salts are frequently used[2]. For a completely biobased and green coating system these driers should be replaced by environmentally friendly biobased ones. Another important challenge is stabilization of the overall formulation. In an aqueous based wood coating formulation surfactants or stabilizers are required in order to prepare a stable system. Current solutions are in use, though these are based on raw materials from fossil resources.

Acknowledgement

This PhD project is funded by the Danish National Advanced Technology Foundation (DNATF) and the Department of Chemical and Biochemical Engineering, Technical University of Denmark.

References

1. N.F. Jones, Alkyd Resins, Ullmann's Encyclopedia of Industrial Chemistry. Wiley-VCH, 2003.
2. R.V. Gorkum, E. Bouwman, Coordination Chemistry Reviews 249 (2005) 1709–1728.



Anne Veller Friis Nielsen

Phone: +45 4525 6892
E-mail: avfn@kt.dtu.dk

Supervisors: Anne S. Meyer
Anis Arnous

PhD Study
Started: September 2012
To be completed: September 2015

Phytate and Phytase Enzyme Kinetics

Abstract

Phytase enzymes are widely used in modern agriculture as an additive to feed of non-ruminant animals, e.g. swine and poultry. The natural substrate of phytases is phytate, which is present in high levels in various plant-based foods, where it binds macro- and micronutrients, notably phosphate, making the nutrients unavailable for absorption by the animals. Upon *in vivo* phytase-catalysed hydrolysis of phytate, these nutrients can be released, leading to increased growth of the animals. However, phytase kinetics is highly dependent on substrates and reaction conditions, making kinetic investigations of genuine substrates at physiologically relevant conditions an important issue.

Introduction

Phytase enzymes (EC 3.1.3.26 and EC 3.1.3.8) are widely used in modern agriculture as an additive to feed for non-ruminant animals (mainly swine and poultry) as a substitution for or supplement to the added inorganic phosphorous, which increase growth (weight gain per kg of feed) of the animals. Extra supply of phosphate is required in monogastric animals due to their inherent inability to utilise the phosphorous in the form that is present in plant-based feed. Together with the increasingly limited availability of phosphorous globally and thus the rising prices of inorganic phosphorous, as well as a pressure to limit the release of phosphate in the manure from animals leading to phosphate runoff, the use of phytases has become feasible in feed applications.

Phytate

50-85 % of the plant phosphorous content is stored in globoids present in the aleurone layer of the grain (wheat and barley). These globoids consist by weight of 40 % phytate (salt of phytic acid), 46 % proteins, 8 % phosphorous in addition to stored minerals and water [1].

The phytate molecule consists of a myo-inositol ring (six carbon ring with an alcohol group on each carbon)

that has been esterified on each alcohol group with a phosphate group; see structure (acid form) in Figure 1.

Most of the phosphate groups are negatively charged at physiologically relevant pH values, thus accounting for the ionic interactions between phytate and proteins in the previously mentioned globoids. These negative charges also account for the ability of phytate to chelate other nutrients, e.g. carbohydrates, lipids and minerals [2].

All these nutrients (in feed, primarily phosphate) can be released upon phytate hydrolysis, where phosphate ions are cleaved off from the inositol ring. This hydrolysis can be catalysed by phytases.

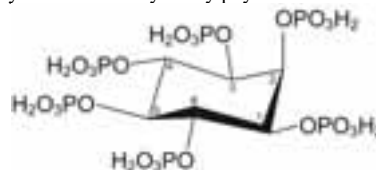


Figure 1: Chemical structure of phytic acid.

Phytases and phytase kinetics

Phytase-catalysed hydrolysis of phytate from feed releases inorganic phosphate and lower inositol phosphates as well as chelated nutrients.

Phytases can generally be classified according to catalytic mechanism, pH profile and/or the order of which they release the different phosphate groups during hydrolysis of phytate. The two most common classes in the last-mentioned group are 3-phytases and 6-phytases, the number indicating the number of the carbon atom in the inositol ring at which dephosphorylation is initiated. After release of the first phosphate ion, the enzyme proceeds in a counterclockwise direction by hydrolysing the following phosphate ester bonds, until it reaches the axially positioned phosphate group (on the C2 of the inositol ring, see Figure 1), towards which the phytases generally have low affinity. Therefore, complete dephosphorylation is rarely observed and a mix of lower inositol phosphates will often be the product of enzymatic phytate hydrolysis. This means that phytase kinetics is not simple to evaluate due to the ambiguous roles of inositol phosphates as both products and substrates of the phytase. When measuring phytase activity in practice, a colorimetric determination of inorganic phosphate is often used as this is fairly fast and simple (e.g. [3], [4]). This method, however, does not give a very detailed picture of the actual mechanism of phytase action and other methods including chromatographic separation followed by quantification of the lower inositol phosphates are therefore sometimes employed.

Phytase substrates

Another important issue related to the evaluation of phytase kinetics is the choice of substrate. In most cases, the chemically pure phytate salt (often sodium phytate) is used for kinetics evaluations as opposed to phytate from genuine substrates, where it is bound in the previously mentioned protein globoids. Bohn et al. demonstrated a significant difference in kinetic parameters of wheat phytase when using these forms of phytic acid, possibly indicating the globoids are less accessible as substrate resulting in a lower degree of dephosphorylation [1]. Tang et al. showed that phytases from wheat, *Aspergillus ficuum* and *Bacillus subtilis* were unable to catalyse the hydrolysis of e.g. aluminium and iron phytate salts, but on the other hand readily catalysed the hydrolysis of e.g. magnesium and calcium phytate salts [5]. Both of these studies show the importance of deriving the relevant phytase kinetics on genuine substrates and that the choice of substrate has a great impact on the result of the evaluation. pH is generally a great factor in determining the activity of different enzymes, but for phytases the pH can have an additional influence on the observed rates of catalysis due to decreased stability of phytate complexes at low pH values. This means that hydrolysis is more favourable in these conditions, as the phytase has easier access to the phosphate ester bonds, when the phytic acid is soluble and uncharged.

Phytase stability

When phytases are used in animal feed, the catalysis primarily occurs in the gastric ventricle of the animals, where the phytate complex as mentioned above is more susceptible to hydrolysis due to increased solubility and uncharged status at the low pH. However, this hostile environment poses a whole new set of challenges for the phytases as they need to be robust both with regard to pH and the digestive enzymes present in the gastric environment, primarily the protease pepsin. Commercial phytases for feed applications are primarily derived from microorganisms (both fungi and bacteria), generally have relatively high activities at the gastric pH (refer to Table 1) and many have also been selected for their proteolytic stability.

Table 1: Different commercially available phytases, their origin and pH optima.

Product name	Phytase origin	pH opt.
Ronozyme NP	<i>Peniphora lycii</i>	4.5 [6]
OptiPhos	<i>Eschericia coli</i>	2.5-5.5 [6]
Natuphos	<i>Aspergillus ficuum</i>	2 & 5.5 [6]
Phyzyme XP	<i>Eschericia coli</i>	2.5-5.5 [6]
Ronozyme HiPhos	<i>Citrobacter braakii</i>	3-4.5 [7]
Wheat phytase	Wheat bran	5.5 [7]

Conclusions

As described, phytase kinetics among other factors is highly dependent on the phytase origin, the pH of the solution and the specific substrate form used for kinetics evaluation. Therefore, different combinations of these parameters will be tested in order to evaluate the performance of different phytases for hydrolysis of phytate from genuine plant substrates.

References

1. L. Bohn, L. Josefsen, A. S. Meyer, S. K. Rasmussen, J. Agric. Food Chem. (55) (2007) 7547–7552.
2. K. Zyla, D. R. Ledoux, T. L. Veum, J. Agric. Food Chem. (43) (1995) 288–294.
3. A. J. Engelen, F. C. van der Heeft, P. H. G. Randsdorp, E. L. C. Smit, J. AOAC Int. (77) (1994) 760–764.
4. J. K. Heinonen, R. J. Lahti, Anal. Biochem. (113) (1981) 313–317.
5. J. Tang, A. Leung, C. Leung, B. L. Lim, Soil Biol. Biochem. (38) (2006) 1316–1324.
6. T. T. Tran, R. Hatti-Kaul, S. Dalsgaard, S. Yu, Anal. Biochem. (410) (2011) 177–84.
7. S. M. Brejnholt, G. Dionisio, V. Glitsoe, L. K. Skov, H. Brinch-Pedersen, J. Sci. Food Agric. (91) (2011) 1398–1405.



Mads Møller Nielsen

Phone: +45 4525 6819
E-mail: mon@kt.dtu.dk

Supervisors: Søren Hvilsted
Katja Jankova

PhD Study
Started: Marts 2010
To be completed: February 2013

Hydrocarbon Architectures for Fuel Cell Membranes

Abstract

An array of non-fluorous macromolecular architectures is prepared from analogous polysulfone-based macroinitiators. Graft copolymers are synthesized by atom transfer radical polymerization (ATRP) of styrene from a modified polysulfone (PSU). The polystyrene is sulfonated and membranes prepared by solvent casting. The macroinitiator is also azide-functionalized so that it can be used for the introduction of non-polymeric, linear and branched side chains by “click” chemistry. Membranes of these are evaluated by fundamental membrane properties like ion exchange capacity, water uptake, and proton conductivity in order to determine their potential as proton exchange membranes (PEM) for fuel cells (FC). The main objective is however to show how relatively few handles and the same chemical strategy can be used to obtain diverse polymeric compounds. These handles comprise the graft site density, nature of side chains, length of grafts and choice of protogenic group.

Introduction

Countries generating excess electricity outside the peak hours, e.g. by wind power, can use the excess electricity to run electrolysis of water. Thereby energy is stored as hydrogen that can be used in fuel cells in the automotive industry as an alternative to gasoline and the internal combustion engine. Besides, proton exchange membrane fuel cell (PEMFC) vehicles show great potential through factors such as local zero pollution, reduced cost to the formation of the fuel and the fact that they are not restricted by the Carnot cycle.

Fuel cells have been commercialized for several years now, and the number of units shipped has increased tremendously with PEMFCs topping the list [1]. PEMFCs have found widespread use as portable, stationary and transport related power generators as they can provide anything from single watts up to kilowatts. Figure 1 illustrates how hydrogen and oxygen via an electrochemical process are turned into electrical energy with water as sole byproduct over a proton conducting polymer membrane, the PEM.

General requirements to PEMs are that they must be chemically, thermally and mechanically stable, they must have low gas permeability and should show moderate water sorption behavior. Current commercial PEMs are perfluorosulfonic acids (PFSA), where a fluorous hydrophobic backbone contributes to the chemical and mechanical stability of the membrane, and tethered sulfonic acid groups contribute to the proton conductivity (phosphonic acid is typically chosen when the operating temperature is above the boiling point of water). Figure 2 shows an illustration of how proton

conduction occurs through ion rich water channels [2]. Despite good overall properties, PFSA suffer from limitations when it comes to the gas permeability and performance at temperatures above 80 °C – besides being rather expensive to produce. Hence extensive research is carried out on finding viable alternatives for future generations of PEMs.

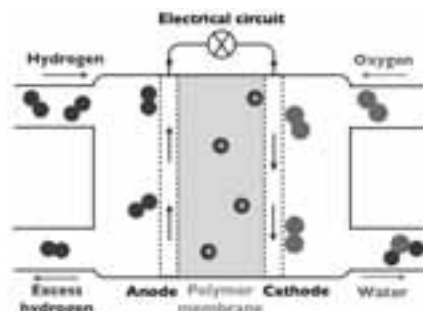


Figure 1: Simplified illustration of a PEMFC. The electrodes contain a gas diffusion layer and the catalyst.

Alternatives to PFSA are many, from phosphonic acid functionalized polybenzimidazoles [3], when the PEMFC is operated at higher temperatures, over low temperature solutions based on sulfonic acid functionalized block copolymers [4], graft copolymers [5] and polyarylene ethers [6].

The present work is centered on hydrocarbon-based compounds where various side chains are attached to the same backbone: a commercially available PSU,

Udel[®] (see Figure 3). The synthetic strategy is to chemically modify the PSU to contain a chloromethyl group so that 1) the atom transfer radical polymerization (ATRP) [7] macroinitiator can be used as starting point for graft copolymer structures, or 2) the chlorine is substituted with an azide by which copper-catalyzed azide-alkyne 1,3-cycloaddition (CuAAC, or “click” chemistry) [8,9] can be performed. By this approach pre-synthesized (sulfonated or unsulfonated) alkyne-terminated compounds can be attached. These compounds include polymers [9], sulfonated linear molecules of various lengths and aliphatic dendrons [10]. Especially the selection of potential synthetic routes is a strong asset as PEM polymers are amphiphilic by nature, which often complicates solubility dependent synthetic steps. Membrane properties are included for the structures with short linear or branched side chains relative to benchmark membrane Nafion[®] 212, a membrane of roughly similar thickness as the produced hydrocarbon membranes.

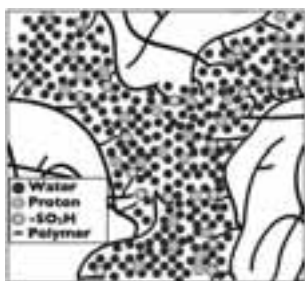


Figure 2: Proton conduction takes place through ionic water channels by various mechanisms.

Important membrane properties are the ion exchange capacity (IEC) [mmol/g], a measure for the ionic concentration in the dry membrane, which for the non-polymeric side chains is calculated from ¹H NMR according to Equation 1. DP_{PSU} is the degree of polymerization of the PSU backbone, DS is the degree of sulfonation, f is the functionality (1 or 2 in this case) and \overline{M}_n (incl. $-SO_3H$) is the number average molecular weight of the end product determined by gel permeation chromatography.

$$IEC = \frac{DP_{PSU} \times DS \times f}{\overline{M}_n \text{ (incl. } -SO_3H)} \times 1000 \quad (1)$$

The second fuel cell key property that is investigated here is water uptake (wt%), a measure for the amount of water in the wet membrane, as shown in Equation 2. m_{wet} is the weight of the wet membrane and m_{dry} is the weight of the dry membrane.

$$\text{water uptake} = \frac{m_{wet} - m_{dry}}{m_{dry}} \times 100 \quad (2)$$

The third property is proton conductivity (σ), which is measured by use of a bench with two electrodes, a DC power supply and two multimeters. Here I is the current, l is the distance between the two electrodes, U is the voltage and A is the area of the cross-section of the membrane.

$$\sigma = \frac{I \cdot l}{U \cdot A} \quad (3)$$

Specific objectives

The red line of the project is the layout of synthetic strategies that are used in the creation of new macromolecular architectures in the context of PEMs. This is done through lab-scale syntheses, conventional characterization and basic testing of membrane properties, e.g. ion exchange capacity (IEC), water sorption and proton conductivity.

Results and discussion

The synthetic pathway from PSU to PEM candidate synthesized by ATRP is shown in Figure 3.

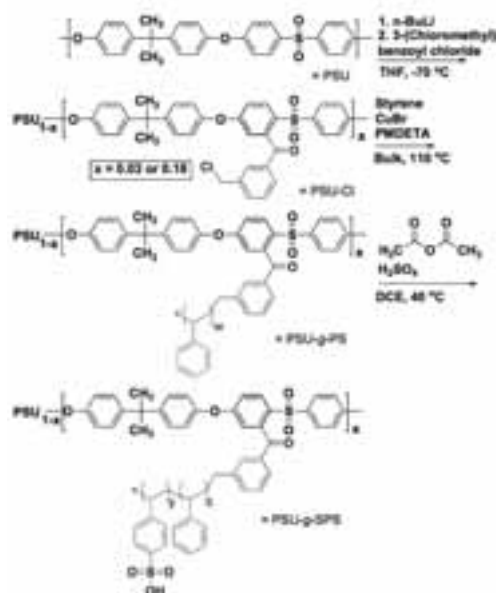


Figure 3: Synthetic pathway from PSU over the PSU-Cl macroinitiator for ATRP and finally to graft copolymers with sulfonated moieties.

The *ortho* position to the O=S=O group of PSU is lithiated upon which the lithiated sites are quenched with the electrophile 3-(chloromethyl)benzoyl chloride in obtaining the macroinitiator, PSU-Cl. Various graft site densities (GD) are produced. For the purpose of grafting from, GDs utilized are 3% and 18%, whereas those applied for the purpose of “clicking” side chains onto azide functionalized PSU, are 18%, 25%, 54% and 67%. Lower GDs are used for the grafts than for the

non-polymeric side chains, in order to obtain a more beneficial ionic-to-hydrophobic content. The more ionic groups introduced as side chains, the fewer there should be. Styrene is grafted from **PSU-CI** to 47 repeat units per chain (DP_{PS}) at $GD = 3\%$ and $DP_{PS} = 10$ at $GD = 18\%$. Sulfonation is done with acetyl sulfate, which is prepared by mixing acetic anhydride with concentrated sulfuric acid. Characterization is performed by use of gel permeation chromatography (GPC), Fourier transform infrared spectroscopy (FTIR) and proton nuclear magnetic resonance (1H NMR).

Azide functionalization was obtained by stirring **PSU-CI** in *N,N*-dimethylformamide (DMF) with NaN_3 overnight. 1H NMR spectra of PSU, **PSU-CI** and **PSU-N₃** are shown in Figure 4.

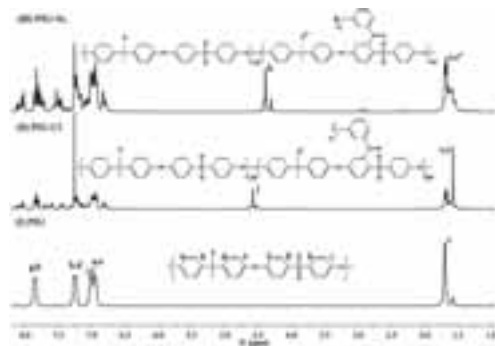


Figure 4: 1H NMR spectra of I) PSU, II) **PSU-CI** and III) the azide functionalized PSU, **PSU-N₃**.

The “click” reaction between pre-sulfonated alkyne-functionalized molecules was verified with 1H NMR and FTIR. Figure 5 shows FTIR spectra of PSU, **PSU-N₃** and the non-polymeric side chain systems.

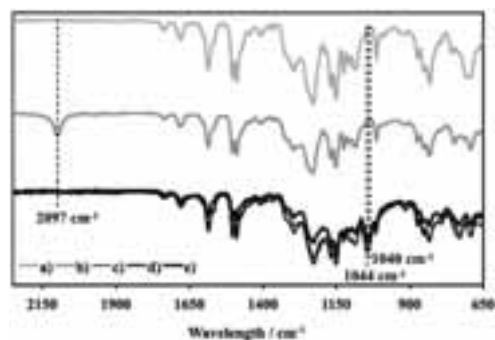


Figure 5: IR spectra of a) **PSU-CI**, b) **PSU-N₃**, c) **PSU-1fS**, d) **PSU-1fL** and e) **PSU-2f**.

Various “click” products are shown in Figure 6, the non-polymeric linear side chain structures **PSU-1fS** (the shortest side chain) and **PSU-1fL** (the longest side chain) and the bisulfonated dendronised structure **PSU-2f**. The graft structure **PSU-g-PFS** [9] is an example of parallel work going on in our group on phosphonated

partially fluorinated compounds, introduced to illustrate the diversity in the architectures that can be synthesized by following the same chemical strategy.

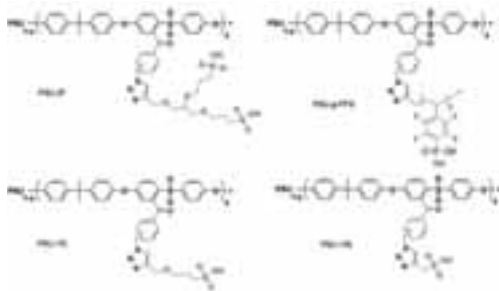


Figure 6: “Click” products synthesized.

In elucidating their potential as PEM candidates water uptake and proton conductivity of the non-polymeric architectures are registered. Figure 7A shows how **PSU-1fS** and **PSU-1fL** in the IEC-range of 0.47-1.06 mmol/g do not exceed 2 mS/cm. Within a similar IEC-interval, **PSU-2f** shows conductivities from 12 to 62 mS/cm. There is a kink in the curve from IEC = 0.74 mmol/g to 0.84 mmol/g at which both water uptake (Figure 7B) and conductivity increase remarkably. The reason is believed to be the resulting structural changes that lead to increased percolating of the water system and hence easier proton migration. N212 is included for the sake of comparison with a benchmark PFSA.

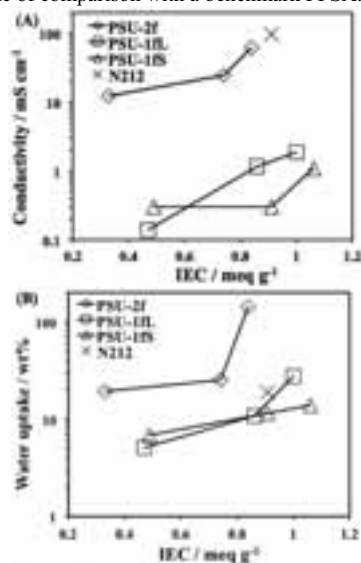


Figure 7: IEC plotted against (A) proton conductivity and (B) water uptake for **PSU-1fS**, **PSU-1fL**, **PSU-2f** and Nafion[®] 212 (N212).

The water uptake of N212 is in the order of the linear side chains that show low conductivity and the

conductivity of N212 is in the order of the dendronised structure, which takes up much more water.

Even though such a direct comparison between the hydrocarbon membranes and a commercial benchmark membrane appears to disfavor the presented hydrocarbon membranes, what is important to remember is that all PSU structures have undergone no further investigations that are believed to elucidate the exact behavior of the systems when changing parameters like GD, the investigation of higher generation dendrons of higher density of sulfonic acid groups. Besides, the membranes have not been attempted optimized. However, what has been investigated is a selection of widely different architectures that exhibit completely different membrane performances. Increasing the local concentration of sulfonic acid groups clearly has a tremendous influence.

Investigations are ongoing on the influence of DG and DP_{PS} of **PSU-g-SPS**. A motivating factor is the observation from PSU-g-PFS, which show how increasing water uptake and conductivity follow increasing IEC (by increasing chain length) [9].

Conclusions

An extensive array of PSU-based macromolecular structures is prepared by use of ATRP and “click” chemistry. The short side chain compounds **PSU-1fS** and **PSU-1fL** show low water uptakes and proton conductivity, which suggests that the ionic contents are probably too low. Higher IEC values are obtainable by increasing the DG. The dendronised structure **PSU-2f** shows a tremendous increase in both water uptake and proton conductivity from IEC = 0.74 mmol/g to 0.84 mmol/g. The assumed improvement in water percolation warrants further investigations of analogous dendronised systems. Homogenous membranes of the graft copolymer structure **PSU-g-SPS** are prepared by solvent casting at elevated temperatures. These will be investigated further in future. Overall, the combination of good film forming properties of PSU and the variety in macromolecular architectures that can be obtained by tuning a relatively small number of parameters is promising. Should they turn out to be imperfect candidates for PEMs – partly due to the model study aspect of the molecular design – they could be interesting applicants on other areas where selective membranes are needed, e.g. water purification.

Acknowledgements

S. Takamuku (LU), I. Dimitrov and I. Javakhishvili (both DTU) are acknowledged for their collaboration. Danish Council for Strategic Research funded the work through contract 09-065198.

References

1. D. Carter, M. Ryan, J. Wing, Fuel Cell Industry Review 2012, www.fuelcelltoday.com, 28.11.12.
2. K. D. Kreuer, J. Membr. Sci. 185 (2001) 29-39.

3. Q. Li, J. O. Jensen, R. F. Savinell, N. J. Bjerrum, Prog. Polym. Sci. 34 (2009) 449-477.
4. Y. A. Elabd, M. A. Hickner, Macromolecules 44 (1) (2011) 1-11.
5. E. M. W. Tsang, Z. Zhang, A. C. C. Yang, Z. Shi, T. J. Peckham, R. Narimani, B. J. Frisken, S. Holdcroft, Macromolecules 42 (24) (2009) 9467-9480.
6. C. H. Park, C. H. Lee, M. D. Guiver, Y. M. Lee, Prog. Polym Sci 36 (2011) 1443-1498.
7. K. Matyjaszewski, J. Xia, Chem. Rev. 101 (9) (2001) 2921-2990.
8. S. Hvilsted, Polym. Int. 61 (4) (2012) 485-494.
9. I. Dimitrov, S. Takamuku, K. Jankova, P. Jannasch, S. Hvilsted, Macromol. Rapid Commun. 33 (16) (2012) 1368-1374.
10. M. M. Nielsen, I. Dimitrov, S. Takamuku, P. Jannasch, K. Jankova, S. Hvilsted, submitted (2012).



Kristian Petersen Nørgaard

Phone: +45 4525 2843
E-mail: kpno@kt.dtu.dk

Supervisors: Søren Kiil
Kim Dam-Johansen
Pere Català, Hempel A/S

PhD Study

Started: January 2011
To be completed: December 2013

Design and Testing of Robust and Efficient Intumescent Coatings

Abstract

Fire protective intumescent coatings swell when exposed to heat, i.e. a fire. The swelled coating forms a thermally insulating porous char, which protects the substrate from the heat. In buildings with load bearing steel constructions, this is especially important, due to a reduced strength of the steel at temperatures around 400 to 550 °C. The swelling of the coating happens according to a complex sequence which involves, not only the coating, but also the surroundings. Therefore, the focus of this project is mainly on effects of changes in outer parameters. In this yearbook contribution, the newest published results on shock heating and char characterization are presented.

Introductions

In the event of a fire, intumescent fire protective coatings swell to an insulating char. Like other coating systems, development of intumescent coatings requires considerations of the coating life time, the architectural properties and the compatibility with other coatings. In addition to these parameters, the significant risks to human life and assets have led to demanding third party approval requirements. These requirements pose an increased challenge to the formulators of intumescent coatings. Therefore, fast screening tests and understanding of mechanisms is a focus area of the intumescent coatings researchers [1,2]. A potentially promising principle of fast screening tests is the use of shock heating and cooling. This is important in the hydrocarbon fires, where explosion like fires occur with high pressure jet flames. However, for so-called cellulosic fires, the interest in shock heating may not be limited to fast development tests, but also special cases where unreacted char is exposed to the high temperature of fire. One such case could be a crack in the char. This situation is illustrated in figure 1. An aspect of shock heating and fast screening tests is the char characterization. In this project, chars have been studied according to the mechanical resistance against compression. In literature, previous studies of mechanical stability has especially been studied by a Russian research group [3,4,5] studying aspects of mechanical stability of intumescent chars.

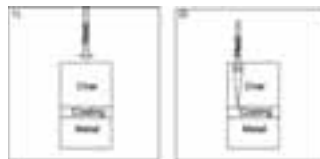


Figure 1: Illustrative drawing of cracking char

Experimental

A generic acrylic intumescent coating was used. Free films were prepared by draw down with a CoatMaster 509 MC from Erichsen. The substrate was overhead transparencies from Erhvervs-skolernes forlag. The dry film thickness was measured to be 147 µm, and circular samples with a diameter of 14 mm were cut with a metal template. Samples were placed in two sizes of cylindrical alsint crucibles from W. Haldenwagner. The large crucibles had a height of 40 mm and 26 mm, respectively. The small crucibles had height and diameter of 30 mm and 16 mm, respectively. Shock heating is obtained by insertion of the samples into a preheated muffle oven (Nabertherm LVT 5/11/180). After insertion of the sample into the oven, the temperature increases from 900 °C to 1100 °C in 300 seconds. Following the fast heating a TA XT plus – Texture analyzer from Stable Microsystems was used to measure the maximum vertical expansion and the work necessary to compress the samples after heating. A cylindrical piston with a diameter of (2 mm) was set to move at a constant speed of 0.1 mm/s and 500 data

points were recorded per second. The principle of the texture analyzer is shown in figure 2. The distances can be measured and used to calculate the height of the char. A strain gauge load cell records the force exerted by the sample.

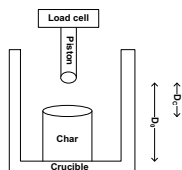


Figure 2: Drawing of Texture Analyzer. D_0 and D_C are the distance to crucible and char.

To investigate if the storage of the char affected the properties, tests where the samples were moved to a desiccator after heating and until compression were made.

Selected results and discussion

In Nørgaard et al. [6] the work of destruction, in mJ, to reach 90% (W_{90}) through the char was studied. An interesting finding was that storage of the char in a desiccator decreased the standard deviation of W_{90} . Initially three repetitions were made but following the result evaluation, repetitions with air storage was increased without this changing the standard deviation. Figure 3 shows the standard deviations, for experiments performed in large and small crucibles. This finding may be important for evaluation of char properties after heating. Other properties such as expansion were not affected by the storage in desiccator.

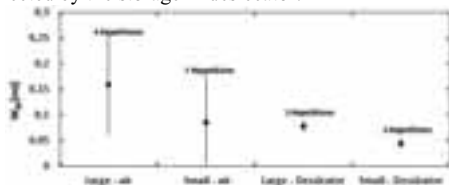


Figure 3: W_{90} in mJ. The samples are $147\mu\text{m}$. Standard deviations and number of repetitions are shown.

Another finding from Nørgaard et al. [6] is that the dimensionless force profile through the char follows the same pattern after shock heating for the samples. The force profile is large at the outer layer, then there is a zone with lower resistance and after approximately 90% of the distance the force increases steeply due to debris material. The dimensionless force is the measured force at a given position divided by the maximum measured force. The length fraction is the fraction of the distance.

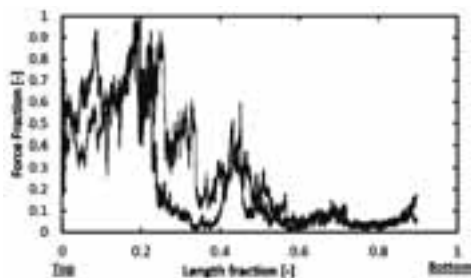


Figure 4: Dimensionless force curve. The curves show the force behavior 2 measurements. After [6].

Conclusive remarks

The method of shock heating and evaluation of chars, provide a potentially useful method to evaluate the chars. However, the method has yet to be calibrated with test results from test furnaces to know the full potential as screening test. Considerations regarding post heating storage of the chars are important for the resistance against compression. The force profile is also seen to follow a certain behavior in dimensionless form.

Acknowledgments

Financial support by the Hempel Foundation is gratefully acknowledged.

References

1. M. Jimenez, S. Duquesne, S. Bourbigot, *Ind. Eng. Chem. Res.* 45 (2006) 4500-4508.
2. M. Jimenez, S. Duquesne, S. Bourbigot, *Ind. Eng. Chem. Res.* 45 (2006) 7475-7481.
3. I.S. Reshetnikov, M.y. Yablokova, E.V. Potapova, N.A. Khalturinskij, V. Y. Chernyh, L.N., *J. Appl. Polym. Sci.* 67 (1998) 1827-1830.
4. A.A. Berlin, N.A. Khalturinskij, I.S. Reshetnikov, M.Y. Yablokova, in: M. Le Bras, G. Camina, S. Bourbigot, R. Delobel (Eds.), *Fire Retardancy of Polymer: The Use of Intumescence*, Cambridge: The royal Society of Chemistry, 1998.
5. I.S. Reshetnikov, A.N. Garashchenko, V.L. Strakhov, *Polym. Adv. Technol.* 11 (2000) 392-397.
6. K.P. Nørgaard, K. Dam-Johansen, P. Català, S. Kiil, *Progress in Organic Coatings* (accepted-07/2012)

List of Publications

K.P. Nørgaard, K. Dam-Johansen, P. Català, S. Kiil, *Progress in Organic Coatings* (accepted-07/2012)

K.P. Nørgaard, K. Dam-Johansen, P. Català, S. Kiil, *European Coatings Journal* 06/2012. (Also translated to publication in *Russian Coatings Journal*).

Presentation at "European Coatings conference – Fire retardant coatings", Berlin, 13th and 14th of March 2012.

Poster presentation at 8th COSI conference, Noordwijk, 25th to 26th of June 2012.



Brian Kjærgaard Olsen

Phone: +45 4525 2830
 E-mail: bria@kt.dtu.dk

Supervisors: Anker Degn Jensen
 Francesco Castellino, Haldor Topsøe A/S

PhD Study
 Started: June 2011
 To be completed: June 2014

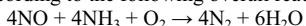
Deactivation of Selective Catalytic Reduction Catalysts in Biomass Fired Power Plants

Abstract

Selective catalytic reduction of nitrogen oxides by ammonia over vanadia based catalysts has proved to be an effective method for reducing the emissions from stationary, coal fired sources. However, during firing of biomass accelerated deactivation of these catalysts has been observed. This is due to the release of alkali elements, such as potassium, which can react with acidic sites on the catalyst. In order to obtain a more in-depth understanding of the deactivation mechanism, a systematic study on the relationship between acidic sites and the alkali uptake has been commenced.

Introduction

Selective catalytic reduction (SCR) of nitrogen oxides (NO_x) with ammonia (NH₃) is a well established method for controlling the NO_x emissions from stationary sources such as coal fired heat and power plants [1,2]. In the presence of oxygen (O₂), nitrogen oxide (NO) is catalytically converted into molecular nitrogen (N₂) according to the following overall reaction [1]:



The most widely used catalysts for stationary applications consists of titania (TiO₂) supported vanadia (V₂O₅), promoted with either tungsten oxide (WO₃) or molybdenum oxide (MoO₃), in the shape of honeycomb monoliths [2].

Topsøe *et al.* [3-5] proposed a widely accepted mechanism for the SCR reaction over V₂O₅ based catalysts. The mechanism, which is schematized in Figure 1, consists of two catalytic cycles, each of which involves a type of active site – the so called Brønsted acid sites (V⁵⁺-OH) and the redox sites (V⁵⁺=O).

In a time with great focus on the release of carbon dioxide (CO₂), firing (or co-firing) of biomass (straw, wood chips etc.) and waste products such as sewage sludge and municipal waste, is being applied in order to reduce the net CO₂ emissions.

Unfortunately, the industrially applied SCR catalysts have a significantly reduced life-time when used in connection with such fuels. The shortened duration of the catalysts is due to an accelerated deactivation by a high amount of poisonous components in the fuels. Alkali and alkaline earth metals, which can be present in

biomass in high concentrations, are examples of components that can severely deactivate commercial SCR catalysts [6].

Potassium, released e.g. during firing of straw, may reach the SCR catalyst in the form of aerosols of potassium chloride (KCl) or potassium sulfate (K₂SO₄) which deposit on the catalyst surface and diffuse into the pore system [7]. It is believed that potassium, due to its alkaline nature, poisons the SCR catalyst by reacting with the acidic V⁵⁺-OH sites [8,9]. Research has furthermore shown that the reducibility of V⁵⁺ species is inhibited upon alkali poisoning [10].

While the effect of alkali metal on commercial SCR catalysts is generally understood, a more systematic study of the deactivation mechanism has yet to be performed. Such a study will provide useful information during development of new alkali resistant catalysts and/or improved means of operation.

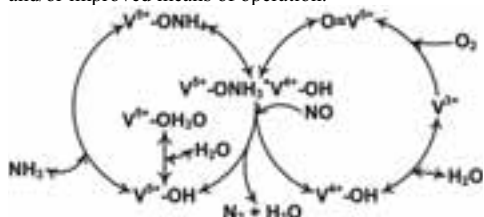


Figure 1: The proposed mechanism for the reduction of NO by NH₃ over V₂O₅ based catalysts. Adapted from [5].

Specific Objectives

The main objective of this PhD study is to investigate the influence of catalyst composition on the rate of deactivation during alkali poisoning. It is particularly of interest to study the relationship between surface -OH sites and the rate of alkali penetration.

Results and Discussion

A series of plate shaped SCR catalyst, supplied by Haldor Topsøe A/S, have been exposed to a KCl aerosol for 600 hours in a bench scale SCR reactor at 350 °C. The catalysts were based on fiber reinforced TiO₂ impregnated with V₂O₅ to various levels (0-9 wt.%). Some of the plates were doped with WO₃ as well.

The aerosol was created by injecting an aqueous solution of KCl, through a two fluid nozzle, into the hot flue gas from a natural gas burner. Cooling of the gas resulted in the nucleation of fine KCl particles which were carried by the flue gas to the catalyst section. A schematic overview of the SCR exposure pilot is presented in Figure 2.

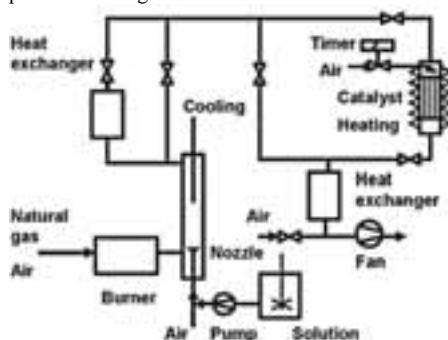


Figure 2: Schematic drawing of the SCR exposure pilot. Adapted from [9].

The activity of the exposed catalysts will be measured and compared to that of fresh ones in order to quantify the poison resistance as a function of composition. To assess the mobility of potassium at the given exposure temperature, the potassium concentration through the thickness of the catalyst plates will be measured by scanning electron microscopy in combination with energy dispersive X-ray spectroscopy (SEM-EDX).

A study on how the concentration and injection rate of KCl solutions affect the resulting aerosol has been performed. Three different KCl solutions (3.7, 7.4 and 22.2 g/L) and different injection rates (420, 210 and 140 mL/h) were used. The respective number based aerosol size distribution was measured by a scanning mobility particle sizer (SMPS). Volume based size distributions, calculated from the SMPS measurements, are presented in Figure 3. From the figure it can be seen that doubling the amount of entrained KCl, in one case, doubles the total volume of particles, as one might expect. This, however, does not appear to be true when using a solution of a high KCl concentration and a low injection rates (e.g. 22.2 g/L at 140 mL/h). The reason for this

might be due to formation of larger particles which lie outside the measuring range of the SMPS.

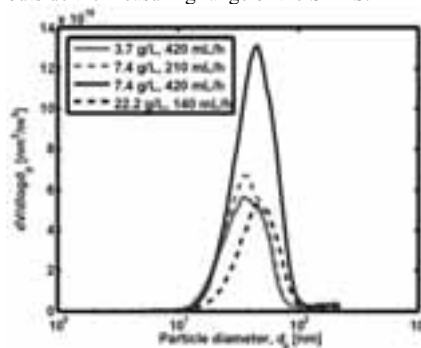


Figure 3: Volume based particle size distributions. Calculated from SMPS data.

A model describing the SCR reaction through a single monolith channel is being developed. At the moment of writing the model can describe the steady-state concentrations of NO and NH₃ along the channel as well as through the catalyst wall. The ultimate goal is to be able to describe the transient concentration profiles of reacting species as well as of potassium during potassium poisoning.

Conclusion

V₂O₅ based SCR catalysts are widely used for limiting NO_x emissions from e.g. coal fired power plants. Alkali metals released during combustion of biomass have proved to severely shorten the lifetime of these catalysts, thus it is of interest to conduct a thorough study on the deactivation mechanism.

Acknowledgements

This PhD project is a part of the GREEN Research Center for Power Generation from Renewable Energy) financed by the Danish Council for Strategic Research.

References

1. H. Bosch, F. Janssen, *Catal. Today* 2 (1988), 369-532
2. P. Forzatti, *Appl. Catal. A* 222 (2001), 221-236
3. N.-Y. Topsøe, *Science* 256 (1994), 1217-1219
4. N.-Y. Topsøe, J.A. Dumesic, H. Topsøe, *J. Catal.* 151 (1995), 241-252
5. J.A. Dumesic, N.-Y. Topsøe, H. Topsøe, Y. Chen, T. Slabiak, *J. Catal.* 163 (1996), 409-417
6. Y. Zheng, A.D. Jensen, J.E. Johnsson, *Ind. Eng. Chem. Res.* 43 (2004), 941-947
7. Y. Zheng, A.D. Jensen, J.E. Johnsson, *Appl. Catal. B* 60 (2005), 253-264
8. J.P. Chen, R.T. Yang, *J. Catal.* 125 (1990), 411-420
9. Y. Zheng, A.D. Jensen, J.E. Johnsson, J.R. Thøgersen, *Appl. Catal.* 83 (2008), 186-194
10. L. Chen, J. Li, M. Ge, *Chem. Eng. J.* 170 (2011), 531-537



Sharat Kumar Pathi

Phone: +45 4525 2923
 E-mail: skp@kt.dtu.dk

Supervisors: Kim Dam-Johansen
 Jytte Boll Illerup
 Weigang Lin
 Klaus Hjuler, FLSmidth A/S

PhD Study
 Started: January 2010
 To be completed: December 2012

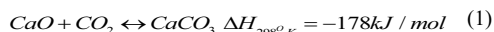
CO₂ Capture from Cement Production by Carbonate Looping

Abstract

The carbonate looping process is a promising technology for CO₂ emission reduction, which may be particularly suitable for the cement industry as calcined raw meal could be efficient for CO₂ capture. A process model was developed to study the integration of carbonate looping at a cement plant using raw meal as sorbent. Carbonate looping experiments were carried out using fluidized bed reactor and TGA equipment. The results from experiments at mild calcination conditions showed similar carbon capture capacity for both limestone and a clay/limestone mixture used to simulate raw meal as sorbent. However, at realistic calcination conditions large differences in the carbon capture capacity of limestone and simulated raw meals were observed, dependent on temperature, CO₂ concentration and sorbent composition. A correlation was observed between the surface area of the sorbent and the carbon capture capacity. Apparently the bed inventory has no significant effect on the performance of the carbonator, whereas the optimal carbonation temperature and inlet calcium to carbon ratio were dependent on the fraction of active sorbent. The experimental results were used to develop a steady state carbonator model, which can be used for optimization of the carbonate looping process.

Introduction

According to Intergovernmental Panel on Climate Change, carbon capture from large stationary sources is considered as the mid-term mitigating option for climate change [1]. Cement industry is one of the major sources of CO₂, which emits CO₂ both from combustion of fuel and calcination of limestone. One of the promising technologies for carbon capture is the carbonate looping process, where the main reaction is the reversible calcination of limestone,



Limestone is the major ingredient in the raw meal for cement clinker production. Application of raw meal as sorbent for carbon capture might be relatively easy to integrate with the cement plant. Most studies of the carbonate looping process have focused on applying various natural occurring limestone as sorbent, for which similar decay profiles have been found. However, no studies have been realized so far on applying cement raw meal as sorbent for carbon capture, a concept that probably may be affected by the interaction between major clinker forming compounds. A schematic representation of the integration of carbonate looping with the cement plant is shown in Figure 1.

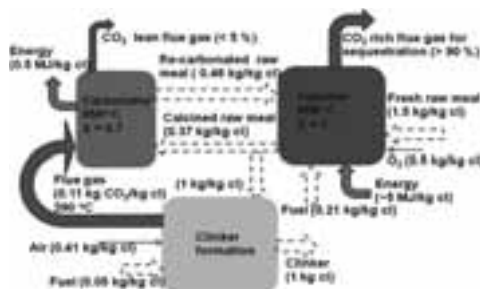


Figure 1: Schematic representation of mass and energy balance for de-carbonization of cement plant using raw meal as sorbent [2]. “cl” means “clinker”

Specific objectives

The objective of this project is to investigate the application of raw meal as sorbent for carbon dioxide capture from the calcinations of raw meal and the cement kiln. In order to achieve the objective, the work is divided into experimental part and modeling part:

Experimental work:

1. Investigate application of raw meal as sorbent for carbon capture and understand the decay mechanism of limestone in raw meal.
2. Re-carbonation behavior in the fluidized bed reactor at different operating conditions.

Modeling work:

1. Process modeling of carbonate looping process integrated with the cement process. This model could be used for optimization of the carbonate looping process and for investigating the influence of important parameters
2. Reactor modeling to investigate the performance of a fluidized bed reactor as carbonator.

Experimental

The experiments were conducted in setups of different scale: 1) Thermo gravimetric analyzer (TGA) for simulating looping conditions; 2) Tubular furnace for sorbent sintering studies, and 3) Fluidized bed reactor for investigating reactor performance (Figure 2).

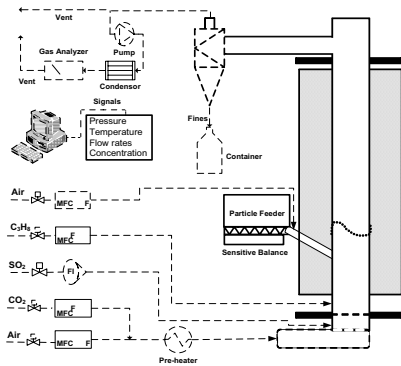


Figure 2: Schematic representation of the fluidized bed reactor experimental setup.

Looping cycle experiments

Experiments were performed in the fluidized bed reactor using a mixture of 30 % (w/w) clay in limestone (termed simulated raw meal) to simulate the behavior of raw meal as sorbent.

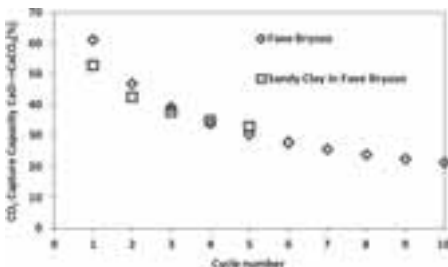


Figure 3: Comparison of CO₂ capture capacity of limestone and simulated raw meal (clay with limestone), calcined in fluidized bed reactor at 850°C in air.

Figure 3 summarizes the CO₂ capture capacity with respect to cycle number for both limestone and mixture of clay in limestone. The decay in CO₂ capture capacity is similar for limestone and simulated raw meal at mild conditions (studied due to temperature limitation in the fluidized reactor cycle experiments). In order to investigate the influence of realistic calcination conditions (950 °C in CO₂-rich atmosphere), cycle experiments were performed in a fast heating rate TGA apparatus.

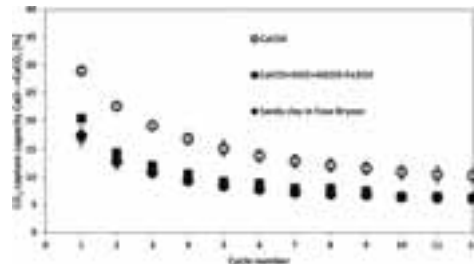


Figure 4: Comparison of CO₂ capture capacity of limestone, synthetic raw meal and simulated raw meal in TGA at realistic calcination conditions (950°C, 84 vol. % CO₂).

Figure 4 shows the CO₂ capture capacity of limestone mixed with clay compared to pure limestone. The trend in CO₂ capture capacity is similar with respect to cycle number, but the capture capacity of limestone mixed with clay is lower than of the pure limestone. Since clay is a complex component, cycle experiments were also performed with limestone mixed with the main components of raw meal (termed synthetic raw meal). The CO₂ capture capacity of the synthetic raw meal was similar to limestone with clay, indicating the adverse effect of clay and main components of raw meal on the capture capacity of limestone.

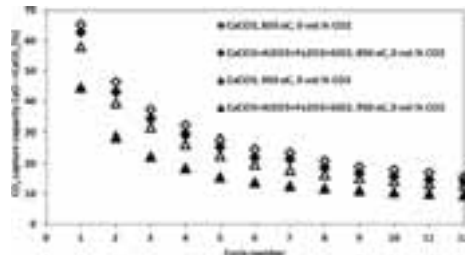


Figure 5: Comparison of the carbon capture capacity of limestone and synthetic raw meal at 850 and 950°C.

The effect of the calcination temperature on the capture capacity (in nitrogen atmosphere) is shown in Figure 5. The capture capacity is significantly lower at 950°C, indicating that at higher temperature the amount of active calcium is reduced due to interactions between limestone and the oxides of Al, Fe and Si. The capture capacity is even lower when calcining in CO₂-rich

atmosphere (figure 4), which is probably caused by enhanced sintering in presence of CO₂.

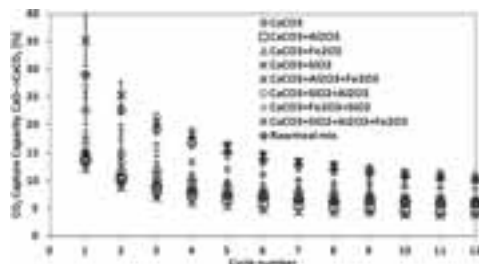


Figure 6: CO₂ capture capacity of limestone compared with binary, tertiary and quadruple mixtures as well as industrial raw meal.

Since the synthetic raw meal has four components it was not clear which of these components contribute most to the decay in the CO₂ capture capacity. Figure 6 show the decay in TGA experiments with all possible combinations containing limestone and other main components of raw meal, including an industrial raw meal. The results indicate that sorbents containing Fe₂O₃ and Al₂O₃ (such as industrial raw meal) are subject to most decay.

In order to analyze the reason for this decay, BET surface area measurements were carried out for all mixtures after calcination at realistic conditions in a tubular furnace.

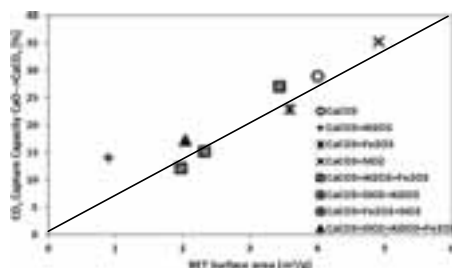


Figure 7: CO₂ capture capacity of sorbent mixtures with respect to their surface area (measured after the first calcination).

Figure 7 shows the CO₂ capture capacity of limestone of the mixtures with respect to their measured BET surface area. There appears to be a correlation between the surface area and the carbon capture capacity of the sorbent. Surprisingly, the presence of pure silica seems to have a positive effect on the surface area and so also on the CO₂ capture capacity.

Performance of Carbonator

The sorbent looping experiments using the fast heating rate TGA apparatus and the fluid bed reactor, respectively, show that raw meal can be used as a sorbent for CO₂ capture. The other objective of the project is to investigate the performance of the fluidized bed carbonator reactor.

The performance of the carbonator was investigated in the fast fluidization regime. For practical reasons and to reduce experimental errors, particle re-circulation was simulated by continuous feeding of sorbent into the reactor. The experiments were performed with highly deactivated sorbent (pure lime), calcined at 1100°C for 2 hr (surface area 1.5 m²/g compared to 4 m²/g of the limestone calcined at 950°C in CO₂ rich atmosphere). The CO₂ capture efficiency was estimated based on ratio of outlet to inlet CO₂ flow and the degree of re-carbonation of lime particles in the fluidized bed reactor at steady state conditions.

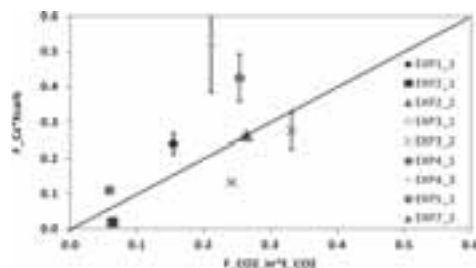


Figure 8: Sorbent conversion versus CO₂ absorbed in the carbonator evaluated for different experiments in the fluidized bed carbonator at steady state conditions.

Figure 8 shows the closure of the mass balance of the carbonator based on the sorbent conversion and gas absorbed for different experiments at steady state. The deviation for some of the experiments might be due to wide distribution of particle which results in non uniform conversion of these particles based on their residence time.

The performance of the carbonator was evaluated at different bed inventories, inlet Ca/C ratio (by changing particle re-circulation rate) and temperatures. The results obtained with different bed inventories (600-700 g & 1000-1200 g) showed no significant effect on the performance of the carbonator.

Figure 9 shows the influence of re-circulation rate on the carbon capture efficiency, i.e. the Ca/C ratio is increased from 1.5 to 3.7. The low performance of the carbonator was due to the low fraction (< 0.15) of active lime used for CO₂ capture. Based on the active fraction the active Ca/C ratio was only 0.2 to 0.5.

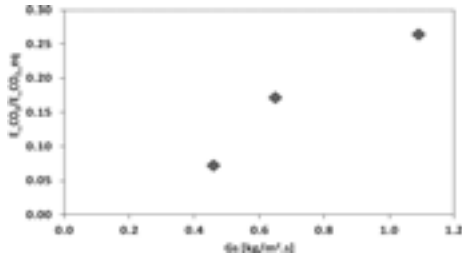


Figure 9: Carbon capture efficiency with respect to particle re-circulation rate.

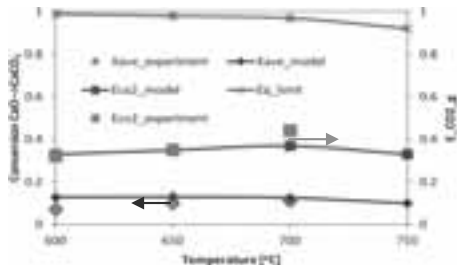


Figure 10: Carbon capture efficiency with respect to carbonator temperature at steady state operation compared with model results.

The effect of the carbonation temperature on the performance of the carbonator was evaluated because increasing temperature has two contradictory effects: i) the rate of reaction increases, whereas ii) the equilibrium conversion of CaO to CaCO₃ decreases. The experiments performed at 600, 650 and 700°C, indicated that the carbonator performance increased slightly with temperature (Figure 10).

Similar results were obtained from steady state modeling of the carbonator up to 700 °C. At 750°C, the calculated CO₂ capture efficiency dropped slightly, indicating the effect of reaction equilibrium. However, this should be taken with care as in the present case the CO₂ capture capacity of lime used is very low. Further experiments are required to conclude further on the effect of temperature.

Conclusions

Carbonate looping process was investigated using a fluidized bed reactor and a fast TGA apparatus. Based on the results following conclusions can be derived:

1. Raw meal can be used as sorbent for CO₂ capture integrated with cement production.
2. Cement raw meal has relatively low carbon capture capacity due to sintering.
3. Sintering of limestone was caused not only by CO₂ at higher temperature but also by Al₂O₃ and Fe₂O₃ contained in raw meal.

4. CO₂ capture was feasible with highly deactivated sorbent using a fast fluidized bed reactor at different operation conditions.
5. The experimental results were used to obtain the key parameters in modeling the fluidized bed carbonator.
6. The reactor performance mainly depends on the calcium to carbon ratio and the carbonation temperature.
7. Further experiments are required to conclude on the effect of temperature, CO₂ concentration and the active fraction of the sorbent.

Acknowledgement

This project is a part of Research Platform on New Cement Production Technology financed by Danish National Advanced Technology Foundation, FLSmidth A/S and DTU.

References

1. Metz B., et al., Special report on Carbon Dioxide Capture and Storage (IPCC), Cambridge University Press, 2005.
2. Pathi S. K., et al., Carbonate Looping for De-Carbonization of Cement plants, 13th International Congress on the Chemistry of Cement, 2011.

**Michael Jønch Pedersen**

Phone: +45 36 43 70 56

E-mail: mjped@kt.dtu.dk

Supervisors: Kim Dam-Johansen

Søren Kiil

Tommy Skovby, H. Lundbeck A/S

Michael J. Mealy, H. Lundbeck A/S

Industrial PhD Study

Started: August 2011

To be completed: July 2014

Design of Continuous Reactor Systems for API Production

Abstract

Grignard alkylation to a carbonyl functional group is a very important method for forming new carbon-carbon bond in pharmaceutical organic synthesis chemistry. Using an ester as carbonyl source usually results in the dialkylated product, and the formation of a tertiary alcohol upon quenching with diluted acid. However, ongoing research indicates that monoalkylated product can be achieved by stabilizing the magnesium alkoxide at very low temperature.

Introduction

The pharmaceutical industry has experienced a significant change over the last decade, especially concerning the manufacturing methods applied. Continuous manufacturing and flow chemistry are believed to cause a major impact on the industry, allowing more safe process, cheaper production, enable chemistry previous not though possible to be run, to mention a few. H. Lundbeck A/S has great believe in these new methods, and has already two continuous reactor setup operating in full-scale.

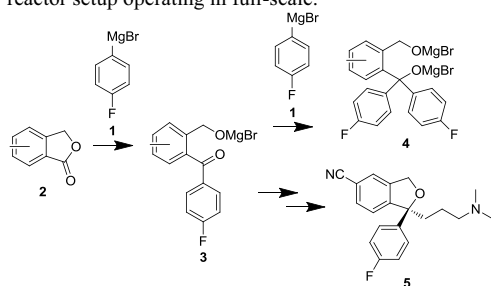


Figure 1: The synthesis step of an intermediate in the active pharmaceutical ingredient **5** Cipralex®. A Grignard alkylation between phthalide **2** and 4-fluorophenylmagnesium bromide **1** forms the desired ketone intermediate **3**. A double alkylation is known to take place resulting in formation of bisadduct **4**.

Chemistry like Grignard reactions are highly suited for being run in flow, due to their exothermic behavior and fast reaction kinetics. Furthermore, it is a widely applied

method for formation of new carbon-carbon bond. The synthesis of the antidepressant (**5**) in Figure 1 illustrates a classic Grignard alkylation that is currently done in batch production at Lundbeck.

The reaction between 4-fluorophenylmagnesium bromide (**1**) and phthalide (**2**), results in the formation of magnesium alkoxide ketone intermediate (**3**). Upon an intramolecular rearrangement, the magnesium alkoxide **3** ring-opens that release a second carbonyl group that can react with a second Grignard **1**, and form the dialkylated bisadduct (**4**), an undesired byproduct.

The reactions can be described as a competitive consecutive reaction:



Usually competitive consecutive reactions are overcome by intensifying the mixing to avoid formation of the undesired products. However, if the consecutive part of the reaction proceeds at a faster reaction rate, this is not enough. Reaction between Grignard reagents and ester carbonyls are in general known to react approximately 100 times slower than Grignard reagents and ketone and aldehyde carbonyls. In the literature, reaction between phthalide and Grignard reagents are known to proceed until the dialkylated product, with exception for highly substituted phthalide derivatives. In contradiction to this, it has been reported by Nicaise et al. [1] that a stable magnesium alkoxide of a 1,2-diester has been achieved at -78 °C.

Results

Micro reactor technology has during the last decade proven it worth for achieving valuable knowledge about chemical synthesis. Additional, syntheses previous unable to run in batch systems have been shown possible to run in flow.

Applying micro reactor technology to the synthesis illustrated in Figure 1, the mixing sensitivity that typical is a challenge in competitive consecutive reaction has been overcome. The setup is illustrated in Figure 2.

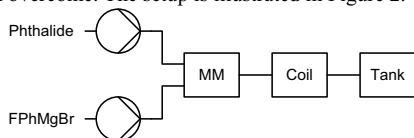


Figure 2: The principle layout of the setup. Two Harvard syringe pumps are used for the two reactants (4-fluorophenylmagnesium bromide (FPhMgBr) (1) and phthalide (2)). The reactants are mixed in the micromixer module (MM) and have an additional residence time in a coil before they reaction mixture enters the collection tank where the quench is performed.

The two reactants 1 and 2 are mixed by the splitting and combining principle, after the micromixer, and coil (ID 0.04'' and length 70 cm) is used for adding the residence time for the synthesis before entering a collection vessel where additional reaction time progresses before sample preparation by quench with 0.5 M HCl, and workup is performed.

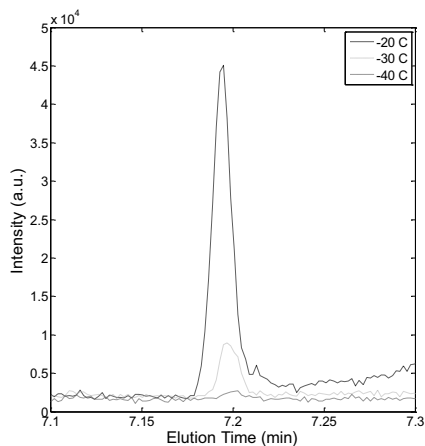


Figure 3: The effect of the temperature for the formation of the undesired dialkylated bisadduct 4. At -40 °C it has been possible to suppress the formation.

Figure 3 shows the GC analysis for 3 temperature steps (-20 °C, -30 °C and -40 °C) and two equivalence of Grignard 1 with 1 hour of reaction time in batch vessel before quench. The peak at 7.2 min is determined by mass spectrometer to be bisadduct 4, and it disappears at

low temperatures. This indicates that the ketone intermediate 3 does not ringopen at this temperature. For all 3 temperatures, mostly the desired product ketone intermediate 3 is formed. If the synthesis was carried out at 20 °C, only a peak at 7.2 min is detected. Despite the great results based on selectivity, using 2 equivalence of Grignard 1 is not desirable, neither the long reaction time. Search for more optimal reaction condition is ongoing, and promising results indicates that using tubular reactor for the entire reaction time, instead of a storage vessel, have positive effect on both the conversion and reaction time. And full consumption of Grignard can be achieved in less than 20 minutes at -40 °C, still having high selectivity of the desired product.

Conclusion

Using micro reactor technology for enhancing of mixing and controlling the temperature, selectivity between mono- and dialkylated phthalide products has been achieved. Applying temperatures below -40 °C, it is possible to favor the monoalkylated phthalide product over the dialkylated for a Grignard alkylation. To achieve the selectivity of the monoalkylated phthalide product, initial good mixing and efficient temperature control have been important. Both terms serve to avoid the formation of hot spot either of concentration of reactants and products or temperature during the reaction. The improvement of these conditions can be ascribed to the micro reactor technology, known to be well suited for heating and mixing sensitive reactions. The found stabilization of the magnesium alkoxide ketone intermediate may help improving the yield of the commercial synthesis step of the Cipralext, as well other alkylation reactions between organometals and ester carbonyls.

Reference

1. O.J.C. Nicaise, et al., Stable enols from Grignard addition to 1,2-diester: serendipity rules, *Tetrahedron* 59 (34) (2003) 6433-6443

List of Publication

M.J. Pedersen, T.L. Holm, J.P. Nielsen, T. Skovby, M.J. Mealy, K. Dam-Johansen, S. Kiil, Grignard Alkylation in a Continuous Heterogeneous Reactor Setup, FROST3, Budapest, Hungary, 2011.

K.M. Christensen, M.J. Pedersen, K. Dam-Johansen, T.L. Holm, T. Skovby, S. Kiil, Design and operation of a filter reactor for continuous production of a selected pharmaceutical intermediate, *Chem. Eng. Sci.* 71 () (2012) 111-117.

A. Cervera-Padrell, J. Nielsen, M.J. Pedersen, K.M. Christensen, A. Mortensen, K. Dam-Johansen, S. Kiil, K. Gernaey, Monitoring and control of a continuous Grignard alkylation reaction for the synthesis of an active pharmaceutical ingredient intermediate using in-line NIR spectroscopy, *Org. Process Res. Dev.* 16 (5) (2012) 901-914.

**Thomas Petersen**

Phone: +45 4174 8010
E-mail: tpet@kt.dtu.dk

Supervisors: Ole Hassager
Thorvald Ullum,
GEA Process Engineering A/S
Jakob Sloth,
GEA Process Engineering A/S

Industrial PhD Study

Started: September 2012
To be completed: August 2015

Model of Stickiness in Spray Drying

Abstract

Wall deposits are a primary concern in the design of spray drying equipment and the most troublesome type is a result of a property known as stickiness. The cause for stickiness is currently not determined conclusively and no accurate models exist for describing stickiness in spray drying quantitatively. It is the purpose of this study to understand the phenomena causing stickiness in spray drying, using modelling tools and rheological measuring equipment. Finally a model which can accurately predict stickiness for the purpose of equipment design is to be produced.

Introduction

Spray drying is a well described method for drying particles used in many applications, ranging from food and dairy, through chemicals to pharmaceuticals. Amongst other things it has the advantage of relatively low drying temperatures and well-controlled, uniform particle size distribution. In spite of this some challenges remain with the method, one of the most dominant of which is wall deposits [1]. Deposits can occur for various reasons depending on the condition of the impacting droplet or particle and various techniques are already in use in order to avoid it. Wet particle-wall impact is avoided by use of controlled flow conditions and dry particles that are deposited because of contributions from Van der Waals and electrostatic forces can be removed by using pneumatic hammers or air brushes. However one type of wall deposits remains a problem, namely those caused by what is known as stickiness in the industry. The term stickiness refers to the condition when a material sticks to another surface, caused by a combination of adhesive and cohesive forces. Several studies of this material have shown that stickiness of a substance occurs at a temperature close to and above its glass transition temperature T_g – a point at which a substance changes from a glassy (below) to a rubbery (above) state – some of which are reviewed in [2]. However the range of temperatures (even within the same study) varies between 5-40 °C with no conclusive reason given. Furthermore most of these measuring techniques fail to match the conditions seen during spray drying. As such the phenomena determining

stickiness in spray drying remain unidentified and an accurate measuring technique has yet to be published.

Specific Objectives

The purpose of this study is to identify the phenomena determining stickiness. This will be done through both experimental work and mathematical modelling.

The modelling will be used in early phases to investigate which phenomena could describe observations in literature. This will require a detailed literature study and different types of models. These models will be used in combination with rheological measurements in order to identify which characteristics cause this apparent relation between stickiness and glass transition.

A more accurate experimental technique will be designed in order to mimic the conditions during spray drying more accurately while allowing the isolation of various parameters.

Finally a detailed model of the phenomena is to be developed in order to improve current equipment design such that wall deposits caused by stickiness can be minimized or avoided completely while accomplishing economically optimum operation.

Results and Discussion

The initial modelling will be to study formation and break-up of liquid bridges. In [3] a method for measuring stickiness is presented but more importantly a theory for the relation between glass transition and stickiness is presented which also takes into account the

varying temperature difference between stickiness occurring and T_g . Here it is suggested that the determining parameter is in fact viscosity which decreases rapidly for increasing temperature just above T_g . This allows for the formation of liquid bridges between a particle of the sticky substance to a wall or another particle. As such initial model studies using a Finite Element Method (FEM) with the Level Set Method (LSM) will look into the formation and break-up of liquid bridges at various viscosities. This will be combined with simple rheological experiments used to investigate how the viscosity varies near the glass transition temperature. Based on this it should be possible to determine whether liquid bridges are a primary or minor factor in determining overall stickiness.

A look into the existing stickiness measuring techniques will reveal that they are often associated with a number of problems that make them different from conditions experienced by a particle in spray drying during sticking [2]. The best example is the so-called stirring technique in which a dry powder is stirred with a rod while slowly being wetted at constant temperature. At a certain point the force required to stir the rod will increase sharply and this temperature and moisture content will make up the so-called sticky-point. This technique shows limited reproducibility but there are more distinct problems with it that exemplify the methods used in the literature. First off the technique uses an initially dry powder and wets it. During drying it is obvious that this is reversed and because the surface properties are most likely what causes stickiness this may be an important error. The second point is that the stirring technique uses a significant number of particles, which makes it difficult to evaluate the stickiness for a single particle meaning it is difficult to discern which phenomena causes the behaviour. An example of where these two problems have been attempted solved is shown in figure 1. Here a particle is dried using equipment at GEA Process Engineering A/S which measures drying conditions accurately and then moved into contact with a plate. Stickiness is then evaluated optically. Figure 1 shows a sticky particle. This method however does not solve the third major problem with the typical technique and showed low reproducibility in the current set-up.

Thirdly the system is much less dynamic than the impact of particles with equipment wall during spray drying. This means that the kinetic energy is much lower and contact times are much higher meaning stickiness would most likely occur much easier in the stirring technique than during spray drying. Another technique called the particle gun measuring technique ([4]) exists where a dry particle is shot through a moist gas before it hits a plate. The amount of material stuck to the wall is the measure of the degree of stickiness. This technique solves problems 2 and 3, but the conditions for the drops are not as well-known and the first problem is not solved either. As such it is desired to develop a technique during this project which can

measure stickiness of particles that are being dried before impacting a wall.

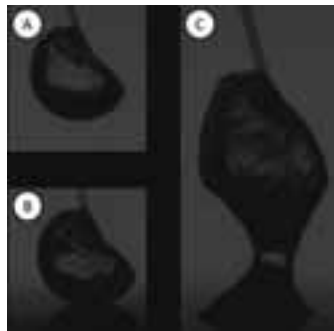


Figure 1: Picture exemplifying a sticky particle. A: Partially dried particle hangs from a pin. B: The particle is moved into contact with a plate. C: The liquid bridge is unbroken and the particle sticks to the plate.

Conclusions

An accurate model would allow improved equipment design for avoiding stickiness in spray drying during operation. Such a model would require knowledge of the phenomena which determine stickiness; however this is not currently available.

Some published results suggest a relation between the change in viscosity occurring at particle temperature just above T_g , which suggest that the primary cause is formation of strong liquid bridges between particle and wall. Whether this is actually the case can be explored using CFD tools and rheological measuring equipment. Similar approaches can be used to investigate the influence of other parameters on stickiness.

Acknowledgements

This project is carried out in cooperation between GEA Process Engineering A/S and the DPC group at DTU Chemical Engineering. Furthermore it is partially funded by the Danish Industrial Ph.D. Fellowship Programme administered by the Danish Agency for Science Technology and Innovation.

References

1. K. Masters, Deposit-Free Spray Drying: Dream or Reality? Proc. Tenth International Drying Symposium IDS '96; Vol. A, 52-60; Krakow, Poland, 1996
2. B. Adhikari, T. Howes, B.R. Bhandari, V. Truong, International Journal of Food Properties, 4 (1) (2001) 1-33
3. K.D. Foster, J.E. Bronlund, A.H.J. (Tony) Paterson, Journal of Food Engineering, 77 (4) (2006) 997-1006
4. J.Y. Zuo, A.H. Paterson, J.E. Bronlund, R. Chatterjee, International Dairy Journal, 17 (3) (2007) 268-273



Jason Price

Phone: +45 4525 2992
E-mail: japr@kt.dtu.dk

Supervisors: John M Woodley
Jakob Kjøbsted Huusom
Mathias Nordblad

PhD Study

Started: September 2011
To be completed: October 2014

Sensitivity Analysis Applied to Kinetics of Enzymatic Biodiesel Production

Abstract

Currently enzymatic catalysts are not used in commercial-scale biodiesel production. This is mainly due to non-optimized process designs. Process modelling can be a valuable tool to help support the enzymatic biodiesel process development. Integral in the simulation step is the availability of reliable models. In this case, the kinetic models describing the transesterification reaction is of importance. This work demonstrates the usefulness of sensitivity and uncertainty analysis in the kinetics of enzymatic biodiesel production to prioritize sources of uncertainty and quantify their impact on modelling simulations which can be used for process prediction, design, and optimization.

Introduction

Biodiesel, a promising renewable fuel, is essentially the fatty acid alkyl monoesters derived from renewable feedstock's, such as vegetable oils, animal fats, etc. The major reaction in biodiesel production that decides the process route is the transesterification of the vegetable oil or animal fat into fatty acid alkyl esters (FAAE), the primary product (see Figure 1). This process reduces the viscosity of the vegetable oil to a value closer to that of petroleum diesel fuel while the cetane number and heating value are saved. This makes biodiesel a strong candidate to supplement petroleum diesel, as their characteristics are generally similar to that of petroleum diesel [1].

Excellent reviews of research activities in the field of enzymatic biodiesel production are given by [2, 3]. The common thread in these articles is, compared to the conventional base-catalysed biodiesel process the enzymatic process is considered a "green reaction", requires less energy and is also highly selective producing less by-products and waste. The production of biodiesel using a biocatalyst eliminates the disadvantages of the alkali catalysed process by producing a product of very high purity with less or no downstream operations. For feed high in free fatty acids if alkali catalyst are used the free fatty acids react with the catalyst to form soaps. This causes the formation of emulsions, which will make the separation process difficult. The soap formed furthermore binds to the alkali catalyst, so the addition of extra catalyst is necessary. This is where the advantage of using a lipase catalyst is apparent, given lipase are capable of

converting the free fatty acids contained in waste oils to esters.

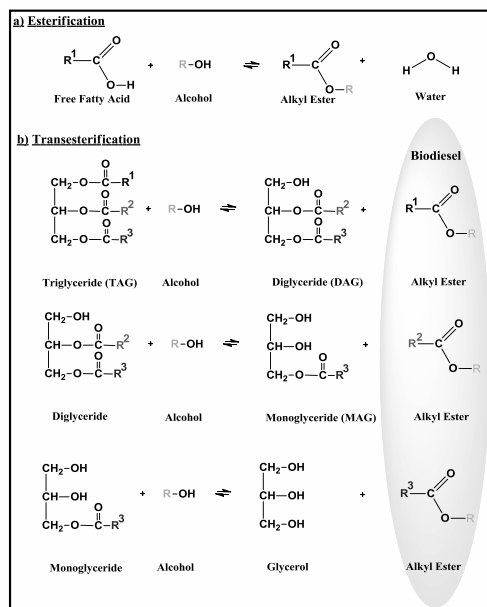


Figure 1 Simplified transesterification reaction. (R^1 , R^2 and R^3 represent linear fatty acid chains with 12 to 24 carbon atoms which can be saturated or unsaturated. R is an alkyl group of the alcohol.)

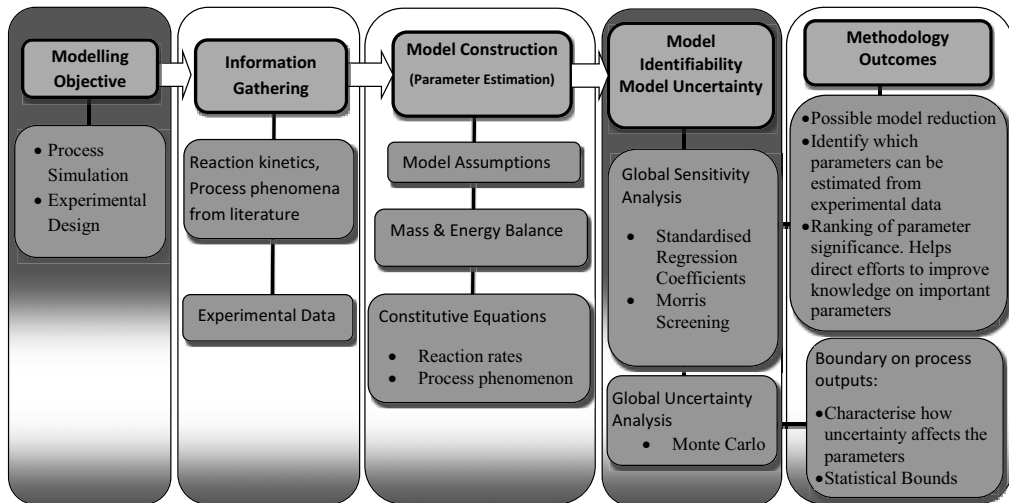


Figure 2 Methodology used in this work

However there are hurdles to industrial implementation such as the inactivation of enzyme with the alcohol substrate, issues with enzyme reuse, enzyme stability and the higher cost of the enzyme compared to chemical based catalyst. Our viewpoint is that modelling can be a valuable tool to help support the enzymatic biodiesel process development in terms of improved enzyme stability, control strategies to mitigate enzyme inactivation and also aid in the formulation of innovative process designs. Integral in the simulation step is the availability of reliable models. In this case, the kinetic models describing the transesterification reaction is of importance. Descriptions of the various kinetic models for enzymatic transesterification of vegetable oils are quite numerous [1, 4, 5].

The gap in previous work to the best of our knowledge is none of these models describing enzymatic transesterification have been statistically analysed to ascertain the quality and the working bounds of the model. This remains as a weak point in their credibility and hence applicability for design purposes, which sets the stage for this study.

Methods

The kinetic model investigated is one proposed by Cheirsilp *et al.* who investigated the transesterification of palm oil with ethanol using an immobilized lipase on a micro-porous polypropylene support, Lipase PS (from *Pseudomonas sp.*). They proposed three different kinetic mechanisms, but the third mechanism they proposed was able to capture the main process dynamics. The differential equations using the third kinetic mechanism for the batch transesterification reaction can be seen in Table 1.

In this study, focus is placed on using statistical tools during the modelling process to achieve better understanding and ascertain the reliability of the kinetic models used [6]. For the uncertainty analysis the

standard Monte Carlo procedure is used to propagate and analyse the uncertainty in the model parameters. To evaluate and rank the output variance of the model with respect to the model parameters, Standard Regression Coefficients (SRC) and Morris screening is used for the sensitivity analysis. The methodology used can be seen in Figure 2.

Table 1 Differential equations used in the simulations

Component	Differential equations Cheirsilp <i>et al.</i>
Triglyceride	$\frac{d[T]}{dt} = -(V_{mT}[W] + V_{eT}[AI])[T][E^{-1}]$
Diglyceride	$\frac{d[D]}{dt} = \{(V_{mT}[W] + V_{eT}[AI])[T] - (V_{mD}[W] + V_{eD}[AI])[D]\}[E^{-1}]$
Monoglyceride	$\frac{d[M]}{dt} = \{(V_{mD}[W] + V_{eD}[AI])[D] - (V_{mM}[W] + V_{eM}[AI])[M]\}[E^{-1}]$
Glycerol	$\frac{d[G]}{dt} = (V_{mM}[W] + V_{eM}[AI])[M][E^{-1}]$
Free Fatty Acid	$\frac{d[F]}{dt} = \{(V_{mT}[T] + V_{mD}[D] + V_{mM}[M])[W] - V_{eF}[F][AI]\}[E^{-1}]$
Biodiesel	$\frac{d[B]}{dt} = (V_{eT}[T] + V_{eD}[D] + V_{eM}[M] + V_{eB}[F])[AI][E^{-1}]$
Water	$\frac{d[W]}{dt} = -(V_{mT}[T] + V_{mD}[D] + V_{mM}[M])[W][E^{-1}]$
Alcohol	$\frac{d[AI]}{dt} = -(V_{eT}[T] + V_{eD}[D] + V_{eM}[M] + V_{eB}[F])[AI][E^{-1}]$
Free Enzyme	$E^{-1} = \frac{E_T}{\left(1 + K_{mT}T + K_{mD}D + K_{mM}M + K_{mF}F + \left(\frac{AI}{K_I}\right)\right)}$
	Model outputs: 8
	Kinetic Parameters: 12

Results and Discussion

Monte Carlo Simulations: The uncertainty in the model outputs to the parameter uncertainty of the model is represented using the mean along with the 5th and 95th percentile of the distribution of each model output at each time instant obtained from the 500 dynamic simulations (to produce the 500 samples of the input parameter space, Latin hypercube sampling is used given its conceptual simplicity, ease of implementation

and dense stratification over the range of each sampled variable [7]). Only the typically measured variables (Triglycerol, Diglycerol, Monoglycerol, Free Fatty Acid and Fatty Acid Alkyl Esters) during the transesterification reaction are reported. The interpretation of these results in Figure 3 is straightforward; the higher the uncertainty band (95th and 5th percentiles), the worse the model prediction quality is.

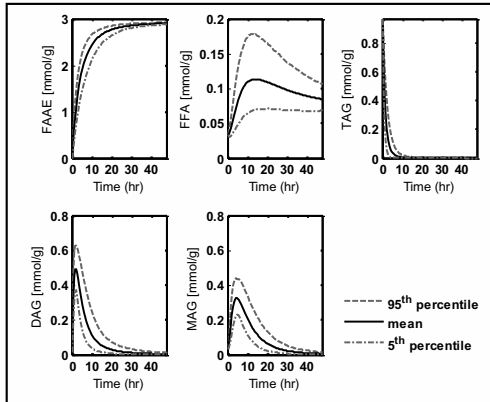


Figure 3 Uncertainty analysis of the model predictions (The mean and the 5th and 95th percentiles are obtained from performing 500 Monte Carlo simulations).

A look at the Cumulative distribution function (CDF) paints a better picture of how acceptable the model outputs are. For example, from Figure 3 the variance in the model outputs visually appear quite large between the times 5 to 15 hrs. Choosing the time of 12 hrs the CDF (Figure 4) shows the DAG concentration has a mean value of 0.08 mmol/g with a standard deviation of 0.05 mmol/g. This is a quite wide variation compared to the FFAE concentration which has a mean value of 2.55 mmol/g with a standard deviation of 0.14 mmol/g. Depending on the application this may or may not be acceptable.

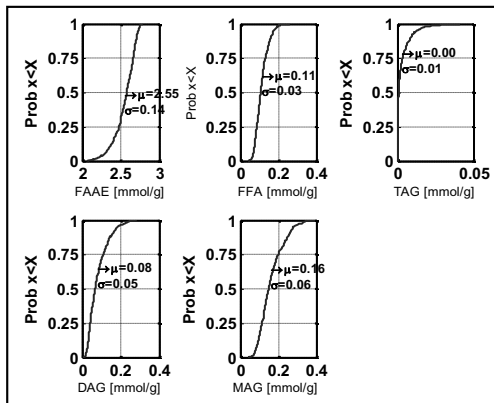


Figure 4 Cumulative distribution function of the 5 model outputs at a time of 12 hrs.

The value of this analysis is the decision maker could now put bounds on their analysis. Take the example an engineer who wishes to do an economic evaluation on the final FFAE yield. At the reaction end time of 48 hrs the FFAE concentration has a mean value of 2.90 mmol/g with a standard deviation of 0.01 mmol/g. In the economic evaluation the decision maker now has statistical meaningful bounds on which to base further calculation.

Sensitivity Analysis - Standardised Regression Coefficients (SRC): For the calculation of the Standardised Regression Coefficients and the Morris screening a scalar output is needed. A meaningful property of time-series (3.5 hrs) for the model output needs to be determined and the choice was made to focus on the model outputs at a time when there were dynamic changes in the model outputs. The degree of linearization indicated by the coefficient of model determination (R^2 value) obtained from the linear least squares fitting was over 0.8. This indicates that the linearized model was able to explain most of the variance in five model outputs investigated, and hence, the corresponding coefficients can reliably be used to assess the importance of the input parameters on the model outputs.

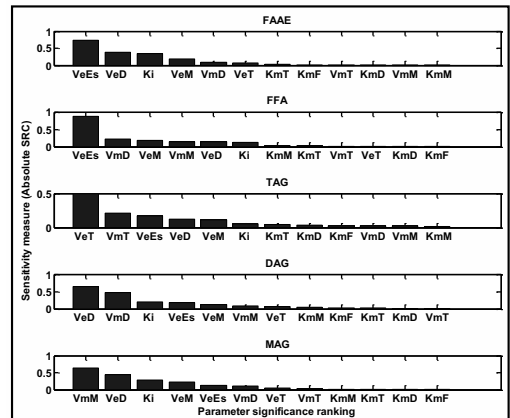


Figure 5 The ranked absolute $\beta_{j,k}$ values of the parameters influencing the transesterification reaction

The SRCs were ranked for each output, and a summary of the ranking is given in Figure 5. Analysing the model outputs the FFAE model output is most influenced by the alcohol inhibition Ki along with VeT, VeD and VeM, the rate constants for ethanolysis of TAG, DAG and MAG, respectively. For the FFA model output the most influential parameters are VeEs (the rate constant for esterification of FFAE), Ki, VmT, VmD and VmM (the rate constants for hydrolysis of TAG, DAG and MAG, respectively). This is in good agreement with the local sensitivity analysis performed by Cheirsilp et al. and helps lend credence to the hypothesis that the hydrolysis reaction produces free fatty acid prior to the esterification and the ethanolysis reaction which directly produce the fatty acid ethyl

ester. This analysis can be applied to the other outputs and what it shows is that for the five measured model outputs, the parameters K_mT , K_mD , K_mM , K_mF ; the equilibrium constants for TAG, DAG, MAG and FFA, are insensitive and hence will be quite difficult to estimate. The Morris screening results are not shown but also confirmed the results obtained from the SRC analysis.

Looking closer at the 12 parameters, K_i is the only parameter that has a significant effect on all the five model outputs. This is fully understandable given K_i is related to the alcohol inhibition. Given the competitive inhibition mechanism it is expected if the enzyme is bound to an alcohol molecule the resulting decrease in enzyme activity should affect all the model outputs.

Use of the kinetic models in enzymatic biodiesel simulation: The results from the uncertainty analysis showed that the parameter estimates for Cheirsilp *et al.* model has great potential to be used in their system for predictive purposes such as yield determination of FFAE and tracking the entire transesterification reaction given the tight confidence intervals in the areas of interest. However if it is wished to determine the FFA concentration halfway through the reaction the confidence intervals are too large and indicates poor parameter estimates given the experimental data they used or there is a particular phenomenon that is not being accounted for. It should be noted that given the reaction mixture changes during the reaction (e.g. viscosity), it is most likely the rate constants also change during the reaction and the rate constants found during the parameter estimation are just average values.

The two sensitivity methods helped to distinguish the most influential parameters in the model. Ranking of the parameter helps to direct efforts to which parameters focused need to be placed. This could then be used for possible model reduction. Another important outcome is being able to identify which parameters can be estimated from experimental data. In this case focus needs to be placed in estimating K_mT , K_mD , K_mM and K_mF . The engineering application of being able to characterize the parameter uncertainty in the model, being able to identify which parameters can be estimated from experimental data and use of the linear models from the SRC analysis are quite valuable.

Conclusions

The main points gleaned from this work are:

1. The Monte Carlo simulations on the parameter estimates provide a measure of the quality of the parameter estimates and could also be linearized satisfactorily ($R^2 > 0.8$), meaning the complex model can be replaced by a simple multivariate linear model.
2. The sensitivity analysis helped to detect influential and non-influential parameters to the model outputs. This can be used to help us improve the quality of the parameter estimates if effort is directed to improve our knowledge of the important parameters.

Future work

There are many different aspects in the sensitivity and uncertainty analysis that could be developed on. Two points that immediately stand out are:

1. The process inputs could have also been added to the analysis. It is known the different components in the oil (TAG, DAG, FFA etc.) can vary in concentration and this could also be investigated to ascertain the effects on the model outputs.
2. The analysis could have also included the glycerol, alcohol and water concentrations to ascertain if the parameters have a significant effect on the model outputs and need to be included in the measurements to be able to uniquely identify certain parameters.

Acknowledgments

The project is just part of a wider initiative with Novozymes A/S and linked to the existing team of researchers at DTU, Århus University, Emmelev A/S and Novozymes A/S working on next-generation biodiesel processes.

References

1. Al-Zuhair, S.: Production of Biodiesel by Lipase-Catalyzed Transesterification of Vegetable Oils: A Kinetics Study. *Biotechnol. Prog.* 21(5), 1442–1448 (2005).
2. Fjerbaek, L., Christensen, K.V., Norddahl, B.: A review of the current state of biodiesel production using enzymatic transesterification. *Biotechnol. Bioeng.* 102(5), 1298–1315 (2009).
3. Ghaly, A.E., Dave, D., Brooks, M.S., Budge, S.: Production of biodiesel by enzymatic transesterification: Review. *American Journal of Biochemistry and Biotechnology*. *American Journal of Biochemistry and Biotechnology* 6(2), 54–76 (2010)
4. Cheirsilp, B., H-Kittikun, A., Limkatanyu, S.: Impact of transesterification mechanisms on the kinetic modeling of biodiesel production by immobilized lipase. *Biochem. Eng. J.* 42(3), 261–269 (2008).
5. Fedosov, S.N., Brask, J., Pedersen, A.K., Nordblad, M., Woodley, J.M., Xu, X.: Kinetic model of biodiesel production using immobilized lipase *Candida antarctica* lipase B. *Journal of Molecular Catalysis B: Enzymatic* 85–86, 156–168 (2012).
6. Sin, G., Gernaey, K.V., Lantz, A.E.: Good modeling practice for PAT applications: Propagation of input uncertainty and sensitivity analysis. *Biotechnol. Progress* 25(4), 1043–1053 (2009).
7. Helton, J., Davis, F.: Latin hypercube sampling and the propagation of uncertainty in analyses of complex systems. *Reliability Engineering & System Safety* 81(1), 23–69 (2003).



Ke Qin

Phone: +45 4525 2890

E-mail: ke@kt.dtu.dk

Supervisors: Anker Degn Jensen
Peter Arendt Jensen
Weigang Lin

PhD Study

Started: January 2009

To be completed: September 2012

Characterization of Residual Particulates from Biomass Entrained Flow Gasification

Abstract

Biomass gasification experiments were carried out in a bench scale entrained flow reactor, and the produced solid particles were collected by a cyclone and a metal filter for subsequent characterization. During wood gasification, the major part of the solid material collected in the filter is soot. Scanning electron microscopy (SEM) images coupled with energy dispersive spectroscopy (EDS) show agglomerated nano-size spherical soot particles (< 100 nm) which are very rich in carbon. In comparison to wood gasification, the soot content in the filter sample from straw gasification is quite low, while the contents of KCl and K_2SO_4 in the filter sample are high. During gasification of dried lignin, the filter sample mainly consists of soot and non-volatilizable inorganic matter. SEM images of the parent wood particles and the derived char samples show that they have similar structure, size and shape but the derived char particle surface looks smoother indicating some degree of melting. The reactivity of the organic fraction of the samples was determined by thermogravimetry, and it was found that char was more reactive than soot with respect to both oxidation and CO_2 gasification. Surprisingly, the soot produced at a higher temperature is more reactive than the soot produced at a lower temperature.

Introduction

In entrained flow gasification the fuel conversion includes pyrolysis, char and soot oxidation and gasification by CO_2 and H_2O , and gas phase reactions. Among these, char and soot gasification are the conversion limiting steps because the heterogeneous reactions are slower than the initial pyrolysis and the gas phase reactions. In previous experiments of biomass (wood and straw) entrained flow gasification, we found a low yield of char (< 0.1 wt %) at 1000 °C while no char was left at higher reactor temperatures. On the other hand, soot was always observed in the syngas in the temperature range of 1000 – 1400 °C. Thus, in comparison to char gasification, soot gasification appears to be a slower process and hence determines the overall fuel conversion of the gasification process and influences the syngas quality. Therefore, knowledge on soot conversion is needed but presently only little is known about the properties of soot particles emitted from biomass entrained flow gasification. The objective of the present work was to characterize the residual solid particles obtained from biomass entrained flow gasification and particularly determine the reactivity of the soot and char particles.

Experimental

Biomass (wood, straw, and dried lignin) gasification experiments were conducted in an entrained flow reactor. The detailed information about the experimental setup and fuel can be found elsewhere [1]. The solid particles collected by the cyclone and metal filter during entrained flow gasification were analyzed by various analytical techniques. Simultaneous thermal analysis (STA) was employed to determine different fractions of the samples. In each analysis, 5 mg samples were loaded in a platinum crucible and heated at 10 °C/min to the final setting temperature in a thermogravimetric apparatus. The applied temperature program and gas environment is shown in Figure 1. Based on the STA analysis, different fractions of the solid particles, such as moisture, organic matters, volatilizable inorganic compounds, and residual ash, can be identified. The organic matters in the cyclone and filter samples are defined as char and soot respectively. For volatilizable inorganic compounds, different species, such as KCl and K_2SO_4 , can be identified on the basis of their evaporating temperatures. The amount of organic matters in the filter sample is defined as soot. Scanning electron microscopy (SEM) with energy dispersive X-

ray spectroscopy (EDS) was employed to obtain the size, morphology, and elemental distribution of the solid particles.

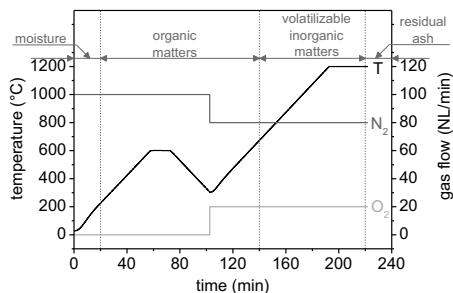


Figure 1: Temperature program and gas environment used for solid particles analysis

The kinetics of the soot and char collected from wood entrained flow gasification were derived by non-isothermal measurements in the thermogravimetric apparatus. In a measurement, approximate 1 mg sample was loaded in an alumina crucible and heated at 5 – 10 °C/min from room temperature to 800 °C during oxidation or to 1100 °C during gasification. The total gas flow was 100 mL/min. Three different O₂ and CO₂ concentrations were selected in the measurements.

The sample conversion in the temperature range of oxidation or gasification was defined as

$$\alpha = \frac{w_i - w}{w_i - w_f} \quad (1)$$

where w was the sample weight at a certain reaction temperature T , w_i was the initial sample weight at the start of oxidation or gasification, and w_f was the final sample weight at the end of oxidation or gasification. The non-isothermal fuel conversion can be described by using an n th order reaction model with the rate constant given by the Arrhenius equation

$$\frac{d\alpha}{dT} = \frac{1}{\beta} k(1 - \alpha)^n = \frac{1}{\beta} P_g^m A_0 e^{\left(\frac{-E}{RT}\right)} (1 - \alpha)^n \quad (2)$$

where β is the heating rate, P_g is the O₂ or CO₂ partial pressure, A_0 is the pre-exponential factor, E is the activation energy, R is the ideal gas constant, and m and n are the reaction order with respect to gas phase and solid phase respectively. In the present study, a common integral method presented by Coats and Redfern [2,3] was used to determine the kinetic parameters.

Results and discussion

The weight loss curves (TG) of filter samples obtained from the entrained flow gasification of wood, straw, and dried lignin respectively are shown in Figure 2. In the three entrained flow gasification experiments, the operating parameters were fixed ($T = 1400$ °C; $H_2O/C = 0.5$; $\lambda = 0.3$; $O_2 = 21$ %). During wood gasification, soot (92.6 wt %), is the major component in the filter sample. The temperature (about 1050 °C) at which the inorganic matter starts to vaporize indicates that the major part of the volatilizable inorganic matter in the filter sample is K₂SO₄ (4.2 wt %). During straw gasification, the soot content (11.1 wt %) in the filter

sample is low, while the volatilizable inorganic matter content (sum of KCl and K₂SO₄ is 47.4 wt %) is high. According to the evaporating temperatures of about 700 and 1050 °C, the first volatilizable inorganic matter is KCl (38.2 wt %) and the second is K₂SO₄ (9.2 wt %). KCl and K₂SO₄ were collected together with soot particles by the metal filter, because they appeared in the gas phase during gasification due to the high reactor temperature and then formed solid aerosols when the syngas was cooled. The filter sample obtained from dried lignin gasification mainly consists of soot (44.9 wt %) and residual ash (52.9 wt %). A small amount of volatilizable inorganic matter (1.5 wt %) was mixed with the soot and ash. The lignin ash mainly consists of silica and calcium which are hard to volatilize.

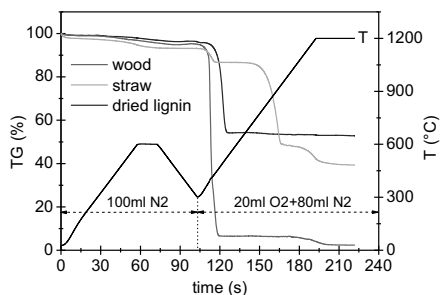


Figure 2: STA analysis of the filter samples obtained from biomass gasification ($T = 1400$ °C, $H_2O/C = 0.5$, $\lambda = 0.3$, $O_2 = 21$ %)

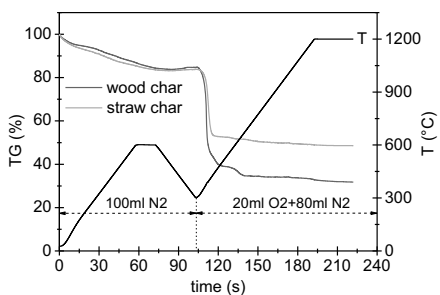


Figure 3: STA analysis of the cyclone samples obtained from wood and straw gasification respectively ($T = 1000$ °C, $H_2O/C = 0.5$, $\lambda = 0.3$, $O_2 = 21$ %)

During wood and straw entrained flow gasification, char particles were found in the cyclone only at 1000 °C. The weight loss curves (TG) of cyclone samples obtained from entrained flow gasification of wood and straw respectively with fixed operating parameters ($T = 1400$ °C; $H_2O/C = 0.5$; $\lambda = 0.3$; $O_2 = 21$ %) is shown in Figure 3. The cyclone sample from straw gasification has higher ash content than that from wood gasification because of the higher ash content in straw. Besides, compared with the filter sample, we found that the ash content in the cyclone sample was higher.

Two filter samples, obtained from wood and straw gasification respectively, which were already analyzed by STA and shown in Figure 2, were further investigated by SEM with EDS analysis. Figure 4 shows

the SEM image with EDS spectrum of the filter sample obtained from wood gasification ($T = 1400\text{ }^{\circ}\text{C}$; $\text{H}_2\text{O}/\text{C} = 0.5$; $\lambda = 0.3$; $\text{O}_2 = 21\%$). In the STA analysis, we found soot (92.6 wt %) is the major component in the filter sample. In the SEM image, it can be observed that the single soot particles are nano-sized carbon spheres ($< 100\text{ nm}$) which are agglomerated together to form clusters and chains of spheres. This is agreement with the structure of soot reported in the literature [4], where it was also shown that there was no visual difference observed between soot produced at 1200 and 1400 $^{\circ}\text{C}$ during wood (beech sawdust) pyrolysis in a drop tube furnace. The wood filter sample is almost homogenous. The EDS spectrum of this sample reveals that it is very rich in carbon because of the very high soot content, and includes traces of oxygen, silica, sulfur, and potassium due to low fractions of K_2SO_4 and SiO_2 being present. The obtained results by SEM with EDS are in qualitative agreement with the results obtained by STA.

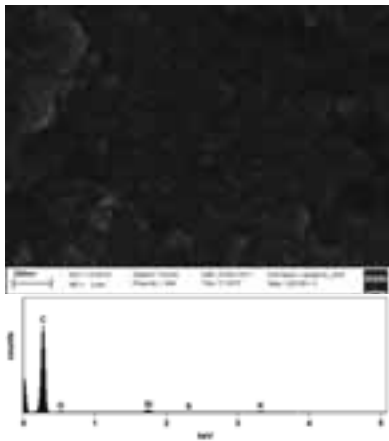


Figure 4: SEM image with EDS spectrum of the filter sample obtained from wood gasification ($T = 1400\text{ }^{\circ}\text{C}$, $\text{H}_2\text{O}/\text{C} = 0.5$, $\lambda = 0.3$, $\text{O}_2 = 21\%$)

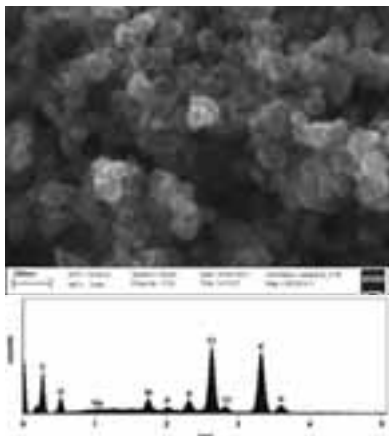
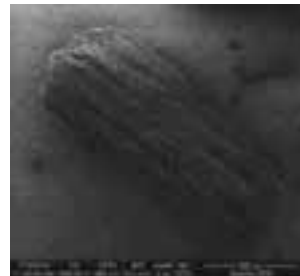


Figure 5: SEM images with EDS spectra of the filter sample obtained from straw gasification ($T = 1400\text{ }^{\circ}\text{C}$, $\text{H}_2\text{O}/\text{C} = 0.5$, $\lambda = 0.3$, $\text{O}_2 = 21\%$)

Figure 5 shows the SEM image with EDS spectrum of the filter sample obtained from straw gasification ($T = 1400\text{ }^{\circ}\text{C}$; $\text{H}_2\text{O}/\text{C} = 0.5$; $\lambda = 0.3$; $\text{O}_2 = 21\%$). The straw filter samples are almost homogenous. However, compared with the wood filter sample, the particle size of the straw filter sample looks larger ($> 100\text{ nm}$) and the shapes of the particles are irregular instead of spherical. This is probably because of the larger amount of KCl and K_2SO_4 present which adsorb on the surface of the soot particles. The EDS spectrum of this filter sample shows that carbon, oxygen, silica, phosphor, and sulfur are observed and potassium and chlorine are present in significant amounts. The EDS result of the straw filter sample is in accordance with its STA result.

The SEM images of the parent wood particle used as fuel and the derived char samples collected by the cyclone during wood entrained flow gasification ($T = 1000\text{ }^{\circ}\text{C}$; $\text{H}_2\text{O}/\text{C} = 0.5$; $\lambda = 0.3$; $\text{O}_2 = 21\%$) are shown in Figure 6. Both the parent wood particles and the derived char particles have a layered structure with a loose and porous texture. Furthermore, the size and shape of the derived char particle are similar to that of the parent wood particle, thus complete melting of the char particles does not take place. However, in comparison to the wood particle, the surface of the derived char particle looks smoother, which probably indicates partial melting.



(a) fuel



(b) char

Figure 6: SEM image of the parent wood particle and the derived wood char particle (cyclone sample) obtained from gasification (operating parameters: $T = 1000\text{ }^{\circ}\text{C}$; $\text{H}_2\text{O}/\text{C} = 0.5$; $\lambda = 0.3$; $\text{O}_2 = 21\%$)

In the experiments of wood gasification at 1000 – 1400 $^{\circ}\text{C}$, unconverted char was found only at 1000 $^{\circ}\text{C}$, while soot was always observed in the whole studied temperature range. Thus, the reactivity of the five wood soot samples obtained at 1000 – 1400 $^{\circ}\text{C}$ and the wood

char sample produced at 1000 °C were compared. The weight loss curves for the oxidation (10 vol % O₂ in N₂) and gasification (10 vol % CO₂ in N₂) of these samples are shown in Figure 7. During both oxidation and gasification, the conversion of the soot produced at a higher temperature takes place at a lower temperature in the STA measurements. This reveals that both the oxidation reactivity and gasification reactivity of soot increase when the soot is produced at high temperature. This is surprising since the reactivity of solid carbonaceous fuel normally decreases with increasing pyrolysis temperature. However, the potassium content is higher in the soot produced at a higher temperature. Therefore the higher reactivity of soot produced at a higher temperature may be related to the presence of potassium, perhaps as intercalated species in the carbon, which is known to catalyze gasification reactions [5]. Moreover, it also can be observed that the char produced at 1000 °C is more reactive than the soot produced at the same temperature as well as the soot produced at higher temperatures.

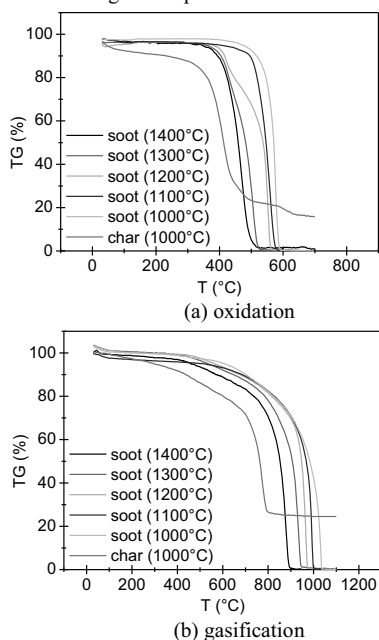


Figure 7: Weight loss curves for the oxidation and gasification of the wood soot obtained from at 1000 – 1400 °C and the wood char obtained from gasification at 1000 °C (10 vol % O₂ or CO₂ in N₂)

Conclusions

During wood gasification, the major part of the collected solids on the filter is soot. The SEM image with the EDS spectrum of the wood filter sample obtained at 1400 °C shows that the soot particles appear as agglomerated nano-size carbon spheres (< 100 nm) that are rich in carbon. Under the same operating condition, in comparison to wood gasification, the filter sample obtained from straw gasification has low soot

content and high KCl and K₂SO₄ contents, and the particles appear as irregular crystals (> 100 nm). The filter sample obtained from the dried lignin gasification experiment mainly consisted of soot and nonvolatilizable inorganic matter due to the lignin ash being rich in silica and calcium. The SEM images of the parent wood particle and the derived char samples show that both of them have a layered structure with a loose and porous texture. Their similarity indicates that complete melting of char did not take place in the conducted entrained flow gasification experiment (T = 1000 °C). In the study on the kinetics and reactivity of the soot and char, we found that the char is more reactive than soot for both oxidation and gasification, probably due to a less ordered structure of carbon in the char compared to the soot. This difference in reactivity partly explains why char is generally fully converted in the conducted entrained flow gasification experiments while soot is not. Moreover, the soot produced at a higher temperature is more reactive than the soot produced at a lower temperature, and the char produced at 1000 °C is more reactive than the soot produced at the same temperature as well as the soot produced at higher temperatures.

References

- [1] Qin K, Jensen PA, Lin W, Jensen AD. Biomass gasification behavior in entrained flow reactor: gas product distribution and soot formation. *Energy & Fuels* 2012;26:5992-6002.
- [2] Coats A, Redfern J. Kinetic parameters from thermogravimetric data. *Nature* 1964;201:68-9.
- [3] Popescu C, Segal E. Critical considerations on the methods for evaluating kinetic parameters from nonisothermal experiments. *Int J Chem Kinet* 1998;30:313-27.
- [4] Septien S, Valin S, Dupont C, Peyrot M, Salvador S. Effect of particle size and temperature on woody biomass fast pyrolysis at high temperature (1000–1400 °C). *Fuel* 2012.
- [5] Wen WY. Mechanisms of alkali metal catalysis in the gasification of coal, char, or graphite. *Catalysis Reviews—Science and Engineering* 1980;22:1-28.

List of Publications

1. Ke Qin, Weigang Lin, Peter Arendt Jensen, Anker Degn Jensen. High temperature entrained flow gasification of biomass. *Fuel* 93 (2012): 589 – 600.
2. Ke Qin, Peter Arendt Jensen, Weigang Lin, Anker Degn Jensen. Biomass gasification behavior in an entrained flow reactor: gas product distribution and soot formation. *Energy and Fuels* 26 (2012): 5992 – 6002.
3. Ke Qin, Weigang Lin, Søren Fæster, Peter Arendt Jensen, Hao Wu, Anker Degn Jensen. Characterization of residual particulates from biomass entrained flow gasification. *Energy and Fuels* (accepted)

**Siqiang Qin**

Phone: +45 4525 2835
E-mail: siq@kt.dtu.dk

Supervisors: Søren Kiil
Brian Brun Hansen

PhD Study

Started: June 2010
To be completed: May 2013

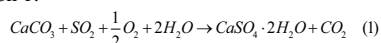
Analysis and quantification of foaming phenomena in wet FGD plants

Abstract

Spontaneous foaming can cause a range of operational problems in industrial processes such as wet flue gas desulphurisation (FGD) at power plants. This work investigates the performance of selected antifoaming agents on foams generated by adipic acid, egg white albumin (protein), and sodium dedecyl sulfate (SDS) at conditions of relevance for wet FGD. The investigations include long-term (up to 110 hrs) lab-scale experiments in a standard Birkman column with variations in salt concentration and pH. SDS and protein are powerful foaming agents which, in the absence of antifoaming agents, will foam strongly causing column overflow at a gas velocity of 0.014 m/s, while adipic acid (1.5 g/L) forms a weak foam even at high gas velocities (0.02 m/s). The addition of antifoaming agents breaks any existing foam and causes an induction period without foaming, after which the foam gradually will begin to reappear. The impact of foaming agents on SO₂ removal efficiency has furthermore been studied in a wet FGD pilot plant. Foaming generated by SDS transferred gypsum and limestone particles to the foam layer and decreased desulfurization degree 10-12% compared to a base case experiment without foaming.

Introduction

Stricter emission control legislation on acid gases (SO₂, HCl, and HF) has caused coal and oil-fired power plants to install high efficiency flue gas desulphurisation (FGD) systems, especially wet FGD in recent years. In wet FGD plants, the flue gas containing SO₂ and other acidic gases enters the wet FGD absorber and is brought into contact with alkaline limestone slurry to remove SO₂. The overall chemical reaction is described by equation 1:



Foaming (dispersion of gas in a liquid matrix) can be an operational problem in wet FGD plants, where it can interfere with the liquid level measurement and the online density measurement. This can result in gypsum scaling, excessive solid concentrations, carryover of slurry into the duct work and the booster fan, and potential cavitation of recycle pumps. When discovered, foaming can be controlled by antifoam addition, but the required dosage and the duration of its effect can vary with time.^{[1][2]}

Experimental procedure

This investigation of foaming and antifoaming agents at wet FGD conditions has been carried out in Birkman

lab-scale set-up and in a wet FGD pilot plant. The Birkman setup is a bubble column, which can be used for studies of foaming as a function of gas flow rate (see Figure 1). SDS, egg white albumin (protein), and adipic acid were chosen as foaming agents. Several different commercial antifoam formulations have been tested in this work and two were selected, in addition to a pure vegetable oil, for further studies. The influence of pH, salt and gypsum concentration is furthermore investigated. The wet FGD pilot plant is shown in Figure 2. The wet FGD pilot plant consist of a 7 meter PVC tube absorber (inner diameter of 0.033 m), which simulate a single channel in the packing zone of a packed wet FGD scrubber.

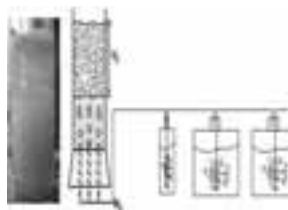


Figure 1: Birkman column with humidifiers.

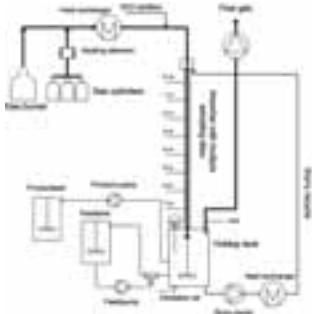


Figure 2: Outline of wet FGD pilot plant.^[3]

Results

SDS experiments

SDS is a powerful foaming agent capable of producing considerable foam volumes. Experiments with low concentration (0.005 g/L) and addition of two commercial antifoams (Nalco FM-37, Foamtrol 2290) at a low gas velocity (0.005 m/s) showed brief initial foaming followed by 10 hrs of negligible foaming. In the case of high Nalco FM-37 a limited extent of foaming returned after 10 hrs. Addition of high levels of rapeseed oil (50 g/L) was unable to affect SDS foaming.

Egg white albumin (protein) experiments

Figure 3 shows the total liquid and foam height of two experiments with 2 g/L protein and 6.4 g/L Nalco FM-37 demonstrating a similar induction time (~ 50 min) and development in foam height as a function of time. After app. 2 hrs the foam peaked, followed by a rapid decline and the onset of an additional increase in foam height after app. 3 hrs and stabilization (8-11 cm foam) after app. 7 hrs.

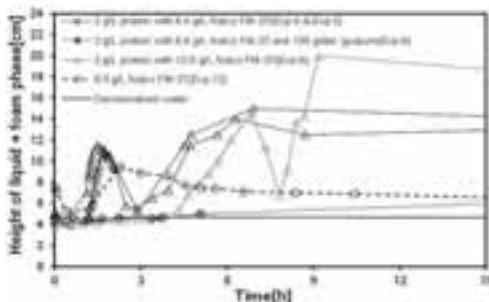


Figure 3: Foaming behavior of protein solution (2 g/L) with Nalco FM-37 (6.4 g/L (two experiments) and 12.9 g/L) and pure 6.4 g/L Nalco FM-37 at a flow velocity of 0.014 m/s.

An increased antifoam dosage (12.9 g/L Nalco FM-37) prolonged the induction time to 5 hrs and increased the resulting maximal foam height to 16 cm, but the overall development was similar. Pure antifoam (6.4 g/L) causes an initial peak in foam height similar to when mixed with protein solution, but subsequently decline without another increase in foam height. The presence of gypsum particles (100 g/L) alongside Nalco FM-37

limited the foam layer to < 2 cm and prevented the sequence of foam growth and decline observed in the absence of particles.

Wet FGD pilot plant experiments

The impact of foaming agents on SO₂ removal efficiency has furthermore been studied in a wet FGD pilot plant (Figure 2). A base case experiment without foaming was able to obtain a 91% desulfurization degree, this decreased 10-12% after addition of 0.13 g SDS/L. The onset of foaming furthermore transferred gypsum and limestone particles to the foam layer, thereby affected limestone availability in the absorber.

Conclusions and further work

Wet FGD foaming has been simulated with SDS, egg white albumin and adipic acid in a series of long-term lab-scale foaming and antifoaming tests. The powerful SDS and egg white albumin foaming could be controlled by commercial antifoams, but these could also generate some extent of foaming by themselves when used at high concentrations. Foaming in a wet FGD pilot plant generated by SDS transferred gypsum and limestone particles to the foam layer and decreased the desulfurization degree by 10-12% compared to a base case experiment without foaming. Future work will focus on the influence, persistence and mechanisms of different foaming agents and antifoams in wet FGD plants.

References

- [1] Soud, H.N. Developments in FGD. IEA Coal Research, London, 2000.
- [2] Thiele, R. Experimental Investigation of Foaming in a Packed Tower for Sour Water Stripping. I& EC Research 42 (7), 2003. 1426-1432.
- [3] Brian B. Hansen. Performance of a wet flue gas desulfurization pilot plant under oxy-fuel conditions. I& EC Research 50 (8), 2011, pp 4238-4244.

Acknowledgments

CHEC is financially supported by the Technical University of Denmark, DONG Energy A/S, Vattenfall A/S, FLSmidth A/S, Hempel A/S, Energinet.dk, the Danish Research Council for Technology Sciences, the Danish Energy Research Program, the Nordic Energy Research Program, and EU. This project is a part of the 'Våd røggasafsvovling 2009-2014' Research Platform financed by DONG Energy A/S and Vattenfall A/S.

**Alberto Quaglia**

Phone: +45 4525 2812

E-mail: aq@kt.dtu.dk

Supervisors: Gürkan Sin
Rafiqul Gani
Bent Sarup, Alfa Laval**PhD Study**

Started: June 2010

To be completed: May 2013

Incremental Refinement of Process Design

Abstract

The design, development and reliability of a chemical product and the process to manufacture it, need to be consistent with the end-use characteristics of the desired product.

One of the common ways to match the desired product-process characteristics is through trial and error based experiments which can be expensive and time consuming. An alternative approach is the use of a systematic model-based framework in product-process design, replacing some of the time consuming and/or repetitive experimental steps.

In this approach, the development of a computer-aided tools for product-process design is very important for analysis, design, and/or identification of feasible chemical product candidates because it allows one to consider processing issues during the development of the product.

In general the use of process simulation tools is not common in the food and biofuels industries, much due to the complexity of fundamental modeling of thermodynamics and transport properties of the involved chemical species and their interactions. This project aims at introducing a paradigm shift in product-process design through application of Process Systems Engineering (PSE) tools.

Introduction

For processing companies, the synthesis and design of optimal processing network includes all the strategic and tactical decisions such as the selection of raw materials and products portfolio, as well as the synthesis and design of the processing network and the optimization of the material flows through it. The solution of this problem requires extensive cross-functional co-ordination through the enterprise, as well as business management, operational and engineering expertise, resulting thereby to large multi-dimensional problems.

Recent developments in Process System Engineering have focused on managing the complexity of different company functions by integrating them in an enterprise-wide model.

The goal of the integration is the simultaneous solutions of the different layers of enterprise-wide problems, to i) reduce the effort needed to solve the problem while improving the reliability of the solution and ii) increase the impact of analysis techniques such as uncertainty and sensitivity analysis by extending their

scope to the whole problem, including the cross-functional issues.

In this contribution, we propose an integrated Business and Engineering framework for synthesis and design of enterprise-wide processing networks. In our framework, an adopted formulation of the transshipment problem is integrated with a superstructure², leading to a Stochastic Mixed Integer Non Linear Program (sMINLP), which is solved to determine simultaneously the optimal strategic and tactical decisions with respect to the processing network, the material flows, raw material and product portfolio.

The framework is complemented with all methods and tools necessary for its execution, including i) a data structure for efficient data-flow, ii) a generic structural model for description of each process alternative considered in the superstructure, starting with simple models and customizable in an incremental manner to more complex forms, iii) a library of algorithms to solve the deterministic and the stochastic problem, and iv) results analysis techniques to provide further insights for the decision making with respect to sustainability, management of the uncertainty and R&D prioritization. A case study illustrating the application of the framework to the synthesis and design of soybean

processing, including 43 process alternatives and 20 candidate products (food, feed and intermediate for pharmaceuticals) leading to the formulation of more than 300,000 equations is presented. The problem is solved both in deterministic conditions (for a given and a priori known market conditions) and under market price uncertainty, which results in a stochastic programming problem. The robustness of the optimal solution and the value of stochastic solution are discussed, and strategies to manage the consequences of the uncertainty for decision making at business and engineering levels are proposed.

The Framework

An integrated Business and Engineering framework for Computer-Aided Synthesis and Design of Processing Network has been developed and applied to the synthesis of soybean processing network.

A graphical representation of the framework is given in Figure 1.

In the workflow the problem is first defined and formulated as a MINLP (step 1, 2, 3), and then solved to determine simultaneously the optimal selection of raw materials, of product portfolio and of processing path, as well as the optimal material flow through the network.

The objective of step 1 is to define the synthesis/design problem. Also, project purpose (new product/process, process improvement, retrofit), performance metrics and objective function structure are defined at this stage.

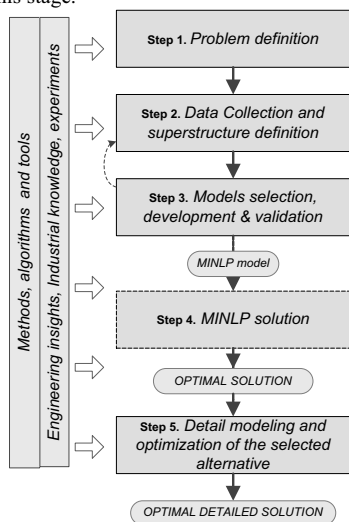


Figure 1: Systematic framework for Synthesis and Design of Processing Network.

In Step 2 all the existing knowledge (industrial know-how, engineering insights, commercial knowledge...) relevant to the problem is collected. Being this knowledge multidisciplinary and

multisource, particular emphasis is given to reconciliation and systematization, as well as to the development of an appropriate infrastructure for efficient data management, composed by a superstructure representing different flowsheet alternatives, structural constraints list, compounds and unit operations inventory and databases of reconciled data, structured in such a way to be accessible from all project levels [1]. Furthermore, performances metrics of similar and competing processes/products are collected for benchmark purposes.

All submodels needed for the multiscale model formulation are generated in step 3 (in collaboration with the Integrated Product-Process Design project). These include physical properties, unit operations, operational and investment cost and sustainability models; a systematic model generation framework is used to ensure consistency among the different models and scales. In order to cope with the lack of consolidated models and of public available data typical of this industry segment, an iterative procedure is followed for incremental model refinement and validation, based on uncertainty and sensitivity analysis to identify the model parameters which have the biggest impact on the model output and to estimate the uncertainty on model output due to parameter errors. Design of experiments techniques are then used to plan experiments in order to maximize the information gain with limited number of trials. Experimental results are added to the databases compiled in step 2 and used for model identification in step 3. The procedure is iterated until model output uncertainty is considered acceptable.

Generic input output models can be employed to describe each process interval included in the superstructure, especially to employ the tool for screening purposes at early project stage [2].

All the model equations together with the constraints and the objective function are collected in a MINLP model, which is solved in step 4, employing one of the consolidated MINLP solution techniques.

If relevant, the selected alternative can be further investigated and optimized by detail modeling and optimization, with the use of traditional process modeling and optimization methods and tools. Performances metrics are calculated for the selected optimal options and are compared against the benchmark.

Depending on the project purpose defined at level 1, project financial indicators (such as IRR, NPV etc) can be calculated for the selected option and used as inputs for project management decision.

The framework is applied to the flowsheet synthesis and design problem for soybean oil extraction and refining. According to the above described approach, the problem is formulated and solved to determine the optimal processing network for the vegetable oil extraction and refining (including biodiesel production and various options for byproducts valorization), as well as the optimal material flows to each processing step.

Case Study: Soybean Processing

Soybean (*Glycine max*) has become one of the most important agricultural commodities with a steadily increasing global production, which reached 248 MMT in 2009 [3].

Soybean can be used as raw material for a wide range of food, feed and pharma products: soybean oil is widely used as cooking or dressing oil, but can also have feed or technical applications, as well as raw material for biodiesel production. Extracted soy-beans are a cheap source of protein, used to displace animal protein in a wide range of feed and food products.

Several soy by-products have high end applications due to their functionality: soy lecithin is used in food and pharma applications as emulsions stabilizer, and tocopherols are sold as antioxidant both for pharmaceutical applications or as natural preservatives for packaged food. Other by-products such as hulls and fatty acids are mostly used as feed ingredients [4].

Average soybean composition is reported in Table 1.

Table 1: Average US Soybean Composition (dry basis) [5].

Component	Weight fraction	Standard Deviation
Protein	40.69%	0.51
Lysine	2.56%	0.11
Methionine	0.57%	0.03
Cysteine	0.72%	0.06
Tryptophane	0.52%	0.05
Threonine	1.54%	0.07
Oil	21.38%	0.64
Ash	4.56%	0.34
Carbohydrate	29.4%	3.29

Being a low margin operation, soybean processing profitability can be achieved only by optimizing the allocation of the different seed components to commercially valuable products and by-products. The wide spectrum of potential products and their mutual influence make the determination of the optimal resource allocation a not trivial task. Moreover, because of agricultural commodities market volatility, this problem needs to be solved frequently in order to have up-to-date solutions.

For these reasons, we estimate that the soybean industry sector in particular (and in general all the agro industrial sector) could benefit of the development and the application of the Integrated Business and Engineering framework.

The case study has been developed in collaboration with Alfa Laval.

For sake of simplicity, the production of biodiesel has been considered out of the scope of the case study, and therefore not included in the superstructure. In the following paragraph, a brief description of each step in the methodology will be given.

Step 1: Problem definition.

The problem is defined as a resources allocation problem, assuming the availability of 2 soybean supplies of different quality and no topological constraint given by pre-existing processing plants. The selected optimality condition is Gross Operating Margin.

Step 2: Data collection and superstructure definition

The knowledge and data relevant to the problem are collected by integrating the information available in the open literature with the industrial knowledge of Alfa Laval.

The superstructure, composed by 65 intervals, is reported in Figure 1. More detailed explanation of each of the processes considered in the superstructure can be found in [6].

The list of components includes 24 process components and 11 utilities components.

Step 3: Model selection and validation

The generic model process description model described by Zondervan for the synthesis of optimal biorefinery is employed for to model each of the considered process intervals [2]. Such an approach is based on simple input output models, describing any processes as a succession of 5 tasks: 1) inlet mixing, 2) utilities application, 3) reaction, 4) wastes separation, 5) outlet.

Step 4: MINLP solution

All the equations generated by the above described steps are grouped to generate a large scale MINLP problem. Problem statistics are reported in Table 2.

Table 2: Case study problem statistics

Total number of parameters:	163,750
Total number of process constraints equations:	159,250
Number of logical constraints	15
Number of binary variables	65
Number of continuous variables	174,378
Number of activation constraints	6,825
Objective function	1
Optimization problem size	166,091
Indicators (calculated after the solution)	147,875
Total number of equations	313,966

Step 5: Detail modeling and optimization

Even though this step is extremely important for the industrial application of the methodology, it has not been included in the scope of the case study since it does not represent a scientific challenge, being a well-known procedure for which methods and tools are available and consolidated.

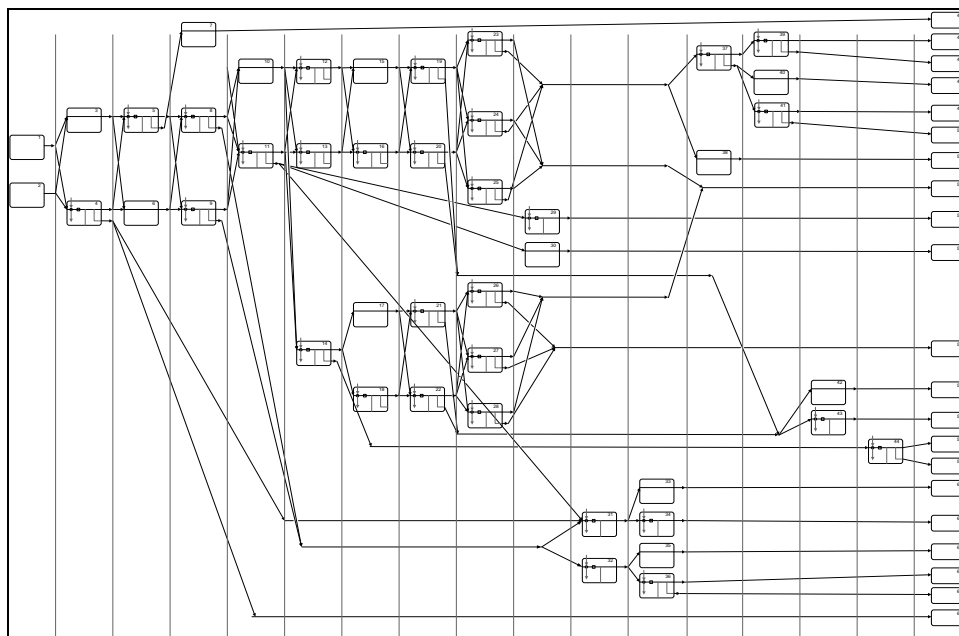


Figure 2: Soybean Processing Superstructure

Current Status and Future Perspective

The MINLP problem formulated with the above mentioned methodology is implemented in GAMS and solved with the use of standard MINLP solver DICOPT [7].

Results analysis and validation is being performed, via comparison of the optimal results with industrial standards.

Future developments include the solution of the problem under different scenarios, as well as the extension of the generic process model to include a wider range of processes.

Moreover, sensitivity analysis to determine the most influent parameters on the final solution, as well as the adaptation of the framework for the solution under uncertainty of parameters will be performed.

References

- [1] R. Singh, K. Gernaey, R. Gani, *Computers & Chemical Engineering* 33 (2009) 22–42.
- [2] E. Zondervan, M. Nawaz, A.B. de Haan, J.M. Woodley, R. Gani, *Computers & Chemical Engineering*, 35 (2011) 1752-1766.
- [3] P. Thoennes, 2009, "Oilseeds, Oils and Meals" in *Food Outlook - June 2009* FAO.
- [4] M.N. Riaz, *Soy Applications in Food*, CRC Press, 2005.

[5] F. Shahidi (ed), *Bailey's Industrial Oil and Fat Products*, Volume 2 (6th Edition), John Wiley & Sons, Hoboken, New Jersey, 2006.

[6] F. Shahidi (ed), *Bailey's Industrial Oil and Fat Products*, Volume 5 (6th Edition), John Wiley & Sons, Hoboken, New Jersey, 2006.

[7] J. Viswanathan, I.E. Grossmann, *Computers and Chemical Engineering*, 14 (1990), 769-782.

List of Publications

1. A. Quaglia, B. Sarup, G. Sin, R. Gani, *Computers and Chemical Engineering*, (submitted)
2. C.A. Diaz-Tovar, A.A. Mustaffa, A. Hukkerikar, A. Quaglia, G. Sin, G. Kontogeorgis, B. Sarup, R. Gani, *Computer Aided Chemical Engineering*, 29 (2011), 256-260



Hemalata Ramesh

Phone: +45 4525 2958
E-mail: hemra@kt.dtu.dk

Supervisors: John M. Woodley
Mathias Nordblad
Pär Tufvesson
Ulrika Törnvall

PhD Study
Started: October 2011
To be completed: September 2014

Design and use of scale-down reactors for assessing operational stability of oxidases

Abstract

Oxidases have been identified as the next generation biocatalysts owing to their ability to perform fantastic chemistry. Whilst the chemistry is great, they often suffer from practical limitations when it comes to scale-up of these reaction. These limitations arise from the loss of catalyst stability while supplying oxygen. Although the overall effect of oxygen supply on the stability is known, it is seldom studied in detail. This article explains the stability effects on oxidases and the use of reactors to study the contributing effects.

Introduction

Oxidases [E.C. 1.x.x.x] are gaining focus as fantastic biocatalysts for oxidation reactions compared to their chemical counterparts owing to their high selectivity [1]. One central consideration with reactions catalyzed by oxidases is that they require oxygen. Since the solubility of oxygen in aqueous solution is low, oxygen often has to be supplied in gaseous form to the reaction mixture to make the reaction feasible [2]. However, hand-in-hand with the oxygen supply issue goes the problem of maintaining catalyst activity and stability [3]. Possible explanations to the loss of activity/stability due to oxygen supply could be i) the amino acid residues in the protein get oxidized and/or the protein is affected by entrainment in the gas-liquid interface [4]. The purpose of this work is therefore to suggest different ways to assess the independent effects of these factors on the stability of the catalysts by means of scale-down reactors and to further validate them with experiments.

Factors affecting stability of oxidases

The low stability of oxidases is often one of the key parameters preventing the scale-up of the reactions. The various factors are outlined in Figure 1. It should be noted that other factors such as storage stability are neglected in this study. pH and plasmid stability are assumed to be enough for the process because biocatalysts are generally engineered to be stable in these aspects. Oxygen concentration has a direct effect on the protein stability depending on the amount of oxidizable amino acids that are accessible in the enzyme. The oxidization of amino acid residues (eg.

methionine and cysteine) can cause structural changes leading to inactivation of the biocatalyst [5]. The effect of oxygen concentration can be studied separate from bubble size by using nitrogen to reduce the concentration of oxygen.

Hydrogen peroxide inactivation is a phenomenon known for years [6]. It is seen to cause inactivation to both soluble and immobilized enzymes. It is therefore desirable to remove the peroxide from the microenvironment of the catalyst, which is often done by using a catalase together with the oxidase. This would then in turn affect the oxygen concentration that is experienced by the enzyme.



Figure 1: Factors affecting stability of oxidases

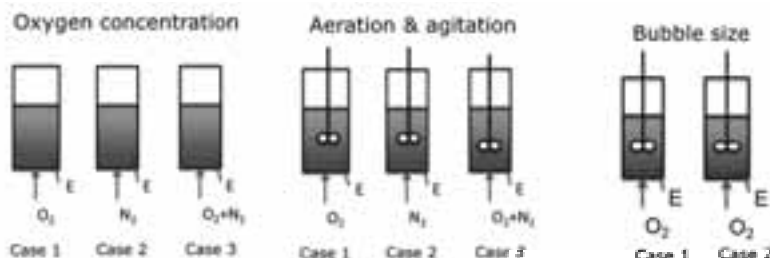


Figure 2: Understanding deactivation of oxidases

Often, external supply of oxygen is desired for an industrial reaction using oxidases. The gas-liquid interface thus formed destabilizes the enzyme [4]. By changing the size of the bubbles, the effect of surface area of gas-liquid interfaces on the stability can be studied.

Shear is a term that is often used loosely to describe the effect of stirring on the catalyst. It has been seen that shear can cause inactivation of the biocatalyst, although this phenomena is not expected in whole-cell biocatalysis [7]. By altering the stirring speed in a stirred tank reactor, the effect of shear on the catalyst can be studied.

Scale-down reactors for stability assessment

In order to study these effects independently, it is desired to expose the catalyst to industrially relevant conditions and assess the stability in a methodical manner. Also, it is desirable to assess the deactivation in such a way that it mimics large scale-operation. In order to do so, scale-down reactors are to be used. This means that to study the effect of shear in a stirred tank reactor, the catalyst must be exposed to stirring that ranges from 0.5 to 1.5 kW/m³ while the supply of air/oxygen should be in the range of 0.5 to 1.5 vvm [8].

Figure 2 depicts the use of scale-down reactors in elucidating the contributing effects to the stability of the catalyst. In order to study the effect of oxygen concentration, the catalyst's activity is first measured using a particular assay. Then, the catalyst is exposed to different concentrations of oxygen and nitrogen. The loss in activity is then measured by performing an activity assay again. The loss in activity can be used to calculate the half-life of the catalyst for the set reaction condition.

Similarly, experiments for determining the effects of other contributing effects can be conducted. The understanding gained by doing these experiments can then be used to make an operational window as shown in Figure 3. This would then enable us to choose process conditions suitable for implementing oxidase-based biocatalysis.

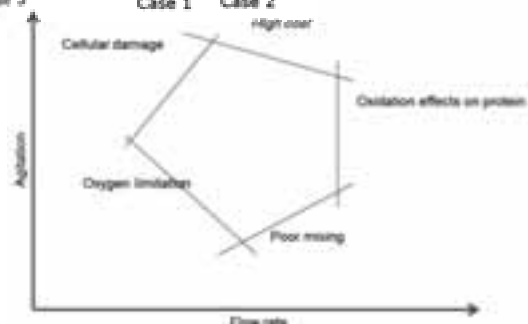


Figure 3: Operational window for the oxidases based on agitation and flow rates

Conclusions

The use of scale-down reactors and assessing independent factors on the stability will help us understand deactivation of the catalyst in a more systematic manner. Once a specific working range is identified, it can be used to operate biocatalysis in an efficient manner by closely controlling the most sensitive parameter. It is noteworthy that the effects of other environmental factors such as substrate and product toxicity need to be assessed in addition to oxygen effects to get a more precise operational window for the use of oxidases.

References

1. F. Hollomann, I. W.C.E. Arends, K. Buehler, A. Schallmeyer, B. Bühler. *Green Chemistry* 12 (2011) 226-265.
2. W. A. Duetz, J. B. van Beilen, B. Witholt. *Current opinion in biotechnology* 12 (2001) 419-425.
3. S.G. Bruton *Trends in Biotechnology* 21(12) (2003) 543-549.
4. B. A. Saville, S. Persi. *Canadian journal of chemical engineering*. 70 (1992) 1143-1148.
5. E.R. Stadtman, R.L. Levine. *Amino acids* 25(2003) 207-218.
6. P.F. Greenfield, J. R. Kittrell, R. L. Laurence. *Analytical Biochemistry* 65 (1975). 109-124.
7. C.B. Elias and J.B. Joshi. *Advances in biochemical engineering*. 59 (1998). 47-71.
8. A. Nienow in: M. Berovic, S- Enfors (Eds.), *Comprehensive bioprocess engineering*, European federation on biotechnology, Ljubljana, 2010, p. 179.



Claus Maarup Rasmussen

Phone: +45 4525 2829
 E-mail: CMA@kt.dtu.dk

Supervisors: Kim Dam-Johansen
 Karsten H. Clement
 Klaus Hjuler, FLSmidth

PhD Study
 Started: January 2010
 To be completed: June 2014

Preheater Design for High Energy Efficiency and Low Emissions

Abstract

The aim of this PhD project is to develop and test new a preheating concept for use in the cement industry, which is economically more beneficial than the existing in terms of capital and/or operational costs. A new design has been tested in several experimental setups, including a hot bench scale setup with a particle feed rate at around 100 kg/hr. Semi-continuous heat exchange experiments with inlet temperatures close to 800°C shows that the particles can be heated more to 500 °C in a four stage process. For comparison with the industrial process the solid load and a stage transport efficiency, defined as the mass stream of particles that experiences a heat exchange followed by a separation from the gas divided by amount of particles fed to a given stage, are important parameters. The stage transport efficiencies have been experimentally estimated to be between 0.5 and 0.6. The solid load is similar in the experiments and the industrial process. Work continues on estimating the size of full scale process equipment and understanding the mechanisms of the internal processes in details.

Introduction

In the modern cement plant, the preheating of particles is carried out in a series of cyclones arranged in a counter current pattern where the cold raw meal is fed to the top cyclone, and the hot process flue gases is introduced to the bottom cyclone. The counter current pattern ensures high particle temperatures after preheating.

Figure 1 provides a schematic drawing of a typical modern pyroprocessing unit. Typical operation conditions of the preheater are provided in Table 1.

Table 1: Operation conditions for a standard industrial preheater [1, 2, 3].

Solid / gas	$T_{Gas,inlet}$	ΔT_{Par}	$\eta_{Transport}$
≈ 1 (kg/kg)	890°C	$\approx 600^\circ\text{C}$	0.75 – 0.95

The basic layout for the preheating process is more than fifty years old [4], and parameters such as pressure drop, power consumption, heat loss, maintenance requirements and environmental impact have been optimized within the limitations of the overall design. However, the existing process design has some inherent disadvantages, such as:

- High capital costs due to the necessary height and structural strength of support structure for the preheating process equipment

- Relatively high heat loss from unit surfaces and through hot dust and gases leaving the system.
- Not capable of efficiently operating at solid load different from the design criteria i.e. the process is not adaptable to different operation conditions.

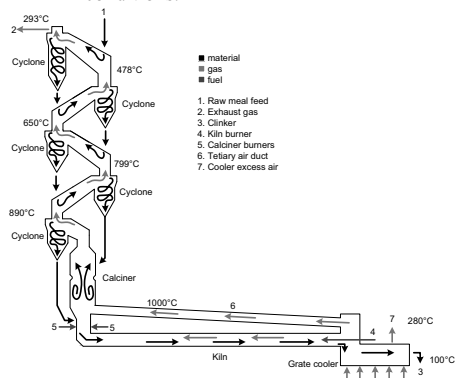


Figure 1: Schematic drawing of a typical pyroprocessing unit in a cement plant.

Alternative preheater process designs may be more suitable than the existing as cement manufacturers face an increasingly restrictive legislation with respect to

emissions of NO_x, SO₂, Hg and possibly also CO₂ in the future, increasing energy prices and the wish for using alternative fuel sources, etc.

To compete with the existing plant layout, this new design must be overall more economically favorable; either cheaper to operate or/and construct. Key words of for a new design could be:

- Compact, modular and scalable unit design (smaller dimensions and lower capital costs)
- Higher energy efficiency than existing design (lower heat losses or better utilization of the thermal energy)
- Acceptable operation over a range of solid load
- Better emission control.

Alternative Preheater Design

A study of the heat exchange processes between particles and gas combined with a close cooperation with FLSmith A/S resulted in several ideas for new pre-kiln concepts.

The most promising concept is a gas/solid heat exchanger process with a design radically different from the cyclone based preheaters. A patent application has been filed for this new design, here after referred to as a modular two dimensional heat exchanger (M2DHX).

The overall design feature of the new heat exchanger is that it consists of planar surfaces and simple geometries. The operation principle is analogous to the existing preheating process, consisting of a series of alternating mixing and separation processes of particles and gas. There are, however, several advantages of modular M2DHX design compared to the cyclone based:

- Lower stage height and smaller total equipment size.
- Lower total pressure drop
- Equipment can be constructed of prefabricated modules for lowering of capital costs
- Possibility for integration of membrane walls for steam (and power) production.

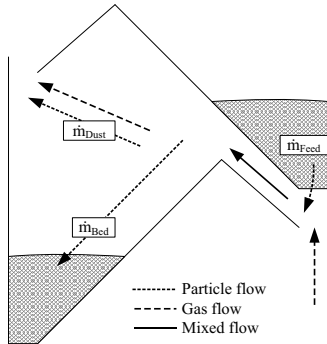


Figure 2: Schematic drawing of the new preheater design. Names are shown for particle streams.

A schematic drawing of a single stage of the new design is provided in Figure 2. In each stage, the rising

hot gases meet falling colder particles, which are entrained in the gas. The gas and particles then heat exchange in a co-current process. The gas and particles is then separated in the separation chamber where the particles are transported to the bottom of the chamber to form a moving particle bed. The hot gases leave the chamber at the top. This process is repeated in each stage of the heat exchange process.

Once the basic stage unit of the equipment has been scaled, equipment with various production rates and number of heat exchange stages can easily be designed.

Stage efficiency considerations

To summarize the efficiency of particle transport in each stage, a stage transport efficiency can be applied:

$$\eta_{Transport} = \eta_{Entrain} \cdot \eta_{Separation} = \frac{\dot{m}_{Bed} + \dot{m}_{Dust}}{\dot{m}_{Feed}} \cdot \frac{\dot{m}_{Bed}}{\dot{m}_{Bed} + \dot{m}_{Dust}} = \frac{\dot{m}_{Bed}}{\dot{m}_{Feed}}$$

where $\eta_{Transport}$ is the stage transport efficiency of particles, $\eta_{Entrain}$ and $\eta_{Separation}$ are particle transport efficiencies of the two internal transport processes (entrainment and separation), \dot{m}_{Bed} , \dot{m}_{Dust} , \dot{m}_{Feed} are the mass flow of particles to the bed, not-separated dust and feed from the particle bed above the actual stage (see Figure 2). The stage transport efficiency equals the product of the entrainment and separation efficiencies.

The stage transport efficiency is of importance in terms of evaluating the performance of the M2DHX. If $\eta_{Transport}$ is low, the overall performance of the system is reduced, despite an efficient heat exchange in each stage. To illustrate this, simple energy and mass calculations on a four stage heat transfer unit with ideal energy transfer in each stage have been performed. Computational parameters are provided in Table 2.

Table 2: Parameters for energy and mass balances of four stage heat exchanger.

Parameter	Value
Gas inlet temperature	790°C
Particle inlet temperature	20°C
Ambient temperature	20°C
Solid load	1
C _{p, Particles}	900 J/Kg/K
C _{p, Air}	1120 J/Kg/K
$\eta_{Entrain} = \eta_{Separation} = \sqrt[4]{\eta_{Transport}}$	

The computation shows, as seen in Figure 3, that the maximum energy that can be transferred to the particles, $\eta_{Energy, max}$, is around 65 % of energy in the gas at inlet conditions. This value is reduced to 58 %, if a heat loss of 15 % of the input energy is applied. The maximum values also decrease with decreasing $\eta_{Transport}$.

The driving force for the energy transport between gas and particles depends on the number of heat exchange processes (stages), the ratio between hot and cold sources (solid/gas ratio), the heat loss and stage transport efficiency.

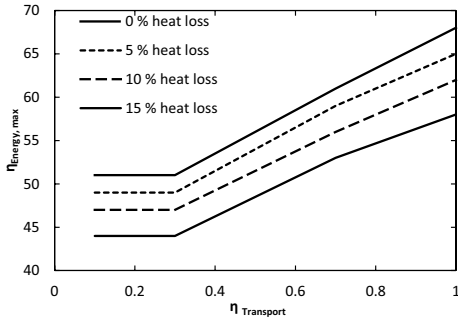


Figure 3: Computed maximum energy transfer in a four stage heat exchanger with ideal heat transfer.

Experimental setups

To verify the behavior and performance of the M2DHX design, a series of tests has been performed in different setups. The main points of interest are to understand the particle flow properties and evaluate the entrainment and separation processes.

To be able to reproduce the behavior of the industrial process and to identify potential flowability problems, the particle matter used was raw meal, received from FLSmidth. The gas used was compressed air.

Initial tests were performed in a cold single stage lab-scale setup and a cold four stage lab-scale setup in order to study the particle and gas flows.

A hot 100 kg particles/hour bench scale setup with an interchangeable number of stages (one, two or four) has been used to verify the observations from cold tests, further investigate the entrainment and separation processes as well as provide data for the thermal performance, particle flowability, and process characterization at inlet gas temperatures up to 800°C.

The hot test setup is a semi-continuous system. The particles and gas are continuously fed to the heat exchanger and the heated particles after leaving the heat exchanger are collected in bins. The limited size of the bins, capable of holding up to approximately 150 kg each, causes the particle flow to be stopped and the bins emptied approximately every 1½ to 2 hours. The hot gas and entrained dust leaves the system for cooling and filtration before being sent to the stack.

At the beginning of each experiment, the entire setup is heated to thermal equilibrium by the hot gas only before initiating the particle flow. Once the particle flow is started, the setup cools until a new operative steady state is reached. Operation is continued a period of time, typically 30 minutes, and the steady state data is recorded at used in the data treatment. An example of a continuous data sampled is provided in Figure 4.

Results and discussion

The results from the cold tests showed that it is possible to obtain stage transport efficiencies of up to 0.7 at a solid loads around 0.95 and a characteristic gas velocity = 4 m/s. These experiments were isothermal, why only particle and gas transport could be evaluated.

To evaluate the thermal performance and particle flowability at high temperatures, several experiments have been carried out on the hot bench scale test rig, including:

- Proof of concept: Continuous running of system at inlet conditions >800 °C.
- Investigation of thermal performance
- Investigation of internal processes (heat exchange, entrainment and separation processes)
- A total of 35 experiments have been performed, of which 10 were used to investigate only gas flow patterns.

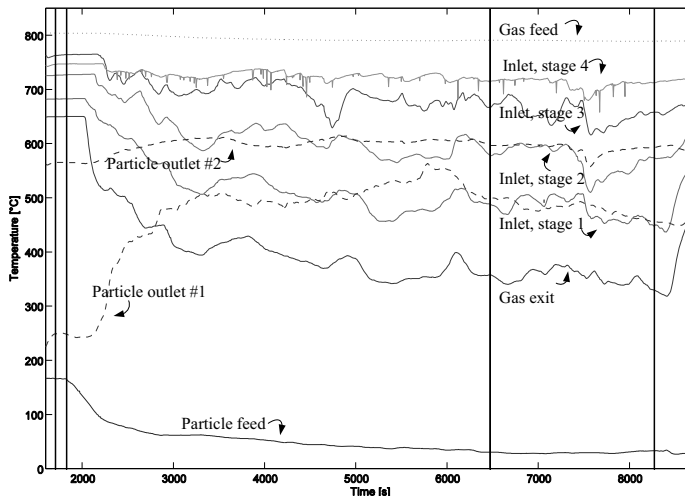


Figure 4: Dynamic data for Experiment No 1. Steady state data is obtain from $t = 6500$ to 8300 s. The two vertical solid lines at $t = 1650$ and 1750 s indicate the steady state conditions before starting the particle flow. Temperatures are measured in each stage and in the inlet and outlet streams

Selected results from three experiments at high temperature are provided in Table 3 and 4. The experiments were carried out with a particle flow rate between 74 and 94 kg/hr.

Table 3 and 4 contains selected data from three high temperature experiments.

Table 3: Experimental conditions and particle temperature increase in the four stage heat exchanger.

No	Solid / gas	$T_{Gas,inlet}$	ΔT_{Par}
1	0.98	790°C	485°C
2	1.2	790°C	502°C
3	0.94	707°C	544°C

Table 4: Particle distribution data of four stage heat exchanger.

No	Particle outlet #1	Particle outlet #2	Dust
1	0.46	0.13	0.41
2	0.55	0.13	0.32
3	0.39	0.07	0.54

The tests showed the measured particle temperature increments were around 500°C, indicating that the particles were heated by the hot gas in several heat exchange processes. The anticipated problems with assuring a stable flow of particles at temperatures above 500°C were only observed in minor degree as the system was stable and could be run for periods of more than one and a half hour without major stability issues. It was however observed that the flowability of the particle beds were deteriorated at temperatures above 500 °C and required external forces for them to flow (hammering).

Experiments were also performed to examine the two major internal transport related processes in the system; entrainment and separation of particles. Videos of the process indicate that the gas velocities as well as the local solid loads are important.

The mechanism of the separation process has been identified as a local super saturation of particles in the gas stream, followed by a relatively weak inertial separation.

The stage transport efficiency in the hot system was measured to range between 0.50 to 0.65 at characteristic gas velocities between 3 and 8 m/s.

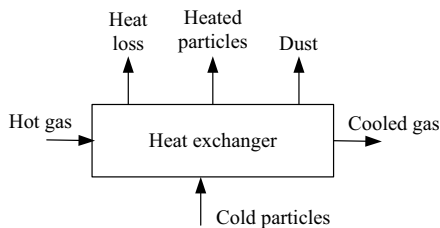


Figure 5: Overall energy balance for the heat exchanger.

Investigating and closing the energy balance over the system reveals that the heat loss to the surroundings is between 10 and 20% of the supplied energy in the hot

gas and that $\eta_{Energy, max}$ is measured to be between 29% and 42%. The remaining energy leaves the system in the gas (40 - 56%) and dust (12 - 14%). Figure 5 contains a schematic drawing of the system used for the energy balance.

Conclusion

The experiments performed on the hot bench scale setup showed that the basic principle of the new heat exchanger design preforms as expected in terms of operational stability and flow patterns.

When comparing the performance of the M2DHX with the industrial process, it is evident that optimized industrial process performs better, as expected. However the current design of the M2DHX is not optimized in terms of separation efficiency or heat exchange and the data collected from the experiments shows that especially the separation efficiency needs to be improved to be able to compete with the industrial process on performance. A comparison and summary is provided in Table 5.

Table 5: Comparison of industrial, experimental and ideal processes [1, 2, 3].

	Cyclone preheater	M2DHX	Ideal HX
Solid / gas	≈ 1	0.94 - 1.12	1
$T_{Gas,inlet}$	890°C	790°C	790
ΔT_{Par}	$\approx 600^\circ\text{C}$	$\approx 500^\circ\text{C}$	$\approx 700^\circ\text{C}$
$\eta_{Transport}$	0.75 - 0.95	0.50 - 0.65	1
$\eta_{Energy, max}$	N/A	30-42 %	62 %

Future work

The data collected from the experiments will be used to understand in detail and describe the internal processes of the system. Especially the separation process is of interest from a modeling and optimization point of view. Estimates of size and functionality of a full scale plants should be made. Production rates of interest range from pilot scale (50 tpd cl (tons clinker per day)) to full scale applications 5000 tpd cl.

Acknowledgements

This project is a part of the Research Platform on Future Cement Technology financed by Danish National Advanced Technology Foundation, FLSmidth A/S and DTU.

References

- 1 J. P. Hansen, SO₂ Emissions from Cement Production, DTU Department of Chemical Engineering, 2003
- 2 FLSmidth A/S sales material, Dry Process Kiln Systems, 2003.
- 3 KHD Humboldt Wedag sales material, Burning technology – Preheater, 2012.
- 4 J. I. Bhatti, Innovation in Portland Cement Manufacturing, Portland Cement Association (2004), p. 224

**Dominik Bjørn Rasmussen**

Phone: +45 4525 2922
E-mail: dbjra@kt.dtu.dk

Supervisors: Anker Degn Jensen
Jakob Munkholt Christensen
Anders Riisager, DTU Chemistry
Jan Rossmeisl, DTU Physics
Burçin Temel, Haldor Topsøe A/S
Poul Georg Moses, Haldor Topsøe A/S

PhD Study

Started: December 2011
To be completed: December 2014

Selective and Efficient Synthesis of Ethanol from Dimethyl Ether and Syngas

Abstract

In the present study the reaction mechanism of methyl acetate (MA) synthesis from dimethyl ether (DME) and syngas over Mordenite is studied by density functional theory (DFT). The results indicate that ketene may be formed as an intermediate and in the main channel of mordenite it is the only species that can react to acetyl. In the side pocket of mordenite the formation of acetyl can also occur via an alkylmium cation. Those findings are consistent with the observation that zeolites with smaller channels than the 12 membered rings are more resistant to coke formation.

Introduction

In the view of the steadily increasing prices of fossil fuels and the vulnerability of the global economy to disruption of oil supplies, it is evident that the demand for alternative fuels will increase. Ethanol (EtOH) can play an important role in this context as gasoline additive or substitute. Catalytic conversion of syngas to ethanol is an interesting option due to its flexibility considering the feedstock and energy efficiency.

Recently, a novel, two-step process has been demonstrated, where DME and CO first react to form MA, which in turn is hydrogenated to EtOH and methanol (MeOH) [1-4]. The main benefit of this method is its unprecedented selectivity towards ethanol, which cannot be obtained with other known processes. The principal challenge that needs to be solved before this method can find industrial use is an increase of the rate of MA synthesis. The following hydrogenation of MA to MeOH and EtOH is facile.

A number of acidic zeolites such as H-MOR, H-FER and H-ZSM5 may act as selective (> 99 mol %) catalyst for synthesis of MA [5-7] and Mordenite was identified to have the highest activity.

Mordenite contains three types of cavities: 1) the main channel, circumscribed by 12 Si atoms (12 membered ring = 12 MR), 2) 8-MR parallel to the main channel and 8-MR side pockets, which do not interconnect the 12-MR. Previous experimental [6] and theoretical [8, 9] studies indicate that the side pockets

are the sole active sites in DME carbonylation and that the surface is completely methylated at steady-state operation. To investigate the effects of the channels on MA synthesis, all relevant species and reactions are studied in this work, both in the main channel and in the side pocket.

Specific Objective

In this work the reaction mechanism of DME carbonylation over Mordenite is studied at the atomic level with DFT. The study involves calculation of the adsorption energies of all relevant reaction species. Additionally, activation energy barriers for formation of the most stable (most abundant) reaction intermediates are calculated.

During the project experiments will be performed to test the theoretical results. The knowledge gained from the theoretical work will be used to improve the catalyst.

Methods

All calculations were performed using the GPAW DFT program with a (1,1,2) k-point mesh and a real grid spacing of 0.18 Å. The RPBE functional was used. The positions of all atoms were optimized until the residual force component was below 0.03 eV/Å. In carbonylation reactions the formation energies of the initial/final state (E_f) and the transition state (E_a) were calculated relative to the system with a methyl group

adsorbed in the main channel and a CO molecule in vacuum. For reactions of DME with surface acetyl, the reference system was extended by a DME molecule in vacuum.

Mordenite and in the main channel it is the only intermediate that can react to acetyl.

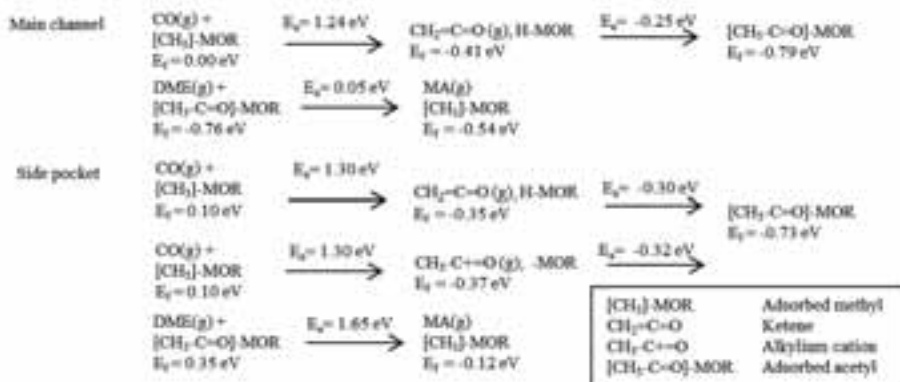


Figure 1: Formation energies of the key species for DME carbonylation on Mordenite in the initial, final and transition states, in the main channel and the side pocket.

Results and Discussion

Figure 1 shows that the formation of surface acetyl proceeds through a ketene molecule and a Brønsted acid site both in the main channel and in the side pocket. In the side pocket acetyl formation can also occur via an alkylm cation. Figure 2 shows a ketene molecule and an alkylm cation in the side pocket. In the main channel the alkylm cation is not stable and spontaneously reacts to a ketene molecule and a Brønsted acid site. The reaction of CO with the surface methyl is the rate limiting reaction step. The energy barrier for the reaction of DME with acetyl to form MA in the main channel is 1.60 eV lower than in the side pocket. A similar result was reported by Boronat et. al. [9]. Mordenite is known to undergo a fast deactivation, which is attributed to coke formation in the main channel, whereas zeolites with smaller channels are more stable [10]. Deactivation of Mordenite may be related to the presence and oligomerization of ketene in a similar manner as proposed for the H-Beta zeolite [11]. This process is more likely to occur under anhydrous conditions, like in the present case, since water readily transforms ketene to acetic acid [12].

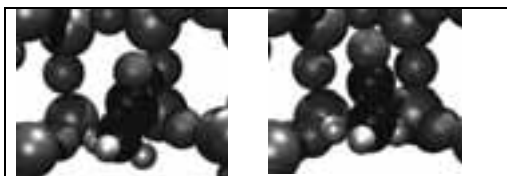


Figure 2: Side pocket, left: alkylm cation, right: ketene at a Brønsted acid site.

Conclusion

The present work shows that ketene may be formed as an intermediate under DME carbonylation over

These findings are consistent with the observation that zeolites with smaller channels than 12-MR are more resistant to coke formation.

Acknowledgments

The project is financed by DTU and the Catalysis for Sustainable Energy research initiative (CASE), funded by the Danish Ministry of Science, Technology and Innovation.

References

- [1] X. San, Y. Zhang, W. Shen, N. Tsubaki, *Energy Fuels* 23 (2009) 2843-2844.
- [2] X. Li, X. San, Y. Zhang, T. Ichii, M. Meng, Y. Tan, N. Tsubaki, *ChemSusChem* 3 (2010) 1192-1199.
- [3] Y. Zhang, X. San, N. Tsubaki, Y. Tan, J. Chen, *Ind. Eng. Chem. Res.* 49 (2010) 5485-5488.
- [4] G. Yang, X. San, N. Jiang, Y. Tanaka, X. Li, Q. Jin, K. Tao, F. Meng, N. Tsubaki, *Catal. Today* 164 (2011) 425-428.
- [5] P. Cheung, A. Bhan, G.J. Sunley, E. Iglesia, *Angew. Chem. Int. Ed.* 45 (2006) 1617-1620.
- [6] A. Bhan, A.D. Allian, G.J. Sunley, D.J. Law, E. Iglesia, *J. Am. Chem. Soc.* 129 (2007) 4919-4924.
- [7] P. Cheung, A. Bhan, G.J. Sunley, D.J. Law, E. Iglesia, *J. Catal.* 245 (2007) 110-123.
- [8] M. Boronat, C. Martinez-Sanchez, D. Law, A. Corma, *J. Am. Chem. Soc.* 130 (2008) 16316-16323.
- [9] M. Boronat, C. Martinez, A. Corma, *Phys. Chem. Chem. Phys.* 13 (2011) 2603-2612.
- [10] J. Liu, H. Xue, X. Huang, Y. Li, W. Shen, *Catal. Lett.* 139 (2010) 33-37.
- [11] M.L.M. Bonati, R.W. Joyner, M. Stockenhuber, *Microporous Mesoporous Mater.* 104 (2007) 217-224.
- [12] C.L. Padro, C.R. Apesteguia, *Catal. Today* 107 (2005) 258-265.



Helle Christine Ravn

Phone: +45 4525 6892
E-mail: hcrv@kt.dtu.dk

Supervisors: Anne S. Meyer
Lars G. Kiørboe

PhD Study

Started: December 2010
To be completed: June 2014

Large Scale Enzymatic Extraction of Pectic Dietary Fibers

Abstract

Pectin is a heteropolysaccharide known for its gelling properties induced by strong binding power for calcium cations, but also for its complex and diverse structure that form the basis of structures considered as dietary fibers. Dietary fibers based on pectic substances can be partially solubilised by applying chelating agents, as calcium will form complexes with the chelating agent and thereby increase the enzymatic solubilisation of pectic substances with dietary fiber properties. Possibly, the usage of the calcium chelating agents enhances the release of pectic dietary fibers. The potential of ethylenediaminetetraacetic acid (EDTA), citric acid, oxalic acid, and phosphate as calcium chelating agents is discussed here, and the ionic character of the chelating agent, i.e. degree of protonation, is crucial for the loosening of the pectin substrate complex to create better availability for enzyme modifications.

Introduction

Pectin is a diverse structural polysaccharide found in plant cell walls – approximately 30% of this polysaccharide is found in the primary cell walls of the majority of higher plants. Pectin is a collective name for heteropolysaccharides that consists predominately of galacturonic acid. In food products such as jams and dairy products, pectin is applied as a gelling agent. In the industrial production of pectin the pectin is extracted chemically from lemon peel and/or apple pomace. Besides serving as a gelling agent, the diversity and complexity of pectin makes pectin an excellent source of soluble dietary fiber, because of the presence of substitution groups such as COOH [1].

Although mainly lemon and apple pomace are used in commercial pectin production other plant cell wall material may serve as a source for enzymatic extraction of pectic dietary fibers. Processing of many agricultural feedstocks generates large amounts of low value waste streams that incorporate cell wall residues containing pectin e.g. potato pulp and sugar beet pulp.

One of the ways in which pectin forms gels is in the presence of calcium ions. The conformation of this gel can be described by the egg-box model (see Figure 1). The egg-box model illustrates how stretches of negatively charged homogalacturonan are stabilized by ionic interactions with calcium – these interactions generate a continuous network (gel) [1] [2]. However, the formation of egg-box structures might limit the availability of homogalacturonan as a substrate for

enzymatic modifications and degradation. In order to increase the availability of homogalacturonan stretches for enzymatic modifications and degradations the egg-box structure can be broken or loosened by applying chelating agents [2] [3].

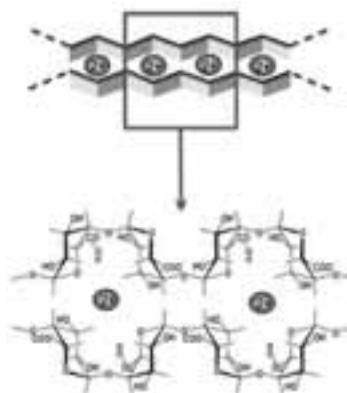


Figure 1: A schematic illustration of the egg-box structure [1].

Objectives

The objective of this Ph.d. project is to develop a large scale process for enzymatic extraction of pectic dietary fibers from potato pulp. The low value of potato pulp

makes the waste stream attractive for upgrade to high-value product as soluble pectic dietary fibers. Presumably applying chelating agents in the process will promote extension of the enzymatic degradation and modification increasing the yield of pectic dietary fibers.

Chelating agents

The loosening of the egg-box structure by chelating agents is believed to be associated through cooperative binding of calcium ions, which are situated in the egg-box [2] [3].

Chelating agents can form strong water-soluble metal complexes with calcium. The metal ion is bound tightly to the ligand and the strength of this complex can be estimated through a stability constant (see Table 1). In general, chelating agents form 1:1 complexes with metal ions. Increasing the stoichiometric concentration of the chelating agent to values greater than 1:1 increases the stability of the chelate complex [4].

Ethylenediaminetetraacetic acid (EDTA) is known for its ability to form complexes with di- and trivalent cations and is the most commonly used metal complexing agent in the food industry. It is used in concentrations of 33 to 800 ppm [4].

In food citric acid is widely used as an acidulant, because of its solubility, low cost and low toxicity, but it can also be applied in food products as a chelating agent. Like citric acid, oxalic acid is a carboxylic acid. Carboxylate ligands are due to their ionic character favored in the formation of complexes with alkali metal ions. The values of formation constants of these species are strongly dependent on the number of carboxylate groups in the chelating agent molecule. This is illustrated in Table 1, where citric acid is compared with oxalic acid [5].

Table 1: Stability constants of 1:1 calcium complexes formed in the presence of citric acid, phosphate, oxalic acid, and EDTA [4] [5].

Chelating agent	pK _a	Protonation (ligand)	log K _{stab.}
Citric acid	pK _a (1) = 3.09	C ₆ H ₈ O ₇	-
	pK _a (2) = 4.74	C ₆ H ₇ O ₇ ⁻	1.1
	pK _a (3) = 5.40	C ₆ H ₆ O ₇ ²⁻	2.81
		C ₆ H ₅ O ₇ ³⁻	4.65
Phosphate	pK _a (1) = 2.15	H ₃ PO ₄	-
	pK _a (2) = 7.20	H ₂ PO ₄ ⁻	1.41
	pK _a (3) = 12.33	HPO ₄ ²⁻	2.64
		PO ₄ ³⁻	-
Oxalic acid	pK _a (1) = 1.18	C ₂ H ₂ O ₄	-
	pK _a (2) = 2.22	C ₂ HO ₄ ⁻	-
		C ₂ O ₄ ²⁻	3.27
EDTA	-	EDTA ⁴⁻	10.69

The effectiveness of the carboxylate ligands is depending on the pH value in the process (see Table 1). The higher the pH the higher the deprotonation of the

carboxylate ligands, and thereby the carboxylate ligands become more charged, which increases the stability of the complex with calcium [5].

Like citric acid, phosphate is an acidulant used in the food industry, but many other applications of phosphates are due to their complexing behavior [6]. Stability data on the calcium complex formation of phosphates shows a similar tendency regarding the stability of the calcium complex. The number of charges involved in the complex formation seems to be one of the best ways to evaluate the potential of ligands for calcium complex formation.

Conclusion

The work is ongoing. The preliminary data indicate, as expected, that the hypothesis that chelating agents may affect the enzymatic solubilization of pectin appear to be valid also in practical enzymatic solubilization of pectinaceous substrate - including potato pulp. The ionic character of the chelating agent, i.e. degree of protonation, is crucial for the stability of the pectin substrate complex, and the significance of this effect appear to shift - or broaden the optimum for the enzymatic solubilisation of dietary fibres from potato pulp.

Acknowledgements

The project is funded by KMC, Brande.

References

1. F. Munarin, M.C. Tanzi, P. Petrini, *Int. J. Biol. Macromol.* 51 (2012) 681–689.
2. V.J. Morris, A. Gromer, A.R. Kirby, *Struct. Chem.* 20 (2009) 255-261.
3. L.V. Thomassen, D.M. Larsen, J.D. Mikkelsen, A.S. Meyer, *Enzyme Microb Tech* 49 (2011) 289-297
4. J.R. Hart, in *Ullmann's Encyclopedia of Industrial Chemistry*, Wiley Verlag, 2011, 573-578.
5. P.G. Daniele, C. Foti, A. Gianguzza, E. Prenesti, S. Sammartan, *Coord. Chem. Rev.* 252 (2008) 1093–1107.
6. K. Schrödter, G. Bettermann, T. Staffel, F. Wahl, T. Klein, T. Hofmann, in *Ullmann's Encyclopedia of Industrial Chemistry*, Wiley Verlag, 2008, 679-724.

List of Publications

H.C. Ravn, M.L. Damstrup, A.S. Meyer, *Biocatal Agr. Biotechnol* 1 (2012) 273-279.



Rolf H. Ringborg

Phone: +45 61663013
E-mail: Rolri@kt.dtu.dk

Supervisors: John Woodley
Ulrich Krühne
Krist V.Gernaey

PhD Study

Started: October 2012
To be completed: September 2015

μ -Tools for Development of ω -Transaminase Processes

Abstract

The focus of this project is to develop μ -technology and toolboxes that can be used for feasibility screening of new processes. The development will focus on the enzyme ω -transaminase, this catalyst has shown challenging difficulties in relation to thermodynamics and economic feasibility. It is believed that the use of microtechnological methods will contribute to the exploitation of ω -transaminase based technology significantly. Microtechnology will reduce the quantity of expensive and/or scarce resources needed for evaluation of potential process candidates. The technology should also potentially help to reduce the development time of biocatalysis based processes. The project is part of a European collaboration called BIOINTENSE and also features a consortium of 14 partners

Introduction

Biochemical process development is currently based on screening. The investigation is most likely performed in shake flasks or in well plates. These techniques often yield poor control and low data density (end-point measurements). Most of all is highly labor intensive and yields often in an uncertain foundation for selection. It is the vision of this project to fabricate an easy building block process tool, that will yield the possibility to quickly and with high confidence analyze the potential of a biocatalyst. For transaminase processes it is explicitly essential to have a flexible design space as each reaction requires a unique design. The project will therefore focus on development of such a platform as a tool for transaminase exploitation. The biocatalyst ω -transaminase (ω -TA) is asymmetrically exchanging a ketone with an amine group [1], see **Figure 2**.

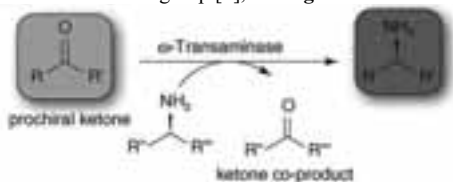


Figure 1: Asymmetric synthesis of prochiral ketones [1]

This transformation produces chiral amines of 99% enantiomeric excess (ee), which is essential for the production of pharmaceuticals [2]. Compared to traditional organic chemistry this feature is

unprecedented, that normally produces racemic mixtures. These mixtures are very difficult to separate due to the similarity between the two enantiomers. On top of that, the maximum yield is halved as one of the aminated enantiomers renders useless [3]. The unfavorable downstreaming and loss of product is the downside of traditional amination. The downside to ω -TAs is that they have in many cases unfavorable thermodynamics, yielding low product concentration. It will therefore be a requirement to shift the equilibrium to the more advantageous side. In this project, both standard and newly developed procedures of product removal, substrate delivery and even cascade reactions will be tested. An example of a cascade reaction is the synthesis of 1-phenylamine from acetophenone is conducted L-alanine as amine donor (see **Figure 2**).

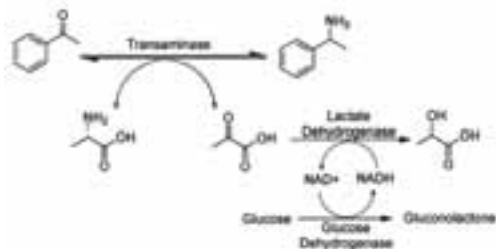


Figure 2: displaying the reaction scheme for synthesis of 1-phenylamine by ω -TA [4]

The amine donor will be converted to pyruvate as a co-product and can further be removed by lactate dehydrogenase (LDH). The LDH reaction is NADH dependent and NADH has to be regenerated for the process to become economically feasible. Glucose dehydrogenase (GDH) can be added and will promote the NADH regeneration. This specific cascade reaction, consisting of three biocatalyst facilitated reactions, is shown in the reaction scheme, in **Figure 2**. The complexity of the transaminase reactions is high and requires accordingly a high level of control. This can be provided with microscale equipment due to the miniaturization. When changing from lab to micro scale the majority of the effects can be described by. In particular the smaller intrinsic volume, larger surface-to-area ratio and small characteristic length. The microchannels will have well defined laminar flow, where heat and mass transfer will mainly be governed by diffusion/convection. Furthermore the heat and mass transfer will also be rapidly completed due to short diffusion distances (channel width).

The science of biocatalysts is based on empirically validated models, and the most effective way to obtain data for these is by screening, which is another reason to use microscale setups. Due to the small volumes it is possible to reduce the substrate and enzyme consumption significantly. This is especially suitable for screening of biocatalysts, as newly expressed enzymes will only be available in small quantities. The developed platform is therefore envisaged to be a very cost effective method for biocatalyst evaluation. The following parameters have been identified by the PROCESS group in order to reach overall economy of a biocatalytic process (**Table 1**).

Table 1: Success factors for the economic feasibility of a biocatalytic process [5]

Biocatalyst formulation	
Retention of activity	High
Stabilization	Improve catalyst productivity > 5 times
Reaction	
Product concentration	>50 g/L
Catalyst productivity	100-250 g product/ g free enzyme (crude) 50-100 g product/g immob. Enzyme
Stereoselectivity	> 98% ee
Yield	>90%

These parameters will be used as a minimum requirement for the development of the platform. A protocol will hereafter be made for data collection, the procedure will be done in an iterative manner where a structured framework will be developed and tested. This is done to direct future labwork towards collecting only essential data for process development.

Specific Objectives

- Develop a microtechnology platform with reactor, analytics and downstreaming.
- Numerical evaluation of the platform by computational fluid dynamics
- Create protocols for experiments and data collection
- Test and develop ω -TA process
- Create a decision algorithm for biocatalytic process development
- Investigate methods for shifting the equilibrium towards product formation
- Evaluate sources of amine donors

Results, Discussion and Conclusions

The projects consortium consists of leading scientists and companies within transaminase and microtechnology. It has competences within fabrication, process development, sensor development, computational fluid dynamics, microreactor development, strain engineering, enzyme expression etc. The project is made with a very pragmatic view on the problem of biocatalyst development, the consortium associated with the project has also been chosen strictly related to the technology that they offer. Integrating the different parts of the consortium yields great possibilities for a success of the project. The end product is desired to be more than a Ph.D thesis, it should be a biocatalyst process development manual. It should be noted that the technology's scope is focused at the fine chemical and pharmaceutical industry as these will be the main producers of optical pure solutions of chiral amines.

Acknowledgements

Many thanks to the European Union for funding this project.

References

1. D. Koszelewski, K. Tauber, K. Faber and W. Kroutil, Trends in Biotechnology 28 (2010) 324-332.
2. J. M. Woodley, Trends in Biotechnology, 26 No. 6 (2008) 321-327
3. P. Tufvesson, J. Lima-Ramos, J. S. Jensen, N. Al-Haque, W- Neto, J. M. Woodley, Biotechnology and Bioengineering, 108 (2011) 1479-1493.
4. M. D. Truppo and N. J. Turner, Org. Biomol. Chem. 8 (2010) 1280-1283.
5. P. Tufvesson, W. Fu, J. S. Jensen, J. M. Woodley, Food Bioprod. Process, 83 (2010) 3-11



Inês Pereira Rosinha

Phone: +45 4525 2993
E-mail: inros@kt.dtu.dk

Supervisors: Ulrich Krühne
John Woodley
Krist V. Gernaey
Anders Daugaard

PhD study
Started: November 2012
To be completed: October 2015

Topology optimization in biocatalytic reactions using miniaturized reactors

Abstract

Biocatalytic processes seem to be the alternative route for pressing global challenges of the chemical synthesis of intermediates for pharmaceutical products. Most of the catalytic reactions take place under unfavourable equilibrium conditions such as product and reactant inhibition. This project will focus on the development of microreactor configurations and the optimization of the spatial distribution of immobilized enzymes in order to overcome this limitation. A range of miniaturized reactors fabricated with different materials will be studied with the help of structured kinetic models and computational fluid dynamics (CFD) models. This will include how specific reactor geometries and the immobilization of enzymes in optimized patterns influence the biocatalytic reactions.

Introduction

Chiral amines are one of the crucial substances for the production of pharmaceutical drugs and agrochemicals. Although some chemical processes to produce chiral amines already exist, biocatalysis has been considered as an alternative process due to its advantages. Biocatalytic processes using ω -transaminase (ω -TA) as biocatalyst have several advantages such as mild reaction conditions, high stereoselectivity and high enantioselectivity. [1, 2] However, the unfavourable equilibrium and substrate and product inhibition problems are usually the major drawback [3]. The challenge in asymmetric syntheses that involve ω -transaminase is to shift the equilibrium to the product side. The chosen model reaction, to produce a chiral amine, is catalysed by the ω -transaminase by cascade reaction as shown in the Figure 1. The chiral product 1-phenylethylamine is synthesized from acetophenone by using a ω -transaminase. L-alanine is the amino donor which is, in the same reaction converted into pyruvate. Pyruvate is removed and converted to lactate by a second enzyme lactate dehydrogenase (LDH) in order to shift the equilibrium to the product side. The LDH reaction is NADH-dependent. Consequently, a third enzyme, glucose dehydrogenase (GDH), is added to the system in order to promote the NADH regeneration [4].

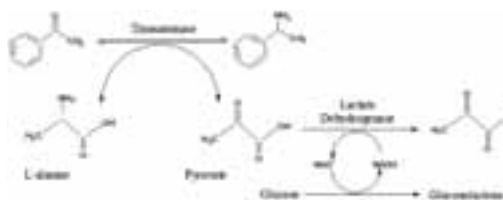


Figure 1 - Cascade reaction: synthesis of 1-phenylethylamine from acetophenone, with reduction of pyruvate to lactate.

Enzymes are expensive and often they are only available in very small quantities, which make large scale or even bench-scale screening of different reaction parameters infeasible. Therefore, miniaturized systems, enabling the high throughput or content screening of process parameters, reaction kinetics, solvents or material properties, are desirable but not yet broadly used in this field.

Topology optimization for bioprocesses at microscale has shown that changing the spatial distribution of immobilized enzymes can potentially lead to microreactors with significantly higher productivity than conventional reactor designs where the immobilized biomass is homogeneously distributed on the reactor surface [5].

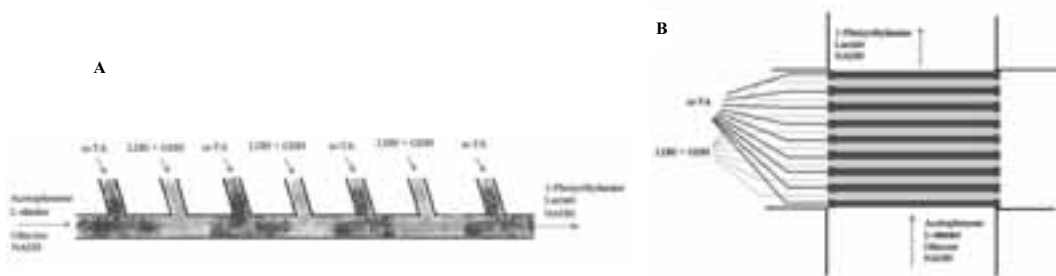


Figure 2 – Reactor configurations : A) microchannel reactor and B) cross-over reactor.

Case studies

Two microbioreactor configurations will be for instance studied and optimized: microchannel reactor and cross-over reactor, which presented in the Figure 2. The microchannel reactor is a capillary where the inlet and the outlet are located at the ends of the reactor. The entrances on the side of the channel are exclusively used for the enzyme immobilization to the walls of the reactor by e.g. covalent bonds. The enzymes are immobilized switching between a layer of ω -transaminase and a layer of dehydrogenase and glucose dehydrogenase. The reactants will flow through the channel and react with the different layers of enzymes. The control of the enzyme placement is controlled by microfluidic principles.

The cross-over reactor consists of a more complicated microfluidic flowscheme. On the side, there are capillaries connected which are used only for immobilization of the enzymes. In this reactor, the enzymes are immobilized in lanes, switching between a lane of ω -transaminase and a lane of dehydrogenase and glucose dehydrogenase. The reactants will run cross-over the layers of enzymes and the transamination and the removal of pyruvate will take place alternately. The alignment between the layers is a result from the guidance between the streams of ω -TA and the streams of LDH/GDH. This guidance is used to obtain the desired trajectory and width of enzyme lanes [6].

Both reactors are designed such that the reactants contact first the ω -transaminase and afterwards the dehydrogenase and glucose dehydrogenase which provide the removal of pyruvate.

Specific objectives

This project will focus on an integrated approach of model based and experimental investigation of the best microbioreactor configuration. With the help of structured kinetic models, Computational Fluid Dynamic (CFD) models and fabrication of miniaturized reactors in different materials, several parameters will be studied and optimized.

For the microchannel configuration, the following parameters will be optimized: flow conditions, channel shape and dimensions, the amount of alternating

enzyme layers and spatial distribution of immobilized enzymes inside of the reactor.

For the cross-over configuration, the following parameters will be optimized: flow conditions, width of enzyme lanes, the amount of alternated enzyme lanes and spatial distribution of immobilized enzymes in the reactor.

Conclusions

With this approach, innovative reactor configurations can be developed where it is possible to remove the inhibitive product *in-situ*. This means the process can be operated without using extra equipment to remove this product, with reduced reactor volume and reduced catalyst and substrate costs, reducing equipment and process costs.

References

1. Wenda S, Illner S, Mell A, Kragl U. Industrial Biotechnology - the future of green chemistry? *Green Chemistry* 13 (2011) 3007-3047
2. Shin JS, Kim BG. Kinetic modeling of ω -transamination for enzymatic kinetic resolution of α -methylbenzylamine. *Biotechnol Bioeng* 60 (1998) 534-540
3. Shin JS, Kim BG. Comparison of the ω -transaminases from different microorganisms and application to production of chiral amines. *Biosci Biotechnol Biochem* 65 (2001) 206-211
4. Koszelewski D, Tauber K, Faber K, Kroutil W. ω -Transaminases for the synthesis of non-racemic α -chiral primary amines. *Trends in Biotechnol* 28 (2010) 324-332
5. Shäpper D, Lencastre Fernandes R, Lantz AE, Okkels F, Bruus H, Gernaey KV. Topology optimized Microbioreactors. *Biotechnol Bioeng* 108 (2011) 786-796
6. Brevig T, Krühne U, Kahn RA, Ahl T, Michael Beyer, Pedersen LH. Hydrodynamic guiding for addressing subsets of immobilized cells and molecules in microfluidic systems. *BMC Biotechnol* 3 (2003) 1-10



Suriyati Saleh

Phone: +45 4525 2927
E-mail: ss@kt.dtu.dk

Supervisors: Kim Dam-Johansen
Peter Arendt Jensen

PhD Study
Started: January 2010
To be completed: June 2013

Influence of biomass chemical properties on torrefaction process

Abstract

Torrefaction is a thermal pretreatment technique for improving the properties of herbaceous and woody biomass in order to deal with such problems as high moisture content, low energy density, poor grindability, and high bulk volume. The objective of this study is to investigate the influence of different biomass chemical properties towards torrefaction characteristics. Different types of biomass with different chemical properties were torrefied in a simultaneous torrefaction and grinding reactor to improve the properties of the biomass to be used as a fuel for pulverized fired boiler.

Introduction

Heat and power production from biomass in Denmark has most cases been based on grate-fired units and co-firing of straw and coal in suspension-fired power stations. However, 100% utilization of biomass in high efficient suspension fired power stations has become an interesting option in order to reduce the greenhouse gas emissions and to increase the use of renewable energy. Suspension-fired units have a higher electrical efficiency compared to traditional grate-fired units. However, problems with handling, pulverizing and ash related operational limitations make the use of biomass on suspension fired boilers without co-firing with fossil fuels complicated. There is a need for a pretreatment process that can minimize problems with particle size reduction and ensure that a high superheater temperature can be used and thereby a high electrical efficiency obtained. Pretreatment by torrefaction is a process of thermal degradation of biomass at a relatively low temperatures and low heating rate of less than 50 °C min⁻¹ under inert conditions whereby the grindability is improved.

The concept used in this study is the integration of a torrefaction pretreatment process with a suspension-fired boiler. Torrefaction of biomass is done simultaneously with grinding by using metal balls in the torrefaction chamber. By employing the simultaneous torrefaction and grinding process, the finely grinded fuels can be supplied to the boiler, and a gas fuel with a low amount of corrosive species can be produced. This gaseous fuel can be applied to ensure a high superheater

temperature and thereby an efficient electricity production.

An ideal biomass pretreatment method would provide the heating value of the biomass for the boiler, but in a way such that the fuel is easily pulverized. In order to achieve this goal, a simultaneous torrefaction and grinding process will be used as a pretreatment method. The main objective for the current study is to investigate the influence of chemical properties on torrefaction characteristics of several biomass samples.

Experimental work

The torrefaction experiments were conducted by using a simultaneous torrefaction and grinding reactor. The conversion of all biomass samples independent of particle size and reactor properties have been carried out in a Simultaneous Thermal Analysis (STA). They were pyrolyzed in a nitrogen atmosphere at 5 K/min up to 600 °C. Six raw biomass samples with particle size less than 4 mm were used. The biomass samples were wheat straw, miscanthus, spruce wood chips, beech wood chips, pine wood chips, and spruce bark. They have different distribution of ash, hemicellulose, cellulose and lignin as shown in tables 1 and 2. In addition, to further investigate the influence of K content, straw and spruce chips were pretreated (washing and alkali impregnation), and then torrefied in STA and the torrefaction reactor. These biomass samples were torrefied at 270 °C for 90 minutes in the simultaneous reactor. A continuous flow of nitrogen is used to keep the system inert. The weight of the char was measured

in order to determine the mass loss of the samples. In order to study the grindability of the torrefied biomass, the torrefied products were sieved into different size fractions and the particle size distribution is evaluated. D_{50} values were obtained from the particle size distribution curves.

Table 1: Composition of the raw biomass

Component (wt% dry)	Straw	Miscant -hus	Bark (Spruce)	Spruce chips	Beech chips	Pine chips
Ash	5,57	2,26	4,98	0,34	0,64	0,5
C	45,93	47,97	49,66	48,88	48,50	53,2
H	5,86	5,92	5,63	6,23	6,05	6,2
N	0,64	0,28	0,34	<0,1	<0,1	0,1
S	0,111	0,039	0,03	0,004	0,009	0,05
Cl	0,19	0,181	0,01	0,003	0,004	0,005
K	0,904	0,485	0,184	0,036	0,128	0,056
Si	1,4	0,45	0,318	0,007	0,005	0,05
Al	0,006	0,008	0,073	0,003	0,002	0,01
P	0,095	0,02	0,034	0,003	0,005	0,007
Fe	0,008	0,008	0,053	0,002	0,002	0,003
Mg	0,079	0,055	0,081	0,011	0,028	0,029
Ca	0,433	0,13	1,29	0,104	0,134	0,1
Na	0,011	0,003	0,01	<0,001	0,001	0,005

Table 2: Carbohydrate analysis for raw biomasses

Components (wt% dry)	Straw	Miscanthus	Spruce chips	Beech chips	Pine chips	Bark (Spruce)
Xylan-based hemicelluloses	23,1	18,1	5,6	16,2	5,1	3,9
Mannan-based hemicelluloses	0	0	11,0	2,3	10,0	4,0
Other hemicelluloses	2,3	2,0	1,8	2,7	5,4	5,0
Total hemicelluloses	25,4	20,1	18,4	21,2	20,5	12,9
Cellulose	42,7	48,5	45	40,8	38,6	24,1
Lignin	17,3	22,4	27,6	23,8	29,2	36,8
Ash	4,2	1,0	0,3	0,5	0,4	5,4
Extractives	3,2	4,3	1,0	1,0	4,7	5,7
Residuals	7,3	3,7	7,8	12,8	6,7	15,0

Results and Discussion

1. Influence of chemical properties on solid yield of torrefied product

The results from pyrolysis of raw biomass in the STA is shown in Figure 1. The char yields are obtained from the thermal gravimetric (TG) curves while the peak temperature (maximum conversion) are obtained from the derivative thermal gravimetric (DTG) curves. Figures 2 to 4 show the influence of potassium (K) content on peak temperature and char yield resulted from torrefaction process.

A simple relation between peak pyrolysis conversion temperature and K content can be observed in Figure 2. A raw biomass with the lowest K content shows the highest peak temperature which is 354 °C for spruce chips. Straw with the highest K content has the lowest peak temperature at 322 °C. Biomass impregnated with KCl shows a similar result as straw, with the peak

temperature of 319 °C. This is in agreement with Fahmi et al [1] who reported that the alkali metals present in the biomass has an ability to lower the degradation temperatures. This clearly shows that potassium has a catalytic influence on the pyrolysis process, decreasing the temperature of maximum conversion, resulting in the decrease of solid yield as shown in figures 3 and 4. The addition of KCl did not result in a pyrolysis behaviour similar to the raw sample. This may partly due to the fact that minerals other than potassium were washed off the raw sample, and this gave an influence on the pyrolysis behaviour [2].

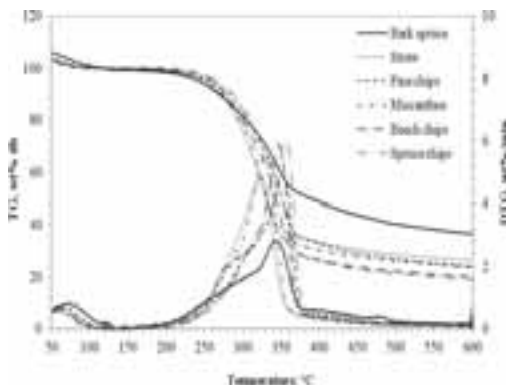


Figure 1: TG-DTG curves for different biomasses pyrolyzed in STA at 5K/min in nitrogen atmosphere

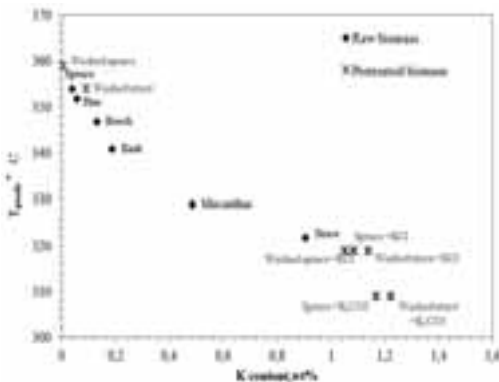


Figure 2: Influence of biomass K content on peak temperature (maximum conversion rate) measured by TGA

Influence of the feedstock K content on char yield (from STA) at 270 °C and 300 °C is shown in Figure 3. A high char yield is obtained for the biomass samples with a low K content. An increase of K content from 0 to 0.2wt% caused a significant decrease in char yield, while only a small influence is observed for a higher K content. Some cases with the addition of KCl and K_2CO_3 into biomass gave a large influence on char yield. This result shows that the alkali metals in biomass

have a catalytic effect on pyrolysis process, which is in agreement with the work conducted by Saddawi et al [3].

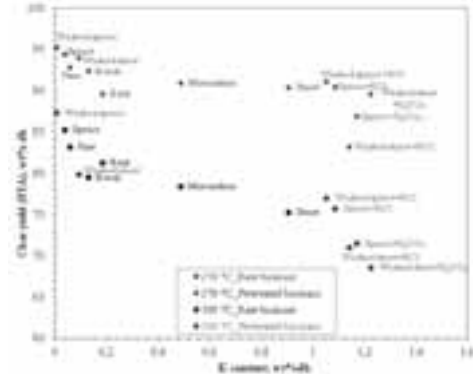


Figure 3: Influence of biomass K content on char yield obtained at 270 °C and 300 °C (pyrolysis in STA)

After analyzing the results from STA, all biomass samples, including the alkali impregnated straw and spruce chips were torrefied in the simultaneous torrefaction and grinding reactor. Torrefaction of raw biomass were conducted at 270 °C and 300 °C for 90 minutes. In Figure 4, the influence of K content on char yields from torrefaction of biomass is shown. A decreasing amount of char yield is observed as the K content in biomass increases in both systems. This results show that the alkali metal has a large catalytic influence on the pyrolysis process, thus the maximum conversion occur at a lower temperature, resulting in decrease of solid yield for both temperatures. Another important point from this investigation is that the addition of KCl and K₂CO₃ into the washed straw did not result in a pyrolysis behavior completely similar to that of the raw straw sample. This may partly be due to the minerals other than potassium were washed off the raw sample, and this gave an influence the pyrolysis behavior. Furthermore, the potassium added as KCl was probably not distributed in the sample in the same way as the naturally occurring potassium, and possibly because not all potassium in the straw was present as KCl [2].

Figure 5 shows the relationship between the solid yield of torrefied biomass, and the lignocelluloses composition and potassium contents in the raw biomasses. All biomasses have reasonably similar lignocelluloses compositions, except for bark spruce, that has a relatively higher lignin content (36.8wt%) and a relatively low hemicellulose content (12.9wt%). With an exception for the case of bark spruce, there is seen an increased release of volatiles (and thereby a lower solid yield) when the biomass potassium content is increased. The bark has a relatively higher solid yield at these temperatures because of the higher lignin content, since lignin is the main contributor for the char formation. The same results were also obtained by Raveendran et al [5] and D. Lv [6], and they concluded that potassium

in biomass is not the only factor that influence the char yield. A relatively higher lignin content in biomass will contributed to the higher char yield after pyrolysis process [5].

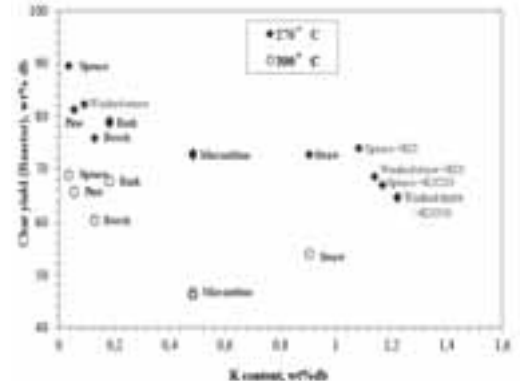


Figure 4: Influence of biomass K content on char yield obtained at 270 °C and 300 °C (torrefaction in simultaneous reactor)

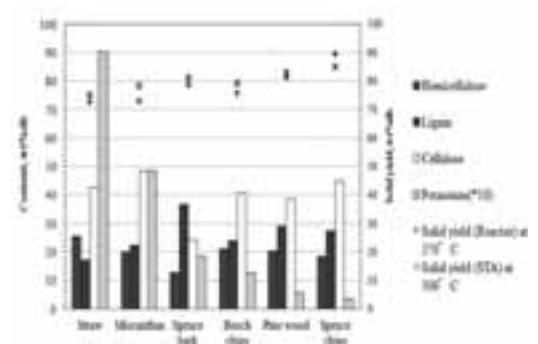


Figure 5: Composition of lignocelluloses materials and potassium in raw biomass. The cross markers represent the solid yield of torrefied biomass at 300 °C from STA and 270 °C from torrefaction reactor

2. Influence of K content on grindability of torrefied biomass

The grindability of torrefied biomass is important with respect to obtaining a high burn out of the fuel supplied to a suspension fired boiler. Thus, it is the aim of this work to study the influence of different biomass properties on the grindability of the produced char. The grindability of biomass was discussed by using the relative d₅₀ value reduction. The d₅₀ value is the particle size at which 50wt% of the particles in a sample are smaller than that size. The relative reduction of d₅₀ by torrefaction can then be used as a measure of the grindability of a torrefied biomass.

The influence of K content on d₅₀ reduction of torrefied biomass is evaluated and presented in Figure 6. A linear relationship between d₅₀ reduction and K content is observed for the raw biomass with a low K content (up to 0.3wt% K content). However, no clear

relationship is observed for the impregnated biomass. Figure 7 shows a relationship of d_{50} reduction and mass loss of torrefied biomass. A linear correlation is observed between d_{50} reduction and mass loss of torrefied biomass (without KCl and K_2CO_3 additions).

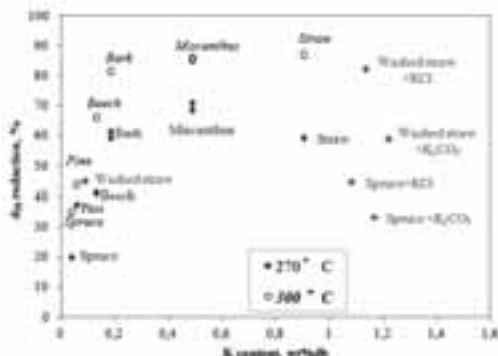


Figure 6: Influence of K content on d_{50} reduction of torrefied biomass

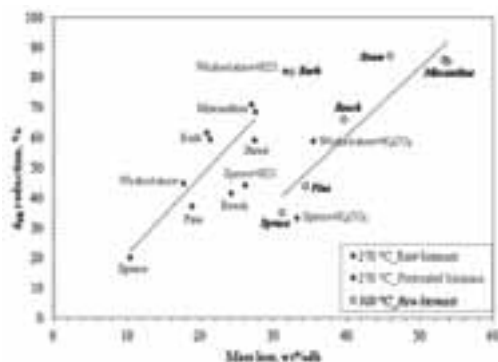


Figure 7: Relationship between d_{50} reduction and mass loss of torrefied biomass with different K content

Conclusions

The biomass potassium content has a catalytic influence on the torrefaction process. The results from this study show that the conversion is strongly influenced by the presence of potassium in the biomass. Biomass samples with higher potassium content have a lower peak maximum conversion temperature, resulting in a lower char yield at the temperatures investigated. The solid yield produced by the torrefaction process do not only depends on the potassium (K) content, but also the biomass lignocelluloses compositions play an important role in the char formation. A biomass with a high lignin content produces relatively smaller amounts of volatiles and thereby a higher char yield. Meanwhile, a biomass with a high potassium content seems to obtain a larger improvement in grindability when it is torrefied. Especially an increase of the biomass potassium content from 0 to 0.3wt% seems to influence the grindability strongly.

References

1. Fahmi, R., Bridgwater, A.V., Donnison, I., Yates, N., Jones, J.M., TG-FTIR Study of lignin and inorganic species in biomass on pyrolysis oil yields, quality and stability, *Fuel* 87 (2008) 1230 – 1240.
2. Jensen, A., Dam-Johansen, K., Wo'jtowicz, M.A., Serio, A., TG-FTIR Study of the Influence of Potassium Chloride on Wheat Straw Pyrolysis, *Energy & Fuels* 12 (1998) 929 – 938
3. Saddawi, A., Jones, J.M., Williams, A., Influence of alkali metals on the kinetics of the thermal decomposition of biomass, *Fuel Process. Technol.* (2012) DOI:10.1016/j.fuproc.2012.05.014
4. Raveendran, K., Ganesh, A., Khilari, K.C., Influence of mineral matter on biomass pyrolysis characteristics, *Fuel* 74 (1995) 1812 – 1822.
5. Lv, D., Xu, M., Liu, X., Li, Z., Yao, H., Effect of cellulose, lignin, alkali and alkaline earth metallic species on biomass pyrolysis and gasification, *Fuel Process. Technol.* 91 (2010) 903 – 909.

Acknowledgement

The author acknowledges the financial support by the Ministry of Higher Education (MoHE) of Malaysia, Universiti Malaysia Pahang (UMP) and by the company Energinet.dk.

**Lei Shang**

Phone: +45 2132 4979
E-mail: lesh@risoe.dtu.dk
Discipline:

Supervisors: Jesper Ahrenfeldt
Ulrik Birk Henriksen
Jens Kai Holm, Dong Energy

PhD Study

Started: January 2010
To be completed: December 2012

Upgrading Fuel Properties of Biomass Fuel and Waste by Torrefaction

Abstract

Torrefaction is a mild temperature (200-300°C) pretreatment of biomass in an inert atmosphere, which has received increased attention in recent years applying to upgrade fuel properties. During the process, the biomass loses moisture and a proportion of the volatile content, and becomes dry, darker, and brittle. Torrefied biomass is more hydrophobic, has a higher calorific value and is easier to grind.

Introduction

Biomass, as a kind of sustainable energy resource, has recently gained more focus from both politically and scientific view. However, these biomass sources will need special attention and more expensive solutions in terms of storage, handling, milling and feeding compared to existing systems used for coal. Especially in pulverised firing systems [1], size reduction of biomass material is much more demanding than for coal due to its fibrous and more tenacious structure. Other challenges with biomass include low energy density and great inhomogeneity of biomass fuels. Torrefaction is a technique to improve the energy density of biomass, which involves the heating of biomass to moderate temperatures in the absence of oxygen and under atmospheric pressure. During the treatment, biomass starts to decompose and release combustible torrefaction gas together with moisture. Thereby, the energy density of the torrefied biomass is increased. Moreover, during the torrefaction the structure of the torrefied biomass is changed to be more brittle, and thus much easier to be ground [2-4]. This effect would lower the energy demand during size reduction of the biomass prior to the combustion or pelletization. Furthermore, if combine torrefaction with pelletization, it will significantly increase the energy density of biomass fuels and thus energy and emission savings could be made in the transport of fuel.

The process of torrefaction has been known for processing of wood since about 1930. Previous research [5-8] shows that the result of the torrefaction process depends on the temperature, heating rate, time and composition of the biomass heated, and the amount of

hemicelluloses is a major factor for how the material will react during torrefaction. Because hemicellulose is reactive at lower temperatures than the other main components of biomass, lignin and cellulose. However, the full extent of these reactions is unknown. Meanwhile, the knowledge of torrefaction is not clearly defined yet. For example, different temperature ranges of torrefaction are found in literature, there is lack of detailed understanding about chemistry occurring during torrefaction, and no mathematical model that can be directly used for predicting the mass yield of solids in real production was developed, etc. Regarding the combination of torrefaction and pelletization, it was first proposed by Energy Research Centre of Netherlands in 2005 [4]. So far only a few studies have been published about the pelletizing properties of torrefied biomass [11-13], and no other publications about the quality of torrefied pellets (different from pellets made from torrefied biomass) have been found. The aim of this project is to understand torrefaction and the property changes of biomass caused by torrefaction at different operation conditions. The goal was to achieve a product that could be used for co-firing in large scale utility boilers. Further aims were to combine the pelletizing process with torrefaction to achieve a product with even higher energy density and durability.

Specific Objectives

This project can be mainly divided into 3 parts: 1) characterize the property changes (grindability, hygroscopicity, cell wall composition, etc) of wheat straw, wood chips, and wood pellets caused by torrefaction; 2) investigate the quality of pellets made from torrefied biomass and pellets that are torrefied

subsequent to pelletization; 3) study the degradation kinetics and devolatilization of wheat straw and develop a method for predicting the mass yield and energy yield of feedstock in real production.

Experimental

Torrefaction was held by placing oven dried samples in an air tight metal container that could be heated in an oven to the desired temperature. Nitrogen was pumped through the sample container. The temperature of the oven was measured in the centre of the chamber and was used for temperature control. The heating rate programmed for the oven was 6 °C/min. The residence time of the torrefaction process starts when the material temperature has reached the set temperature until it starts to cool down. Torrefaction was carried out at 200 to 300°C. Anhydrous weight loss (AWL) was determined as the sample weight loss after torrefaction. 3 different biomass materials have been torrefied, they are wood chips, wood pellets and wheat straw.

Grindability of biomass fuels were tested on a standard Hardgrove grinder by feeding 50 cm³ samples with particle size between 0.6-1.18 mm. The equivalent Hardgrove Index was determined by Eq. (1), which was obtained in our earlier work from the reference coal samples:

$$HGI_{\text{equiv}} = \frac{(wt.\% + 5.2521)}{0.3577} \quad (1)$$

Where *wt.%* is the weight percent of the ground product passing the 75 µm sieve. The specific energy required for grinding was determined on a bench scale disc mill. Higher heating value (HHV) was determined on a bomb calorimeter. Hygroscopicity of biomass fuels were measured by placing samples in 3 different relative humidity, and recording the weight change once a week. Gas products evolution during torrefaction was studied on a mass spectrometer coupled TGA, which allows analyzing the evolved gas on-line. The heat-induced chemical modification of wheat straw was monitored by both Attenuated Total Reflectance (ATR) – FT-IR spectroscopy and chemical analysis of cell wall composition.

Results and Discussion

HHV and AWL for 3 biomass on dry and ash free basis (daf) are shown in Figure 1. It is not a liner relationship between AWL and HHV/energy yield. There is more energy and mass loss at torrefaction temperatures ranging from 250 to 300 °C compared to from 200 to 250 °C. Energy yield was defined as the ratio between total thermal energy retained in the torrefied samples and in the oven dried samples. For tested biomass species, the same AWL corresponds to a similar fraction of energy loss in the samples during torrefaction.

The results of equivalent Hardgrove Grindability Index for different biomass samples torrefied at different temperatures are shown in Figure 2. The grindability of torrefied wood pellets was not improved satisfactorily according to HGI results, while the grindability of wheat straw was proved to be enhanced by the

torrefaction treatment most. In order to achieve similar grindability as coal, torrefaction temperature of above 240 °C would be needed for wheat straw and wood chips, and 290 °C would be required for wood pellets.

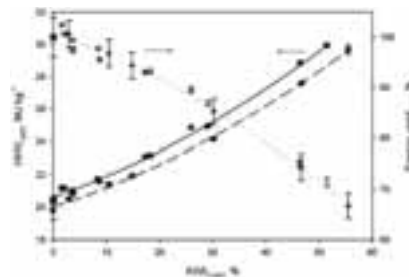


Figure 1: Higher heating value for wheat straw (●), wood pellets (■) wood chips (▲), and energy yield for wheat straw (+), wood pellets (-), wood chips (×) vs. anhydrous weight loss (torrefaction was carried out from 200 to 300 °C with every 20 °C interval) [9].

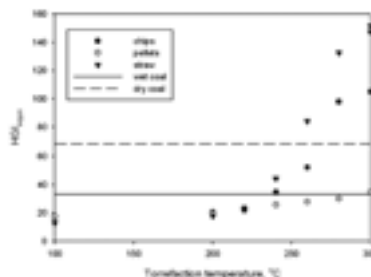


Figure 2: Results of Hardgrove Grindability test for biomass torrefied at different temperatures (2h), coal in wet and dry condition were also tested as reference [9].

Figure 3 shows the results of specific energy requirement of grinding pellets and wood chips torrefied at different degrees. Different from the HGI results, wood chips consumed more grinding energy than pellets, except for the highest AWL (about 50%) where energy use in grinding these two fuels are tend to be close. It means that HGI tests do not have direct correlation with energy consumption during grinding. Moreover, energy use for both wood chips and pellets showed a sharp decrease in the first 25% and 10% AWL respectively, and then followed by decreases with lower rates. Therefore, these two AWLs can be suggested as the optimal torrefaction condition to achieve the maximum energy saving during grinding while maintain as much HHV as possible. Particle size distribution analysis showed that torrefied wood chips ended up with much higher percent of fines (75 µm) than pellets after grinding, and the higher torrefaction temperature the higher percent of fines. This is consistent with the results from HGI.

Hygroscopicity study showed that when relative humidity increased, equilibrium moisture content (EMC) of all samples (wood chips, wood pellets and

Where the biomass is denoted 'A', and 'B' is the intermediate compound, which is a solid with a reduced degree of polymerization. 'V1' and 'V2' are volatiles; 'C' is the solid residue. In order to verify the model, experimental data were compared with model results from both TGA tests and in a batch reactor. The temperature recorded in the center of the reactor was used as the input for the model to calculate the residual mass, assuming heat transfer from the wheat straw surface to the center is much faster than the heating rate of the oven ($6\text{ }^{\circ}\text{C min}^{-1}$). Model and experimental results are shown in Figure 6. Gas products during torrefaction of wheat straw (250 and $300\text{ }^{\circ}\text{C}$) detected were water, CO , CO_2 , formic acid, formaldehyde, methanol, acetic acid, methyl chloride, traces of hydrogen sulfide and carbonyl sulfide were also found.

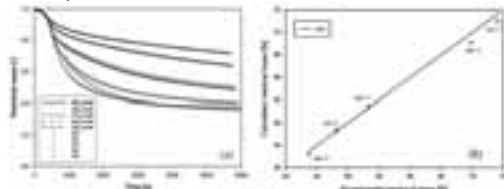


Figure 6: Experimental and modeled relative weight of wheat straw (daf) vs. time for (a) tests run on TGA at heating rate of 10 K min^{-1} ; (b) torrefaction of wheat straw in a batch reactor [16].

Conclusions

It is proved that energy density, grindability, and hygroscopicity of biomass fuels were improved by means of torrefaction. Moreover, the correlation between these properties and degree of torrefaction was also established. The bonds formed during pelletization outlast the torrefaction quite well. In practice, once the kinetic parameters have been obtained from the TGA test, the mass yield in the real torrefaction facility can be predicted by simply knowing the temperature profile of the sample.

Acknowledgements

This work was financially supported by ENERGINET.DK and the ForskEL program (Project 2009-1-10202, Torrefaction of Biomass).

References

1. T. Bridgeman, J. Jones, A. Williams, D. Waldron, *Fuel* 89 (12) (2010) 3911-3918.
2. T. Bridgeman, J. Jones, I. Shield, P.T. Williams, *Fuel* 87 (6) (2008) 844-56.
3. B. Arias, C. Pevida, J. Feroso, MG. Plaza, F. Rubiera, J.J. Pis, *Fuel Process Technol* 89 (2008) 169-75.
4. PCA. Bergman, Combined torrefaction and pelletisation: the TOP process. Report ECN-C--05-073, ECN (2005).
5. J. Deng, G. Wang, J. Kuang, Y. Zhang, Y. Luo, *J Anal Appl Pyrolysis* 86 (2009) 331-7.
6. S. Sadaka, S. Negi, *Environ Prog Sustainable Energy* 28 (2009) 427-34.

7. J.S. Tumuluru, S. Sokhansanj, C.T. Wright, J.R. Hess, R.D. Boardman, A review on biomass torrefaction process and product properties. INL/CON-11-22634.
8. PCA. Bergman, AR. Boersma, RWH. Zwart, JHA. Kiel. Torrefaction for biomass co-firing in existing coal-fired power stations. Report ECN-C--05-013, ECN, Petten (2005a).
9. L. Shang, W. Stelte, R.Z. Zhang, T. Thomsen, L.S. Bach, J. Ahrenfeldt. Physical and chemical property changes of 3 biomass fuels caused by torrefaction, conference paper: WSED Next: 29.Feb - 2.Mar 2012, Wels, Austria.
10. L. Shang, J. Ahrenfeldt, J.K. Holm, AR. Sanadi, S. Barsberg, T. Thomsen, W. Stelte, U.B. Henriksen, *Biomass Bioenerg*, 40 (2012) 63-70.
11. MJC. Van der Stelt, H. Gerhauser, JHA. Kiel, KJ. Ptasiński, *Biomass Bioenerg* 35(9) (2011) 3748-62.
12. W. Stelte, C. Clemons, J.K. Holm, A.R. Sanadi, J. Ahrenfeldt, L. Shang, et al., *Biomass and Bioenerg* 35 (11) (2011) 4690-8.
13. P. Gilbert, C. Ryu, V. Sharifi, J. Swithenbank, *Fuel* 88(8) (2009) 1491-7.
14. L. Shang, N.P.K. Nielsen, J. Dahl, W. Stelte, J. Ahrenfeldt, J.K. Holm, T. Thomsen, U.B. Henriksen, *Fuel Process Technol*, 101(2012) 23-28.
15. C. Di Blasi, M. Lanzetta, *J Anal Appl Pyrol*, 40 (1997) 287-303.
16. L. Shang, J. Ahrenfeldt, J.K. Holm, S. Barsberg, R.Z. Zhang, Y.H. Luo, H. Egsgaard, U.B. Henriksen, *J Anal Appl Pyrol*, under review.

List of Publications

1. W. Stelte, C. Clemons, J.K. Holm, A.R. Sanadi, J. Ahrenfeldt, L. Shang, U.B. Henriksen, *Biomass Bioenerg*, 35 (11) (2011) 4690-4698.
2. L. Shang, W. Stelte, R.Z. Zhang, T. Thomsen, L.S. Bach, J. Ahrenfeldt. Physical and chemical property changes of 3 biomass fuels caused by torrefaction, oral presentation in WSED Next: 29.Feb - 2.Mar 2012, Wels, Austria.
3. L. Shang, J. Ahrenfeldt, J.K. Holm, AR. Sanadi, S. Barsberg, T. Thomsen, W. Stelte, U.B. Henriksen, *Biomass Bioenerg*, 40 (2012) 63-70.
4. L. Shang, N.P.K. Nielsen, J. Dahl, W. Stelte, J. Ahrenfeldt, J.K. Holm, T. Thomsen, U.B. Henriksen, *Fuel Process Technol*, 101(2012)23-28.
5. L. Shang, W. Stelte, J. Ahrenfeldt, J.K. Holm, R.Z. Zhang, Y.H. Luo, S. Barsberg, T. Thomsen, L.S. Bach, U.B. Henriksen, *Biomass Bioenerg*, under revision.
6. L. Shang, J. Ahrenfeldt, J.K. Holm, S. Barsberg, R.Z. Zhang, Y.H. Luo, H. Egsgaard, U.B. Henriksen, *J Anal Appl Pyrol*, under review.
7. W. Stelte, A.R. Sanadi, L. Shang, J.K. Holm, J. Ahrenfeldt, U.B. Henriksen, *BioResources*, 7 (3) (2012) 4451-4490.
8. W. Stelte, N.P.K. Nielsen, L. Shang, J. Dahl, A.R. Sanadi, H.O. Hansen, *Biomass Bioenerg*, under revision.



Laura Snip

Phone: +45 4525 2990
E-mail: lasn@kt.dtu.dk

Supervisors: Krist V. Gernaey
Ulf Jeppsson (Lund University)
Xavier Flores Alsina (Lund University)
Benedek Plósz, DTU Environment
Ulrich Krühne

PhD Study
Started: May 2012
To be completed: April 2015

Practical Application of Models in the Urban Water System: Simulation Based Scenario Analysis

Abstract

Nowadays a wastewater treatment plant is challenged to not only provide clean water but also to take its carbon footprint into account. Another ‘new’ challenge is the removal of so called micropollutants. In order to further optimize the performance of the wastewater treatment plant a good understanding of the production of greenhouse gases and the removal of micropollutants is required. Modeling these processes contributes to the development of a proper understanding of the main mechanisms involved, and enables to test different plant operation scenarios on their efficiency in silico. As a result new evaluation tools can be developed concerning the production of greenhouse gases and the concentration of micropollutants.

Introduction

With the increasing awareness of global warming also wastewater treatment plants (WWTPs) have to monitor their production of greenhouse gases (GHGs). In a WWTP, three different GHGs are produced, namely CO₂, CH₄ and N₂O. The global warming potential (a measurement to compare the effect of different chemicals on the global warming) of CH₄ is 23 kg equivalent CO₂ and that of N₂O is 296 [1]. This shows that a small production of N₂O will have a higher impact compared to a small production of CO₂ and therefore it is important to take those emissions into account.

Besides GHG emissions, a WWTP has a relatively new challenge. Indeed, the development of methods to measure chemicals at low concentrations has resulted in a growing awareness of the presence of micropollutants in the aquatic environment. These micropollutants can originate from medication, illicit drugs and personal care products. Recent studies have shown that these chemicals can influence aquatic life by inducing sex reversal and/or intersexuality [2], or that the reproductive behavior is reduced [3]. WWTPs are traditionally not designed to remove micropollutants; however a change in operational conditions such as increasing the sludge retention time can increase the removal of micropollutants in a WWTP [4].

In order to face these challenges the Benchmark Simulation Model 2 (BSM2) will be extended to include the processes concerning GHGs and micropollutants.

The BSM2 is a general plant wide model of a WWTP that was developed in order to compare different control strategies [5]. The model includes a plant layout, shown in Figure 1, a simulation model, influent loads, test procedures and evaluation criteria. When using the same plant layout, influent loads, test procedures and evaluation criteria, the outcome of different control strategies will be comparable.

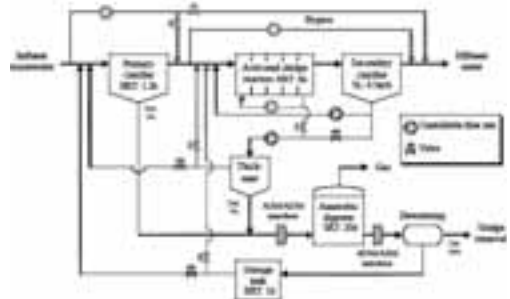


Figure 1: A schematic overview of the plant layout of BSM 2.

Objectives

The objective of this PhD study is to extend the BSM2 with processes involving the greenhouse gas production and processes concerning the micropollutants. Once this extension is made different scenarios will be compared according to newly developed evaluation tools. These evaluation tools should include criteria concerning GHG emissions and micropollutants besides the current

effluent quality index and operational cost index,. Also, different control strategies will be tested to investigate potential improvements of plant operation.

Carbon footprint of the WWTP

Nitrous oxide is being produced in a WWTP as an intermediate during heterotrophic denitrification, which is an anoxic process. Also it can be produced in the aerobic tanks by ammonia oxidizing bacteria. This can happen during nitrifier denitrification and by chemical reactions; however it is not yet known precisely how these processes work and to what extent they contribute to the overall production of N_2O [6]. Ni *et al.* [7] have developed four different mathematical models that can describe the N_2O production. These models can be seen in Figure 2, and will be added to the BSM2 in order to account for N_2O production by ammonia oxidizing bacteria.

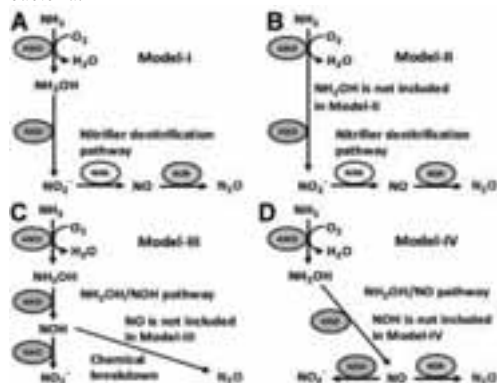


Figure 2: Four different mathematical models to describe N_2O production by ammonia oxidizing bacteria. A and B show the nitrifier denitrification pathway and C and D show the chemical formation of N_2O [7].

For now the CO_2 production is mainly calculated by conversion factors and the CH_4 production by the anaerobic digester is already calculated in the BSM2. The emissions that are taken into account when calculating the carbon footprint are emissions during i) treatment, namely biotreatment, endogenous respiration, BOD oxidation, nitrification (CO_2 credit) and nitrogen removal; ii) energy use of the plant; iii) sludge digestion; iv) sludge disposal; v) power credit by use of biogas; and vi) chemical usage. The emissions during the building of the WWTP are not taken into account as those are not controllable. Once the BSM2 is extended with the production of GHGs, different control strategies can be compared in order to decrease the carbon footprint of the plant.

Micropollutants

There are many different micropollutants present in the water with each compound having its own characteristics. Therefore every compound has to be modeled with different parameters. However the same

processes are responsible for the removal of the micropollutants. The processes removing the micropollutants are sorption and biotransformation [8]. Other processes that also occur with the micropollutants are desorption and retransformation into parent compound. These processes can take place in the aerobic and in the anoxic phase; however there are different parameters for the aerobic and anoxic phase. These processes will lead to three different forms of the micropollutant in the wastewater, namely the liquid form, the sorbed form, and the conjugated form. There is then also a fraction of the micropollutants that can not be removed because it is sequestered. These are just the processes concerning the micropollutants in the activated sludge reactors. To model the fate of the micropollutants in a plant wide context, also the behavior in the influent water and the anaerobic digester should be taken into account.

There are different studies on the removal of micropollutants in a WWTP, however not all include a mathematical model and the published models differ largely. Also the verification of the model might not be accurate as large variations in the measurements can exist. The sampling, sample preparation and the measurement itself can be different in the reported studies [9]. Therefore implementation of models concerning the fate of micropollutants has to be done with consideration. Once the implementations are done, the optimization of the plant operation can be done, by comparing different control strategies.

References

1. IPPC, Climate Change 2001: The Scientific Basis, Cambridge University Press, 2001, chapter 4.
2. A. Lange, G.C. Paull, T.S. Coe, Y. Katsu, H. Urushitani, T. Iguchi, C.R. Tyler, Environmental Science and Technology, 43 (4) (2009) 1219-1225.
3. T.S. Coe, P.B. Hamilton, D. Hodgson, G.C. Paull, J.R. Stevens, K. Sumner, C.R. Tyler, Environmental Science and Technology, 42 (13) (2008) 5020-5025.
4. M. Clara, N. Kreuzinger, B. Strenn, O. Gans, H. Kroiss, Water Research, 39 (1) (2005) 97-106.
5. U. Jeppsson, M.-N. Pons, I. Nopens, J. Alex, J. Copp, K.V. Gernaey, C. Rosen, J.-P. Steyer, P.A. Vanrolleghem, Water Science and Technology, 56 (8) (2007) 67-78.
6. M.J. Kampschreur, H. Temmink, R. Kleerebezem, M.S. Jetten, M.C. van Loosdrecht, Water Research, 43 (2009) 4093-4103.
7. B.-J. Ni, Z. Yuan, K. Chandran, P.A. Vanrolleghem, S. Murthy, Biotechnology and Bioengineering, 110 (1), (2013) 153-163
8. B.Gy. Plósz, K.H. Langford, K.V. Thomas, Biotechnology and Bioengineering, 109 (11) (2012) 2757-2769
9. A.C. Johnson, T. Ternes, R.J. Williams, JP. Sumpter, Environmental Science and Technology, 42 (15) (2008) 5390-5399

**Eike Marie Thaysen**

Phone: +45 51801481
E-mail: emth@kt.dtu.dk

Supervisors: Iver Jakobsen
Per Ambus

PhD Study

Started: August 2010
To be completed: July 2013

Climate Change Mitigation by Transport of CO₂ to Aquifers beneath Croplands

Abstract

The potential for mitigating CO₂-induced climate change through storage of CO₂ in aquifers was investigated by measuring carbon dioxide partial pressure (pCO₂), dissolved inorganic carbon (DIC) and carbon dioxide exchange in unplanted soil mesocosms (controls) and in mesocosms planted with barley. DIC flux to the groundwater was correlated to drainage volume and amounted to 17± 2.5 mg C m⁻² d⁻¹ in control mesocosms. Higher pCO₂ in mesocosms planted with barley also resulted in a higher DIC flux to the aquifer being 27 ± 0.3 mg C m⁻² d⁻¹.

Introduction

Worldwide concern about climate change and the effects on the future environment requires a better understanding of the global carbon (C) cycle [1]. In addition to large-scale C cycling, leaching losses of dissolved C from soils turned out to affect annual C budgets of croplands, but estimates of carbon losses are few [2]. A proportion of the C leached from soils is in the form of DIC and the amount of CO₂ dissolved into the groundwater varies with the pCO₂, initial pH and temperature [3]. However, our understanding of production and transport of CO₂ in the soil and of how these processes are affected by changes in meteorological and soil variables is incomplete [1]. In this work we measured CO₂ fluxes in a soil mesocosm system to increase current knowledge on CO₂ transport in soils and to investigate the potential for DIC storage in aquifers beneath croplands.

Specific Objectives

The objective was to assess the effect of a typical crop on soil CO₂ content and DIC transport to aquifers as compared to CO₂ fluxes in unplanted soil. Four replicate mesocosms were filled with coarse sand and incubated in a climate chamber. Barley (*Hordeum vulgare L.*) was grown in mesocosms 1 and 2 while mesocosms 3 and 4 remained unplanted. Results are exemplified by mesocosms 2 and 4. The pCO₂ in the soil air at different depths, soil respiration and photosynthesis as well as the C storage (defined as the amount of DIC in the drainage) was determined at regular intervals.

Results and Discussion**Soil Air CO₂ Content**

The pCO₂ under growth of barley increased steadily with plant age and peaked at 8% at ~25 cm depth 56 days after sowing (Fig.1A). On the day of the last measurement, 69 days after seeding, but before plant maturity, pCO₂ in soil air had dropped to 5%. Measured peak CO₂ levels in mesocosms with barley were 3-5% higher than observed in the field under barley cultivation in a sandy soil [4] and in a study on a silt loam soil addressing CO₂ dynamics concentrations under actively growing winter wheat [5].

In control mesocosms, pCO₂ was ~1 order of magnitude lower than in planted mesocosms at 0.3-1% (Fig.1B). The control mesocosms showed slightly decreasing CO₂ levels with time. Results for control mesocosms were in agreement with the CO₂ content of 0.5-1% in unplanted silt loam soil under field conditions [5]. In both control mesocosms and mesocosms with barley the pCO₂ was strongly reduced at 6-7 cm depth due to loss by diffusion.

CO₂ Exchange

CO₂ production (the CO₂ flux measured under darkness) of planted mesocosms increased slightly up to 45 days after planting. A subsequent boost in ecosystem respiration coincided with a high-intensity irrigation event of 69 mm (Fig. 2A). Mean respiration rates throughout the experimental period were 24±18 μmol m⁻² s⁻¹. A maximum respiration rate of 51 μmol m⁻² s⁻¹

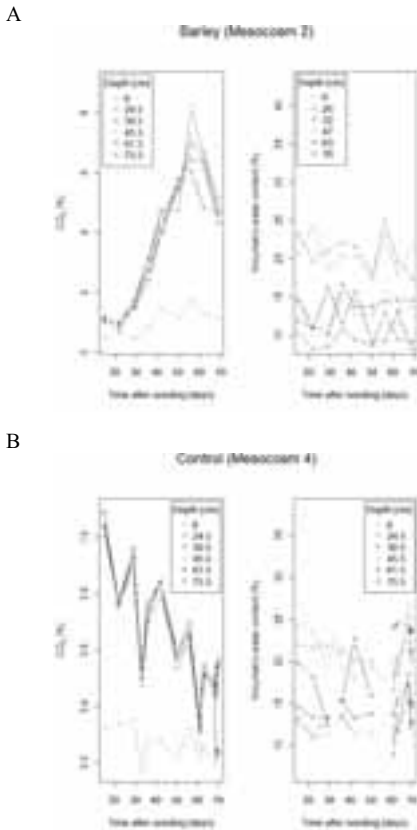


Figure 1. Profiles of the volumetric percentage of CO₂ in the soil air and soil moisture content in mesocosms with barley (A) and control mesocosms (B) at consecutive days after sowing.

was observed on day 72. Soil surface temperatures were 20-24°C at daytime. Somewhat higher respiration rates of 86-143 $\mu\text{mol m}^{-2} \text{s}^{-1}$ were observed after a 23-mm rain event few days after disk-incorporation of wheat residues [6] but the bulk of reported respiration rates measured under growing crops at temperatures >20°C are 10 times lower, e.g. [5]. With temperatures being comparable to the other studies, the considerably higher respiration rates from the mesocosms were probably caused by the high irrigation rates that by far exceeded rates at field conditions and by, the generally high soil CO₂ contents.

The CO₂ respiration from control mesocosms was 0.1-3 $\mu\text{mol m}^{-2} \text{s}^{-1}$ throughout the whole experimental period, except for -0.5 to -3 $\mu\text{mol m}^{-2} \text{s}^{-1}$ at days 61, 72 and 78 (Fig 2B). Mean respiration rates throughout the experimental period were $0.2 \pm 1.5 \mu\text{mol m}^{-2} \text{s}^{-1}$. In contrast to planted mesocosms, control mesocosms did not respond significantly to high irrigation amounts. The soil respiration rates of control mesocosms were in the lower range of what has previously been reported for

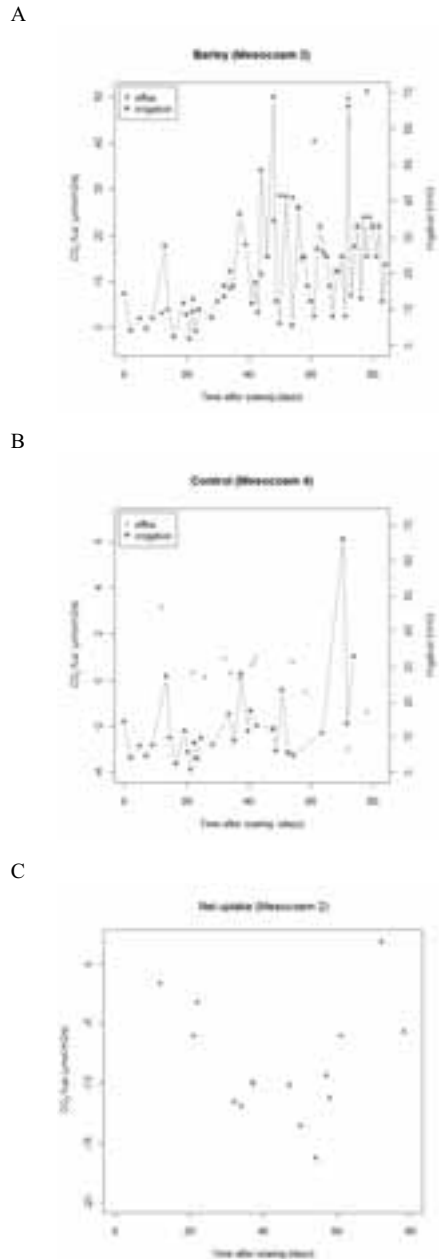


Figure 2. CO₂ production and daily irrigation amounts in mesocosms with barley (A) and in control mesocosms (B). Net uptake of CO₂ in planted mesocosms over time is shown in C.

unplanted soil, e.g. 1.3-4 $\mu\text{mol m}^{-2} \text{s}^{-1}$ [7]. Although the top surface soil of the mesocosms was loosened regularly, frequent watering with nutrient solution

caused growth of algae in the upper few cm of the soil. The photosynthetic activity of the algae is likely to have caused slightly reduced values for CO₂ production at the end of the experiments.

Net CO₂ uptake by planted mesocosms (the CO₂ flux measured under light) varied considerably due to daily variation in photosynthesis rates. Net uptake showed a trend towards increased uptake with plant age up to 54 days after sowing (Fig. 2C). Thereafter it decreased to values similar to those observed 20 days after sowing. The decline in net uptake reflected a decreased ratio between gross photosynthesis and soil respiration and was associated with declining CO₂ contents in the soil air after day 56 (Fig. 1A).

Carbon Storage

Carbon storage varied considerably over time in both unplanted and planted mesocosms, as did the drainage (Fig. 3). Gaps in the figure are due to missing samples, but nevertheless a pattern in DIC leaching is visible. As anticipated, total leached C depended on the drainage volume in both control and planted mesocosms. In an equilibrated carbonated system, the volumetric concentration of CO₂ in the soil solution exceeds the volumetric concentration in the air by a factor of 5-10 [8]. Hence, under equal incubation conditions, the higher partial pressures of CO₂ in mesocosms with barley were expected to increase DIC concentrations in soil water and drainage. At individual time points, the higher pCO₂ in mesocosms with barley had no clear effect for the C storage (Fig. 3), but the mean cumulative amount of 37±6 mg C leached from planted mesocosms was significantly higher than the corresponding amount of 22±3 mg C leached from control mesocosms. The cumulative drainage was 127±9 mm and 149±12 mm for mesocosms with barley and control mesocosms, respectively. Due to the lack of plant mediated transpiration more water passed faster through unplanted mesocosms and moved considerable amounts of DIC to the aquifer even at low soil air CO₂ contents.

Extrapolating mesocosm data on CO₂ storage under barley to a growth period of 3.5 month in the field suggests an aquifer storage of 2.8±0.2 g C m⁻² yr⁻¹. This is similar to a reported mean annual DIC flux to the groundwater of 2.0 g C m⁻² under winter barley and winter wheat at drainages of ~87.5 mm yr⁻¹ [9]. Higher DIC leaching losses of 16±4 g C m⁻² yr⁻¹ were reported for two European cropland soils with silt loam texture at increased drainages of 582 mm yr⁻¹ [2].

The Deviation between Results from Mesocosm and Field Studies

There are several possibilities to explain why soil CO₂ contents were higher in planted mesocosms than in the field. Mesocosms were kept at air temperatures of 18°C, creating soil temperatures approximately 10°C higher than in the field. Such difference would have caused higher root respiration and soil microbial activity in the

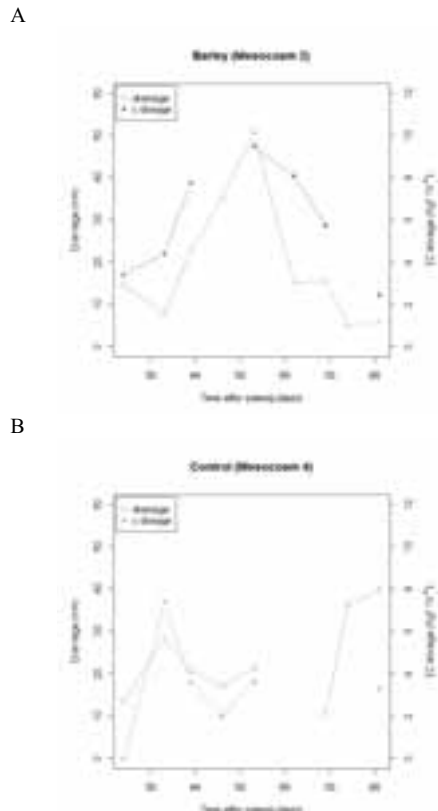


Figure 3. Weekly drainage and C storage from mesocosms planted with barley (A) and control mesocosms (B).

mesocosms than in the field. In control mesocosms that were irrigated with nutrient solution, organic carbon would soon become the limiting factor for microbial respiration, as initial amounts were low (3% C). In planted mesocosms, microbes were continuously fed with C from root exudates and dying roots. Furthermore, if the rhizosphere priming effect is increased at higher temperatures as was indicated by [10] this could also explain the higher pCO₂ in planted mesocosms.

In addition, planted mesocosms were irrigated frequently, applying total daily irrigation amounts that exceeded “normal” rain events by up to ~10 times. While a big part of this water was transpired (>50% at all times in planted mesocosms), water content in the topsoil averaged 20% during experiments (data not shown). Field surface soil moisture content of a sandy soil is likely lower than in mesocosms due to less frequent rain episodes and fast drainage of the coarse-sanded soil of the study. Lower water content in the topsoil causes more soil CO₂ to escape to atmosphere due to eased diffusion, lowering pCO₂ at depth.

Despite high soil CO₂ contents and intensive irrigation in our study, including two high-intensity rain events of 68.5 and 66 mm, CO₂ was not retrieved at elevated rates in the saturated bottom zone. However, our DIC storage estimate of 2.8 g C m⁻² yr⁻¹ does neither comprise periods without plant cover nor leaching to groundwater under root degradation. CO₂ levels in the soil air under wheat were reported to be highest under root degradation, reaching 6-8% [5]. During periods when water transport to the aquifer is increased due to absence of plant transpiration, such high CO₂ levels are therefore expected to cause significant DIC transport to the aquifer.

Conclusions

The soil pCO₂ in mesocosms planted with barley reached levels of 8% while control soil mesocosms had pCO₂ values between 0.3-1%. Soil pCO₂ during growth of barley was higher than in comparable field studies, probably due to a combination of elevated soil temperatures, optimal nutrient supply and an intensive irrigation scheme. Soil pCO₂ in control mesocosms was comparable to field conditions, but was probably limited by low amounts of labile soil organic carbon. Our results show that at rather constant and high soil surface temperatures (>20°C), irrigation is the controlling factor for CO₂ efflux. DIC transport to the groundwater was correlated to drainage volume both with and without plants. Mean cumulative fluxes of DIC leached from mesocosms with barley amounted to 27± 0.3 mg C m⁻² d⁻¹ and were higher than fluxes from control mesocosms of 17± 2.5 mg C m⁻² d⁻¹, indicating higher carbon storage potential in aquifers under cropped agricultural land. High soil air CO₂ contents did not increase DIC storage compared to what has been reported by other studies, but results might be influenced by the lack of data on DIC storage during root degradation.

Acknowledgements

I would like to thank my supervisors Iver Jakobsen and Per Ambus as well as Søren Jessen (KU) for guidance and support.

References

1. R. Jassal, A. Black, *Agr. Forest Meteorol.* 130 (3-4) (2005) 176-192.
2. R. Kindler, J. Siemens, et al., *Glob Change Biol* (2010) 1-11.
3. I. Clark, P. Fritz, *Environmental Isotopes in Hydrogeology*, CRC Press LLC, Boca Raton, FL, USA, 1997.
4. S. Jessen, Personal Communication on CO₂ levels in the unsaturated zone at the field site at Voulund, Denmark. E.M. Thaysen, Copenhagen.
5. G.A. Buyanovsky, G.H. Wagner, *Soil Sci Soc Am J*, 47 (1983), 1139-1145.
6. P.J. Bauer, J.R. Frederik, et al., *Soil Respiration Rates After 25 Years of No Tillage*, 26th

Southern Conservation Tillage Conference for Sustainable Agriculture, Auburn University, Raleigh, NC, USA, 2004.

7. L. Weihermüller, J.A. Huisman, et al., 2009, *Vadose Zone J.* 8 (3) (2009) 772-782.
8. M. Maier, H. Schack-Kirchner, et al., *Agr. Forest Meteorol.* 151 (12) (2011) 1723-1730.
9. J. Siemens, A. Pacholski, et al., *Biogeochemistry* 108 (2012) 135-148.
10. B. Zhu, W. Cheng, *Glob Change Biol* 17 (2011) 2172-2183.

**Rasmus Trane**

Phone: +45 4525 2809

E-mail: rt@kt.dtu.dk

Supervisors: Anker D. Jensen
Søren Dahl, Haldor Topsøe A/S**PhD Study**

Started: August 2010

To be completed: August 2013

Catalytic Steam Reforming of Bio-Oil to Hydrogen Rich Gas

Abstract

Steam reforming (SR) of bio-oil can be used to produce syngas or hydrogen in a sustainable manner. However carbon deposition is one the major hurdles and it leads to catalyst deactivation. Several means of lowering carbon deposition by changing the catalyst formulation has been investigated in SR of ethanol. Addition of CeO₂, ZrO₂, and K could decrease carbon deposition and in some cases also increase conversion. Carbon deposition could also be decreased by adding sulfur, however, the reforming activity decreased as well.

Introduction

Liquid fuels, like diesel and gasoline, contain hydrocarbons and currently the only route for producing these fuels in a sustainable manner is from biomass. Biomass has a low energy density making transportation of untreated biomass costly. However, bio-oil can be produced through pyrolysis of biomass and has an energy density up to 10 times higher than bulk biomass. This makes bio-oil interesting as an energy carrier. However, bio-oil is not suited for direct use due to a low heating value and poor storage stability, and therefore needs upgrading.

Prospective upgrading methods are steam reforming of bio-oil, which can be used to produce syngas or H₂ or hydrodeoxygenation, where the oxygen is removed from the bio-oil, which results in a crude oil-like product [1-3]. Both options will provide sustainable alternatives to conventional fossil fuel based processes. SR of bio-oil can be performed over supported Ni or noble metals catalysts, where high degrees of conversion and high yields of the desired products can be achieved. However, carbon deposition causes short lifetimes of catalysts and new catalysts or processes must be developed to make SR of bio-oil feasible [3-5]. Steam reforming of ethanol has been investigated initially. Ethanol was chosen as a model compound of bio-oil, because it has a functionality which is found in bio-oil and it has tendency to form carbon, which is one of the major problems in SR of bio-oil

Specific objectives

This Ph.D. projects aims to find catalysts or operating conditions for SR of oxygen containing hydrocarbons,

which enables operation with low carbon deposition. Several model feeds will be investigated along with the effect of catalysts poisons like sulphur.

Experimental

MgAl₂O₄ were prepared by dissolving Mg(NO₃)₂ in H₂O and mixing with alumina (Puralox TH-150, 150 m²/g). The slurry was dried over night at 110 °C and then calcined at 900 °C for 8 hours.

Catalysts were prepared by incipient wetness impregnation. MgAl₂O₄, CeO₂, and CeZrO₄ were impregnated with approx. 8 wt% Ni. Ni(NO₃)₂·6H₂O was dissolved in a minimum amount of water. The solution was mixed with the dry carrier material and stirred. After this the wet particles were dried at 110 °C over night and calcined at 800 °C for 2 h.

Addition of CeO₂, ZrO₂, and K were done by co-impregnation with the nitrates of the compounds and Ni(NO₃)₂·6H₂O on MgAl₂O₄ followed by drying and calcination.

Sulfur was added by impregnation with K₂SO₄ or H₂SO₄ on Ni-CeO₂/MgAl₂O₄ followed by drying at 110 °C over night.

The experimental setup used for testing the SR of ethanol consisted of two bubble columns connected to a quartz tube with the catalyst bed inside a three-zone furnace as shown in figure 1.

In the bubble columns N₂ flows were saturated with ethanol or water at 60 °C and 79 °C, respectively. This gave a feed gas with approx. 3 mole% ethanol and 39 mole% H₂O in N₂.

The reactor effluent was passed through a condenser operated at 10 °C before passing the analysis section

consisting of a Variant Micro-GC CP-4900 with two TCD's for the permanent gasses and a NGA 2000 on-line gas analyzer for CO, CO₂, and O₂.

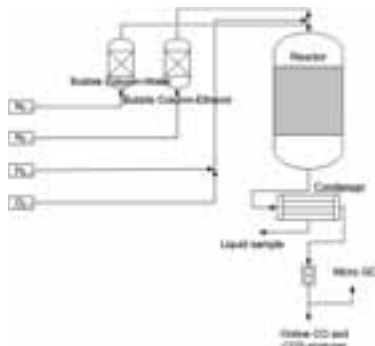


Figure 1: Flowsheet for the setup used to investigate the SR of ethanol.

Results and discussions

Initially the conversion and product distribution at temperatures between 400 and 700 °C were investigated for several different supports for Ni. The offgas concentrations and conversions as function of temperature in SR of ethanol over Ni/CeZrO₄/MgAl₂O₄ can be seen in figure 2. The conversion increased with temperature along with the concentration of CO and H₂. The CO₂ and CH₄ concentration decreased with temperature while the ethene concentration had a maximum at 500 °C. This behavior was similar for the different support materials and resembled the thermodynamic equilibrium where CO and H₂ are favored at high temperatures. These trends were similar for all the tested catalysts.

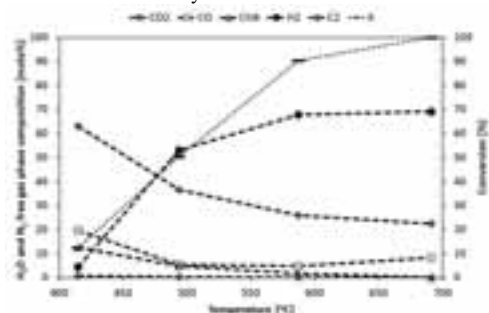


Figure 2: Exit concentrations as function of temperature over Ni/CeZrO₄/MgAl₂O₄. WHSV=12.8 h⁻¹; S/C=5.8; 8.2 wt% Ni. N₂ as balance.

The conversion as function of temperature over Ni on different support materials can be seen in figure 3. Here it can be seen that Ni/Ce_{0.6}Zr_{0.4}O₂ had the highest conversion and therefore seemed interesting. The high conversion might be ascribed to increased water dissociation over CeZrO₄, which aids in carbon gasification [5]. Apparently stable operation for at least 24 h could be achieved at 600 and 700 °C for this

catalyst. Furthermore it was found that the addition of 10 wt% of both CeO₂ and ZrO₂ to a Ni/MgAl₂O₄ had a beneficial effect on the conversion as shown in figure 3. This might be due to a similar effect as for CeZrO₄. Ni/CeO₂ had the lowest conversion at high temperatures, while Ni/MgAl₂O₄ had a conversion between Ni/MgAl₂O₄ and Ni/Ce_{0.6}Zr_{0.4}O₂.

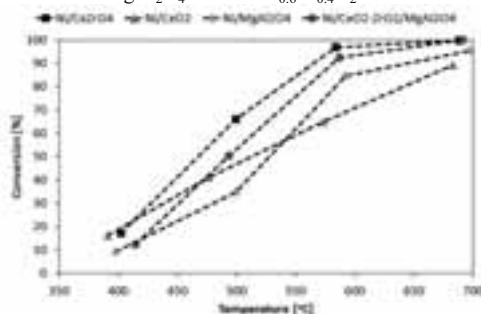


Figure 3: The conversion as function of temperature for selected catalysts. Experimental conditions: S/C: 5.3-6.0; Temp.: 400-700 °C; WHSV= 12.8-14.0 h⁻¹; Ni loading: 8.0-8.5 wt%.

It was chosen to test the different catalysts at approx. 600 °C in order to determine differences in carbon deposition and activity. At this temperature full conversion was not achieved, which lead to higher potential for forming carbon deposits and therefore it is easier to distinguish differences in catalytic performance.

The conversion as function of time over Ni supported on four different support materials tested at 590 °C can be seen in figure 4. All the tested catalysts showed a more or less pronounced decrease in conversion with time. The deactivation was most pronounced for Ni/CeO₂ and Ni/MgAl₂O₄ while especially Ni/Ce_{0.6}Zr_{0.4}O₂ had a very low drop in conversion. An eight hour experiment has also been conducted on the same catalyst where no deactivation was apparent.

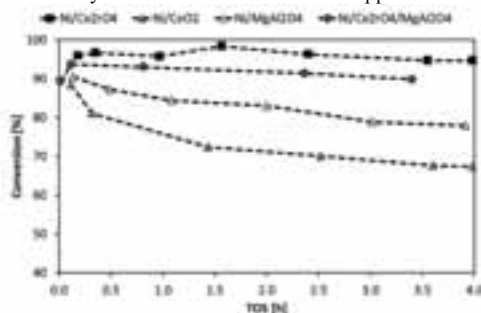


Figure 4: Conversion as function of time at 580°C for Ni on four different supports. Experimental conditions: S/C: 5.3-6.0, Temp.: 579-585 °C, m_{Cat}=0.50 g, Ni loading: 8.0-8.2 wt%, F_T=1.5-1.6 NL/min, x_{Eth}=3.2-3.5 %, x_{H2O}=38.6-39.2 %, N₂ as balance.

The cause of deactivation was most likely due to either sintering or carbon deposition or both. In order to determine if sintering could be a problem, the BET surface area and XRD Ni-particle size were measured before and after an experiment and the results are shown in table 1. The surface area for Ni/CeO₂ and Ni/Ce_{0.6}Zr_{0.4}O₂ decreased by factor of roughly 3 and 2, respectively, while the Ni particle size increased by a factor of 3 and 2, respectively. This shows that sintering of both the metal particles and the support materials takes place. For Ni/MgAl₂O₄ and Ni/CeZrO₄/MgAl₂O₄ the surface areas did not decrease significantly, while the Ni particle size increased by a factor of 1.5 for both of the catalysts. The change in Ni particle size for all the catalysts showed that sintering did occur. However, the two spinel based catalysts seemed more stable as the changes in BET surface areas and Ni particle size were less pronounced over a 60-70 h experiment.

Table 1: Comparison between BET surface area and XRD Ni particle size before and after a temperature dependence experiment with 60-70 h on stream.

Catalyst	BET surface area [m ² /g]		Ni particle size [nm]	
	Fresh	Spent	Fresh	Spent
Ni/CeZrO ₄	90	42	15-20	20-28
Ni/CeO ₂	113	37	10	27
Ni/MgAl ₂ O ₄	69	66	7	11
Ni/CeZrO ₄ /MgAl ₂ O ₄	63	53	6	9

The other possible cause of deactivation was carbon deposition and the amounts of carbon formed on each of the catalysts determined by TPO are shown in table 2. Ni/Ce_{0.6}Zr_{0.4}O₂ had the highest carbon deposition of 1.5 mole C/mole C_{Feed}·100 or 96 mg/(g_{Cat}·h), which may seem contradictory to the fact that it remained stable and active over time. However, the carbon could be whiskers on this catalyst, which is known not to decrease the catalytic activity [6]. The formation of carbon whiskers was confirmed by TEM images of spent Ni/Ce_{0.6}Zr_{0.4}O₂. The other catalysts had much lower carbon depositions in range of 0.2 to 0.4 mole C/mole C_{Feed}·100 or 15-26 mg/(g_{Cat}·h). It was found that adding CeO₂-ZrO₂ to Ni/MgAl₂O₄ could decrease carbon deposition from 26 to 15 mg/(g_{Cat}·h). This decrease could be due to reaction of coke with O-species on CeZrO₄ during operation or due to an increased amount of OH-species on the support. Ni/CeO₂, Ni/MgAl₂O₄, and Ni/CeZrO₄/MgAl₂O₄ had nickel particles with a particle size of 6-10 nm while Ni/Ce_{0.6}Zr_{0.4}O₂ had nickel particles with diameter of 15-20 nm. Therefore the lower amount of carbon on Ni/CeO₂, Ni/MgAl₂O₄, and Ni/CeZrO₄/MgAl₂O₄ compared with Ni/Ce_{0.6}Zr_{0.4}O₂ could be due to smaller Ni particles, which lowers the risk of formation of carbon whiskers [6; 7].

Deactivation by sintering and carbon deposition was apparent for all of the tested support materials.

Therefore others changes to catalysts formulation and operating conditions were investigated as well.

The carbon deposition as function of the temperature for Ni/MgAl₂O₄ and Ni/Ce_{0.6}Zr_{0.4}O₂ can be seen in figure 6 for experiments with 4 h on stream. The experiments for Ni/Ce_{0.6}Zr_{0.4}O₂ at 400 and 500 °C were stopped after 2 h on stream due to carbon build up causing a large pressure drop over the reactor.

Table 2: Comparison of carbon deposited on the catalysts during a 4 hour experiment at approx. 600 °C. Experimental conditions: S/C: 5.3-6.0, Temp.: 579-585 °C, m_{Cat}=0.50 g, Ni loading: 8.0-8.2 wt%, FT=1.5-1.6 NL/min, x_{Eth}=3.2-3.5 %, x_{H2O}=38.6-39.2 %, N₂ as balance.

Catalyst	Carbon deposition	
	[mg/(g _{Cat} ·h)]	[% of C in feed]
Ni/CeZrO ₄	96	1.5
Ni/CeO ₂	19	0.3
Ni/MgAl ₂ O ₄	26	0.4
Ni/CeZrO ₄ /MgAl ₂ O ₄	15	0.2

The carbon deposition on both Ni/MgAl₂O₄ and Ni/Ce_{0.6}Zr_{0.4}O₂ had a maximum at 500 °C. For Ni/MgAl₂O₄ it decreased with temperature from 94 to 0.2 mg/(g_{Cat}·h) when increasing the temperature from 506 to 741 °C. For Ni/Ce_{0.6}Zr_{0.4}O₂ a significant decrease from 552 to 0.4 mg/(g_{Cat}·h) in carbon deposition was observed when increasing the temperature from 495 to 755 °C. The maximum in carbon deposition coincided with the maximum of ethene in the offgas, which is not unexpected as ethene is as potent coke precursor.

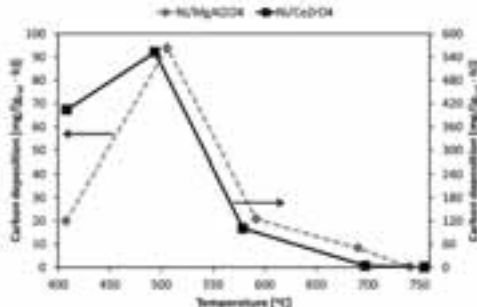


Figure 5: Carbon deposition as function of temperature over Ni/MgAl₂O₄ and Ni/Ce_{0.6}Zr_{0.4}O₂ over a 4 h experiment. 400 °C and 500 °C experiment for Ni/Ce_{0.6}Zr_{0.4}O₂ was stopped after 2 h due to risk of blockage. Experimental conditions: S/C: 5.5-6.2, Temp: 408-755 °C, m_{Cat}=0.50 g, Ni loading: 8.1-8.2 wt%, F_T=1.5 NL/min, x_{Eth}=3.2-3.6 %, x_{H2O}=38.8-39.0 %, N₂ as balance.

These results suggest that higher temperatures lower the risk of carbon formation, which could be due to increased rate of both SR reactions and carbon

gasification, which lowers the risk of carbon accumulation on the catalyst surface.

Changes to the catalyst formulation of Ni/MgAl₂O₄ were investigated to see the effects of K, CeO₂, and ZrO₂ on conversion and carbon deposition. The effect of the different promoters is summarized in figure 6. Carbon deposition decreased for all of the combinations shown figure 6 and in some cases the conversion increased as well. Addition of K and CeO₂ did not influence the conversion but carbon deposition was decreased in both cases. The addition of both CeO₂ and K increased conversion and had the second lowest carbon deposition. These effects might be ascribed to an increased gasification of carbon. Furthermore, increased water dissociation has been observed on CeZrO₄, which would contribute to a higher conversion and lower carbon deposition as observed for Ni/CeZrO₄/MgAl₂O₄ and Ni-K/CeZrO₄/MgAl₂O₄. The TPO curves for combustion of carbon on the different promoted catalysts showed that the oxidation of carbon was moved to lower temperatures compared with Ni/MgAl₂O₄. Ni-K/CeZrO₄/MgAl₂O₄ showed carbon oxidation at lowest temperature of 385 °C compared with 560 °C for Ni/MgAl₂O₄.

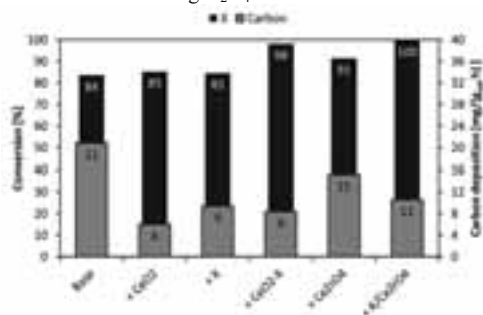


Figure 6: Comparison of the average conversion and carbon deposition for Ni/MgAl₂O₄ with different additives. Experimental conditions: S/C: 5.6-6.1, Temp.: 579-592 °C, m_{Cat}=0.50 g, Ni loading: 8.0-8.3 wt%, FT=1.5 NL/min, x_{Eth}=3.2-3.6 %, x_{H2O}=38.8-39.0 %, N₂ as balance.

Sulfur is known to bond strongly to Ni and the most active sites in SR are step sites. Addition of sulfur to catalysts might bind to step sites and hereby lower the activity of the catalysts but also carbon deposition as carbon accumulation might be lowered. Addition of small amounts of sulfur to the catalyst was investigated and the conversion, carbon deposition, and yield of carbon oxides (CO_x) as function of sulfur in the catalyst is shown in figure 7. It was found that the CO_x-yield decreased with increasing amounts of sulfur on the catalysts, indicating a loss in activity. The carbon deposition was lower with sulfur present and it had a minimum at 0.03 wt% S. Therefore it appears that sulfur can be used to block sites on the catalyst and hereby inhibit carbon deposition. A loss in activity was observed as a decrease in the yield of CO_x. The

observed increase in conversion with addition of sulfur could be ascribed to K as impregnation with H₂SO₄, showed similar trends, but no increase in conversion.

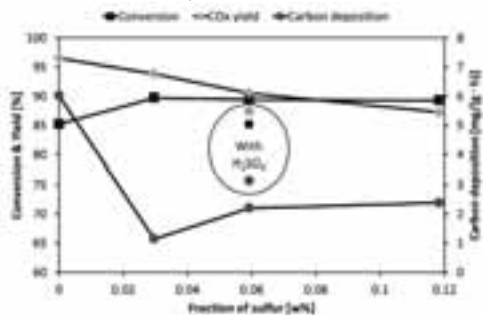


Figure 7: Conversion, carbon deposition, and yield of carbon oxides as function amount of sulfur on Ni-CeO₂/MgAl₂O₄. Curves are guides for the eye. TOS= 4 h, Temp.= 600°C, S/C≈6, WHSV≈13 h⁻¹, 8.3 wt% Ni.

Conclusion

The SR of ethanol was investigated over several Ni-based catalysts and was found to be a challenge as deactivation by both carbon deposition and sintering was observed for all the tested catalysts.

Additives like CeO₂ and K can be used to lower the carbon deposition with no influence on the activity of the catalyst. Combination of ZrO₂, CeO₂ and K induces both an increase in conversion and decrease in carbon deposition.

Addition of sulfur could also decrease carbon deposition, however a decrease in reforming activity was observed.

References

- G.W. Huber, S. Iborra, A. Corma, Chem. Rev. 106 (2006) 4044-4098
- P.M. Mortensen, J.-D. Grunwaldt, P.A. Jensen, K.G. Knudsen, A.J. Jensen, Appl. Catal. A: General 407 (2011) 1-19
- R. Trane, S. Dahl, M.S. Skjøth-Rasmussen, A. D. Jensen, Int. J. Hydrogen Energy 37 (2012) 6447-6472
- A. C. Basagiannis, X. E. Verykios, Cat. Today. 127 (2007) 256-264
- C. Rioche, S. Kulkarni, C. Meunier, J.P. Breen, R. Burch, Appl. Catal. B., Environ. 61 (2005) 130-139
- D. L. Trimm, Catal. Today 37 (1997) 233-238
- J. R. Rostrup-Nielsen in: G. Ertl, H. Knözinger, F. Schüth, J. Weitkamp (Eds.), Handbook of Heterogeneous Catalysis, Wiley-VCH, 2008, p. 2882

List of Publications

- R. Trane, S. Dahl, M. S. Skjøth-Rasmussen, A. D. Jensen, Int. J. Hydrogen Energy 37 (2012) 6447-6472



Trung Ngoc Trinh

Phone: +45 4525 2853

E-mail: tnt@kt.dtu.dk

Supervisors: Kim Dam-Johansen

Peter Arendt Jensen

PhD Study

Started: January 2010

To be completed: March 2013

Fast Pyrolysis of Lignin

Abstract

Fast pyrolysis of lignin from an ethanol plant with a lignin content of 79 wt% daf was successfully pyrolysed on a pyrolysis centrifugal reactor without the plugging of the feeder, however after an hour of operation plugging at the cooling nozzle was observed was investigated on a pyrolysis centrifugal reactor (PCR). A maximal organic oil yield of 31 wt% db is obtained at temperatures of 500 – 550 °C, reactor gas residence time of 0.8 s and feed rate of 5.6 g/min when pyrolysis conditions of the lignin PCR were investigated.

Introduction

Lignin with a typical biomass weight fraction of 15 – 33 wt% is the second most abundant biomass component in biomasses¹ and account for up to 40 % of the biomass energy content. Lignin has a complex, amorphous cross-linked and three-dimensional, highly branched structure² and is formed by a number of chemical groups such as aromatic rings, phenolic, aliphatic, alcohol and methoxy groups.² Lignin is mainly produced by the pulp and paper industry and in the near future it will also appear as a by-product from a bio-ethanol industry. The potential of lignin produced as a residue in the paper industry is more than 50 million tons/year. But only about 2% of the lignin residue is used as commercial products for producing lignosulphonates (1.000.000 tons/year) and kraft lignins (less than 100.000 tons/year).³ Most of the lignin is burned to generate energy for the pulp mills. Thus lignin is considered as a potential source for bio-oil production by fast pyrolysis.

The research on fast pyrolysis of lignin show some initial promising results for lignin utilization.^{4,6} However plugging/agglomeration in the fuel feeder system of fluidized bed reactor and condenser have been observed and is probably due to low melting point of lignin and viscous oil.^{5,6} Also a low bio-oil yield of lignin fast pyrolysis (20 – 58 wt% db)⁵⁻⁷ has been obtained compared to that of wood fast pyrolysis⁸⁻¹⁰. Thus efforts on reactor modifications or new reactor designs for conventional fast pyrolysis are conducted to

overcome these barriers in and enhance the bio-oil yield.

The pyrolysis centrifugal reactor (PCR), a type of ablative reactor, has been developed at the CHEC center at DTU Chemical engineering.¹⁴ By a high centrifugal force, biomass particles can gain a heating rate of 200 – 2000 K/s.¹⁴ The main advantage of this concept compared to fluid bed reactors is a compact design that uses a low flow rate of carrier gas and pyrolyse biomass without a heat carrier (sand). Also the PCR can treat relatively large biomass particles.

The PCR use centrifugal forces for obtaining a high heat transfer rate and movement of solid particles in the reactor. The PCR may provide less problems with plugging/agglomeration in the feeder compared to fluidized bed reactors. Only little information of effects of lignin fast pyrolysis conditions with respect to temperature, gas residence time and feed rate on product yields. Thus the objectives of this work were to provide detailed knowledge on the lignin fast pyrolysis process.

Experimental setup

The pyrolysis centrifugal reactor was developed at the CHEC center (Technical University of Denmark) and is described in detail elsewhere.¹⁴ A sketch of the PCR is presented in figure 1 and pictures of the reactor are showed in figure 2. The lignin is introduced into the reactor by a screw feeder. Pyrolysis of lignin takes place inside the reactor, whereby char, bio-oil and gas are produced. The char particles are collected by cyclones heated up 500 °C. The bio-oil is condensed in a bubble chamber filled with isopropanol as a condensing

solvent. The temperature in the bubble chamber is controlled to be 30 – 50 °C by means of a cooling water system. The light oil fraction and aerosols are further condensed by a coalescer filled with rockwool. A recycled gas product is pumped back to maintain a desired reactor gas residence time (0.5 – 5 s). Before entering the reactor, the gas is heated up to around 500 – 550 °C. The gas products are dried by a water condenser and a gas filter to totally remove liquid before entering a gas meter.

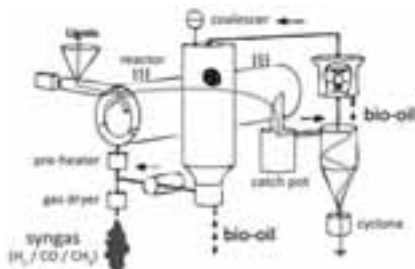


Figure 1: The sketch of the pyrolysis centrifugal reactor (PCR).

The liquid fraction collected from the bubble chamber, coalescer and water condenser is filtered through a Whatman filter paper (pore size of 5 µm). The char left on the filter is washed thoroughly by ethanol and then dried in an oven at 100 °C. The bio-oil yield is determined from the liquid that passed through the filter paper. The char yield is determined from the chars collected in the cyclones and the char left on the filter paper. The gas measured from the gas meter is used to calculate the gas yield by the ideal gas equations.



Figure 2: The reactor (A) is shown with insulation and electrical heating elements removed, reactor wall (B) and rotor (C) after few hour run of lignin pyrolysis.

Results

Table 1 shows the lignin properties. The lignin has volatile content of 61.2 wt% db (determined at 950 °C) and an ash content of 12.1 wt% db and a relatively low potassium content of 0.13 wt% db. The potassium content is important as it is found to influence the pyrolysis process through catalysis that increase the char formation and decrease the production of bio-oil.¹⁸⁻

²⁰ The lignin was collected from a wheat straw ethanol plant it was thus treated and washed several times, consequently although the lignin has the high ash content, it contains a relatively low potassium content when compared to virgin wheat straw.²⁰ The lignin sample has a Klason lignin content of 78.8 wt% daf.

Table 1: The lignin properties.

Moisture (%wt)	4.7
Volatile (% wt dry basis)	61.2
Fixed carbon (% wt dry basis)	26.7
Ash (wt% dry basis)	12.1
HHV (MJ/kg on dry basis)	23.9
Elemental content (%wt dry basis)	
C	57.8
H	5.7
O ^a	23.6
N	1.2
Cl	0.02
S	0.14
Ca	0.43
K	0.13
Na	0.28
Klason lignin (wt% daf)	78.8
Cellulose (wt% daf)	8.3
Hemicellulose (wt% daf)	3.6

Figure 3 shows the TGA and DTG profiles of the lignin sample. The thermal decomposition appears in a temperature range of 150 – 550 °C. A main temperature peak at 350 °C and a shoulder at 220 °C were observed in the DTG curve. The peak and the shoulder are believed to corresponding to decompositions of lignin having a content of 79 wt% daf^{5,6} and hemicellulosic components^{5,21}, respectively. The TGA and DTG of lignin results are consistent with data in the literature.^{5,6}

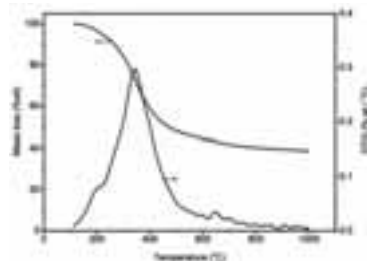


Figure 3: TGA and DTG profiles of lignin.

Lignin is generally been found to be more difficult to use in fast pyrolysis reactor than a wood.⁶ Pluggings/agglomerations in the feeder of fluidized bed reactors are reported when pyrolysing a pure lignin material.^{5,6} The PCR lignin fast pyrolysis experiments were observed to be more difficult than that of wood, straw, or algae²² because of plug formations in the tubes between the reactor and the condenser. A plug at pot outlet (char pot) was observed within 10 minutes at a pyrolysis temperature of 400 °C and a feed rate of 10.4 g/min. Melting of the char at low temperature and consequently agglomeration of unconverted lignin at pot

outlet probably cause the plugging. The phenomenon disappears when the reaction temperature is higher than 450 °C.

However a plugging of the nozzle connecting the cyclone and the condenser appeared after a 60 - 70 minutes operation at the runs conducted at temperatures higher than 450 °C. This means that long lignin pyrolysis tests (several hours) are still not possible. The deposit contains probably heavy tar and fine lignin char particles (particles with a size smaller than 10 µm that cannot be separated efficiently in the cyclone). The nozzle has a low temperature and this may cause the plugging. With the current PCR configuration, the cooling water system of the condenser cannot keep a low constant temperature (less than 50 °C) of the liquid for a long test (several hours). Light components of bio-oil and isopropanol (the cooling solvent) are gradually lifted out of a condenser at the temperature higher than 50 °C. This leads to an increase of oil viscosity in condenser which probably cause of the plugging of nozzle. Furthermore, the nozzle diameter of 4.8 mm seems to be small. The limitations are probably solved by modifications of the condenser's cooling system and nozzle.

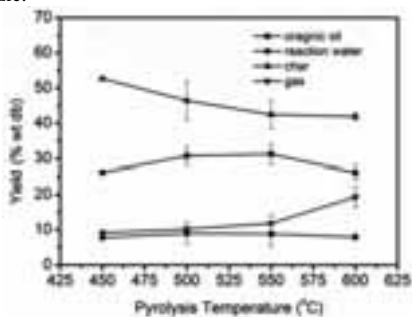


Figure 4: The effect of pyrolysis temperature at reactor gas residence time of 0.8 s, feed rate of 10.4 g/min.

In this study the experiments with PCR lignin pyrolysis were successfully performed with constant operation conditions: an rotor speed of 8870 rpm, a reactor gas residence time of 0.8 second (and 4.2 s for investigations of the influence of reactor gas residence time), a total experimental time of 50 - 62 minutes, a total feed consumption of 204 - 481 g lignin for each run and feeder rates of 4.1 - 10.4 g/min. The results of the effect of changed pyrolysis conditions with respect to temperature, reactor gas residence time and feed rate on product yields distribution are presented in figure 4 - 6. The effect of temperature on lignin pyrolysis product yield trends are observed to be similar to that of wood pyrolysis.¹⁵ A maximal organic oil yield of 30 - 31 wt% db is obtained at temperatures of 500 - 550 °C (see figure 6). A decrease of the organic oil yield from 31 to 25 wt% db is observed when the temperature is increased from 550 to 600 °C. The decrease of the organic oil yield together with a large increase of the gas yield indicates that secondary reactions are important at temperatures higher than 550 °C. That the

secondary reactions are important at high temperatures is consistent to other studies.^{12,17} A decrease of the char yield from 53 to 40 wt% db and an increase of the gas yield from 9 to 20 wt% db were obtained. In contrast the water reaction yield of 8 wt% db seems not to be significantly influenced by the pyrolysis temperature. The reactor gas residence time has a large influence on the organic oil yield and gas yield (see figure 5). The organic oil yield decreases from 31.2 to 17.8 wt% db and the gas yield increase from 11.8 to 24.3 wt% db when reactor gas residence time increases from 0.8 to 4.2 s. Cracking of organic vapors (secondary reactions) to generate non-condensable gases increase with a longer gas residence time.^{12,17}

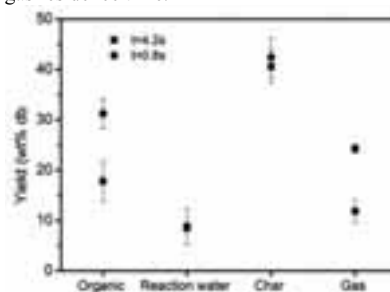


Figure 5: The effect of reactor gas residence time at temperature of 550 °C, feed rate of 10.4 g/min.

The feed rate is often investigated to determine a maximal capacity of a reactor for bio-oil production obtaining a given yield. A reciprocal relation among feed rate, pyrolysis temperature and bio-oil yield are found in the literature.¹⁶ An increase of the feed rate at a constant temperature is known to slightly increase bio-oil yield^{13,16} in fluidized bed reactors. However a further increase of the feed rate will reduce the heating rate of biomass particles, leading to a decreased bio-oil yield. In this study the feed rate is investigated in a range of 4.1 - 10.4 g/min. The organic oil yield obtains a maximum of 34 wt% db at a feed rate of 5.6 g/min (see figure 6). The yield slightly decreases from 34 to 31 wt% db with an increasing feed rate from 5.6 to 10.4 g/min.

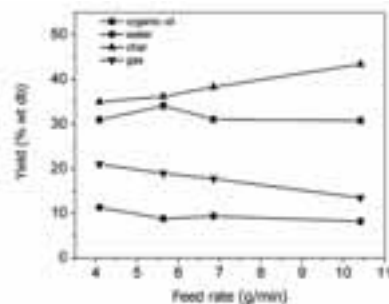


Figure 6: The effect of feed rate at reactor gas residence time of 0.8 s, temperature of 550 °C.

The maximal organic oil yield of 34 wt% db, a char yield of 36 wt% db was obtained at the temperature of

550 °C, reactor gas residence time of 0.8 s and a feed rate of 5.6 g/min. The char yield is 10 wt% lower than the TGA char yield at 550 °C (46 wt% db) and 3 wt% lower than the TGA char yield at 950 °C (39 wt% db) (see figure 3). This indicates that the lignin PCR fast pyrolysis probably obtained optimal conditions for a maximal bio-oil yield.

Table 2: The relation of the lignin, ash content and potassium content of biomasses and the bio-oil and char yields.

Sample	Lignin content (wt% daf)	Ash content (wt% db)	K content (wt% db)	Yield (wt % db) ^(a)			Tech ^(b) - Temp	Ref
				Bio-oil	Char	Gas		
Wood								
Beech	22	0.7	0.12	67	10	23	FBR, 470 °C	10
Spruce	29	0.4	0.04	67	10	23	FBR, 470 °C	10
Poplar aspen	16	0.4	-	76	14	11	FBR, 500 °C	9
Willow	20	1.3	0.20	69	21	9	FBR, 507 °C	8
Lignin								
Straw lignin	79	12	0.13	43	36	19	PCR, 550 °C	This study
ETEK Lignin	~50	0.2 – 0.6	0.02	58	27	10	FBR, 530 °C	6
ALM lignin	94	1.1 - 1.3	0.04	31	49	5.7	FBR, 530 °C	6
Alcell lignin	96	0	-	39	43	21	FBR, 500 °C	5
Granit lignin	90	<2	-	48	39	15	FBR, 500 °C	5
Organosolv lignin	96	0.0	-	55	36	15	FBR, 500 °C	5
Organosolv lignin	95	0.1	-	52	31	17	FBR, 500 °C	5

The feedstock ash influences the pyrolysis products distribution of biomasses.^{8,11,12,19} However the roles of the individual ash components on the pyrolysis process are not well understood. Potassium has been found to considerably catalyse the pyrolysis^{8,19,20} by decreasing the bio-oil yield and increase the gas and char yield,^{8,11} whereas silicate seems to be inactive to pyrolysis of biomass. The feedstock lignin content has a major influence on the product distribution.^{8,11} The lignin component produce a low bio-oil yield and a high char yield compared to cellulose.^{5,6} Table 2 summaries a relation of ash, potassium and lignin contents, and product yields of wood and lignin pyrolysis. With a low potassium content (less than 0.12 wt% db) and a lignin content of 16 – 29 wt% daf, wood fast pyrolysis often provides a high bio-oil yield of 67 – 77 wt% db.⁸⁻¹⁰ Thus wood is considered as the best material for producing bio-oil. Lignin samples from ethanol and paper plants that have a negligible potassium content (less than 0.13 wt% db)^{5,6} and high lignin content of 79 – 96 wt% daf and relatively low bio-oil yields of 31 – 55 wt% db for fast pyrolysis. It is seen that the lignin content has the considerably effect on the bio-oil yield.

Conclusion

A residual lignin sample from an ethanol plant with a lignin content of 79 wt% daf was successfully pyrolysed on a pyrolysis centrifugal reactor without the plugging

of the feeder, however after an hour of operation plugging at the cooling nozzle was observed. The effects of pyrolysis conditions as temperature (450 – 600 °C), reactor gas residence time (0.9 and 4.2 s) and feed rate (4.1 - 10.4 g/min) on trends of product yields were relatively similar to those of wood fast pyrolysis. The optimal pyrolysis conditions of lignin PCR to obtain a maximal organic oil yield is a temperature of 550 °C, a reactor gas residence time of 0.8 s and a feed rate of 5.6 g/min. The maximal organic oil yield of 34 wt% db is however much lower than that of wood fast pyrolysis.

References

- (1) Bridgwater, A. V. *Therm. Sci.* **2004**, *8*, 21-49.
- (2) Buranov, A. U., Mazza, G. *Ind. Crops Prod* **2009**, *28*, 237-259.
- (3) Gosselink, R. J. A.; de Jong, E.; Guran, B.; Abacherli, A. *Industrial Crops and Products* **2004**, *20*, 121-129.
- (4) S. Baumlin et al. *International Journal of Hydrogen Energy* **31**, **2006**, 2179– 2192
- (5) P.J. de Wild. *Journal of Analytical and Applied Pyrolysis* **2012**, *93*, 95–103
- (6) D.J. Nowakowski. *Journal of Analytical and Applied Pyrolysis* **88**, **2010**, 53–72
- (7) *Front. Environ. Sci. Eng.* **2012**, *6*, 295–303
- (8) Fahmi, R.; Bridgwater, A. V.; Donnison, I.; Yates, N.; Jones, J. M. *Fuel* **2008**, *87*, 1230-1240.
- (9) Scott, D. S.; Plskorz, J.; Radleln, D. *Ind.Eng.Chem.Process Des.Dev* **1985**, *24*, 581-588.
- (10) Azeez, A. M.; Meier, D.; Odermatt, J. ê.; Willner, T. *Energy Fuels* **2010**, *24*, 2078-2085.
- (11) Oasmaa, A.; Solantausta, Y.; Arpiainen, V.; Kuoppala, E.; Sipilä, K. *Energy Fuels* **2009**, *24*, 1380-1388.
- (12) Michael L. Boroson, Jack B. Howard, John P. Longwell, William A. Peters. *AIChE Journal* **1989**, *35*, 120-128.
- (13) Hyun Ju Park, Young-Kwon Park, Jong-In Dong, Joo-Sik Kim, Jong-Ki Jeon, Seung-Soo Kim, Jinsoo Kim, Byungho Song, Junhong Park, Kyung-Jin Lee. *F U E L P R O C E S S I N G T E C H N O L O G Y* **9 0 (2 0 0 9) 1 8 6 – 1 9 5**.
- (14) Bech, N.; Larsen, M. B.; Jensen, P. A.; Dam-Johansen, K. *Biomass and Bioenergy* **2009**, *33*, 999-1011.
- (15) Bridgwater, A. V. *Biomass and Bioenergy* **2012**, *38*, 68-94.
- (16) Ofci D. Mante , Foster A. Agblevor. *b i o m a s s a n d b i o e n e r g y* **3 5 (2 0 1 1) 4 4 1 7 e 4 4 2 5**.
- (17) L. Fagbemi, L. Khezami, R. Capart. *Applied Energy* **69 (2001)** 293–306.
- (18) Fahmi, R.; Bridgwater, A. V.; Donnison, I.; Yates, N.; Jones, J. M. *Fuel* **2008**, *87*, 1230-1240
- (19) Abdullah, N.; Gerhauser, H. *Fuel* **2008**, *87*, 2606-2613.
- (20) Jensen, A.; Dam-Johansen, K.; Wojtowicz, M. A.; Serio, M. A. *Energy Fuels* **1998**, *12*, 929-938.
- (21) Sanchez-Silva, L.; Lopez-Gonzalez, D.; Villanor, J.; Sanchez, P.; Valverde, J. L. *Bioresource Technology* **2012**, *109*, 163-172.
- (22) Trinh, N. T.; Jensen, P. A.; Dam-Johansen, K.; Knudsen, N.O.; Sørensen, H. R.; Hvilsted, S. A Comparison of Lignin, Macroalgae, Wood and Straw Fast Pyrolysis. Submitted to *Engery and Fuel*

Acknowledgments

CHEC is financially supported by the Technical University of Denmark, DONG Energy A/S, Vattenfall A/S, FLSmidth A/S, Hempel A/S, Energinet.dk, the Danish Research Council for Technology Sciences, the Danish Energy Research Program, the Nordic Energy. Financial support of this PhD study by DONG energy A/S and Energinet.dk is gratefully acknowledged.



Anna Trubetskaya

Phone: +45 4525 2952
E-mail: atru@kt.dtu.dk

Supervisors: Peter Glarborg
Peter Arendt Jensen
Anker Degn Jensen

PhD Study
Started: April 2012
To be completed: March 2015

Single Biomass Particle Combustion and Fuel Characterization

Abstract

Coal fired power plants contribute significantly to greenhouse gas emissions, particularly CO₂. An attainable way to reduce CO₂ emissions is to replace coal with biomass in power plants. Biomass has traditionally been fired in grate and fluidized bed boilers, while the experience with pure pulverized biomass combustion is limited. The objective of this PhD research is to establish accurate simplified one-dimensional mathematical models, which will be possible to use for the prediction of main combustion processes for biomass particles of different sizes and shapes. The accuracy of these models will be validated against the experimental data provided by measurements on entrained-flow reactors at DTU and Stanford University.

Introduction

Biomass as an environmentally friendly and CO₂ neutral fuel is increasingly used for power production. On the global scale biomass contributes currently roughly 10 % to the primary energy demand [1].

Biomass combusted in boiler can be used for the production of heat, power and electricity. There are a variety of biomass residues available around the world. The most abundant of these are crops, forestry and livestock residues [2].

The most common ways of biomass combustion in power plants are grate firing and pulverized wood combustion. Suspension firing of pulverized fuel has been used for coal combustion for many decades. One of the challenges by using biomass in a suspension firing plant is the presence of large top size biomass particles (0.5-2 mm) where the coal particles size are maximum 0.1-0.3 mm, and this could cause problems with the flame stability and burnout.

Although the amount of literature dealing with the combustion of coal and coal char is overwhelming, research concerning the combustion of biomass char has not been carried out to a similar extent.

Objectives

A major focus of this work is to investigate the different stages of a single particle biomass combustion behavior (ignition, pyrolysis and char oxidation) for particles of different type, size and shape with the development of two accurate simplified one-dimensional mathematical single-particle models for biomass particles of size (< 1 mm) and size (> 1mm) based on conservation of mass, energy and momentum. Both one-dimensional models will be modified in the way to be used as a part of CFD calculation.

The accuracy of two models will be validated against the experimental data provided by measurements on entrained-flow reactors at DTU (5 kW) and Stanford University (for 100 mg/h).

Project

In this project, two simplified models will be developed to predict the main characteristics of single biomass particles combustion. Saastamoinen [3] studied the burning of pulverized biomass in a large scale utility boiler originally designed for a coal combustion, and found out that particle loses much of its weight during drying and pyrolysis by following direction of the gas flow when much weight has been lost. Saastamoinen [4] concluded that pyrolysis does not take place uniformly inside

of the particle, and the calculations are sensitive to particle shape and size during the investigation of a large aspect ratio effect on the carbon burnout. Yang [5] confirmed that the isothermal assumption is no longer valid when the pulverized particle size exceeds 150-200 μm . Lu [6] investigated the particle shape and size influence combustion dynamics, including drying, heating rate and reaction rate. Lu [7] concluded that the spherical mathematical approximations for fuels during thermal treatments poorly represent the combustion behavior when particles exceed 200-300 μm . Haseli [8] established several simplified models of preheating, pyrolysis and char combustion for the prediction of a thermally thin single biomass particle. The behavior of a thermally thick single particle was considered only for the preheating stage. The simplified models of Haseli [8] consider non-sphericity of a single particle only during preheating and pyrolysis.

In this project, the influence of particle shape and size will be considered in two simplified models. Based on the simplified models for preheating, pyrolysis and char oxidation, the first model will be established to predict a thermally thin single biomass particle behavior, while the second model will be used to predict the behavior of thermally thick single biomass particle. The effects of particle size and shape, heating conditions on combustion dynamics of a single biomass particle will be investigated using the developed models.

On the basis of two established models, calculations to determine the necessary residence time of the particle in the combustion chamber to enable a complete biomass char burnout (for the defined boundary conditions) will be performed. The models will be made to estimate the ignition time for different particle sizes.

The results will be validated against own experimental data and compared with the previous results from the literature.

The final combustion model will be simplified in an algebraic way to validate the preheating, pyrolysis and char combustion models in CFD. The application of this model in combination with CFD simulations can enable a simulation and optimization of the furnace geometry as well as of the residence times necessary for the fuel particles in the combustion chamber with the benefit to reduce time of consuming test runs [9]. Special attention will be given to the relation of chemical kinetics and transport phenomena for both single particles and reactors.

Because the biomass combustion is influenced markedly by feedstock nature, char-preparation

conditions, the detailed analysis of milling and drying processes will be applied in this work.

The morphology of wood and straw particles has a significant impact on the chemical and physical processes in the combustion. The porosity, sphericity, surface area and volume will be characterized for the biomass particles in details before a single particle enter the furnace and after the combustion process is completed. With the included particle geometric information (particle aspect ratio, volume, and surface area), the models can be modified to simulate the combustion process of biomass particles of any shape.

Acknowledgements

This PhD project is a part of the GREEN Research Center (Center for Power Generation from Renewable Energy) financed by the Danish Strategic Research Council.

References

1. M. Kaltschmitt, Biomass for energy in Germany: status, perspectives and lessons learned, *Journal of Sustainable Energy and Environ. Special Issue* (2011) 481-490.
2. M. Balat, G. Ayar, Biomass Energy in the World, Use of biomass and Potential Trends, *Energy Sources*, 27 (10) (2006) 931-940.
3. J. Saastamoinen, M. Aho, A. Moilanen, L.H. Sørensen, S. Clausen, M. Berg, Burnout of pulverized biomass particles in large scale boiler-Single particle model approach, *Biomass and Energy* 34 (2010) 728-736.
4. L.H. Sørensen, J. Saastamoinen, J. E. Hustad, Evaluation of char reactivity data by different shrinking-core models, *Fuel* 75 (1996), 1294-1300.
5. Yao B. Yang, V.N. Sharifi, J. Swithenbank, A. Williams, Combustion of a single particle of biomass, *Chemosphere* 42 (2001) 481-490.
6. Hong Lu, E. Ip, J. Scott, P. Foster, M. Vickers, L. Baxter, Effects of particle shape and size on devolatilization of biomass particles, *Fuel*, 89 (2010) 1156-1168.
7. Hong Lu, Experimental and modeling investigations of biomass particle combustion, PhD thesis, Brigham Young University (2006).
8. Yousef Haseli, Modeling Combustion of Single Biomass Particle, PhD thesis, Eindhoven University of Technology (2012).
9. A. Elfasakhany, X.S. Bai, Modeling of pulverized wood combustion: a comparison of different models, *Progress in Fluid Dynamics* 6 (2006) 188-199.
10. W.R. Chan, M. Kelbon, B.B. Krieger, Modeling and experimental verification of physical and chemical processes during pyrolysis of large biomass particle, *Fuel* 64 (1985) 1505-1513.



Anna Katrine Vangsgaard

Phone: +45 4525 2910

E-mail: akv@kt.dtu.dk

Supervisors: Gürkan Sin

Krist V. Germaey

Barth F. Smets, DTU Environment

PhD Study

Started: September 2010

To be completed: August 2013

Framework for Construction of Multi-scale Models for Biological Wastewater Treatment Processes - Autotrophic Nitrogen Conversion

Abstract

In wastewater treatment technologies, employing biofilms or granular biomass, processes might occur at very different spatial and temporal scales. Model development for such systems is typically a tedious, complicated, and time consuming task, which involves selecting appropriate model equations for the different scales, making appropriate and simplifying assumptions, connecting them, analyzing and solving the model equations numerically, and performing parameter estimations if necessary. In this study, a structured framework for modeling such systems is developed. It aims to support the user at the various steps and to reduce the time it takes to generate a model ready for application. An implementation of the framework is illustrated using a case study, which considers treatment of a nitrogen-rich wastewater via the nitrification-anammox process by a granular biofilm system.

Introduction

Models are playing an increasingly important role in design, optimization, and control of wastewater treatment plants and processes. Models have successfully been used for many purposes, from design to supporting process operation and control of treatment plants, or as tools to evaluate the performance of a specific treatment technology. An area which has been receiving increased attention is the application of models as a tool for design of experiments when investigating new and emerging processes. By utilizing models for this purpose, the practical experiments can be better targeted towards a specific goal of the study or towards testing a specific hypothesis. As a consequence, it is expected that the number of experiments to be performed can be reduced, which will decrease the manpower needs and the cost of process development. In addition, the effect of operating conditions can be explored and help direct practical experiments towards obtaining optimal process performance. For all the above mentioned purposes, development of appropriate and reliable models is of great importance. A systematic framework generating models in an efficient and structured way has therefore been developed in this work. The framework is illustrated by a case study regarding biological conversion of nitrogen in an autotrophic environment. The overall aim of this project

is to develop a detailed model capturing process performance and microbial composition in biofilm systems performing autotrophic nitrogen conversion. This is done by development of detailed models for the involved bacterial groups and integrating them into complete ecosystem models, which describe how the major microbial groups interact. This insight will be used to design experiments in which relevant operational conditions will be identified and tested, and to design control structures for the process. The relevant conditions are those under which the nitrogen removal process is optimized through the development of selection pressure, resulting in a targeted nitrogen removal or enhancement of specific microbial groups.

Methods

In biofilm systems, processes happen at very different spatial scales, as opposed to in completely mixed reactors where all reactions often are assumed to happen at the same spatial scale. Modeling biofilm systems typically involves three spatial scales (Xavier et al., 2005); individual cells, biofilm, and reactor scale, as shown in Figure 1. On the individual or cellular scale (10^{-5} - 10^{-6} m) the growth and metabolism of the microorganisms are captured. On the biofilm scale (10^{-4} - 10^{-3} m) the spatial location of the bacteria is described, and also the transport of soluble and particulate compounds is included here. At the reactor scale (10^{-1} -

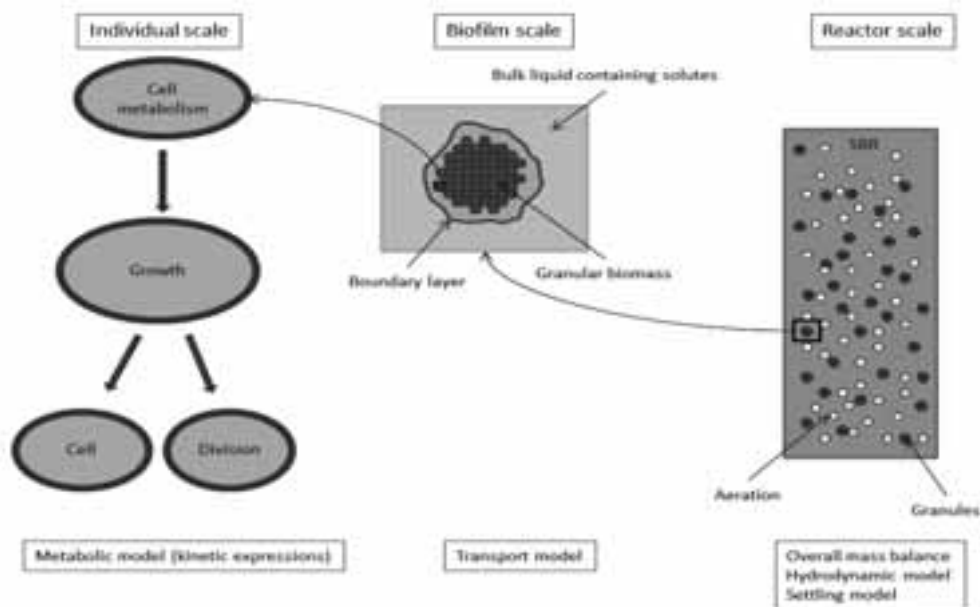


Figure 1. Conceptual model of an SBR with granular biomass, as an example of a multi-scale model. Three spatial scales are considered; the individual or cellular, biofilm, and reactor scale (adapted from Xavier et al., 2005).

10^0 m) the overall mass balances are considered along with the hydrodynamic conditions in the reactor. At the cellular scale, individual cells, a subset of a functional group (e.g. specific species of ammonium oxidizing bacteria (AOB)), or an entire functional group of microorganisms (e.g. AOB) can be modeled. If individuals are considered, a certain differentiation in their metabolism might be assumed, whereas if a subset or an entire functional group is modeled, their metabolism can be assumed to be identical. The latter is termed the lumped approach and can be solved along with the transport equations at the biofilm scale.

A framework that supports the model construction at the different scales as well as linking them to each other has been developed, by studying the workflow typically involved in development of multi-scale systems (see Figure 2). The first step consists of defining the overall modeling objective. The second step is gathering system information such as for example physical and operational conditions of the system. From this information the main assumptions can be established in the third step. Subsequently, the model scenarios of interest should be defined, including which spatial scales and processes are of relevance. From this definition the individual models to be constructed can be derived. Each of the individual models are either taken from previous studies, if such exist, or they are constructed following the workflow depicted on the right side of Figure 2. First the specific model objective for the individual model and then the corresponding identifiability analysis of the model parameters are

conducted as necessary. The model is then calibrated to experimental data by adjusting the sensitive parameters. Finally, when the individual model has been validated, it is "exported" back into the multi-scale modeling workflow. The individual models are then linked to each other by defining the data that need to be transferred from one spatial scale to the next and vice versa. The multi-scale model system can now be solved by defining appropriate initial and boundary conditions.

Case study. Complete autotrophic nitrogen removal (CANR), is a relatively new treatment technology, which combines partial nitrification with anaerobic ammonium oxidation (anammox). Nitrification is performed by ammonium oxidizing bacteria (AOB), which convert ammonium to nitrite. The anammox process is performed by anaerobic ammonium oxidizing bacteria (AnAOB), by oxidizing ammonium using nitrite as the terminal electron acceptor. For wastewaters containing high concentrations of nitrogen and low organic carbon to nitrogen ratios, such as sludge digester effluent, landfill leachate, or special industrial wastewaters, conventional nitrification-denitrification is either not a very efficient treatment process or a rather costly process. CANR combining partial nitrification (eq. 1) with anaerobic ammonium oxidation (eq. 2) can overcome these difficulties, because the requirement for aeration is lowered and the need for addition of organic carbon is eliminated (Strous et al., 1997). Meanwhile, the sludge production and the need for treatment of excess sludge are significantly lowered.

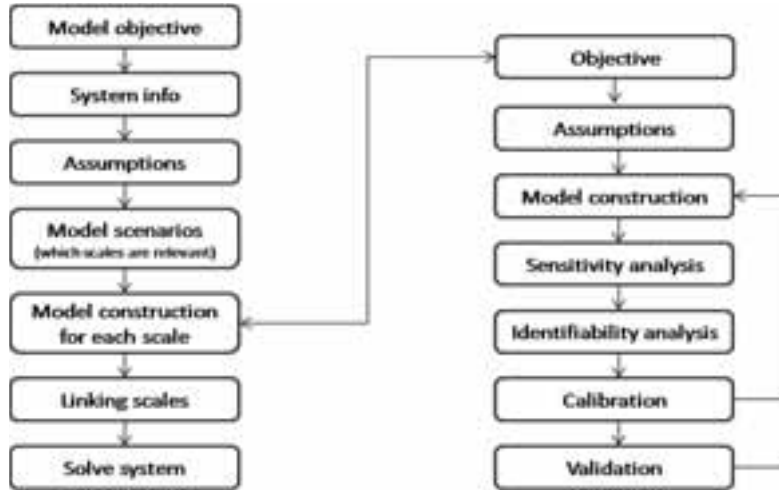
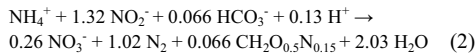
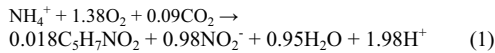


Figure 2. Workflow scheme for multi-scale modeling (left) and identification of the individual models (right) (adapted from Heitzig et al, 2010).



An environment where both groups of bacteria can co-exist can be created in biofilms or granular biomass, where both anoxic and aerobic conditions are created in a stratified structure. In the outer layers AOB will grow, consume oxygen, and prevent oxygen from penetrating further than a certain depth, while producing substrate for the AnAOB. In the anoxic inner biofilm layers, the AnAOB will be present.

In this case study the overall model objective is to study the microbial composition of granules containing AOB and AnAOB along with the bacterial groups competing with them for substrate, namely nitrite oxidizing bacteria (NOB) and heterotrophic bacteria (HB), growing on organic material originating from bacterial decay. The model is capturing a 1-dimensional spherical biofilm. The maximum biofilm thickness, number of granules, and reactor volume are all constant parameters with certain values (system info). The advective transport of soluble compounds is ignored, and all particulates (bacterial groups and inert material) are solely transported by advection as in the benchmark biofilm model no. 3 (Wanner et al., 2006). The bacterial species are assumed to have a uniform metabolism (assumptions). The mass balances in the cellular and biofilm scale can thus be solved simultaneously (Figure 3). The model scenario considered therefore includes two scales; the biofilm and reactor scales. The individual models for the conversion and transport of soluble and particulate compounds can be seen in eq. 3

and 4, respectively. The soluble and particulate mass balance in the reactor scale (eq. 7) is linked to the biofilm scale by the flux through the boundary layer between the biofilm and the bulk liquid (eq. 5 and 6, respectively).

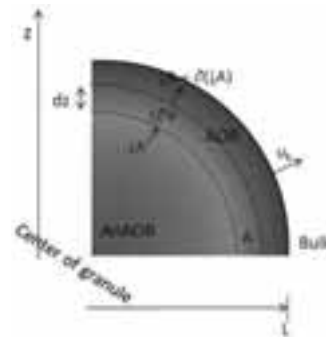


Figure 3. Conceptual model of a slice of a granule illustrating the biofilm scale with the transport, microbial metabolism, and positions indicated.

The mass balance for soluble compounds in spherical coordinates is given by:

$$\frac{\partial S_i}{\partial t} = D_{\text{bio},i} \frac{1}{z^2} \frac{\partial}{\partial z} \left(z^2 \frac{\partial S_i}{\partial z} \right) + r_i \quad (3)$$

S_i is the concentration of the soluble compound i inside the biofilm, z is the radial distance from the center of the granule, r_i is the conversion rate, and $D_{\text{bio},i}$ is the diffusion coefficient in the biofilm.

The mass balance for particulate compounds:

$$\frac{\partial X_i}{\partial t} = -\frac{\partial(X_i u_F)}{\partial z} + r_i \quad (4)$$

X_i is the concentration of the particulate species i , u_F is the advective velocity, and r_i is the conversion rate.

Assuming flux continuity, the flux of soluble compounds at the biofilm/liquid interface is given by:

$$j_{\text{bio},S_i} = \frac{D_i}{L_B} (S_{i,\text{bulk}} - S_{i,L}) \quad (5)$$

Where D_i is the diffusivity in water, L_B is the thickness of the mass transfer boundary layer, $S_{i,\text{bulk}}$ is the concentration in the bulk liquid, and $S_{i,L}$ is the concentration at the biofilm/liquid interface.

The flux of particulate species can be describe as:

$$j_{\text{bio},X_i} = -u_D X_{i,L} \quad (6)$$

Where u_D is the detachment velocity and $X_{i,L}$ is the concentration of the particulate at the biofilm/liquid interface.

The reactor mass balance is given as:

$$\frac{dC_{i,\text{bulk}}}{dt} = \frac{Q_{\text{in}} C_{i,\text{in}} - Q_{\text{out}} C_{i,\text{bulk}} - j_{\text{bio},i} A}{V_{\text{reactor}}} + r_{i,\text{bulk}} \quad (7)$$

Where C denotes the concentration of either a soluble or a particulate species, Q represents a flow rate (inflow, Q_{in} , or outflow, Q_{out}), A is the total surface area of the granules, V_{reactor} is the volume of the entire reactor, and $C_{i,\text{in}}$ is the influent concentration.

Results

A generic multi-scale modeling framework was implemented in the Matlab software (Vangsgaard et al., 2011), and can be customized for the needs of biofilm systems by adapting the features of the software according to the work flow identified for multi-scale biofilm modeling, as shown in Figure 2.

By solving the constructed model, a stratified structure and the specific location of the bacteria is obtained (Figure 4).

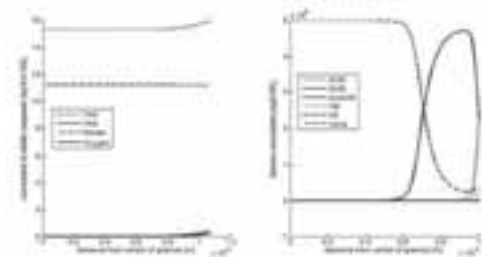


Figure 4. Soluble and biomass concentrations inside the biofilm matrix obtained from a simulation.

While the case study is used to highlight the framework and the software support for multi-scale model development, more detailed and complex model systems, e.g. by inclusion of additional microbial species and a higher number of soluble compounds, can easily be constructed in the future.

Conclusions

A framework for construction of multi-scale models of biofilms used in biological wastewater treatment processes has been constructed. The framework is implemented in the Matlab software. It is flexible and efficient, which allows for generation of customized models for a broad range of applications from design of experiments for new processes to process design, control, and optimization.

Acknowledgements

The author would like to thank the Technical University of Denmark for financial support as well as the Danish Agency for Science, Technology and Innovation for funding through the Research Centre for Design of Microbial Communities in Membrane Bioreactors (09-067230).

References

1. Heitzig, M., Sin, G., Glarborg, P., Gani, R., 2010. In: Pierucci, S., Buzzi Ferraris, G. (Eds.), 20th European Symposium on Computer Aided Process Engineering - ESCAPE20. Elsevier.
2. Strous, M., VanGerven, E., Zheng, P., Kuenen, J.G., Jetten, M.S.M., 1997. *Water Research* 31, 1955-1962.
3. Xavier, J.B., Picioreanu, C., van Loosdrecht, M.C.M., 2005. *Environmental Microbiology* 7, 1085-1103.
4. Wanner, O., Eberl, H. J., Morgenroth, E., Noguera, D. R., Picioreanu, C., Rittmann, B. E., van Loosdrecht, M. C. M. (2006) *Mathematical Modeling of Biofilms - IWA Scientific and Technical Report*, IWA Publishing.
5. Vangsgaard, A.K., Mauricio-Iglesias, M., Gernaey, K.V., Smets, B.F., Sin G., 2011. *IWA Symposium on Systems Analysis and Integrated Assessment*, 8th IWA Watermatex conference proceedings, pages: 687-690.

List of Publications

1. Vangsgaard, A.K., Mauricio-Iglesias, M., Gernaey, K.V., Smets, B.F., Sin, G., 2012. *Bioresour Technol* 123, 230-241.
2. Vangsgaard, A.K., Gernaey, K.V., Sin, G., Mutlu, A.G., Smets, B.F., 2012. *Dansk Kemi* 93(10), 16-18.



Sindhu Vudayagiri

Phone: +45 4525 6825

E-mail: sivu@kt.dtu.dk

Supervisors: Anne Ladegaard Skov
Ole Hassager

PhD Study

Started: August 2011

To be completed: July 2014

Factors affecting surface and release properties of thin PDMS films

Abstract

Polydimethylsiloxane (PDMS) elastomers are commonly used as dielectric electroactive polymers (DEAP). DEAP films are used in making actuators, generators and sensors. In the large scale manufacture of DEAP films, the PDMS elastomer mixture is applied to the substrate (carrier web) and then peeled off the substrate after the elastomer has cured completely. [1] The process of release from the substrate is not as smooth as it is desired, and induces considerable pre-strain and defects in the film which affects the performance of the films as actuators. To ease the process of release, release agents in the form of sprays or liquids cannot always be used. The current research is directed towards investigating factors affecting the peel force and release of thin, corrugated polydimethylsiloxane films used in DEAP films. It has been shown that doping the PDMS films with small quantities of perfluoroether allylamide (PFE) lowered the surface energy which could ease the release. This is further investigated together with an evaluation of the resulting change in actuator performance. The relationship between the adhesive energy, surface energy, Young's modulus and peel force of the films is analyzed.

Introduction

The peel force required to peel a film from a substrate is a complex function of geometry, the mechanical properties of the film and the substrate, thickness of the film, interfacial cohesive properties and also the friction between the surfaces.

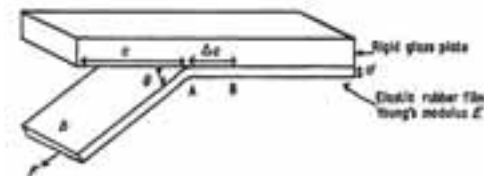


Figure 1. Peeling an elastomer film from a rigid substrate [2]

Consider an elastomer film of thickness d which is being peeled from a rigid substrate at a peel angle θ with a force F (Figure1). The elastomer has a Young's modulus E . The adhesive energy between the film and the glass substrate is R . Consider a unit length Δc of the film being peeled from the substrate between the points A and B. [2] The width of the film at any given point is b . The three contributions to the energy changes involved in the peeling process are

- 1) Surface energy - due to creation of new surfaces $[-bR\Delta c]$

- 2) Potential energy- due to the movement of the applied force $[F(1-\cos\theta)]$

- 3) Elastic energy -due to extension of the film in the direction of the applied force. $\left[\frac{F^2 \Delta c}{2bdE}\right]$

Adding up these contributions and assuming energy conservation the following equation is obtained.[2]

$$-bR\Delta c + F(1 - \cos\theta)\Delta c + \frac{F^2 \Delta c}{2bdE} = 0 \quad \dots\dots (1)$$

From the equation (1) the adhesive energy R can be calculated. R is different from surface energy, work of adhesion or any thermodynamic quantity and R gives an estimate of the adhesive force between the substrate and the film. If the R between the substrate and the elastomeric film is high, then the force F required to peel the film will also be high.

Experimental

18 samples are made by mixing Elastosil RT-625 (a commercially available RTV silicone[9:1]), 2) Powersil Fluid TR50 (15%) and 3) Inhibitor PT 88 (0.8%) respectively, obtained from Wacker Chemie AG, Germany. The films are doped with 1% PFE. The PFE (KDP-4645) was supplied by DuPont Krytox Performance Lubricants, USA. The films are subjected to rheological tests, peel tests, permittivity tests and contact angle tests.

Calculation of Adhesive force 'R'

Using the peel equation (2), the adhesive energy R is calculated. [2]

$$\left(\frac{F}{b}\right)^2 \frac{1}{2dE} + \left(\frac{F}{b}\right)(1 - \cos\theta) - R = 0 \quad \dots\dots (2)$$

$$E = 2G(1 + \nu) \quad \dots\dots (3)$$

Where, G is the static shear modulus and ν is the poisson ratio.

The F is obtained from the peel tests and the E is calculated from the equation (3). The value of G ($G = G' (\omega \rightarrow 0)$) [3] is obtained from the rheological tests and the poisson ratio (ν) for silicone elastomers (rubber) taken as 0.5. The maximum value of F is used for all calculations in order to estimate the maximum R between the film and the substrate during the processing. A comparison of samples 2 and 12 clearly shows that as the E increased, the R decreased. [Sample 2 has $F = 0.016\text{N/mm}$, $E = 0.18\text{MPa}$, and the calculated $R = 27\text{N/m}$. Sample 12 has $F = 0.022\text{N/mm}$, $E = 0.10\text{MPa}$ and the calculated $R = 61.7\text{N/m}$.]

Results & Conclusions

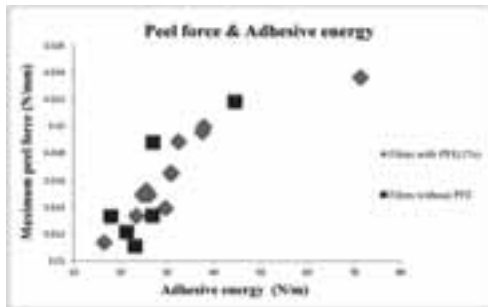


Figure 2. Relationship of the adhesive energy R and peel force F

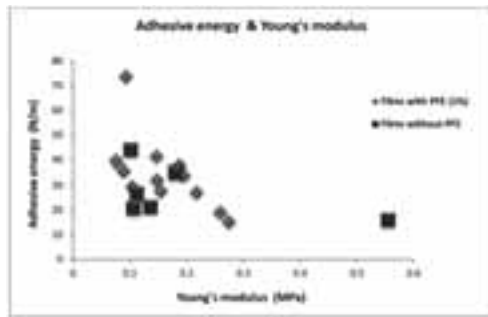


Figure 3. Relationship of the adhesive energy R and Young's modulus E

From Figure 2 and 3 one can understand the relationship of the E , R and F . From Figure 2 it is observed that as the F increased the value of R also increased. To lower peel force, the adhesive energy needs to be lowered.

From Figure 3, it is observed that R and E are related inversely, in accordance to equation (1). As the E of the samples increased, their R value decreased, thus making their release easier. Though surface energy, F and R at the interface are related through the action of surface forces, the relation is not obvious. [4] The relationship of F , R , E and release can be understood further from the theory proposed by Johnson, K.L. et al. [4] Every surface has a surface energy resulting from the action of surface forces. When two surfaces are in intimate contact, these surface forces act as attractive (adhesive) forces. The strength of the attractive (adhesive) force between two surfaces depends on the contact surface area. [4] Interfacial gaps due to surface asperities or dust particles will strongly influence the adhesion between the surfaces because the attractive forces decrease rapidly with increasing separation.[4] Materials with low elastic modulus, will even out easily against a substrate and make very good contact. Therefore they are strongly adhered to the substrate. [4] Hence, to peel the film off, one needs to overcome the adhesive forces and apply a high F . To make the release easier, the contact at the interface needs to be reduced to prevent the surfaces from adhering strongly. That is what release agents like oils and surfactants do, namely reducing the good contact to ease the release of a surface from another surface. On the contrary, materials with high Young's modulus will not flatten out against another surface and cannot make an intimate contact, hence, less adhesive force. The addition of PFE to the Elastisol RT-625 did not influence the storage modulus G' much, as seen from the time sweeps. The dielectric permittivity of the samples was also not modified by the addition of PFE. Though the surface energy reduced by the addition of PFE, the peel force values did not decrease. The reason for this is because the elastic contribution to the peel force is much higher than the potential and the surface energy contribution. So, tuning the elasticity of the networks is actually the easiest path for reducing the release problems of thin silicon films, when other solutions like using a release agent is not an option.

Acknowledgements

The Danish National Advanced Technology Foundation for the financial support.

Key words carrier web, DEAP, elastomers, PDMS, release, surface energy

References

- [1] Kiil, E. and Benslimane, M.Y. Scalable industrial manufacturing of DEAP. Proc. of SPIE, San Diego, California, USA. 72870R-1 – 72870R-10 (2009).
- [2] Kendall, K. Thin-film peeling-the elastic term. Journal of Physics D: Applied Physics. 8(13): 1449–1452(1975).
- [3] Morrison, F.A. Understanding Rheology, ISBN13: 9780195141665 (Oxford University Press, 2001)
- [4] Johnson, K.L., Kendall, K. and Roberts, A.D. Surface Energy and the Contact of Elastic Solids. Proceedings of the Royal Society A: Mathematical, Physical and Engineering Sciences. 324(1558): 301–313 (1971).

**Qiongxiao Wu**

Phone: +45 4525 2837
E-mail: qw@kt.dtu.dk

Supervisors: Anker Degn Jensen
Jan-Dierk Grunwaldt, Karlsruhe Institute
of Technology (Germany)
Burcin Temel, Haldor Topsøe A/S
Jakob Munkholt Christensen

PhD Study
Started: January 2010
To be completed: December 2012

CO hydrogenation over Cu-Ni catalysts

Abstract

This work provides a systematic study of Cu-Ni catalysts for liquid fuel synthesis from biomass-derived syngas. Based on both density functional theory (DFT) calculations and activity tests for CO hydrogenation, Cu-Ni alloys supported on SiO₂ have been found to be promising methanol synthesis catalysts. Hence, systematically studies on Cu-Ni catalysts have been carried out in a next step: the influence of (1) the support using carbon nanotubes, ZrO₂, SiO₂ and Al₂O₃ (2) the Cu/Ni ratio; 3) the pretreatment of catalysts; 4) the operating conditions, e.g., temperature, H₂/CO ratio, and CO₂ co-feeding; 5) catalyst preparation methods such as incipient wetness impregnation, co-precipitation or deposition-co-precipitation. In addition, various in situ characterization techniques such as XAS, XRD, TEM and FTIR together with DFT calculations have been applied for understanding the structure-activity relationships of Cu-Ni catalysts at simulated reaction conditions.

Background

The rapid development of the world over the last century is based on easy-access to inexpensive fossil fuels, and this era is coming to the end [1]. The demand for energy around the world is growing rapidly [2]; meanwhile, it is obvious that the emission of CO₂ that follows the use of fossil fuels is threatening the climate of the earth [3]. Arguably this makes the development of sustainable energy solutions the most scientific and technical challenge of our time. The previous Danish Minister of Science Helge Sander has granted DKK 120 million to scientists at the Technical University of Denmark to support the development of novel methods for converting sustainable energy from the sun and wind into fuels under the “Catalysis for Sustainable Energy (CASE)” initiative [4]. This Ph.D. project is among one of the sustainable approaches – ‘Fuel synthesis from biomass-derived syngas’.

The present project was built on the following two aspects:

1. Combination of experimental and computational catalyst screening

Suitable reference systems have been prepared and tested for benchmarking in the syngas conversion. In parallel, a rational design of possible catalysts has been performed by computational methods (carried out by CASE partners) and it has been directly linked with the synthesis of the proposed catalyst candidates, followed by catalyst testing, and use of the resulting experimental data as input to more detailed calculations, i.e.

development of an integrated experimental and computational catalyst discovery process. This approach is schematically shown in Figure 1.

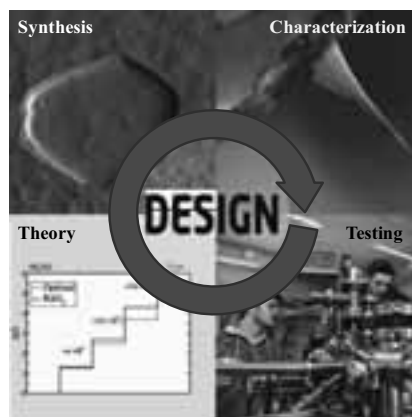


Figure 1 Illustration of the approach of catalyst development.

2. Structure-activity relationship by electron microscopy and in situ diffraction and spectroscopy

State-of-the-art electron microscopy, diffraction and spectroscopic methods play a significant role in the establishment of structure-activity relationships for reactions in this project. In situ X-ray adsorption

spectroscopy (XAS), X-ray diffraction (XRD), transmission electron microscopy (TEM) and Fourier transform infrared spectroscopy (FTIR) have been combined for understanding the structure of catalysts in simulated reaction conditions.

In this project, the focus has been on methanol and partly on higher alcohol synthesis from synthesis gas or syngas, a mixture of CO, H₂ and CO₂. Theory (DFT) and experiments have been combined for developing new catalysts for methanol and higher alcohol syntheses. The following systematic studies on this catalyst system have been carried out:

- i. DFT calculations and experimental activity investigation;
- ii. Effect of supports: carbon nanotubes, ZrO₂, SiO₂ and Al₂O₃;
- iii. Effect of Cu/Ni ratio;
- iv. Effect of pretreatment of catalysts;
- v. Effect of preparation methods such as incipient wetness impregnation, co-precipitation and deposition-co-precipitation.

Specific Objectives

This work aims at providing a systematic study of Cu/Ni catalysts for alcoholic fuel synthesis from biomass-derived syngas.

Results and Discussion

1. DFT calculations and experimental activity investigation [5]

Our partners in CASE have developed an analytical micro kinetic model that assumes hydrogenation of CO and methoxy as being rate determining and constructed a volcano-relationship for methanol synthesis that is based on scaling relations and hence maps out the activity towards methanol as a function of ΔE_C and ΔE_O (carbon and oxygen binding energies). A comparison with the rates for methane formation gives a selectivity map between methane and methanol. A number of binary alloys were screened as leads for methanol synthesis candidates and identified Cu-Ni alloys as being interesting [5], as shown in Figure 2.

The calculated candidates, Cu-Ni alloy catalysts, have been prepared via incipient wetness impregnation and tested in a fixed-bed continuous-flow reactor for CO hydrogenation. The metal area-based activity for a Cu-Ni/SiO₂ catalyst indeed is at the same level as the Cu/ZnO/Al₂O₃ model catalyst. It even has a slightly higher selectivity to methanol than the model methanol synthesis catalyst during CO hydrogenation. The high activity and selectivity of silica supported Cu-Ni alloy catalyst agrees with the fact that the DFT calculations identified Cu-Ni alloy catalyst as highly active and selective catalysts for the hydrogenation of CO to form methanol. Additionally, no deactivation was observed, but instead an activation process is observed during a total 73 h test of time on stream for the Cu-Ni alloy catalyst [5].

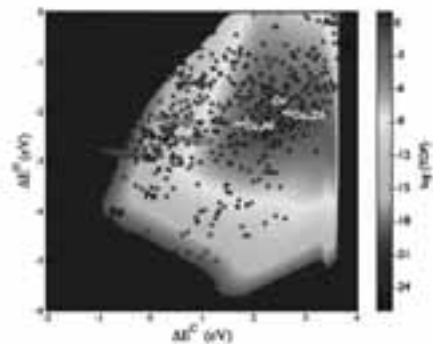


Figure 2 Theoretical activity volcano for the production of methanol from CO and H₂. The turnover frequency is plotted as a function of carbon and oxygen binding energies. The carbon and oxygen binding energies for the stepped surfaces of selected transition metals are depicted. Small circles depict calculated carbon and oxygen binding energies for a range of binary alloys. Two different steps for either of Cu₃Ni and CuNi₃ alloys are depicted in red; the Cu step of Cu₃Ni is depicted in white. Cu and the AB step of Cu₃Zn are depicted in black. Reaction conditions are 523 K, 45 bar H₂, 45 bar CO, and 10 bar methanol [5].

2. Effect of support materials [6]

CO hydrogenation has been investigated over Cu-Ni supported on different carriers (SiO₂, CNT, ZrO₂ and γ -Al₂O₃) and has been shown to display major differences in product selectivity.

Table 1 Behavior of Cu-Ni catalysts over different supports during CO hydrogenation at steady state. Experimental conditions: P = 100 bar, T=250 °C, and H₂/CO = 1.0 vol/vol.

Catalysts	GHSV ¹⁾ [h ⁻¹]	X _{CO} ²⁾ [%]	CO ₂ -free selectivity [mol %]				Activity ³⁾ mol m ⁻² s ⁻¹
			MeOH	C ₂ -OH	HCs ⁴⁾	DME	
Cu-Ni/SiO ₂	2000	2.4	99.2	0.4	0.4	0.0	1.3·10 ⁻⁷
Cu-Ni/CNT	7500	2.6	98.9	0.1	0.5	0.5	2.0·10 ⁻⁷
Cu-Ni/Al ₂ O ₃	2000	5.0	5.6	0.0	12.5	81.9	2.1·10 ⁻⁷
Cu-Ni/ZrO ₂	2000	9.8	80.8	1.0	11.2	7.0	2.0·10 ⁻⁷
Cu/ZnO/Al ₂ O ₃	16000	7.2	99	0.4	0.1	0.5	2.7·10 ⁻⁷

¹⁾ Gas hourly space velocity. ²⁾ CO conversion. ³⁾ Area-based activity: CO conversion rate per metal surface area of catalysts. ⁴⁾ Hydrocarbons

It has been found that the SiO₂ and CNT supported catalysts show a very high selectivity to methanol – around 99 mol % and low selectivity to hydrocarbons (< 0.5 mol %) at all temperatures tested. Among the catalysts, which are highly selective to methanol, the metal area-based activities on both Cu-Ni/CNT and Cu-Ni/SiO₂ catalysts are comparable to the model industrial Cu/ZnO/Al₂O₃ catalyst. The other supports tested, γ -Al₂O₃ and ZrO₂, influence the Cu-Ni alloy selectivity strongly by making more by-products (hydrocarbons and DME) than methanol. In particular, the γ -Al₂O₃ supported catalyst contains a significant amount of acid sites (333 μ mol g⁻¹) and produces predominantly DME, which is probably due to the dehydration of methanol produced initially by the Cu-Ni alloys. The ZrO₂ supported catalyst also contains a high amount of acid sites (309 μ mol g⁻¹), however, it produces largely hydrocarbons above 275 °C. The ability of solids to facilitate acid-catalyzed reactions depends not only on

the amount of acid sites but also on their strength. Alumina is naturally a better catalyst than zirconia for DME formation from methanol. In addition, ZrO₂ itself is able to convert methanol and DME into hydrocarbons. It is therefore not surprising that the γ -Al₂O₃ supported catalyst exhibits much higher DME selectivity than the ZrO₂ supported catalyst.

3. Effect of catalyst pretreatment [7]

Cu-Ni/SiO₂ catalysts in connection with different calcination and reduction procedures have been compared with a conventional Cu/ZnO/Al₂O₃ catalyst in the synthesis of methanol from synthesis gas (CO/H₂) in the presence and absence of carbon dioxide.

In general, the synthesized Cu-Ni alloy catalysts that are prepared by incipient wetness impregnation are active and highly selective (~99 mol %) for methanol synthesis during CO hydrogenation.

The pretreatment of incipient wetness-impregnated catalysts has a significant influence on Cu-Ni particle sizes and the alloy formation itself and consequently on its catalytic activity. Calcination of the impregnated catalyst leads to a broader particle size distribution and bigger particles compared to that of direct reduction of the impregnated catalyst. By reducing impregnated Cu-Ni catalyst in a more dilute H₂ gas (2 mol % H₂/N₂, compared to the same catalyst reduced at 20 mol % H₂/N₂) the amount of Cu that segregate from the Cu-Ni particles could be decreased. In addition the Cu and Cu-Ni particle sizes are smaller. Consequently, this increases the overall productivity of methanol. However, the metal area-based activity of methanol formation on the Cu-Ni catalyst is comparable to a conventional Cu/ZnO/Al₂O₃ model catalyst regardless of the catalyst pretreatment (calcination and reduction procedures) after impregnation.

Addition of 3 mol % CO₂ to the H₂/CO leads to a significant loss of activity (17% to 48%, depending on temperature). Density functional theory calculations show in accordance with previous surface science studies that oxygen as one of the intermediates from water gas shift reaction could induce segregation of Ni to the first layer by its adsorption on the surface. Hence, this could be one of the reasons of the unusual detrimental influence of CO₂ on the catalytic performance.

3. Effect of catalyst preparation method [8]

Silica supported bimetallic Cu-Ni alloy catalysts have been prepared via the incipient wetness impregnation, co-precipitation, and deposition-co-precipitation methods and tested for CO hydrogenation. The formation of bimetallic Cu-Ni alloy nanoparticles during reduction has been studied with in situ XRD, which shows that co-precipitation and deposition-co-precipitation methods are more efficient than the impregnation method for preparation of small and homogeneous Cu-Ni alloy nanoparticles. A clear difference in structure among these three catalyst precursors can be observed in the TEM images and particle size distributions (**Error! Reference source not found.**).

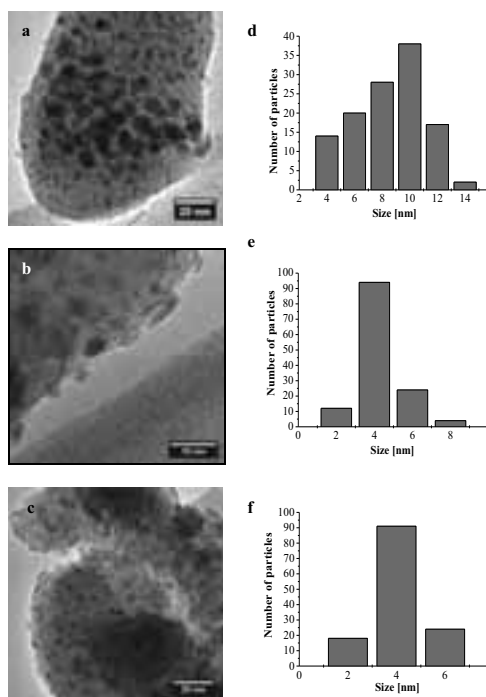


Figure 3 TEM images of (a) Cu-Ni/SiO₂-IWI, (b) Cu-Ni/SiO₂-Dep-Copr, and (c) Cu-Ni/SiO₂-Copr and particle size distributions of (d) Cu-Ni/SiO₂-IWI, (e) Cu-Ni/SiO₂-Dep-Copr, and (f) Cu-Ni/SiO₂-Copr samples.

For CO hydrogenation, the selectivity towards methanol is always higher than 99 mol % and the metal area-based activity to methanol over these Cu-Ni catalysts are at the same level, which are less dependent on the preparation approaches, while the productivity of methanol is significantly influenced by the preparation methods. The methanol productivity increases in the order of impregnation < co-precipitation < deposition-co-precipitation. The methanol productivity is about 3 fold higher over the deposition-co-precipitated catalyst than the impregnated catalyst. A maximum methanol productivity of 0.66 kg kg_{cat}⁻¹ h⁻¹ and corresponding selectivity of 99.2 mol % have been achieved for a Cu₂Ni₁/SiO₂ catalyst prepared via the deposition-co-precipitation method. The increase in methanol productivity is caused predominantly by a decrease in particle size of the active metal alloy particles in combination with a low content of residual alkali metal (Na) from the coprecipitation agent.

3. Effect of Cu/Ni ratio [9]

Silica supported bimetallic Cu-Ni nanomaterials with different compositions of Cu and Ni (20 wt % Cu+Ni, Cu/(Cu+Ni)=0, 10, 25, 50, 66.7, 75, and 100 mol %) have been prepared by incipient wetness impregnation method without calcination before reduction. The formation processes of Cu-Ni alloy nanoparticles have been followed by in situ XRD, XAS, TEM, and mass spectrometry measurements. In situ reduction of Cu-Ni alloys on both XRD and XAS have

revealed a strong interaction between Cu and Ni, resulting in improved reducibility as compared to monometallic Ni.

Silica supported Cu-Ni alloys, at high nickel concentrations a homogeneous solid solution of Cu and Ni are formed, whereas at lower nickel contents copper and nickel are separately aggregated and form metallic Cu and Cu-Ni alloy phases. At the same reduction conditions, the particle sizes of reduced Cu-Ni alloys decrease with the increase in Ni content. Ni can enhance the sintering stability of metallic Cu significantly.

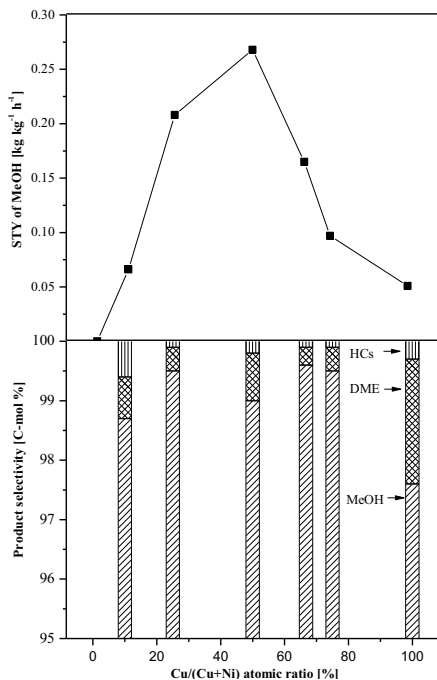


Figure 4 Space time yield of methanol (top) and selectivity of products (bottom) over Cu-Ni catalysts with different atomic ratios of Cu/Ni at steady state. The operating conditions are: P = 100 bar, T=275 °C, GHSV = 4000 h⁻¹, Feed: H₂/CO=1, vol/vol.

The Cu-Ni alloys with different Cu/Ni ratios have been tested for CO hydrogenation. All Cu-Ni alloys produce mainly methanol during CO hydrogenation regardless of the Cu/Ni ratio. These tested Cu-Ni alloy catalysts show similarities in the selectivity mainly towards methanol (~99 mol %), while exhibiting differences in methanol productivity, which follows a 'volcano-type' relationship and reaches the maximum in the molar ratio of 1. It seems that the Cu-Ni alloy catalysts have a similar type of site regardless of Cu/Ni ratio, which are able to selectively hydrogenate CO to methanol, while the amount of this type of sites are different in the surface. This needs to be further investigated.

Conclusion

The following observations have been made: 1) Cu-Ni on SiO₂, ZrO₂, γ-Al₂O₃, and CNT make different products. 2) Cu-Ni alloys (supported on SiO₂ and CNT) are very active and selective catalysts for CO hydrogenation to methanol. 3) Cu_xNi_{1-x} (x=0 to 1) alloys always produce mainly methanol regardless of the Cu/Ni ratio. 4) Pretreatment of impregnated catalysts - with/without a calcination step and different reduction gas compositions have significant influence on Cu-Ni alloy formation and consequently on its activity. 5) Addition of 3 mol % CO₂ to the H₂/CO leads to a significant loss of activity of Cu-Ni catalysts. 6) The methanol productivity increases in the order of impregnation < co-precipitation < deposition-co-precipitation. 7) There is no apparent catalyst deactivation observed during the tested time on stream (40-100 h), contrary to the observation for the commercial methanol synthesis catalyst.

Acknowledgements

This specific work was financially supported by CASE, Catalysis for Sustainable Energy. The work was carried out in collaboration between the CHEC centre, Haldor Topsøe, Center for Electron Nanoscopy (CEN) of DTU, Institute of Chemical Technology and Polymer Chemistry of Karlsruhe Institute of Technology, and Center for Interface Science and Catalysis, SLAC National Accelerator Laboratory (The United States). Thank you for all the supports. Finally, ANKA (Karlsruhe) and ESRF (Grenoble) is gratefully acknowledged for beam time and the EU and DANSCAT for experiment financial support for the synchrotron.

References

- [1] M. Tsoskounoglou, G. Ayerides, E. Tritopoulou, *Energy Policy* 36 (2008) 3797.
- [2] M. Asif, T. Muneer, *Renew. Sustain. Energy Rev.* 11 (2007) 1388.
- [3] R. Quadrelli, S. Peterson, *Energy Policy* 35 (2007) 5938.
- [4] Catalysis for sustainable energy, www.case.dtu.dk
- [5] F. Studt, F. Abild-Pedersen, Q. Wu, A.D. Jensen, B. Temel, J.D. Grunwaldt, J.K. Nørskov, *J. Catal.* 293 (2012) 51.
- [6] Q. Wu, G.L. Chiarello, L.D.L. Duchstein, J.M. Christensen, J.B. Wagner, B. Temel, J.D. Grunwaldt, A.D. Jensen, article in preparation.
- [7] Q. Wu, L.D.L. Duchstein, F. Studt, J.M. Christensen, C.F. Elkjær, J.B. Wagner, S. Dahl, B. Temel, J.D. Grunwaldt, A.D. Jensen, article in preparation.
- [8] Q. Wu, L.D.L. Duchstein, J.M. Christensen, C.D. Damsgaard, J.B. Wagner, B. Temel, J.D. Grunwaldt, A.D. Jensen, article in preparation.
- [9] Q. Wu, G.L. Chiarello, L.D.L. Duchstein, J.M. Christensen, C.D. Damsgaard, J.B. Wagner, B. Temel, J.D. Grunwaldt, A.D. Jensen, article in preparation.

**Rui Xue**

Phone: +45 4525 2993
E-mail: rxue@kt.dtu.dk

Supervisors: John M. Woodley
Anne S. Meyer
Jørn D. Mikkelsen

PhD Study

Started: December 2010
To be completed: November 2013

Reactor and Process Design for Multi-enzymatic Synthesis

Abstract

Enzyme cascades (which mimic nature) using two or more enzymes sequentially for the synthesis of useful chemical compounds are attracting increasing interest as a potential means of production. Such schemes overcome many of the conventional problems integrating biocatalysis into chemical synthetic schemes, such as changes of media, temperature and pH. In this project, the synthesis of sialic acid derivatives and useful oligosaccharides will be taken as an example for the design of an enzyme cascade. Laboratory scale-down tests will be carried out to characterize the enzymatic systems. Engineering tools for selection of reactors and processes for multi-enzymatic synthesis will be developed.

Introduction

During the past decade, biocatalysis has become increasingly attractive for the development of more efficient and cleaner chemical synthetic processes [1]. Higher selectivity and specificity, as well as the use of mild reaction conditions in general gives an excellent 'green' profile to reactions catalyzed by enzymes. Enzymatic synthesis can either involve a single enzyme or can make use of more than one enzyme operating either sequentially or in parallel for the synthesis of more complex compounds (Figure 1) [2,3].

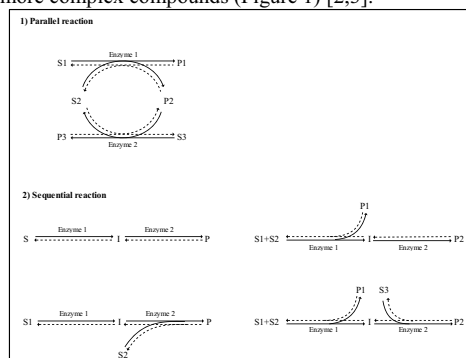


Figure 1: Scheme of different multi-enzymatic reactions. S: substrate, I: intermediate, P: product [3].

The interesting concept of using multi-enzymatic synthesis mimics the chemical processes in nature.

According to the applications, multi-enzymatic systems can be classified into four categories, including cofactor regeneration (parallel reactions), equilibrium shift (sequential reactions), renewable biomass feedstock degradation (mixed reactions) and macromolecule synthesis (mixed reactions). Multi-enzymatic processes have been deemed as an alternative to chemical-catalysis in the production of a number of pharmaceuticals and fine chemicals. In principle, they may also be applied in the field of bulk chemicals (and even biofuels and bio-polymers), although the cost structure in these sectors makes application challenging [3].

The purpose of this project is to develop tools for the selection of synthetic routes, reactors, processes and operations for the reactions which involve multi-step biocatalysis.

Process options

Multi-enzymatic syntheses can be carried out in either a single reactor or several reactors. In theory, for an n-step multi-enzymatic reaction, the number of possible processes is 2^{n-1} . Hence, reducing the size of the search space is highly desirable [3]. Developing an engineering tool to accelerate the selection process is one of the main goals in this project.

For the reactions in which the combination of enzymes may come from different hosts, the enzymes may not share similar optimal temperatures, optimal pH values and other conditions, or even more importantly they may not have similar reaction rates at similar

concentrations of reagents. Hence, it might be preferable to divide the cascade into several groups [3, 4].

On the other hand, a one-pot process uses more than one enzyme in a single reactor. The concentrations of the intermediates are usually low so that the possibility of intermediate inhibition may be reduced. Additionally, one-pot processes may also reduce downstream processing and operating costs [5]. However, the limitation of a one-pot process is that the conditions in each reaction (such as media, temperature, pH, catalyst stability) should be well balanced and optimized for maximum productivity [3].

Reactor options

The selection of an optimal reactor for an enzymatic reaction is usually based on cost, space, mass transfer, kinetics, and reusability of the catalyst [6, 7]. The same principles apply for multi-enzymatic processes.

The number of factors affecting the kinetics of a multi-enzymatic reaction is much more than that in a kinetic model for a single enzymatic reaction. The evaluation and selection of reactors for a multi-enzymatic process, based on the kinetic model, is therefore more difficult. Experimental work can be carried out to examine the performance of different reactors. For the purposes of understanding the mechanisms of the biocatalysis and better experimental design, however, it is also important to establish the theoretical basis first [3]. Integral kinetic models describing the reactions in different reactors are desirable and give rise to a new challenge in the project.

Strategy

The project will be achieved by fulfilling the tasks in two platforms.

Experiment

The case studies involve the synthesis of sialic acid and human milk oligosaccharides.

Sialic acid has been attracting much interest due to its potential applications for the compounds of interest in the pharmaceutical industry [8]. The reactions involved in the production of sialic acid are shown in Figure 2. Both of the reactions are thermodynamically unfavorable in the desired direction. Human milk oligosaccharides are complex glycans that are highly abundant in human breast milk. They have prebiotic, anti-adhesive, anti-microbial and cell surface glycome-modifying effects [9]. Several attempts to synthesize the HMOs have been carried out due to their rare natural origin and unique biological function. However, only low yields have been achieved.

In this project, different routes of producing these compounds will be investigated. Characterization of different enzymes used in the system and study of kinetics and thermodynamics for different reactions will be taken into account.

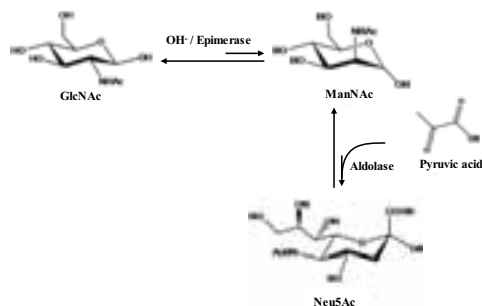


Figure 2: Scheme of the reactions involved in the synthesis of sialic acid.

Modeling

Engineering tools for reactor/process selection for multi-step biocatalysis will be developed. Based on the experimental data, reliable and integral kinetic models will be proposed for future applications and validation of different developed engineering tools.

Acknowledgements

The author would like to express her gratitude to Technical University of Denmark and 'HMO' project for the financial support.

List of publication

1. R. Xue, J.M. Woodley, *Bioresour. Technol.* 115 (2012) 183-195.
2. R. Xue, J.D. Mikkelsen, A.S. Meyer, J.M. Woodley, 10th International Symposium on Biocatalysis and Biotransformations, Giardini Naxos, Sicily, Italy, 2011.
3. R. Xue, J.D. Mikkelsen, A.S. Meyer, J.M. Woodley, Zing Conference on Biocatalysis, Occidental Grand Xcaret Hotel, Xcaret, Mexico, 2012.

References

1. D.J. Pollard, J.M. Woodley, *Trends Biotechnol.* 25 (2007) 66-73.
2. A. Bruggink, R. Schoevaart, T. Kieboom, *Org. Process Res. Dev.* 7 (2003) 622-640.
3. R. Xue, J.M. Woodley, *Bioresour. Technol.* 115 (2012) 183-195.
4. D. Monti, E.E. Ferrandi, I. Zanellato, L. Hua, F. Polentini, G. Carrea, S. Riva, *Adv. Synth. Catal.* 351 (2009) 1303-1311.
5. P.A. Santacoloma, G. Sin, K.V. Gernaey, J.M. Woodley, *Org. Process Res. Dev.* 15 (2010) 203-212.
6. J.F.A. Fernandes, M. McAlpine, P.J. Halling, *Biochem. Eng. J.* 24 (2005) 11-15.
7. J.M. Woodley, M.D. Lilly, in: J.M.S. Cabral, D. Best, L. Boross, J. Tramper (Eds.) *Applied Biocatalysis*, Harwood Academic, 1994, p. 371.
8. R. Schauer, *Glycoconj. J.* 17 (2000) 485 - 499.
9. L. Bode, *Nutr. Rev.* 67 (2009) S183-S191.



Nor Alafiza Yunus

Phone: +45 4525 2910

E-mail: noy@kt.dtu.dk

Supervisors: Rafiqul Gani
John M. Woodley
Krist V. Gernaey

PhD Study

Started: July 2010

To be completed: July 2013

An Integrated Methodology for Design of Tailor-Made Blended Products: Lubricant Base Oil

Abstract

A systematic methodology is developed to design tailor-made blended products. The methodology has three stages; product design, process identification and experimental verification. Only the product design stage is considered in this work. The objective of this stage is to screen and select suitable chemicals to be used as building blocks in the mixture design, and then to propose the blend formulations that fulfill the desired product attributes. The result is a set of blends that match the constraints, the compositions, values of the target properties and information about their miscibility. The methodology has been applied to design several blended products. A case study on design of lubricant base oil is highlighted. The objective is to identify base oil mixtures that satisfy their target properties with at least similar or better performance compared to conventional products.

Introduction

Nowadays, design of chemical-based products is becoming more challenging due to uncertainty in raw materials supply and changes in environmental regulations. Moreover, industry and consumers are now much more focused on environmentally friendly products. They prefer products that not only can perform better, are more effective, and/or last longer, but also have a minimal adverse effect on the environment. Due to the environmental concern, many chemical-based products are now designed to be greener products. Substituting the conventional raw materials (crude oils) with bio-based chemicals is a step towards a green product. Nevertheless, the selection of the raw materials and bio-based chemicals, and formulation of products with new ingredients requires more efforts, cost and resources to find the best raw materials and product formulation. Therefore, the integrated methodology is developed, specifically for blended products, so that it can screen the suitable ingredients in formulations, and thus propose the blends/mixtures to be tested experimentally. This method is able to quickly screen the ingredients and identify the most promising blends. It thus could reduce the cost and resources consumption for a specific product design.

In order to fulfill consumer needs, products need to be designed such that all the consumer needs and product

functions are matched in an economically sustainable manner. Note that the blended products (liquid formulations) need to satisfy a set of product attributes (related to product needs) and a set of constraints related to blend stability, functionality, etc. Selection of the suitable ingredients is vital in product design since it determines the product's performance. In order to design tailor-made blended products, an integrated methodology to design mixture/blended products has been developed. The methodology has three stages: 1) product design, 2) process identification, and 3) experimental verification. In the first stage, which will be presented here, a computer-aided methodology is implemented to quickly identify and evaluate the most promising blend candidates. Subsequently, the ability to produce the chemicals used as the components in the mixtures is analyzed. This will form the base for design of experiments needed for verification. The latter two stages are not considered here.

Integrated Methodology

Figure 1 illustrates the three-stage methodology, where the details of the methodology are explained elsewhere [1]. Here, the product design stage is explained in detail. It consists of 4 main tasks. First, the design problem is defined where the product needs are identified, translated into target properties and given target values.

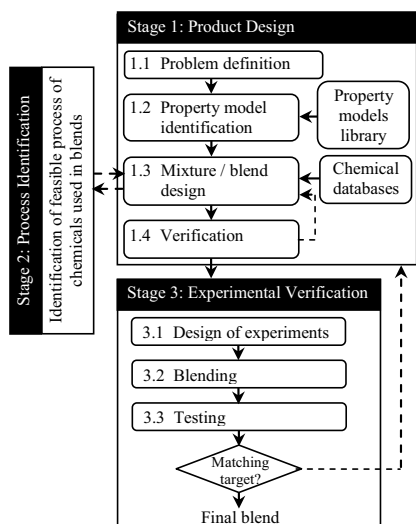


Figure 1: Integrated methodology

Secondly, target property models are retrieved from a property model library developed specifically for this methodology. Thirdly, a mixture/blend design algorithm is applied to obtain the mixtures/blends that match the set of constraints (design targets). Fig. 2 illustrates the details of this task, where a decomposition based solution strategy is employed to solve the mixture/blend problems in the product design stage. The problem is divided into four levels;

Level 1(L1): Preliminary screening of the mixture based on the pure component properties without involving any calculations.

Level 2(L2): Checking the mixture stability since it is very important in chemical-based (product) formulation design. Totally immiscible and partially miscible mixtures must be rejected.

Level 3(L3): The optimal composition range of each mixture is calculated to satisfy the linear property constraints. Here, the mixtures and their compositions are identified.

Level 4(L4): The result from L3 is used as input to the optimization problem in L4, and the problem is solved to give the mixtures that satisfy the non-linear constraints.

The result is a set of blends that match the constraints, as well as their compositions, the value of the target properties of the blends and information about their miscibility. Finally, the mixture target property values are verified by means of rigorous models.

General Problem Formulation

The blend problem is formulated as a Mixed Integer Non-Linear Programming (MINLP) problem, where the specified objective function is to be optimised, subject to product attributes (target properties) and process specifications. Considering the multiple types of

constraint equations, the general blend problem is formulated as:

$$\min/\max f_{obj}(x, y, C, Q, E, S)$$

Subject to

$$\text{Mixture constraints: } g_1(x, y) \leq 0$$

$$\text{Target property constraints: } \xi_{LB} \leq g_2(x, y, \varphi) \leq \xi_{UB}$$

$$\text{Process model constraints: } g_3(x) = 0$$

$$x \in \{x | x \in R^n, 0 \leq x \leq 1\}$$

$$y \in \{0,1\}$$

Where f_{obj} is the objective function either to minimize or maximize the composition x , type of mixture y , cost C , product performance Q , environment E , or sustainability factors S ; y is a binary integer variable, which is linked to the identities of the chemicals; x is a continuous variable, which is related to the mixture compositions; while φ corresponds to pure properties; ξ_{LB} and ξ_{UB} represent the lower and upper bounds of property constraints; g_1 , g_2 and g_3 represent the mixture constraints (for example miscibility and solubility of the mixture), the target property constraints and the process model constraints, respectively.

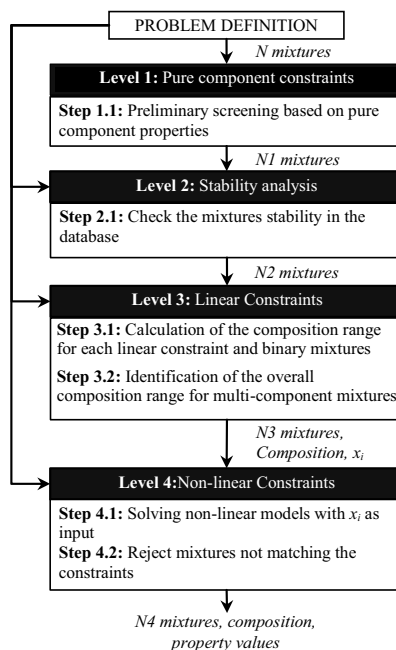


Figure 2: Mixture/blend design methodology (Stage 1, Task 1.3)

Case Study: Design of Lubricant Base Oil Mixtures

Problem formulation: Lubricants are widely used to reduce friction between two moving surfaces, e.g. in engines. Formulated lubricants are the mixture of base oil and additives. Base oil is the main component in a lubricant, where it can represent between 65-98 percent

of the lubricant. Meanwhile, an amount of additives is added according to the severity of the application. Additives are required to enhance certain criteria of a lubricant, for example, viscosity modifier, antiwear, dispersants, and form inhibitor.

The base oil properties influence the lubricant attributes, where they vary according to respective sources. The most common base oil sources are: petroleum, synthetic and biological, i.e. originating from plants or animals [2]. Mineral oils derived from petroleum are the most widely used base oils. On the other hand, synthetic oils are man-made oils with superior properties, thereby performing well in extreme conditions. Vegetable oils are easily degraded. They have poor oxidative stability and cold flow properties, making them suitable only for low demand applications. Comparing various types of base oils, it can be concluded that synthetic oils have excellent physical and chemical properties, but are expensive, while mineral oils are cheaper but less environmentally friendly, and vegetable oils are biodegradable but have poor oxidative stability and cold flow properties [3]. Therefore, the objective of this work is to design mixtures of base oils that combine good lubricant properties with low environmental impact at a reasonable production cost.

Task 1.1: Problem Definition

The new base oil mixtures should have good lubrication performance, where the mixture is able to lubricate and prevent wear, function properly at high temperature and flow continuously at low temperature. It should have a suitable specific gravity for handling purposes, low flammability limit to avoid fire within the lubrication system for reasons of safety, and low volatility to reduce lubricant loss to the environment, thereby reducing the environmental pollution. In addition, the base oil mixtures must be stable, meaning that the mixtures do not oxidize to form deposits in the system to be lubricated, and must be single-phase mixtures. The base oil mixture is designed as a single grade oil for gasoline engines to be used in a hot climate with average ambient temperatures of around 27°C.

In order to achieve the above-mentioned objective, a set of chemicals from basic lube feedstocks (hydrocarbon) and bio-based chemicals are used as building blocks. The mixtures of base oil may comprise mineral oil components, vegetable oils as well as bio-based chemicals to form binary, ternary or multi-component mixtures. The first task is to translate the product needs into target properties and then to set the target values. The following properties are considered; lubrication

and wear prevention is measured by viscosity; resistance to high temperature is represented by the relationship between viscosity and temperature, measured as the viscosity index; the ability to maintain the mixture as a liquid at a low temperature is measured by the pour point; specific gravity and density are needed for handling purposes; product safety in terms of fire precaution is controlled by the flash point; the volatility is measured by the amount of vapor loss from the lubricant system at 250°C (according to ASTM D5800-10); and the stability of a blend is evaluated from the Gibbs energy of mixing. Also, excessive lubricant oxidation can be avoided by reducing the amount of aromatics and unsaturated chemicals. On the other hand, paraffins are preferred because they have a high melting point temperature making them suitable for high-temperature applications. The base oil needs, translated target properties and their target values are given in Table 1.

Task 1.2: Property Model Identification

The required mixture property models are retrieved from the property model library. A linear mixing rule is used to predict some mixture properties. The general linear mixing rule is represented by Eq. 1.4, where TP is the target property, x_i is the composition of component i , and ϕ_i represent the pure properties of component i . In this work, viscosity of the mixture is predicted using this equation, where TP and ϕ_i are substituted with lv and lv_i respectively.

Some of the mixture properties are predicted using correlations, for example, the viscosity index (VI). This correlation is given by Eq. 1.5, where U is the kinematic viscosity of the mixture at 40°C, while L and H represent the kinematic viscosity of 0 and 100 VI oils, respectively. Values of L and H are taken from Rizvi [2], by using the viscosity of blend oil at 100°C as reference.

The pour point is not an additive property. Therefore, pour point blending indices are used to predict the pour point of mixtures, where a linear mixing rule on volume basis is employed. Equations 1.6-1.8 are used to determine the pour point of the blends, where PP_i and BI_i are the pour point and blending index of component i , respectively. BI_B represents the blending index of the mixture. The corresponding pour point of the pure component is the melting point, which is used throughout this work [4].

Equations 1.12-1.17 are flash calculations, which are used to estimate the lubricant volatility. Here F represents the feed, L the liquid and V the amount of

Table 1: The needs of base oil mixture, translated target properties and target values

Need	Property	Symbol	Unit	Target value
1 Able to lubricate and prevent wear	Viscosity, 100°C	ν	cSt	4.12 – 12.5
2 Able to function properly at a high temperature	Viscosity Index	VI	-	> 80
3 Able to flow at the surrounding temperature	Pour point	PP	C	< 25
4 Handling purposes	Specific gravity, 15°C	SG	-	0.80 – 0.91
5 Safety	Flash point	FP	C	> 220
6 Environmental	Volatility, 250°C	V/F	%	< 15

vapor; z_i , x_i and y_i are feed, liquid and vapor fractions, respectively. K_i is the equilibrium constant, P_i^{sat} is the saturated pressure of component i , P is the pressure of the system, and A_i , B_i , and C_i are Antoine constants for component i .

Task 1.3: Mixture/blend Design

The base oil formulation design is formulated as a mathematical problem by minimizing the cost subject to mixture constraints, target properties and process specifications (also represented as constraints). Considering all the constraints, the base oil problem is formulated as follows:

$$\text{minimize } f_{obj}(C, x) \quad \dots (1.1)$$

Subject to,

Mixture constraints:

$$\frac{\Delta G^{mix}}{RT} = \sum_i^{NC} x_i \ln x_i + \frac{G^E}{RT} \quad \dots (1.2)$$

$$\frac{d^2 G^{mix}}{dx^2} > 0 \quad \dots (1.3)$$

Target property constraints:

$$TP = \sum_i^{NC} x_i \varphi_i \quad \dots (1.4), \quad VI = \frac{L-U}{L-H} \times 100 \quad \dots (1.5)$$

$$BI_L = PP_L^{0.08} \quad \dots (1.6), \quad BI_B = \sum_i^{NC} x_i BI_i \quad \dots (1.7)$$

$$PP_B \leq BI_B^{0.08} \quad \dots (1.8), \quad 1/\rho_B = \sum_i^{NC} (x_i/\rho_i) \quad \dots (1.9)$$

$$SG \leq \frac{\rho_B}{\rho_w} \quad \dots (1.10), \quad \sum_i^{NC} \frac{x_i \gamma_i P_i^{sat}(T)}{P_{i,fp}^{sat}} - 1 = 0 \quad \dots (1.11)$$

$$Fz_i = Lx_i + Vy_i \quad \dots (1.12), \quad y_i = K_i x_i \quad \dots (1.13)$$

$$K_i = P_i^{sat}/P \quad \dots (1.14), \quad \ln P_i^{sat} = A_i - B_i/(T - C_i) \quad \dots (1.15)$$

$$P_{dew} = 1 / \sum_i^{NC} (y_i/P_i^{sat}) \quad \dots (1.16),$$

$$\sum_i^{NC} \frac{z_i K_i}{1 + V(K_i - 1)} - 1 = 0 \quad \dots (1.17)$$

Process model constraints:

$$\sum_i^{NC} x_i - 1 = 0 \quad \dots (1.18)$$

This problem is solved using the mixture/blend design methodology as illustrated in Figure 2. Initially, a total of 44 basic lube feedstock compounds were used to formulate 946 binary mixtures. At the first level, L1 of screening, 93% of the mixture candidates were rejected based on their pure properties (only 63 binary mixtures remained). At L2, 3 out of 63 were removed because they are unstable. At L3, the compositions of the remaining 60 mixtures were optimized to satisfy the linear constraints. Then, this composition range is used as input at L4 to calculate the optimal mixtures that also satisfy the non-linear constraints. Only 33 mixtures were found to satisfy all constraints. Fig. 3 illustrates this reduction of the number of mixture candidates for ternary and quaternary mixtures.

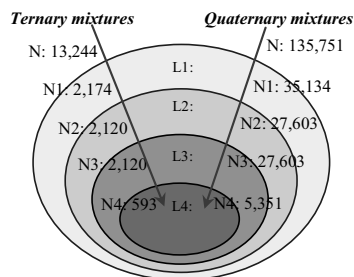


Figure 3: Number of mixture candidates

There are many mixtures at L4 that satisfied all the constraints. The mixtures are then optimized further to obtain a minimum cost. The mixtures with lower costs are identified as listed in Table 2. The bio-based chemicals, propane-1,2,3-triol (C35) and cis-9-Octadecenoic acid (C39) are present in each of the design (blends) mixtures.

Table 2: Base oil for different types of mixtures with their estimated properties

Mixture	Comp.	x_i	Cost (\$/L)	v (cSt)	VI	Pp (K)	SG	Fp (C)
Binary mixture	C13	0.56						
	C35	0.44	7.80	4.12	95	263	0.9790	221.15
Ternary mixture	C10	0.08						
	C20	0.54	6.88	4.12	101	273	0.9781	292.07
	C35	0.38						
Quaternary mixture	C13	0.58						
	C26	0.05						
	C35	0.36	6.63	4.12	108	283	0.9778	292.82
	C39	0.01						

C10: 3-Methyleicosane C13:2-Methyltricosane C20: 3-Ethyltetracosane C35: propane-1,2,3-triol C26: 1H-Dibenz[*a,i*]fluorene, eicosahydro- C39 : cis-9-Octadecenoic acid

Conclusions and Future Work

An integrated methodology to design blended products has been applied for design of base oil mixtures. A decomposition approach is used to solve the blending problem, and systematically reduces a large number of blend candidates. The bio-based chemicals derived from renewable resources are used in the base oil mixtures, which yields a more sustainable product. In the future, the base oil mixture design will be extended for lubricant design by adding additives which can enhance the base oil attributes. Furthermore, the methodology will be tested and validated for other types of blended products to extend the capability of the methodology.

References

- Yunus, N. A., Gernaey, K.V., Woodley, J.M., and Gani, R. (2011). ESCAPE22 proceeding, Elsevier, p. 752-756.
- Rizvi, Syed Q. A. (2009). Comprehensive Review of Lubricant Chemistry, Technology, Selection, and Design. ASTM International.
- Wilson, B. (1998). Lubricants and functional fluids from renewable sources. Industrial Lubrication and Tribology, 50(1), 6.
- Lynch, T. R., (2008). Process Chemistry of Lubricant Base Stocks. United States. Taylor and Francis Group..

**Shizhong Zhang**

Phone: +45 4525 2853
E-mail: shiz@kt.dtu.dk

Supervisors: Søren Kill
Kim Dam-Johansen
Sten Nørkjær
Hempel A/S

PhD Study
Started: September 2011
To be completed: August 2014

Wind Turbine Blade Coatings with Anti-Erosion Properties

Abstract

Rain erosion is one of the main destructive factors leading to physical failure of wind turbine blade coatings. The whirling-arm rig as one of the most popular rigs in the paint industry for blade coating evaluation is expensive and time consuming to operate. At this stage, a new rain erosion test rig was designed and constructed. The new rig is cheap, small and easy to be operated. It can test 22 samples simultaneously which is an essential expectation.

Introduction

Wind turbine blade coatings play a critical role in determining the durability and performance efficiency. It protects them from exposure to rain, solid particle, dust, UV radiation, salt water, extreme temperature fluctuation and ice accumulation. Rain droplet impacting is one of the most important factors causing erosion. Rain field properties including droplet temperature, droplet shape, droplet size and density, attack angles, impact velocity and impact time can influence the erosion process in different ways [1]. It is difficult to perform the real erosion test for aircrafts and wind turbine blades, therefore, material anti-erosion properties are normally tested on an artificial erosion testing rig, which can provide an experimental simulation on the coating erosion process and predict the lifetime [2].

The most representative devices of liquid impingement testing are rotating disk-and-jet (namely wheel-and-jet) repetitive impact apparatus, and whirling arm-and-spray (namely rotating arm) distributed impact apparatus. Historically, the first was the wheel-and-jet method, which has been used in various forms since 1920 [3]. Whirling arm devices were developed from wheel-and-jet approach for higher-velocity testing. A complex single impact GRCI hydrometeor facility was used to study waterdrop impact mechanism in 1976; it can achieve well-formed waterdrop impact, so precisely controlled parameters could come true, this allows detailed study of both liquid and solid [27]. There are also other types of waterjets impact facilities used by different researchers. Apparatus useful for some specific investigation as rocket sleds and nylon bead impact.

A distinction is made between “distributed impact tests” and “repetitive impact tests”. Devices using sprays or simulated rainfields fall into the first category, and most using jets into the second. Another method for distinction is made between the “single impact test” and “multiple impact tests”. But here a new distinction method is proposed, it distinguishes all the liquid erosion facilities by the number of sources that impact a specimen during the test, for example, devices using one nozzle or needle etc. are called single impact-source device, and more than one will be called multiple impact-source devices.

Whirling-arm test method is an effective research tool for guiding exploratory development of rain erosion resistant material, and its results are regarded as an unwritten standard by paint companies. But the setup occupies large space due to its necessity with big radius to achieve high speeds in simulated rain. It is also expensive to construct and operate such big equipment.

Specific Objectives

The first stage of this project is to build a new set up whose test results should be able to be correlated with the whirling-arm test results. The rig should be small, cheap to construct and easy to operate to aid the screening test of the new coating development. As an easy way to simulate the rain erosion, single impact-water jet is the very first one constructed in history, and it has also been proved to be an effective way for liquid erosion simulation. Our new rig design was started from investigating the even distributed water jet and to make necessary modification to find out the proper conditions for creating the same erosion ranking as whirling-arm.

Results and Discussion

The first design of the new rig is shown in Figure 1; a wheel rotating in a chamber can hold 22 panels. A water bath with 100 L water under the chamber is to control temperature in order to investigate the temperature effect on the erosion process, and the water will be sucked by a high pressure pump to create high pressure water at maximum 200 bars, then panels will be impacted and eroded. A high speed camera on the wall can record the whole erosion process and as one of the most important parameters, the start of the erosion can be detected.

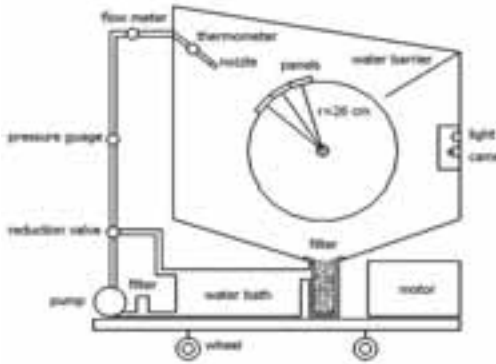


Figure 1: New water jet erosion rig design from cross sectional view.

Three coatings, each with 3 duplicates were tested with new erosion test rig under 200 bar water pressure. The rig was stopped for visual evaluation and taking picture every 20 minutes, it can be seen in Figure 2 that each coating was eroded but shows different erosion pattern.

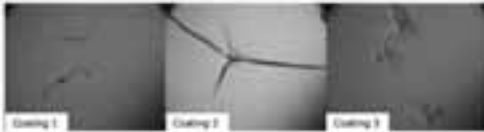


Figure 2: Trial test of new rig with three different coatings.

Before the test, each of the panels were photographed by a digital camera and pictures were taken every 20 minutes, all the photos were analyzed by Image J which is a powerful image analysis program that can measure the area of a complex object. In this case, the cracks or pits on coatings can be measured and the failure fraction for the same surface area of 9 coatings can be ranked. The ranking is shown in **Error! Reference source not found.** It can be seen that coating 1 failed much faster than coating 2, while there was no failure found on coating 3 over 280 minutes. However, this method gives the opposite results to whirling-arm test in which coating 1 showed the best anti-erosion performance.

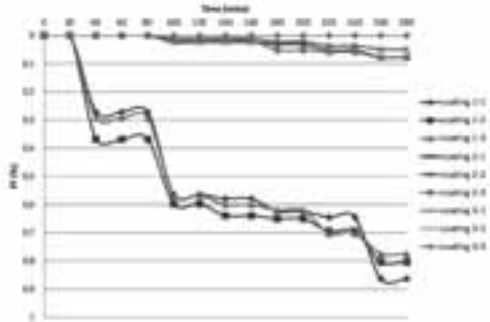


Figure 3: Failure fraction versus time of 9 coatings

Conclusions

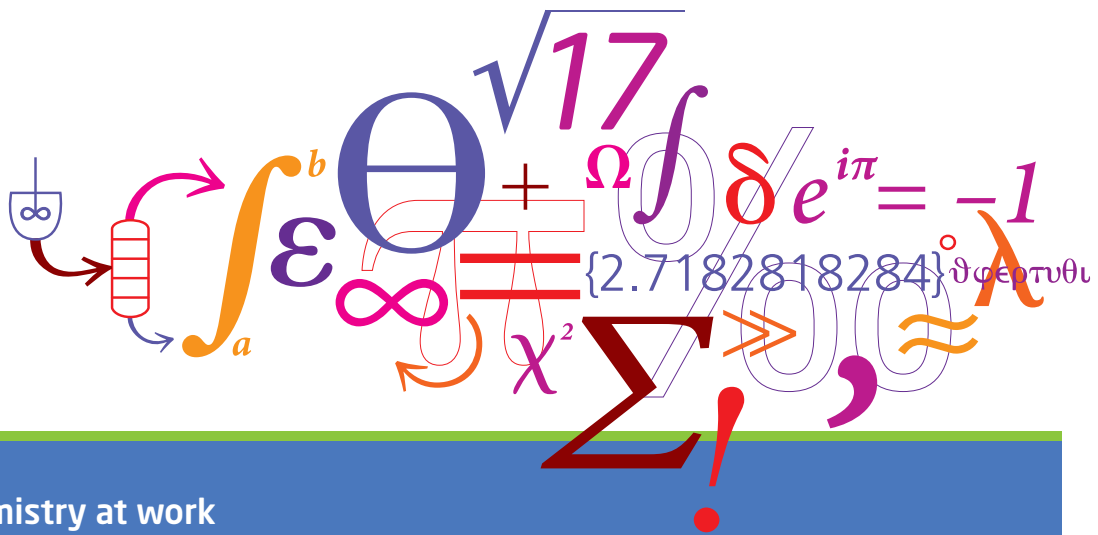
A new cheap, small and easy operating erosion test rig was constructed; it can test 22 samples each time. All these can fulfill the requirements of the project, but the test showed opposite results to the whirling-arm test. According to literature survey, erosion is a complex process; the difference might be from the water jet speed, size and shape or the relaxation time. The rig is to be modified in the following stage in terms of these concerns.

Acknowledgement

The project is financially supported by the Technical University of Denmark and The Hempel Foundation.

References

1. O. G. Engel, Mechanism of Rain Erosion, Report No. 53-192, Wright Air Development Center, 1953.
2. The free library, Coatings critical for wind energy efficiency, <http://www.thefreelibrary.com>.
3. J.E. Field, Wear. 233-235 (1999) 1-12
4. W. F. Adler, Wear. 233-235 (1999) 25-38



Chemistry at work

Bio Engineering

Catalysis

Combustion and Environmental Engineering

Ecosystem Modelling and Sustainability

Engineering Thermodynamics

Enzyme Technology

Petroleum Engineering

Polymer Technology

Process Technology and Unit Operations

Product Design

Reaction and Transport Engineering

Systems Engineering

Department of Chemical
and Biochemical Engineering

DTU Building 229
Søltofts Plads
DK-2800 Kgs. Lyngby
www.kt.dtu.dk